This Page is Inserted by IFW Indexing and Scanning Operations and is not part of the Official Record

BEST AVAILABLE IMAGES

Defective images within this document are accurate representations of the original documents submitted by the applicant.

Defects in the images include but are not limited to the items checked:

- ☐ BLACK BORDERS
- ☐ IMAGE CUT OFF AT TOP, BOTTOM OR SIDES
- ☐ FADED TEXT OR DRAWING
- ☐ BLURRED OR ILLEGIBLE TEXT OR DRAWING
- ☐ SKEWED/SLANTED IMAGES
- ☐ COLOR OR BLACK AND WHITE PHOTOGRAPHS
- ☐ GRAY SCALE DOCUMENTS
- ☐ LINES OR MARKS ON ORIGINAL DOCUMENT
- ☐ REFERENCE(S) OR EXHIBIT(S) SUBMITTED ARE POOR QUALITY
- ☐ OTHER: _____

IMAGES ARE BEST AVAILABLE COPY.
As rescanning these documents will not correct the image problems checked, please do not report these problems to the IFW Image Problem Mailbox.

Pergamon

Tetrahedron Letters 43 (2002) 8721–8725

TETRAHEDRON LETTERS

Co-crystal structures of 4,7-phenanthroline and carboxylic acids: synthon competition and prediction

Ning Shan, Elaine Batchelor and William Jones*

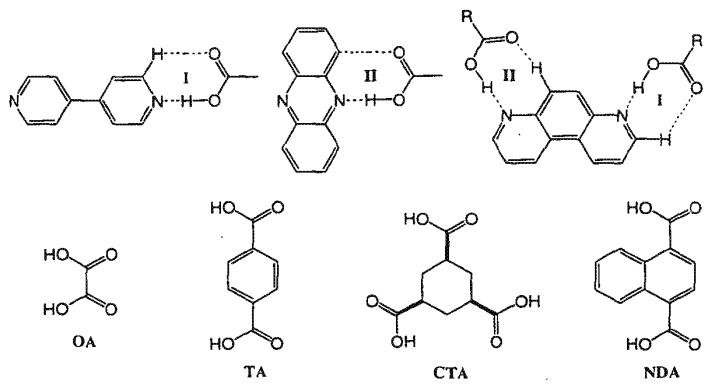
Department of Chemistry, University of Cambridge, Lensfield Road, Cambridge CB2 1EW, UK

Received 30 July 2002; accepted 26 September 2002

Abstract—Co-crystal formation of 4,7-phenanthroline and various carboxylic acids allows a study of the effect of supramolecular synthon competition. © 2002 Elsevier Science Ltd. All rights reserved.

The ultimate goal of crystal engineering is to pre-design solid-state structures based only on a knowledge of molecular structure.[1,2] The supramolecular synthon approach, in which desired supermolecules are formed and/or assembled using previously identified robust intermolecular interactions, is advantageous in that it offers a considerable simplification in the design of crystal structures.[3] In the co-crystal structures of carboxylic acids with 4,4′-bipyridine and phenazine, for example, O–H···N strong hydrogen bonds and weak C–H···O interactions create synthons **I** and **II**, respectively (Scheme 1).[4] For other bases (building blocks), however, a competition between choices of synthon may arise. In the case of 4,7-phenanthroline (**Ph**),[5] for example, hydrogen atoms on two chemically different sp^2 C atoms can be used to form C–H···O interactions (Scheme 1), giving rise to either synthon **I** or **II**. A search of the Cambridge Structural Database (CSD)[6] reveals that no organic **Ph** co-crystal structure has been reported to date, so that the preference for synthon **I** or **II** in carboxylic acid/**Ph** co-crystals is unknown.

A semi-empirical quantum mechanical calculation to determine the preferred synthon in carboxylic acid/**Ph** co-crystals was therefore undertaken. The AM1 approximation, successfully used elsewhere in studies of hydrogen bond arrangements in organic complexes, was adopted.[7] In order to simplify the calculation, a model structure of oxalic acid (**OA**) and **Ph** (**OA+Ph**) was built and geometrically optimised, using the *Cerius*^{2} program.[8] Several restraints were applied: (1) both molecules were constrained to be planar; (2) the H-bond angle of the strong O–H···N interactions was fixed at 180°, with the value of the O···N distances varying between 2.45 and 3.25 Å; (3) the angle between



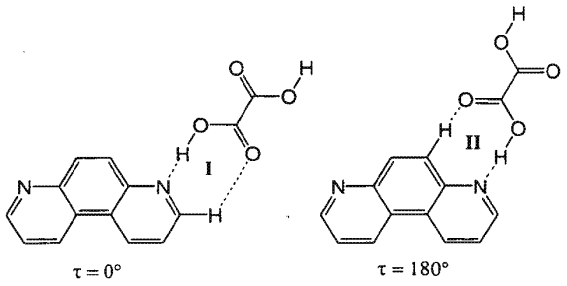
Scheme 1.

* Corresponding author. Tel.: +44-1223-336468; fax: +44-1223-336362; e-mail: wj10@cam.ac.uk

0040-4039/02/$ - see front matter © 2002 Elsevier Science Ltd. All rights reserved.
PII: S0040-4039(02)02140-8

UM00011802
NOVARTIS EXHIBIT 1017
Novartis v. Regents, IPR2023-01346
Page 548 of 4460

two molecules (τ) was fixed at 0° (synthon **I**), 90 or 180° (synthon **II**), as shown in Scheme 2. Hydrogen-bonding energies (HBE) were calculated for each possible supramolecular entity using the MOPAC interface[9]—details are given in Table 1.[10] For all three values of τ, an increase in the O···N distances results in the HBE values decreasing. Only small HBE differences, for the same O···N distances, are observed between formation of $\tau=0°$ (synthon **I**) and that of $\tau=90°$, while the HBE for $\tau=180°$ (synthon **II**) suggests that this arrangement is significantly less stable.



Scheme 2.

Table 1. Hydrogen-bonding energies (HBE) of oxalic acid/**Ph** dimers (kcal/mol) (**OA**+**Ph**)

$D_{O\cdots N}$ (Å)	$\Delta_{\text{Heat of formation}}$	$\Delta_{\text{Heat of formation}}$	$\Delta_{\text{Heat of formation}}$
τ	0° (synthon **I**)	90°	180° (synthon **II**)
2.45	8.267	10.137	82.389
2.55	3.616	5.493	58.793
2.65	0.639	2.427	41.377
2.75	−1.079	0.576	28.488
2.85	−1.961	−0.457	18.812
2.95	−2.369	−1.016	11.486
3.05	−2.551	−1.339	6.04
3.15	−2.637	−1.551	2.203
3.25	−2.67	−1.694	−0.287

Synthon **I**, therefore, would appear to be thermodynamically preferred over synthon **II** in carboxylic acid/**Ph** co-crystal structures.

To compare the theoretical prediction with actual crystal structures, an aliphatic dicarboxylic acid, **OA**, an aromatic dicarboxylic acid, terephthalic acid (**TA**), as well as a tricarboxylic acid, *cis*, *cis*-cyclohexane-1,3,5-tricarboxylic acid (**CTA**), were each separately co-crystallized with **Ph**. The resulting co-crystals, **OA·Ph**, **TA·Ph** (both molar ratio 1:1) and **CTA·2Ph** (molar ratio 1:2), were obtained by slow evaporation at room temperature from a 1:1 acid/**Ph** solution in dimethylsulfoxide (DMSO), tetrahydrofuran (THF) and methanol, respectively (Scheme 1).

In agreement with the HBE calculation, *all* acids and bases interact via synthon **I**. In the structure of **OA·Ph**,[11] zigzag tapes are formed via synthon **I**, involving O–H···N and C–H···O interactions [O···N, H···N, O–H···N: 2.657(4), 1.64 Å, 175.8°; C···O, H···O, C–H···O: 3.259(4), 2.49 Å, 127.3°].[12,13] The torsion angle between carboxylic acid group and aromatic ring is ca. 12.8°. Fig. 1 shows the supramolecular sheets formed by the linkage of adjacent tapes. Zigzag supramolecular tapes formed using synthon **I** also exist in the structure of **TA·Ph** [O···N, H···N, O–H···N (x–0.5, y, $-z$+0.5): 2.724(2), 1.71 Å, 171°; C···O, H···O, C–H···O (x+0.5, y, $-z$+0.5): 3.234(3), 2.59 Å, 117°]. In **TA**, the torsion angle between the carboxylic acid group and the aromatic ring (C–O–N–C) is ca. 38.5°, and results in significantly buckled infinite supramolecular sheets, generated by inter-tape C–H···O hydrogen bonds. In the structure of **CTA·2Ph**, the three carboxylic acid groups on the **CTA** molecule interact with three **Ph** molecules using synthon **I**. With the linkage of synthon **I**, a two-acid–four-base unit is produced and adopts a 'chair' conformation (Fig. 2). These supramolecular units pack forming stacks along the a-axis in a close packed manner. These three structures, therefore, support the idea that synthon **I** is indeed preferred to synthon **II** in these acid:base co-crystals.

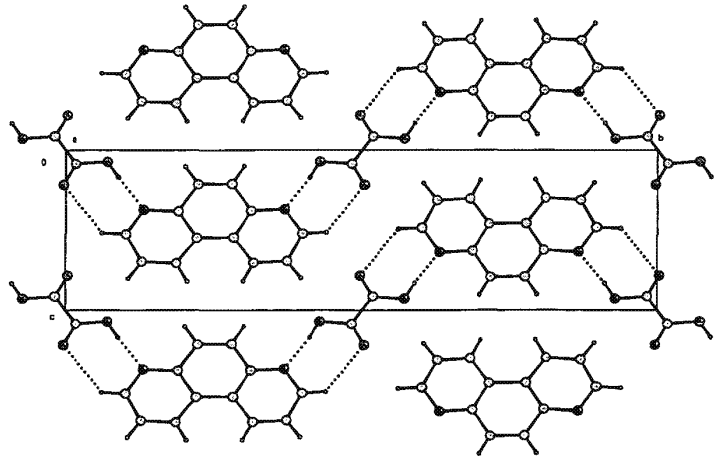


Figure 1. Projection onto (100) showing the supramolecular sheet in the structure of **OA·Ph** involving synthon **I**.

UM00011803
NOVARTIS EXHIBIT 1017
Novartis v. Regents, IPR2023-01346
Page 549 of 4460

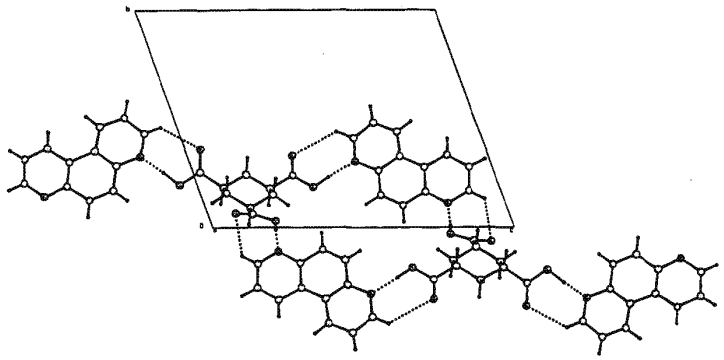


Figure 2. Projection onto (100) showing the two-acid-four-base unit in the structure of **CTA·2Ph**. These units stack along the *a*-axis in a close packed manner.

The crystal structure of **Ph** with 1,4-naphthalenedicarboxylic acid (**NDA**) has also been studied. Interestingly, when co-crystals of **NDA** and **Ph** (**NDA·2Ph**) are obtained by slow evaporation at room temperature from a 1:1 (acid:base) molar ratio solution in *N,N'*-dimethylformamide (DMF), synthon **II** is observed with one carboxylic acid group [O···N, H···N, O–H···N: 2.649(2), 1.64 Å, 173°; C···O, H···O, C–H···O: 3.319(2), 2.62 Å, 122°], whilst the other carboxylic acid group adopts synthon **I** [O···N, H···N, O–H···N ($-x$, $-y+2$, $-z+1$): 2.626(2), 1.62 Å, 169°; C···O, H···O, C–H···O ($-x$, $-y+2$, $-z+1$): 3.638(2), 3.21 Å, 105°] (Fig. 3).

In order to rationalise the presence of synthon **II** in **NDA·2Ph**, further AM1 calculations were carried out using models of **TA+Ph**, **CTA+Ph** and **NDA+Ph**, with similar criteria to those used in the case of **OA+Ph**. For **TA** and **CTA** molecular pairs, similar results to that of **OA+Ph** were obtained. In the case of **NDA+Ph**, however, for the same O···N distances, smaller HBE differences are observed in all cases between models of $\tau = 0°$ (synthon **I**) and $\tau = 180°$ (synthon **II**) in **NDA+Ph** (Table 2). This would suggest that, in the case of **NDA·2Ph**, the energy difference between synthon **I** and **II** is likely to be less important during crystallization.

We are not aware of a systematic study having been made of the choice of supramolecular arrangement among two or more possible synthons with the same functional groups, and we describe this as *synthon competition*. In this study, the hydrogen bond arrangements adopted in the majority of carboxylic acid/**Ph** crystal structures, synthon **I**, can be regarded as the result of synthon competition. The actual results of the various competing synthon units determine the specific geometry of supramolecular assemblies in the structures and hence the overall packing arrangements. Our results, furthermore, demonstrate good agreement between experiment and calculation, suggesting that the AM1 approximation can be a practical way to predict the results of synthon competition.

Acknowledgements

We are grateful for a DWEF Cambridge Scholarship and ORS Award (N.S.) as well as financial assistance

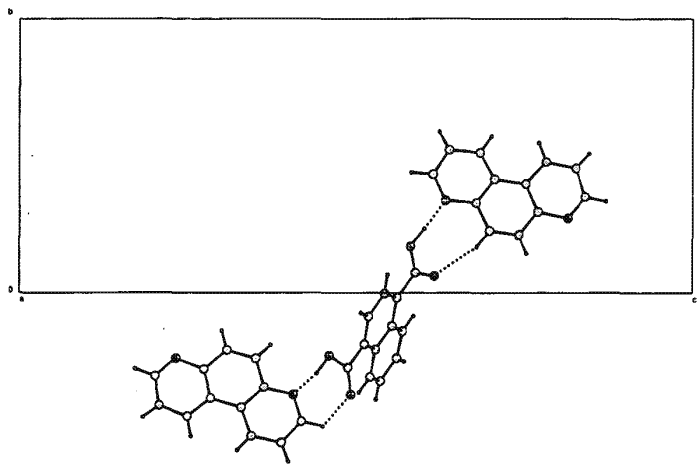
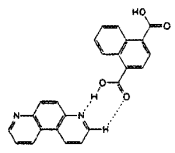
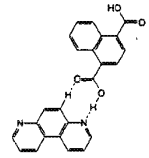
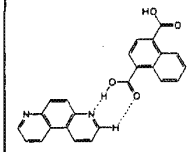
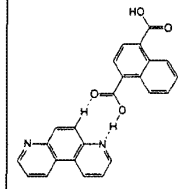


Figure 3. Projection onto (100) of **NDA·2Ph** showing the one-acid-two-base unit formed by synthons **I** and **II**.

UM00011804
NOVARTIS EXHIBIT 1017
Novartis v. Regents, IPR2023-01346
Page 550 of 4460

Table 2. Hydrogen-bonding energies (HBE) of 1,4-naphthalenedicarboxylic acid/**Ph** pairs (kcal/mol) (**NDA**+**Ph**)[a]

$D_{O\cdots N}$/Å	$\Delta_{Heat\ of\ formation}$	$\Delta_{Heat\ of\ formation}$	$\Delta_{Heat\ of\ formation}$	$\Delta_{Heat\ of\ formation}$	$\Delta_{Heat\ of\ formation}$
τ	0° (synthon I)	90°	180° (synthon II)	0° (synthon I)	180° (synthon II)
Scheme					
2.45	10.026	12.347	31.927	9.338	30.877
2.55	5.148	7.101	20.12	4.923	19.005
2.65	1.863	3.5	11.538	2.022	10.37
2.75	-0.187	1.187	5.674	0.278	4.465
2.85	-1.39	-0.235	1.953	-0.691	0.712
2.95	-2.085	-1.113	-0.246	-1.214	-1.509
3.05	-2.504	-1.687	-1.472	-1.514	-2.752
3.15	-2.771	-2.084	-2.125	-1.705	-3.417
3.25	-2.933	-2.356	-2.44	-1.822	-3.741

[a]Note relative positions of naphthalene rings.

from EPSRC towards the purchase of the CCD diffractometers. We also thank Dr. V. R. Pedireddi for a helpful discussion regarding the energy calculations and Dr. J. E. Davies for data collection.

References

1. Desiraju, G. R. *Crystal Engineering: The Design of Organic Solids*; Elsevier: Amsterdam, 1989; pp. 1–25.
2. Bond, A. D.; Jones, W. In *Supramolecular Organization and Materials Design*; Jones, W.; Rao, C. N. R., Eds.; Cambridge University Press: Cambridge, 2002; pp. 391–443.
3. Nangia, A.; Desiraju, G. R. *Acta Cryst.* **1998**, *A54*, 934–944.
4. (a) Shan, N.; Bond, A. D.; Jones, W. *Cryst. Eng.* **2002**, *5*, 9–24; (b) Batchelor, E.; Klinowski, J.; Jones, W. *J. Mater. Chem.* **2000**, *10*, 839–848.
5. Bond, A. D.; Shan, N.; Jones, W. *Acta Cryst.* **2001**, *E57*, o145–o146.
6. CCDC, the Cambridge Structural Database, ConQuest 1.4, Cambridge, UK, 2002.
7. (a) Dannenberg, J. J. *Chem. Mater.* **1990**, *2*, 635–636; (b) Vinson, L. K.; Dannenberg, J. J. *J. Am. Chem. Soc.* **1989**, *111*, 2777–2781; (c) Dannenberg, J. J.; Evleth, E. M. *Int. J. Quantum Chem.* **1992**, *44*, 869–885; (d) Turi, L.; Dannenberg, J. J. *J. Phys. Chem.* **1993**, *97*, 12197–12204.
8. Cerius[2], Accelrys Ltd., Cambridge, UK.
9. Dewar, M. J. S.; Zoebisch, E. G.; Healy, E. F.; Stewart, J. J. P. *J. Am. Chem. Soc.* **1985**, *107*, 3902–3909.
10. HBEs have been calculated by subtracting the heats of formation of the two monomers from that of the pair. Even though a large amount of this energy is due to H-bonding in the pair, the contributions of other types of interactions, e.g. van der Waals interactions and induced and permanent dipole–dipole interactions, can also be significant. Thus, these intermolecular binding energies are collectively termed as the HBE.
11. X-Ray diffraction data (Mo-Kα $\lambda=0.7107$ Å) were collected at 180(2) K using a Nonius Kappa CCD diffractometer equipped with an Oxford Cryosystems system. Data reduction and cell refinement were performed with the programs *DENZO* (University of Texas, Southwestern Medical Center at Dallas, HKL Denzo and Scalepack, USA, 1997) and *COLLECT* (Nonius, B. V. Delft, The Netherlands, 1998) and multi-scan absorption corrections were applied with the program *SORTAV* (Blessing, R. H. *Acta Cryst.* **1995**, *A51*, 33–38). Structures were solved by direct methods using *SHELXS*-97 (University of Göttingen, Germany, 1997) and refined on F^2 against all data using *SHELXL*-97 (University of Göttingen, Germany, 1997). All non-hydrogen atoms were refined with anisotropic displacement parameters. Hydrogen atoms bonded to C or N atoms were placed geometrically and were allowed to ride during subsequent refinement with an isotropic displacement parameter fixed at 1.2 times U_{eq} for the atoms to which they were attached. Hydrogen atoms bonded to O were located in difference Fourier maps and refined isotropically without restraint.

Crystal data for **OA·Ph**: $C_7H_5NO_2$, $M=135.12$, colourless plate, monoclinic, space group $P2_1/m$, $a=3.7136(7)$, $b=23.455(5)$, $c=6.7199(13)$ Å, $\beta=92.57(3)°$, $V=584.7(2)$ Å^3, $Z=4$, $D_{calcd}=1.535$ Mg/m^3, $\mu=0.115$ mm^{-1}, $F(000)=280$, crystal size $0.30\times0.10\times0.04$ mm^3, 3477 reflections collected, 1048 independent reflections ($R_{int}=0.0783$), $R_1=0.0751$, $wR_2=0.2059$ for $I>2\sigma(I)$, $R_1=0.1085$, $wR_2=0.2335$ for all data.

UM00011805
NOVARTIS EXHIBIT 1017
Novartis v. Regents, IPR2023-01346
Page 551 of 4460

Crystal data for **TA·Ph**: $C_{10}H_7NO_2$, $M=346.33$, colourless block, orthorhombic, space group *Pnma*, $a=13.3988(9)$, $b=30.798(3)$, $c=3.7657(2)$ Å, $V=1553.9(2)$ Å^3, $Z=8$, $D_{calcd}=1.480$ Mg/m^3, $\mu=0.105$ mm^{-1}, $F(000)=720$, crystal size $0.16\times0.10\times0.10$ mm^3, 5129 reflections collected, 1639 independent reflections ($R_{int}=0.0596$), $R_1=0.0489$, $wR_2=0.0935$ for $I>2\sigma(I)$, $R_1=0.1038$, $wR_2=0.1103$ for all data.

Crystal data for **CTA·2Ph**: $C_{33}H_{28}N_4O_6$, $M=576.59$, colourless block, triclinic, space group $P\text{-}1$, $a=7.2332(4)$, $b=12.3119(9)$, $c=16.4902(13)$ Å, $\alpha=108.891(3)$, $\beta=100.998(4)$, $\gamma=93.412(4)°$, $V=1352.23(16)$ Å^3, $Z=2$, $D_{calcd}=1.416$ Mg/m^3, $\mu=0.099$ mm^{-1}, $F(000)=604$, Crystal size $0.12\times0.12\times0.05$ mm^3, 11327 reflections collected, 4731 independent reflections ($R_{int}=0.0851$), $R_1=0.0580$, $wR_2=0.1090$ for $I>2\sigma(I)$, $R_1=0.1344$, $wR_2=0.1364$ for all data.

Crystal data for **NDA·2Ph**: $C_{36}H_{24}N_4O_4$, $M=576.59$, yellow plate, monoclinic, space group $P2_1/c$, $a=7.3810(2)$, $b=12.1035(5)$, $c=30.1798(11)$ Å, $\beta=90.074(2)°$, $V=2696.14(17)$ Å^3, $Z=4$, $D_{calcd}=1.420$ Mg/m^3, $\mu=0.095$ mm^{-1}, $F(000)=1200$, crystal size $0.40\times0.18\times0.07$ mm^3, 14929 reflections collected, 5527 independent reflections ($R_{int}=0.0522$), $R_1=0.0500$, $wR_2=0.1032$ for $I>2\sigma(I)$, $R_1=0.0994$, $wR_2=0.1213$ for all data.

Crystallographic data have been deposited with the Cambridge Crystallographic Data Centre as supplementary publication numbers CCDC 190657–190660. Copies of these data can be obtained free of charge on application to CCDC, 12 Union Road, Cambridge, CB2 1EZ, UK (fax: +44(0)1223-336033 or e-mail: deposit@ccdc.cam.ac.uk).

12. Intermolecular bond distances and angles to H atoms were normalised to standard neutron-derived distances along the bond vectors derived from the X-ray results.
13. Allen, F. H.; Kennard, O.; Watson, D. G.; Brammer, L.; Orpen, A. G.; Taylor, R. *J. Chem. Soc., Perkin Trans. 2* **1987**, S1–S19.

UM00011806
NOVARTIS EXHIBIT 1017
Novartis v. Regents, IPR2023-01346
Page 552 of 4460

Pergamon

Crystal Engineering 5 (2002) 9–24

Crystal Engineering

www.elsevier.com/locate/cryseng

Crystal engineering using 4,4′-bipyridyl with di- and tricarboxylic acids

N. Shan, A.D. Bond, W. Jones *

Department of Chemistry, University of Cambridge, Lensfield Road, Cambridge CB2 1EW, UK

Received 14 July 2001; received in revised form 13 September 2001; accepted 13 September 2001

Abstract

The X-ray structures of four co-crystals of 4,4′-bipyridyl (Bipy) with two dicarboxylic acids and two tricarboxylic acids are described. A coupling (**I**) involving O–H···N and C–H···O interactions, previously seen in co-crystals of carboxylic acids with other heterocyclic bases, is again shown to be involved in the formation of supramolecular structures. Bipy with isophthalic acid, 1,4-naphthalenedicarboxylic acid and 1,3,5-cyclohexane-tricarboxylic acid forms 1:1 complexes. Tapes of acid:base components are formed via coupling **I**; these tapes extend to form supramolecular sheets via O–H···O and/or C–H···O interactions. With tricarballylic acid, a co-crystal with stoichiometry 3:2 (acid:base) is generated, with a four-acid-four-base cyclic motif (involving coupling **I**) as the elementary supramolecular unit. Two previously reported co-crystals of Bipy with trimesic acid and 2,5-di-n-hexylterephthalic acid are also discussed, as well as a CSD search for coupling **I** in mono-and poly-carboxylic acid/Bipy complexes. © 2002 Elsevier Science Ltd. All rights reserved.

Keywords: Crystal engineering; Supramolecular tapes; Hydrogen bonding; 4,4′-Bipyridyl; Dicarboxylic acid; Tricarboxylic acid; Co-crystals

1. Introduction

This work forms part of a continuing study of the design of organic acid:base co-crystals and in particular the role of hydrogen bonding in the creation of specific supramolecular structures. As with most studies of this type, the long-term objective

* Corresponding author.
E-mail address: wj10@cam.ac.uk (W. Jones).

1463-0184/02/$ - see front matter © 2002 Elsevier Science Ltd. All rights reserved.
PII: S1463-0184(02)00002-3

UM00011807
NOVARTIS EXHIBIT 1017
Novartis v. Regents, IPR2023-01346
Page 553 of 4460

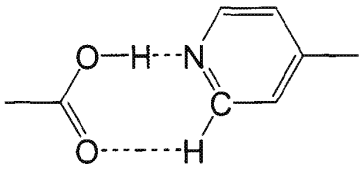
is to define robust procedures for the design of organic crystals possessing desirable chemical and physical properties [1,2]. Crystal engineering and/or supramolecular design requires the efficient creation of molecular assemblies by means of specific intermolecular (i.e. non-covalent) interactions [3].

Synthons and couplings are terms frequently used to describe groups of non-covalent interactions linking together molecular units. Crystal engineering, therefore, requires identification of those synthons or couplings that may be considered reliable and robust [4]. The hydrogen bond is among the most reliable of intermolecular interactions and several reviews have addressed the role of hydrogen bonding in crystal engineering [5,6]. In the case of acid:base co-crystals, Batchelor et al. [7] have recently used a strong/weak hydrogen-bond coupling based on O–H···N/C–H···O interactions to create supramolecular tapes using carboxylic acids and phenazine.

Various papers have reported the use of Bipy as a design component in crystal engineering [8]. When co-crystallised with carboxylic acid groups, the pyridyl nitrogen atoms can interact with the carboxyl -OH to form O–H···N hydrogen bonds. Additionally, the pyridyl *ortho*-H may form a C–H···O hydrogen bond with the carbonyl oxygen, leading to the formation of coupling **I** (Scheme 1). The Cambridge Structural Database (CSD) [9] has 14 examples of Bipy and carboxylic acid co-crystals to date. Here we examine further the robustness of coupling **I** in Bipy co-crystals with di- and tri-carboxylic acids. Specifically, two dicarboxylic acids (isophthalic acid, IPA and 1,4-naphthalenedicarboxylic acid, NDA) as well as two tricarboxylic acids (1,3,5-cyclohexane-tricarboxylic acid, CTA and tricarballylic acid, TCA) are used (Scheme 2). The packing of some other co-crystals of Bipy with di- and tri-carboxylic acids existing in the CSD are also included in the discussion. Finally, a CSD search of Bipy co-crystals with general carboxylic acids has been carried out and the results are discussed.

2. Experimental

The starting materials with purity of ca. 98% were obtained from Aldrich and were used without further purification. Mixtures of Bipy and the acids were prepared from either *N,N*-dimethylformamide (DMF) or methanol. The input ratios of acid

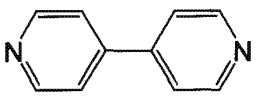


Coupling **I**

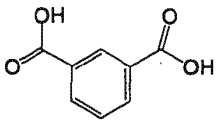
Scheme 1.

UM00011808
NOVARTIS EXHIBIT 1017
Novartis v. Regents, IPR2023-01346
Page 554 of 4460

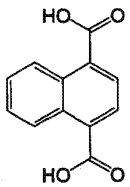
Scheme 2



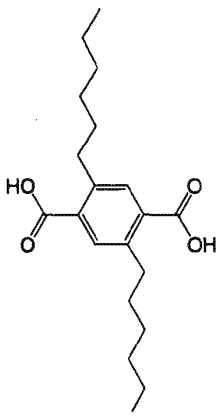
4,4'-bipyridyl
(Bipy)



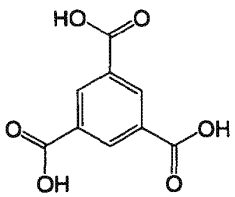
Isophthalic Acid (IPA)



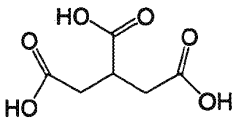
1,4-Naphthalenedicarboxylic Acid (NDA)



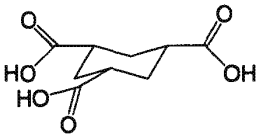
2,6-Di-n-hexylterephthalic Acid (HTA)



Tremesic Acid (TMA)



Tricaballylic Acid (TCA)



Cyclohexane-1r,3cis,5cis-
tricarboxylic Acid (CTA)

Scheme 2

UM00011809
NOVARTIS EXHIBIT 1017
Novartis v. Regents, IPR2023-01346
Page 555 of 4460

and base were 1:1 for the di-acids and 2:3 for the tri-acids. The solutions were left to evaporate slowly at room temperature in air. X-ray diffraction data were collected using a Nonius Kappa CCD diffractometer equipped with an Oxford Cryosystems cryostream. Data were collected at 180(2) K for **2a** and **3a**, but crystals of **2b** and **3b** were observed to crack at this reduced temperature, and data were collected for these at 230(2) K. Data reduction and cell refinement were performed with the programs *DENZO* [10] and *COLLECT* [11], and multi-scan absorption corrections were applied with the program *SORTAV* [12]. Structures were solved by direct methods using *SHELXS*-97 and refined on F^2 against all data using *SHELXL*-97 [13] The crystallographic data are summarised in Table 1. All non-hydrogen atoms were refined with anisotropic displacement parameters. Hydrogen atoms bonded to carbon were placed geometrically and allowed to ride during subsequent refinement with an isotropic displacement parameter fixed at 1.2 times U_{eq} of the atoms to which they are attached. Hydrogen atoms bonded to O or N were located in difference Fourier maps and refined isotropically with the O–H and N–H distances restrained to 0.84(2) and 0.88(2) Å, respectively. These bond distances are intended to provide the best fit to the X-ray data, but do not reflect the true position of the hydrogen nucleus. For discussion of intermolecular distances and angles involving hydrogen atoms, the positions of the hydrogen atoms were normalised to standard neutron-

Table 1
Crystallographic data for the various complexes

Identification code	**2a**	**2b**	**3a**	**3b**
CCDC Deposit No.	179739	179740	179741	179742
Empirical formula	$C_{18}H_{14}N_2O_4$	$C_{22}H_{16}N_2O_4$	$C_{19}H_{20}N_2O_6$	$C_{21}H_{20}N_3O_6$
Formula weight	322.31	372.37	372.37	410.40
Solvent	DMF	DMF	Methanol	Methanol
Temperature/K	180(2)	230(2)	180(2)	230(2)
Wavelength/Å	0.71073	0.71073	0.71073	0.71073
Crystal system	Monoclinic	Triclinic	Monoclinic	Triclinic
Space group	*P2/c*	$P\bar{1}$	$P2_1/n$	$P\bar{1}$
a/Å	9.7977(3)	10.4170(4)	8.3209(4)	8.8093(10)
b/Å	6.8620(3)	15.1751(5)	25.3410(13)	10.9581(17)
C/Å	22.7713(7)	17.8681(4)	8.7105(3)	11.3238(17)
α/°	90	70.479(2)	90	95.793(5)
β/°	100.897(2)	83.103(2)	109.312(3)	111.601(8)
γ/°	90	86.249(2)	90	100.613(8)
V/Å3	1503.35(9)	2641.98(15)	1733.35(14)	981.8(2)
Z	4	6	4	2
Density (calculated)	1.424 g cm^{-3}	1.404 g cm^{-3}	1.427 g cm^{-3}	1.388 g cm^{-3}
Absorption coefficient	0.102 mm^{-1}	0.098 mm^{-1}	0.107 mm^{-1}	0.103 mm^{-1}
Reflections collected	13930	31633	9819	6555
Independent reflections	3444	12014	3031	2667
R_{int}	0.0672	0.0449	0.0455	0.0645
*R*1 [$I > 2\sigma(I)$]	0.0487	0.0753	0.0421	0.0821
*wR*2 [$I > 2\sigma(I)$]	0.1038	0.1691	0.0880	0.2069

UM00011810
NOVARTIS EXHIBIT 1017
Novartis v. Regents, IPR2023-01346
Page 556 of 4460

derived distances [14] along the bond vector derived from the X-ray results. *CERIUS*^{2} [15] and *RPLUTO* [16,17] were used to visualise the structures.

For the co-crystal **2b**, one pyridyl ring in one Bipy molecule exhibited positional disorder in the plane of the molecule. This result was reproduced with different data sets collected from several different crystals. Refinement of the pyridyl ring in a single orientation requires the geometry to be constrained and gives rise to anisotropic displacement parameters with large components in the molecular plane and $R1$ ca. 14%. This arrangement also results in a curious "bifurcated" geometry in which the nitrogen atom of the pyridyl ring points exactly between the two oxygens of the neighbouring carboxylic acid group. Refinement with the pyridyl ring disordered over two orientations is considerably more satisfactory: no geometric restraints are required for either orientation, the site occupancy factors refine to 50% and it is possible to refine all atoms anisotropically, reducing $R1$ to ca. 7.5%. In addition, this arrangement gives rise to two approximately linear O–H···N hydrogen-bond geometries. The C–O bond distances of the neighbouring carboxylic acid group (C(12) − O(3) = 1.241(4)Å and C(12) − O(4) = 1.242(4)Å) do not facilitate distinction between the C=O and C–OH groups, and this was modelled, therefore, with H disordered equally over the two oxygen atoms. It is not possible, however, to distinguish any positional disorder for the other pyridyl ring in the Bipy molecule.

2.1. CSD Searches

Searches were carried out using the 2001 release of the Cambridge Structural Database (CSD) [9] using *ConQuest* version 1.2 [18]. Those structures with $R1 > 0.1$ were discarded, as were organometallic entries. Hydrogen atom positions were normalised. The visualisation package *CERIUS*^{2} was used to analyse the retrieved structures.

3. Results

3.1. Co-crystal structure 2a (Bipy:IPA)

1:1 Co-crystals of Bipy and IPA crystallise in the space group $P2/c$ (Table 1). The atomic numbering scheme is shown in Fig. 1(a). An extended zigzag tape is generated via coupling **I**, Fig. 1(b). A summary of the hydrogen bond parameters for **2a** is given in Table 2. The C–H···O interaction within the coupling (O2···H13A 2.37 Å; O4···H18A 2.55 Å) helps maintain co-planarity of the carboxylic acid group and pyridyl plane; the dihedral angles between the carboxylic plane O1, C7, O2 and pyridyl plane C13, C9, N1 and between the carboxylic plane O3, C8, O4 and pyridyl plane C14, C18, N2 are ca. 3.6° and ca. 10.4°, respectively. Tapes align parallel to each other forming planar supramolecular sheets via C–H···O hydrogen bonds (O2···H9A 2.66 Å; O4···H14A 2.21 Å), Fig. 1(c). No significant hydrogen bonding exists between the sheets.

UM00011811
NOVARTIS EXHIBIT 1017
Novartis v. Regents, IPR2023-01346
Page 557 of 4460

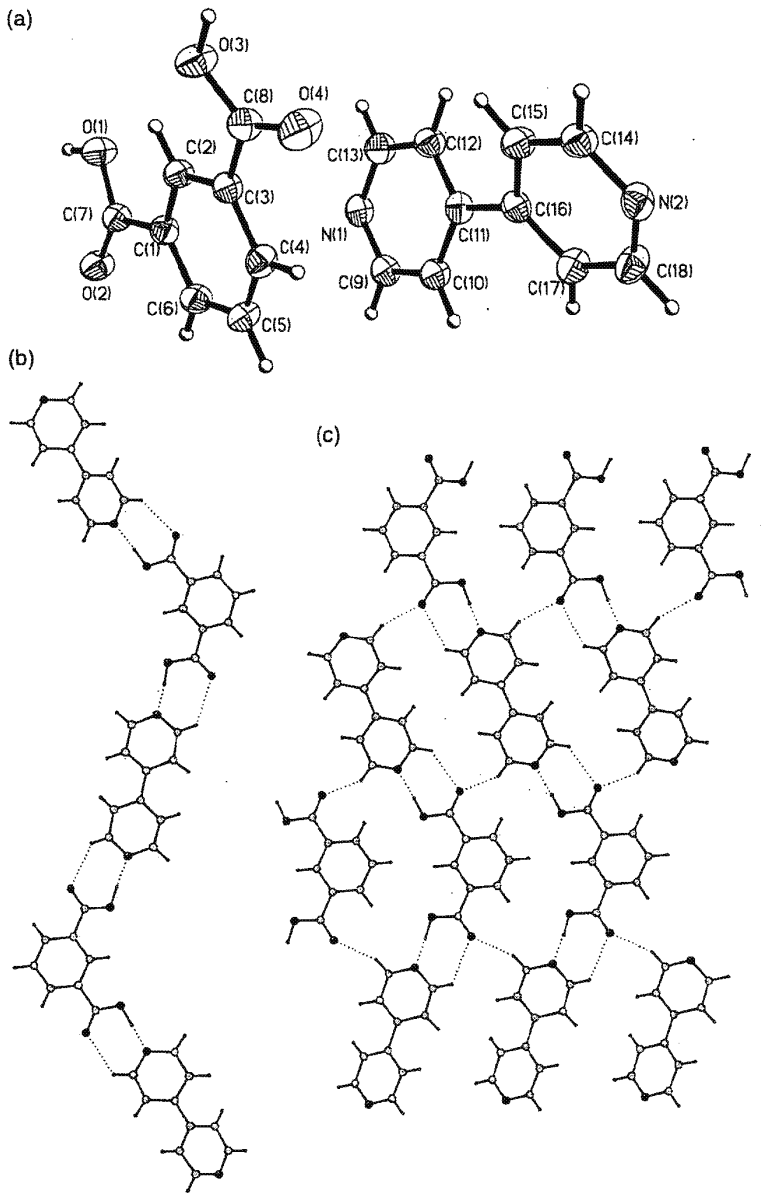


Fig. 1. (a) Atomic numbering scheme of the asymmetric unit of **2a**. (b) The zigzag tape formed through coupling **I**. (c) The supramolecular sheet formed *via* inter-tape hydrogen bonds.

UM00011812
NOVARTIS EXHIBIT 1017
Novartis v. Regents, IPR2023-01346
Page 558 of 4460

Table 2
Selected hydrogen bond parameters for the various complexes

Co-crystal	D–H···A	H···A/Å	D···A/Å	D–H···A	Symmetry operator[a]
2a	O1–H100···N1	1.64	2.6533(17)	177.7	$-x+2, -y-1, -z$
	C13–H13A···O2	2.37	3.159(2)	128.5	$-x+2, -y-1, -z$
	O3–H101···N2	1.61	2.6259(17)	175.7	$-x+1, y-1, z+0.5$
	C18–H18A···O4	2.55	3.255(2)	122.4	$-x+1, y+1, 0.5-z$
2b	O2_1–H2_1···N1_1	1.68	2.696(2)	174.4	
	C17_1–H17A_1···O1	2.52	3.260(3)	124.8	
	O4_1–H4_1···N2_1	1.67	2.683(3)	172.2	$x, y+1, z-1$
	C18_1–H18A_1···O3_1	2.76	3.438(3)	120.6	$x, y-1, z+1$
	O3_2–H3_2···N2′_2	1.65	2.670(7)	173.3	$x, y+1, z-1$
	C22′_2–H22C_2···O4_2	2.55	3.180(8)	116.0	$x, y-1, z+1$
	O3_2–H3_2···N2_2	2.15	3.059(8)	147.4	$x, y+1, z-1$
	O4_2–H4_2···N2_2	1.65	2.670(7)	174.0	$x, y+1, z-1$
	C18_2–H18B_2···O3_2	2.64	3.229(9)	113.7	$x, y-1, z+1$
	O4_2–H4_2···N2′_2	2.15	3.053(9)	147.6	$x, y+1, z-1$
	O2_2–H2_2···N1_2	1.58	2.591(2)	171.9	
	C13_2–H13B_2···O1_2	2.73	3.421(3)	121.5	
	O2_3–H2_3···N1_3	1.69	2.696(4)	168.4	$x, y-1, z+1$
	C13_3–H13C_1···O1_3	2.92	3.392(5)	106.4	$x, y+1, z-1$
	O4_3–H4_3···N2_3	1.57	2.590(3)	174.5	
	C18_3–H18D_3···O3_3	2.58	3.269(3)	121.2	
3a	O2-H100···N1	1.61	2.608(2)	163.6	
	C10–H10···O1	3.31	3.889(2)	114.8	
	O4–H101···N2	1.62	2.627(2)	169.5	$-x+1.5, y+0.5, -z-0.5$
	C17–H17···O3	3.24	3.804(2)	113.6	$-x+1.5, y-0.5, -z-0.5$
	O6–H102···O4	1.92	2.8486(19)	150.4	$x, y, z+1$
	C2–H2A···O5	2.74	3.829(2)	173.5	$x, y, z-1$
3b	O2–H2···N1	1.60	2.614(4)	174.0	$x+2, y, z+1$
	C7–H7···O1	2.59	3.305(4)	123.0	$x-2, y, z-1$
	O4–H4···N3	1.63	2.633(5)	166.7	
	C17–H17···O3	2.63	3.347(6)	123.2	
	O6–H6···N2	1.59	2.588(5)	167.2	
	C12–H12···O5	2.63	3.335(5)	122.1	

[a] Symmetry operators apply to acceptor atoms.

UM00011813

NOVARTIS EXHIBIT 1017
Novartis v. Regents, IPR2023-01346
Page 559 of 4460

3.2. Co-crystal structure 2b (Bipy:NDA)

Crystals of the 1:1 complex **2b** adopt the space group $P\bar{1}$. Fig. 2(a) shows the atomic numbering scheme for one of the three acid:base residues in the asymmetric unit (Fig. 2(b)). Essentially linear supramolecular tapes (Fig. 2(c)) are formed via coupling **I** (Table 2). C–H···O interactions exist, with H···O distances ranging from 2.52 to 2.92 Å. As a result, coupling **I** is relatively distorted with the dihedral angle between the carboxylic group and pyridyl ring varying between 6.9° and 25.2°. Tapes pack parallel to each other forming planar sheets and the inter-tape weak C–H···O interactions also exist (H···O 2.30 Å), Fig. 2(d). The naphthalene rings are twisted from the plane of the supramolecular sheets, and adjacent sheets are stacked such that these rings occupy cavities in the neighbouring sheets.

3.3. Co-crystal structure 3a (Bipy:CTA)

The 1:1 complex **3a** adopts the space group $P2_1/n$ (Table 1). The atom numbering scheme is given in Fig. 3(a). Molecules assemble into crinkled tapes with the curvature of the tape reflecting the *meta* arrangement of the carboxylic acid groups within CTA. In this case, the C–H···O interactions are extended considerably compared with the other co-crystals discussed (H···O 3.31 Å). The angle between the carboxylic acid group and pyridyl ring is 6.5° (Fig. 3(b)). The tapes interact so that crinkled sheets are formed, Fig. 3(c). Strong O–H···O hydrogen bonds exist between carboxylic acid groups in adjacent tapes (Table 2). Additionally, weak C–H···O hydrogen bonds (Table 2) between carboxyl oxygen and cyclohexyl hydrogen are also present (Fig. 3(c)). As shown in Fig. 3(d), the complete structure of **3a** is formed by close packing of the supramolecular sheets.

3.4. Co-crystal structure 3b (Bipy:TCA)

Bipy co-crystallises with TCA in the ratio 3:2 to yield crystals in the space group $P\bar{1}$ (Fig. 4(a)). The supramolecular structure is formed by coupling **I**. Details of the O–H···N/C–H···O hydrogen bonds are provided in Table 2. The elementary supramolecular structure is a four-acid-four-base ring (Fig. 4(b)) which is perpendicular to the *b* axis. These rings are linked further via coupling **I** to form extended tapes. No significant hydrogen bonding exists between the tapes; the total crystal structure is formed by close packing (Fig. 4(c)).

4. Discussion

4.1. Description of co-crystal structures of Bipy with dicarboxylic acids

Tape arrangements are observed in the co-crystals of **2a** and **2b**. In both cases, the ratio of acid and base is 1:1 and molecules are linked by coupling **I**. The geometry of the tapes reflects the geometry of the linking acids in a predictable manner. Two

UM00011814
NOVARTIS EXHIBIT 1017
Novartis v. Regents, IPR2023-01346
Page 560 of 4460

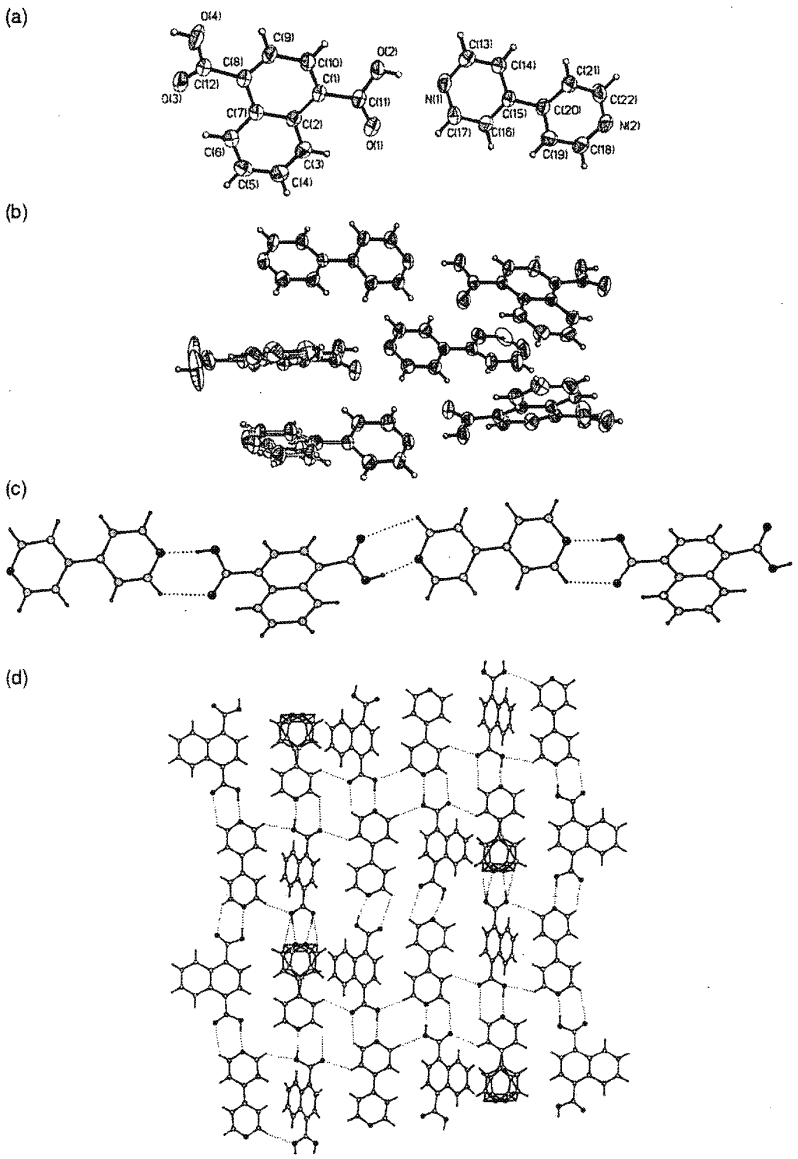


Fig. 2. (a) Atomic numbering scheme of one residue of the asymmetric unit of **2b**. (b) The asymmetric unit containing three independent residues. (c) The tape formed by coupling **I**. (d) The planar sheet formed by tapes by weak C–H···O interactions.

UM00011815
NOVARTIS EXHIBIT 1017
Novartis v. Regents, IPR2023-01346
Page 561 of 4460

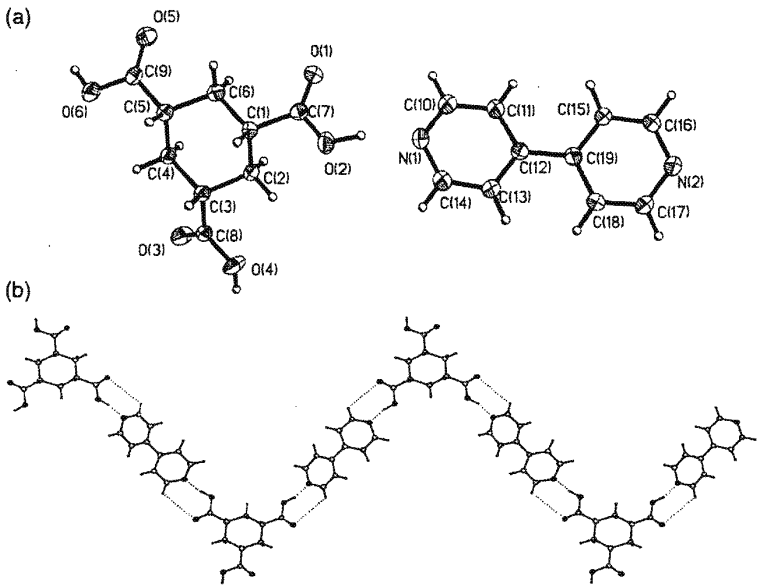


Fig. 3.ab (a) Atomic numbering scheme of the asymmetric unit of **3a**. (b) The zigzag tape formed by coupling **I**.

general types of tapes are shown in Scheme 3, with the tape of **2a** being zigzag while that of **2b** linear. As shown in Fig. 1(c) and Fig. 2(d), C–H···O hydrogen bonds link parallel tapes to create supramolecular sheets. Usually pyridyl hydrogen atoms take part in such interactions. The same arrangement has been observed previously in the complex of Bipy and 2,5-di-n-hexylterephthalic acid (HTA) (**2c**, Fig. 5 [19]).

4.2. Description of co-crystal structures of Bipy with tricarboxylic acids

By contrast with dicarboxylic acid co-crystals, there is much more variety within the structures of tricarboxylic acid co-crystal structures. All of the pyridyl rings take part in coupling **I** with carboxylic acid groups, and the geometry of the acids dictates the overall crystal structures. **3a** forms the 1:1 co-crystal and its behaviour is very similar to the co-crystals of the dicarboxylic acids. Crinkled carbon rings of CTA molecules in **3a** determine the relative positions of carboxyl moieties, and the geometry of the supramolecular sheets is affected accordingly, Fig. 3(c).

The structure of **3b** shows that when co-crystallising tricarboxylic acids with bases in ratio 2:3, rings can be formed. Six-acid-six-base rings have been observed previously in the 2:3 co-crystal of TMA and Bipy (**3c**, [20]). Comparison of the structures of **3b** and **3c** reveals clearly that the supramolecular structure is dependent on

UM00011816
NOVARTIS EXHIBIT 1017
Novartis v. Regents, IPR2023-01346
Page 562 of 4460

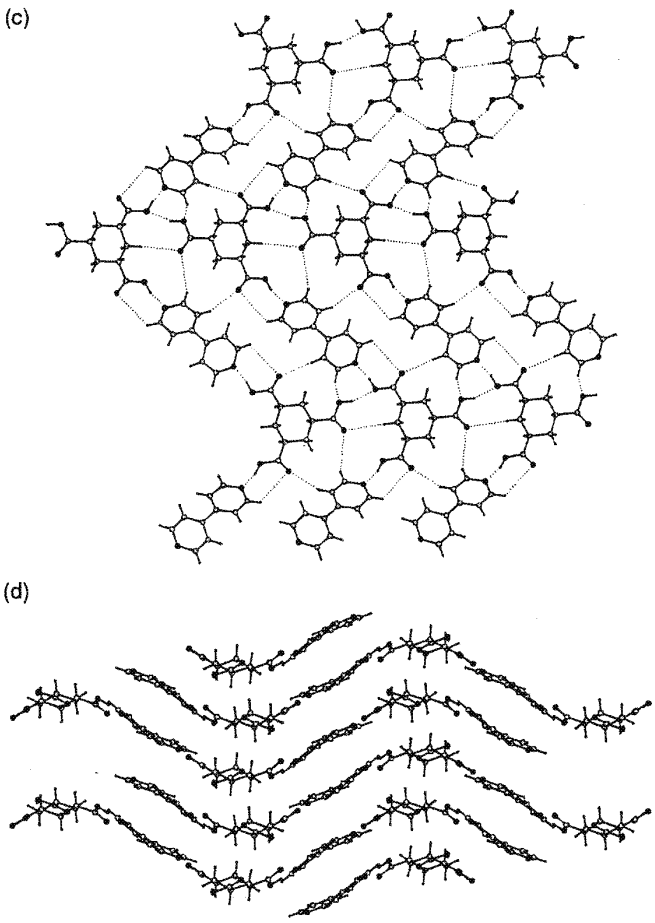


Fig. 3.cd (c) The supramolecular sheets formed by tapes via weak hydrogen bonds. (d) The side view and packing diagram of crinkled supramolecular sheets.

the geometry of the tricarboxylic acid. The three-fold symmetric planar geometry of TMA gives rise to planar six-acid-six-base rings with three-fold symmetry. In **3b**, however, the geometry of the TCA molecule gives rise to four-acid-four-base rings (Scheme 4). A two-acid-two-base cyclic non-covalent structure formed by thiodiglycolic acid and Bipy via coupling **I** has also been reported by Pedireddi et al. [21]. In **3b**, however, the cyclic structure is enlarged to form a four-acid-four-base ring. In addition, supramolecular tapes are formed in **3b** based on these cyclic units.

UM00011817
NOVARTIS EXHIBIT 1017
Novartis v. Regents, IPR2023-01346
Page 563 of 4460

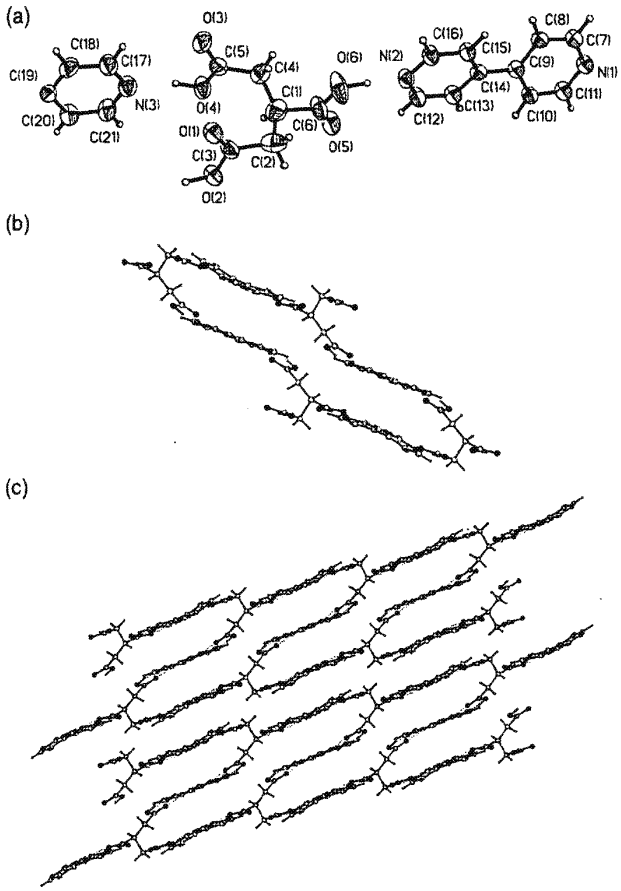
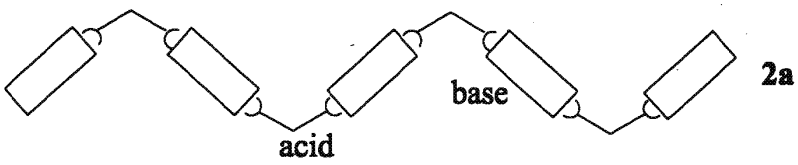


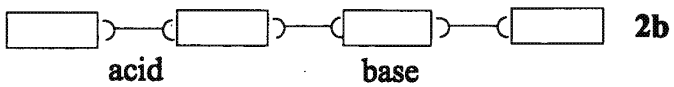
Fig. 4. (a) Atomic numbering scheme of the asymmetric unit of **3b**. (b) The basic four-acid-four-base ring in the structure of **3b**. (c) Packing of tapes in the crystal structure of **3b**.

4.3. A CSD search of carboxylic acid:Bipy co-crystals with coupling I

Although coupling **I** is observed in all of the six crystal structures considered, this does not necessarily imply that it will be present in all co-crystals of Bipy and carboxylic acids. To investigate the general robustness of coupling **I**, a search of the CSD was undertaken. 14 examples of Bipy co-crystals with carboxylic acids were identified. Of these complexes, 4 involved mono-carboxylic acids [22], 9 involved dicarboxylic acids [19,21,23] and one involved trimesic acid [20]. Interestingly, *all* 14 structures possess coupling **I**. Details of the geometry of coupling **I** from the CSD search are displayed in Fig. 6. For the O–H···N interactions: (a) H···N distances vary between ca. 1.60 and 1.75 Å while the mean value of the distances is ca. 1.65

UM00011818
NOVARTIS EXHIBIT 1017
Novartis v. Regents, IPR2023-01346
Page 564 of 4460





Scheme 3

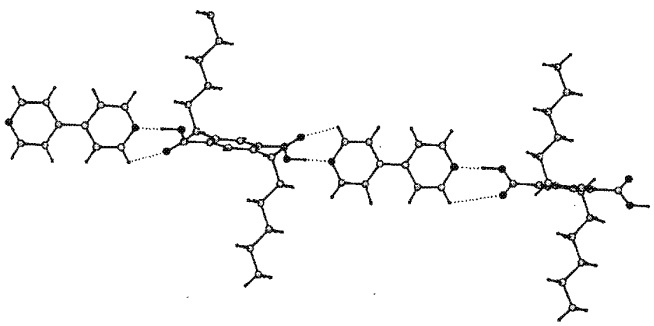


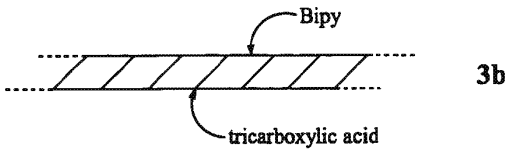
Fig. 5. The supramolecular tape formed by coupling **I** in the structure of **2c**.

Å; (b) most of the N···O distances are focused between 2.60 and 2.65 Å; (c) the O–H···N angles lie in the range 165°–180°. For the C–H···O interactions, the mean values of the H···O and C···O distances are ca. 2.8 and 3.5 Å, respectively, while the C–H···O angles mainly lie between 100° and 130°.

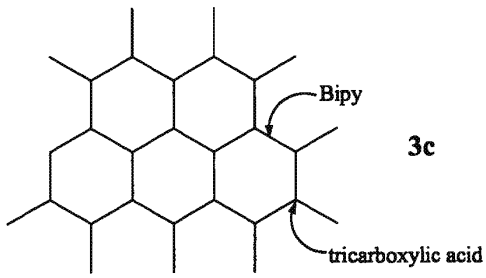
4.4. Comments on coupling I in the co-crystals of Bipy with carboxylic acids

Clearly, coupling **I** is a predictable and robust motif in the structures of co-crystals of Bipy with carboxylic acids. The strong O–H···N interaction plays the main role in controlling the one-dimensional supramolecular assemblies of the co-crystals. The C–H···O interactions are weaker and more readily distorted, as seen in the example of the structure of **2c**. In **2c**, O–H···N hydrogen bonds exist (Fig. 5), but the long alkyl side-chains on the benzene ring of terephthalic acid force the pyridyl and benzene ring to be almost perpendicular to each other. As a result, the H···O distance

UM00011819
NOVARTIS EXHIBIT 1017
Novartis v. Regents, IPR2023-01346
Page 565 of 4460



3b



3c

Scheme 4

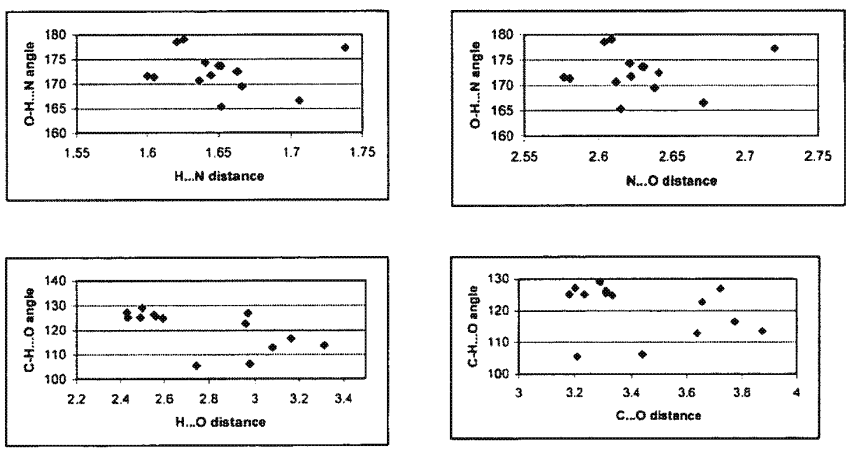


Fig. 6. (a) The geometry of O–H···N interactions in coupling I in the CSD. (b) The geometry of C–H···O interactions in coupling I in the CSD.

(3.03 Å) in the C–H···O interaction is at the long end of the typical range (in typical C–H···O interactions, the C···O separations occur in the range 3.0–4.0 Å, with H···O separations in the range of 2.2–3.0 Å [24]).

UM00011820
NOVARTIS EXHIBIT 1017
Novartis v. Regents, IPR2023-01346
Page 566 of 4460

5. Conclusion

Coupling **I** was successfully applied in the design of supramolecular tapes of dicarboxylic acids with 4,4′-bipyridyl. The geometry of the O–H···N interaction is generally predictable, but the geometry of the weaker C–H···O hydrogen bonds may be affected by the geometry of the acid molecules. Furthermore, the shapes of the supramolecular tapes can be affected. For tricarboxylic acid co-crystals, coupling **I** also can be found, but the supramolecular motifs are more variable. This suggests the final structures of the co-crystals are the result of competition between various factors including coupling **I** and the geometry of the acid molecules.

Acknowledgements

We wish to thank DWEF Cambridge Scholarship and ORS Award for financial support to NS and EPSRC for funding (ADB) and assistance with the purchase of the diffractometer.

References

[1] W. Jones, Organic Molecular Solids: Properties and Applications, in: CRC Press, New York, 1997.
[2] G.R. Desiraju, Crystal Engineering: The Design of Organic Solids, in: Elsevier, Amsterdam, 1989.
[3] J.-M. Lehn, Supramolecular Chemistry, in: VCH, Weinheim, 1995.
[4] G.R. Desiraju, Angew. Chem., Int. Ed. Engl. 34 (1995) 2311.
[5] a) G.A. Jeffrey, W. Saenger, Hydrogen Bonding in Biological Structures, in: Springer-Verlag, Berlin, 1991. b) C.B. Aakeroy, K.R. Seddon, Chem. Soc. Rev. 22 (1993) 397. c) M.J. Zaworotko, Chem. Soc. Rev. 23 (1994) 283. d) L. Leiserowitz, Acta Cryst. B32 (1976) 775. e) E. Weber, J. Mol. Graphics 7 (1989) 12. f) J.C. MacDonald, G.M. Whitesides, Chem. Rev. 94 (1994) 2383. g) M.C. Etter, J. Am. Chem. Soc. 104 (1982) 1095.
[6] V.R. Pedireddi, W. Jones, A.P. Chorlton, R. Docherty, Chem. Commun. (1996) 997.
[7] E. Batchelor, J. Klinowski, W. Jones, J. Mater. Chem. 10 (2000) 839.
[8] a) A. Ranganathan, et al., J. Mol. Struct. 522 (2000) 87. b) V.R. Pedireddi, S. Chatterjee, A. Ranganathan, C.N.R. Rao, J. Am. Chem. Soc. 119 (1997) 10867. c) V.R. Pedireddi, A. Ranganathan, S. Chatterjee, Tetra. Lett. 39 (1998) 9831. d) B. Moulton, M.J. Zaworotko, Chem. Rev. 101 (2001) 1629. e) A.J. Lough, P.S. Wheatley, G. Ferguson, C. Glidewell, Acta Cryst. B56 (2000) 261.
[9] F.H. Allen, J.E. Davies, J.J. Galloy, O. Johnson, O. Kennard, C.F. Macrae, E.M. Mitchell, G.F. Mitchell, J.M. Smith, D.G. Watson, J. Chem. Inf. Comput. Sci. 31 (1991) 187.
[10] Z. Otwinowski, W. Minor, Methods Enzymol. 276 (1997) 307.
[11] Nonius COLLECT, Nonius BV, Delft, The Netherlands, 1998.
[12] R.H. Blessing, Acta Cryst. A51 (1995) 33.
[13] G.M. Sheldrick, SHELXS97 and SHELXL97, University of Göttingen, Germany, 1997.
[14] F.H. Allen, O. Kennard, D.G. Watson, L. Brammer, A.G. Orpen, R. Taylor, J. Chem. Soc., Perkin Trans. 2 (1987) S1–S19.
[15] Molecular Simulations Inc., San Diego, CA, 1995.
[16] http://www.ccdc.cam.ac.uk/prods/rpluto/index.html.
[17] F.H. Allen, O. Johnson, C.F. Macrae, J.M. Smith, W.D. Motherwell, J.J. Galloy, D.G. Watson, R.S. Rowland, R.S. Edington, P.R. Garner, S.E. Davies G.F. Mitchell, Cambridge Structural Database System, Volume 4, Analysis and Display Procedures, GSTAT and PLUTO, 1992, Chapter 5, 5.

UM00011821
NOVARTIS EXHIBIT 1017
Novartis v. Regents, IPR2023-01346
Page 567 of 4460

[18] ConQuest Version 1.2, Cambridge Crystallographic Database Center, 2001.
[19] C. Meiners, S. Valiyaveettil, V. Enkelmann, K. Mullen, J. Mater. Chem. 7 (1997) 2367 (Refcode: PULWUO).
[20] C.V.K. Sharma, M.J. Zaworotko, Chem Commun (1996) 2655. (Refcode: RAPHAR).
[21] V.R. Pedireddi, S. Chatterjee, A. Ranganathan, C.N.R. Rao, Tetrahedron 54 (1998) 9457 (Refcode: SOVBOU; SOVDIQ; SOVFIS; SOVFOY; SOVHEQ).
[22] a) P.S. Wheatley, A.J. Lough, G. Ferguson, C. Glidewell, Acta Cryst. C55 (1999) 1489 (Refcode: BEQWAV); b) V.R. Pedireddi, A. Ranganathan, S. Chatterjee, Tetra. Lett. 1998 (9831) 39 (Refcode: FIHYEA; FIJCIK; FIJCUW).
[23] a) S. Chatterjee, V.R. Redireddi, C.N.R. Rao, Tetra. Lett. 1998 (2843) 39 (Refcode: GIPQAX; GIPQEB); b) J.J. Kane, R.F. Liao, J.W. Lauher, F.W. Fowler, J. Am. Chem. Soc. 117 (1995) 12003 (Refcode: ZINZUR).
[24] G.R. Desiraju, Comprehensive Supramolecular Chemistry 6 (1996) 1.

UM00011822
NOVARTIS EXHIBIT 1017
Novartis v. Regents, IPR2023-01346
Page 568 of 4460

Pergamon

Tetrahedron Letters 43 (2002) 3101–3104

TETRAHEDRON LETTERS

Supramolecular synthons in the co-crystal structures of 2-aminopyrimidine with diols and carboxylic acids

Ning Shan, Andrew D. Bond and William Jones*

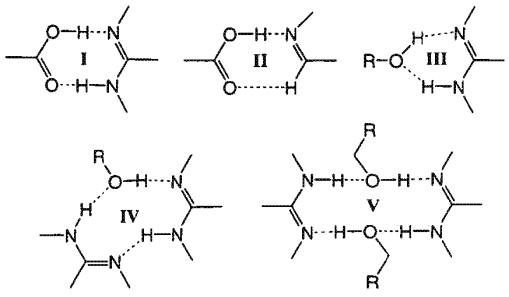
Department of Chemistry, University of Cambridge, Lensfield Road, Cambridge CB2 1EW, UK

Received 5 February 2002; revised 26 February 2002; accepted 8 March 2002

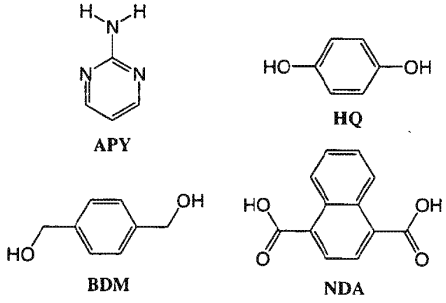
Abstract—The co-crystal structures of 2-aminopyrimidine (**APY**) with diols have been analysed and poly-component hydrogen bond arrangements have been found. In addition, a novel supramolecular synthon has been identified and rationalised in the co-crystal structure of **APY** and 1,4-naphthalenedicarboxylic acid (**NDA**). © 2002 Elsevier Science Ltd. All rights reserved.

The role of hydrogen bonding in crystal engineering and the creation of desired supramolecular structures is well established.[1–4] So-called strong hydrogen bonds, such as O–H···O, N–H···O and O–H···N interactions,[5] play a particularly important structure-directing role. Furthermore, those supramolecular arrangements that possess proportionally more strong hydrogen bonds are likely to be favoured amongst possible alternative arrangements. When designing supramolecular tapes involving carboxylic acids and *N*-heterocycles, therefore, synthon **I** is likely to be preferred to synthon **II**—synthon **I** creating two strong hydrogen bonds whereas synthon **II** is composed of one weak (C–H···O) and one strong hydrogen bond.

In the Cambridge Structural Database (CSD),[6] 22 structures have been reported to date for co-crystals involving 2-aminopyrimidine (**APY**). Of these, 21 involve **APY** co-crystallised with molecules possessing at least one carboxylic acid group and in each structure, synthon **I** is observed.[7] Thus, from the existing crystallographic data, it is possible to predict with reasonable confidence at least the local supramolecular arrangement in carboxylic acid/**APY** co-crystals, i.e. interaction via synthon **I**. Despite the abundance of carboxylic acid/**APY** co-crystals within the CSD, there is little information concerning the types of synthons or supramolecular structures that **APY** will form with other types of functional groups. Diols, for example, are of interest from the viewpoint of crystal engineering because they can be considered as being derived from carboxylic acids with the carbonyl group (C=O) omitted. The carbonyl group is clearly essential in the formation of synthon **I**. In the absence of appropriate crystal structures, a possible new synthon (synthon **III**), which retains the original O–H···N interaction in synthon **I** and creates a new N–H···O interaction, might be predicted as the likely hydrogen bond arrangement in diol/**APY** co-crystals (Schemes 1 and 2).



Scheme 1.



Scheme 2.

* Corresponding author. Tel.: +44-1223-336468; fax: +44-1223-336362; e-mail: wj10@cam.ac.uk

0040-4039/02/$ - see front matter © 2002 Elsevier Science Ltd. All rights reserved.
PII: S0040-4039(02)00511-7

UM00011823
NOVARTIS EXHIBIT 1017
Novartis v. Regents, IPR2023-01346
Page 569 of 4460

To investigate this hypothesis, two representative diols, hydroquinone (**HQ**) and 1,4-benzenedimethanol (**BDM**),[8] were co-crystallised with **APY**. Two co-crystals in the molar ratio 1:2 (**HQ·2APY** and **BDM·2APY**)[9] were obtained by slow evaporation at room temperature from a 1:1 diol/**APY** solution in ethanol.

It transpires that synthon **III** is found in neither of the two diol/**APY** co-crystals, and instead larger cyclic hydrogen-bonded motifs are formed. In the structure of **HQ·2APY** (Fig. 1) molecules assemble in an $R_3^3(10)$ trimer arrangement (synthon **IV**) involving N–H···N, N–H···O and O–H···N hydrogen bonds [N···N, H···N, N–H···N ($-x$, y–0.5, $-z$+0.5): 3.06, 2.18 Å, 144°; N···O, H···O, N–H···O ($-x$, y+0.5, $-z$+0.5): 3.00, 2.13 Å, 144°; O···N, H···N, O–H···N: 2.76, 1.78 Å, 174°].[10,11] This supramolecular hydrogen-bonded ring adopts an 'envelope' conformation similar to that for cyclopentane, and results in a noticeable non-linear arrangement for the N donor hydrogen bond. Infinite supramolecular sheets are formed exclusively using synthon **IV**.

In the structure of **BDM·2APY** (Fig. 2), an $R_4^4(12)$ hydrogen-bonded cyclic synthon exists (synthon **V**) involving two **APY** molecules and two **BDM** molecules. An inversion centre exists within the ring and a *boat-like* conformation is adopted, in which a pair of O–H···N and N–H···O hydrogen bonds exist [N···O, H···O, N–H···O: 2.91, 2.03 Å, 143°; O···N, H···N, O–H···N ($-x$+1, $-y$+2, $-z$+1): 2.83, 1.86 Å, 173°]. Again supramolecular sheets are formed, in which molecules are linked by synthon **V** as well as **APY** $R_2^2(8)$ dimers with C_i symmetry [N···N, H···N, N–H···N ($-x$, $-y$+2, $-z$): 3.03, 2.04 Å, 168°].

The absence of synthon **III** in these two diol/**APY** structures may be rationalised in part by the poor directionality of the N–H···O hydrogen bond (theoretically ca. 130°) that would exist within such a synthon—especially when considered in competition with more geometrically favourable synthons such as **IV** and **V**. Similarly, it is noteworthy that in the presence of carboxyl groups (C=O), synthon **I** is more preferable than synthon **IV** and **V** in the molecular assemblies of carboxylic acid/**APY** co-crystals.

As part of a more general study, we have also been interested in co-crystals formed with 1,4-naphthalenedicarboxylic acid (**NDA**).[12] On the basis of existing crystallographic data, we would predict that synthon **I** would be the *only* direct hydrogen bond arrangement between the carboxylic acid group and **APY** in **NDA·APY** co-crystals. Interestingly, when co-crystals of **APY** and **NDA**[9] are obtained from slow evaporation at room temperature from a 1:1 (acid:base) molar ratio in *N*,*N*-dimethylformamide, synthon **III** is observed [N···O, H···O, N–H···O: 3.17, 2.42 Å, 130°; O···N, H···N, O–H···N ($-x$–1, $-y$+1, $-z$+3): 2.65, 1.67 Å, 159°]. As shown in Fig. 3, supramolecular sheets are

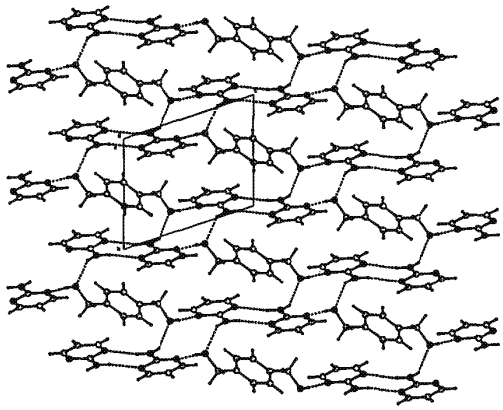


Figure 2. The supramolecular sheet in the co-crystal structure of **BDM·2APY** involving synthon **V**.

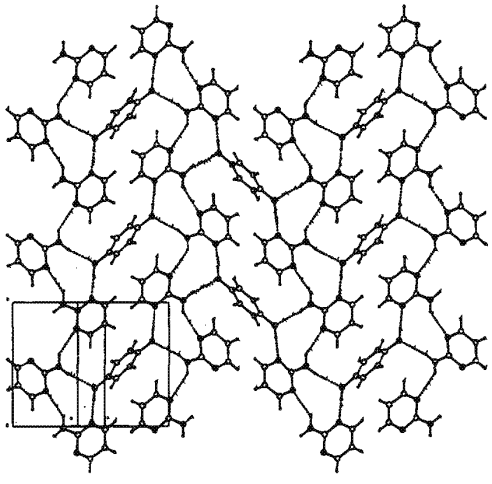


Figure 1. The supramolecular sheet in the co-crystal structure of **HQ·2APY** involving synthon **IV**.

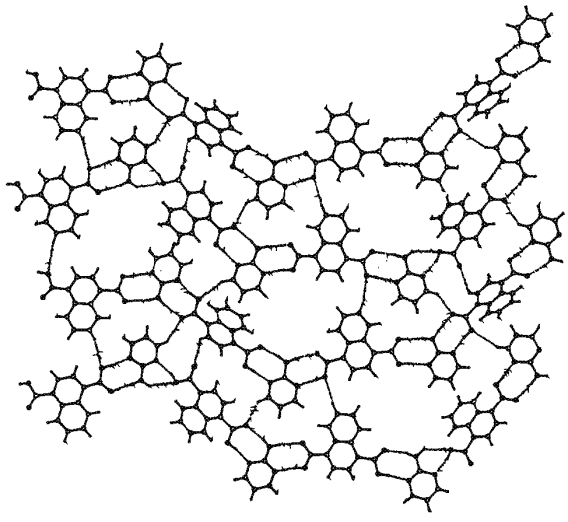


Figure 3. The supramolecular sheet in the co-crystal structure of **NDA·APY** involving synthon **I** and synthon **III**.

UM00011824
NOVARTIS EXHIBIT 1017
Novartis v. Regents, IPR2023-01346
Page 570 of 4460

formed by the alternate packing of two distinct tapes, one of them formed entirely by synthon I while the other tape involves both synthon I and III. Tapes interact via C–H···O interactions to form supramolecular sheets.

The structure of the terephthalic acid (TA)/APY co-crystal reported in the CSD allows us to rationalise the existence of synthon III in NDA·APY. In TA·APY,[13] supramolecular tapes are formed via synthon I. In addition, tapes assemble via inter-tape C–H···O interactions to create supramolecular sheets (Fig. 4). In NDA·APY, however, supramolecular tapes formed *only* by synthon I cannot, unlike TA, pack efficiently because of the asymmetry created by the naphthalene ring on NDA. Synthon III is then utilised as an alternative choice for close packing. Additionally, the existence of synthon III may result from the presence of the carboxyl group, which may prevent the formation of other geometrically more favourable synthons such as synthons IV and V. Clearly therefore, under appropriate conditions synthon III becomes viable.

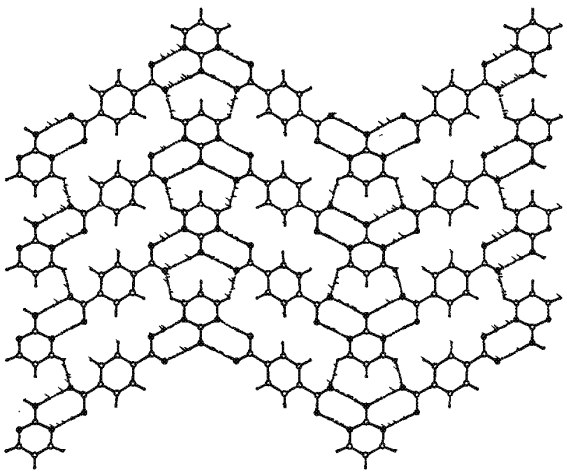


Figure 4. Projection of the supramolecular sheet in the co-crystal structure of TA·APY involving synthon I.

Acknowledgements

We are grateful for a DWEF Cambridge Scholarship and ORS Award (N.S.) as well as the financial assistance from EPSRC with purchase of the CCD diffractometers. We also thank Dr. J. E. Davies for data collection.

References

1. Jones, W. *Organic Molecular Solids: Properties and Applications*; CRC Press: New York, 1997; pp. 181–194.
2. Bond, A. D.; Jones, W. In *Supramolecular Organization and Materials Design*; Jones, W.; Rao, C. N. R., Eds.; Cambridge University Press: Cambridge, 2002; pp. 391–443.
3. Etter, M. C. *Acc. Chem. Res.* **1990**, *23*, 120–126.
4. Aakeroy, C. B.; Seddon, K. R. *Chem. Soc. Rev.* **1993**, *22*, 397–407.
5. Desiraju, G. R. In *Comprehensive Supramolecular Chemistry*; MacNicol, D. D.; Toda, F.; Bishop, R., Eds.; Pergamon Press: Oxford, 1996; Vol. 6.
6. CCDC, The Cambridge Structural Database, ConQuest 1.3, Cambridge, UK, 2001.
7. Among these, five contain synthon I but with proton transfer between the carboxylic acid group and the aromatic N atom on the pyrimidine ring.
8. Shan, N.; Jones, W. *Acta Crystallogr.* **2001**, *E57*, o1233–o1234.
9. X-Ray diffraction data (Mo-K_α $\lambda=0.7107$ Å) were collected at 180(2) K using a Nonius Kappa CCD diffractometer equipped with an Oxford Cryosystems cryostream. Data reduction and cell refinement were performed with the programs DENZO (University of Texas, Southwestern Medical Center at Dallas, HKL Denzo and Scalepack, USA, 1997) and COLLECT (Nonius, B. V. Delft, The Netherlands, 1998) and multi-scan absorption corrections were applied with the program *SORTAV* (Blessing, R. H. *Acta Crystallogr.* **1995**, *A51*, 33–38). Structures were solved by direct methods using SHELXS-97 (University of Göttingen, Germany, 1997) and refined on F^2 against all data using SHELXL-97 (University of Göttingen, Germany, 1997). All non-hydrogen atoms were refined with anisotropic displacement parameters. Hydrogen atoms bonded to C or N atoms were placed geometrically and were allowed to ride during subsequent refinement with an isotropic displacement parameter fixed at 1.2 times U_{eq} for the atoms to which they were attached. Hydrogen atoms bonded to O were located in difference Fourier maps and refined isotropically without restraint.
   Crystal data for HQ·APY: $C_7H_8N_3O$, $M=150.16$, colourless block, monoclinic, space group $P2_1/c$, $a=7.3831(5)$, $b=8.8495(6)$, $c=10.8365(4)$ Å, $\beta=93.621(4)°$, $V=706.61(7)$ Å^3, $Z=4$, $D_c=1.412$ Mg/m^3, $\mu=0.100$ mm^{-1}, $F(000)=316$, crystal size 0.39×0.23×0.23 mm^3, 4984 reflections collected, 1576 independent reflections ($R_{int}=0.0387$), $R_1=0.0397$, $wR_2=0.0984$ for $I>2\sigma(I)$, $R_1=0.0485$, $wR_2=0.1046$ for all data, extinction coefficient 0.108(10).
   Crystal data for BDM·APY: $C_8H_{10}N_3O$, $M=164.19$, colourless block, triclinic, space group $P\text{-}1$, $a=6.5880(5)$, $b=7.4197(6)$, $c=9.3465(6)$ Å, $\alpha=103.588(4)$, $\beta=107.958(4)$, $\gamma=102.109(3)°$, $V=402.29(5)$ Å^3, $Z=2$, $D_c=1.355$ Mg/m^3, $\mu=0.094$ mm^{-1}, $F(000)=174$, crystal size 0.35×0.23×0.09 mm^3, 3981 reflections collected, 1822 independent reflections ($R_{int}=0.0376$), $R_1=0.0429$, $wR_2=0.1075$ for $I>2\sigma(I)$, $R_1=0.0563$, $wR_2=0.1160$ for all data.
   Crystal data for NDA·APY: $C_{16}H_{13}N_3O_4$, $M=311.29$, yellow block, monoclinic, space group $P2_1/n$, $a=11.7912(3)$, $b=17.7583(6)$, $c=27.8061(8)$ Å, $\beta=98.430(2)°$, $V=5759.5(3)$ Å^3, $Z=16$, $D_c=1.436$ Mg/m^3, $\mu=0.106$ mm^{-1}, $F(000)=2592$, crystal size 0.23×0.18×0.18 mm^3, 25986 reflections collected, 9846 independent reflections ($R_{int}=0.0607$), $R_1=0.0509$, $wR_2=0.1167$ for $I>2\sigma(I)$, $R_1=0.1023$, $wR_2=0.1389$ for all data.

UM00011825
NOVARTIS EXHIBIT 1017
Novartis v. Regents, IPR2023-01346
Page 571 of 4460

Crystallographic data have been deposited with the Cambridge Crystallographic Data Centre as supplementary publication numbers CCDC 176101–176103. Copies of these data can be obtained free of charge on application to CCDC, 12 Union Road, Cambridge, CB2 1EZ, UK (fax: +44(0)1223-336033 or e-mail: deposit@ccdc.cam.ac.uk).

10. Bond distances and angles to H atoms were normalised to standard neutron-derived distances along the bond vectors derived from the X-ray results.
11. Allen, F. H.; Kennard, O.; Watson, D. G.; Brammer, L.; Orpen, A. G.; Taylor, R. *J. Chem. Soc., Perkin Trans. 1* **1987**, S1–S19.
12. Shan, N.; Bond, A. D.; Jones, W. *Cryst. Eng.* **2002**, in press.
13. Goswami, S.; Mahapatra, A. K.; Ghosh, K.; Nigam, G. D.; Chinnakali, K.; Fun, H.-K. *Acta. Crystallogr.* **1999**, *C55*, 87–89.

UM00011826
NOVARTIS EXHIBIT 1017
Novartis v. Regents, IPR2023-01346
Page 572 of 4460

British Journal of Experimental Pathology Vol. 27 p46-54 (1946)

We are indebted to the Chief Scientific Officer, Ministry of Supply, for permission to publish this paper, and to numerous colleagues, at Porton and elsewhere, for stimulating discussions.

REFERENCES.

BELOFF, A., AND PETERS, R. A.—(1945) *J. Physiol.*, **103**, 461.
BERGMANN, M., AND NIEMANN, C.—(1938) *J. biol. Chem.*, 122, 577.
BIER, O., AND E SILVA, M. R.—(1938) *C. R. Soc. Biol., Paris*, 129, 769, 773, 1138.
DUTHIE, E. S., AND CHAIN, E.—(1939) *Brit. J. exp. Path.*, 20, 417.
MENKIN, V.—(1936) *J. exp. Med.*, 64, 485.—(1938*a*) *Ibid.*, 67, 129.—(1938*b*) *Ibid.*, 67, 145.—(1938*c*) *Ibid.*, 67, 153.—(1940) *Dynamics of Inflammation*, New York (Macmillan).

FURTHER OBSERVATIONS ON THE CHEMOTHERAPY OF EXPERIMENTAL GAS GANGRENE: FLAVAZOLE, MARFANIL, V187 AND V335.

J. McINTOSH AND F. R. SELBIE.

From the Bland-Sutton Institute of Pathology, Middlesex Hospital, London, W. 1.

Received for publication January 15, 1946.

RECENT publications have shown that the mortality rate in clostridial gas gangrene is still high, in spite of the use of powerful therapeutic agents and improved surgical technique. There is, however, the reassuring finding of MacLennan and Macfarlane (1944) that in the Sicilian and Italian campaign the mortality rate fell from 70 to 30 per cent coincident with an improvement in the general standard of treatment, and that the mortality rate was lowest among those who received adequate surgical and antitoxin treatment within 6 hours of diagnosis. There have also been very favourable reports of the value of treatment with penicillin, but we and others have observed fatalities even in cases where complete sterilization of the clostridial infection was attained, and in spite of adequate antitoxin dosage. As has been suggested recently by MacLennan and Macfarlane (1945*a*, *b*), these deaths may have been due, not to the direct effects of the clostridial infection, but to some toxic substance derived from the damaged muscle.

It is thus evident that the treatment of established gas gangrene is still a major problem, and in view of the fact that the incidence of gas gangrene has been between 0·3 and 1·0 per cent of all United Kingdom and Empire troops wounded in the different campaigns of this war, it is all the more important that efficient prophylactic measures should be employed. The great success of tetanus toxoid in abolishing tetanus has suggested the use of prophylactic injection of toxoid prepared from the clostridia of gas gangrene. However, difficulties have been encountered in the large-scale preparation of potent toxoid, so that this method of protection is still in the experimental stage. We therefore

UM00011827
NOVARTIS EXHIBIT 1017
Novartis v. Regents, IPR2023-01346
Page 573 of 4460

consider that an essential prophylactic measure is the immediate treatment of all wounds with an antiseptic capable of preventing the development of gas gangrene infection, in addition to the removal of all devitalized tissues which might promote the growth of bacteria.

With the aim of finding drugs suitable for this purpose we have investigated the therapeutic action of a large number of substances in experimental gas gangrene infections in mice. The mouse is perhaps not the most suitable animal for the experimental study of gas gangrene infection, in that it requires a very much larger number of organisms to produce a fatal infection in the mouse than in the guinea-pig. However, by the choice of suitable strains of clostridia we have been able to obtain consistent results by intramuscular injection over a number of years. Uncertainties which might arise from variations in the amount of preformed toxin in the inocula have been avoided by using washed organisms suspended in a solution of calcium chloride. This method has the further advantage that it produces an overwhelming bacterial invasion of the tissues at an early stage of the infection, and thus provides a highly suitable test for therapeutic substances.

In a previous communication we have shown that highly active substances against *Cl. welchii* and *Cl. septicum* infections are penicillin and sulphathiazole respectively, whereas *Cl. oedematiens* infection is less responsive to treatment (McIntosh and Selbie, 1943). On the basis of our findings we have recommended a powder mixture containing 1 part of proflavine and 99 parts of sulphathiazole as a prophylactic application to wounds (McIntosh, Selbie, Hudson, Patey, Parkes, McMullen and Pile, 1944). Since then a further series of drugs has been tested, and an account of the results obtained with the more active of these will be given here.

EXPERIMENTAL.

The Drugs Tested.

The drugs which have proved active in this series of tests are four new acridine compounds, two sulphone compounds, and marfanil.

Acridine compounds.—Two of the new acridine compounds, nitracrin (5-amino-2-nitro-7-ethoxyacridine, Albert and Gledhill, 1942) and suproflavine (2 : 8-diamino-1 : 9-dimethylacridine, Albert, Rubbo, Goldacre, Davey and Stone, 1945) were supplied by Dr. A. Albert of Sydney University. The two others, which have been prepared by the Research Laboratories of Boots, Ltd., are acridine-sulphathiazole compounds, flavazole (2 : 8-diaminoacridine-sulphathiazole or proflavine-sulphathiazole) and 5-aminoacridine-sulphathiazole. An account of the favourable results obtained with flavazole in the treatment of infected wounds has already been published (McIntosh, Robinson, Selbie, Reidy, Blake and Guttmann, 1945).

Sulphones.—The two sulphones are V187, or *p*-methylsulphonylbenzamidine hydrochloride, and V335, or *p*-methylsulphonylbenzylamine hydrochloride, both synthesized by Evans, Fuller and Walker (1944) in the course of work on the chemotherapy of typhus. These authors have shown that V187 and V335 are similar to the related compound marfanil in their therapeutic activity against *Cl. welchii* infection in guinea-pigs, and that V187 and marfanil are equally active against *Cl. septicum* and *Cl. oedematiens*.

UM00011828
NOVARTIS EXHIBIT 1017
Novartis v. Regents, IPR2023-01346
Page 574 of 4460

Marfanil.—Marfanil, or *p*-sulphonamidobenzylamine hydrochloride (Miller, Sprague, Kissinger and McBurney, 1940; Klarer, 1941) has been shown by Domagk (1942), Evans, Fuller and Walker (1944), and Hamre, Walker, Dunham, van Dyke and Rake (1944) to have considerable activity against experimental anaerobic infections, and has been used prophylactically by the German army.

Bacteriostatic properties.

Bacteriostatic tests of these drugs have been made in an infusion meat extract with 1 per cent Witte peptone, which does not inhibit sulphonamide activity. Several strains of each of a number of aerobic and anaerobic organisms were sown in this medium in the presence of two-fold dilutions of the drugs, and the results were read after incubation for 24 hours.

The results of these tests are shown in Table I, where it will be noted that sulphathiazole is exceptional in this series of drugs in that it is highly specific in its action against the clostridia, being highly active against *Cl. septicum* and only moderately active against the other two. All the other drugs are highly active against all three clostridia and, although most of the drugs are somewhat more active against *Cl. oedematiens*, the bacteriostatic titres of each drug against the three clostridia lie within fairly narrow limits. On the other hand there are wide differences in the bacteriostatic activities of these drugs against the aerobic organisms. Marfanil, V187, V335, sulphathiazole and penicillin are all relatively much less effective against certain aerobic organisms, particularly the Gram-negative bacilli, whereas the acridine compounds show a more uniform and high activity against all the organisms tested. It is also of interest that the acridine-sulphathiazole compounds have lost none of the bacteriostatic activity of their components, and have even greater activity against *Proteus* and *Ps. pyocyanea.*

TABLE I.—*Bacteriostatic Concentration* in vitro *in mg. per* 100 c.c.

	Cl. welchii.	*Cl. septicum.*	*Cl. oedematiens.*	*Staph. aureus.*	*Strept. pyogenes.*	Coliforms.	*Ps. pyocyanea.*	*Proteus.*
Flavazole	0·6	0·15	0·3	0·6	0·08	0·6–10	2·5–5	0·3–2·5
5-aminoacridine sulphathiazole	1·25	0·15	0·6	1·25	0·3	0·6	2·5–10	1·25
Proflavine	0·6	0·15	0·15	0·6–1·2	0·15	2·5–10	10–40	1·2–2·5
Suproflavine	0·15	0·08	0·02	0·6	0·01	0·6–2·5	2·5–5	0·6–1·25
Nitracrin	0·15	0·08	0·04	0·6	0·3	2·5	20–40	20–40
V187	12·5	0·8	0·4	250	1·2	400–800	400–800	400–800
V335	1·5	0·8	0·8	40–80	1·2	500–2000	250–2000	500–2000
Marfanil	7·5	3·0	1·5	100–1000	2·5	200	75	1000
Sulphathiazole	200	0·4	200	0·6	0·15–0·6	0·6–40	40	40
Penicillin	0·008	0·008	0·001	0·001	0·0005	—	—	—

Toxicity.

With all the substances tested except penicillin an endeavour has been made to maintain a constant relationship between dosage and toxicity by limiting the therapeutic test dose to about $\frac{1}{4}$ to $\frac{1}{3}$ of the maximum tolerated dose by the same injection route. For this purpose mice are injected intramuscularly with increasing quantities of the drug, and the least quantity which causes death is regarded as the maximum tolerated dose. The results of these tests can be judged from the therapeutic doses chosen (Table II). An interesting finding is

UM00011829
NOVARTIS EXHIBIT 1017
Novartis v. Regents, IPR2023-01346
Page 575 of 4460

that the proflavine-sulphathiazole compound, flavazole, is about 20 times less toxic than proflavine by the intramuscular route whereas, by its constitution, it would be expected to be only half as toxic. Further tests, however, by injection into the peritoneal cavity have shown a much smaller difference in toxicity, so that the discrepancy may be largely ascribed to the much lower solubility of flavazole.

The local toxicity of the drugs has also been examined by the histological method previously described (Selbie and McIntosh, 1943). In the therapeutic doses used, nitracrin, suproflavine and 5-amino-acridine-sulphathiazole are somewhat more toxic than proflavine, whereas flavazole, marfanil, V187 and V335 are about equal to proflavine in toxicity.

Therapeutic Experiments.

Method of testing.

The strains used, *Cl. welchii*, B.S.I. 186 and S 107, *Cl. septicum*, B.S.I. 84, and *Cl. oedematiens*, B.S.I. 193 (Jolly) and B.S.I. 194 (H.I.), and the method of testing the therapeutic efficacy of drugs are the same as those previously described (McIntosh and Selbie, 1943). In each therapeutic experiment 4 to 6 groups of mice are injected intramuscularly in the thigh with 0·2 c.c. of washed organisms suspended in a 2·5 per cent solution of calcium chloride, the infective dose being sufficient to kill all untreated mice within 18 hours and usually about 100 minimal lethal doses. One group of mice is left untreated and the remaining groups are treated 1 hour later each with a different drug, which is injected in solution or suspension in quantities of 0·1 or 0·2 c.c. at the site of the infective inoculation.

The daily incidence of deaths is then noted, and at the end of 3 days, after which deaths are few, an estimate of the efficacy of the drugs in postponing or preventing death is made on the basis of the average number of days survived per mouse over the 3-day period. This figure is obtained by adding up the number of whole days survived by the mice and dividing by the number of mice in the group (Whitby, 1937). Thus in an experiment comprising 6 mice, if 2 mice are dead at 1 day, 1 at 2 days, and 1 at 3 days, leaving 2 survivors, the number of whole days survived is $1 \times 1 + 1 \times 2 + 2 \times 3$, giving a total of 9 for 6 mice and an average of 1·5 per mouse. A more convenient method is to express this figure as the percentage of total survival over 3 days, so that the result of this particular experiment is expressed as 50 per cent ($9/18 \times 100$) of 3 days survived. This method of estimation is a more accurate measure of therapeutic efficiency than the crude survival rate at 3 days, since it allows for the delay in death to the second or third day of treated mice that failed to survive the full 3-day period of observation, and it is of particular relevance here because all the untreated mice died within 24 hours.

Results.

The results of our therapeutic tests against the three chief causal organisms of gas gangrene are shown in Fig. 1 and Tables II and III. These experiments have included parallel tests on penicillin, proflavine and sulphathiazole for purposes of comparison. As will be seen from the results, the activities of these substances against the three anaerobic infections have been comparable with

UM00011830

NOVARTIS EXHIBIT 1017
Novartis v. Regents, IPR2023-01346
Page 576 of 4460

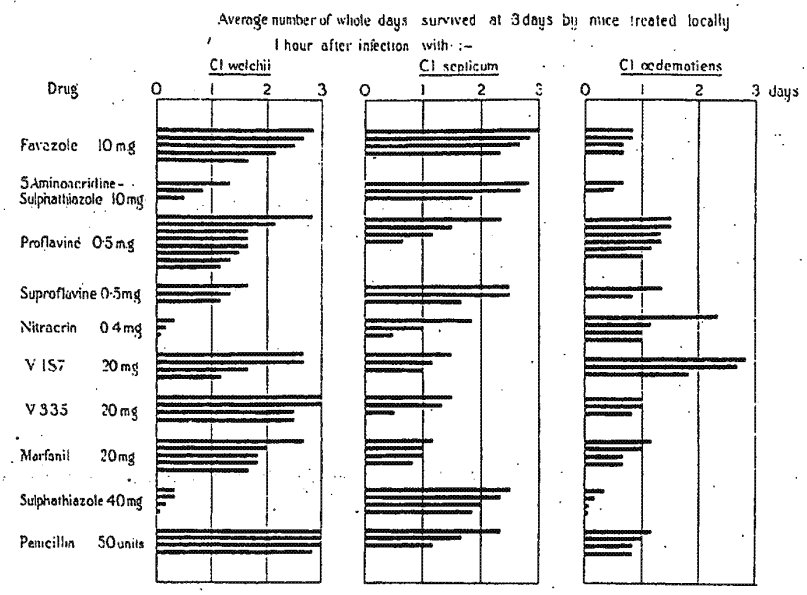


FIG. 1.—Each horizontal line represents one therapeutic test in which 6 mice were treated locally 1 hour after infection; the length of the line indicates the average number of days survived per mouse at the end of 3 days. (For "Favazole" read "Flavazole.")

those obtained previously (McIntosh and Selbie, 1943), so that the conditions of infection and response to therapy do not appear to have altered in any material respect.

The individual tests, each comprising 6 mice, are shown in Fig. 1, where the results are expressed as the average number of whole days survived by the mice at the end of 3 days. It has already been mentioned that the several tests for each drug were made in separate experiments, so that Fig. 1 shows the degree of variation in the response to treatment from one experiment to another. Although this variation has been considerable in a few instances, the results as a whole would appear to be sufficiently uniform to warrant the further analysis presented in Tables II and III.

It is evident from Tables II and III that the three clostridial infections vary greatly in their sensitivity to chemotherapeutic treatment. In the first place, *Cl. oedematiens* infection is in general much less responsive to treatment than the two other infections, in spite of the fact that this organism is at least as sensitive to the direct action of all the drugs used except sulphathiazole (Table I). In the second place, as shown in Table III, the order of efficacy of the drugs varies greatly from one organism to another. Thus, the most active drugs against *Cl. welchii* infection are penicillin and V335, against *Cl. septicum* flavazole, and against *Cl. oedematiens* V187. If, on the other hand, the average efficacy of drugs on all three anaerobes is considered, the most effective are flavazole,

UM00011831
NOVARTIS EXHIBIT 1017
Novartis v. Regents, IPR2023-01346
Page 577 of 4460

TABLE II.—*Effect of Local Treatment 1 Hour after Infection with Cl. welchii, Cl. septicum and Cl. oedematiens.*

Drug.	*Clostridium.*	Number of mice.	Survivors at 3 days. No.	Survivors at 3 days. %	Average number of days survived.	Per cent of 3 days survived.
Flavazole 10 mg.	*welchii*	30	23	77	2·4	79
	septicum	24	20	83	2·7	90
	oedematiens	24	0	0	0·8	25
5-Aminoacridine-sulphathiazole 10 mg.	*welchii*	18	2	11	0·9	30
	septicum	18	13	72	2·4	81
	oedematiens	12	0	0	0·6	19
Proflavine 0·5 mg.	*welchii*	48	21	44	1·8	58
	septicum	24	2	8	1·4	47
	oedematiens	36	3	8	1·3	44
Suproflavine 0·5 mg.	*welchii*	18	4	22	1·4	46
	septicum	18	7	39	2·2	74
	oedematiens	12	0	0	1·1	36
Nitracrin 0·4 mg.	*welchii*	18	0	0	0·2	6
	septicum	18	4	22	1·1	37
	oedematiens	24	4	17	1·4	46
V187 20 mg.	*welchii*	24	14	58	2·0	68
	septicum	18	0	0	1·2	41
	oedematiens	18	11	61	2·4	81
V335 20 mg.	*welchii*	24	21	88	2·8	92
	septicum	18	0	0	1·1	37
	oedematiens	18	0	0	0·9	31
Marfanil 20 mg.	*welchii*	30	15	50	2·0	68
	septicum	24	0	0	1·0	33
	oedematiens	24	0	0	0·9	29
Sulphathiazole 40 mg.	*welchii*	24	0	0	0·2	7
	septicum	24	11	46	2·2	72
	oedematiens	24	0	0	0·1	4
Penicillin 50 units	*welchii*	24	23	96	3·0	99
	septicum	18	5	28	1·7	57
	oedematiens	24	0	0	1·0	32
Nil (control mice)	*welchii*	90	0	0	0	0
	septicum	72	0	0	0	0
	oedematiens	60	0	0	0	0

penicillin and V187 with averages of 63 to 65 per cent, the next are V335, suproflavine and 5-aminoacridine-sulphathiazole with averages of 50 to 53 per cent, and the least efficacious are marfanil, nitracrin and sulphathiazole with averages of 28 to 43 per cent.

Some interesting relationships are found when the therapeutic values of the individual drugs are considered. Flavazole is of greater value than either of its components, proflavine and sulphathiazole, against *Cl. welchii* and *Cl. septicum* infections, whereas it is only of intermediate value against *Cl. oedematiens*. 5-Aminoacridine-sulphathiazole is similar to flavazole in its activity against *Cl. septicum* and *Cl. oedematiens*, but is much less active against *Cl. welchii*. Proflavine, as has been noted before (McIntosh and Selbie, 1943), is exceptional

UM00011832
NOVARTIS EXHIBIT 1017
Novartis v. Regents, IPR2023-01346
Page 578 of 4460

TABLE III.—*Comparative Efficacy of Drugs Against Anaerobic Infections Expressed as Percentage of 3 Days Survived by Treated Mice.*

Per cent of 3 days survived.	*Cl. welchii.*	*Cl. septicum.*	*Cl. oedematiens.*
100	Penicillin (99) V335 (92)	Flavazole (90) 5-Aminoacridine-sulphathiazole (81)	V187 (81)
80	Flavazole (79) V187 (68) Marfanil (68)	Suproflavine (74) Sulphathiazole (72)	
60	Proflavine (58) Suproflavine (46)	Penicillin (57) Proflavine (47) V187 (41)	Nitracrin (46) Proflavine (44)
40	5-Aminoacridine-sulphathiazole (30)	Nitracrin (37) V335 (37) Marfanil (33)	Suproflavine (36) Penicillin (32) V335 (31) Marfanil (29) Flavazole (25)
20	Sulphathiazole (7) Nitracrin (6)		5-Aminoacridine-sulphathiazole (19)
0			Sulphathiazole (4)

in that it has a moderately high activity against all three types of infections. Of the other acridines tested in this series suproflavine is similar to proflavine except that it is somewhat more active against *Cl. septicum*, while nitracrin is inferior against *Cl. welchii* and *Cl. septicum*, perhaps because of its low solubility.

The results obtained with marfanil, V187 and V335 are of interest in that they are closely related compounds, and would therefore be expected to have similar chemotherapeutic properties. This expectation is upheld in the almost equal activity of marfanil and V187 against *Cl. welchii*, of marfanil and V335 against *Cl. oedematiens*, and of all three drugs against *Cl. septicum* infection. On the other hand V335 and V187 are much more active against *Cl. welchii* and *Cl. oedematiens* infections respectively.

The varying sensitivity of these infections to drugs is also shown in the parallel tests with penicillin and sulphathiazole. Penicillin, in the dosage used, is highly effective against *Cl. welchii* and less effective against *Cl. septicum* and *Cl. oedematiens*, while sulphathiazole is highly active against *Cl. septicum*, and is of little or no value against the two other clostridia.

UM00011833

NOVARTIS EXHIBIT 1017
Novartis v. Regents, IPR2023-01346
Page 579 of 4460

DISCUSSION.

A comparison of the relative bacteriostatic titres against *Cl. welchii*, *Cl. septicum* and *Cl. oedematiens* of the various drugs used in these experiments (Table I) and the relative efficacy of these drugs against the corresponding infections in mice (Table III) shows that bacteriostatic activity does not necessarily bear a close relationship to chemotherapeutic activity. A high specificity in the in-vitro tests is shown only by sulphathiazole in that it is highly active against *Cl. septicum* and only moderately active against the two other clostridia, and this specificity of action is also shown in the therapeutic tests. With the other drugs of this series the bacteriostatic tests show an almost equal activity for each drug against all three clostridia, whereas the chemotherapeutic tests show great differences in their therapeutic efficiency for the three corresponding infections with the exception of proflavine.

The wide differences that have been found here in the chemotherapeutic activity of drugs against experimental gas gangrene, and in particular, the varying order of efficacy of the drugs from one clostridium to another, may be due to differences in the metabolism of these organisms which, although they have much in common, are recognized as having distinct biological properties. If this is true it would then appear that these differences in metabolism have more decisive effects in determining drug sensitivity in the treatment of infections than in bacteriostatic tests where, as has been shown here, only sulphathiazole of a number of drugs had any specificity in its action against these three clostridia. In therapeutic experiments, however, other factors come into play in determining the effect of chemotherapy, such as invasiveness and toxin production, and these may largely account for the relative insensitivity of *Cl. oedematiens* infection to drug action.

As it is evident, from the results presented here and previously, that no particular drug does at present or is likely in the future to prove a panacea for clostridial infections, we are still convinced of the necessity of using a mixture of drugs for the prophylaxis of clostridial infections in wounds. Such a mixture should be capable of dealing with all the organisms, both aerobic and anaerobic, likely to be met with in wounds, including the Gram-negative bacilli which may promote conditions suitable for the onset of gas gangrene infection.

For this purpose we originally selected a mixture of an acridine (1 per cent proflavine) and sulphathiazole as the most potent and readily available drugs. More recently after clinical trial we suggested that the proflavine in the mixture might be replaced by the new acridine flavazole (2 per cent), which is somewhat less toxic than proflavine and more active against *Proteus* and *Ps. pyocyanea*. This mixture can be enhanced in its activity against *Staphylococcus aureus* and other organisms by the addition of penicillin (McIntosh, Robinson, Selbie, Reidy, Blake and Guttmann, 1945).

SUMMARY.

A number of substances have been tested for their therapeutic activity against *Cl. welchii*, *Cl. septicum* and *Cl. oedematiens* infections in mice.

The results, summarized in Table III, show that these infections differ greatly in their sensitivity to chemotherapeutic substances, and for this reason no one drug can be regarded as an adequate prophylactic against these three infections. An efficient wound antiseptic must therefore consist of a mixture of drugs.

UM00011834
NOVARTIS EXHIBIT 1017
Novartis v. Regents, IPR2023-01346
Page 580 of 4460

Against *Cl. welchii* infection the most active of the chemotherapeutic substances tested are penicillin and V335; against *Cl. septicum* flavazole (proflavine-sulphathiazole compound), and against *Cl. oedematiens* infection the sulphone V187.

REFERENCES.

ALBERT, A., AND GLEDHILL, W.—(1942) *J. Soc. chem. Ind., Lond.*, **61**, 159.
Idem, RUBBO, S. D., GOLDACRE, R. J., DAVEY, M. E., AND STONE, J. D.—(1945) *Brit. J. exp. Path.*, **26**, 160.
DOMAGK, G.—(1942) *Klin. Wschr.*, **21**, 448.
EVANS, D. G., FULLER, A. T., AND WALKER, J.—(1944) *Lancet*, ii, 523.
HAMRE, D. M., WALKER, H. A., DUNHAM, W. B., VAN DYKE, H. B., AND RAKE, G.—(1944) *Proc. Soc. exp. Biol., N.Y.*, **55**, 170.
KLARER, J.—(1941) *Klin. Wschr.*, **20**, 1250.
MCINTOSH, J., ROBINSON, R. H. M., SELBIE, F. R., REIDY, J. P., BLAKE, H. E., AND GUTTMANN, L.—(1945) *Lancet*, ii, 97.
Idem AND SELBIE, F. R.—(1943) *Ibid.*, i, 793.
Iidem, HUDSON, R. V., PATEY, D. H., PARKES, T., MCMULLEN, H. L., AND PILE, G. C. L.—(1944) *Ibid.*, i, 591.
MACLENNAN, J. D., AND MACFARLANE, M. G.—(1944) *Brit. med. J.*, i, 683.
Idem AND MACFARLANE, R. G.—(1945*a*) *Lancet*, ii, 301.—(1945*b*) *Ibid.*, ii, 328.
MILLER, E., SPRAGUE, J. M., KISSINGER, L. W., AND MCBURNEY, L. F.—(1940) *J. Amer. chem. Soc.*, **62**, 2099.
SELBIE, F. R., AND MCINTOSH, J.—(1943) *J. Path. Bact.*, **55**, 477.
WHITBY, L. E. H.—(1937) *Lancet*, i, 1517.

TUMOURS PRODUCED BY 2-ANTHRAMINE.

F. BIELSCHOWSKY.

From the Department of Pathology and the Field Laboratory, University of Sheffield.

Received for publication January 22, 1946.

THE three aromatic amines, 2-naphthylamine, 2-anthramine and 2-aminofluorene, have been found to induce distant tumours. Hueper and Wolfe (1937) and Bonser (1943) obtained neoplasms of the bladder by feeding 2-naphthylamine to dogs, Shear (1938) hepatomas in mice after injection of 2-anthramine, and Bielschowsky (1944) liver tumours by painting the skin of rats with a solution of 2-aminofluorene in acetone. In this connection some compounds chemically related to 2-naphthylamine may be mentioned. Hueper (1942) discovered the carcinogenic activity of 2-amino-1-naphthol, and Cook, Hewett, Kennaway and Kennaway (1940) found that 2 : 2′-azo-naphthalene and 2 : 2′-diamino-1 : 1′-dinaphthyl produce liver tumours in mice. The last two compounds can be considered intermediaries between 2-naphthylamine and 3 : 4 : 5 : 6-dibenzcarbazole, the carcinogenic activity of which was discovered by Boyland and

UM00011835

NOVARTIS EXHIBIT 1017
Novartis v. Regents, IPR2023-01346
Page 581 of 4460

This Page is Inserted by IFW Indexing and Scanning Operations and is not part of the Official Record

BEST AVAILABLE IMAGES

Defective images within this document are accurate representations of the original documents submitted by the applicant.

Defects in the images include but are not limited to the items checked:

- ☐ BLACK BORDERS
- ☐ IMAGE CUT OFF AT TOP, BOTTOM OR SIDES
- ☐ FADED TEXT OR DRAWING
- ☐ BLURRED OR ILLEGIBLE TEXT OR DRAWING
- ☐ SKEWED/SLANTED IMAGES
- ☐ COLOR OR BLACK AND WHITE PHOTOGRAPHS
- ☐ GRAY SCALE DOCUMENTS
- ☐ LINES OR MARKS ON ORIGINAL DOCUMENT
- ☐ REFERENCE(S) OR EXHIBIT(S) SUBMITTED ARE POOR QUALITY
- ☐ OTHER: _____

IMAGES ARE BEST AVAILABLE COPY.
As rescanning these documents will not correct the image problems checked, please do not report these problems to the IFW Image Problem Mailbox.

Inorganica Chimica Acta [redacted] v. 198-200, p. 613-21 (1992)

Magnetochemistry of the tetrahaloferrate(III) ions 6. Crystal structure and magnetic ordering in $[(pyH)_3Cl][FeCl_4]_2$

Roey Shaviv, Carol B. Lowe
Department of Chemistry, University of Illinois at Chicago, Chicago, IL 60680 (USA)

Jalal A. Zora, Christer B. Aakeröy, Peter B. Hitchcock, K. R. Seddon
School of Chemistry and Molecular Science, University of Sussex, Brighton BN1 9QJ (UK)

and Richard L. Carlin*
Department of Chemistry, University of Illinois at Chicago, Chicago, IL 60680 (USA)

Abstract

The crystal structure, magnetic susceptibilities and specific heat of the title compound were determined by X-ray diffraction, susceptometry between 1.2 and 20 K, and adiabatic calorimetry between 1.5 and 39 K, respectively. The material is found to be a canted antiferromagnet with a critical temperature of 2.212 K. A λ-feature in the heat capacity at that temperature and an apparent break in the susceptibility curves are indicative of the manifestation of long-range order. A large degree of short-range order is observed to persist above the critical temperature, however. The compound crystallizes in the orthorhombic space group *Pbca* ($Z=8$, $a=13.040(2)$, $b=15.929(2)$, $c=27.014(5)$ Å and $V=5611.2$ Å^3). Bond lengths average 2.184(5) and 2.185(2) Å for Fe(1)–Cl and Fe(2)–Cl, respectively, within the slightly distorted tetrahedra. Single crystal magnetic susceptibility measurements of the sample show behavior consistent with that of a three-dimensional Heisenberg antiferromagnet with a small ferromagnetic peak whose maximum is identified at 2.00(1) K. This behavior is indicative of sublattice canting. A fit of the data from high temperature series expansions for a Heisenberg $S=5/2$ simple cubic lattice gives $|J|/k_B=0.084(1)$ K with $g=2.00$.

Introduction

As part of an investigation of the magnetic interactions in a series of compounds containing iron(III), we examined the compound of empirical formula $(pyH)_3Fe_2Cl_9$. Once thought to contain the triply-bridged binuclear complex, [tri-μ-chlorobis-trichloroferrate(III)]$^{3-}$ [1], the compound was studied by Earnshaw and Lewis [2] as part of their investigation of the distance dependence of magnetic interactions between metal atoms. The assumption at that time was that the metal–metal interactions in a triply-bridged dimer complex should be stronger than in a similar di- or mono-bridged species. Magnetic susceptibility data measured between 93 K and room temperature were fit to the equation for a binuclear $S=S'=5/2$ interaction [3]:

$$\chi_A=(3K/T)[55+30\exp(10x)+14\exp(18x)+5\exp(24x)+\exp(28x)]/[11+9\exp(10x)+7\exp(18x)+5\exp(24x)+3\exp(28x)+\exp(30x)]+N(\alpha) \quad (1)$$

where $K=N_0g^2\mu_B^2/3k_B$ and $x=-J/k_BT$. The symbols g, N_0, μ_B and k_B represent the spectroscopic splitting factor, Avogadro's number, the Bohr magneton and Boltzmann's constant, respectively; $N(\alpha)$ is the temperature independent paramagnetic term, J is the exchange constant and T the absolute temperature. A good fit of the data to this function was obtained with values of $J/k_B=-1.7$ K, $g=2.09$, and $N(\alpha)$ taken to be zero. This small interaction was interpreted in terms of a distortion of the octahedra on formation of the binuclear complex in such a way as to cause the iron atoms to move apart. Another conclusion was that the chlorine bridging group was not as effective as an oxygen bridge in enhancing the interaction between metals,

*Author to whom correspondence should be addressed.

0020-1693/92/$5.00

© 1992 – Elsevier Sequoia. All rights reserved

UM00011837
NOVARTIS EXHIBIT 1017
Novartis v. Regents, IPR2023-01346
Page 583 of 4460

since with oxygen a π-bonding mechanism can operate in the M–L–M (metal–ligand–metal) system.

In a later report, Ginsberg and Robin [3] extended the magnetic susceptibility measurements on $(pyH)_3Fe_2Cl_9$ to lower temperatures, and presented optical and Mössbauer spectra of the compound. These data provided evidence to the fact that the iron is present only as tetrahedral $[FeCl_4]^-$. While the two sets of magnetic susceptibility measurements [2, 3] agreed well over the common temperature region, substantial deviation of the data from the theoretical fit to eqn. (1) below liquid nitrogen temperature was found [3] and no fit to the equation over the entire temperature range with any set of J/k_B and g values could be obtained. Between 90 and 298 K, the newer data set was fit to eqn. (1), with $|J|/k_B = 1.6$ K and $g = 2.00$. It was therefore concluded that the observed exchange coupling in $(pyH)_3Fe_2Cl_9$ is simply a weak antiferromagnetic long-range interaction, with a Weiss constant of $\theta = -4$ K, similar to the interaction in $[(C_2H_5)_4N][FeCl_4]$, and not a pairwise metal–metal interaction [3]. No attempt was made to fit the data to any other theoretical magnetic interaction model.

In order to provide further evidence for a non-dimeric structure, the optical thin-film spectrum of the pyridinium compound was compared to its solution spectrum in acetone, and to that of $[(CH_3)_4N][FeCl_4]$ [3]. The spectra were found to be identical, with the optical density in the $[FeCl_4]^-$ bands of $(pyH)_3Fe_2Cl_9$ twice that of an equimolar solution of $[(CH_3)_4N][FeCl_4]$. The magnitude of the isomer shift for $(pyH)_3Fe_2Cl_9$ in the Mössbauer spectrum was closer to that of the tetrahedral $[(CH_3)_4N][FeCl_4]$ than that for iron(III) chloride, which has octahedral coordination.

Recent studies of magnetic exchange interactions in a set of isostructural compounds with the stoichiometry $A_3Fe_2X_9$ (A = [4-X(py)H]$^+$, X = Cl or Br), have revealed canted antiferromagnetism for substances containing discrete metal ion complexes [4]. The telling weak ferromagnetic peak occurs in the magnetic susceptibility data for measurements in which the applied field is directed perpendicular to the easy axis along a crystallographic axis, namely b, for these nominally antiferromagnetic materials.

It will be seen from our X-ray results that $(pyH)_3Fe_2Cl_9$ does indeed contain discrete $[FeCl_4]^-$ ions, but is not isostructural with the other $A_3Fe_2X_9$ compounds previously reported [4–7]. The magnetic measurements show that the antiferromagnetic exchange is weak in $(pyH)_3Fe_2Cl_9$, for it orders at only 2.212 K, but evidence of canting is still present. The magnetic susceptibility measurements for the pyridinium compound reveal a weak ferromagnetic contribution along the c crystallographic direction, unlike in the 4-halo-substituted pyridinium compounds [4]. This report contains the synthesis, complete crystal structure, and single crystal and powder magnetic susceptibility studies for $[(pyH)_3Cl][FeCl_4]_2$, with a calculated theoretical fit of the magnetic data obtained and a look at the plausible superexchange paths. The critical temperature for long-range order and the extent of short-range order are best determined by specific heat measurements. No previous such measurements of this compound have been reported. Thus the specific heat of the title compound was also measured between 1.5 and 39 K using adiabatic calorimetry.

Experimental

Preparation of $[(pyH)_3Cl][FeCl_4]_2$

The method of preparation was similar to that used by Weinland and Kiszling [1]. Anhydrous iron(III) chloride or iron(III) chloride hexahydrate and pyridinium chloride were each dissolved in dilute hydrochloric acid and then mixed together (molar ratio 1:2). The yellow–brown solution was placed over conc. H_2SO_4 at room temperature and produced large prismatic single crystals after 4 to 6 days. The yellow–green hygroscopic crystals were then collected by filtration, and dried *in vacuo*. *Anal.* Calc. for $C_{15}H_{18}Cl_9Fe_2N_3$: C, 26.85; H, 2.70; Cl, 47.55; Fe, 16.64; N, 6.26. Found: C, 27.03; H, 2.67; Cl, 47.47; Fe, 16.31; N, 6.20%.

Crystal alignment procedures

Crystals (25–80 mg) for magnetic susceptibility measurements were chosen and aligned using a polarizing microscope. Smaller crystals suitable for X-ray analysis were also aligned by X-ray precessional photographic methods. The single crystals were sealed with a thin layer of Apiezon N grease before mounting in the

TABLE 1. Crystallographic data for $[(pyH)_3Cl][FeCl_4]_2$

Chemical formula	$C_{15}H_{18}Cl_9Fe_2N_3$
Formula weight (g/mol)	671.1
Crystal class	orthorhombic
Space group	*Pbca*
Sample temperature (°C)	25
a (Å)	13.040(2)
b (Å)	15.929(2)
c (Å)	27.014(5)
V (Å^3)	5611.3
Z	8
λ (Å)	0.71069
ρ_{calc} (g cm^{-3})	1.59
μ (Mo Kα) (cm^{-1})	19.1
Structure solution package	MULTAN
Thermal parameters	anisotropic on all non-H atoms
$R(F)$	0.053
$R_w(F^2)$	0.063
Total reflections measured	4565
$\|F^2\| < \sigma(F^2)$	2248

UM00011838
NOVARTIS EXHIBIT 1017
Novartis v. Regents, IPR2023-01346
Page 584 of 4460

TABLE 2. Fractional atomic coordinates ($\times 10^4$) for $[(pyH)_3Cl][FeCl_4]_2$ with e.s.d.s given in parentheses and fractional atomic coordinates for hydrogen atoms ($\times 10^3$) introduced at calculated positions

Atoms	x	y	z
Fe(1)	8456.0(9)	162.5(7)	7440.9(4)
Fe(2)	2993.1(8)	2536.8(7)	5040.8(4)
Cl(1)	8023.5(18)	−931.5(14)	6994.8(10)
Cl(2)	8017.1(18)	1283.6(14)	7022.4(9)
Cl(3)	10113.1(17)	177.3(17)	7564.2(9)
Cl(4)	7721.1(19)	157.6(21)	8160.7(9)
Cl(5)	2223.8(16)	1498.5(13)	5418.0(8)
Cl(6)	2609.0(18)	3748.5(13)	5372.5(9)
Cl(7)	4651.5(16)	2331.4(13)	5071.3(9)
Cl(8)	2557.6(20)	2520.6(15)	4261.8(8)
Cl(9)	5755.1(19)	7524.0(14)	3365.6(9)
N(1)	4983(5)	5982(4)	3947(2)
C(2)	5429(6)	5396(5)	3705(3)
C(3)	5273(7)	4604(5)	3820(3)
C(4)	4655(7)	4403(5)	4201(4)
C(5)	4189(6)	5021(6)	4460(3)
C(6)	4368(6)	5824(5)	4329(3)
N(7)	5092(5)	9153(4)	3875(2)
C(8)	4109(6)	9141(6)	3795(3)
C(9)	3508(6)	9705(6)	4012(4)
C(10)	3924(7)	10293(6)	4302(4)
C(11)	4954(8)	10301(5)	4386(3)
C(12)	5548(6)	9724(6)	4168(3)
N(13)	4800(7)	7342(4)	2327(2)
C(14)	3867(8)	7593(6)	2208(4)
C(15)	3531(7)	7476(7)	1742(6)
C(16)	4186(11)	7168(7)	1430(4)
C(17)	5128(11)	6939(7)	1568(3)
C(18)	5389(6)	7031(6)	2007(4)
H(N1)	508	654	386
H(2)	589	554	344
H(3)	561	417	364
H(4)	456	383	429
H(5)	374	490	473
H(6)	405	627	451
H(N7)	550	874	373
H(8)	382	874	357
H(9)	278	970	396
H(10)	352	1072	446
H(11)	526	1072	459
H(12)	627	972	422
H(N13)	502	740	267
H(14)	341	786	244
H(15)	286	758	162
H(16)	406	708	109
H(17)	567	671	134
H(18)	605	688	212

susceptometer, to protect them from moisture. Powder samples (about 100 mg) were obtained by grinding small single or poly-crystals with a mortar and pestle in a dry atmosphere. In some cases the powder sample was further dried using a vacuum line. Magnetic susceptibility measurements in the temperature ranges 1.4–4.2 K and 2.0–25 K proceeded as described earlier [4].

Crystal structure

Room temperature X-ray data was collected using an Enraf-Nonius CAD4 diffractometer in a θ–2θ mode for a crystal of dimensions $0.25\times0.20\times0.18$ mm. Unit cell and refinement parameters are listed in Table 1. A total of 4565 reflections was measured for $2<\theta<23°$, $+h$, $+k$, $+l$; and 2248 unique reflections with $|F^2|>\sigma(F^2)$ were used in the refinement. No crystal decay was observed and no absorption correction was made.

The Fe and Cl atoms were located by direct methods using MULTAN, and the C and N atoms were found on difference maps. Refinement was by full matrix least-squares with anisotropic temperature factors, except for the H atoms which were held fixed at calculated positions (C–H and N–H at 0.95 Å) with B_{iso} of 6.0 Å^2. The weighting scheme was $w=1/\sigma^2(F)$ and the final residuals were $R=0.053$ and $R'=0.063$. A final difference map was featureless. Programs used were from the Enraf-Nonius SDP-Plus package. Fractional atomic coordinates with their standard deviations and isotropic temperature factors are given in Table 2. The associated anisotropic thermal parameters are included in Table 3.

TABLE 3. Thermal parameters ($\times 10^3$) for $[(pyH)_3Cl][FeCl_4]_2$ in the form: $\exp[-2p^2(U_{11}h^2a^{*2}+U_{22}k^2b^{*2}+U_{33}l^2c^{*2}+2U_{12}hka^*b^*+2U_{13}hla^*c^*+2U_{23}klb^*c^*)]$

Atom	U_{11}	U_{22}	U_{33}	U_{12}	U_{13}	U_{23}
Fe(1)	57(1)	80(1)	87(1)	−3(1)	1(1)	2(1)
Fe(2)	61(1)	58(1)	81(1)	−2(1)	6(1)	−2(1)
Cl(1)	102(2)	80(1)	143(2)	−9(1)	−10(2)	−12(1)
Cl(2)	105(2)	78(1)	123(2)	−2(1)	−15(2)	9(1)
Cl(3)	59(1)	150(2)	116(2)	4(1)	−3(1)	−15(2)
Cl(4)	86(2)	209(3)	96(2)	−20(2)	16(1)	6(2)
Cl(5)	78(1)	79(1)	103(2)	−14(1)	2(1)	15(1)
Cl(6)	96(2)	71(1)	128(2)	9(1)	20(1)	−17(1)
Cl(7)	61(1)	83(1)	124(2)	−1(1)	5(1)	−14(1)
Cl(8)	111(2)	115(2)	82(1)	0(2)	−10(1)	10(1)
Cl(9)	111(2)	70(1)	102(1)	2(1)	11(1)	−8(1)
N(1)	81(4)	57(4)	107(5)	0(4)	−9(4)	−2(4)
C(2)	80(5)	96(6)	83(5)	9(5)	12(5)	3(5)
C(3)	121(7)	75(5)	123(7)	26(6)	18(6)	−12(6)
C(4)	117(7)	66(5)	142(8)	−8(6)	−3(7)	29(5)
C(5)	80(6)	133(8)	100(6)	−18(6)	18(5)	13(6)
C(6)	69(5)	106(6)	101(6)	14(5)	5(5)	−41(5)
N(7)	104(5)	67(4)	99(5)	26(4)	21(4)	−2(4)
C(8)	83(6)	97(6)	125(7)	−24(5)	5(6)	−21(6)
C(9)	64(5)	125(7)	148(8)	15(6)	1(6)	−24(7)
C(10)	115(7)	79(6)	161(8)	31(5)	47(6)	−13(6)
C(11)	130(8)	73(5)	100(6)	−6(6)	−2(6)	−21(5)
C(12)	66(5)	115(7)	102(6)	7(5)	−12(5)	6(6)
N(13)	143(7)	75(5)	89(5)	3(5)	−8(5)	−7(4)
C(14)	149(8)	95(7)	171(8)	13(6)	88(6)	−8(7)
C(15)	68(5)	97(7)	335(16)	8(6)	−47(8)	23(9)
C(16)	325(14)	100(7)	161(8)	−55(9)	−144(8)	21(7)
C(17)	252(13)	171(9)	91(6)	−5(10)	35(8)	−77(6)
C(18)	71(6)	92(6)	215(10)	7(5)	5(7)	−54(7)

UM00011839
NOVARTIS EXHIBIT 1017
Novartis v. Regents, IPR2023-01346
Page 585 of 4460

Specific heat

Heat capacity measurements were carried out in an adiabatic calorimetric cryostat. The experimental apparatus and pertinent operating techniques have been previously described [8]. The polycrystalline sample was ground with a mortar and pestle and pelleted, into two pellets, to fit the inside of the calorimeter. Rapid thermal equilibrium was facilitated by threading the pellets with about 0.5 g of fine copper wire. Thermal contact between the pellets and the gold plated OFHC copper calorimetric vessel was provided by a thin layer of Apiezon N grease. The sample used was synthesized especially for the calorimetric experiment and was not the same sample used in the determination of the magnetic susceptibilities. In all about 12.25 g samples were used, which correspond to 0.01825 mol, when 671.101 g/mol is selected as the molecular mass.

During the course of the experiment 100 data points were taken using the standard heat pulse technique. Thermal equilibrium time, for each individual point, was between 3 and 6 min. The precision of a single point was better than 0.1% above the transition region and about 0.7% below it, where temperature increments were significantly smaller.

Results and discussion

Crystal lattice structure

One molecular formula contains three pyridinium cations, two $[FeCl_4]^-$ tetrahedra and one chloride ion which is strongly bonded to the three pyridinium cations. Intramolecular bond distances and angles are shown in Table 4. The two separate tetrachloroferrate(III) groups describe slightly distorted tetrahedra, with an average of 2.184 Å for Fe(1)–Cl bond lengths and 2.185 Å for the corresponding Fe(2)–Cl lengths. These values are comparable with those reported earlier [4] (literature mean = 2.175(9)). Bond angles for Cl–Fe–Cl within the anions range from 107.0 to 112.1°, with the normal tetrahedral average of 109.5°. In this material the tetrahedra are not aligned with two- or three-fold axes parallel to any crystallographic axis, as with some other tetrahaloferrate(III) structures [4–7].

With $Z = 8$, the 16 $[FeCl_4]^-$ tetrahedra in each unit cell form four two-dimensional layers which are roughly perpendicular to the *c* axis. Two-dimensional magnetic ordering seen in many layer-type structures is not expected in this case, because the inter-layer separation is only 6.75 Å. This distance is not very different from the shortest Fe- - -Fe distance of 6.53 Å found along the *a* direction within the planes. A sketch showing relative Fe- - -Fe distances within the unit cell and the tetrahedral staggered ABAC layer stacking is given in Fig. 1. Between-layer Fe- - -Fe contacts shown in the drawing range from 7.808 to 8.188 Å. Within the A layers the Fe- - -Fe distances along the *b* direction are 8.562 Å, however within the B and C layers adjacent ferric ions along *b* are 8.831 Å distant. Overall three-dimensional magnetic order is predicted for $(pyH)_3Fe_2Cl_9$. However, with very favorable superexchange paths lacking, the transition is likely to occur at low temperatures. No such transition was reported earlier [3] though the magnetic susceptibility measurements span the temperature range from 298 down to 1.4 K. On the other hand, our results indicate a transition at about 2 K. We will show that this apparent discrepancy arises from the fact that the temperature increments between the data points measured by Ginsberg and Robin near the critical temperature region (at 1.4 and 4.2 K) are too large.

Within the pyridinium rings, bond distances and angles are normal, with averages of r(C–N) 1.31, r(C–C) 1.33 Å, and (∠s) 119.9±4°, respectively. The three pyridinium rings depicted in Fig. 2 are arranged in propeller-like fashion about the free halide. Short H- - -Cl contacts between nitrogen bound H atoms and

TABLE 4. Intramolecular distances (Å) and angles (°) for $[(pyH)_3Cl][FeCl_4]_2$ with e.s.d.s given in parentheses

Distances (Å)			
Fe(1)–Cl(1)	2.192(3)	Fe(1)–Cl(2)	2.190(3)
Fe(1)–Cl(3)	2.187(2)	Fe(1)–Cl(4)	2.168(3)
Fe(2)–Cl(5)	2.186(2)	Fe(2)–Cl(6)	2.186(2)
Fe(2)–Cl(7)	2.189(2)	Fe(2)–Cl(8)	2.180(2)
N(1)–C(2)	1.280(10)	N(1)–C(6)	1.331(10)
C(2)–C(3)	1.315(12)	C(3)–C(4)	1.347(13)
C(4)–C(5)	1.352(13)	C(5)–C(6)	1.348(13)
N(7)–C(8)	1.301(11)	N(7)–C(12)	1.345(11)
C(8)–C(9)	1.329(13)	C(9)–C(10)	1.337(13)
C(10)–C(11)	1.362(13)	C(11)–C(12)	1.339(12)
N(13)–C(14)	1.320(13)	N(13)–C(18)	1.257(13)
C(14)–C(15)	1.35(2)	C(15)–C(16)	1.30(2)
C(16)–C(17)	1.34(2)	C(17)–C(18)	1.242(15)
Cl(9)–H(1)	2.23	Cl(9)–H(7)	2.20
Cl(9)–H(13)	2.12		
Angles (°)			
Cl(1)–Fe(1)–Cl(2)	107.3(1)	Cl(1)–Fe(1)–Cl(3)	110.3(1)
Cl(1)–Fe(1)–Cl(4)	112.1(1)	Cl(2)–Fe(1)–Cl(3)	109.2(1)
Cl(2)–Fe(1)–Cl(4)	110.5(1)	Cl(3)–Fe(1)–Cl(4)	107.5(1)
Cl(5)–Fe(2)–Cl(6)	111.83(9)	Cl(5)–Fe(2)–Cl(7)	108.83(9)
Cl(5)–Fe(2)–Cl(8)	108.7(1)	Cl(6)–Fe(2)–Cl(7)	110.1(1)
Cl(6)–Fe(2)–Cl(8)	110.3(1)	Cl(7)–Fe(2)–Cl(8)	107.0(1)
C(2)–N(1)–C(6)	122.1(7)	N(1)–C(2)–C(3)	120.7(8)
C(2)–C(3)–C(4)	120.0(8)	C(3)–C(4)–C(5)	119.5(8)
C(4)–C(5)–C(6)	118.5(8)	N(1)–C(6)–C(5)	119.2(8)
C(8)–N(7)–C(12)	123.0(7)	N(7)–C(8)–C(9)	119.8(8)
C(8)–C(9)–C(10)	119.6(8)	C(9)–C(10)–C(11)	120.3(8)
C(10)–C(11)–C(12)	119.4(8)	N(7)–C(12)–C(11)	117.9(8)
C(14)–N(13)–C(18)	121.1(9)	C(13)–C(14)–C(15)	118.9(9)
C(14)–C(15)–C(16)	116.0(1)	C(15)–C(16)–C(17)	122.0(1)
C(16)–C(17)–C(18)	119.0(1)	N(13)–C(18)–C(17)	122.0(1)
H(1)–Cl(9)–H(7)	107	H(1)–Cl(9)–H(13)	106
H(7)–Cl(9)–H(131)	114		

UM00011840
NOVARTIS EXHIBIT 1017
Novartis v. Regents, IPR2023-01346
Page 586 of 4460

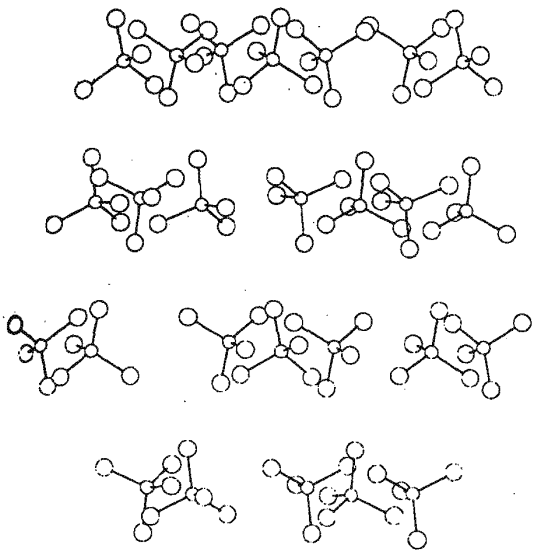


Fig. 1. The packing of the tetrahedra in the orthorhombic unit cell of $[(pyH)_3Cl][FeCl_4]_2$. The layers are shown successively in the order CABA.

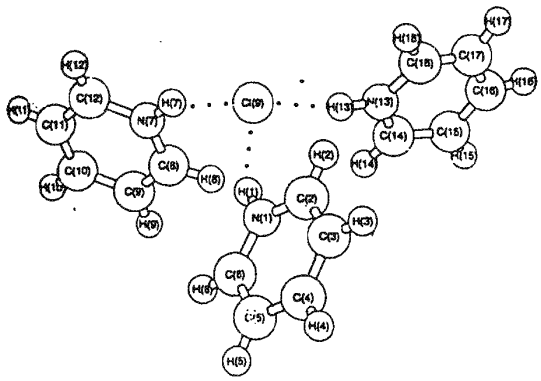


Fig. 2. Hydrogen bonding and pyridinium ion arrangement in the $[(pyH)_3Cl]^{2+}$ cation.

Cl(9) averaging 2.18 Å, disclose strong H bonding. The average N–H- - -Cl distance is 3.076 Å, close to values given [9] for hydrazinium(2+) dichloride (3.10 ± 0.02 Å) and hydroxylaminium(1+) chloride (3.16 ± 0.02 Å). A range of H- - -Cl(9)- - -H angles between 106 and 114° indicate near tetrahedral H-bond coordination to Cl(9). The discrete nature of the strong hydrogen bonds to the chloride ion leads to the recognition of the cation $[(pyH)_3Cl]^{2+}$, similar to that observed in the 4-chloropyridinium analogue [4]. This stable entity completes the tetrahedral coordination sphere around the chloride ion by the formation of a weak hydrogen bond (r(H ... Cl)2.746 Å) to an H3 proton of a neighboring $[(pyH)_3Cl]^{2+}$ cation, thus forming a three-dimensional hydrogen-bonded cationic network. There are no hydrogen bonds between $[(pyH)_3Cl]^{2+}$ and the $[FeCl_4]^-$ units.

The individual hydrogen bonds in the $[(pyH)_3Cl]^{2+}$ cation are longer than those in pyridinium chloride (r(N ... Cl) 2.95 Å) [10], reflecting the charge depletion at the chloride center when it receives four hydrogen bonds.

Zero-field magnetic susceptibilities

The zero-field susceptibility data with the *ac* field H (ν = 155 Hz) aligned along the crystal a, b and c axes are shown in Fig. 3. No correction for demagnetization was required for the small values of the susceptibility. Single crystal data are shown for temperatures between 1.1 and 4.2 K and measurements of polycrystalline powder are shown for the temperature range 1.1–24 K. It is clear that the material undergoes long range three-dimensional antiferromagnetic order at about 2 K. An out-of-phase component χ'' was detected between approximately 1.5 to nearly 2.1 K. The susceptibility increases as temperatures drop and attains a maximum value of 0.55 emu mol^{-1} at T = 2.3 K. A second maximum is seen in the data at T = 2.00 K as the development of weak ferromagnetic alignment occurs, corresponding to the χ'' observation. Below this temperature the susceptibility decreases, but does not extrapolate to zero for T = 0 K for any of the $H \| a$, b, c measurements. For an orthorhombic crystal the easy axis must follow one of the crystallographic axes, determined only experimentally [11]. The data which approach the smallest values of χ are the values measured for $H \| a$, indicating that the easy axis is probably coincident with the a axis direction, with deviation due to misalignment of

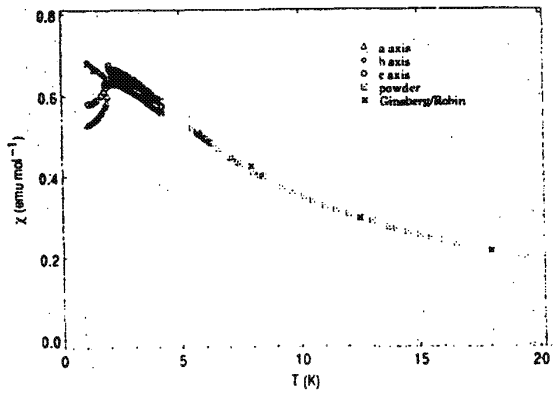


Fig. 3. The magnetic susceptibility curves for $(pyH)_3Fe_2Cl_9$. The measurements along the a, b and c axes are illustrated by triangles, diamonds and circles, respectively; powder data are represented by squares. The lowest temperature data of Ginsberg and Robin [3] are shown as x.

UM00011841
NOVARTIS EXHIBIT 1017
Novartis v. Regents, IPR2023-01346
Page 587 of 4460

the crystal or some impurity. Misalignment is not unlikely, as we note a small component of the weak ferromagnetic peak in data measured with the field along the *a* direction as well. An impurity which might cause an increase in the susceptibility below T_c could be a very small amount of $(pyH)_5Fe_2Cl_{11}$, which we have found does not order above 1.1 K.

From the present data it may be concluded that the compound orders as a canted antiferromagnet. With the moments aligned toward the *a* axis, canting occurs toward the *c* axis with a very small net moment along *c*. Since tetrahedral iron(III) salts generally have isotropic *g* values with small zero field splitting and spin orbit coupling effects, the Heisenberg model will apply here. Three-dimensional ordering is clearly present from the susceptibility data and we use a high temperature series expansion [12] to fit the data. In this way we obtain an adequate fit with $g=2.02$, and $J/k_B=-0.084(1)$ K. The fit is based on a simple cubic lattice with six nearest neighbors. This is a reasonable lattice approximation if the important interactions shown in Fig. 1 are those parallel to *a* and those running diagonally between tetrahedra in the *bc* plane. It is not known whether the pyridinium rings increase magnetic isolation along any of the pathways pictured.

The data presented here are in basic agreement with those of Ginsberg and Robin [3]. The presence of three-dimensional order was not noted by the earlier studies due to the lack of data at low enough temperatures, and the infrequency of the data points measured. Curie–Weiss plots of the three data sets yield θ values of -4, 8 and -4 K for the Ginsberg and Robin, Earnshaw and Lewis and the present data, respectively. The close agreement in the Weiss constant for two of the data sets is gratifying, given the variation in temperature regions measured. A very good fit to the high temperature series expansion for the $S=5/2$ sc Heisenberg model was obtained using the three data sets combined over the large temperature span of 3 to 300 K (Fig. 4). Parameters obtained for the combined data were $g=2.00$ and $J/k_B=-0.084(1)$ K.

The theoretical predictions given below are a good reference as to how well this compound behaves as a simple cubic $S=5/2$ Heisenberg antiferromagnet. According to Puertolas *et al.* [13]

$$\chi_{max}|J|/N_0g^2\mu_B^2=0.0394(1) \quad (2)$$

$$k_BT(\chi_{max})/|J|S(S+1)=3.07(1) \quad (3)$$

$$k_BT_c/|J|S(S+1)=2.84(1) \quad (4)$$

where all of the parameters have their previously defined meanings. Substituting our experimental values for χ_{max}, $T(\chi_{max})$, T_c, and that of $|J|/k_B$ obtained from our high temperature series fit, we calculate ratios of parameters for eqns. (2) through (4) of 0.0379, 3.01 and 3.14,

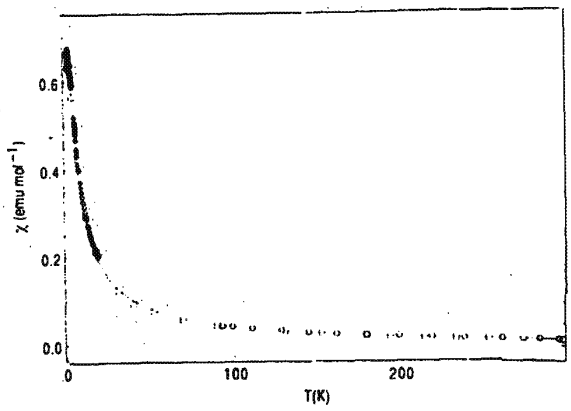


Fig. 4. Comparison of magnetic susceptibility measurements from three sources. The circles are data taken by Earnshaw and Lewis [2], the squares are from Ginsberg and Robin [3] and the diamonds are from this work. The solid line is a theoretical fit, explained in the text.

respectively. Though it appears contradictory because of the weak ferromagnetism, the presence of which implies a certain degree of anisotropy, the substance appears to follow the Heisenberg model quite well. The physical significance of this argument is questionable, however, in light of the complex nature of the magnetic susceptibility near the critical temperature. The two maxima observed in the data and the fact that the susceptibility may not be extrapolated to zero at 0 K for any of the axes strongly suggests that the nature of the magnetic interactions is complicated and may not be accounted for by a simple model.

Two mechanisms have been previously proposed to account for weak ferromagnetism [14]. One involves single ion anisotropy and the other mechanism involves anisotropic spin–spin coupling. The second mechanism is operative in the canted antiferromagnet α-Fe_2O_3 and we consider this further.

For antisymmetric spin couplings to exist, certain requirements are necessary. In all cases the symmetry must be sufficiently low. Moriya gives rules for determining when *d*, the coupling constant vector between two ions A and B, is non-zero and also for determining its possible directions [14]. Following these rules for this orthorhombic system with space group *Pbca*, we can make the following observations based on symmetry. (i) It is readily evident from Fig. 1 that no inversion center exists between neighboring Fe(III) tetrahedral ions along the *a*, *b* or *c* axes. This means that *d* may be non-zero for this crystal space group. There is, however, inversion symmetry between tetrachloroferrate(III) ions along the face diagonals in the *a*–*b* plane. Consequently no canting is allowed between these sites. (ii) There is a mirror plane separating adjacent ions along the *b* crystallographic direction. This effectively

UM00011842
NOVARTIS EXHIBIT 1017
Novartis v. Regents, IPR2023-01346
Page 588 of 4460

TABLE 5. Molar heat capacities of bis[pyridinium tetrachloroferrate(III)]·pyridinium chloride ($M = 671.101$ g mol^{-1})

T (K)	$C_{p,m}/R$[a]	T (K)	$C_{p,m}/R$	T (K)	$C_{p,m}/R$	T (K)	$C_{p,m}/R$	T (K)	$C_{p,m}/R$
Series I		2.013	3.4095	1.998	3.0486	4.760	0.9356	13.961	4.9629
1.575	2.0196	2.046	3.4724	2.038	3.3419	5.039	0.9323	14.678	5.4342
1.601	1.9858	2.080	3.6223	2.071	3.6785	5.324	0.9452	15.438	5.9429
1.639	1.8252	2.113	3.7807	2.099	3.7416	5.616	0.9735	16.232	6.4871
1.684	2.0439	2.144	3.9885	2.126	3.8423	5.919	1.0190	17.070	7.0704
1.755	2.3311	2.173	4.1722	2.152	4.0269	6.238	1.0831	17.946	7.6911
1.843	2.6425	2.202	4.2236	2.176	4.2140	6.568	1.1608	18.879	8.3461
1.921	2.9292	2.231	3.9125	2.198	4.3908	6.921	1.2608	19.860	9.0368
1.990	3.2845	2.265	3.1751	2.221	4.1836	7.287	1.3763	20.893	9.7686
2.052	3.5480	2.307	2.8620	2.312	2.9501	7.667	1.5102	21.979	10.5354
2.135	3.9342	2.352	2.5935	2.465	2.1540	8.062	1.6621	23.128	11.3195
		2.401	2.3823	2.606	1.9385	8.473	1.8373	24.334	12.1177
Series II		2.452	2.2013	2.750	1.6637	8.906	2.0331	25.599	12.9734
1.629	2.1664	2.516	2.0743	2.939	1.5090	9.361	2.2508	26.926	13.9095
1.677	2.0213			3.131	1.3479	9.840	2.4948	28.235	14.8947
1.739	2.2644	Series III		3.324	1.2386	10.346	2.7661	29.643	15.9389
1.801	2.5271	1.712	2.1462	3.541	1.1461	10.868	3.0599	31.206	17.0227
1.852	2.6780	1.785	2.4819	3.754	1.0820	11.427	3.3886	32.844	18.0676
1.898	2.8449	1.846	2.6556	4.004	1.0168	12.013	3.7367	34.595	19.1045
1.938	2.9995	1.901	2.8500	4.260	0.9722	12.634	4.1135	36.424	20.1404
1.977	3.2314	1.951	3.0771	4.496	0.9465	13.280	4.5238	38.358	21.1264

[a] $R = 8.3144$ J K^{-1} mol^{-1}.

confines the d term in $d[S_i x S_j]$ to be parallel to the a–c plane. The value of d is estimated to be of the order of $\Delta g/g$ times the superexchange interaction, where $\Delta g = g - 2$. This value can be very small, for example $\Delta g/g \approx 1 \times 10^{-3}$ in α-Fe_2O_3 [15]. Susceptibility measurements indicate that the easy axis is probably along a. Therefore, a d term along c would meet all symmetry requirements and remain perpendicular to the easy axis, effectively causing the spins to tilt slightly away from the a axis toward c. A net moment would then be observable along the c direction for a simple two-sublattice system [16].

Specific heat

The experimental molar specific heat of $[(pyH)_3Cl][FeCl_4]_2$ along with the sample's thermal history during the course of the calorimetric experiment are listed in Table 5 and plotted in Fig. 5. The experimental heat capacity is the sum of the lattice and the excess contributions. In $[(pyH)_3Cl][FeCl_4]_2$, all excess heat capacity may be assigned to the magnetic ordering process. A resolution of this heat capacity contribution from the experimental results depends upon a successful resolution of the latter to lattice and excess contributions.

The magnetic and lattice heat capacities were resolved by means of the enhanced Komada/Westrum (KW) method in a manner that was described in the preceding papers in this series [8, 17]. Thus the apparent characteristic temperature θ_{KW} (Fig. 6) was determined over

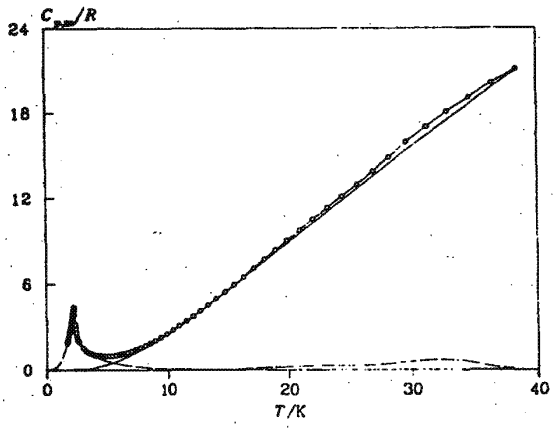


Fig. 5. Specific heat of $[(pyH)_3Cl][FeCl_4]_2$: O–O–O, experimental results; ——, lattice heat capacity; – – –, magnetic heat capacity.

the entire temperature range of the experiment, 26.25 K was assigned as the characteristic temperature for the compound and the lattice heat capacity (Fig. 5) was evaluated on the basis of this value. A minimum in the apparent characteristic temperature is observed at the vicinity of 2 K and a second local minimum is present near 32 K. The two minima are reflected in the two maxima in the magnetic heat capacity (calculated by subtracting the lattice contribution from the experimental data) and are associated with long- and short-range ordering, respectively. The long-range mag-

UM00011843
NOVARTIS EXHIBIT 1017
Novartis v. Regents, IPR2023-01346
Page 589 of 4460

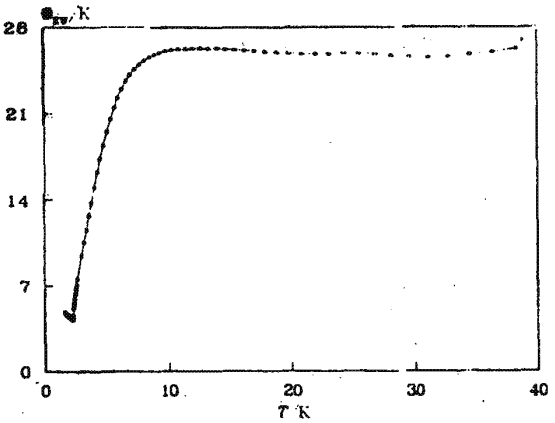


Fig. 6. Apparent characteristic temperature, θ_{KW}, for the title compound.

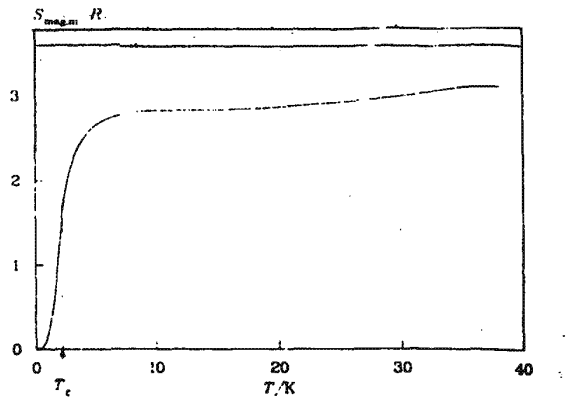


Fig. 7. Magnetic entropy of $[(pyH)_3Cl][FeCl_4]_2$. The critical temperature, 2.212 K, is indicated by the solid vertical line. The upper limit for the magnetic entropy, 3.5835R, is indicated by the horizontal dashed line.

netic order gives rise to a λ-feature in the magnetic heat capacity, whose maximum is identified at 2.212 K, which is selected as the critical temperature (Fig. 5). The low temperature segment of the transition does not follow the behavior predicted by spin wave theory as the magnetic heat capacity increases almost linearly with temperature between 1.6 and 2.0 K. The magnetic heat capacity below the critical temperature was extrapolated to 0 K by using the data between 1.6 and 1.8 K to produce a distribution function which was, in turn, used to reproduce the magnetic heat capacity over that range. The same distribution function was then used to extrapolate the heat capacity curve from 1.6 to 0 K, under the constraint of a T^3 dependence approaching absolute zero temperature. A polynomial fit between 0 K and the critical temperature yielded $1.518R$ for the magnetic entropy at the critical temperature. This value is only 42% of the total theoretical magnetic entropy of $3.584R$. The fact that less than half of the magnetic ordering takes place below the critical temperature indicates that short-range phenomena play an important role in the magnetic ordering process.

Short-range order manifests itself with a broad maximum in the vicinity of 31.5 K. Only about a third of the ordering entropy is associated with short-range order. This may explain the lack of evidence for short-range order in the magnetic susceptibility data. The experimental data do not extend to high enough temperatures to allow a complete analysis of the short-range contribution. We cannot, therefore, be certain about the exact exchange pathways responsible for the phenomena. We note, however that anticipated short-range order provided the original motivation for the study of this material [2, 3]. The conclusion that the compound is a simple antiferromagnet should be revised in light of these data. Short-range order is found to be a common feature in this series of tetrahaloferrates(III). Thus, $(pyH)_3Fe_2Br_9$ displays short-range order while $[4\text{-}Br(py)H]_3Fe_2Cl_9$ has the ordering phenomena equally divided between short- and long-range order. Of the materials studied in this chemical system to date, only $[4\text{-}Cl(py)H]_3Fe_2Cl_9$ does not display an important degree of short-range order.

The critical temperature, as identified by the specific heat experiment appears about 0.21 K higher than the temperature at which the weak ferromagnetic peak in the magnetic susceptibility is identified. However, at the vicinity of the critical temperature, the resolution of the magnetic susceptibility experiment is not sufficient to provide an unequivocal interpretation of the data. The ordering process appears to result in at least two maxima in the susceptibility data between 2 and 2.3 K. This indicates that the magnetic interactions, on the microscopic scale, are complex and may not be reproduced by a simple model. The atypical shape of the magnetic heat capacity over that temperature region, i.e. the almost zero curvature, reaffirms this observation. The critical temperature, 2.212 K, was, therefore, identified solely on the basis of the maximum in the magnetic heat capacity. We note, however, that the two measurements were not made on the same sample. Small differences in impurity levels and thermal history may also account for the difference in the critical temperatures.

The excess entropy over the entire temperature region of the experiment is $3.09R$ (Fig. 7). This value represents the entropy associated with the long-range order and the portion of the entropy associated with the short-range order that lies in the experimental temperature range. Thus only about 86% of the total magnetic entropy is within our range.

UM00011844
NOVARTIS EXHIBIT 1017
Novartis v. Regents, IPR2023-01346
Page 590 of 4460

Conclusions

The compound $(pyH)_3Fe_2Cl_9$ behaves as a canted antiferromagnet with very weak exchange. Canting appears to be towards the *c* axis when the *a* axis is identified as the easy axis. The exchange interactions in this compound are among the weakest yet found for these tetrachloroferrates(III), with the possible exception of $(pyH)_5Fe_2Cl_{11}$, which has not yet been fully characterized. It is notable that $(pyH)_3Fe_2Cl_9$ and its counterpart, $(pyH)_5Fe_2Cl_{11}$, are the only two salts of the $[4\text{-}X(py)H]_3Fe_2Cl_xBr_{9-x}$ family (here, X may be Cl, Br or H) which are known to have orthorhombic structures. While the ferromagnetic peak in the susceptibility data is found at 2.00 K, a second maximum at 2.5 K is also found and the critical temperature for long-range order is identified at 2.212 K from the λ-feature in the magnetic specific heat, and a large degree of short-range order is observed. Analysis according to the high-temperature series expansion yields $|J|/k_B = 0.084$ K and $g = 2.02$.

Supplementary material

A table of observed and calculated structure factors for $(pyH)_3Fe_2Cl_9$ (11 pages) is available from the authors.

Acknowledgements

The work in Chicago was supported in part by the Solid State Chemistry Program of the Division of Materials Research of the National Science Foundation, under Grants DMR-8515224 and DMR-8815798. We also thank Basrah University and the Iraqi government for the award of a scholarship. Acknowledgement is made to the Donors of the Petroleum Research Fund, administered by the American Chemical Society, and the BP Venture Research Unit for the partial support of this research.

References

1 R. F. Weinland and A. Kiszling, *Z. Anorg. Chem., 120* (1922) 220.
2 A. Earnshaw and J. Lewis, *J. Chem. Soc.,* (1961) 396.
3 A. P. Ginsberg and M. B. Robin, *Inorg. Chem., 2* (1963) 817.
4 J. A. Zora, K. R. Seddon, P. B. Hitchcock, C. B. Lowe, D. P. Shum and R. L. Carlin, *Inorg. Chem., 29* (1990) 3302.
5 J. C. Deaton, M. S. Gebhard and E. I. Solomon, *Inorg. Chem., 28* (1989) 877.
6 M. L. Hackert and R. A. Jacobson, *Acta Crystallogr., Sect. B, 27* (1971) 1658.
7 C. B. Lowe, R. L. Carlin, A. J. Schultz and C.-K. Loong, *Inorg. Chem., 29* (1990) 3308.
8 R. Shaviv, K. E. Merabet, D. P. Shum, C. B. Lowe, D. Gonzalez, R. Burriel and R. L. Carlin, *Inorg. Chem.,* in press.
9 G. C. Pimental and A. L. McClellan, *The Hydrogen Bond,* W. H. Freeman, San Francisco, CA, 1960, pp. 290–291.
10 C. Rerat, *Acta Crystallogr., 15* (1962) 427.
11 R. L. Carlin, *Magnetochemistry,* Springer, Berlin, 1986.
12 L. J. de Jongh and D. J. Breed, *Solid State Commun., 15* (1974) 1061.
13 J. A. Puertolas, R. Navarro, F. Palacio, J. Bartolome and R. L. Carlin, *Phys. Rev. B, 26* (1982) 395.
14 T. Moriya, in G. T. Rado and H. Suhl (eds.), *Magnetism,* Vol. 1, Academic Press, New York, 1963, pp. 93–96.
15 T. Moriya, *Phys. Rev., 120* (1960) 91.
16 R. L. Carlin, C. B. Lowe and F. Palacio, *An. Quim., 87* (1991) 5.
17 R. Shaviv and R. L. Carlin, *Inorg. Chem., 31* (1992) 710.

UM00011845
NOVARTIS EXHIBIT 1017
Novartis v. Regents, IPR2023-01346
Page 591 of 4460

Heparin is infrequently used in this regard due primarily to the necessity for parenteral administration. This situation could possibly be changed by formulation of heparin with a nontoxic sulfated surfactant.

REFERENCES

(1) R. H. Engel and M. J. Fahrenbach, *Proc. Soc. Exptl. Biol. Med.*, 129, 772(1968).

(2) R. H. Engel and S. J. Riggi, *ibid.*, 130, 879(1969).

(3) D. S. Robinson and P. M. Harris, *Quart. J. Exptl. Physiol.*, 44, 80(1959).

(4) G. E. P. Box and K. B. Wilson, *J. Roy. Stat. Soc., Ser. B.*, 13, 1(1951).

(5) T. A. Loomis, *Proc. Soc. Exptl. Biol. Med.*, 101, 447(1959).

(6) E. Windsor and G. E. Cronheim, *Nature*, 190, 263(1961).

(7) D. M. Graham, T. P. Lyon, J. W. Gofman, H. B. Jones, A. Yankley, J. Simonton, and S. White, *Circulation*, 4, 663(1951).

(8) H. Engelberg, *ibid.*, 10, 604(1954).

ACKNOWLEDGMENTS AND ADDRESSES

Received January 17, 1969, from the *Department of Metabolic Chemotherapy, Lederle Laboratories, American Cyanamid Company, Pearl River, NY 10965*

Accepted for publication February 26, 1969.

The authors wish to thank Mr. J. Haynes for the statistical analyses, Mr. E. Shinal and Dr. R. Nash for the enteric-coated capsules, and Mr. T. Van Trabert and Miss A. Greening for invaluable technical assistance.

* Present address: Battelle Memorial Institute, Duxbury, MA 02332

† To whom all correspondence should be addressed.

Structural Studies on Complexes IV: Crystal Structure of a 1:1 5-Chlorosalicylic Acid and Theophylline Complex

ELI SHEFTER

Abstract □ Single crystal X-ray diffraction methods were utilized in obtaining the crystal and molecular structure of a 1:1 association complex between 5-chlorosalicylic acid and theophylline. The crystals are monoclinic (space group P $2_1/c$) with cell parameters of a = 7.845 Å.; b = 9.636 Å.; c = 21.185 Å.; and β = 92.20°. The crystals contain a significant fraction of the impurities 3,5-dichloro- and 3-chlorosalicylic acid. Hydrogen bonds are the major attractive forces between the components of the complex. A relatively strong hydrogen bond exists between the carboxyl group of 5-chlorosalicylic acid and N(9) of theophylline (2.682 Å.). The theophylline molecules are in a dimeric arrangement by virtue of centrosymmetrically related hydrogen bonds between N(7) and TO(10). The packing arrangement of the molecules suggests that the stacking forces are similar to those in a caffeine:5-chlorosalicylic acid complex.

Keyphrases □ Complexes—structural studies □ 5-Chlorosalicylic acid-theophylline complex—crystal, molecular structure □ Diffractometry—5-chlorosalicylic acid-theophylline complex □ Hydrogen bonding—5-chlorosalicylic acid-theophylline complex

Spectroscopic, kinetic, and a variety of other physical chemical methods have been used successfully to obtain valuable information on the nature and strength of intermolecular association complexes between a wide variety of biological compounds (1). However, these methods are generally unable to provide detailed descriptions of the complex at the atomic level. For this, one may in some instances resort to the direct method of X-ray diffraction. Though this technique requires crystalline complexes, whose structures may be somewhat different from those in solution, the results are quite useful when correlated to solution data. It is through such correlations that a clear picture of various molecular association complexes involving pharmaceutically important molecules may emerge.

The interactions of salicylates and other biological materials containing *pi* systems with xanthine derivatives have been studied quite extensively in solution. The thermodynamic parameters of such complexes obtained by Higuchi *et al.* (2, 3) suggest that "hydrophobic" forces aside from hydrogen bonding play a significant role. Donbrow and Jan (4) have indicated that xanthine–hydroxybenzoic acid complexes may involve a donor-acceptor-type mechanism. In a crystallographic study on the 1:1 complex between 5-chlorosalicylic acid and caffeine, the idea of "polarization bonding" was put forth (5). Although the primary intermolecular force in that solid-state complex is hydrogen bonding, some evidence was found for a localized interaction between the α-β unsaturated ketone portion of the xanthine and the *pi* system of the salicylic acid molecule. Even with the wide variety of experimental data now available on such complexes and postulated models for the interactions (for a theoretical model see reference (6)), the interactions in these complexes have not been elucidated with sufficient detail to draw definitive conclusions on their molecular nature.

The present report concerns a structural study on a 1:1 complex formed between theophylline and 5-chlorosalicylic acid. This structure was determined with the hope of providing further insight into the molecular nature of the "polarization" forces, and also to learn more about the role hydrogen bonds play in stabilizing such complexes.

EXPERIMENTAL

Prism-shaped crystals of the 1:1 complex were obtained by dissolving equal molar quantities of theophylline (Matheson, Coleman and Bell, Inc.) and 5-chlorosalicylic acid (Eastman Kodak practical grade) in an alcohol-water solution and allowing the solution to

UM00011846
NOVARTIS EXHIBIT 1017
Novartis v. Regents, IPR2023-01346
Page 592 of 4460

Table I—Positional and Thermal Parameters with (in Parentheses) their Respective Standard Deviations × 10⁴[a]

Atom	x/a	y/b	z/c	b_{11}	b_{22}	b_{33}	b_{12}	b_{13}	b_{23}
				Theophylline					
TN1	10848(5)	2307(4)	1478(2)	118(6)	100(5)	15(1)	14(9)	−12(4)	1(3)
TC2	10310(6)	3675(6)	1581(2)	128(8)	112(6)	17(1)	4(11)	−4(4)	−7(4)
TN3	9397(5)	4318(4)	1108(2)	135(6)	75(4)	20(1)	−2(8)	−13(4)	−20(3)
TC4	8975(5)	3602(5)	562(2)	109(7)	97(5)	15(1)	0(10)	−11(4)	2(4)
TC5	9519(6)	2269(5)	473(2)	126(7)	88(5)	16(1)	27(10)	−3(4)	−3(4)
TL6	10510(6)	1529(5)	937(2)	131(7)	92(5)	15(1)	13(10)	−23(4)	−8(3)
TN7	8800(5)	1870(4)	−99(2)	164(7)	89(4)	16(1)	70(9)	−25(4)	−9(3)
TC8	7909(6)	2952(5)	−321(2)	157(8)	109(6)	12(1)	21(12)	−35(5)	−8(4)
TN9	7977(5)	4044(4)	67(2)	148(7)	89(4)	19(1)	37(9)	−23(4)	−3(3)
TO10	11003(5)	337(4)	896(2)	242(8)	93(4)	19(1)	82(9)	−43(4)	−5(3)
TC11	11693(7)	1599(7)	2018(2)	176(10)	168(8)	16(1)	−29(15)	−38(5)	7(5)
TO12	10638(5)	4251(5)	2081(2)	236(8)	150(6)	20(1)	49(11)	−47(4)	−45(4)
TC13	8791(9)	5750(6)	1190(3)	283(4)	82(6)	30(2)	60(14)	5(8)	−23(5)
				5-Chlorosalicylic acid					
Cl5	6448(3)	−1149(2)	799(1)	373(5)	122(2)	54(1)	151(5)	−103(3)	5(2)
Cl3	7516(18)	2472(18)	2903(6)	354(30)	322(27)	29(3)	175(47)	−33(14)	44(14)
C1	5229(6)	2754(6)	1226(2)	124(8)	126(7)	20(1)	1(12)	−7(5)	14(5)
C2	5945(7)	2906(7)	1831(3)	159(9)	158(8)	19(1)	−11(14)	−25(5)	12(5)
C3	6809(7)	1792(8)	2118(3)	168(10)	220(11)	21(1)	−25(17)	−35(6)	30(6)
C4	6972(7)	5898(7)	1805(3)	178(10)	148(8)	31(1)	−1(15)	−44(7)	65(6)
C5	6250(8)	410(6)	1200(3)	191(11)	114(7)	32(2)	34(14)	−21(7)	38(6)
C6	5363(6)	1494(6)	915(2)	142(8)	128(7)	21(1)	18(12)	−32(5)	25(5)
C7	4301(6)	3927(6)	921(2)	136(8)	117(6)	20(1)	−1(11)	−7(5)	4(4)
O1	3637(5)	3665(4)	356(2)	195(7)	94(4)	23(1)	53(9)	−37(4)	12(3)
O2	4138(6)	5056(5)	1184(2)	282(10)	135(6)	27(1)	79(12)	−41(5)	−14(4)
O3	5818(7)	4074(6)	2166(2)	281(10)	207(8)	24(1)	28(14)	−52(5)	−29(5)

[a] Temperature factor = exp $[-(b_{11}h^2 + b_{22}k^2 + b_{33}l^2 + b_{12}hk + b_{13}hl + b_{23}kl)]$.

evaporate. The following crystallographic data were measured for this material:

a = 7.845 (0.001) Å.
b = 9.636 (0.002) Å.
c = 21.185 (0.003) Å.
β = 92.20 (0.01)°

Density (measured by flotation) = 1.46 g./cm.³
Density (calculated assuming a 1:1 complex containing one full chlorine) = 1.468 g./cm.³
Z = 4 (number of molecules of complex in unit cell)
Space group $P2_1/c$

The stationary crystal-stationary counter method (7) was used to collect the intensity data on a diffractometer[1] equipped with goniostat. A set of balanced Ross filters (Ni against Co) were used for monochromatization of the Cu radiation. The crystal (dimensions 0.4 × 0.3 × 0.1 mm.) was mounted with [1 0 0] parallel to the *Phi* axis of the diffractometer. In the range of data measurement (limit 150° in *two theta*), 2,338 reflections of the 3,306 unique data had peak intensities that were significantly greater than their respective background. An approximate correction was made for absorption, based on the anisotropy of transmission of the X-rays as a function of the angle *Phi*. This function was measured for the (2 0 0) reflection at *Chi* equal to 90°. Aside from this correction, the appropriate Lorentz polarization factor and a factor to correct for α_1-α_2 splitting (25) were applied to convert an intensity to its structure factor amplitude, $|F_o|$. The $|F_o|$'s were placed on an absolute scale by Wilson's method, and normalized structure factors, $|E|$'s were computed.

The symbolic addition procedure was utilized to derive a set of phases for 292 reflections having $|E|$ values greater than 1.60. The method makes use of the Sayre relationship (8), which is essentially the same as the formula of Hauptman and Karle (9). Three linearly independent reflections (2 1 −3; 2 1 −2; 3 1 16) were selected as the origin-determining reflections on the basis that they have large values of $|E|$ and enter into many combinations for the application of the Sayre equation. Four reflections having a magnitude of $|E|$ greater than 3.0 (4 2 −5; 6 2 11; 6 3 −8; 2 8 7) were allowed to take up the 16 possible permutations of their phases. The phases of the other 285 reflections were determined for each of the 16 sets of starting phases using a program written by Robert Long (10). An E-map (11) was computed using the set of phases for the 292 data with the highest consistency index (10, 12). The position of 16 nonhydrogen atoms were positively located in this synthesis. A three-dimensional Fourier synthesis phased on these atoms enabled the other nonhydrogen atoms to be positioned in the lattice.

During the initial refinement by least-squares and difference electron-density maps, an atom other than hydrogen appeared to be attached to C3 of the salicylic acid molecule. The distance of this peak to C3 suggested that it was a chlorine atom with only a partial occupancy factor (peak height ~ 1 e/Å.³). The atomic site occupancy factor of the two chlorines were refined by least-squares along with their isotropic temperature factors. The site occupancy factor obtained for the chlorine bound to C3 was only 0.15 while that in Position 5 was 0.93. The practical grade of 5-chlorosalicylic acid in all likelihood is a mixture of the 5-chloro-, 3-5 dichloro- and 3-chloro- compounds, resulting from chlorination of salicylic acid. The crystalline complex reflects the varying portions of the chloro derivatives of salicylic acid, and can be considered as a solid solution of these compounds.

The hydrogen atoms were located in difference electron-density syntheses and included in the final cycles of least-squares refinement with isotropic temperature factors. All the other atoms were refined anisotropically, during which the site occupancy factors for the two chlorines were fixed at their respective values. A modification of the Gantzel, Sparks and Trueblood block diagonal least-squares program (unpublished) was utilized for this purpose. The weighting scheme in the final stages of refinement was $w^{-1} = (|F_o| - 3)/12^2 + 1$, designed such that $(w\Delta^2)$ is constant over the whole range of $|F_o|$'s.[2] The unobserved data were given zero weight. The final R value for the observed data is 0.087 (for all data 0.134). The atomic parameters and their estimated standard deviations (*ESD*'s) are listed in Tables I and II. A tabulation of the structure factors has been deposited in the Health Sciences Library of this University and may be obtained from the librarian on request.

With the exception of hydrogen, the atomic scattering factors used throughout the above calculations are those presented in *Reference 13*. The form factors for hydrogen are those published by Stewart *et al.* (14).

[1] General Electric XRD-6.

[2] $|F_o|$ is on absolute scale.

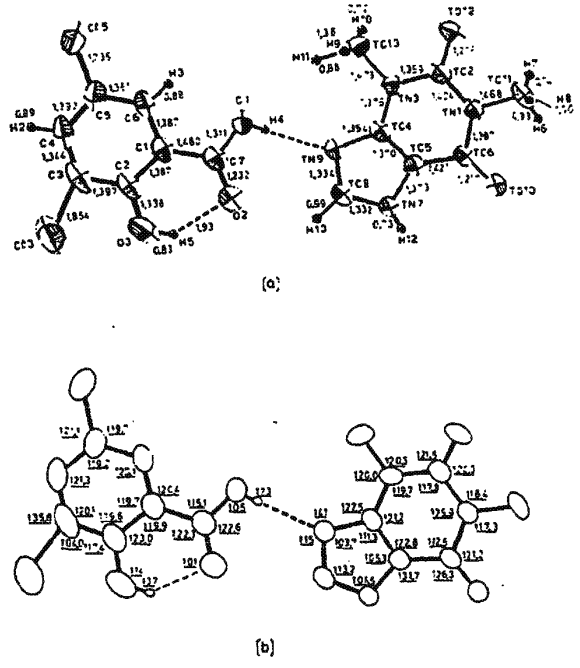
UM00011847
NOVARTIS EXHIBIT 1017
Novartis v. Regents, IPR2023-01346
Page 593 of 4460

Table II—Parameters for Hydrogen Atoms with Their *ESD*'s in Parentheses

Atom	$x/a \times 10^3$	$y/b \times 10^3$	$z/c \times 10^3$	B_{iso}, Å.²
H2	750(8)	−13(7)	199(3)	5.8(1.5)
H3	495(8)	152(7)	52(3)	5.8(1.5)
H4	331(9)	426(7)	25(3)	6.6(1.6)
H5	546(8)	475(6)	196(3)	5.2(1.4)
H6	1242(10)	104(8)	179(4)	8.1(2.1)
H7	1234(8)	207(7)	217(3)	5.2(1.5)
H8	1075(8)	104(7)	219(3)	6.3(1.6)
H9	880(9)	650(7)	65(3)	6.8(1.6)
H10	950(12)	616(9)	131(4)	9.7(2.5)
H11	769(14)	559(13)	122(5)	13.8(3.2)
H12	907(5)	123(4)	−25(2)	1.5(0.7)
H13	724(7)	290(6)	−72(3)	4.6(1.2)

The thermal parameters of the nonhydrogen atom were analyzed by the method of Schomaker and Trueblood (15). The *Uij's* calculated for the two molecular species, assuming that each behaves as a "rigid body," are in good agreement with their observed thermal parameters. The root mean-square difference between the calculated and observed values of the *Uij's* is 0.004 Å.² for theophylline and 0.005 Å.² for 5-chlorosalicylic acid including the partially occupied chlorine attached to C3; these differences are the same order of magnitude as the *ESD*'s of the *Uij's*. The translational and librational components of the thermal motion for theophylline are approximately 20% less than those computed for the salicylic acid residue. This reflects the greater number of intermolecular hydrogen bonds in which the theophylline molecule participates. The change in bond lengths and angles resulting from the thermal motion were all less than 1.5 times the *ESD*'s for the respective bonds, the corrections were therefore deemed to be unnecessary for the present discussion.

The bond lengths and angles obtained from the least-squares refined parameters are shown in Fig. 1. The *ESD*'s for the atom-to-atom distances are on the average 0.008 Å., and for the angles 0.4°. Those bonds involving hydrogens have an error of 0.1 Å. The angles about the hydrogen atoms are not given (because of their relatively high uncertainty, ±3°), except where the discussion warrants such information. Figure 1 also shows the atomic labels that are used throughout the discussion.



(a)

(b)

Figure 1—*Intramolecular bond lengths (a) and angles (b). The thermal motion of the individual atoms is represented by the ellipsoids.*

DISCUSSION OF RESULTS

The theophylline moiety has intramolecular bond distances and angles that are quite similar to those found in theophylline monohydrate crystals (16); none differ by more than 2 *ESD*'s. There is however, a significant difference between the planarity of the xanthine residues in the two structures. The atoms comprising the purine nucleus in the hydrated crystal are essentially coplanar, while in the complex there is a marked degree of puckering (see Table III). The pyrimidine and imidazole portions of the purine system are each planar within the limits of the errors in the atomic positions of the respective atoms. The 5- and 6-membered rings are however tilted from coplanarity about the C4—C(5) bond by 3.7°. This distortion of the purine system could possibly result from intermolecular packing forces, such as polarization bonding between the xanthine and the salicylic acid residue. In the 1:1 complex of caffeine with 5-chlorosalicylic acid (12), the pyrimidine and imidazole portions of the xanthine are also bent in a similar manner; distortion from planarity is 3.2°. TO12 and TC11 are significantly displaced from the plane of the pyrimidine ring, while TO10 and TC13 are essentially coplanar with this ring. Nonbonded intra- and intermolecular contacts may in all probability account for the distortions of these two exocyclic atoms from the pyrimidine ring.

In general the molecular parameters of the salicylic acid residue correspond with those found for the 5-chlorosalicylic acid moiety of the caffeine complex (12) and for salicylic acid itself (17). The differences that exist between the bond lengths and angles in this

Table III—Least-Squares Planes[a]

Atoms Comprising l.s. Plane	Displacement, Å.	Other Atoms	Displacement, Å.
TN1	0.027	TO10	0.009
TC2	0.035	TC11	0.216
TN3	−0.024	TO12	0.109
TC4	−0.035	TC13	−0.012
TC5	−0.045	H12	−0.010
TC6	−0.015	H13	0.241
TN7	−0.013		
TC8	0.037		
TN9	0.007		
$-0.8422\,X - 0.3381\,Y + 0.4199\,Z + 6.5311$ Å. $= 0$			
TN1	0.001	TN7	0.098
TC2	0.009	TC8	0.143
TN3	−0.015	TN9	0.090
TC4	0.010	TO10	0.016
TC5	0.000	TC11	0.152
TC6	−0.006	TO12	0.051
		TC13	−0.002
$-0.8551\,X - 0.3385\,Y + 0.3927\,Z + 6.6999$ Å. $= 0$			
TC4	0.004	TN1	0.156
TC5	−0.004	TC2	0.164
TN7	0.003	TN3	0.059
TC8	−0.001	TC6	0.072
TN9	−0.002	H12	−0.12
		H13	0.03
$-0.8247\,X - 0.3379\,Y + 0.4536\,Z + 6.4065$ Å. $= 0$			
C2	−0.009	C7	−0.014
C2	−0.002	O1	0.014
C3	0.011	O2	−0.016
C4	−0.009	O3	0.023
C5	−0.003	Cl3	0.023
C6	0.011	Cl5	−0.014
		H2	0.02
		H3	−0.07
		H4	−0.04
		H5	−0.13
		TN9[b]	0.025
$-0.8644\,X - 0.3197\,Y + 0.3881\,Z + 3.2917$ Å. $= 0$			

[a] The equations of the least-squares planes were calculated according to the method of Schomaker *et al.* (24). [b] This is the nitrogen that is involved in the hydrogen bond with O1.

UM00011848
NOVARTIS EXHIBIT 1017
Novartis v. Regents, IPR2023-01346
Page 594 of 4460

structure and those observed in the other two salicylic acid structures are only significant about the C3, C4, and C5 atoms of the phenyl ring. The poorer agreement in this region of the molecule most likely reflects the solid solution phenomena, *i.e.* presence of 3-chloro- and 3,5-dichlorosalicylic acid.

The C5—Cl5 length is in excellent agreement with values reported (18) for a number of aromatic C—Cl bonds. The distance between C3 and Cl3, on the other hand, is considerably longer than the commonly found value. The angles about C3 deviate substantially from trigonal symmetry whereas those about C5 do not. An explanation for the unusual bonding parameters found for Cl3, undoubtedly resides in the small occupancy factor associated with this site. It is believed that the standard deviations for the positional parameters of Cl3 are greatly underestimated because of the use of the block diagonal approximation and the very low occupancy factor associated with this atom.

The least-square plane calculated through the phenyl ring of 5-chlorosalicylic acid indicates that the molecule is planar within experimental error (*cf.* Table III). The atomic displacements are greatest (but are not highly significant) in the vicinity of the intramolecular hydrogen bond between O2 and O3. A comparable situation also is found in the salicylic acid structure.

Hydrogen bonds appear to be the predominant stabilizing forces behind this solid-state association complex. These interactions are illustrated in Fig. 2. The weakly basic nitrogen (TN9) of theophylline participates in a relatively strong hydrogen bond with the proton from the carboxyl group of 5-chlorosalicylic acid. The 2.682 ± 0.006 A. length between the N and O is somewhat longer than the similar interaction observed in the caffeine complex (2.644 ± 0.007). The difference in the strength of this hydrogen bond in the two crystalline complexes most probably reflects the variation in the basic character of N9 of the two xanthine molecules. There is also a hydrogen bond between the TN7 hydrogen of one theophylline and TO10 of a centrosymmetrically equivalent molecule. The same bonding situation also was found in theophylline monohydrate, but the N to O distance is 0.04 A. shorter in the present instance. The hydrogen bonding scheme (*i.e.*, the two unique hydrogen bonds) is compatible with the infrared data of Cook (19, 26) on analogous solid-state complexes.

In Fig. 2 the dotted lines show the only other intermolecular contacts involving hydrogen atoms that are shorter than a nonbonded contact between the respective atoms. The sum of the van der Waals radii of hydrogen and oxygen is 2.6 A. (20). A recent article on the topic of C H hydrogen interactions by Donohue (21) suggests that

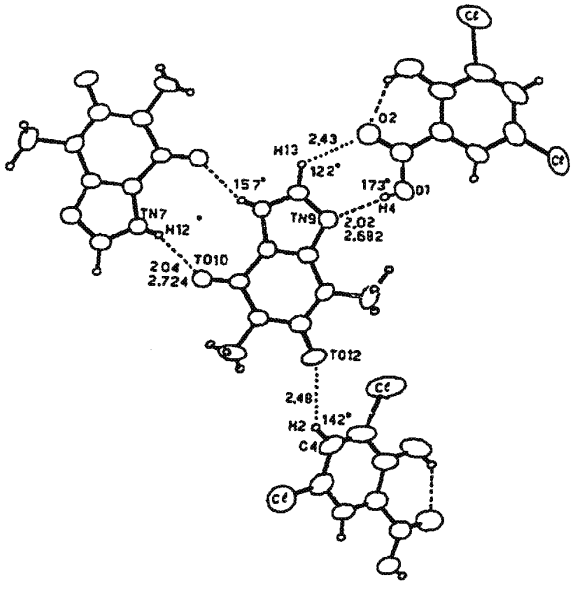


Figure 2-- *A view of the molecular species in the crystal lattice showing the hydrogen bonding network (dashed lines). Dotted lines are relatively short C-H . . . O contacts.*

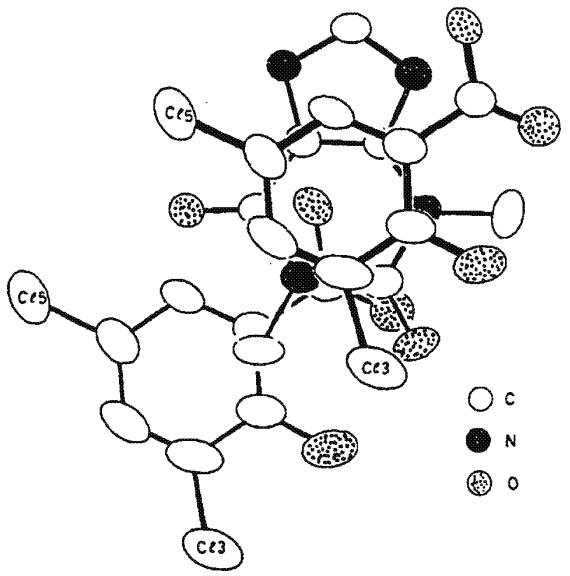


Figure 3--*The stacking arrangement of the 5-chlorosalicylic acid molecules about theophylline. The salicylic acid molecule with the heavier bonds is above the xanthine, while the other is below in this illustration.*

a 2.4 A. contact between hydrogen and oxygen is a more realistic minimum value for a normal van der Waals contact between these two atoms. It is thus felt that the C—H . . . O contacts shown in Fig. 2 are not hydrogen bonds of the type postulated by Sutor (22). Verification of such hydrogen bonds must be determined by other physical chemical measurements, *e.g.*, infrared data.

In a previous report it was postulated that in certain association complexes (5), the α-β unsaturated ketone portion of a molecule may be involved in polarization bonding with the *pi* system of the other component of the complex. This was shown to be possibly valid in the case of the 1:1 crystalline complex between caffeine and 5-chlorosalicylic acid. In another crystallographic study on an acridine-cytosine complex (23), where neither component has the α-β unsaturated ketone residue, the only apparent intermolecular forces were of the hydrogen bond variety. The stacking arrangement about the theophylline molecule in the present structure, shown in Fig. 3, has certain features that are analogous to those observed in the caffeine complex. The phenyl ring of the salicylic acid moiety that is above theophylline in this illustration, overlaps the TC4, TC5, and TC6 atoms. In light of the variation in the hydrogen bonding schemes of the two xanthine complexes, the stacking orientations are remarkably homologous. The atoms TC5 and TC4 are closer to the phenyl ring (average 3.41 ± 0.01 A.) than the other members of the xanthine system. The possibility thus exists that a weak attraction exists between the portion of theophylline containing these atoms and the *pi* electrons of the salicylic acid may cause the observed puckering of the xanthine. A parallel situation was also found in the caffeine-5-chlorosalicylic acid complex. The packing arrangement and the mode of puckering of the purine nucleus lend support to the idea that a localized attractive force polarization bonding exists between the phenyl ring and the α-β unsaturated ketone portion of the xanthine in this complex (5).

Other crystallographic analyses of complexes are underway in this laboratory, which hopefully will permit more definitive descriptions of these interactions to be made.

REFERENCES

(1) "Molecular Associations in Biology," B. Pullman, Ed., Academic Press, New York, N. Y., 1968.

(2) T. Higuchi and J. L. Lach, *J. Am. Pharm. Assoc., Sci. Ed.*, **43**, 349(1954).

UM00011849
NOVARTIS EXHIBIT 1017
Novartis v. Regents, IPR2023-01346
Page 595 of 4460

(3) T. Higuchi and D. A. Zuck. *ibid.*, 41, 10(1952); *ibid.*, 42, 132(1953).
(4) M. Donbrow and Z. A. Jan. *J. Pharm. Pharmacol., Suppl.*, 17, 129S(1965).
(5) E. Shefter. *J. Pharm. Sci.*, 57, 350(1968).
(6) R. S. Schnaare and A. N. Martin. *ibid.*, 54, 1707(1965).
(7) T. F. Furnas and D. Harker. *Rev. Sci. Instr.*, 26, 449(1955).
(8) D. Sayre. *Acta Cryst.*, 5, 60(1952).
(9) H. Hauptman and J. Karle. "Solution of the Phase Problem I. The Centrosymmetric Crystal." ACA monograph No. 3. Polycrystal Book Service. Pittsburgh, Pa., 1953.
(10) R. E. Long. Ph.D. thesis. University of California. Los Angeles. 1965.
(11) I. L. Karle, H. Hauptman, J. Karle, and A. B. Wing. *Acta Cryst.*, 11, 257(1958).
(12) E. Shefter. *J. Pharm. Sci.*, 57, 1163(1968).
(13) "International Tables for X-ray Crystallography," vol. III. Kynoch Press. Birmingham, England. p. 202.
(14) R. F. Stewart, E. R. Davidson, and W. T. Simpson. *J. Chem. Phys.*, 42, 3175(1965).
(15) V. Schomaker and K. N. Trueblood. *Acta Cryst.* B24, 63 (1968).
(16) D. J. Sutor. *ibid.*, 11, 83(1958).
(17) M. Sundaralingam and L. H. Jensen. *ibid.*, 18, 1053(1965).
(18) G. Gafner and F. H. Herbstein. *ibid.*, 15, 1081(1962).
(19) D. Cook, personnal communication.
(20) L. Pauling. "The Nature of the Chemical Bond." 3rd ed., Cornell University Press. Ithaca. N. Y., 1960.
(21) J. Donohue, in "Structural Chemistry and Molecular Biology." A. Rich and N. Davidson, Eds., W. H. Freeman, San Francisco, Calif., 1968, p. 443.
(22) D. J. Sutor. *J. Chem. Soc.*, 1963, 1105.
(23) E. Shefter. *Science*, 160, 1351(1968).
(24) V. Schomaker, J. Waser, R. E. Marsh, and G. Bergman. *Acta Cryst.*, 12, 600(1959).
(25) A. Tulinsky, C. R. Worthington, and E. Pignataro. *ibid.*, 12, 623(1959).
(26) D. Cook and Z. R. Regner. *Can. J. Chem.*, 46, 3055(1968).

ACKNOWLEDGMENTS AND ADDRESSES

Received February 6, 1969, from the *Department of Pharmaceutics, School of Pharmacy, State University of New York at Buffalo, NY 14214*

Accepted for publication March 3, 1969.

Presented to Basic Pharmaceutics Section, APhA Academy of Pharmaceutical Sciences, Montreal meeting, May 1969.

This investigation was supported by a National Cancer Institute grant No. CA-10104. The author is indebted to the SUNY/B Computing Center (partially supported by N.S.F. grant GP-7318 and P.H.S. grant PO7FR0012605) for computing services; to Mrs. Phyllis Sackman for her technical assistance; to Dr. C. K. Johnson for making his ORTEP program available; to Professor K. N. Trueblood for his thermal analysis routine; and to Prof. Philip Coppens for a number of interesting discussions.

Nuclear Magnetic Resonance and Rheological Studies on the Thixotropic Properties of Montmorillonite–Water Systems

ARTHUR H. KIBBE and OSCAR E. ARAUJO

Abstract □ Several proposed mechanisms of the thixotropic behavior of montmorillonite-water systems were evaluated. The effects of temperature, reshearing, concentration, and storage time on these systems were studied by means of NMR and rheological measurements. The specific parameters used were the change in line width of the NMR spectrum and the static yield values obtained from the rheograms. The results indicate clear agreement with the theory that the colloidal particles upon contact adhere to form a spacious matrix resembling a house of cards.

Keyphrases □ Montmorillonite–water systems—rheology □ Thixotropic behavior—montmorillonite–water systems □ Stability—montmorillonite-water systems □ NMR spectroscopy—analysis

Montmorillonite–water systems have long been under study by physical chemists and more recently by the pharmaceutical industry because of their unique thixotropic behavior.

Hause and Reed (1) found that as little as 0.05% bentonite was sufficient to stop gas bubbles from rising to the surface.

Norton and Johnson (2) studied the properties of monodispersed clay-water systems and calculated the thickness of the water film, finding it to be approximately two molecules thick.

Freundlich (3), von Engelhardt (4), and Hause (5) assume that there are long-range electrical forces which permit the individual particles to act over distances of the order of 10^3 Å. This would be similar to the type of structure found in a magnet where all the free electrons of the iron are lined up in the same direction.

Usher (6), Kuhn (7), and Hofmann (8) prefer a mechanical picture of thixotropy in which the particles touch one another, adhere on contact, and build up a spacious matrix resembling a house of cards.

Macy (9), McBain (10), and Grim and Cuthbert (11) explain the rheological mechanism of montmorillonite mixtures by assuming that the aqueous layer which surrounds the clay particle becomes rigid as if it had crystallized into ice.

Williamson (12) reviewed the physical relationship between clay and water systems and concluded that the "ice" theory is the least satisfactory explanation for the rigidity of the water film on clay.

The strength of thixotropic gels increases with decreasing particle size. Brownian molecular motion is nonexistent in truly thixotropic systems and the particles which have ceased to move seem to be clearly separated from each other by water (12).

In 1945 Ewing (13) felt that bentonite had become of such importance in pharmaceutical preparations that he

UM00011850
NOVARTIS EXHIBIT 1017
Novartis v. Regents, IPR2023-01346
Page 596 of 4460

This Page is Inserted by IFW Indexing and Scanning Operations and is not part of the Official Record

BEST AVAILABLE IMAGES

Defective images within this document are accurate representations of the original documents submitted by the applicant.

Defects in the images include but are not limited to the items checked:

- ❑ BLACK BORDERS
- ❑ IMAGE CUT OFF AT TOP, BOTTOM OR SIDES
- ❑ FADED TEXT OR DRAWING
- ❑ BLURRED OR ILLEGIBLE TEXT OR DRAWING
- ❑ SKEWED/SLANTED IMAGES
- ❑ COLOR OR BLACK AND WHITE PHOTOGRAPHS
- ❑ GRAY SCALE DOCUMENTS
- ❑ LINES OR MARKS ON ORIGINAL DOCUMENT
- ❑ REFERENCE(S) OR EXHIBIT(S) SUBMITTED ARE POOR QUALITY
- ❑ OTHER: _____

IMAGES ARE BEST AVAILABLE COPY.
As rescanning these documents will not correct the image problems checked, please do not report these problems to the IFW Image Problem Mailbox.

Acta Cryst. (1982). B**38**, 2309–2311

Structure of 2,4-Diamino-5-(3,4,5-trimethoxybenzyl)pyrimidine–5,5-Diethylbarbituric Acid (1:1)

BY NOBUYUKI SHIMIZU AND SADAO NISHIGAKI

Pharmaceutical Institute, School of Medicine, Keio University, Shinjuku-ku, Tokyo 160, *Japan*

YOSHINOBU NAKAI

Faculty of Pharmaceutical Sciences, Chiba University, Chiba 260, *Japan*

AND KENJI OSAKI

Faculty of Pharmaceutical Sciences, Kyoto University, Kyoto 606, *Japan*

(*Received* 24 *February* 1982; *accepted* 26 *March* 1982)

Abstract. $C_{14}H_{18}N_4O_3.C_8H_{12}N_2O_3$, $M_r = 474{\cdot}5$, monoclinic, $C2/c$, $a = 12{\cdot}509$ (10), $b = 16{\cdot}532$ (7), $c = 22{\cdot}627$ (29) Å, $\beta = 94{\cdot}56$ (13)°, $U = 4664{\cdot}4$ Å^3, $D_x = 1{\cdot}352$, D_m (n-hexane/CCl_4) = 1·349 Mg m^{-3}, $Z = 8$, $\mu = 0{\cdot}965$ mm^{-1}, $F(000) = 2016$, Cu $K\alpha$ radiation, $\lambda = 1{\cdot}54178$ Å. Full-matrix least-squares refinement resulted in a final conventional R index of 0·073 for 3660 observed reflections. 2,4-Diamino-5-(3,4,5-trimethoxybenzyl)pyrimidine (DTMBP) and 5,5-diethylbarbituric acid (DBA) are alternately linked by hydrogen bonds to form an endless chain in the **b** direction.

Introduction. DTMBP is an antifolate drug and DBA is a hypnotic drug. This investigation was undertaken as part of a series of structural studies of molecular complexes between different drugs. Single crystals (m.p. 497 K) of the title compound were grown from a solution of equimolar quantities of DTMBP and DBA in ethanol–acetone by slow evaporation of the solvent. Lattice constants were calculated by least squares from the diffractometrically determined θ values of 20 reflections. Intensity measurements were performed on a computer-controlled single-crystal diffractometer (Rigaku AFC-5, graphite-monochromated Cu $K\alpha$ radiation, ω–2θ scan) up to $2\theta = 145°$ using a crystal with dimensions 0·3 × 0·3 × 0·5 mm. A total of 3660 independent structure factors [$F_o \geq 3{\cdot}0\sigma(F_o)$] were observed and used in this analysis. The phase problem was solved by direct methods using *MULTAN* 78 (Main, Hull, Lessinger, Germain, Declercq & Woolfson, 1978); the E map computed with the set of best consistency (COMBFOM = 3·0000) revealed 33 of 34 non-hydrogen atoms. The one remaining atom [C(14)] was located after a Fourier synthesis.

Table 1. *Positional parameters and equivalent isotropic thermal parameters* (*Hamilton*, 1959), *with e.s.d.'s in parentheses*

	x	y	z	B_{eq} (Å^2)
DTMBP				
N(1)	0·0839 (3)	0·1806 (2)	0·6917 (1)	3·26
C(1)	0·1459 (3)	0·2263 (2)	0·7294 (1)	2·89
N(2)	0·1468 (2)	0·3077 (2)	0·7300 (1)	2·89
C(2)	0·0803 (3)	0·3454 (2)	0·6889 (1)	2·94
C(3)	0·0112 (3)	0·3024 (2)	0·6474 (1)	2·98
C(4)	0·0174 (3)	0·2201 (2)	0·6519 (2)	3·19
N(3)	0·2119 (3)	0·1883 (2)	0·7694 (2)	4·25
N(4)	0·0827 (3)	0·4265 (2)	0·6890 (1)	4·07
C(5)	−0·0646 (3)	0·3429 (2)	0·6019 (2)	3·48
C(6)	−0·0173 (3)	0·3684 (2)	0·5446 (1)	2·92
C(7)	−0·0879 (3)	0·3918 (2)	0·4971 (2)	3·33
C(8)	−0·0501 (3)	0·4146 (2)	0·4441 (2)	3·41
C(9)	0·0606 (3)	0·4135 (2)	0·4371 (2)	3·40
C(10)	0·1298 (3)	0·3921 (2)	0·4845 (2)	3·66
C(11)	0·0913 (3)	0·3685 (2)	0·5381 (2)	3·53
O(1)	−0·1123 (2)	0·4395 (2)	0·3954 (1)	4·25
O(2)	0·0980 (3)	0·4416 (2)	0·3848 (1)	4·42
O(3)	0·2400 (2)	0·3976 (2)	0·4828 (1)	5·74
C(12)	−0·2262 (4)	0·4420 (3)	0·3997 (2)	5·00
C(13)	0·0754 (4)	0·3887 (3)	0·3339 (2)	5·50
C(14)	0·2904 (4)	0·3472 (4)	0·4435 (3)	7·48
DBA				
C(15)	0·3700 (3)	0·3517 (2)	0·8491 (2)	3·48
C(16)	0·3192 (3)	0·4758 (2)	0·7958 (2)	3·29
C(17)	0·4647 (3)	0·4851 (2)	0·8729 (2)	3·49
C(18)	0·4494 (3)	0·3973 (2)	0·8906 (2)	3·25
N(5)	0·3060 (3)	0·3950 (2)	0·8085 (1)	3·44
N(6)	0·3997 (3)	0·5161 (2)	0·8272 (1)	3·59
O(4)	0·3599 (3)	0·2790 (2)	0·8518 (1)	5·53
O(5)	0·2625 (2)	0·5082 (2)	0·7564 (1)	4·31
O(6)	0·5323 (2)	0·5273 (2)	0·8991 (1)	4·87
C(19)	0·4005 (4)	0·4033 (3)	0·9527 (2)	4·48
C(20)	0·3841 (4)	0·3221 (3)	0·9834 (2)	5·46
C(21)	0·5581 (3)	0·3542 (3)	0·8953 (2)	4·24
C(22)	0·6109 (5)	0·3510 (3)	0·8372 (3)	6·51

0567-7408/82/082309-03$01.00 © 1982 International Union of Crystallography

UM00011852
NOVARTIS EXHIBIT 1017
Novartis v. Regents, IPR2023-01346
Page 598 of 4460

The structure was refined by full-matrix least-squares calculations with parameters grouped in three blocks including anisotropic temperature factors for the non-hydrogen atoms and isotropic temperature factors for the H atoms to yield $R = 0.073$. Extinction corrections were applied (Zachariasen, 1967) with the isotropic mode. The H atoms of C(13), C(14) and C(20) were not clearly seen in the difference synthesis. Neutral-atom scattering factors were obtained from *International Tables for X-ray Crystallography* (1974). Positional parameters are in Table 1.*

Discussion. Fig. 1 shows the structure of the title compound. Table 2 lists bond distances and valence angles. Table 3 contains selected best planes and deviations of atoms from them and dihedral angles.

The bond lengths and angles in the DTMBP part are in good agreement with those of DTMBP itself (Koetzle & Williams, 1976). Planes (1) and (2) of DTMBP are planar within experimental error.

Torsion angles C(2)–C(3)–C(5)–C(6) and C(3)–C(5)–C(6)–C(7) are 84·3 (4) and 168·0 (3)° respectively, compared to the corresponding angles of −89·4 (1) and 153·3 (1)° found by Koetzle & Williams, and to the values −67·5 (4) and 122·1 (4)° from our previous result for DTMBP–*o*-sulfobenzoimide (1:1) monohydrate (Shimizu & Nishigaki, 1982). The bond distances and angles of the DBA moiety are in agreement with those of DBA itself (Craven, Vizzini & Rodrigues, 1969). O(4) deviates from plane (3) by

* Lists of structure factors, anisotropic thermal parameters and H-atom positional parameters have been deposited with the British Library Lending Division as Supplementary Publication No. SUP 36831 (12 pp.). Copies may be obtained through The Executive Secretary, International Union of Crystallography, 5 Abbey Square, Chester CH1 2HU, England.

Table 2. *Bond distances* (Å) *and bond angles* (°), *with e.s.d.'s in parentheses*

DTMBP

N(1)–C(1)	1·340 (4)	C(6)–C(11)	1·378 (5)
N(1)–C(4)	1·345 (5)	C(7)–C(8)	1·376 (7)
C(1)–N(2)	1·346 (5)	C(8)–C(9)	1·406 (6)
C(1)–N(3)	1·333 (5)	C(8)–O(1)	1·361 (5)
N(2)–C(2)	1·350 (4)	C(9)–C(10)	1·370 (6)
C(2)–C(3)	1·416 (5)	C(9)–O(2)	1·387 (5)
C(2)–N(4)	1·341 (5)	C(10)–C(11)	1·396 (7)
C(3)–C(4)	1·366 (5)	C(10)–O(3)	1·385 (5)
C(3)–C(5)	1·501 (5)	O(1)–C(12)	1·436 (6)
C(5)–C(6)	1·527 (6)	O(2)–C(13)	1·456 (6)
C(6)–C(7)	1·391 (5)	O(3)–C(14)	1·404 (7)

C(1)–N(1)–C(4)	116·6 (3)	C(7)–C(6)–C(11)	119·2 (3)
N(1)–C(1)–N(2)	125·0 (3)	C(6)–C(7)–C(8)	120·6 (4)
N(1)–C(1)–N(3)	117·6 (3)	C(7)–C(8)–C(9)	120·3 (4)
N(2)–C(1)–N(3)	117·4 (3)	C(7)–C(8)–O(1)	125·1 (3)
C(1)–N(2)–C(2)	116·8 (3)	C(9)–C(8)–O(1)	114·7 (4)
N(2)–C(2)–C(3)	122·4 (3)	C(8)–C(9)–C(10)	118·8 (4)
N(2)–C(2)–N(4)	116·6 (3)	C(8)–C(9)–O(2)	119·6 (4)
C(3)–C(2)–N(4)	121·0 (3)	C(10)–C(9)–O(2)	121·3 (4)
C(2)–C(3)–C(4)	115·0 (3)	C(9)–C(10)–C(11)	120·8 (4)
C(2)–C(3)–C(5)	123·4 (3)	C(9)–C(10)–O(3)	122·0 (4)
C(4)–C(3)–C(5)	121·6 (3)	C(11)–C(10)–O(3)	117·1 (4)
N(1)–C(4)–C(3)	124·2 (3)	C(6)–C(11)–C(10)	120·3 (4)
C(3)–C(5)–C(6)	116·1 (3)	C(8)–O(1)–C(12)	117·4 (3)
C(5)–C(6)–C(7)	117·9 (3)	C(9)–O(2)–C(13)	114·6 (3)
C(5)–C(6)–C(11)	122·9 (3)	C(10)–O(3)–C(14)	118·5 (3)

DBA

C(15)–C(18)	1·513 (6)	C(17)–N(6)	1·364 (5)
C(15)–N(5)	1·371 (5)	C(17)–O(6)	1·214 (5)
C(15)–O(4)	1·211 (5)	C(18)–C(19)	1·580 (7)
C(16)–N(5)	1·379 (5)	C(18)–C(21)	1·531 (6)
C(16)–N(6)	1·360 (5)	C(19)–C(20)	1·533 (7)
C(16)–O(5)	1·218 (5)	C(21)–C(22)	1·518 (8)
C(17)–C(18)	1·522 (5)		

C(18)–C(15)–N(5)	118·4 (3)	C(15)–C(18)–C(19)	107·6 (3)
C(18)–C(15)–O(4)	122·0 (4)	C(15)–C(18)–C(21)	110·3 (3)
N(5)–C(15)–O(4)	119·6 (4)	C(17)–C(18)–C(19)	103·9 (3)
N(5)–C(16)–N(6)	117·5 (3)	C(17)–C(18)–C(21)	109·4 (3)
N(5)–C(16)–O(5)	120·4 (3)	C(19)–C(18)–C(21)	111·8 (4)
N(6)–C(16)–O(5)	122·1 (3)	C(15)–N(5)–C(16)	124·9 (3)
C(18)–C(17)–N(6)	118·6 (3)	C(16)–N(6)–C(17)	125·8 (3)
C(18)–C(17)–O(6)	121·1 (4)	C(18)–C(19)–C(20)	115·1 (4)
N(6)–C(17)–O(6)	120·3 (3)	C(18)–C(21)–C(22)	113·6 (4)
C(15)–C(18)–C(17)	113·7 (3)		

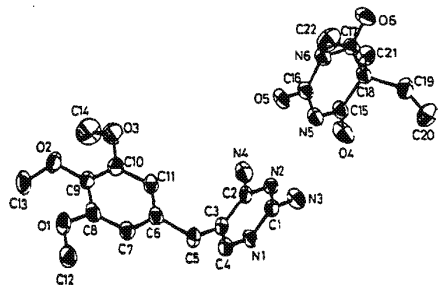


Fig. 1. Molecular structure of the title compound.

Table 3. *Least-squares planes and deviations* (Å) *of atoms from them and dihedral angles*

The planes are expressed in the form $lx + my + nz = d$ in Å.

DTMBP

Plane (1)

$-0.767744x + 0.003668y + 0.640746z = 10.162057$

N(1) −0·005 (5), C(1) −0·001 (5), N(2) 0·005 (4), C(2) −0·005 (5), C(3) −0·005 (5), C(4) 0·006 (5), N(3)* −0·004 (5), N(4)* −0·021 (5), C(5)* 0·009 (5)

Plane (2)

$-0.033759x - 0.949567y - 0.311741z = -9.576522$

C(6) 0·004 (6), C(7) −0·002 (6), C(8) −0·007 (6), C(9) 0·013 (6), C(10) −0·011 (6), C(11) 0·002 (6), C(5)* 0·025 (6), O(1)* −0·032 (4), O(2)* −0·080 (6), O(3)* −0·132 (4)

DBA

Plane (3)

$-0.719466x + 0.240296y + 0.651634z = 11.716209$

C(15) −0·070 (5), C(16) 0·028 (5), C(17) −0·012 (5), C(18) 0·060 (5), N(5) 0·029 (4), N(6) −0·035 (4), O(4)* −0·225 (4), O(5)* 0·037 (4), O(6)* −0·034 (4)

Dihedral angles (°)

(1) ∧ (2) 100·21 (5) (1) ∧ (3) 13·89 (15) (2) ∧ (3) 114·02 (15)°

* Atoms not included in the plane calculations.

UM00011853
NOVARTIS EXHIBIT 1017
Novartis v. Regents, IPR2023-01346
Page 599 of 4460

Table 4. *Intermolecular hydrogen bonds (distances in Å, angles in degrees)*

Donor	Acceptor		
N(6)–H*E*(ii)	N(1)*A*(i)	N(6)–H	0·99 (3)
		N(6)···N(1)	2·763 (5)
		H···N(1)	1·78 (3)
		N(6)–H···N(1)	176 (3)
N(3)–H(1)*A*(i)	O(5)*E*(ii)	N(3)–H(1)	0·83 (3)
		N(3)···O(5)	3·056 (5)
		H(1)···O(5)	2·24 (3)
		N(3)–H(1)···O(5)	166 (4)
N(3)–H(2)*A*(i)	O(4)*B*(i)	N(3)–H(2)	0·95 (4)
		N(3)···O(4)	2·933 (6)
		H(2)···O(4)	2·01 (4)
		N(3)–H(2)···O(4)	165 (4)
N(5)–H*B*(i)	N(2)*A*(i)	N(5)–H	0·95 (4)
		N(5)···N(2)	2·940 (5)
		H···N(2)	2·00 (4)
		N(5)–H···N(2)	171 (3)
N(4)–H(1)*A*(i)	O(5)*B*(i)	N(4)–H(1)	1·05 (4)
		N(4)···O(5)	2·943 (5)
		H(1)···O(5)	1·91 (4)
		N(4)–H(1)···O(5)	168 (4)

Symmetry code: (i) x,y,z; (ii) $0·5 - x, -0·5 + y, 1·5 - z$. (*A*) DTMBP. (*B*) and (*E*) DBA.

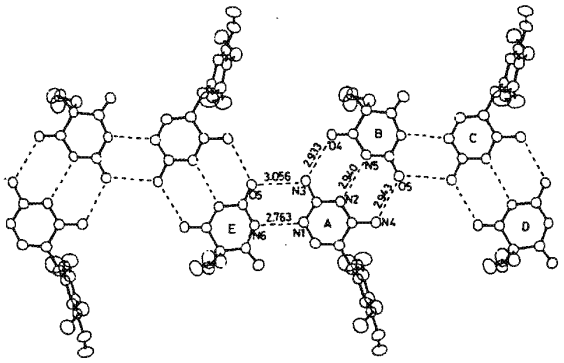


Fig. 2. Packing diagram of the title compound (*A*, *C*: DTMBP; *B*, *D*, *E*: DBA). (Distances are in Å.)

0·225 (4) Å. The angles C(15)–C(18)–C(19)–C(20) and C(15)–C(18)–C(21)–C(22) are 63·3 (3) and 63·4 (4)°, respectively. Table 4 gives the hydrogen-bonding parameters. A packing diagram is shown in Fig. 2. The shortest N(1)···H–N(6) contact between DTMBP(*A*) and DBA(*E*) is 2·763 (5) Å, which is considerably shorter than the sum of the radii, 3·0 Å (Pauling, 1960). O(6) does not participate in any hydrogen bonds. DTMBP molecules have a tendency to form dimers – as Koetzle & Williams found in DTMBP, and we found in DTMBP–*o*-sulfobenzoimide (1:1) monohydrate – *via* the hydrogen bond N(4)···N(2); DBA molecules also have a tendency to form dimers (NH···C=O), as observed in DBA by Craven *et al.* (1969), and in the DBA–caffeine (2:1) complex by Craven & Gartland (1970).

In the present crystal, however, DTMBP and DBA are alternately linked to form an endless chain (*–A–B–C–D–*) by characteristic hydrogen bonds, which apparently contribute significantly to the stabilization of this crystal; this is probably why its melting point (497 K) is so high. No significant contacts exist between molecules of the same kind (DTMBP···DTMBP, DBA···DBA).

We wish to thank Professor Toyozo Uno of Kyoto University for many helpful suggestions during the course of this work, and also Dr Keiichi Yamaguchi, Chiba University, for collecting the diffraction data. The calculations were performed using the programs *MULTAN* 78 (Main *et al.*, 1978), *ORTEP* (Johnson, 1965) and *UNICS* (1967) at the Computer Center, University of Tokyo.

References

Craven, B. M. & Gartland, G. L. (1970). *J. Pharm. Sci.* **59**, 1666–1670.

Craven, B. M., Vizzini, E. A. & Rodrigues, M. M. (1969). *Acta Cryst.* B**25**, 1978–1993.

Hamilton, W. C. (1959). *Acta Cryst.* **12**, 609–610.

International Tables for X-ray Crystallography (1974). Vol. IV. Birmingham: Kynoch Press.

Johnson, C. K. (1965). *ORTEP*. Report ORNL-3794. Oak Ridge National Laboratory, Tennessee.

Koetzle, T. F. & Williams, G. J. B. (1976). *J. Am. Chem. Soc.* **98**, 2074–2078.

Main, P., Hull, S. E., Lessinger, L., Germain, G., Declercq, J. P. & Woolfson, M. M. (1978). *MULTAN* 78. *A System of Computer Programs for the Automatic Solution of Crystal Structures from X-ray Diffraction Data*. Univs. of York, England, and Louvain, Belgium.

Pauling, L. (1960). *The Nature of the Chemical Bond*, 3rd ed., p. 260. Ithaca: Cornell Univ. Press.

Shimizu, N. & Nishigaki, S. (1982). *Acta Cryst.* B**38**, 1834–1836.

UNICS (1967). *The Universal Crystallographic Computation Program System*, edited by T. Sakurai. Tokyo: The Crystallographic Society of Japan.

Zachariasen, W. H. (1967). *Acta Cryst.* **23**, 558–564.

UM00011854
NOVARTIS EXHIBIT 1017
Novartis v. Regents, IPR2023-01346
Page 600 of 4460

Indian Journal of Chemistry
Vol. 37B, May 1998, pp. 429 - 432

Solid state reaction between 8-hydroxyquinoline and *p*-nitrobenzoic acid

N B Singh*, Ms Renu Singh & Ms Kalpana Singh
Department of Chemistry University of Gorakhpur, Gorakhpur-273009, India

Received 10 October 1997; accepted (revised) 24 March 1998

8-Hydroxyquinoline reacts with *p*-nitrobenzoic acid in solid state forming 1:1 molecular complex. In solid state the diffusion of 8-hydroxyquinoline occurs towards *p*-nitrobenzoic acid and the process of diffusion is not vapour phase dominated process. Micro structural studies have indicated that reaction during solid state may be nucleation controlled process. Reaction products obtained from solution and solid state reaction are identical and their is a hydrogen bonding between the components in the reaction product.

In recent years considerable interest have developed in the study of organic reactions in the crystalline state.[1-9] Many such reactions have been studied from the synthetic and mechanistic point of view. Recently a few solid state reactions of 8-hydroxyquinoline with anhydrides [10] and also with metal salts [11] have been studied with a view to understand the mechanism of diffusion of 8-hydroxyquinoline molecules into the crystal lattice of the other reacting components. However due to non availability of the crystal structures of the reaction products, the exact mechanism could not be understood. In this paper solid state reaction between *p*-nitrobenzoic acid and 8-hydroxyquinoline has been studied with a view to understand the mechanism of reaction and the nature of reaction product.

Materials and Purification

8-hydroxyquinoline (A.R. Merck) was purified by repeated distillation under reduced pressure. The purified sample melts at 75°C.

p-Nitrobenzoic acid (A.R. CDH) was used without further purification. The melting point was found to be 242°C. 8-Hydroxyquinoline and *p*-nitrobenzoic acid are abbreviated as 8-HQ and *p*-NBA respectively.

Preparation of reaction product from solution— *p*-nitrobenzoic acid (*p*-NBA) (0.5566 g) and of 8-hydroxyquinoline (8-HQ) (0.4833 g) were dissolved in methanol separately. Both the solutions were warmed and mixed. After 24h very thin yellow colour crystals were obtained, m.p. 180°C.

Preparation of reaction product from solid-state reaction—Solid powders of 8-HQ and *p*-NBA were mixed thoroughly in 1:1 molar ratio in an agate mortar and kept in an incubator at 50°C for a week with occasional mixing and crushing. The reaction product was yellow in colour and melted sharply at 171°C.

Methods

The electronic spectra of 8-HQ, *p*-NBA and mixture of the two in 1:1 molar ratio were recorded in DMF (0.02*M*). The I.R. spectra of 8-HQ, *p*-NBA and the reaction products obtained from solution and solid-state reaction were recorded in Nujol mull.

The powder X-ray diffraction patterns and DTA data of the 8-HQ, *p*-NBA and the reaction products obtained from solution and solid-state reactions were recorded.

Microstructural studies were also made[12]. A clean slide was kept at 245°C in an oven and a small amount of *p*-NBA was placed over the slide which immediately melted. The temperature of the oven was lowered down up to 242°C and crystallised in one direction with the help of a cover slip in such a way that a very thin layer of *p*-NBA crystallised. This was examined under microscope and photographed.

The slide of *p*-NBA was kept on the top of the beaker filled with vapours of 8-HQ and covered

UM00011855
NOVARTIS EXHIBIT 1017
Novartis v. Regents, IPR2023-01346
Page 601 of 4460

with big beaker and kept at 70°C for different time intervals. *p*-NBA reacted with vapours of 8-HQ and change in microstructure was photographed.

Kinetics of solid -state reaction between *p*-nitrobenzoic acid and 8-hydroxyquinoline in capillary (reactions in contact)—The detailed method for studying the reaction is described elsewhere[13]. A pyrex glass capillary was used for the purpose. One end of the capillary was sealed with the help of sealing wax. Half of the capillary was filled with *p*-nitrobenzoic acid (particle size <100 mesh) and the remaining half of the capillary was filled with 8-hydroxyquinoline (particle size < 100 mesh) in such a way that *p*-nitrobenzoic acid and 8-hydroxyquinoline came in close contact. At the junction of the two components, the reaction started with a colour change (intense yellow). The kinetics was followed by measuring the thickness of the reaction product at different intervals of time with the help of a travelling microscope at different temperatures (40, 50, 55 and 60°C).The kinetics was also studied when the reactants were separated by air gaps. Reaction occured at the surface of *p*-nitrobenzoic acid

Kinetic studies between *p*-nitrobenzoic acid (solid) and 8-hydroxyquinoline (vapour)—In order to understand the inner penetration of 8-hydroxyquinoline into the crystal lattice of *p*-nitrobenzoic acid, the reaction of *p*-nitrobenzoic acid (solid) was carried out with 8-hydroxyquinoline (vapours) gravimetrically. The detailed method for studying out the reaction is described elsewhere[14]. The kinetics was followed by noting the increase in weight of *p*-nitrobenzoic acid at different intervals of time at different temperatures 50, 55, 60 and 65°C.

Results and Discussion

Before we speculate on the mechanism of diffusion and solid-state reactivity, it is desirable to characterise the reaction product. When *p*-nitrobenzoic acid and 8-hydroxyquinoline were mixed in solid-state in 1:1 molar ratio, immediately an yellow colour developed, indicating that reaction occurred in solid state. When solutions of *p*-nitrobenzoic acid and 8-hydroxyquinoline in methyl alcohol were mixed in 1:1 molar ratio, thin yellow coloured crystals were obtained.

The X-ray diffraction patterns of the components and the reaction products obtained by solid-state reaction and from methanol were recorded. The reaction product obtained from methanol showed sharp intense and new peaks indicating that there is a formation of new compound with a definite crystal lattice. The diffraction patterns of the reaction product obtained by solid-state reaction is almost identical to that of the product obtained from methanol except that the intensities of the peaks are very low. The results show that the reaction products obtained from solution and solid-state reactions are identical but the reaction in solid-state is slow.

When vapours of 8-hydroxyquinoline were allowed to react with solid *p*-nitrobenzoic acid at 65°C, the final increase in weight of *p*-nitrobenzoic acid corresponded to reaction product $(8\text{-HQ})_1.(p\text{-NBA})_1$ The differential thermal analyses of the product $(8\text{-HQ})_1.(p\text{-NBA})_1$ obtained from solid state reactions and solution were recorded. An endotherm at 179.6°C in the case of $(8\text{-HQ})_1.(p\text{-NBA})_1$ obtained from solution corresponds to its melting point. On the other hand DTA of $(8\text{-HQ})_1.(p\text{-NBA})_1$ obtained from solid-state reactions shows 3 endotherms at 75.9°C, 170.0°C and 240.8°C corresponding to the melting of unreacted 8-hydroxyquinoline, product $(8\text{-HQ})_1.(p\text{-NBA})_1$ and unreacted *p*-nitrobenzoic acid. This shows that reaction is incomplete in solid-state and decrease in melting points is due to impurities of the components. The results show that the reaction product obtained from solution and solid-state reaction are identical.

Since the reaction product is coloured, one can expect a CT interaction between the two components. The UV spectra of the reaction product in DMF does not give any new band indicating that either the charge transfer interaction is absent or very weak interaction is present. However the IR spectral studies of the reactants and the product gave some information regarding the nature of interactions. It is already reported that 8-hydroxyquinoline in the solid state exists as dimer and the association is due to hydrogen bonding[15]. Due to reaction the dimeric structure of 8-hydroxyquinoline is broken and the W = O group of *p*-nitrobenzoic acid is hydrogen bonded with the hydrogen atom of -OH group of 8-hydroxyquinoline and at the same time nitrogen atom of 8-hydroxyquinoline is hydrogen bonded

UM00011856
NOVARTIS EXHIBIT 1017
Novartis v. Regents, IPR2023-01346
Page 602 of 4460

with hydrogen atom of -COOH group of *p*-nitrobenzoic acid.

When powders of 8-hydroxyquinoline and *p*-nitrobenzoic acid were kept in glass capillary in contact, the start of the reaction was indicated by the formation of an yellow coloured boundary at the point of contact. As the reaction proceeded, boundary moved towards *p*-nitrobenzoic acid, indicating that 8-hydroxyquinoline is the diffusing species. The kinetics was followed by measuring the thickness of the product layer as a function of time and the kinetic data obeyed the Eq. (1)

$$\xi = k_1 t^n \quad \ldots (1)$$

where ξ is the thickness of the product layer at time t, k_1 and n are constants. k_1 is temperature dependent and hence an apparent rate constant related to diffusion coefficient. The validity of Eq. 1 is tested by plotting log ξ vs. log t where straight lines are obtained .The values of k_1 and n are given in Table 1. The energy of activation was calculated from Arrhenius plot and was found to be 30.1 *kJ* mol^{-1}. The energy of activation value is much lower than the heat of sublimation of 8-hydroxyquinoline (108.7 *kJ* mol^{-1})[16]. This shows that the diffusion of 8-hydroxyquinoline molecules towards *p*-nitrobenzoic acid is not a vapour phase diffusion dominated process. Diffusion may occur through surface migration. It has been pointed out by Patil *et al.*[17] that volatility is not the only factor affecting the solid-state reactivity. For example, methyl quinone reacted relatively rapidly with the unsubstituted hydroquinone and also the unsubstituted quinone reacted readily with methyl hydroquinone.

When the kinetics were studied by creating air-gaps of different length, kinetic data were again fitted by Eq. 1. For this case k_1 and n are referred to as k_1' and n'. The values of k_1' is decreased with the increase of the length of air-gap. The variation of rate constant (k_1') with length of air-gap (d) is given by Eq. 2.

$$k_1' = Ae^{-pd} \quad \ldots (2)$$

where A and p are constants. When log k_1' is plotted against d, a straight line is obtained .The kinetic parameters are given in Table II. The rate constant on extrapolation to zero air-gap comes out to be 3.63 x 10^{-2} cm h^{-1} which is much less than the rate of reaction when the reactants are in contact (4.67 x 10^{-2} cm h^{-1}) at 60 ± 1°C. This simply shows that during migration of 8-hydroxyquinoline towards *p*-nitrobenzoic acid apart from vapour phase diffusion some easier mode of migration such as surface migration is also involved. The surface migration of 8-HQ over the glass surface is not uncommon.[18]

Table I—Effect of temperature on the kinetic parameters of Eq. (1)
Particle size < 100 mesh

Temperature (°C)	k_1 x 10^2 (cm/h)	n	E (kJ. mol^{-1})
40	2.5	0.24	
50	3.6	0.24	
60	4.1	0.24	
70	4.7	0.24	30.1

Table II—Effect of air - gaps on the kinetic parameters of Eq. (3.1)
Temperature = 60 ± 1°C; Particle size < 100 mesh

d (cm)	k_1' x 10^2 (cm/h)	n'
1.190	2.0	0.37
0.800	2.5	0.41
0.500	3.0	0.40
0.194	3.3	0.41

When d=0 on extrapolation $k_1' = 3.6 \times 10^{-2}$ cm/h; k_1(contact)=4.7 x 10^{-2} cm /h

The process of inner penetration of 8-hydroxyquinoline into the crystal lattice of *p*-nitrobenzoic acid can be understood by gravimetric studies. The kinetic data obeyed the Eq. (3)

$$\Delta W/W_0 = k_2 t \quad \ldots (3)$$

where ΔW is the increase in weight of *p*-nitrobenzoic acid at any time *t*, W_0 is the initial weight of *p*-nitrobenzoic acid and k_2 is the rate constant. The validity of Eq. (3) is tested by plotting $\Delta W/ W_0$ vs *t*. when straight lines are obtained. The values of k_2 calculated from these plots are listed in Table III. The energy of activation calculated from Arrhenius plot is found to be 78.7 kJ. mol^{-1}. During the course of diffusion of 8-hydroxyquinoline towards *p*-nitrobenzoic acid, the following two processes will occur simultaneously: (i) Migration of 8-hydroxyquinoline over the surface of *p*-nitrobenzoic acid, and (ii) Inner penetration into crystal lattice of *p*-nitrobenzoic acid.

UM00011857
NOVARTIS EXHIBIT 1017
Novartis v. Regents, IPR2023-01346
Page 603 of 4460

Table III—Inner-diffusion of 8-hydroxyquinoline (vapour) in *p*-nitrobenzoic acid (solid) increase in weight, gravimetric technique following Eq. (3)

Temperature (°C)	$k_2 \times 10^3$ (g/h)	E ($kJ.\ mol^{-1}$)
50	0.63	
55	0.85	78.7
60	1.05	
65	1.42	

Out of the above two processes, the first is much faster and easier as compared to the second one. Microscopic studies give informations only for the first process whereas gravimetric studies account for both processes. Since inner penetration in organic solids is difficult, it will require higher energy of activation as shown by gravimetric studies.

During solid-state reactions, very little structural changes occur. This can be confirmed by complete structural determinations. In the absence of structural data some idea can be made from microstructural changes. The microstructure of *p*-nitrobenzoic acid shows that small crystallites are joined together indicating that strcture is probably globular in nature. When *p*-nitrobenzoic acid was exposed to the vapours of 8-hydroxyquinoline for 30 minutes, long and thin crystals of the product were observed .This indicated that the growth of the product is mainly in one direction which shows that the solid-state reaction is a nucleation controlled process

The overall results show that 8-HQ reacts with *p*-NBA both in solid state and solution forming 1:1 hydrogen bonded molecular crystalline complex. During solid state reaction, 8-HQ diffuses towards *p*-NBA and the process of diffusion is not vapour phase dominated process. Microstructural studies have shown that the solid state reaction might be nucleation controlled process.

Acknowledgement

The authors are thankful to UGC, New Delhi for financial support.

References:

1 Singh N B, Singh R J & Singh N P, *Tetrahedron*, 15 1994, 6441.
2 Paul I C, & Curtin D Y, *Science* 19, 1975,187.
3 Green B S, Lahav M., Rabinowich D., *Acc. Chem. Res.*, 12, 1979 154.
4 Hasegawa M, *Chem. Rev.*, 83, 1983, 507.
5 Gillepsie R J & Day P, *Philos. Trans. Royal Soc. London*, 1985, 314.
6 Bym S R, *Solid state of drugs*, (Academic Press, New .York),. 1982.
7 Williams J M, bens M A, wang H, Leung P C N, Emge T J, GeiseV & Carlson K D, *Acc. Chem. Res.*, 18, 1985, 261.
8 Singh N B, Singh R P, Singh J & Singh H C, *J. Solid State Chem.*, 33, 1980,391.
9 Beg M A., Ahmad A & Aksari A, *J. Solid State Chem.*, 68, 1987,22.
10 Rastogi R P, Singh N B & Singh R P *Indian. J. Chem.*, 1977, 941.
11 Dubey B L & Tiwari N, *Indian J Chem.*, 30A, 1991, 855.
12 Singh N B & Singh N B, *J. Crystal Growth*, 28, 1975,267.
13 Rastogi R P, Bassi P S & Chaddha S L, *J. Phys. Chem.*, 66, 1962, 2707 .
14 Rastogi R P, Bassi P S & Chaddha S L, *J. Phys. Chem.*, 67, 1963,2569.
15 Prout C K & Wheeler A G, *J.Chem.Soc.,(A)*, 1967,469.
16 *Lange's handbook of chemistry*, 13th Edn. (McGraw Hill Book Company, New York), 9-153, 9-158.,1985.
17 Patil A O, Curtin D Y & Paul I C, *J. Am. Chem. Soc.*, 106, 1984, 348.
18 Rastogi R P, Singh N B & Singh R P, *Ind. J. Chem.*, 1977, 941.

UM00011858
NOVARTIS EXHIBIT 1017
Novartis v. Regents, IPR2023-01346
Page 604 of 4460

This Page is Inserted by IFW Indexing and Scanning Operations and is not part of the Official Record

BEST AVAILABLE IMAGES

Defective images within this document are accurate representations of the original documents submitted by the applicant.

Defects in the images include but are not limited to the items checked:

- ☐ BLACK BORDERS
- ☐ IMAGE CUT OFF AT TOP, BOTTOM OR SIDES
- ☐ FADED TEXT OR DRAWING
- ☐ BLURRED OR ILLEGIBLE TEXT OR DRAWING
- ☐ SKEWED/SLANTED IMAGES
- ☐ COLOR OR BLACK AND WHITE PHOTOGRAPHS
- ☐ GRAY SCALE DOCUMENTS
- ☐ LINES OR MARKS ON ORIGINAL DOCUMENT
- ☐ REFERENCE(S) OR EXHIBIT(S) SUBMITTED ARE POOR QUALITY
- ☐ OTHER: _____

IMAGES ARE BEST AVAILABLE COPY.
As rescanning these documents will not correct the image problems checked, please do not report these problems to the IFW Image Problem Mailbox.

Acta Crystallographica Section C
Crystal Structure Communications
ISSN 0108-2701

The 1:1 adduct of 4-aminobenzoic acid with 4-aminobenzonitrile

Graham Smith,[a]* Raymond C. Bott[a] and Daniel E. Lynch[b]

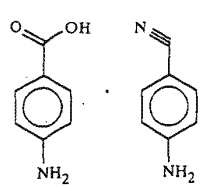
[a]Centre for Instrumental and Developmental Chemistry, Queensland University of Technology, GPO Box 2434, Brisbane 4001, Australia, and [b]School of Natural and Environmental Sciences, Coventry University, Coventry CV1 5FB, England
Correspondence e-mail: g.smith@qut.edu.au

Received 31 January 2000
Accepted 19 June 2000

The 1:1 adduct of 4-aminobenzoic acid (PABA) with 4-aminobenzonitrile (PABN), $C_7H_7NO_2 \cdot C_7H_6N_2$, consists of a primary centrosymmetric cyclic hydrogen-bonded PABA dimer interaction [O···O 2.640 (3) Å] peripherally linked into chains by weaker hydrogen bonds *via* a head-to-tail PABN interaction [N···N 3.179 (4) and N···O 3.062 (4) Å], and is linked between the chains by amine-N (PABN) to amine-N (PABA) interactions [N···N 3.233 (5) Å]. No proton transfer occurs.

Comment

4-Aminobenzoic acid (PABA) is an important biological molecule, being an essential bacterial cofactor involved in the synthesis of folic acid (Robinson, 1966), as well as acting as an antagonist to the action of the drug sulfonilamide in competition for essential growth metabolites (Pauling & Hayward, 1964). As a simple organic molecule which promotes the extension of hydrogen-bonded network structures it has no equal, having associations with neutral molecules such as 4-nitropyridine *N*-oxide (Lechat, 1984), 1,3,5-trinitrobenzene (Lynch *et al.*, 1994) and urea (Smith, Baldry *et al.*, 1997), with Lewis bases such as 4-(4-nitrobenzyl)pyridine (Smith, Lynch *et al.*, 1997), and with carboxylic acids such as 2,4,6-trinitrobenzoic acid (Lynch *et al.*, 1992*a*), (2,4-dichlorophenoxy)acetic acid (Lynch *et al.*, 1992*b*), 2-(carboxyphenoxy)acetic acid (Byriel *et al.*, 1991) and 3,5-dinitrosalicylic acid (Smith *et al.*, 1995).



(I)

The ability of strong carboxylic acids to protonate the amine group of PABA often results in the formation of acid–

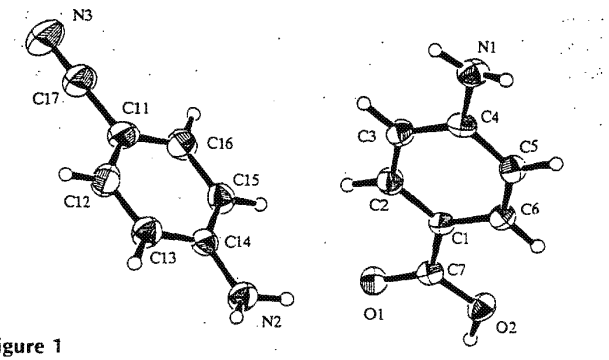


Figure 1
The molecular configuration of adduct (I) and the atom-numbering scheme, showing 30% probability displacement ellipsoids. H atoms are drawn as small spheres of arbitrary radii.

(PABA)$_2$ associations in which one PABA is protonated while the second is not. This is found in the adduct with 3,5-dinitrosalicylic acid. In a review of the adducts of PABA (Smith, Lynch *et al.*, 1997), the most common primary associative mode was recognized as the *A*–*A* homodimer, in which the two PABA molecules form a cyclic hydrogen-bonded dimer [graph set $R_2^2(8)$; Etter, 1990], such as is found in the parent acid (Lai & Marsh, 1967) and in the adduct with (2,4-dichlorophenoxy)acetic acid. The less common form is the *A*–*B* [$R_2^2(8)$] heterodimer, which is found with the (2-carboxyphenoxy)acetic acid adduct.

Our previous work has involved the adducts of PABA with carboxylic acids and with Lewis bases, and was extended in the present study to include 4-aminobenzonitrile (PABN), a

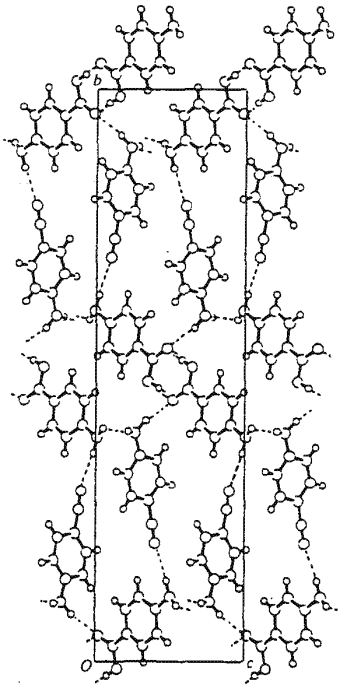


Figure 2
The packing in the unit cell of (I) viewed down the *a* axis, showing the hydrogen-bonding interactions as broken lines.

 © 2000 International Union of Crystallography • Printed in Great Britain – all rights reserved

UM00011860
NOVARTIS EXHIBIT 1017
Novartis v. Regents, IPR2023-01346
Page 606 of 4460

molecule not unlike PABA, having potential for hydrogen-onding extension *via* the cyanide group. We present here the crystal structure analysis of the 1:1 PABA–PABN adduct, (I).

In adduct (I), the PABA molecules form the common primary *A*–*A* cyclic hydrogen-bonded dimers across crystallographic inversion centres [O2—HO2···O1($1-x, -y, -z$) 2.640 (3) Å and 173 (3)°]. Weaker secondary interactions link these dimer units along the *b* direction (Fig. 2) through both the cyanide and amino groups of the PABN molecule [N1—H10···N3($-1+x, \frac{1}{2}-y, \frac{1}{2}+z$) 3.179 (5) Å and 164 (3)°; N2—H20···O1 3.062 (4) Å and 159 (3)°]. These chains are held together by lateral hydrogen bonds between the PABA and PABN amine groups [N1—H11···N2($-1+x, y, 1+z$) 3.233 (5) Å and 139 (3)°].

Experimental

The synthesis of (I) was carried out by refluxing equimolar (2 mmol) amounts of 4-aminobenzoic acid and 4-aminobenzonitrile for 15 min at *ca* 350 K in 95% ethanol (20 ml). Crystals of (I) were obtained after evaporation of the solvent at room temperature.

Crystal data

$C_7H_7NO_2{\cdot}C_7H_6N_2$
$M_r = 255.28$
Monoclinic, $P2_1/c$
$a = 4.860\ (3)$ Å
$= 32.543\ (4)$ Å
$= 8.538\ (3)$ Å
$\beta = 94.79\ (4)°$
$V = 1345.6\ (8)$ Å^3
$Z = 4$
$D_x = 1.260$ Mg m^{-3}
Mo $K\alpha$ radiation
Cell parameters from 25 reflections
$\theta = 10$–$20°$
$\mu = 0.087$ mm^{-1}
$T = 153$ K
Prismatic, colourless
$0.3 \times 0.2 \times 0.2$ mm

Data collection

Rigaku AFC-7*R* diffractometer
ω scans with profile analysis
2723 measured reflections
2372 independent reflections
1614 reflections with $I > 1.5\sigma(I)$
$R_{int} = 0.074$
$\theta_{max} = 25°$
$h = 0 \rightarrow 5$
$k = 0 \rightarrow 38$
$l = -10 \rightarrow 10$
3 standard reflections
frequency: 150 min
intensity decay: none

Table 1
Selected geometric parameters (Å, °).

O1—C7	1.240 (3)	N2—C14	1.368 (4)
O2—C7	1.319 (3)	N3—C17	1.127 (4)
N1—C4	1.379 (4)		
C2—C1—C7	119.3 (3)	O2—C7—C1	115.1 (3)
C6—C1—C7	122.1 (3)	C12—C11—C17	119.5 (4)
N1—C4—C3	120.5 (3)	C16—C11—C17	121.6 (4)
N1—C4—C5	121.0 (3)	N2—C14—C13	121.2 (3)
O1—C7—O2	122.1 (3)	N2—C14—C15	120.5 (3)
O1—C7—C1	122.7 (3)	N3—C17—C11	179.5 (6)

Refinement

Refinement on F
$R = 0.045$
$wR = 0.043$
$S = 1.795$
1614 reflections
193 parameters
H atoms treated by a mixture of independent and constrained refinement
$(\Delta/\sigma)_{max} = 0.002$
$\Delta\rho_{max} = 0.14$ e Å^{-3}
$\Delta\rho_{min} = -0.16$ e Å^{-3}
Extinction correction: Zachariasen (1968) type 2 Gaussian isotropic
Extinction coefficient: 8.001

The parameters of the H atoms involved in hydrogen bonding were refined (HO2, H11, H12, H21 and H22). All other H atoms were allowed for as riding.

Data collection: *MSC/AFC Diffractometer Control Software* (Molecular Structure Corporation, 1993); cell refinement: *MSC/AFC Diffractometer Control Software*; data reduction: *TEXSAN* (Molecular Structure Corporation, 1985); program(s) used to solve structure: *SIR*88 (Burla *et al.*, 1989); program(s) used to refine structure: *TEXSAN*; software used to prepare material for publication: *TEXSAN*.

The authors wish to thank the Australian Research Council and The Centre for Instrumental and Developmental Chemistry (QUT) for financial assistance. Dr Michael Gardner is thanked for collection of diffraction data.

Supplementary data for this paper are available from the IUCr electronic archives (Reference: TA1290). Services for accessing these data are described at the back of the journal.

References

Burla, M. C., Camalli, M., Cascarano, G., Giacovazzo, C., Polidori, G., Spagna, R. & Viterbo, D. (1989). *J. Appl. Cryst.* **22**, 389–393.
Byriel, K. A., Lynch, D. E., Smith, G. & Kennard, C. H. L. (1991). *Aust. J. Chem.* **44**, 1495–1464.
Etter, M. C. (1990). *Acc. Chem. Res.* **23**, 120–126.
Lai, T. F. & Marsh, R. E. (1967). *Acta Cryst.* **22**, 885–893.
Lechat, J. (1984). *Acta Cryst.* A**40**, C-264.
Lynch, D. E., Smith, G., Byriel, K. A. & Kennard, C. H. L. (1992*a*). *Acta Cryst.* C**48**, 533–536.
Lynch, D. E., Smith, G., Byriel, K. A. & Kennard, C. H. L. (1992*b*). *Z. Kristallogr.* **200**, 73–82.
Lynch, D. E, Smith, G., Byriel, K. A. & Kennard, C. H. L. (1994). *Acta Cryst.* C**50**, 2079–2082.
Molecular Structure Corporation (1985). *TEXSAN*. MSC, 3200 Research Forest Drive, The Woodlands, TX 77381, USA.
Molecular Structure Corporation (1993). *MSC/AFC Diffractometer Control Software*. Version 5.1.0. MSC, 3200 Research Forest Drive, The Woodlands, TX 77381, USA.
Pauling, L. & Hayward, R. (1964). *The Architecture of Molecules*, p. 56. San Francisco: W. H. Freeman.
Robinson, F. A. (1966). *The Vitamin Co-factors of Enzyme Systems*, pp. 541–662. London: Pergamon.
Smith, G., Baldry, K. E., Byriel, K. A. & Kennard, C. H. L. (1997). *Aust. J. Chem.* **50**, 727–736.
Smith, G., Lynch, D. E., Byriel, K. A. & Kennard, C. H. L. (1995). *Aust. J. Chem.* **48**, 1133–1149.
Smith, G., Lynch, D. E., Byriel, K. A. & Kennard, C. H. L. (1997). *J. Chem. Cryst.* **27**, 307–317.
Zachariasen, W. H. (1968). *Acta Cryst.* A**24**, 212–216.

UM00011861
NOVARTIS EXHIBIT 1017
Novartis v. Regents, IPR2023-01346
Page 607 of 4460

Aust. J. Chem. **2001**, *54*, 171–175

Interactions of Aromatic Carboxylic Acids with Quinolin-8-ol (Oxine): Synthesis and the Crystal Structures of the Proton-Transfer Compounds with the Nitro-Substituted Benzoic Acids

Graham Smith,[A,B] *Urs D. Wermuth*[A] *and Jonathan M. White*[C]

[A] Centre for Instrumental and Developmental Chemistry, School of Physical Sciences, Queensland University of Technology, GPO Box 2434, Brisbane, Qld. 4001.
[B] Author to whom correspondence should be addressed(e-mail: g.smith@qut.edu.au).
[C] School of Chemistry, University of Melbourne, Parkville, Vic. 3052.

Proton-transfer compounds of quinolin-8-ol (oxine) with the nitro-substituted aromatic carboxylic acids 2-nitrobenzoic acid, $[(C_9H_8NO^+)(C_7H_4NO_4^-)\cdot H_2O]$ (1), 3-nitrobenzoic acid, $[(C_9H_8NO^+)(C_7H_4NO_4)^-]$ (2), 4-nitrobenzoic acid, $[(C_9H_8NO^+)(C_7H_4NO_4^-)(C_7H_5NO_4)]$ (3), 3,5-dinitrobenzoic acid, $[(C_9H_8NO^+)_2(C_7H_3N_2O_6^-)_2\cdot 3H_2O]$ (4), 5-nitrosalicylic acid, $[(C_9H_8NO^+)(C_7H_4NO_5^-)]$ (5) and 3,5-dinitrosalicylic acid, $[(C_9H_8NO^+)(C_7H_3N_2O_7^-)]$ (6) have been prepared and characterized by using both infrared spectroscopy and single-crystal X-ray diffraction methods [(3), (4) and (6)]. In all compounds, protonation of the quinoline nitrogen occurs together with primary hydrogen-bonding interactions involving this group and the carboxylate group of the acid, while further peripheral associations, in the case of the trihydrate (4), also involving the water molecules, result predominantly in simple chain polymeric structures.

Manuscript received: 5 February 2001.
Final version: 30 May 2001.

Introduction

Quinolin-8-ol [8-hydroxyquinoline (oxine)] is well known as a disinfectant and antiseptic agent as well as being a particularly versatile molecule for use in metal complex chemistry. The relative positions of the hetero-nitrogen (pK_a 10.8) and 8-substituted phenol group, together with the acidic nature of the latter (pK_a 4.9), provide the textbook example for selective interaction with metals, giving bis- and tris-chelate complex systems which are often neutral. Under basic conditions, essentially no selectivity is achieved but with pH control, quantitative precipitation is possible, such as with Mg^{2+} where the complex $[Mg(oxine^-)_2]$ is a common weighing form in gravimetric analysis.[1] While neutral divalent metal complexes such as this and $[Pd(oxine^-)_2]$[2] are common, adducts involving metal complexes or metal salts with free oxine are also known, e.g. $\{[Ni(oxine^-)_2]\cdot oxine\}$,[3] $[K^+(oxine^-)\cdot oxine]$[4] and $[K^+(oxine^-)\cdot(oxine)_2]$.[5] In addition, metal complexes with both anionic and neutral coordinated oxine species have been reported, e.g. $\{[Ag(oxine^-)(oxine)]\cdot pyridine\}$[6] and the Ag complex unit in $\{[Ag(oxine)_2]^-(p\text{-toluenesulfonate}^-)\}$.[7]

Neutral adducts with organic compounds are less prevalent, but the structures of stable 1:1 adducts with chloranil[8] and 1,3,5-trinitrobenzene[9] are known together with the 2:1 proton-transfer adduct with 1,2,3-trihydroxybenzene, $[(oxine^-)(thb^-\cdot oxine]$.[10] In the neutral adducts, the oxine forms cyclic $R_2^2(8)$ hydrogen-bonded dimers via the hetero-nitrogen and the phenolic oxygen, with peripheral secondary hydrogen bonds giving polymer structures. This basic dimer is similar to what is found in the crystal structure of the parent oxine.[11]

Previous preliminary work by our group on cocrystals of aromatic carboxylic acids with oxine gave some crystals which proved unsuitable for structural analysis by single-crystal X-ray methods[12] because of an apparent tendency for twinning, while in its adduct with Kemp's triacid (*cis,cis*-1,3,5-trimethylcyclohexane-1,3,5-tricarboxylic acid), $[(oxine^+)_2(C_{12}H_{17}O_6^-)_2\cdot n(oxine)]$,[13] the partial disordered oxine molecule in the lattice was progressively lost during data collection without apparent destruction of the crystallinity of the compound. This matter has been further addressed in this study because of a similar occurrence with one of the reported compounds. Reported here is the preparation and characterization using spectroscopic and single-crystal X-ray diffraction of a series of six proton-transfer compounds of quinolin-8-ol (oxine) with the nitro-substituted aromatic carboxylic acids 2-nitrobenzoic acid (2-nba), $[(oxine^+)(2\text{-}nba^-)\cdot H_2O]$ (1), 3-nitrobenzoic acid (3-nba), $[(oxine^+)(3\text{-}nba^-)]$ (2), 4-nitrobenzoic acid (4-nba), $[(oxine^+)(4\text{-}nba^-)(4\text{-}nba)]$ (3), 3,5-dinitrobenzoic acid (dnba), $[(oxine^+)_2(dnba^-)_2\cdot 3H_2O]$ (4), 5-nitrosalicylic acid (5-nsa), $[(oxine^+)(5\text{-}nsa^-)]$ (5), and 3,5-

UM00011862
NOVARTIS EXHIBIT 1017
Novartis v. Regents, IPR2023-01346
Page 608 of 4460

Aust. J. Chem. **2001**, *54*, 171–175

Interactions of Aromatic Carboxylic Acids with Quinolin-8-ol (Oxine): Synthesis and the Crystal Structures of the Proton-Transfer Compounds with the Nitro-Substituted Benzoic Acids

Graham Smith,[A,B] *Urs D. Wermuth*[A] *and Jonathan M. White*[C]

[A] Centre for Instrumental and Developmental Chemistry, School of Physical Sciences, Queensland University of Technology, GPO Box 2434, Brisbane, Qld. 4001.
[B] Author to whom correspondence should be addressed(e-mail: g.smith@qut.edu.au).
[C] School of Chemistry, University of Melbourne, Parkville, Vic. 3052.

Proton-transfer compounds of quinolin-8-ol (oxine) with the nitro-substituted aromatic carboxylic acids 2-nitrobenzoic acid, $[(C_9H_8NO^+)(C_7H_4NO_4^-)\cdot H_2O]$ (1), 3-nitrobenzoic acid, $[(C_9H_8NO^+)(C_7H_4NO_4)^-]$ (2), 4-nitrobenzoic acid, $[(C_9H_8NO^+)(C_7H_4NO_4^-)(C_7H_5NO_4)]$ (3), 3,5-dinitrobenzoic acid, $[(C_9H_8NO^+)_2(C_7H_3N_2O_6^-)_2\cdot 3H_2O]$ (4), 5-nitrosalicylic acid, $[(C_9H_8NO^+)(C_7H_4NO_5^-)]$ (5) and 3,5-dinitrosalicylic acid, $[(C_9H_8NO^+)(C_7H_3N_2O_7^-)]$ (6) have been prepared and characterized by using both infrared spectroscopy and single-crystal X-ray diffraction methods [(3), (4) and (6)]. In all compounds, protonation of the quinoline nitrogen occurs together with primary hydrogen-bonding interactions involving this group and the carboxylate group of the acid, while further peripheral associations, in the case of the trihydrate (4), also involving the water molecules, result predominantly in simple chain polymeric structures.

Manuscript received: 5 February 2001.
Final version: 30 May 2001.

Introduction

Quinolin-8-ol [8-hydroxyquinoline (oxine)] is well known as a disinfectant and antiseptic agent as well as being a particularly versatile molecule for use in metal complex chemistry. The relative positions of the hetero-nitrogen (pK_a 10.8) and 8-substituted phenol group, together with the acidic nature of the latter (pK_a 4.9), provide the textbook example for selective interaction with metals, giving bis- and tris-chelate complex systems which are often neutral. Under basic conditions, essentially no selectivity is achieved but with pH control, quantitative precipitation is possible, such as with Mg^{2+} where the complex $[Mg(oxine^-)_2]$ is a common weighing form in gravimetric analysis.[1] While neutral divalent metal complexes such as this and $[Pd(oxine^-)_2]$[2] are common, adducts involving metal complexes or metal salts with free oxine are also known, e.g. $\{[Ni(oxine^-)_2]\cdot oxine\}$,[3] $[K^+(oxine^-)\cdot oxine]$[4] and $[K^+(oxine^-)\cdot(oxine)_2]$.[5] In addition, metal complexes with both anionic and neutral coordinated oxine species have been reported, e.g. $\{[Ag(oxine^-)(oxine)]\cdot pyridine\}$[6] and the Ag complex unit in $\{[Ag(oxine)_2]^-(p\text{-toluenesulfonate}^-)\}$.[7]

Neutral adducts with organic compounds are less prevalent, but the structures of stable 1:1 adducts with chloranil[8] and 1,3,5-trinitrobenzene[9] are known together with the 2:1 proton-transfer adduct with 1,2,3-trihydroxybenzene, $[(oxine^-)(thb^-)\cdot oxine]$.[10] In the neutral adducts, the oxine forms cyclic $R_2^2(8)$ hydrogen-bonded dimers via the hetero-nitrogen and the phenolic oxygen, with peripheral secondary hydrogen bonds giving polymer structures. This basic dimer is similar to what is found in the crystal structure of the parent oxine.[11]

Previous preliminary work by our group on cocrystals of aromatic carboxylic acids with oxine gave some crystals which proved unsuitable for structural analysis by single-crystal X-ray methods[12] because of an apparent tendency for twinning, while in its adduct with Kemp's triacid (*cis,cis*-1,3,5-trimethylcyclohexane-1,3,5-tricarboxylic acid), $[(oxine^+)_2(C_{12}H_{17}O_6^-)_2\cdot n(oxine)]$,[13] the partial disordered oxine molecule in the lattice was progressively lost during data collection without apparent destruction of the crystallinity of the compound. This matter has been further addressed in this study because of a similar occurrence with one of the reported compounds. Reported here is the preparation and characterization using spectroscopic and single-crystal X-ray diffraction of a series of six proton-transfer compounds of quinolin-8-ol (oxine) with the nitro-substituted aromatic carboxylic acids 2-nitrobenzoic acid (2-nba), $[(oxine^+)(2\text{-}nba^-)\cdot H_2O]$ (1), 3-nitrobenzoic acid (3-nba), $[(oxine^+)(3\text{-}nba^-)]$ (2), 4-nitrobenzoic acid (4-nba), $[(oxine^+)(4\text{-}nba^-)(4\text{-}nba)]$ (3), 3,5-dinitrobenzoic acid (dnba), $[(oxine^+)_2(dnba^-)_2\cdot 3H_2O]$ (4), 5-nitrosalicylic acid (5-nsa), $[(oxine^+)(5\text{-}nsa^-)]$ (5), and 3,5-

UM00011863
NOVARTIS EXHIBIT 1017
Novartis v. Regents, IPR2023-01346
Page 609 of 4460

dinitrosalicylic acid (dnsa), [(oxine$^+$)(dnsa$^-$)] (6). The crystal structures of three of these [(3), (4) and (6)] have been determined by single-crystal X-ray diffraction methods.

Results

Final atomic coordinates, bond distances and angles, anisotropic thermal parameters and hydrogen atom coordinates for adducts (3), (4) and (6) have been deposited as an Accessory Publication.* Atom numbering schemes for the associated molecule types and the hydrogen-bonding schemes are shown in Figs 1–4.

Discussion

In all compounds reported here, as predicted on the basis of pK_a differences, proton transfer from the carboxylic acid group to the hetero-nitrogen of the oxine molecule occurs, together with primary O···N hydrogen-bond formation between donor and acceptor atoms. However, in none of the compounds do we find a primary cyclic hydrogen-bonded $R_2^2(8)$ A–B heterodimer formed, involving the second carboxylate oxygen and the 8-hydroxy substituent of oxine; nor are there any A–A or B–B homodimers found (as with the parent acids or with oxine itself [11]). Instead, this molecule acts in a bridging mode to link the associated molecular units into chain polymers through hydrogen bonds. In addition, this adduct series with oxine shows a greater tendency for formation of various stoichiometric ratios than any of the previously studied Lewis base types.

[(oxine$^+$)(4-nba$^-$)(4-nba)] (3)

The structure of the 1 : 2 adduct of quinolin-8-ol with 4-nitrobenzoic acid [(oxine$^+$)(4-nba$^-$)(4-nba)] (3) (Fig. 1) comprises an A–A–B repeating unit in which the primary interaction, after proton transfer from the first carboxylic acid to the hetero-nitrogen of oxine, is formation of a single hydrogen bond [N(1)–H(1)···O(7), 2.730(3) Å; N–H···O, 147(3)°]. The second carboxyl oxygen then forms a single hydrogen bond with the carboxyl group of the second (protonated) 4-nba molecule [O(6)···H(1)–O(2), 2.572(3) Å; O···H–O, 170(3)°]. The polymer link is provided by the oxine molecule through the 8-hydroxy group to a carboxylate oxygen of the first 4-nba molecule [O(1)–H(24)···O(6)^a, 2.730(3) Å; O–H···O, 147(3)° (a = 1+x, y, z)], giving a three-centre interaction about O(6). The resulting chains form along the a cell direction (Fig. 2). Neither the second

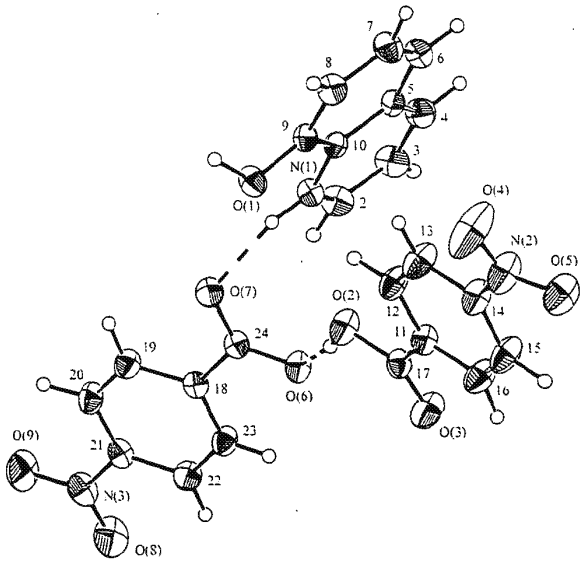


Fig. 1. Molecular configuration and atom numbering for the three molecules in the hydrogen-bonded A–A–B trimer in adduct (3). Unless otherwise indicated, atoms are carbon.

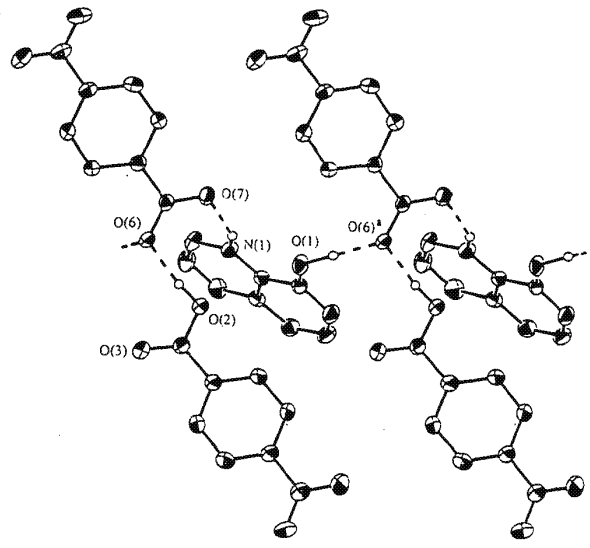


Fig. 2. Extension of the trimer units in (3) through peripheral hydrogen bonds in the a cell direction.

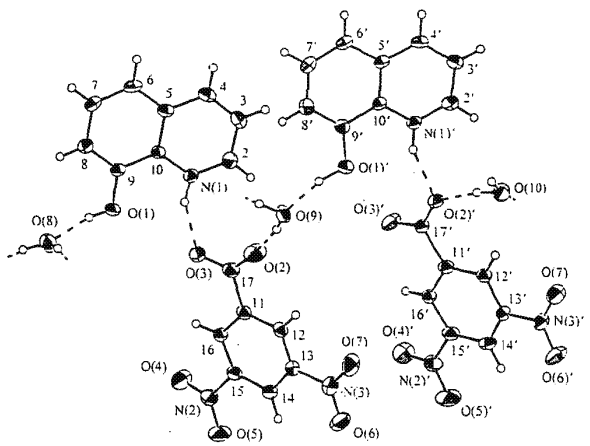


Fig. 3. Atom numbering scheme and hydrogen bonding (shown as broken lines) in the adduct hydrate (4).

*Copies are available, until 31 December 2006, from *Australian Journal of Chemistry—an International Journal for Chemical Science*, P.O. Box 1139, Collingwood, Vic. 3066.

UM00011864
NOVARTIS EXHIBIT 1017
Novartis v. Regents, IPR2023-01346
Page 610 of 4460

carboxyl oxygen of molecule 2 nor the nitro groups of either acid are involved in hydrogen bonding.

[(oxine$^+$)$_2$(dnba$^-$)$_2$·3H$_2$O] (4)

In the 2 : 2 adduct trihydrate of oxine with 3,5-dinitrobenzoic acid, [(oxine$^+$)$_2$(dnba$^-$)$_2$·3H$_2$O] (4), the primary A–B interaction similar to that found in adduct (3) is present in both independent molecule pairs in the asymmetric unit [N(1)–H(11)···O(3), 2.829(3) Å; N–H···O, 156(3)°; N(1′)–H(11′)···O(2′), 2.701(3) Å; N–H···O, 152(3)°]. The A–B pairs are joined into a ribbon polymer (Fig. 3) by peripheral hydrogen bonds to the three water molecules [O(8), O(9), O(10)] linking the carboxyl oxygens and the 8-hydroxy substituent of the oxine molecules [O(2)···H(9A)–O(9), 2.686(3) Å; O···H–O, 169(3)°; O(9)···H(1′)–O(1′), 2.545(3) Å; O···H–O, 165(3)°; O(9)–H(9B)···O(3′)^a, 2.690(3) Å; O–H···O, 175(3)° (a = 1 – *x*, ½+*y*, 1 – *z*); O(2′)···H(10B)–O(10), 2.754(3) Å; O–H···O, 169(3)°; O(8)···H(1)–O(1), 2.671(3) Å; O···H–O, 167(3)°; O(8)–H(8B)···O(3)^b, 2.707(3) Å; O–H···O, 171(3)° (b = –*x*, ½+*y*, 1 – *z*)]. The water molecules also mutually interact [O(8)–H(8A)···O(10)^a, 2.772(3) Å; O–H···O, 175(3)°; O(10)–H(10A)···O(8)^c, 2.958(3) Å; O–H···O, 158(3)° (c = 1+*x*, *y*, *z*)].

No nitro-group participation in hydrogen bonding is found.

[(oxine$^+$)(dnsa$^-$)] (6)

The 1 : 1 proton-transfer compound of oxine with 3,5-dinitrosalicylic acid, [(oxine$^+$)(dnsa$^-$)], is similar to the previously discussed carboxylic acid–oxine cocrystals in having the primary hydrogen-bonded dimeric repeat within all four hetero-pairs in the crystallographic repeating unit (Fig. 4). All interactions between the quinolinium proton and the carboxylate oxygen are dimensionally and geometrically similar [N(1)–H(1)···O(4), 2.730–2.790(9) Å; N–H···O, 149–160(4)°]. Similar extensions to those found in (4) and (5) via strong peripheral hydrogen bonds linking the protons of the 8-hydroxy substituent of oxine with one of the carboxyl oxygens of dnsa are also found [O(1)–H(1)···O(3′′)^a, 2.567(9) Å; O–H···O, 173(3)° (a = 1+*x*, *y*, *z*); O(1′′)–H(1′′)···O(3)^b, 2.562(9) Å; O–H···O, 171(3)° (b = –1+*x*, –1+*y*, *z*); O(1:)–H(1:)···O(3′)^c, 2.591(9) Å; O–H···O, 168(3)° (c = –2+*x*, –1+*y*, *z*); O(1′)–H(1′)···O(3)^d, 2.561(9) Å; O–H···O, 165(3)° (d = *x*, *y*, *z*)]. The result is a hydrogen-bonded chain polymer structure. Unlike a number of the compounds involving the nitrosalicylic acids,[14,15] no interactions involving the nitro oxygens are present. However, this structure shows significant π–π association between the dnsa and oxine molecules, a feature not common among either the neutral or proton-transfer compounds or adducts of the nitro-substituted aromatic carboxylic acids. Also as expected, and similar to the parent acid and its compounds, the intramolecular O(hydroxyl)···O(carboxyl) hydrogen bond is present [O(2)···O(4), 2.462–2.472(8) Å].

Some disorder and minor conformational variation in the nitro groups of the dnsa molecules are present but are not sufficient to contribute to the more serious structural problem (described in Experimental), which manifests itself as pseudo-symmetry (both translation and inversion) among the four sets of molecular pairs in the crystallographic asymmetric unit. By a legal shift of the origin in the space group *Pc* in both the *x* direction (0.390) and the *y* direction (0.063), a pseudo-translation (*x*, ½+*y*, *z*) is created, relating the X, X′′ and X:, X′ pairs. In addition, a pseudo-inversion centre at ($^1/_2$, $^5/_8$, $^1/_2$) would create the $P2_1/c$ cell (with the *b* axis halved) from the previous unsuccessful structure determination attempt.[12] Such pseudo-symmetry identifies the possible presence of a stacking fault or inversion-related twinning. The presence of the 'ghost' oxine may be an artefact of such phenomena if ignored[16] but the computational treatment necessary to handle the problem will not be considered here. This argument, however, would tend to obviate oxine as a contributing factor, having, as previously mentioned, a tendency to act as a labile molecule of crystallization despite its moderate melting temperature (76°C). This was definitely the case with the cyclic 2 : 2 proton-transfer compound with Kemp's triacid where a labile disordered partial unassociated oxine molecule (occupancy ca. 0.9) existed beside the stable dimeric acid–oxine cage structure.[13] Oxine has been observed to undergo intrusive solid-state reaction by diffusion into certain anhydrides,[17] nitrophenols,[18] salicylic acid[19] and metal salts.[20] The formation of the 2 : 1 proton-transfer adduct with 1,2,3-trihydroxybenzene also proceeds in a similar manner by intrusive solid-state reaction.[10] Of possible relevance to the present examples, it was observed that with the nitrophenols,[18] reaction proceeded more readily with increased nitro-group substitution and with increased molecular symmetry. It must be generally assumed that both types of solid-state reaction involving oxine (either intrusive or effusive, usually without crystal breakdown), occur by similar mechanisms.

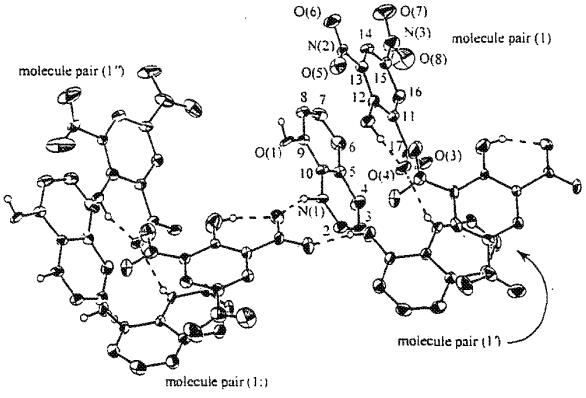


Fig. 4. Atom numbering scheme and hydrogen bonding involving the four independent A–B dimers in the crystallographic repeating unit in the adduct (6).

Experimental

All complexes were prepared from 1 : 1 molar amounts of quinolin-8-ol (0.2 g, 1.4 mmol) and respectively: 2-nitrobenzoic acid (1), 3-nitrobenzoic acid (2), 4-nitrobenzoic acid (3), 3,5-dinitrobenzoic acid

UM00011865
NOVARTIS EXHIBIT 1017
Novartis v. Regents, IPR2023-01346
Page 611 of 4460

(4), 5-nitrosalicylic acid (5) and 3,5-dinitrosalicylic acid (6). Preparations involved heating under reflux for 10 min at ca. 90°C in 20 cm^3 of 95% ethanol, the product being subsequently obtained by the partial or total evaporation of the solvent at room temperature, yielding for (1) large yellow *prisms* (m.p. 88–90°C); for (2), yellow *microcrystals* (m.p. 130–131°C); for (3), yellow *prisms* (m.p. 195–198°C); for (4), yellow *prisms* (m.p. 161–162.5°C); for (5) a yellow *powder* (m.p. 180–182°C); for (6) orange *needles* (m.p. 244–250°C). Elemental analyses indicated 1 : 1 stoichiometries for all adducts except (3) (1 : 2), while (1) was a monohydrate. With (4), the presence of 1.5 waters was found from analysis, later confirmed in the crystal structure determination as a 2 : 2 trihydrate. Found for (1): C, 58.2; H, 4.3; N, 8.5. $C_{16}H_{14}N_2O_6$ requires C, 58.2; H, 4.2; N, 8.5%. Found for (2): C, 61.5; H, 3.8; N, 8.8. $C_{16}H_{12}N_2O_5$ requires C, 61.5; H, 3.8; N, 9.0%. Found for (3): C, 57.7; H, 3.6; N, 8.8. $C_{23}H_{17}N_3O_9$ requires C, 57.6; H, 3.6; N, 8.8%. Found for (4): C, 50.0; H, 3.5; N, 10.8. $C_{32}H_{28}N_6O_{17}$ requires C, 50.0; H, 3.7; N, 10.9%. Found for (5): C, 58.5; H, 3.6; N, 8.3. $C_{16}H_{12}N_2O_6$ requires C, 58.5; H, 3.7; N, 8.5%. Found for (6): C, 51.8; H, 2.9; N, 11.3. $C_{16}H_{11}N_3O_8$ requires C, 51.5; H, 3.0; N, 11.3%.

Attempts to prepare the adduct with 1,3,5-trinitrobenzoic acid using either the general refluxing method in ethanol at elevated temperature or the room-temperature variant (because of the ease of decarboxylation of the acid even at moderate temperature) gave good crystals of the previously described 1 : 1 oxine–1,3,5-trinitrobenzene adduct.[9] Infrared spectra were recorded for all samples as pressed disks in KBr on a Perkin–Elmer Spectrum 1000 Fourier-transform infrared spectrometer.

Crystallography

Crystal Data

(3) $[(C_9H_8NO^+)(C_7H_4NO_4^-)(C_7H_5NO_4)]$, CCDC 164598, mol. wt 479.4, triclinic, space group $P\bar{1}$, a 7.052(2), b 7.497(2), c 21.121(6) Å, α 97.94(2), β 97.35(3), γ 99.45(2)°, V 1077.9(5) Å^3, $F(000)$ 496, Z 2, D_c 1.477 g cm^{-3}, μ(Mo Kα) 1.16 cm^{-1}, temperature 293(2) K. 4089 reflections measured [$2\theta_{max}$ 51°: h, 0 to 8; k, −8 to 8; l, −25 to 24], 3756 unique (R_{int} 0.012). Final R_1* 0.048 (F); wR_2† 0.123 (F^2) [2845 observed with $I > 2.0\sigma(I)$]; S 1.03. Crystal size 0.50 by 0.30 by 0.25 mm; max/min transmission factors. 0.82/0.70.

(4) $[(C_9H_8NO^+)_2(C_7H_3N_2O_6^-)_2{\cdot}3H_2O]$, CCDC 164597, mol. wt 768.6, monoclinic, space group $P2_1$, a 14.9606(6), b 7.4287(5), c 15.633(1) Å, β 102.170(4)°, V 1698.4(2) Å^3, $F(000)$ 796, Z 2, D_c 1.503 g cm^{-3}, μ(Cu Kα) 1.22 cm^{-1}, temperature 293(2) K. 3851 reflections measured [$2\theta_{max}$ 150°: h, −18 to 0; k, 0 to 9; l, −19 to 19], 3705 unique (R_{int} 0.022). Final R_1 0.029 (F); wR_2 0.084 (F^2) [3564 observed with $I > 2.0\sigma(I)$]; S 1.04; absolute structure parameter. 0.01(15). Crystal size 0.43 by 0.30 by 0.23 mm.

(6) $[(C_9H_8NO^+)(C_7H_3N_2O_7^-)]$, CCDC 164599, mol. wt 373.3, monoclinic, space group Pc, a 8.015(2), b 15.010(2), c 26.546(2) Å, β 95.52(2)°, V 3178.8(9) Å^3, $F(000)$ 1536, Z 8, D_c 1.560 g cm^{-3}, μ(Cu Kα) 1.11 cm^{-1}, temperature 293(2) K. 7322 reflections measured [$2\theta_{max}$ 140°: h, −6 to 9; k, −12 to 18; l, −32 to 32], 7103 unique (R_{int} 0.013). Final R_1 0.080 (F); wR_2 0.210 (F^2) [6101 observed with $I > 2.0\sigma(I)$]; S 1.03; absolute structure parameter. 0.4(3). Crystal size 0.78 by 0.21 by 0.14 mm; max/min transmission factors. 0.87/0.64.

Data Collection, Structure Solution and Refinement

X-Ray diffraction data for all compounds were measured on Enraf–Nonius CAD-4 diffractometers by using either crystal-monochromatized Mo Kα X-radiation (λ 0.71073 Å) [compound (3)] or Cu Kα X-radiation (λ 1.5418 Å) [compounds (4) and (6)]. Negligible change in the intensities of three standards monitored throughout the data collection periods for all adducts indicated no significant crystal decomposition. Data were corrected for Lorentz and polarization effects, extinction and for absorption [(3) and (6) only (analytical, Gaussian)]. The structures were solved by direct methods and refined by full-matrix least-squares (on F^2) by using SHELXL-97[21] with anisotropic thermal parameters for all non-hydrogen atoms. Hydrogen atoms involved in the hydrogen-bonding interactions were located by difference methods and both positional and thermal parameters were refined while others were generally included at calculated positions in the refinements as riding models. The values of A and B in the weighting scheme $w = [\sigma^2(F_o)^2+(AP)^2+BP]^{-1}$ {where P = [max. $(F_o^2,0)+2(F_c)^2]/3$} were 0.0783, 0.2461 (3), 0.0593, 0.1264 (4), and 0.1826, 0.7519 (6). With (3), the high thermal motion of the nitro-oxygens of molecule 1 [O(4) and O(5)] resulted in these being modelled over two independent sites with occupancies of 0.80 and 0.20 respectively. Compound (6), which we had previously investigated unsuccessfully crystallographically,[12] when it was found to have what appeared to be bad disorder in the space group $P2_1/c$ with Z 4 in a unit cell with half the present b axial parameter, was resolved in the lower-symmetry space group Pc with Z 8. In this space group, pseudo-symmetry is present with the molecules related by an approximate 2_1 screw operation and inversion symmetry. This is somewhat analagous to, but not as severe as, the modulated structure described for the 1 : 1 proton-transfer adduct of 2,4,6-trinitrobenzoic acid with 2,6-diaminopyridine.[22] In addition, the presence of a partial disordered labile molecule of oxine contributes to the high refinement residual which could be reduced from the table value (R 0.080) to ca. R 0.05 by incorporating electron density equivalent to 90% of a ghost oxine molecule having an occupancy of 0.08. This effect may also be due to the presence of an overriding but inadequately modelled stacking fault or an inversion twin. However, this structural problem could not be further handled in this study and furthermore, the Pc model adequately describes the basic hydrogen-bonded structural framework which is not altered by the presence of the the unasssociated 'ghost oxine'. A similar phenomenon was observed for the structure of the 1 : 1 proton-transfer compound of Kemp's triacid with oxine,[13] in which a partial disordered oxine molecule of crystallization was lost progressively with time during room-temperature data collection, without significant loss in crystallinity.

Conclusions

The series of quinolin-8-ol compounds with the nitro-substituted benzoic acids studied here shows a greater variability in composition and form than any of the other Lewis-base compounds of the same acids previously studied. The incorporation of water into the cocrystal make-up in two of the examples [(1) and (4)] obviously influences the stabilization of the crystal lattice, which in the case of the trihydrate (4) links together rows of oxine and dnba molecules to give an very stable and ordered structure. This is in contrast to the 1 : 1 compound with dnsa (6), where a probable stacking fault is present in the structure, and may be similar to the badly twinned monohydrate (1) where no structural analysis was possible, despite its macro-crystalline morphology. Infrared spectroscopy has also proved useful, as previously noted,[23] for the recognition of proton transfer in compounds of the type found in this series, particularly with those for which crystal structure determinations are not possible e.g. (1), (2) and (5). As with the parallel study involving the same series of acids with the analogous nitrogen base 8-aminoquinoline,[24] disappearance of the characteristic strong C=O stretching frequency at ca. 1700 cm^{-1} is the most definitive sign in the composite spectrum of proton transfer [except in the case of the 1 : 2 adduct (3) where free acid is present]. The accompanying broad =N–H$^+$

*$R_1 = [\Sigma||F_o|-|F_c||]/[\Sigma|F_o|]$.
†$wR_2 = [\Sigma w(F_o^2-F_c^2)^2/\Sigma w(F_o^2)^2]^{1/2}$.

UM00011866
NOVARTIS EXHIBIT 1017
Novartis v. Regents, IPR2023-01346
Page 612 of 4460

absorptions expected in the 2700–2250 cm^{-1} region of the spectrum[25] are invariably unresolved within the broad and extended hydrogen-bonded –OH absorptions centred typically at ca. 3400 cm^{-1} [range: 3391 (2) to 3446 cm^{-1} (6)], similar to those in the parent oxine (3405 cm^{-1}).[26] However, infrared spectroscopy remains a useful tool for the identification of the nature of the interaction in such compounds.

Acknowledgments

The authors acknowledge financial support from the Centre for Instrumental and Developmental Chemistry of the Queensland University of Technology, The Australian Research Council and the University of Melbourne. The referee is thanked for the deconvolution of the pseudo-symmetry problem with compound (6).

References

[1] D. A. Skoog, D. M. Holler, F. J. West, *Analytical Chemistry*, 5th Edn, pp. 76–77, Saunders, New York, **1988**.
[2] C. K. Prout, A. G. Wheeler, *J. Chem. Soc. A* **1966**, 1286.
[3] A. T. Rane, V. V. Ravi, *Indian J. Chem., Sect. A* **1982**, *21*, 311.
[4] D. L. Hughes, M. R. Truter, *J. Chem. Soc., Dalton Trans.* **1979**, 520.
[5] D. L. Hughes, M. R. Truter, *J. Chem. Soc., Dalton Trans.* **1979**, 250.
[6] J. E. Fleming, H. Lynton, *Can. J. Chem.* **1968**, *46*, 471.
[7] G. Smith, J. H. Thomasson, J. M. White, *Aust. J. Chem.* **1999**, *52*, 317.
[8] C. K. Prout, A. G. Wheeler, *J. Chem. Soc. A* **1967**, 469.
[9] E. E. Castellano, C. K. Prout, *J. Chem. Soc. A* **1971**, 550.
[10] N. B. Singh, N. P. Singh, V. A. Kumar, M. Nethaji, *J. Chem. Soc., Perkin Trans. 2* **1994**, 361.
[11] W. W. Wendlandt, G. R. Horton, *J. Inorg. Nucl. Chem.* **1963**, *25*, 247; P. Roychowdhury, B. N. Das, B. S. Basak, *Acta Crystallogr., Sect. B* **1978**, *34*, 1047; S. H. Simonsen, D. W. Bechtel, *Am. Cryst. Assoc., Ser. 2* **1980**, *7*, 23; T.Bannerjee, N. N. Saha, *Acta Crystallogr., Sect. C* **1986**, *42*, 1408.
[12] G. Smith, D. E. Lynch, K. A. Byriel, C. H. L. Kennard, *Aust. J. Chem.* **1995**, *48*, 133.
[13] G. Smith, U. D. Wermuth, J. M. White, *Chem. Commun.* **2000**, 2349.
[14] Smith, D. E. Lynch, K. A. Byriel, C. H. L. Kennard, *Aust. J. Chem.* **1995**, *48*, 1133.
[15] G. Smith, D. E. Lynch, K. A. Byriel, C. H. L. Kennard, *Acta Crystallogr., Sect. C* **1996**, *52*, 231.
[16] S. W. Ng, A. D. Rae, *Z. Kristallogr.* **2000**, *215*, 199.
[17] R. P. Rastogi, N. B. Singh, R. P. Singh, *Indian J. Chem.* **1977**, 941.
[18] N. B. Singh, R. Singh, K. Singh, *Mol. Cryst. Liq. Cryst.* **1999**, *333*, 269.
[19] N. B. Singh, R. Singh, K. Singh, *Z. Phys. Chem.* **2000**, *214*, 179.
[20] B. L. Dubey, N. Tiwari, *Indian J. Chem., Sect. A* **1991**, *30*, 855.
[21] G. M. Sheldrick, *SHELXL–97, Program for Crystal Structure Determination*, University of Göttingen, Federal Republic of Germany, **1997**.
[22] G. Smith, R. C. Bott, A. D. Rae, A. C. Willis, *Aust. J. Chem.* **2000**, *53*, 531.
[23] G. Smith, D. E. Lynch, K. A. Byriel, C. H. L. Kennard, *J. Chem. Crystallogr.* **1997**, *27*, 307; D. E. Lynch, G. Smith, K. A. Byriel, C. H. L. Kennard, *Aust. J. Chem.* **1997**, *50*, 977.
[24] G. Smith, U. D. Wermuth, R. C. Bott, J. M. White, A. C. Willis, *Aust. J. Chem.* **2001**, *54*, 165.
[25] H. Williams, I. Fleming, *Spectroscopic Methods in Organic Chemistry*, 5th Edn, pp. 28–62, McGraw–Hill, London, **1995**.
[26] I. Suryanarayana, B. K. Saikia, *Indian J. Pure Appl. Phys.* **1980**, *18*, 1010; M. S. Afifi, A. A. Azhar, *Egypt. J. Chem.* **1984**, *27*, 385; S. L. Srivastava, M. Prasad, Rihitashava, *Spectrochim. Acta, Sect. A* **1984**, *40*, 681.

UM00011867
NOVARTIS EXHIBIT 1017
Novartis v. Regents, IPR2023-01346
Page 613 of 4460

Pergamon

Tetrahedron 58 (2002) 4837–4849

TETRAHEDRON

Asymmetric synthesis of two new conformationally constrained lysine derivatives

Robert A. Stalker, Tamara E. Munsch, Jacquelyn D. Tran, Xiaoping Nie, Ralf Warmuth,* Alicia Beatty† and Christer B. Aakeröy

Department of Chemistry, Kansas State University, Manhattan, KS 66506-3701, USA

Received 8 November 2001; revised 18 April 2002; accepted 22 April 2002

Abstract—The asymmetric synthesis of the conformationally constrained L- and D-lysine derivatives methyl (1*S*,8*S*)-1-amino-8-tert-butoxycarbonylamino-1,2,3,4,5,6,7,8-octahydroanthracene-1-carboxylate (**4**) and methyl (1*R*,8*S*)-1-amino-8-tert-butoxycarbonylamino-1,2,3,4,5,6,7,8-octahydroanthracene-1-carboxylate (**5**), respectively are described. Application of the Bucherer hydantoin synthesis to the carbonyl group of 2′,3′,4′,5′,6′,7′-hexahydrospiro[1,3-ethylenedithiole-2,1′-anthracen]-8′-one (**18**), which was prepared from 1,8-dichloroanthraquinone (**14**) in nine steps and the deprotection of the masked second ketone of **18** yields *rac*-21. The latter is the precursor for a novel asymmetric reductive amination protocol using (*R*)-phenylglycinol as a chiral amino auxiliary and $NaBH(OAc)_3$ as a reducing agent. Using this procedure, the asymmetric reductive amination of α-tetralone derivatives and indanone proceeds with >95% de. Lower diastereomeric excesses are observed for benzosuberone (16.7% de) and acetophenone (27.3% de). *rac*-21 gave (1′*S*,8′*S*,1(*R*)-**25a** (38% yield) and (1′*R*,8′*S*,1(*R*)-**25b** (44.5% yield) with greater than 52 and 78% de, respectively. Cleavage of the amino auxiliary of (1′*S*,8′*S*,1(*R*)-**25a** and of (1′*R*,8′*S*,1(*R*)-**25b** with lead(IV) tetraacetate and hydrolysis of the hydantoin ring yields the unprotected analogs of **4** and **5**. The latter are transformed into the selectively protected target molecules **4** and **5** through standard protection procedures. The overall yield of the 17- and 18-step synthesis starting from **13** was 0.3% yield for each constrained lysine derivative. © 2002 Elsevier Science Ltd. All rights reserved.

1. Introduction

The design and synthesis of conformationally constrained amino acids[1] and peptidomimetics[2] is of special interest for medicinal and bio-organic chemistry in view of their possible application as potency-enhanced ligands for biological receptors,[3] as probes for mimicry of peptide secondary structures,[4] and as novel structural elements of relevance to bio-materials.[5] Efforts to design and synthesize scaffolds that mimic parts of peptide folds and induce an increased conformational stability have mainly focused on the α-helix and β-hairpin.[1,2,4,6,7]

In particular constrained di- and tripeptides have been used to mimic turn structures, which are parts of these motifs. In addition, the incorporation of α,α-disubstituted glycines into the peptide backbone has led to stabilized helices.[8,9] We have designed the conformationally constrained amino

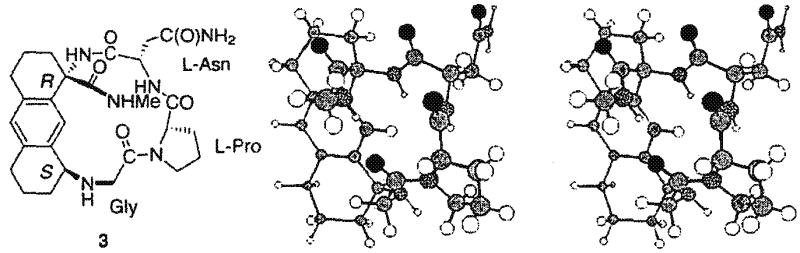


Figure 1. Stereoview of energy-minimized structure of helix-nucleation site 3 (OPLS-AA*,[31] GB/SA water solvation model[25c]); atom coloring: C grey; H white; N dotted; O black.

Keywords: asymmetric reductive amination; constrained amino acid; lysine.

* Corresponding author. Tel.: +1-785-532-6684; fax: +1-785-532-6666; e-mail: warmuth@ksu.edu

† Present address: Department of Chemistry and Biochemistry; University of Notre Dame, Notre Dame, IN, USA.

0040–4020/02/$ - see front matter © 2002 Elsevier Science Ltd. All rights reserved.
PII: S0040-4020(02)00450-7

UM00011868
NOVARTIS EXHIBIT 1017
Novartis v. Regents, IPR2023-01346

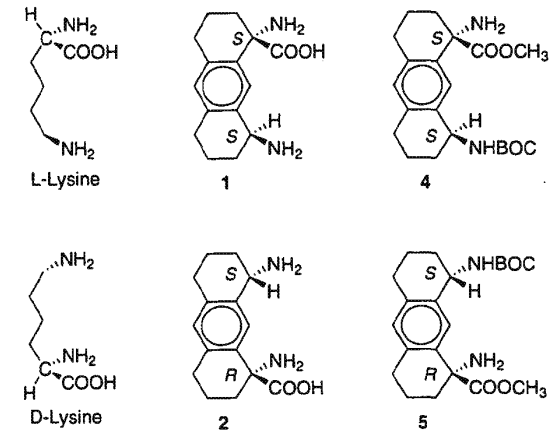
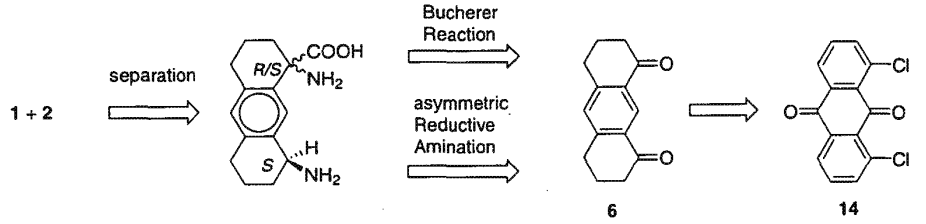


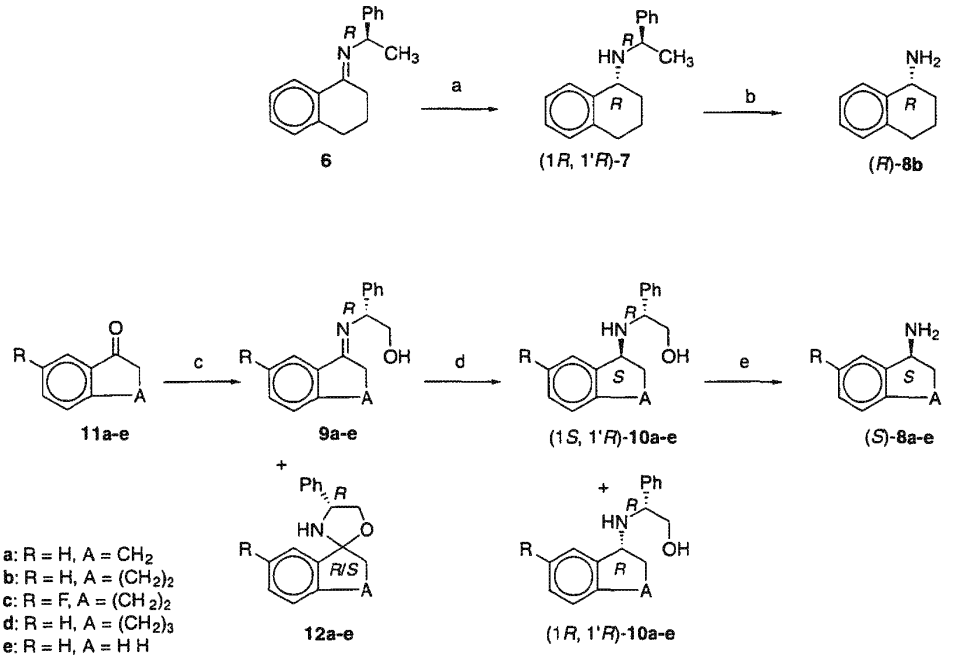
Chart 1.

acids **1** and **2**, which belong to the family of α,α-disubstituted glycines. Our motivation for the design and synthesis of **1** and **2** was twofold. (1) Both **1** and **2** are conformationally constrained L- and D-lysines, respectively,[10] with a completely constrained side chain in the $(+)g$, t, t, $(-)g$ conformation for **1** and $(-)g$, t, t, $(-)g$ conformation for **2**. In lieu of the importance of the lysine side chain for the stability of the α-helix[11] both amino acids are interesting targets for extended studies related to this aspect. For example, model studies show that the protonated ε-amino group of **1** can undergo an $(i, i-3)$-electrostatic interaction with a backbone carbonyl group of an α-helix. (2) Both constrained lysines are interesting rigid building blocks for the design of novel C- and N-terminal peptide helix nucleation sites.[7,11] For example, linking both amino groups of **1** with a Gly-(L)-Pro-(L)-Asn tripeptide leads to a macrocycle **3** that mimics the first turn of an α-helix (Fig. 1) and could strongly stabilize the α-helical conformation of a covalently attached peptide.

In this report, we describe the asymmetric synthesis of **4** and



Scheme 1. Synthetic strategy towards the conformationally constrained lysines **1** and **2**.



Scheme 2. Model studies on the reductive amination of α-tetralone **12**. *Conditions*: (a) $NaBH_4$, EtOH, toluene, −10°C; (b) $Pd/C/H_2$, MeOH, HCl (1N) (c) (*R*)-phenylglycinol, *p*-TsOH, xylenes, reflux; (d) $NaBH(OAc)_3$ THF, 0°C; (e) 1.$Pb(OAc)_4$, MeOH, 0°C; 2. HCl (6N), EtOH, reflux.

UM00011869
NOVARTIS EXHIBIT 1017
Novartis v. Regents, IPR2023-01346
Page 615 of 4460

Table 1. Asymmetric reductive amination of ketones **12a–e**

Entry	Ketone	Ratio[a,b] **10**:**13**	Reducing agent/solvent	Temperature (°C)	Ratio[c] (1*S*,1′*R*)-**11**/(1*R*,1′*R*)-**11** (de)	Yield[d] **11** (%)
1	**12a**	>40:1[e]	$NaBH(OAc)_3$/THF	0	>40:1 (>95%)	84
2	**12b**	86:14[e,f]	$NaBH_4$/EtOH	24	9.5:1 (80.7%)	85
3	**12b**	86:14[e,f]	$NaBH_4$/EtOH	0	9.95:1 (81.7%)	83
4	**12b**	86:14[e,f]	$NaBH_4$/EtOH	−10	9.85:1 (81.6%)	85
5	**12b**	86:14[e,f]	$NaBH(OAc)_3$/THF	0	40:1 (95.1%)	87
6	**12c**	89:11[e,g]	$NaBH(OAc)_3$/THF	24	>40:1 (>95%)	48
7	**12d**	[h]	$NaBH(OAc)_3$/THF	24	1.4:1 (16.7%)	84
8	**12e**	22:78[d,i]	$NaBH(OAc)_3$/THF	0	7:4 (27.3%)	90

[a] Determined from the integrals of the 1′ methine proton signals of the products in the ^1H NMR spectrum of the reaction mixture.
[b] See Ref. 24d,e.
[c] Determined by HPLC.
[d] Yield of isolated product (mixture).
[e] Only *E*-imine was detected.
[f] 10:4 Ratio of diastereomeric 1,3-oxazolidines **13b**.
[g] 7:4 Ratio of diastereomeric 1,3-oxazolidines **13c**.
[h] Complex mixture of *E*-**10**, *Z*-**10**, and two diastereomeric 1,3-oxazolidines (1*S*,1′*R*)-**13** and (1*R*,1′*R*)-**13**.
[i] 2.1:1 Ratio of diastereomeric 1,3-oxazolidines **13e**.

5, which are selectively protected derivatives of **1** and **2** and which are suitable to be incorporated into short host peptides for such model studies (Chart 1).

2. Results and discussion

2.1. Synthetic strategy

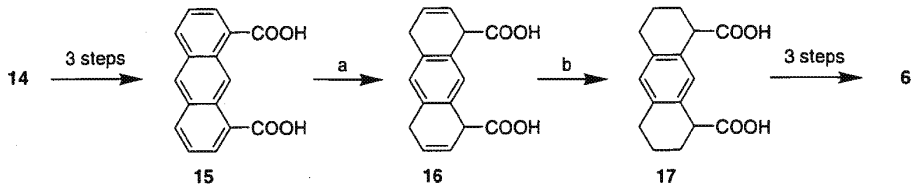
Our strategy for the synthesis of **1** and **2** involves the regioselective conversion of the carbonyl groups of 1,2,3,4,5,6,7,8-tetrahydroanthracene-1,8-dione **6**,[12] into an amino acid group and an amine, respectively (Scheme 1). For the first key transformation, we choose the *Bucherer hydantoin synthesis* followed by the hydrolysis of the hydantoin ring. Even though no asymmetric protocol has been developed for the *Bucherer* reaction, it has been proven highly reliable and high yielding for the synthesis of benzocyclic aryl- and alkyl-amino acids.[13] The subsequent enantioselective reductive amination of the second ketone group of **7** would yield both diastereomeric **1** and **2**, which would have to be separated chromatographically or through crystallization.

2.2. Model study of the asymmetric reductive amination

Based on our outlined synthetic strategy, the reductive amination is a very important step in the reaction sequence. We undertook an investigation using α-tetralone as model compound (Scheme 2). Several methods for the asymmetric reductive amination of ketones had been developed earlier.[14] These include the reduction of imines, oximes, or enamines in the presence of a chiral reducing reagent,[15,16] a chiral hydrogenation catalyst,[17,18] or a hydrosilylation catalyst,[19] asymmetric transaminations,[20] enzymatic methods,[21] and the selective reduction of chiral imines formed from chiral amino auxiliaries and the ketone.[22,23] The latter method has the advantage to yield diastereomeric product mixtures. Often, these mixtures can be separated through column chromatography or crystallization to yield enantiopure amines after cleavage of the auxiliary. A recent investigation of the reduction of (*R*)-α-methylbenzylamine derived imine **7** by Gutman et al. caught our attention (Scheme 2).[23]

Under optimal conditions, the reduction proceeded with excellent 97:3 diastereofacial selectivity. Unfortunately, the subsequent debenzylation using catalytic hydrogenation showed a marginally regioselectivity of 3.5:1 in favor of cleaving the C1′–N bond of **7**. Nevertheless, the high facial selectivity of this reduction lured us to investigate the related reduction of the (*R*)-α-phenylglycinol derived imine **10b**. The use of (*R*)-α-phenylglycinol as the chiral amino auxiliary is very attractive since the C1′–N bond of the expected product **11b** is selectively cleaved with lead (IV) tetraacetate.[24] Imine **10b** was prepared as an equilibrium mixture with the two diastereomeric 1,3-oxazolidines **13b** in greater 90–95% yield by refluxing tetralone and (*R*)-α-phenylglycinol in xylenes in the presence of catalytic amounts of *p*-tolylsulfonic acid.[24e] The reduction of this mixture with $NaBH_4$ in ethanol at room temperature gave in greater than 85% yield a 9.5:1-mixture of diastereomeric amines (1*S*,1′*R*)-**11b** and (1*R*,1′*R*)-**11b** (80.7% de) (Table 1, entry 2). The diastereomeric excess (de) showed little temperature dependence (Table 1, entries 3–4). We reckoned that an increased bulkiness of the reducing agent would improve the facial selectivity. Indeed, reduction of the **10b**/**13b** mixture with freshly prepared $NaBH(OAc)_3$ in THF at 0°C strongly increased the diastereomeric ratio (dr) of (1*S*,1′*R*)-**11b**/(1*R*,1′*R*)-**11b** to 40:1 (95.1 de; 87% isolated yield) (Table 1, entry 5). The subsequent oxidative cleavage of (1*S*,1′*R*)-**11b** using $Pb(OAc)_4$ gave (*S*)-**9** in 63% yield. Thus, this method proved to be a suitable alternative to Gutman's method as well as other asymmetric reductive amination protocols. The stereochemical outcome of the reduction was determined by X-ray crystallography. The use of (*R*)-α-phenylglycinol gives (*S*)-stereochemistry at the new stereogenic center of the major product diastereomer **11b**. This outcome is consistent with the lowest energy conformation of **10b** obtained from a Monte Carlo conformational search (MM2; GB/SA $CHCl_3$ solvent model),[25] which shows a better accessibility of the imine bond from the *re*-face of **10b** to give (*S*)-**9b**.

UM00011870
NOVARTIS EXHIBIT 1017
Novartis v. Regents, IPR2023-01346
Page 616 of 4460

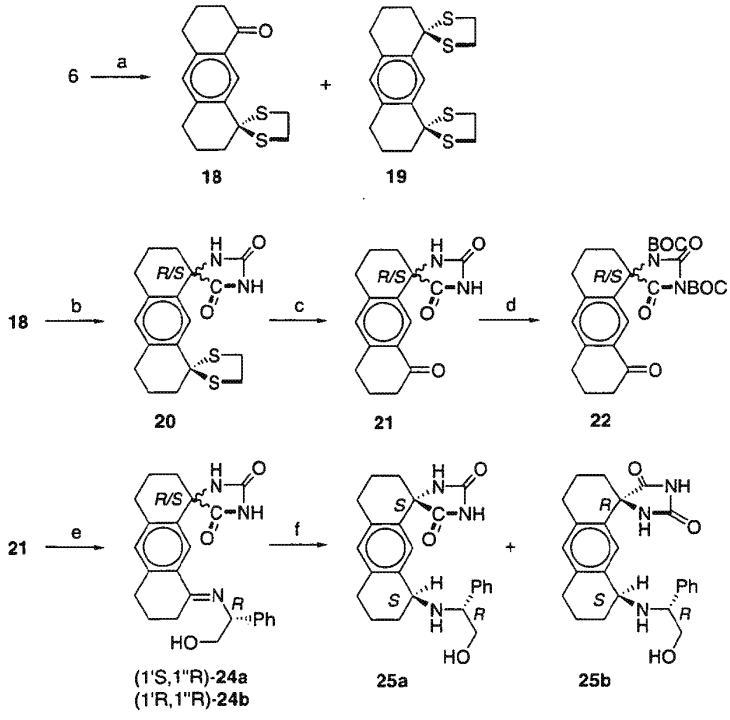


Scheme 3. Synthesis of 1,2,3,4,5,6,7,8-tetrahydroanthracene-1,8-dione **6**. *Conditions*: (a) 1. Li/NH_3 liq.; 2. NH_4Cl; (b) EtOH; $Pd/C/H_2$ 67% yield over 2 steps.

We further tested this approach for the asymmetric reductive amination of other arylketones **12a** and **12c–e** (Table 1, entries 1, 6–8). In each case, the major product diastereomer had (*S*)-stereochemistry at the new stereogenic center, as determined by comparing the optical rotation of the amines **9** after cleavage of the auxiliary with $Pb(OAc)_4$ (47–75% yield) with those reported in the literature.[23] For five and six-membered benzocycloalkanones, we obtained excellent diastereomeric excesses >95%. These high diastereomeric excesses clearly show that the two diastereomeric 1,3-oxazolidines **13** have no negative influence on the diastereofacial selectivity of the reduction. Poor diastereomeric ratios were obtained for benzosuberone **12d** and acetophenone **12e**, which is consistent with similar results for the TMSCN addition to these imines.[24d,e] Whereas the condensation of **12d** with (*R*)-α-phenylglycinol **12a–c** and **12e** yields only the corresponding (*E*)-imine, the formation of both (*E*)-**13d** and (*Z*)-**13d** might contribute to the lower de observed in the reductive amination of **12d**. Both isomeric imines **13d** will have different and most likely opposite diastereofacial selectivities in their reaction with $NaBH(OAc)_3$.

2.3. Synthesis of constrained lysines derivatives

As briefly discussed in Section 1, our strategy for the synthesis of the constrained lysine derivatives **1** and **2** involved the conversion of one carbonyl group of **6** into a racemic fully protected amino acid moiety. Subsequently, application of our asymmetric reductive amination would result in a pair of diastereomers, which we would try to separate chromatographically. For the synthesis of dione **6**, we chose a literature procedure,[12a] which we slightly modified during the course of our investigations (Scheme 3). 1,8-Dichloroanthraquinone **14** was converted in three steps into anthracene-1,8-dicarboxylic acid **15**.[26] We experienced major difficulties in converting **15** into **17** according to the reported three-step literature procedure.[12a] In particular, the Birch reduction of **15** under the published conditions gave very unreliable results in our laboratory. Thus, we modified the conditions of this step.[27] Quenching the Birch reduction with excess solid ammonium chloride gave 1,4,5,8-tetrahydroanthracene-1,8-dicarboxylic acid **16**, which was immediately subjected to a catalytic hydrogenation on Pd/C to afford **17** as a mixture of diastereomers.



Scheme 4. *Conditions*: (a) $HSCH_2CH_2SH$; $BF_3{\cdot}Et_2O$; CH_2Cl_2. (b) KCN; $(NH_4)_2CO_3$; EtOH; H_2O; 130°C. (c) $AgNO_3$; EtOH; THF; H_2O. (d) $(BOC)_2O$; DMAP cat.; THF; rt. (e) (*R*)-phenylglycinol; xylenes; *p*-TsOH cat.; reflux. (f) $NaBH(OAc)_3$; THF; 0°C.

UM00011871
NOVARTIS EXHIBIT 1017
Novartis v. Regents, IPR2023-01346
Page 617 of 4460

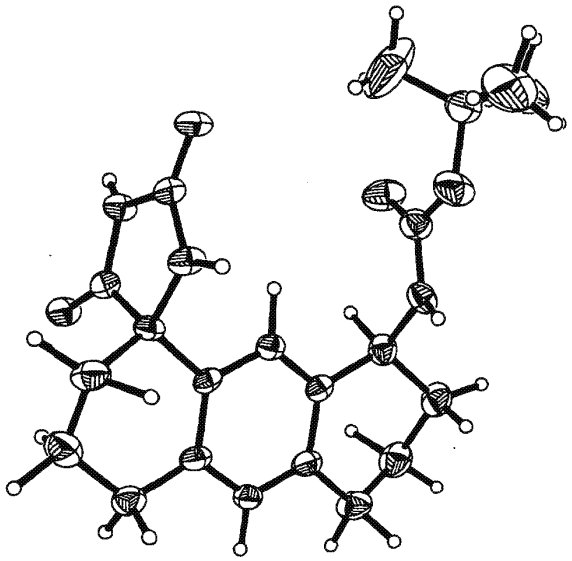
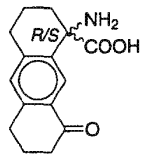


Figure 2. X-Ray crystal structure of diastereomer **26b**.

The total yield of converting **15** to **17** was very reproducible and is comparable to the yield of the reported three-step synthesis. Diacid **17** was further converted into **6** in three steps as described by Caluwe and Pepper.[12a]

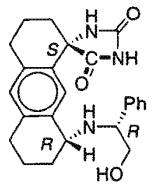
Monoprotection of one carbonyl group of **6** using one equivalent of ethane-1,2-dithiol in the presence of the Lewis acid $BF_3{\cdot}Et_2O$ gave **18** together with small amounts of the diprotected bis-dithiane **19** which could be easily separated by chromatography (Schemes 3 and 4).

Subjection of **18** to typical conditions of a Bucherer hydantoin synthesis (KCN, $(NH_4)_2CO_3$, EtOH, water, 130°C)[13] gave almost quantitatively the racemic hydantoin **20**. The protected carbonyl group of **20** was unmasked using $AgNO_3$ in an ethanol/water/THF (5:3:1) mixture (65% yield). Unfortunately, the arylketone group of **21** was too unstable under the harsh conditions ($Ba(OH)_2$/120°C) required for the hydrolysis of the hydantoin moiety. Thus, we tested a mild hydantoin hydrolysis procedure reported by Rebek and co-workers in which they successfully hydrolyzed a *N,N*-bis-BOC-protected hydantoin at room temperature with aqueous LiOH.[28] The BOC protection of **21** using $(BOC)_2O$ in the presence of catalytic amounts of DMAP afforded **22** in 79% yield. However, treatment of **22** at room temperature with 2N LiOH in THF/water reverted **22** back to **21** rather than forming the desired amino acid **23**.

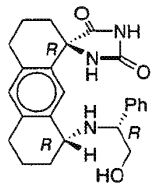


23

After the failure to hydrolyze the hydantoin on this stage of the synthesis, we decided that the conversion of the carbonyl group of **21** into an amino group would render the molecule stable enough. For the reductive amination of **21**, we applied our protocol described above. Heating a solution of **21** and 1.5 equiv. of (*R*)-phenylglycinol in xylenes in the presence of catalytic amounts of *p*-tolylsulfonic acid under constant removal of condensation water afforded a 1:1 mixture of diastereomeric imines **24a** and **24b** in about 80–85% yield as determined from the ^1H NMR spectrum of the crude reaction mixture. Reduction of both imines with $NaBH(OAc)_3$ in THF yielded a 1:1-mixture of two major products. Both products were isolated in 38 and 44.5% yield using normal phase gravity chromatography followed by reversed phase HPLC. Their spectroscopic properties are consistent with those of the diastereomeric amines **25a** and **25b**, which are the expected stereoisomers according to our model investigation. The other two possible diastereomers **25c** and **25d** could not be isolated and must be formed, if at all, in very low yields.



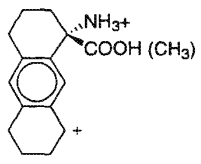
25c



25d

The assignment of the stereochemical relationship between the hydantoin ring at C1′ and the amino group at C8′ of **25a** and **25b** was determined after the cleavage of the chiral auxiliary using lead (IV) acetate. *N*-BOC protection of the generated amino group gave **26a** from **25a** and **26b** from **25b** in 65 and 62% yield, respectively. Fortunately, we were able to grow crystals of **26b** that were suitable for X-ray crystal structure analysis. The crystal structure of **26b** is illustrated in Fig. 2 and shows *R*-configuration at the stereogenic carbon C1′.

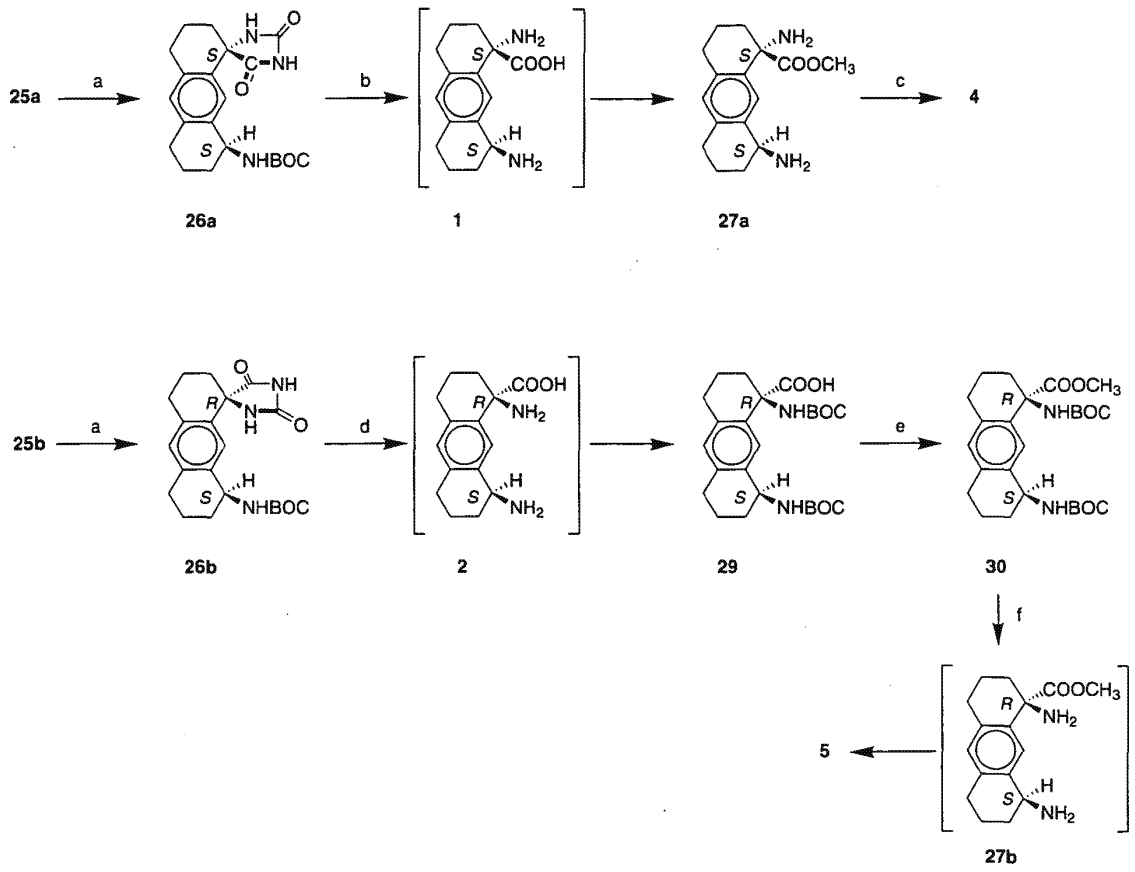
In order to complete the synthesis of **4** (Scheme 5), the hydantoin ring of **26a** was hydrolyzed with aqueous $Ba(OH)_2$ at 125°C. Subsequent heating of crude **1** in methanol in the presence of $SOCl_2$ for 24 h afforded the methyl ester **27a** in 40.5% yield. Selective BOC-protection of the more reactive secondary amine of **27a** under standard conditions gave the desired constrained L-lysine derivative **4**, which is suitably protected to allow its incorporation into a short peptide. The yield of the esterification of crude **1** was disappointingly low. This might result from an acid catalyzed deamination of **1** or **27a** during the esterification as a consequence of the stability of carbocation **28**.



28

Thus, for the synthesis of the constrained D-lysine derivative **5** (Scheme 5), we choose a slightly different route in the hope to improve the overall yield. After hydrolysis of

UM00011872
NOVARTIS EXHIBIT 1017
Novartis v. Regents, IPR2023-01346
Page 618 of 4460



Scheme 5. Final steps of the synthesis of **4** and **5**. *Conditions*: (a) 1. $Pb(OAc)_4$; CH_2Cl_2/MeOH (2:1); 0°C; 2. HCl (2N) reflux; 3. Na_2CO_3, $(BOC)_2O$; dioxane/water (1:1); **26a**: 62% yield, **26b**: 65% yield. (b) 1. $Ba(OH)_2$; water; 125°C; 2. H_2SO_4; 3. $SOCl_2$; MeOH; reflux; 4. Na_2CO_3; 40.5% yield. (c) $(BOC)_2O$; dioxane; 78% yield. (d) 1. $Ba(OH)_2$; water; 125°C; 2. H_2SO_4; 3. $(BOC)_2O$; Na_2CO_3; dioxane/water (1:1); 45% yield. (e) CH_2N_2; ether; quantitative. (f) 1. TFA; 0°C; 2. Na_2CO_3 3. $(BOC)_2O$; dioxane; 65% yield.

hydantoin **26b**, both amino groups of **2** were first protected with a BOC group through the reaction of crude **2** with excess $(BOC)_2O$. The subsequent reaction of **29** with diazomethane afforded **30** quantitatively. Deprotection of both amino groups with trifluoroacetic acid and subsequent selective BOC-protection of the secondary amine of **27b** gave **5** in 65% yield. Unfortunately, the total yield of this sequence did not lead to an improved yield as compared to the shorter sequence used for the preparation of **4** from **26a**.

3. Conclusions

In summary, we have developed a new asymmetric reductive amination protocol for arylalkylketones in which α-phenylglycinol is used as chiral auxiliary and $NaBH(OAc)_3$ as reducing agent. Particularly high diastereomeric excesses are obtained for indanone and tetralone derivatives. This reductive amination protocol was a key step in our synthesis of the new conformationally constrained L-lysine and D-lysine derivatives **4** and **5**, which were prepared starting from 1,8-dichloroanthraquinone **14** through a 17- and 18-step reaction sequence. Both amino acids derivatives are interesting scaffolds to test the important role of the lysine side chain in the conformational stability of secondary peptide structures. They are also useful building blocks for the design and synthesis of novel C- and N-terminal α-helix nucleation sites. Such studies are currently underway in our laboratories.

4. Experimental

4.1. General

1-Indanone, 1-tetralone, and 1-benzosuberone were obtained from Aldrich Chemical Company, and were distilled under reduced pressure prior to use when necessary. 7-Fluoro-α-tetralone was synthesized from fluorobenzene and succinnic anhydride in three steps.[29,30] Dichloromethane, methanol and tetrahydrofuran were freshly distilled from calcium hydride, magnesium methoxide or benzophenone ketyl respectively, under an inert atmosphere. All other reagents were used without further purification. All reactions were conducted under an argon atmosphere unless otherwise stated. ^1H and ^{13}C NMR spectra were obtained using a 400 MHz Varian FT NMR spectrometer or a Varian 200 MHz FT NMR spectrometer.

UM00011873
NOVARTIS EXHIBIT 1017
Novartis v. Regents, IPR2023-01346
Page 619 of 4460

^{1}H NMR spectra were referenced to the residual $CHCl_3$, CHD_2OD, $CHCl_2CDCl_2$, $C_6D_5CD_2H$ or HDO, signals at δ 7.26, 3.31, 5.91, 2.09 or 4.81, respectively. ^{13}C NMR spectra were referenced to the residual $CDCl_3$, $CDCl_2CDCl_2$, or CD_3OD signals at δ 77.3, 74.2, or 49.5, respectively. MALDI-TOF mass spectra were obtained on an IonSpec HiRes MALDI mass spectrometer. High resolution FAB-MS were determined on a ZAB SE instrument with 3-nitrobenzyl alcohol (NOBA) matrix from the mass spectrometry laboratory at the University of Kansas, Lawrence, Kansas. CHN analyses were obtained from Desert Analytics, Tucson, Arizona. Gravity chromatography was performed on Bodman silica gel (70–230 mesh). HPLC was performed on Rainin Varian Dual Pump System. Melting points are uncorrected.

4.2. X-Ray crystallography

Crystalline samples of (1*S*,1′*R*)-**11b** and **26b** were placed in inert oil, mounted on a glass pin, and transferred to the cold gas stream of the diffractometer. Crystal data were collected and integrated using a Bruker SMART 1000 system, with graphite monochromated Mo Kα (λ=0.71073 Å) radiation at 173 K. The structures were solved by direct methods using SHELXS-97 and refined using SHELXL-97 (Sheldrick, G. M., University of Göttingen). Non-hydrogen atoms were found by successive full matrix least squares refinement on F^2 and refined with anisotropic thermal parameters. Hydrogen atom positions were located from difference Fourier maps, and a riding model with fixed thermal parameters (u_{ij}=1.2U_{ij}(eq) for the atom to which they are bonded), was used for subsequent refinements.

4.3. Asymmetric reductive amination of α-tetralone using (*R*)-2-phenylglycinol (*procedure A*)

To a stirred solution of α-tetralone **12b** (15 mmol) in xylenes (30 mL) was added (*R*)-2-phenylglycinol (16.5 mmol) and *p*-tolylsulfonic acid monohydrate (0.5 mol%). The resulting mixture was heated to reflux and maintained there until ^{1}H NMR spectroscopy showed less than 5% **12b** (3–8 h). The reaction mixture is diluted with 15 mL toluene, washed with 10% $NaHCO_3$ (2×10 mL), water (5×10 mL), and brine (10 mL) and is dried over $MgSO_4$. Solvent was removed in vacuo to give a mixture of imine **10b**, oxazolidines **13b** and unreacted **12b** (86:10:4:5 ratio).[24e] For the reduction with $NaBH(OAc)_3$, the crude imine/oxazolidine mixture (1.3 g, 4.8 mmol) was taken up in anhydrous THF (10 mL) and cooled to 0°C under argon. $NaBH_4$ (2.1 g, 5.5 mmol) and glacial acetic acid (0.95 mL, 16.5 mmol) were added and the reaction mixture was stir at 0°C for 2 h. Dichloromethane (10 mL) and saturated $NaHCO_3$ (2 mL) was added. The organic phase was separated and washed with saturated $NaHCO_3$ (4×2 mL), dried over $MgSO_4$ and concentrated to yield 1.3 g of the crude product. The crude diastereomeric mixtures of amines were purified by column chromatography (Silica gel, CH_2Cl_2) to give a mixture of diastereomeric amines (1*S*,1′*R*)-**11b**/(1*R*,1′*R*)-**11b** (1.16 g, 87%). For the reduction with $NaBH_4$, the imine/oxazolidine mixture (100 mg, 0.38 mmol) was dissolved in absolute ethanol (10 mL). The solution was thermally equilibrated at the desired reaction temperature (24, 0, or −10°C) and $NaBH_4$ (3 equiv.) was added. The solution was stirred until all imine and oxazolidines had been reduced (TLC control) and was worked up as described above. The diastereomeric ratio of each reaction was determined by reversed phase HPLC of the crude reaction products (Higgins TARGA C18 column, 4,6×250 mm, 100 mM phosphate buffer pH 2.74/MeOH (55:45), 1 mL/min flow rate, detection at 270 nm). Retention time of major isomer: 26.5 min; retention time of minor isomer: 31.2 min. Both diastereomers were separated by preparative reversed phase HPLC on a TARGA C18 column (250×20 mm) (Higgins Analytical) using 40 mM phosphate buffer pH 2.85/MeOH (60:40) as the mobile phase (15 mL/min flow rate, detection at 285 nm). The product fractions were concentrated, basified with saturated Na_2CO_3 and extracted twice with ether. The combined organic layers were washed with water and with brine, dried over $MgSO_4$ and concentrated to yield the pure diastereomers.

4.3.1. *N*-[(*R*)-2′-Hydroxy-1′-phenylethyl]-(*S*)-1-amino-1,2,3,4,-tetrahydronaphthalene (1*S*,1′*R*)-11b (major diastereomer). Colorless solid; mp 84–86°C; $[\alpha]_D^{24}$=−95.2° (*c* 3.14, MeOH); ^{1}H NMR (400 MHz, $CDCl_3$) δ 7.40–7.27 (m, 6H), 7.2–7.14 (m, 2H), 7.12–7.07 (m, 1H), 3.98 (dd, *J*=4.6, 7.9 Hz, 1H), 3.80 (t, *J*=4.5 Hz, 1H), 3.72 (dd, *J*=4.6, 10.7 Hz, 1H), 3.51 (dd, *J*=7.9, 10.7 Hz, 1H), 2.86–2.64 (m, 2H), 1.94–1.60 (m, 4H) 2.4–1.7 (svb, 2H); ^{13}C NMR (50.29 MHz, $CDCl_3$) δ 142.2, 139.3, 137.4, 129.3, 129.2, 128.8, 127.7, 127.4, 127.0, 125.8, 66.9, 63.2, 54.3, 30.2, 29.1, 18.8; HR-MALDI MS *m/z* ($M+Na^+$) 290.154 (calcd for $C_{18}H_{21}NONa$, 290.152). Anal. calcd for $C_{18}H_{21}NO$: C, 81.16; H, 7.57; N, 5.26. Found: C, 81.17; H, 7.89; N, 5.33.

4.3.2. *N*-[(*R*)-2′-Hydroxy-1′-phenylethyl]-(*R*)-1-amino-1,2,3,4,-tetrahydronaphthalene (1*R*,1′*R*)-11b (minor diastereomer). Colorless oil; $[\alpha]_D^{24}$=+3.5° (*c* 0.34, MeOH); ^{1}H NMR (400 MHz, $CDCl_3$) δ 7.44–7.30 (m, 5H), 7.16–7.06 (m, 4H), 3.99 (dd, *J*=4.6, 9.0 Hz, 1H), 3.71–3.66 (m, 2H), 3.51 (dd, *J*=9.0, 10.8 Hz, 1H), 2.88–2.79 (m, 1H), 2.74–2.60 (m, 1H), 2.4–1.7 (svb, 2H), 2.15–1.9 (m, 2H), 1.77–1.65 (m, 2H); ^{13}C NMR (50.29 MHz, $CDCl_3$) δ 141.0, 139.2, 137.9, 129.4, 129.14, 129.07, 128.1, 127.7, 127.2, 126.2, 67.1, 62.2, 51.7, 29.6, 27.4, 18.5; HR-MALDI MS *m/z* ($M+Na^+$) 290.153 (calcd for $C_{18}H_{21}NONa^+$, 290.152).

4.3.3. *N*-[(*R*)-2′-Hydroxy-1′-phenylethyl]-(*R*)-1-amino-8-fluoro-1,2,3,4,-tetrahydronaphthalene (1*S*,1′*R*)-11c. Application of procedure A to 8-fluoro-1,2,3,4-tetrahydro-1-naphthalone **12c** and (*R*)-phenylglycinol gave crude (1*S*,1′*R*)-**11c**, which was purified by column chromatography (SiO_2, CH_2Cl_2/MeOH (50:1)) to afford (1*S*,1′*R*)-**11c** as a single diastereomer by ^{1}H NMR in 48% yield. Pale yellow oil; $[\alpha]_D^{24}$=−51.8° (*c* 0.79, $CHCl_3$); ^{1}H NMR (400 MHz, $CDCl_3$) δ 7.4–7.28 (m, 5H), 7.08 (dd, *J*=2.4, 9.6 Hz, 1H), 7.03 (dd, *J*=6.0, 7.6 Hz, 1H), 6.86 (dt, *J*=2.4, 8.4 Hz, 1H), 3.97 (dd, *J*=4.1, 8.0 Hz, 1H), 3.78–3.70 (m, 2H), 3.52 (dd, *J*=8.0, 10.8 Hz, 1H), 2.80–2.60 (m, 2H), 2.5 (svb, 2H), 1.90–1.77 (m, 2H), 1.74–1.58 (m, 2H); ^{13}C NMR (100.56 MHz, $CDCl_3$) δ 161.1 (d, $^1J_{CF}$=242 Hz), 142.0, 141.3 (d, $^3J_{CF}$=6.1 Hz), 132.8 (d, $^4J_{CF}$=3.1 Hz), 130.5 (d, $^3J_{CF}$=7.6 Hz), 128.9, 127.8, 127.6, 115.2 (d, $^2J_{CF}$=20.9 Hz), 114.0 (d, $^2J_{CF}$=21.2 Hz), 67.0, 65.2, 54.3 (d, $^4J_{CF}$=1.2 Hz),

UM00011874
NOVARTIS EXHIBIT 1017
Novartis v. Regents, IPR2023-01346
Page 620 of 4460

(m, 2H), 2.12 (sb, 2H), 2.1–1.6 (m, 4H); δ_C (100.56 MHz, $CDCl_3$) δ 161.1 (d, $^1J_{CF}$=243 Hz), 142.8 (d, $^3J_{CF}$=6.1 Hz), 132.5 (d, $^4J_{CF}$=3.0 Hz), 130.5 (d, $^3J_{CF}$=7.7 Hz), 114.4 (d, $^2J_{CF}$=21.0 Hz), 114.0 (d, $^2J_{CF}$=21.3 Hz), 49.9 (d, $^4J_{CF}$= 1.1 Hz), 33.5, 29.0, 20.0; HR-FAB MS *m/z* ($M+H^+$) 166.1027 (calcd for $C_{10}H_{13}FN$, 166.1032).

4.4.6. (*S*)-1-Indanamine ((*S*)-9a). Application of procedure B to (1*S*,1′*R*)-**11a** afforded (*S*)-**9a** as a colorless oil in 47% yield. $[\alpha]_D^{24}$=+16.4° (*c* 1.4, MeOH) ((*R*)-**9a**: $[\alpha]_D^{20}$=−17 (*c* 1.5, MeOH));[23] δ_H(400 MHz, $CDCl_3$) 7.33 (d, *J*=7.6 Hz, 1H), 7.26–7.18 (m, 3H), 4.36 (t, *J*=7.4 Hz, 1H), 3.00–2.86 (m, 1H), 2.83–2.76 (m, 1H), 2.58–2.44 (m, 1H), 1.63 (s, 2H), 1.74–1.65 (m, 1H); δ_C (100.56 MHz, $CDCl_3$) δ 147.7, 143.3, 127.4, 126.7, 124.9, 123.5, 57.5, 37.6, 30.3; HR-FAB MS *m/z* ($M+H^+$) 134.0988 (calcd for $C_9H_{12}N$, 134.0988).

4.4.7. 1-Aminobenzocycloheptane (9d). Application of procedure B to (1*S*,1′*R*)-**11d**/(1*R*,1′*R*)-**11d** (1.4:1) afforded **9d** as a colorless oil in 61% yield. $[\alpha]_D^{24}$=−1.4° (*c* 1.5, MeOH) ((*R*)-**9d**: $[\alpha]_D^{20}$=+26 (*c* 1.125, MeOH));[23] δ_H(400 MHz, $CDCl_3$) 7.42 (d, *J*=7.6 Hz, 1H), 7.21 (dt, *J*=1.6, 5.7 Hz, 1H), 7.15–7.05 (m, 2H), 4.22 (d, *J*= 8.8 Hz, 1H), 2.86–2.78 (m, 2H), 2.04–1.93 (m, 1H), 1.91–1.75 (m, 3H), 1.70–1.38 (m, 4H); δ_C (100.56 MHz, $CDCl_3$) δ 146.0, 141.7, 129.7, 126.6, 126.4, 124.4, 55.0, 37.5, 36.1, 29.1, 27.8.

4.4.8. 1-Phenyl-1-ethylamine (9e). Application of procedure B to (1*S*,1′*R*)-**11e**/(1*R*,1′*R*)-**11e** (7:4) afforded (*S*)-**8e** (23% ee) as a colorless oil (75% yield). $[\alpha]_D^{24}$=−8.0° (*c* 2.36, MeOH) ((*R*)-**9e** (Aldrich Chemical Company, 99%ee): $[\alpha]_D^{20}$=+34.4 (*c* 3.52, MeOH)); δ_H(400 MHz, $CDCl_3$) 7.37–7.22 (m, 5H), 4.12 (q, *J*= 6.6 Hz, 1H, C*H*CH_3), 1.48 (sb, 2H), 1.39 (d, *J*=6.6 Hz, 3H, CH$C\mathit{H}_3$); δ_C (100.56 MHz, $CDCl_3$) δ 148.0, 128.7, 127.0, 125.9, 51.5, 25.9.

4.5. 1,2,3,4,5,6,7,8-Octahydroanthracene-1,8-dicarboxylic acid (17)

Dry tetrahydrofuran (20 mL) was added under argon into a 3-necked, 250 mL flask fitted with a dry ice condenser, gas inlet and low temperature thermometer and was cooled to −70°C using an acetone/dry ice bath. The dry ice condenser was charged with a acetone/dry ice slurry and dry ammonia gas was passed through the cold tetrahydrofuran until the flask was approximately half-full. To this solution, solid anthracene-1,8-dicarboxylic acid[26] (1.21 g, 4.55 mmol) was added under stirring in one portion. The acetone/dry ice bath was removed. Lithium wire (190 mg, 27 mmol) was added in eight portions. Caution: exothermic reaction. Enough time was given to allow each lithium piece to dissolve before the next portion was added. After the addition was complete, the reaction mixture was refluxed for 1 h and was quenched by the addition of solid ammonium chloride (3 g). Caution: the addition of ammonium chloride is very exothermic. The ammonium chloride should be added carefully in small portions. After the addition, the reaction mixture was further stirred at room temperature until all of the ammonia had been evaporated. The tetrahydrofuran was removed under vacuum. The residual solid was suspended in water (20 mL) and was cooled with an ice bath to 0°C. Ice-cold aqueous HCl (6N) was added until pH<1. The precipitated crude 1,4,5,8-tetrahydroanthracene-1,8-dicarboxylic acid **15** was filtered off, washed with water until the filtrate was pH neutral, sucked dry and was used for the next step without further purification. The crude **15** (1.2 g) was dissolved in ethanol (150 mL). Hydrogenation catalyst, 5% Pd on activated charcoal, (1.2 g) was added and the solution degassed twice and purged with hydrogen gas. The solution was shaken under a hydrogen atmosphere (70 psi) for 12 h. After completion of the hydrogenation, the solution was degassed and filtered through a pad of celite. The ethanol was removed in vacuo to leave **17** as a white solid, which was 90 to 95% pure by ^{1}H NMR spectroscopy. It was further purified by crystallization from boiling xylenes to give **17**[12a] as colorless solid (0.83 g, 66.2% yield).

4.5.1. 2′,3′,4′,5′,6′,7′-Hexahydrospiro[1,3-ethylenedithiole-2,1′-anthracen]-8′-one (18) and 2′,3′,4′,5′,6′,7′-hexahydrodispiro[1,3-dithiolane-2,1′-anthracen-8′,2″-[1,3]dithiolane] (19). 3,4,5,6-Tetrahydro-1(2*H*),8(7*H*)-anthracenedione 6 (365 mg, 1.7 mmol) was dissolved in 50 mL dry dichloromethane under argon and cooled to 0°C. Ethane-1,2-dithiol (90%, 0.14 mL, 1.7 mmol) was added via syringe followed by the addition of $BF_3{\cdot}Et_2O$ (86 μL, mmol). The solution was stirred at room temperature under argon. After 24 h, the reaction solution was washed with 5% Na_2CO_3 solution (10 mL), dried over $MgSO_4$, filtered, and concentrated. The residual solid was dissolved in the minimum amount of dichloromethane and was purified by flash-column chromatography on silica gel. The diprotected anthracenedione **19** was eluted with CH_2Cl_2 (192 mg, 37% based on consumed **6**) followed by the monoprotected anthracenedione **17** (214 mg, 52% based on consumed **6**). Unreacted **6** (56 mg) was eluted with CH_2Cl_2/MeOH (9:1). **18**: colorless solid mp 138°C; ^{1}H NMR (400 MHz, $CDCl_3$) δ 8.59 (s, 1H), 6.89 (s, 1H), 3.7–3.42 (m, 4H), 2.88 (t, *J*=6.1 Hz, 2H), 2.81 (t, *J*= 6.4 Hz, 2H), 2.62 (dd, *J*=6.2, 6.9 Hz, 2H), 2.42–2.37 (m, 2H), 2.14–1.98 (m, 4H); ^{13}C NMR (100.56 MHz, $CDCl_3$) δ 197.8, 143.1, 142.9, 139.0, 131.4, 130.4, 128.9, 68.3, 43.8, 41.2, 39.4, 30.0, 29.5, 23.4, 22.9; HR-MALDI MS *m/z* ($M+Na^+$) 313.070 (calcd for $C_{16}H_{18}S_2ONa^+$, 313.069). Anal. calcd for $C_{16}H_{18}OS_2$: C, 66.16; H, 6.25. Found: C, 66.12; H, 6.19. **19**: colorless solid mp 236–238°C; ^{1}H NMR (400 MHz, $CDCl_3$) δ 8.50 (s, 1H), 6.65 (s, 1H), 3.7–3.42 (m, 8H), 2.73 (t, *J*=6.2 Hz, 4H), 2.40–2.37 (m, 4H), 2.01–1.95 (m, 4H); ^{13}C NMR (100.56 MHz, $CDCl_3$) δ 137.4, 136.6, 133.7, 128.7, 68.9, 43.8, 41.0, 29.3, 23.2; HR-MALDI MS *m/z* ($M+Na^+$) 389.051 (calcd for $C_{18}H_{22}S_4Na^+$, 389.050). Anal. calcd for $C_{18}H_{22}S_4$: C, 58.96; H, 6.05. Found: C, 58.37; H, 6.02.

4.5.2. *rac*-2′,3′,4′,5′,6′,7′-Hexahydrodispiro[imidazolidine-4,1′-anthracene-8′,2″-[1,3]dithiolane]-2,5-dione (20). A suspension of **18** (2 g, 6.85 mmol), KCN (2.5 g, mmol) and $(NH_4)_2CO_3$ (13.6 g, mmol) in ethanol/water (4:1) (100 mL) was placed in a steel reactor fitted with a glass liner. The reactor was sealed and the content heated to 130–140°C for 48 h with stirring. After the reactor had cooled to room temperature it was carefully vented in a fume hood and opened. The content was poured into water (400 mL). The precipitated product was filtered off and washed with water (200 mL). The precipitate was dried

UM00011875
NOVARTIS EXHIBIT 1017
Novartis v. Regents, IPR2023-01346
Page 621 of 4460

and suspended in boiling dichloromethane (100 mL). After cooling and standing for 1 h, the suspension was filtered to give 1.8 g of pure **20** as a white solid. The filtrate contained some unreacted **18**, **20** and an unidentified byproduct. All three compounds were separated by silica gel column chromatography. Unreacted **18** (252 mg) was eluted first with CH_2Cl_2, followed by the byproduct (50 mg) with CH_2Cl_2/EtOAc (9:1), followed by **20** (420 mg) with CH_2Cl_2/EtOAc (6:4). The total yield of **20** was 97% based on reacted **18**. Mp 251°C; ^{1}H NMR (400 MHz, $CDCl_3$) δ 7.79 (s, 1H), 7.49 (sb, 1H), 6.8 (s, 1H), 5.6 (s, 1H), 3.6–3.38 (m, 4H), 2.86–2.7 (m, 4H), 2.4–2.25 (m, 4H), 2.08–1.94 (m, 3H), 1.84–1.74 (m, 1H); ^{13}C NMR (100.56 MHz, CD_3OD/$CDCl_3$ (1:2)) δ 178.5, 157.7, 137.7, 137.6 136.8, 130.8, 129.3, 128.8, 68.3, 64.1, 43.4, 40.5, 34.0, 29.0, 28.2, 22.5, 18.7; HR-FABMS *m/z* ($M+H^+$) 361.1033 (calcd for $C_{18}H_{21}N_2O_2S_2$, 361.1044). Anal. calcd for $C_{18}H_{20}N_2O_2S_2$: C, 59.97; H, 5.59; N, 7.77. Found: C, 60.01; H, 5.53; N, 7.78.

4.5.3. *rac*-2′,3′,4′,5′,6′7′-Hexahydrospiro[imidazolidine-4,1′-anthracen-8′-one]-2,5-dione (21). Compound **20** (569 mg, 1.58 mmol) was dissolved in ethanol/water/THF (5:3:1) (90 mL) under gentle warming. To this solution was added a solution of silver(I) nitrate (1.07 g, 6.3 mmol) in ethanol/water/THF (5:3:1) (30 mL). Immediately after the addition, a yellowish precipitate forms. The suspension was stirred in the dark at 45°C for 1 h. Brine (10 mL) was added. The precipitate was filtered off and washed with hot ethanol (30 mL). The filtrate was concentrated to 20 mL and extracted with ethyl acetate (4×30 mL). The combined extracts were dried over $MgSO_4$ and concentrated to give the crude product as a slightly yellowish solid. The crude product was purified by crystallization from boiling ethanol/ethyl acetate to give **21** as a colorless solid (305 mg, 68% yield): mp 274°C; ^{1}H NMR (400 MHz, CD_3OD) δ 7.78 (s, 1H), 7.15 (s, 1H), 2.95 (t, J=6.4 Hz, 2H), 2.88 (t, J=6.0 Hz, 2H), 2.61 (t, J=6.0 Hz, 2H), 2.3–2.0 (m, 5H), 1.94–1.82 (m, 1H); ^{1}H NMR (400 MHz, $CDCl_3$) δ 7.91 (s, 1H), 7.38 (sb, 1H), 7.07 (s, 1H), 5.54 (sb, 1H), 2.95–2.81 (m, 4H), 2.62 (t, J=6.4 Hz, 2H), 2.40–2.30 (m, 2H), 2.15–2.0 (m, 3H), 1.88–1.77 (m, 1H); ^{13}C NMR (100.56 MHz, CD_3OD/DMF_{d7} (1:1)) δ 199.1, 179.5, 158.7, 146.0, 145.7, 134.4, 132.5, 131.1, 126.4, 65.0, 40.0, 35.0, 30.3, 30.2, 24.4, 19.8; HR-FABMS *m/z* ($M+H^+$) 285.1223 (calcd for $C_{16}H_{17}N_2O_3$, 285.1239). Anal. calcd for $C_{16}H_{16}N_2O_3$: C, 67.59; H, 5.67; N, 9.85. Found: C, 67.49; H, 5.64; N, 9.88.

4.5.4. *rac*-*N*,*N*′-bis[*tert*-Butyloxycarbonyl]-2′,3′,4′,5′,6′,7′-hexahydrospiro[imidazolidine-4,1′-anthracen-8′-one]-2,5-dione (22). Ketone **21** (50 mg, 0.176 mmol) was dissolved in dry THF (7 mL) under argon. $(BOC)_2O$ (150 mg, 0.69 mmol) was added and the solution was refluxed for 3 h. The solvent was removed in vacuo. The residual crude product was purified by column chromatography on silica gel (eluant: dichloromethane/ethyl acetate (9:1)) to give **22** as a colorless oil (67 mg, 79% yield) ^{1}H NMR (400 MHz, $CDCl_3$) δ 7.76 (s, 1H), 7.09 (s, 1H), 295–2.78 (m, 3H), 2.66–2.55 (m, 2H), 2.61 (t, J=6.0 Hz, 2H), 2.3–2.0 (m, 5H), 1.94–1.82 (m, 1H), 1.63 (s, 9H), 1.29 (s, 9H); ^{13}C NMR (100.56 MHz, $CDCl_3$ (1:1)) δ 197.5, 168.3, 147.8, 147.7, 145.4, 144.8, 144.5, 131.6, 31.1, 130.4, 123.9, 87.0, 84.8, 65.5, 39.2, 32.1, 29.5, 29.3, 27.94, 27.92 23.3, 19.3; HR-MALDI MS *m/z* 407.159 ($M-CO_2-CH_2=C(CH_3)_2+Na^+$) (calcd for $C_{21}H_{24}N_2O_5Na^+$, 407.158).

4.5.5. (1′*S*,8′*S*,1″*R*)-*N*-[2″-Hydroxy-1″-phenylethyl]-8′-amino-2′,3′,4′,5′,6′,7′,8′-heptahydrospiro[imidazolidine-4,1′-anthracene]-2,5-dione (25a) and (1′*R*,8′*S*,1″*R*)-*N*-[2″-hydroxy-1″-phenylethyl]-8′-amino-2′,3′,4′,5′,6′,7′,8′-heptahydrospiro[imidazolidine-4,1′-anthracene]-2,5-dione (25b). Application of procedure A using **21** (300 mg, 1.06 mmol), (*R*)-phenylglycinol (299 mg, 1.7 mmol), and *p*-tolylsulfonic acid monohydrate (28 mg, 0.13 mmol) to form the intermediate imines (1′*S*,1″*R*)-**24a** and (1′*R*,1″*R*)-**24b**, and $NaBH(OAc)_3$ as reducing agents afforded the crude amines **25a** and **25b**. Column chromatography (silica gel; eluant: $CHCl_3$/ethyl acetate) afforded unreacted **21** (50 mg) and a 1:1-mixture of the diastereomeric amines (336 mg). Both diastereomers were further separated by preparative reversed phase HPLC on a TARGA C18 column (250×20 mm; Higgins Analytical) using water/methanol (20:35) containing 0.1% TFA as the mobile phase (20 mL/min flow rate, detection at 254 nm; retention time of **25a**: 19.6 min, retention time of **25b**: 17.3 min). The product fractions were concentrated by rotavaporation. The residual TFA salts of **25a** and of **25b** were partitioned between saturated aqueous Na_2CO_3 (20 mL) and ethyl acetate (20 mL). The organic layers were separated off. The aqueous layers were extracted with ethyl acetate (4×25 mL each). The combined organic layers were dried over $MgSO_4$, concentrated to give **25a** and **25b**, respectively as white solids. Both diastereomers were recrystallized from ethyl acetate. **25a**: (136 mg, 38% yield) colorless needles; mp 224–226°C; $[\alpha]_D^{24}=-52°$ (*c* 0.31 $CHCl_3$); ^{1}H NMR (400 MHz, $CDCl_3$) δ 7.4–7.16 (m, 5H), 7.10 (s, 1H), 7.03 (sb, 1H), 6.81 (s, 1H), 5.4–3.9 (svb, 3H), 3.86 (dd, J=3.8, 9.0 Hz, 1H), 3.58–3.51 (m, 1H), 3.52 (dd, J=3.8, 11.2 Hz, 1H), 3.33 (m, 1H), 2.8–2.5 (m, 4H), 2.3–2.14 (m, 2H), 1.95–1.5 (m, 6H); ^{13}C NMR (100.56 MHz, $CDCl_3$; 60°C) δ 177.27, 157.05, 142.14, 138.8, 138.51, 136.55, 130.53, 130.28, 128.96, 127.8, 127.75, 126.95, 67.55, 64.87, 64.2, 54.03, 34.57, 30.8, 28.93, 28.76, 19.5, 19.17; HR-FABMS *m/z* ($M+H^+$) 406.2125 (calcd for $C_{24}H_{28}N_3O_3$, 406.2131). Anal. calcd for $C_{24}H_{27}N_3O_3$: C, 71.09; H, 6.71; N, 10.36. Found: C, 71.54; H, 6.50; N, 10.20. **25b**: (159 mg, 44.5% yield) colorless needles; mp 208°C; $[\alpha]_D^{24}=-39.1°$ (*c* 1.39, $CHCl_3$); ^{1}H NMR (400 MHz, $CDCl_3$) δ 7.38–7.16 (m, 5H), 7.18 (s, 1H), 6.83 (s, 1H), 6.66 (sb, 1H), 6.4–3.0 (svb, 3H), 3.80 (dd, J=3.6, 8.8 Hz, 1H), 3.60–3.55 (m, 1H), 3.51 (dd, J=3.6, 11.0 Hz, 1H), 3.33 (dd, J=8.8, 11.0 Hz, 1H), 2.8–2.5 (m, 4H), 2.3–2.18 (m, 2H), 2.0–1.9 (m, 1H), 1.86–1.64 (m, 2H), 1.64–1.50 (m, 3H); ^{13}C NMR (100.56 MHz, $CDCl_3$) δ 178.2, 157.6, 142.0, 136.6, 138.3, 136.4, 130.4, 130.1, 128.8, 127.6, 127.2, 67.2, 64.6, 64.3, 54.2, 34.2, 30.5, 28.8, 28.7, 19.5, 18.9; HR-FABMS *m/z* ($M+H^+$) 406.2131 (calcd for $C_{24}H_{28}N_3O_3$, 406.2131). Anal. calcd for $C_{24}H_{27}N_3O_3$: C, 71.09; H, 6.71; N, 10.36. Found: C, 71.28; H, 6.49; N, 10.40.

4.5.6. (1′,8′*S*)-*N*-[*tert*-Butyloxycarbonyl]-8′-amino-2′,3′,4′,5′,6′,7′,8′-heptahydrospiro[imidazolidine-4,1′-anthracene]-2,5-dione (26b). Application of procedure B to **25b** (133 mg, 0.32 mmol) using dichloromethane/methanol (2:1) as solvent mixture instead of pure methanol, afforded

UM00011876
NOVARTIS EXHIBIT 1017
Novartis v. Regents, IPR2023-01346
Page 622 of 4460

the crude amine **31**, which was *N*-BOC protected without purification. Thus, crude **31** was dissolved in THF (6 mL), methanol (3 mL) and triethylamine (0.5 mL). Solid $(BOC)_2O$ (110 mg, mmol) was added and the solution was stirred at room temperature for 13 h. The solvent was evaporated in vacuo. The residual solid was participated between water (10 mL) and ethyl acetate (10 mL). The organic layer was separated off. The aqueous layer was extracted with ethyl acetate (3×10 mL). The combined organic layers were dried over $MgSO_4$ and concentrated in vacuo. The residual solid was purified by column chromatography (SiO_2, ethyl acetate/dichloromethane (1:2)) to yield pure **26b** (82 mg, 65% yield), which was further recrystallized from chloroform/hexane (1:3). Mp 224°C; $[\alpha]_D^{24}=-23.4°$ (*c* 1.49, MeOH); ^{1}H NMR (400 MHz, $CDCl_2CDCl_2$; 353 K) δ 8.2 (svb, 1H), 7.12 (s, 1H), 6.83 (s, 1H), 6.1 (svb, 1H), 5.0 (svb, 1H), 4.66 (sb, 1H), 2.8–2.6 (m, 4H), 2.25–2.10 (m, 2H), 2.0–1.85 (m, 2H), 1.82–1.71 (m, 4H), 1.38 (s, 9H); ^{13}C NMR (100.56 MHz, $CDCl_2CDCl_2$, 353 K) δ 176.88, 156.50, 155.92, 138.50, 137.00, 136.69, 131.14, 130.15, 126.83, 80.03, 64.54, 49.45 (sb), 34.54, 30.59, 29.17, 28.72, 28.66, 20.1, 19.24; HR-FABMS *m/z* ($M+H^+$) 386.2056 (calcd for $C_{21}H_{28}N_3O_4$, 386.2080).

4.5.7. (1′*S*,8′*S*)-*N*-[*tert*-Butyloxycarbonyl]-8′-amino-2′,3′,4′,5′,6′,7′,8′-heptahydrospiro[imidazolidine-4,1′-anthracene]-2,5-dione (26a). This compound was prepared from **25a** in 62% yield as described for the synthesis of **26b** from **25b**. Colorless solid; mp 248°C; $[\alpha]_D^{24}=-17.0°$ (*c* 0.84, MeOH); ^{1}H NMR (400 MHz, $CDCl_3$) δ 7.35 (sb, 1H), 7.15 (s, 1H), 6.88 (s, 1H), 5.78 (sb, 1H), 4.75–4.55 (m, 2H), 2.9–2.2 (m, 4H), 2.38–2.2 (m, 2H), 2.1–1.1 (m, 6H), 1.47 (s, 9H); ^{13}C NMR (100.56 MHz, $CDCl_3/CD_3OD$ (5:1)) δ 178.7, 157.3, 156.3, 138.0, 136.8, 136.0, 130.9, 130.0, 126.3, 79.7, 64.3, 48.7, 34.3, 30.4, 28.9, 28.5, 28.3, 20.1, 18.9, 18.9; HR-FABMS *m/z* ($M+H^+$) 386.2061 (calcd for $C_{21}H_{28}N_3O_4$, 386.2080).

4.5.8. Methyl (1*S*,8*S*)-1,8-diamino-1,2,3,4,5,6,7,8-octahydroanthracene-1-carboxylate (27a) (*Procedure C*). Hydantoin **26a** (173 mg, 0.61 mmol) and $Ba(OH)_2{\cdot}8H_2O$ (5.85 g, 18.5) were suspended in water (14 mL) and were heated to 120°C for 24 h in a Teflon-lined steel-reactor. After cooling the reactor to room temperature, it was vented, opened and the content was poured into 50 mL of water. The solution is carefully acidified with 1.4 M H_2SO_4 aq. The precipitated $BaSO_4$ was filtered off and washed with water. The filtrate was concentrated. The partially solidified crude **1**. $n H_2SO_4$ was taken up in the minimum amount of methanol and was precipitated with ether, filtered off, washed with ether and dried at high vacuum: ^{1}H NMR (400 MHz, D_2O) δ 7.27 (s, 1H), 7.16 (s, 1H), 4.56 (sb, 1H), 3.0–2.75 (m, 4H), 2.5–2.4 (m, 1H), 2.35–1.8 (m, 7H). The crude **1**·H_2SO_4 was dissolved in dry methanol (20 mL) and was cooled to 0°C under argon. Thionyl chloride (4 mL, mmol) was dropwise added to this stirred solution. After the addition was complete, the reaction solution was refluxed for 24 h. The solvent was evaporated in vacuo. The remaining solid was participated between ethyl acetate and 10% aqueous Na_2CO_3. The organic layer was separated off. The aqueous layer was extracted with ethyl acetate (4×20 mL). The combined organic layers were washed with 10 mL brine, dried over $MgSO_4$ and concentrated. The residual oil was purified by reversed phase HPLC (TARGA C18 20×250 mm (Higgins Analytical); MeOH/water (6:4); flow 20 mL/min, detection at 254 nm; retention time of **27a**=4.5 min) to yield **27a** as a yellowish oil (50 mg, 40.5% yield). $[\alpha]_D^{24}=+60°$ (*c* 0.1, MeOH); ^{1}H NMR (400 MHz, $C_6D_5CD_3$) δ 7.38 (s, 1H), 6.60 (s, 1H), 3.66 (t, *J*=5.6 Hz, 1H), 3.34 (s, 3H), 2.64–2.4 (m, 4H), 2.24–2.16 (m, 1H), 2.05–1.95 (m, 1H), 1.88–1.63 (m, 4H), 1.56–1.43 (m, 1H), 1.4–1.3 (m, 1H), 1.0 (ssb, 4H (NH_2), 4H (H_2O)); ^{13}C NMR (100.56 MHz, $CDCl_3$) δ 178.12, 139.24, 136.51, 136.36, 135.23, 129.91, 126.55, 59.84, 52.85, 49.29, 36.66, 33.35, 29.40, 29.33, 19.80, 19.34; HR-MALDI-MS *m/z* 297.159 ($M+Na^+$) (calcd for $C_{16}H_{22}N_2O_2Na^+$, 297.157).

4.5.9. Methyl (1*S*,8*S*)-1-amino-8-*tert*-butoxycarbonylamino-1,2,3,4,5,6,7,8-octahydroanthracene-1-carboxylate (4). $(BOC)_2O$ (34 mg, 0.156 mmol) was added at room temperature to a solution of **27a** (48 mg, 0.134 mmol) in dry THF (3 mL). The solution was stirred for 10 h at room temperature under argon. The solvent was evaporated in vacuo. The remaining solid was washed with hexanes (2×2 mL) to leave **4** as a slightly yellowish solid (49 mg, 78% yield).

Mp 170°C; $[\alpha]_D^{24}=-14.4°$ (*c* 0.23, MeOH); ^{1}H NMR (400 MHz, $CDCl_3$; 60°C) δ 7.15 (s, 1H), 6.83 (s, 1H), 4.76 (sb, 1H), 4.62 (sb, 1H), 3.71 (s, 3H), 2.82–2.62 (m, 4H), 2.3–2.2 (m, 1H), 2.08–1.74 (m, 9H), 1.49 (s, 9H); ^{13}C NMR (100.56 MHz, $CDCl_3$, 60°C) δ 177.91, 155.73, 137.28, 136.88, 136.22, 135.89, 129.96, 127.33, 79.60, 60.10, 52.58, 48.99, 36.73, 31.00, 29.51, 29.23, 28.82, 20.32, 19.41; HR-MALDI-MS *m/z* 397.212 ($M+Na^+$) (calcd for $C_{21}H_{30}N_2O_4Na^+$, 397.210).

4.5.10. (1*R*,8*S*)-1,8-bis(*tert*-Butyloxycarbonylamino)-1,2,3,4,5,6,7,8-octahydroanthracene-1-carboxylic acid (29). Application of procedure C to **26b** (141 mg, 0.37 mmol) gave crude **2**·$n H_2SO_4$: ^{1}H NMR (400 MHz, D_2O) δ 7.27 (s, 1H), 7.16 (s, 1H), 4.56 (sb, 1H), 3.0–2.75 (m, 4H), 2.5–2.4 (m, 1H), 2.35–1.8 (m, 7H). Crude **2**·$n H_2SO_4$, was dissolved in dioxane/1N NaOH (1:1, 10 mL). This solution was cooled to 0°C. $(BOC)_2O$ (600 mg, 2.75 mmol) was added and the solution stirred at room temperature for 20 h. The solution was concentrated to half of its initial volume. Ethyl acetate (20 mL) was added and the aqueous layer cooled to 0°C and acidified to pH 3 with aqueous citric acid (10%). The organic layer was separated off and the aqueous layer extracted with ethyl acetate (5×25 mL). The combined organic layers were washed with brine (10 mL), dried over $MgSO_4$ and concentrated. The crude product was purified by column chromatography (SiO_2, CH_2Cl_2/ethyl acetate 2:1 to 0:1). The product fractions were concentrated. The remaining solid was crystallized form dichloromethane/hexanes (1:10) to yield **29** as colorless crystals (76 mg, 45% yield). mp 185°C; $[\alpha]_D^{24}=-55.3°$ (*c* 1.36, MeOH); ^{1}H NMR (400 MHz, $CDCl_3$; 60°C) δ 7.37 (s, 1H), 6.83 (s, 1H), 5.7 (sb, 1H), 5.9–3.8 (svb, 1H), 4.9–4.6 (m, 2H), 2.82–2.5 (m, 4H), 2.4–2.32 (m, 1H), 2.12–2.02 (m, 1H), 1.92–1.7 (m, 4H), 1.48 (s, 9H), 1.41 (s, 9H); ^{13}C NMR (100.56 MHz, $CDCl_3$; 60°C) δ 176.14, 156.06, 154.68, 137.69, 137.28, 135.53, 133.93, 130.07, 127.19, 80.14, 60.85, 49.12, 32.89, 30.44, 29.33, 29.18, 28.98, 28.79, 28.69, 20.34, 19.71;

UM00011877
NOVARTIS EXHIBIT 1017
Novartis v. Regents, IPR2023-01346
Page 623 of 4460

HR-MALDI-MS *m/z* 483.247 ($M+Na^+$) (calcd for $C_{25}H_{36}N_2O_6Na^+$, 483.247). Anal. calcd for $C_{25}H_{36}N_2O_6$: C, 65.20; H, 7.88; N, 6.08. Found: C, 65.43; H, 7.77; N, 6.03.

4.5.11. Methyl (1*R*,8*S*)-1,8-bis(*tert*-butyloxycarbonylamino)-1,2,3,4,5,6,7,8-octahydroanthracene-1-carboxylate 30). Carboxylic acid **29** (75 mg, 0.163 mmol) was dissolved in diethyl ether (6 mL) and was cooled to 0°C. Into this solution was condensed an approximately 0.4 M solution of diazomethane in diethyl ether (9 mL), which was prepared from diazald (1 g, 4.6 mmol) using a commercially available Mini-Diazald Kit (Aldrich Chemical Company). The reaction flask was sealed with a rubber septum and was left standing inside a metal can in the back of a well-ventilated fume hood. After 12 h, excess diazomethane was decomposed via the drop-wise addition of glacial acetic acid (100 μL). The solvent was removed under high vacuum to yield **30** as a colorless oil (77 mg, quantitative). $[\alpha]_D^{24}=-32.5°$ (*c* 1.5, MeOH); ^1H NMR (400 MHz, $CDCl_3$; 60°C) δ 7.33 (s, 1H), 6.83 (s, 1H), 5.45 (sb, 1H), 4.75–4.65 (m, 1H), 4.58 (sb, 1H), 3.72 (s, 3H), 2.82–2.5 (m, 5H), 2.38–2.30 (m, 1H), 2.07–1.75 (m, 8H), 1.51 (s, 9H), 1.41 (s, 9H); ^{13}C NMR (100.56 MHz, $CDCl_3$; 60°C) δ 173.97, 155.69, 154.26, 137.51, 137.45, 136.15, 133.86, 130.14, 126.92, 79.83, 79.68, 61.18, 52.94, 49.12, 32.50, 30.78, 29.36, 29.2, 28.82, 28.70, 20.15, 20.03; HR-MALDI-MS *m/z* 497.263 ($M+Na^+$) (calcd for $C_{26}H_{38}N_2O_6Na^+$, 497.262)

4.5.12. Methyl (1*R*,8*S*)-1-amino-8-*tert*-butoxycarbonylamino-1,2,3,4,5,6,7,8-octahydroanthracene-1-carboxylate (5). Ice-cold trifluoroacetic acid (0.5 mL) was added to **30** (27 mg, 0.056 mmol) at 0°C. This solution was left standing in an ice bath for 1 h. The solvent was removed in vacuo. The remaining **27b**·$2CF_3COOH$ was taken up in aqueous saturated Na_2CO_3 (2 mL) and was extracted with ethyl acetate (2×5 mL). The combined organic layers were dried over $MgSO_4$ and concentrated. The remaining crude **27b** was redissolved in dioxane (1 mL). A solution of $(BOC)_2O$ (12.5 mg, 0.057 mmol) dissolved in dioxane (0.2 mL) was added via syringe. The reaction mixture was stirred at room temperature for 2 h until which all **27b** had been consumed (TLC control: SiO_2; mobile phase: ethyl acetate/*n*-butanol/acetic acid/water (2:1:1:1; R_F(**27b**)=0.3; R_F(**5**)=0.8). The solution was concentrated in vacuo. The residual crude product was purified by reversed phase HPLC (TARGA C18 20×250 mm (Higgins Analytical); MeOH/water (7:3); flow 20 mL/min, detection at 254 nm; retention time of **5**=13.9 min) to give **5** as a colorless foam (13 mg, 61% yield). $[\alpha]_D^{24}=-21°$ (*c* 0.32, MeOH); ^1H NMR (400 MHz, $CDCl_3$; 60°C) δ 7.13 (s, 1H), 6.83 (s, 1H), 4.73 (sb, 1H), 4.64 (sb, 1H), 3.71 (s, 3H), 2.8–2.62 (m, 4H), 2.3–2.21 (m, 1H), 2.03–1.75 (m, 9 H), 1.49 (s, 9H); ^{13}C NMR (100.56 MHz, $CDCl_3$; 60°C) δ 179.07, 155.79, 137.16, 137.02, 136.07, 135.96, 130.04, 127.07, 79.73, 60.09, 52.82, 49.17, 36.79, 30.86, 29.59, 29.27, 28.83, 20.22, 19.47; HR-MALDI-MS *m/z* 397.212 ($M+Na^+$) (calcd for $C_{21}H_{30}N_2O_4Na^+$, 397.210).

Acknowledgements

T. E. M. thanks the Kansas State University Center for Basic Cancer Research for an Undergraduate Student Cancer Research Fellowship. R. W. warmly thanks the National Institute of Health for a FIRST AWARD (Grant R01 GM57934-01, NIGMS)

References

1. (a) Hanessian, S.; McNaughton-Smith, G.; Lombart, H.-G.; Lubell, W. D. *Tetrahedron* **1997**, *53*, 12789–12854. (b) Gibson, S. E.; Guillo, N.; Tozer, M. J. *Tetrahedron* **1999**, *55*, 585–616.
2. (a) Fletcher, D. M.; Campbell, M. M. *Chem. Rev.* **1998**, *98*, 763–795. (b) Kemp, D. S. *Trends Biotechnol.* **1990**, *8*, 249–255. (c) Rizo, J.; Gierasch, L. M. *Annu. Rev. Biochem* **1992**, *61*, 387–418. (d) Gante, A. *Angew. Chem., Int. Ed. Engl.* **1994**, *33*, 1699–1720.
3. (a) Hruby, V. J. *Life Sci.* **1982**, *31*, 189–199. (b) Giannis, A.; Kolter, T. *Angew. Chem., Int. Ed. Engl.* **1993**, *32*, 1244–1267. (c) Friedinger, R. M.; Veber, D. F.; Perlow, D. S.; Brooks, J. R. *Science* **1980**, *210*, 656–658. (d) Hirschmann, R. *Angew. Chem., Int. Ed. Engl.* **1991**, *30*, 1278–1301.
4. (a) Halab, L.; Gosselin, F.; Lubell, W. D. *Biopolymers* **2000**, *55*, 101–122. (b) Balaram, P. *Curr. Opin. Struct. Biol.* **1992**, *2*, 845–851. (c) Hruby, V. J.; Slate, C. A. *Adv. Amino Acid Mimetics Peptidomimetics* **1999**, *2*, 191–220. (d) Kahn, M., Ed. Peptide secondary structure mimetics. *Tetrahedron, Symposia-in-Print* **1993**, *50* (49), 3433–3689. (e) Curran, T. P.; Marcaurelle, L. A.; O'Sullivan, K. M. *Org. Lett.* **1999**, *1*, 1225–1228.
5. Gellman, S. H. *Acc. Chem. Res.* **1998**, *31*, 173–180.
6. Schneider, J. P.; Kelly, J. W. *Chem. Rev.* **1995**, *95*, 2169–2187.
7. (a) Kemp, D. S.; Boyd, J. G.; Muendel, C. C. *Nature* **1991**, *352*, 451–454. (b) Kemp, D. S.; Oslick, S. L.; Allen, T. J. *J. Am. Chem. Soc.* **1996**, *118*, 4249–4255. (c) Wallimann, P.; Kennedy, R. J.; Kemp, D. S. *Angew. Chem., Int. Ed. Engl.* **1999**, *38*, 1290–1292. (d) Austin, R. E.; Maplestone, R. A.; Sefler, A. M.; Liu, K.; Hruzewicz, W. N.; Liu, C. W.; Cho, H. S.; Wemmer, D. E.; Bartlett, P. A. *J. Am. Chem. Soc.* **1997**, *119*, 6461–6472. (e) Cabezas, E.; Satterthwait, A. C. *J. Am. Chem. Soc.* **1999**, *121*, 3862–3875. (f) Ösapay, G.; Taylor, J. W. *J. Am. Chem. Soc.* **1992**, *114*, 6966–6973.
8. (a) Paterson, Y.; Rumsey, S. M.; Benedetti, E.; Nemethy, G.; Scheraga, H. A. *J. Am. Chem. Soc.* **1981**, *103*, 2947–2955. (b) Karle, I. L.; Balaram, P. *Biochemistry* **1990**, *29*, 6747–6756. (c) Toniolo, C.; Benedetti, E. *Macromolecules* **1991**, *24*, 4004–4009. (d) Hanson, P.; Millhauser, G.; Formaggio, F.; Crisma, M.; Toniolo, C. *J. Am. Chem. Soc.* **1996**, *118*, 7618–7625. (e) Wysong, C. L.; Yokum, T. S.; McLaughlin, M. L.; Hammer, R. P. *Chemtech* **1997**, 26–33. (f) Straessler, C.; Linden, A.; Heimgartner, H. *Helv. Chim. Acta* **1997**, *80*, 1528–1554. (g) Torrini, I.; Pagani Zecchini, G.; Paglialunga Paradisi, M.; Lucente, G.; Mastropietro, G.; Gavuzzo, E.; Mazza, F.; Pochetti, G.; Traniello, S.; Spisani, S. *Biopolymers* **1996**, *39*, 327–337. (h) Hanson, P.; Martinez, G. V.; Millhauser, G.; Formaggio, F.; Crisma, M.; Toniolo, C.; Vita, C. *J. Am. Chem. Soc.* **1996**, *118*, 271–272. (i) Yokum, T. S.; Gauthier, T. J.; Hammer, R. P.; McLaughlin, M. L. *J. Am. Chem. Soc.* **1997**, *119*, 1167–1168.
9. Obrecht, D.; Altorfer, M.; Bohdal, U.; Daly, J.; Hüber, W.; Labhardt, A.; Lehmann, C.; Müller, K.; Ruffieux, R.;

UM00011878
NOVARTIS EXHIBIT 1017
Novartis v. Regents, IPR2023-01346
Page 624 of 4460

Schönholzer, P.; Spiegler, C.; Zumbrunn, C. *Biopolymers* **1997**, *42*, 575–626.
10. (a) Murray, P. J.; Starkey, I. D. *Tetrahedron Lett.* **1996**, *37*, 1875–1878. (b) Murray, P. J. *Tetrahedron Lett.* **1998**, *39*, 6721. (c) Wang, Q.; Sasaki, N. A.; Potier, P. *Tetrahedron* **1998**, *54*, 15759. (d) Goswami, R.; Moloney, M. G. *Chem. Commun.* **1999**, *23*, 2333–2334.
11. (a) Groebke, K.; Renold, P.; Tsang, Y. K.; Allen, T. J.; McClure, K. F.; Kemp, D. S. *Proc. Natl Acad. Sci. USA* **1996**, *93*, 2025–2029. (b) Williams, L.; Kather, K.; Kemp, D. S. *J. Am. Chem. Soc.* **1998**, *120*, 11033–11043.
12. (a) Caluwe, P.; Pepper, T. *J. Org. Chem.* **1988**, *53*, 1786–1790. (b) Christopfel, W. C.; Miller, L. L. *J. Org. Chem.* **1984**, *49*, 5198–5202.
13. Obrecht, D.; Spiegler, C.; Schönholzer, P.; Müller, K.; Heimgartner, H.; Stierli, F. *Helv. Chim. Acta* **1992**, *75*, 1666–1696.
14. (a) Johansson, A. *Contemp. Org. Synth.* **1995**, *2*, 393–408. (b) Groger, H.; Wilken, J. *Angew. Chem., Int. Ed. Engl.* **2001**, *40*, 529–532.
15. (a) Cho, B. T.; Chun, Y. S. *J. Chem. Soc., Perkin Trans. 1* **1990**, 3200–3201. (b) Inoue, T.; Sato, D.; Komura, K.; Itsuno, S. *Tetrahedron Lett.* **1999**, *40*, 5379–5382.
16. (a) Itsuno, S.; Sakurai, Y.; Shimizu, K.; Ito, K. *J. Chem. Soc., Perkin Trans. 1* **1989**, 1548–1549. (b) Itsuno, S.; Sakurai, Y.; Shimizu, K.; Ito, K. *J. Chem. Soc., Perkin Trans. 1* **1990**, 1859–1863. (c) Sugi, K. D.; Nagata, T.; Yamada, T.; Mukaiyama, T. *Chem. Lett.* **1997**, 493–494.
17. (a) Cheong, Y. N.; Osborn, J. A. *J. Am. Chem. Soc.* **1990**, *112*, 9400–9401. (b) Bolm, C. *Angew. Chem., Int. Ed. Engl.* **1993**, *32*, 232–233. (c) Burk, M. J.; Martinez, J. P.; Feaster, J. E.; Cosford, N. *Tetrahedron* **1994**, *50*, 4399–4428. (d) Uematsu, N.; Fujii, A.; Hashiguchi, S.; Ikariya, T.; Noyori, R. *J. Am. Chem. Soc.* **1996**, *118*, 4916–4917. (e) Buriak, J. M.; Osborn, J. A. *Organometallics* **1996**, *15*, 3161–3169. (f) Schnider, P.; Koch, G.; Prétôt, R.; Wang, G.; Bohnen, F. M.; Krüger, C.; Pfaltz, A. *Chem. Eur. J.* **1997**, *3*, 887–892. (g) Mao, J.; Baker, D. C. *Org. Lett.* **1999**, *1*, 841–843. (h) Hayashi, T.; Ishigedani, M. *J. Am. Chem. Soc.* **2000**, *122*, 976–977.
18. (a) Burk, M. J.; Casy, G.; Johnson, N. B. *J. Org. Chem.* **1998**, *63*, 6084–6085. (b) Zhang, F.-Y.; Pai, C.-C.; Chan; Albert, S. C. *J. Am. Chem. Soc.* **1998**, *120*, 5808–5809.
19. (a) Verdaguer, X.; Lange, U. E. W.; Reding, M. T.; Buchwald, S. L. *J. Am. Chem. Soc.* **1996**, *118*, 6784–6785. (b) Verdaguer, X.; Lange, U. E. W.; Buchwald, S. L. *Angew. Chem., Int. Ed. Engl.* **1998**, *37*, 1103–1107. (c) Hansen, M. C.; Buchwald, S. L. *Org. Lett.* **2000**, *2*, 713–715.
20. Soloshonok, V. A.; Ono, T.; Soloshonok, I. V. *J. Org. Chem.* **1997**, *62*, 7538–7539.
21. Shin, J.-S.; Kim, B.-G. *Biotechnol. Bioeng.* **1999**, *65*, 206–211.
22. (a) Wiehl, W.; Frahm, A. W. *Chem. Ber.* **1986**, *119*, 2668–2677. (b) Schlichter, W. H.; Frahm, A. W. *Arch. Pharm.* **1993**, *326*, 429–436. (c) Lauktien, G.; Volk, F.-J.; Frahm, A. W. *Tetrahedron: Asymmetry* **1997**, *8*, 3457–3466. (d) Sreekumar, R.; Pillai, C. N. *Tetrahedron: Asymmetry* **1993**, *4*, 2095–2100. (e) Cimarelli, C.; Palmieri, G. *Tetrahedron: Asymmetry* **2000**, *11*, 2555–2563.
23. Gutman, A. L.; Etinger, M.; Nisnevich, G.; Polyak, F. *Tetrahedron: Asymmetry* **1998**, *9*, 4369–4379.
24. (a) Mokhallalati, M. K.; Pridgen, L. N. *Synth. Commun.* **1993**, *23*, 2055–2064. (b) Chakraborty, T. K.; Hussain, K. A.; Reddy, G. V. *Tetrahedron* **1995**, *51*, 9179–9190. (c) Chakraborty, T. K.; Reddy, G. V.; Hussain, K. A. *Tetrahedron Lett.* **1991**, *32*, 7597–7600. (d) Ma, D.; Tian, H.; Zou, G. *J. Org. Chem.* **1999**, *64*, 120–125. (e) Warmuth, R.; Munsch, T. E.; Stalker, R. A.; Li, B.; Beatty, A. *Tetrahedron* **2001**, *57*, 6383–6397.
25. (a) Goodman, J. M.; Still, W. C. *J. Comput. Chem.* **1991**, *12*, 1110–1117. (b) Allinger, N. L. *J. Am. Chem. Soc.* **1977**, *99*, 8127–8134. (c) Still, W. C.; Tempczyk, A.; Hawley, R. C.; Hendrickson, T. *J. Am. Chem. Soc.* **1990**, *112*, 6127–6129.
26. Golden, R.; Storck, L. M. *J. Am. Chem. Soc.* **1972**, *94*, 3080–3088.
27. Murthy, R.; Sundar, N.; Rao, G. S. R. S. *Tetrahedron* **1982**, *38*, 2831–2836.
28. Kubik, S.; Meissner, R. S.; Rebek, Jr., J. *Tetrahedron Lett.* **1994**, *35*, 6635–6638.
29. Newman, M. S.; Chatterji, R.; Seshadri, S. *J. Org. Chem.* **1961**, *26*, 2667.
30. Owton, W. M.; Brunavs, M. *Synth. Commun.* **1991**, *21*, 981.
31. Jorgensen, W. L.; Maxwell, D. S.; Tirado-Rives, J. *J. Am. Chem. Soc.* **1996**, *118*, 11225–11235.

UM00011879
NOVARTIS EXHIBIT 1017
Novartis v. Regents, IPR2023-01346
Page 625 of 4460



Donor and acceptor strengths in C—H···O hydrogen bonds quantified from crystallographic data of small solvent molecules

Thomas Steiner*

Department of Structural Biology, Weizmann Institute of Science, Rehovot 76100, Israel

The influence of donor and acceptor strengths on mean distances in C—H···O hydrogen bonds is quantified in a crystallographic database study. Small solvent molecules are used as donors, which are cocrystallized in organic and organometallic crystals. This system provides chemically homogeneous sets of C—H groups, allowing better defined statistical analysis compared to studies based on molecular fragments. Eight kinds of O-atom acceptors are considered, ranging from the very strong acceptor P=O to the weak acceptor M—CO (M = transition metal atom). For the strongest donor considered, chloroform, mean hydrogen bond distances vary by *ca.* 0.5 Å as the acceptor strength is varied from P=O to M—CO. For the weak donor acetone, this variation is only *ca.* 0.1 Å. It is confirmed that even weakly polar C—H groups can donate, and that the O-atoms of M—CO groups can accept C—H···O hydrogen bonds.

The general properties of intermolecular C—H···O interactions are at this time the subject of intense research, and several reviews are already available.[1–5] It is found that C—H···O interactions possess all characteristics of hydrogen bonds, including complex properties such as cooperativity within hydrogen bond arrays.[6] Because carbon acidities span a range of over 50 orders of magnitude, the strength of C—H···O hydrogen bonds covers a wide range which overlaps with 'normal' O—H···O hydrogen bonds for more acidic C—H donors,[7–9] and merges with van der Waals interactions for the weakest C—H donor types. It could be shown that for C—H···O contacts in crystals, mean C···O distances correlate with the conventional C—H acidity (in DMSO).[10] Notably, even for C—H of methyl groups, the angular characteristics of C—H···O contacts show weak preference for linearity, indicating weakly hydrogen-bonding character.[11] Because weak hydrogen bonds are primarily electrostatic interactions, they operate also at long distances exceeding the van der Waals separation: for alkynyl donors, contacts with H···O distances of 2.9 Å still show clearly the spectroscopic effects of hydrogen bonding.[12]

The influence of donor strength on mean C—H···O hydrogen bond distances has been described by Desiraju and co-workers in a series of crystallographic database analyses.[10,13,14] Related data were only recently reported for C—H···Hal^- hydrogen bonds.[15] The influence of acceptor nature is more difficult to quantify, and has long resisted detection from crystallographic data. In a preliminary communication, it was shown that for C—H···O contacts formed by solvent molecules cocrystallized in organic crystal lattices, mean H···O distances clearly depend on the acceptor nature.[16] The system of cocrystallized solvent molecules is exceptionally well suited for such a study because it provides chemically homogeneous sets of C—H donors, such as $CHCl_3$, CH_2Cl_2, *etc.* Furthermore, solvent molecules can relatively freely orient in crystal lattices and effects of steric hindrance are smaller than for C—H donors that are part of larger molecules. In the present contribution, the concept of the initial communication is followed, but the work is expanded to a comprehensive form by including organometallic crystal structures and considering a larger set of acceptors. This does not only widen the scope, but it also increases the number of analysed contacts by almost a factor of four (from 311 to 1183), thereby considerably improving the statistical significance of the results. The study is based on 'normalised' X—H bond lengths, that is on bond lengths adjusted to corresponding neutron diffraction values. This procedure should be generally used in statistical hydrogen bond studies.[17]

It is necessary to give a comment on the terminology used. The quantities that are analysed in crystallographic database studies, *i.e.* distances and angles, are purely geometrical. Mean donor–acceptor separations in D—H···A hydrogen bonds are related to a number of physical and chemical properties of the groups involved, but do not directly measure them. For example, the geometric solid state property of mean H···A separations in crystals is correlated to the chemical property of D—H acidity,[10] but this is only a correlation and not a strict dependency. H···A separations in crystals are influenced by many effects, and acidities vary from solvent to solvent. The terms 'donor strength' and 'acceptor strength' are used here solely to characterise distance properties of donor–acceptor combinations in the solid state, meaning that a strong donor (or strong acceptor) will on average attract a given partner to a shorter distance than a weak one. Characterizing the relationships of strengths to properties such as acidity and basicity in solution, partial charges on H and on O, interaction energy, *etc.*, is non-trivial and not the subject of this study.

Results

To obtain results of statistical significance, only organic solvent molecules can be considered that are found cocrystallized in a relatively large number of crystal structures. Futhermore, these crystal structures must be chemically diverse so that C—H···O interactions are formed with a wide variety of acceptor types. Finally, the solvent molecules must not show a too strong tendency for disorder. Only five kinds of molecules fulfil all these requirements: chloroform, dichloromethane, acetonitrile, dimethyl sulfoxide and acetone. Benzene, unfortunately, is unsuitable because of its notorious tendency to disorder. The terminal alkyne group, C≡C—H, is also included in the set of donors because it is one of the very few molecular residues that is in almost all molecules fully accessible to intermolecular contacts.

* On leave from: Institut für Kristallographie, Freie Universität Berlin, Takustr. 6 D-14195 Berlin, Germany. e-mail: steiner@chemie.fu-berlin.de

UM00011880
NOVARTIS EXHIBIT 1017
Novartis v. Regents, IPR2023-01346
Page 626 of 4460

Compared to the previous communication, the range of acceptor strengths is widened by including the strong acceptors P=O and H_2O, and the weak acceptor M—CO (M = transition metal atom; only terminal CO ligands considered). For the latter functional group, the potential to accept C—H···O hydrogen bonds has been shown only recently.[18,19] Further subdivision of the acceptors, such as (CC)C=O, (NC)C=O, (OC)C=O, instead of >C=O, or primary, secondary and tertiary hydroxy groups instead of C(sp^3)—OH, would be desirable in principle, but is not feasible because of the limited numbers of crystal structures. Many important O-atom acceptors such as C(sp^2)—OH, N—OH, P—OH, —O—O—, bridged CO ligands, could not be considered because the available crystal structures are too few for analysis of statistical significance.

As the first step of the analysis, the sequence of C—H donors strengths is determined based on the mean distances to the acceptors O, N and Cl^-, Table 1 (Cambridge Structural Database,[20] January 1998 update). Because the data for O and N acceptors are averaged over all chemical types of O and N atoms, respectively, this is only a rough initial description. Ideally, the sequence of donor strengths should be the same for all acceptor types, and this is actually observed in Table 1, with the exception of minor uncertainties for the methyl donors. For the three stronger donor types, the sequence is clearly $CHCl_3$ > C≡C—H > CH_2Cl_2, and for the weak methyl donors, it appears to be N≡C—Me > DMSO > acetone.

In the second step, a ranking of strengths is set up for the eight types of O-atom acceptors under study. This is performed by determining mean hydrogen bond distances with the conventional donors H_2O and $-NH_3^+$, which occur in very large numbers of crystal structures, Table 2. The acceptors H_2O, C=O and S=O have very similar mean distances to the donors, but for the other acceptors the ranking of strengths is unambiguous: P=O > H_2O ≥ C=O ≥ S=O > C(sp^3)—OH > C—O—C > $-NO_2$ > M—CO. Within this sequence, the mean hydrogen bond distances vary by *ca.* 0.5 Å from the strongest to the weakest acceptors. The poor acceptor strength of the nitro group is in accordance with a recent database and theoretical study on N/O—H···O_2N hydrogen bonds.[21]

If the six C—H donors in Table 1 are combined with the eight O-atom acceptors in Table 2, this leads to a 6 × 8 matrix of 48 possible donor–acceptor combinations. The mean hydrogen bond distances for these combinations are given in Table 3, the total number of contacts for each acceptor type is given in Table 4. In the lines of Table 3, the effect of donor strength on mean hydrogen-bond distances can be seen, and in the columns the corresponding effect of acceptor strengths. Because donors and acceptors are arranged in sequence of falling strengths, the strongest hydrogen bonds are formed with the combinations in the top left corner, and the weakest hydrogen bonds with those in the bottom right corner of the matrix. When looking at the numerical values, it must be considered that for many of the donor–acceptor combinations, only very few examples occur in crystal structures, leading to large standard uncertainties of the mean contact distances. The effect of donor strengths can be best seen in the lines for C=O, C(sp^3)—OH and C—O—C acceptors, for which the largest numbers of contacts are found, and also in the line for P=O, for which the effect is strongest. Within the lines, the mean H···O and C···O separations systematically increase from the left to the right. The effect of acceptor strength is best seen for the more acidic donors, in particular for chloroform. In essence, the sequences of donor and acceptor strengths that were initially set up in Tables 1 and 2 lead to a self-consistent picture in Table 3. It appears that the sequence of acceptor strengths derived from O/N—H···O hydrogen bonds is fully valid also for C—H···O interactions.

The effect of acceptor strength is qualitatively the same for all kinds of donors, *i.e.*, the mean hydrogen-bond distances systematically increase down the columns from P=O to M—CO. Quantitatively, however, there are large differences between the different donors. If the acceptor strength is reduced from P=O to M—CO, the mean H···O distance increases by 0.52 Å for the strongest donor, $CHCl_3$, but only by 0.12 Å for the weakest, acetone. For the other donor types, this value systematically falls with falling donor strength, Table 5. This shows that hydrogen bonds from strong donors are strongly influenced by variations of acceptor strength, whereas hydrogen bonds from weak donors are influenced only slightly. On the other hand, it is of importance that C—H···O contacts even of the weakest donors in the set are not completely insensitive to variations of acceptor nature (insensitivity would be an indication that such contacts do not

Table 1 Database results:[a] mean H···A and C···A distances/Å in hydrogen bonds of different C—H donors to the acceptors O (all types),[b] N (all types)[b] and Cl^-. The chemically more important distance is H···A

Donor	O acceptors	N acceptors	Cl^- acceptors
Mean H···A distance			
$CHCl_3$	2.31(1) [222]	2.37(3) [32]	2.38(3) [16]
C≡C—H	2.40(2) [145]	2.40(6) [12]	2.56(4) [8]
CH_2Cl_2	2.492(8) [356]	2.53(2) [58]	2.59(3) [34]
N≡C—Me	2.567(9) [323]	2.59(1) [114]	2.72(3) [20]
DMSO	2.56(1) [203]	2.65(2) [18]	2.94 [3]
Acetone	2.60(1) [92]	2.64(3) [11]	2.98 [1]
Mean C···A distance			
$CHCl_3$	3.24(1) [222]	3.34(3) [32]	3.41(2) [16]
C≡C—H	3.35(1) [145]	3.36(5) [12]	3.58(4) [8]
CH_2Cl_2	3.347(8) [356]	3.45(2) [58]	3.54(2) [34]
N≡C—Me	3.40(1) [323]	3.47(2) [114]	3.68(3) [20]
DMSO	3.45(1) [203]	3.57(3) [18]	3.86 [3]
Acetone	3.48(1) [92]	3.63(2) [11]	3.88 [1]

[a] Standard uncertainties are given in parentheses (given only for $n_{H\cdots A} > 3$), data quantities $n_{H\cdots A}$ are given in brackets. Numerical values are given for normalized H-atom positions. [b] Excluded are N and O atoms directly bonded to metal atoms, or carrying a positive charge.

Table 2 Database results:[a] mean H···O and D···O distances/Å in hydrogen bonds of H_2O and $-NH_3^+$ donors to various O-atom acceptors

Acceptor	H_2O donor	C—NH_3^+ donor
Mean H···O distance		
P=O	1.871(7) [374]	1.856(7) [336]
H_2O	1.903(3) [3002]	1.918(8) [325]
>C=O	1.903(3) [3280]	1.918(6) [1035]
>S=O	1.906(7) [650]	1.936(12) [162]
C(sp^3)—OH	1.921(5) [795]	2.00(2) [130]
C—O—C	2.018(11) [307]	2.07(2) [72]
C—NO_2	2.158(12) [175]	2.19(2) [37]
M—CO	2.29 [2]	2.35 [3]
Mean C···O distance		
P=O	2.793(5) [374]	2.817(4) [336]
H_2O	2.808(2) [3002]	2.851(5) [325]
>C=O	2.823(2) [3280]	2.839(3) [1035]
>S=O	2.824(5) [650]	2.859(7) [162]
C(sp^3)—OH	2.834(4) [795]	2.90(1) [130]
C—O—C	2.894(8) [307]	2.94(1) [72]
C—NO_2	2.988(9) [175]	3.05(2) [37]
M—CO	3.04 [2]	3.24 [3]

[a] Standard uncertainties are given in parentheses (given only for $n_{H\cdots O} > 3$), data quantities $n_{H\cdots O}$ are given in brackets. Numerical values are given for normalized H-atom positions.

UM00011881
NOVARTIS EXHIBIT 1017
Novartis v. Regents, IPR2023-01346
Page 627 of 4460

Table 3 Database results:[a] mean H···O and C···O distances/Å in hydrogen bonds of different C—H donors and various O-atom acceptors

	$CHCl_3$	C≡C—H	CH_2Cl_2	N≡C–Me	DMSO	Acetone
Mean H···O distance						
P=O	1.97 [2]	2.02 [5]	2.27(7) [6]	2.40(4) [4]	— [0]	2.49 [2]
H_2O	2.11 [1]	2.11 [3]	2.16 [2]	2.65 [3]	2.73 [3]	2.61(9) [4]
>C=O	2.22(3) [52]	2.29(3) [40]	2.41(2) [123]	2.53(3) [42]	2.52(2) [73]	2.60(2) [67]
>S=O	2.25(6) [21]	2.50(6) [9]	2.40(4) [31]	2.57(3) [14]	2.57(2) [58]	2.53(8) [5]
$C(sp^3)$–OH	2.31(8) [5]	2.40(3) [31]	2.47(11) [4]	2.52(6) [11]	2.52(2) [73]	2.53(19) [4]
C—O—C	2.33(5) [16]	2.45(4) [19]	2.55(2) [57]	2.56(2) [56]	2.65(4) [4]	2.64(3) [14]
$C—NO_2$	2.52(6) [4]	2.63(3) [6]	2.48(4) [15]	2.59(3) [17]	2.60(3) [22]	2.57(5) [5]
M—CO	2.49(3) [20]	2.48(12) [4]	2.57(1) [176]	2.63(3) [21]	— [0]	2.61(2) [29]
Mean C···O distance						
P=O	3.03 [2]	3.06 [5]	3.19(7) [6]	3.36(5) [4]	— [0]	3.30 [2]
H_2O	3.09 [1]	3.15 [3]	3.22 [2]	3.41 [3]	3.61 [3]	3.57(11) [4]
>C=O	3.18(2) [52]	3.28(2) [40]	3.27(2) [123]	3.36(3) [42]	3.43(2) [73]	3.48(2) [67]
>S=O	3.22(5) [21]	3.45(5) [9]	3.31(4) [31]	3.36(4) [14]	3.47(2) [58]	3.39(11) [5]
$C(sp^3)$–OH	3.28(11) [5]	3.35(3) [31]	3.42(7) [4]	3.35(4) [11]	3.43(2) [73]	3.43(15) [4]
C—O—C	3.26(4) [16]	3.35(2) [19]	3.44(2) [57]	3.44(2) [56]	3.63(3) [4]	3.58(4) [14]
$C—NO_2$	3.48(7) [4]	3.45(4) [6]	3.33(4) [15]	3.25(5) [17]	3.47(3) [22]	3.31(5) [5]
M—CO	3.32(4) [20]	3.47(11) [4]	3.40(1) [176]	3.45(4) [21]	— [0]	3.52(3) [29]

[a] Standard uncertainties are given in parentheses (given only for $n_{H\cdots O} > 3$), data quantities $n_{H\cdots O}$ are given in brackets. Numerical values are given for normalized H-atom positions.

represent hydrogen bonds at all: for pure van der Waals contacts, one would expect to find the value 0.0 in Table 5).

Analogous observations can be made for the effect of donor strength on hydrogen bonds to different acceptors. For the strong acceptors P=O and H_2O, the H···O distances increase by *ca.* 0.5 Å if the donor is varied along the lines. For the weak acceptors NO_2 and M—CO, this variation is much smaller, only *ca.* 0.1 Å (Table 6).

It is of some interest to look at the top left corner of Table 3 which contains the strongest hydrogen bonds. It is not surprising that the shortest C—H···O hydrogen bond in the data sample (H···O = 1.88 Å) is formed by the combination of the strongest donor with the strongest acceptor considered, $Cl_3C—H\cdots O=P$. This crystal structure, an organometallic phosphine,[22] is shown in Fig. 1. The second $Cl_3C—H\cdots O=P$ hydrogen bond in the sample is somewhat longer, H···O = 2.06 Å, C···O = 3.14 Å.[23] Remarkably short C—H···O hydrogen bonds are also formed if the alkyne donor, C≡C—H, is combined with the strong acceptors O=P and H_2O; since examples have been discussed in the original literature, they need not be shown here again (ref. 8 for P=O, ref. 9 for H_2O acceptors). Finally, the combination of the chloroform donor and the water acceptor also leads to short C—H···O hydrogen bonding; the only example in crys-

Table 4 The structural data set. Numbers of C—H···O contacts analysed for the different acceptor types (summed over all donors)

Acceptor	$n_{C—H\cdots O}$
P=O	19
H_2O	16
>C=O	397
>S=O	138
$C(sp^3)$—OH	128
C—O—C	166
$C—NO_2$	69
M—CO	250

Table 5 Difference of mean H···O distances/Å to P=O and M—CO acceptors (using data in Table 3)

Donor	$(H\cdots O)_{M—CO}$ minus $(H\cdots O)_{P=O}$
$CHCl_3$	0.52
C≡C—H	0.46
CH_2Cl_2	0.30
N≡C—Me	0.22
Acetone	0.12

Table 6 Difference of the mean H···O distances of hydrogen bonds formed by $CHCl_3$ and acetone to given acceptors (using data in Table 3)

Acceptor	$(H\cdots O)_{CHCl_3}$ minus $(H\cdots O)_{acetone}$
P=O	0.52
H_2O	0.50
>C=O	0.38
>S=O	0.28
$C(sp^3)$—OH	0.22
C—O—C	0.31
$C—NO_2$	0.05
M—CO	0.12

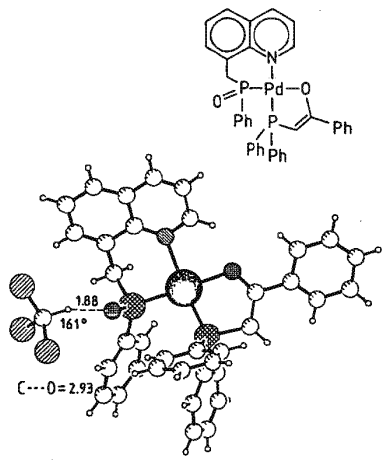


Fig. 1 The shortest hydrogen bond contained in the structural data set, donated from a $CHCl_3$ molecule to a P=O acceptor bonded to a Pd atom. Crystal structure determined by Braunstein and coworkers.[22] Numerical values are given for a normalized H-atom position

UM00011882
NOVARTIS EXHIBIT 1017
Novartis v. Regents, IPR2023-01346
Page 628 of 4460

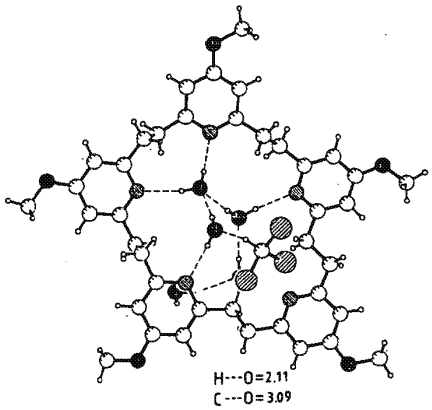


Fig. 2 The only hydrogen bond in the CSD which is donated from $CHCl_3$ to H_2O, occurring in a pyridinophane crystal structure containing one $CHCl_3$ and five water molecules. Crystal structure determined by Vögtle and co-workers.[24] Numerical values are given for a normalized H-atom position

tals is found in a pyridinophane structure containing chloroform as well as water molecules[24] (Fig. 2).

There has been some debate in the recent literature as to whether C—H···N interactions deserve generally the classification as 'hydrogen bonds'.[25–27] The data in Table 1 show that the effect of C—H donor strength in C—H···N contacts is the same as the effect in C—H···O contacts. It is of interest to see whether there is also an effect of N-atom acceptor strength. Because the number of relevant C—H···N contacts in the CSD is about a factor of 10 smaller than that of C—H···O contacts, a detailed analysis similar to that in Table 3 cannot be performed. However, at least for the acceptors C=N—C and N≡C—C, it can be shown that the influence of the acceptor type on H···N distances is similar for C—H···N and O—H···N hydrogen bonds, *i.e.* contacts to C=N—C are systematically shorter than to N≡C—C (Table 7).

Conclusions

It is shown that in intermolecular C—H···O contacts, the mean H···O separations depend strongly on the natures of both contact partners. Earlier studies on donor strengths of different C—H groups are confirmed.[10,13,14] The sequence of acceptor strengths found for conventional O/N—H···O hydrogen bonds (Table 2) is valid also for C—H···O interactions (Table 3). It is, furthermore, confirmed that even weakly polar C—H groups such as those in $-CH_3$ can donate, and that the O atoms of M—CO groups can accept (albeit weak) C—H···O hydrogen bonds.

Table 7 Database results:[a] mean H···N distances/Å in hydrogen bonds of different C—H donors and two kinds of N-atom acceptors. The conventional donor C(sp^3)—OH is included for comparison

	C—N=C	N≡C—C
$CHCl_3$	2.42(5) [16]	2.53 [2]
CH_2Cl_2	2.49(5) [13]	2.59(6) [8]
N≡C—Me	2.60(5) [10]	2.61(1) [112]
DMSO	2.61(2) [8]	2.67(9) [9]
C(sp^3)—OH	1.888(6) [418]	2.02(2) [35]

[a] Standard uncertainties are given in parentheses (given only for $n_{H\cdots O} > 3$), data quantities $n_{H\cdots O}$ are given in brackets. Numerical values are given for normalized H-atom positions.

It has been stated repeatedly that the influence of acceptor strength (or acceptor basicity) on C—H···O hydrogen bond distances is small compared to the influence of donor acidity.[2,16] The results in Table 3 suggest that this view should be modified: it appears that the variation range of mean donor–acceptor distances due to variation of donors (0.5 Å; Table 5) is just as broad as that due to variation of acceptors (0.5 Å; Table 6). Earlier observations have been made for the O-atom types that occur in organic crystals most frequently, such as C=O, C—OH and C—O—C. These represent only a small section of the range of acceptor strengths (and of O-atom basicities), so that the observed variation of mean H···O distances could be only small (*ca.* 0.1–0.2 Å). The early analyses of C—H donor strengths,[13,14] in contrast, did not suffer much from truncating the acidity range: structural data on strong ($CHCl_3$) and very weak ($-CH_3$) C—H donors are readily available in large quantities, so that a pronounced effect of donor strength became immediately obvious.

The functional groups and molecules in Table 3 cover neither the whole range of C—H acidities, nor the whole range of O-atom basicities. Considerably stronger carbon acids than $CHCl_3$ are known, such as HCN, $CH(NO_2)_3$, and $CH(CN)_3$. Notably, in the only crystal structure of a $CH(NO_2)_3$ complex, a very short C—H···O hydrogen bond is formed although the acceptor is one of the weaker types, C—O—C (H···O = 2.00 Å, C···O = 2.94 Å).[7] Similarly, stronger O-atom acceptors than P=O are known, such as $C-O^-$ in phenolate ions.[28] This suggests that the formation of even shorter C—H···O hydrogen bonds should be possible than the shortest known today. Experimentally, this could be realised for example by cocrystallisation of a P=O acceptor molecule such as triphenylphosphinoxide with a carbon acid stronger than $CHCl_3$.

Finally, it is noted that in the preceding short communication, the acceptor $-NO_2$ has been ranked at a high position between C=O and S=O.[16] This is peculiar because in O/N—H···O hydrogen bonds, the acceptor strength of the nitro group is poor.[21] In the present analysis, this ranking is not confirmed and the nitro acceptor is placed at the weak end of the scale, between C—O—C and M—CO. The previous ranking is interpreted as a statistical artifact.

Database Analysis

The study is based on the organic and organometallic crystal structures archived in the Cambridge Structural Database (CSD),[20] January 1998 update with 175093 entries. Only ordered and error-free structures with R-values < 0.08 were used. H-atom positions were normalized using the CSD default X—H bond lengths. M—CO acceptors are defined as carbonyl ligands bonded to exactly one transition metal atom. Carbonyl ligands bonded to more than one metal atom were not considered. O- and N-atom acceptors directly bonded to metal atoms were generally disregarded. D—H···A contacts were considered to distance cut-off values of 2.8 Å for D = C and A = O/N, 3.0 Å for D = C, A = Cl^-, and 2.4 Å for D = N/O and A = O. No angle cut-off criteria were used. Comments and warnings concerning the use of cut-off criteria have been published previously.[2] Because of their structural importance, two crystal structures were included that did not pass the quality criteria defined above: the partially disordered structure of the complex triphenylsilylacetylene–triphenylphosphinoxide containing short C≡C—H···O=P hydrogen bonds,[8] and a structure with R = 0.084 containing a Cl_3C—H···O=P hydrogen bond.[23] The total number of contacts included in Table 3 is 1183, compared to 311 in the corresponding table of the preliminary report.[16]

Acknowledgements

The author thanks the Minerva-Foundation (Munich) for

UM00011883
NOVARTIS EXHIBIT 1017
Novartis v. Regents, IPR2023-01346
Page 629 of 4460

awarding a fellowship at the Weizmann Institute of Science in the laboratory of Professor Joel L. Sussman. Professor Gautam R. Desiraju (Hyderabad) is thanked for discussions, in particular on C—H···N hydrogen bonds.

References

1 T. Steiner, *Cryst. Rev.*, 1996, **6**, 1.
2 T. Steiner, *Chem. Commun.*, 1997, 727.
3 G. R. Desiraju, *Acc. Chem. Res.*, 1991, **24**, 290.
4 G. R. Desiraju, *Acc. Chem. Res.*, 1996, **29**, 441.
5 M. C. Wahl and M. Sundaralingam, *Trends Biol. Sci.*, 1997, **22**, 97.
6 T. Steiner, B. Lutz, J. van der Maas, N. Veldman, A. M. M. Schreurs, J. Kroon and J. A. Kanters, *Chem. Commun.*, 1997, 191.
7 H. Bock, R. Dienelt, H. Schödel and Z. Havlas, *J. Chem. Soc., Chem. Commun.*, 1993, 1792.
8 T. Steiner, J. van der Maas and B. Lutz, *J. Chem. Soc., Perkin Trans. 2*, 1997, 1287.
9 B. M. Kariuki, K. D. M. Harris, D. Philp and J. M. A. Robinson, *J. Am. Chem. Soc.*, 1997, **119**, 12679.
10 V. R. Pedireddi and G. R. Desiraju, *J. Chem. Soc., Chem. Commun.*, 1992, 988.
11 T. Steiner and G. R. Desiraju, *Chem. Commun.*, 1998, 891.
12 T. Steiner, B. Lutz, J. van der Maas, A. M. M. Schreurs, J. Kroon and M. Tamm, *Chem. Commun.*, 1998, 171.
13 G. R. Desiraju, *J. Chem. Soc., Chem. Commun.*, 1989, 179.
14 G. R. Desiraju, *J. Chem. Soc., Chem. Commun.*, 1990, 454.
15 T. Steiner, *Acta Crystallogr., Sect. B*, 1998, **54**, 456.
16 T. Steiner, *J. Chem. Soc., Chem. Commun.*, 1994, 2341.
17 G. A. Jeffrey and W. Saenger, *Hydrogen Bonding in Biological Structures*, Springer, Berlin, 1991.
18 D. Braga, F. Grepioni, K. Biradha, V. R. Pedireddi and G. R. Desiraju, *J. Am. Chem. Soc.*, 1995, **117**, 3156.
19 D. Braga and F. Grepioni, *Acc. Chem. Res.*, 1997, **30**, 81.
20 F. H. Allen and O. Kennard, *Chem. Des. Autom. News*, 1993, **8**, 1.
21 F. H. Allen, C. A. Baalham, J. P. M. Lommerse, P. R. Raithby and E. Sparr, *Acta Crystallogr., Sect. B*, 1997, **53**, 1017.
22 F. Balegroune, P. Braunstein, D. Grandjean, D. Matt and D. Nobel, *Inorg. Chem.*, 1988, **27**, 3320.
23 D. G. Gilheany, D. A. Kennedy, J. E. Malone and B. J. Walker, *J. Chem. Soc., Chem. Commun.*, 1984, 1217.
24 F. Vögtle, G. Brodesser, M. Nieger and K. Rissanen, *Rec. Trav. Chim. Pays-Bas*, 1993, **112**, 325.
25 R. Taylor and O. Kennard, *J. Am. Chem. Soc.*, 1982, **104**, 5063.
26 F. A. Cotton, L. M. Daniels, G. T. Jordan IV and C. Murillo, *Chem. Commun.*, 1997, 1673.
27 M. Mascal, *Chem. Commun.*, 1998, 303.
28 I. Majerz, Z. Malarski and L. Sobczyk, *Chem. Phys. Lett.*, 1997, **274**, 361.

Received in Cambridge, UK, 1st June 1998;
Paper 8/04121K

UM00011884
NOVARTIS EXHIBIT 1017
Novartis v. Regents, IPR2023-01346
Page 630 of 4460

Crystallography Reviews, 2004, Vol. 10, No. 1, pp. 45–56

Taylor & Francis
Taylor & Francis Group

AUTOMATION OF SOLID FORM SCREENING PROCEDURES IN THE PHARMACEUTICAL INDUSTRY – HOW TO AVOID THE BOTTLENECKS

RICHARD STOREY[a,*], ROBERT DOCHERTY[a], PAUL HIGGINSON[a], CHRIS DALLMAN, CHRIS GILMORE[b], GORDON BARR[b] and WEI DONG[b]

[a]*Pharm R&D, Pfizer Global R&D, Ramsgate Road, Sandwich, Kent CT13 9NJ, UK;*
[b]*Department of Chemistry, University of Glasgow, Glasgow G12 8QQ, Scotland, UK*

Solid form selection is one of the key milestones in the development of any new small molecule drug candidate. It is critical not only from a regulatory perspective but also from a drug substance manufacturing and drug product-processing viewpoint. High throughput systems provide a significant increase in the number and diversity of experiments performed on a given compound, and are becoming a central feature of drug development, especially in areas concerned with solid form selection. This paper reports our automation of the polymorph screening procedure in combination with automated isolation of samples. Particular focus is placed on the analysis by high throughput PXRD with associated strategies for analysis, clustering, pattern classification, and visualization

Keywords: Polymorphism; Automated crystallization; High throughput powder diffraction; Automated pattern comparison and classification

Contents

1. INTRODUCTION 46
2. AUTOMATION OF SCREENING EXPERIMENTATION 47
3. LIQUID HANDLING SYSTEM 48
4. ANALYTICAL TOOLS 50
5. PATTERN COMPARISON AND VISUALISATION SOFTWARE 51
6. CONCLUSIONS 54
References 56

*Corresponding author.

ISSN 0889-311X print: ISSN 1476-3508 online © 2004 Taylor & Francis Ltd
DOI: 10.1080/08893110410001664846

UM00011885
NOVARTIS EXHIBIT 1017
Novartis v. Regents, IPR2023-01346
Page 631 of 4460

1. INTRODUCTION

Solid form selection is one of the key milestones in the development of any new small molecule drug candidate. It is critical from not only a drug substance manufacturing standpoint but also from a drug product processing, performance and stability perspective. Regulatory authorities dictate that the solid form of a compound is fully understood. DeCamp (2001) and Byrn *et al.* (1999, 2002) provided excellent overviews of the solid-state chemistry of drug molecules. There is potential for considerable delays during the development or even post-approval issues of a compound, should changes in the solid form be observed, e.g. the anti-viral compound Norvir™ (Chemburker *et al.*, 2000). The importance of intellectual property around polymorphs are well documented (Glaxo Group Limited *versus* Novopharm Limited). The effects on properties of a different solid form of a pharmaceutical compound are summarised in Table I.

Despite much work and progress by leading academics (Desiraju, 1991; Davey, 1997; Gavezzotti, 1997; Bernstein, 2002), there remains a lack of a structural rationale or a theoretical treatment for predicting such observations. Recently Stahly (2003) has shown that of the numerous polymorph screens carried out

- 87% have more than one form
- 51% have multiple polymorphs
- 37% have hydrates
- 31% are solvates

It has been proposed by McCrone (1965) that the number of polymorphic forms known for a given molecule is proportional to the time, money and experiments spent on that compound. Thus by increasing the number of experiments performed during the development of a drug molecule it will be more likely that the large majority of different polymorphs will be identified as shown in Table II. Pharmaceutical companies continue to strive for greater robustness in solid form selection without a significant increase in the resource/timelines required to achieve

TABLE I Summary of properties affected by different solid forms

Drug	*Processing*	*Drug product*
Yield	Milling	Solubility
Filtration	Mixing	Dissolution
Washing	Granulation	Freeze-drying
Habit	Flow	Syringeability
Drying (especially hydrates)	Tabletting	
Intellectual property rights		

TABLE II Summary of number of experiment performed on different compounds in the recent literature

API	*Crystallisations*	*Results*	*Ref.*
Acetaminophen	10 000	Elusive form III identified and characterised beyond debate	Peterson *et al.* (2002)
Norvir	2000	Three new forms identified	Morisette *et al.* (2003)
Sumatriptan succinate	2000	Two new polymorphs identified for material not thought to be polymorphic	Almarsson (2003)
30 Different API	25 000	108 New forms identified	Wu and Desrosiers (2003)

UM00011886
NOVARTIS EXHIBIT 1017
Novartis v. Regents, IPR2023-01346
Page 632 of 4460

this desired level of confidence. Thus there is a definite need for automated procedures during solid form selection. These procedures have been shown to be fruitful in the identification of new forms and recent publications have illustrated the value of such technologies.

During the development of an automated solid form screening system some basic considerations must be taken into account. Firstly, they should automate the best practices and regulatory guidance and not change or compromise the science or process to accommodate ease of automation. Secondly, the design of the actual screen must take into account the potential solid-state chemistry of the drug, the likely intermolecular interactions with solvent, the process conditions and the type of dosage form. Thirdly, single characterisation methods are likely to be a risky proposition and multiple analytical techniques should be employed. Finally, the technology must be specifically designed to eliminate bottlenecks and allow rapid analysis of large quantities of data.

Robotic platforms are traditionally based around liquid handling systems and have provided an increase in the throughput in the screening of novel compounds in a drug discovery environment. During the late 1990s the potential was recognised for utilising these technologies to aid in the preparation, screening and characterisation of salts, polymorphs and hydrates of new chemical entities. As within the chemical discovery environment, simply automating sample preparation will only shift the bottleneck further down the process. To ensure a smooth workflow a fully integrated experimental design, solid form preparation, sampling, analysis and data review strategy are required.

This article reports our automation of the polymorph screening procedure in combination with automated isolation of samples with a particular focus on their analysis by powder X-ray diffraction and pattern classification, analysis and visualisation.

2. AUTOMATION OF SCREENING EXPERIMENTATION

The development of bespoke robotic platforms to perform crystallisations of many samples using different techniques with automated sample isolation and analysis has proved challenging. The majority of robotic systems are focussed on the analysis of liquid preparations and, to allow for solid form analysis, bespoke preparation robots have been specifically designed in collaboration with key partners. These systems have to be as flexible as possible ensuring that their role is not limited and they provide a range of crystallisation environments using equipment comparable to those utilised on a larger scale. This will provide potential for different solid forms to be formed and isolated as well as the ability to challenge the robustness of a process in an attempt to avoid issues on scaling up the process. The robotic designs have focussed on maximising experimental diversity given the limited amount of bulk available at a particular stage in the development process. Figure 1 summarises the different robotic systems, the amount of bulk required to run these systems and how the samples from each of the robots are analysed using common techniques.

Analysis of the samples produced by the robotic workstations provides information on the solid form of the materials produced using accepted solid-state techniques. Of these techniques PXRD provides the 'gold standard' for solid form analysis. Other techniques such as Raman and image analysis are also of great

UM00011887
NOVARTIS EXHIBIT 1017
Novartis v. Regents, IPR2023-01346
Page 633 of 4460

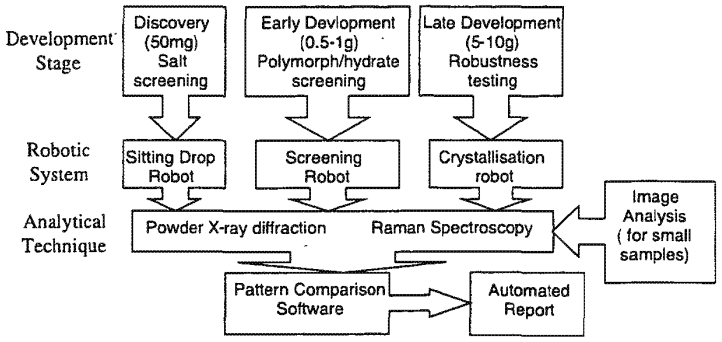


FIGURE 1 Robotic systems available at different stages in development.

value and have been incorporated into a number of automated systems (Peterson *et al.*, 2002; Wu and Desrosiers, 2002). Due to the difficulty of automated sample preparation, fully robotic thermal analysis remains a challenge. However, recent advances by external technology vendors using a combination of a hot stage and optical microscopy has allowed the melting point of compounds to be automatically assessed (Wu and Desrosiers, 2002).

With the introduction of high throughput screening systems the analysis of the data produced is a key concern. Pattern comparison packages have permitted large datasets to be analysed with highly visual interactive output allowing trends in the data to be observed, interpreted and new experiments designed. Such data examination strategies allow the user to relate sample generation condition to polymorphic form, enabling critical parameters in the preparation and edges of failure to be identified.

3. LIQUID HANDLING SYSTEM

The robotic system utilised to perform the polymorph screening procedures is shown in Figs. 2 and 3. It has been specifically designed to allow crystallisations using a realistic scale and procedures that are commonly used for the production of bulk pharmaceuticals. The robotic system is extremely flexible allowing multiple isolations from single reactors as well as a wide range of crystallisation conditions using commonly used crystallisation techniques, e.g. cooling, anti-solvent precipitation and evaporation.

The robotic system has the capability of producing crystallisations from 96 reactors of volume *ca.* 2 ml, in a stirred environment with a wide range of solvents and a wide variety of cooling/stirring regimes as the reactors are separated into eight different zones each of which can be independently heated/cooled/stirred without any cross-talk to adjacent zones. Multiple samples can be taken from the system, which will allow up to 384 samples to be produced from *ca.* 5 g of bulk.

The introduction of a multiple reactor-based system can quite quickly overwhelm any manual analytical processes. Hence a system, which automatically isolates the samples in a format ideal for analysis, had to be devised. As metastable polymorphs have the potential to ripen if left for long periods of time in contact with solvent, it is required

UM00011888
NOVARTIS EXHIBIT 1017
Novartis v. Regents, IPR2023-01346
Page 634 of 4460

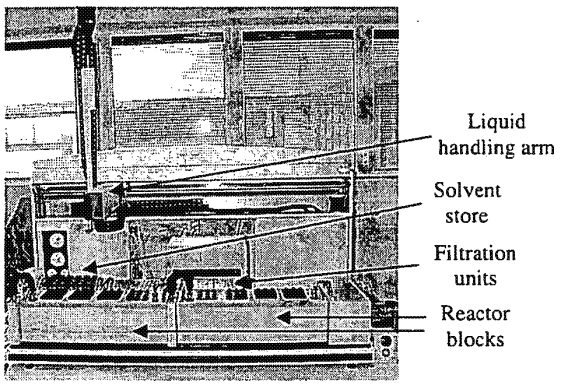


FIGURE 2 Robot pictures.

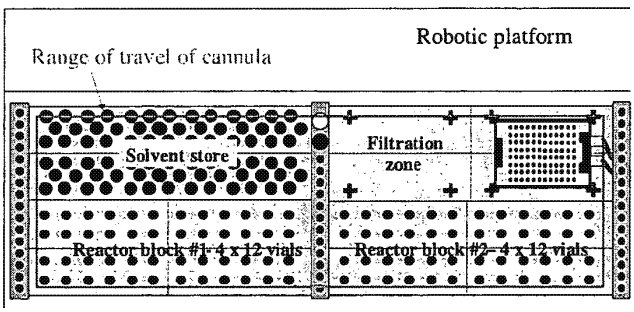


FIGURE 3 Schematic of robotic bed.

to halt any further ripening by isolation of the solids from the solvents using filtration. Once the crystallisation procedure has been completed the samples are isolated from the reactors using a wide bore cannula and deposited on a specifically designed filtration plate. This plate isolates the solids from the reaction slurry by vacuum, onto a substrate ideal for automated analysis, and allows evaporation of the filtrate to dryness producing a further sample, also in a format ideal for automated analysis. The design of the filtration plates utilises 'off the shelf' components ensuring that samples can be easily retained for future reference with barcodes fitted to all plates to maintain sample integrity.

During experimentation the robotic system records a large number of parameters. The ability to recall these parameters to investigate how a sample has been generated is key to the success of the system. In our laboratory we output selected experimental parameters using a specifically designed macro. This exports sample information in a spreadsheet format, which is easily incorporated into the analytical techniques so that processing parameters can be quickly identified. Other automation technologies utilise the storage of experimental design, sample parameters and a results database centrally which allows multiple analytical techniques to access sample preparation information.

UM00011889
NOVARTIS EXHIBIT 1017
Novartis v. Regents, IPR2023-01346
Page 635 of 4460

4. ANALYTICAL TOOLS

Automated sample generation and isolation requires the need for automated analysis to avoid bottlenecks. As mentioned above, single analytical tools are a risky option and multiple techniques provide an extra degree of confidence in the results. Of these techniques PXRD provides the method of choice for solid form analysis. Recent developments in the use of two-dimensional detectors, motorised stages and laser-guided autofocus have dramatically reduced the time for analysis without a major compromise on quality, although peak widths tend to be larger than conventional systems. High throughput software equipped with bar-code readers allows plate dimensions and sample identities to be automatically imported into the data-analysis ensuring sample integrity (Figs. 4 and 5).

Due to the rapid data collection and small sample requirements with the addition of motorised stages and autofocus routines, Raman spectroscopy has also successfully been incorporated into solid form analysis in the automation laboratory (Peterson, 2002). The incorporation of polarised light image analysis with Raman spectroscopy has provided an ideal opportunity to locate automatically and subsequently analyse

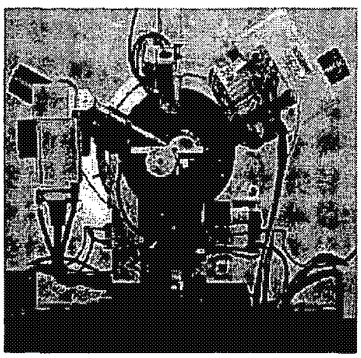


FIGURE 4 Bruker GADDS X-ray diffractometer.

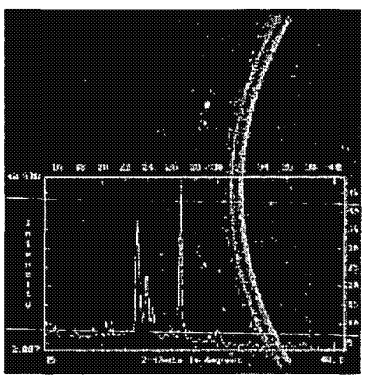


FIGURE 5 Output of a crystalline material analysed by GADDS.

UM00011890
NOVARTIS EXHIBIT 1017
Novartis v. Regents, IPR2023-01346
Page 636 of 4460

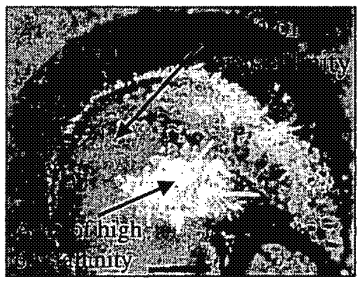


FIGURE 6 Image analysis picture showing areas of high and low crystallinity.

extremely small samples such as those produced from vapour diffusion with minimal user input. In these experiments the samples (as shown in Fig. 6) have areas of high and low crystallinity. Using polarised light microscopy and image analysis software it has been possible to locate the crystalline zones and record their co-ordinates. These crystals can be subsequently relocated, with the help of graticules fitted to the sample well plates for Raman spectroscopic analysis.

5. PATTERN COMPARISON AND VISUALISATION SOFTWARE

Due to the large amounts of data being generated it will quickly become impossible to manually view and interpret the results from automated screens. Furthermore the data collected from high throughput systems have associated problems:

1. Possible poor signal-to-noise ratio.
2. Broad peaks with variable shapes.
3. Strong backgrounds.
4. Problems with amorphous samples.
5. Inherent preferred orientation effects.

The incorporation of robust pattern comparison software and associated visualisation tools are key to interpreting the results and, indeed, without such tools the hardware is of very limited value. Patterns can be compared to each other using a weighted mean of parametric and non-parametric correlation coefficients (the Pearson and Spearman coefficients respectively) using the whole pattern, i.e. every measured data point (Gilmore *et al.*, 2003). From this a correlation matrix, $\boldsymbol{\rho}$, can be derived. This matrix can be converted to a distance matrix, $\mathbf{d}$, via

$$\mathbf{d} = 0.5(1.0 - \boldsymbol{\rho}) \tag{1}$$

Thus highly correlated patterns with large $\boldsymbol{\rho}$ gives small corresponding distance and vice-versa. We can use the matrices $\mathbf{d}$ and $\boldsymbol{\rho}$ as an input to a set of clustering and multivariate data analysis methods (Barr *et al.*, 2003) with associated visualisation tools.

Cluster analysis can arrange the patterns into distinct clusters and display them as a dendrogram. (For a useful introduction to this methodology, see Gordon, 1999.) This simplifies the process of examining the diffraction patterns since all the patterns in a given cluster should be very similar. A typical dendrogram is shown in Fig. 7.

UM00011891
NOVARTIS EXHIBIT 1017
Novartis v. Regents, IPR2023-01346
Page 637 of 4460

In this case we have 21 samples containing five polymorphs and two mixtures. Each pattern begins at the bottom of the plot as a separate class, and these amalgamate in stepwise fashion linked by horizontal tie bars. The height of the tie bar represents a similarity measure as measured by the relevant distance. The samples 20 and 21, believed to be mixtures, are the least tightly linked.

It is necessary to estimate the number of clusters present and so 'cut' the dendrogram, i.e. draw a horizontal line across the graph so that all the tie lines above the cut line are ignored and only the connections below this line are retained. Accurately determining cluster numbers is an unsolved problem, but there are tools which can help. We use estimates based on the eigen-analysis of the correlation and related matrices integrated with techniques based on cluster analysis, especially techniques developed by Goodman and Kruskal (1954), Calinski and Harabasz (1974) and Milligan and Cooper (1985). Again, space precludes any detailed discussion, and the reader is referred to Barr *et al.* (2003) for further information.

The cut line is shown on the dendrogram in Fig. 7, and defines the chosen clusters. The colours given to each cluster can be translated into pie charts, which give the contents of each well in the data measurement system; this is shown in Fig. 8.

The data can also be summarised using three-dimensional plots derived from either metric multi-dimensional scaling or three-dimensional score plots from principal component analysis. There is insufficient space here to discuss these methods but there is a good introduction by Jobson (1992). The metric multi-dimensional scaling plot corresponding to the polymorph data is shown in Fig. 9.

Each sphere in this plot represents a powder diffraction sample; the further the distance apart of the spheres the greater the corresponding distance as measured by Eq. (1) and the lower the corresponding correlation. It can be seen that the patterns form natural clusters. The dendrogram had some evidence that patterns 20 and 21 were less well-linked than others: the sphere corresponding to pattern 21 is isolated from other patterns. However, that of pattern 20 seems quite close to another cluster. Ambiguities of this sort are to be expected, and it is because of this that a raft of techniques is required for high throughput data analysis.

We can clarify the situation further by investigating the possibility of mixtures of polymorphs being present. To do this we define for each cluster with more than one member, the most representative member, i.e. that member which has the minimum mean distance from every other sample in the cluster. These samples are used to generate a pure phases database. Every pattern in the original data set is matched against the entries in this database, and if a significant correlation is found the data are analysed quantitatively via a least-squares procedure using singular value decomposition methods (Gilmore *et al.*, 2003). The results are best displayed in pie chart in Fig. 10.

Patterns 20 and 21 can be seen to correspond to mixtures. We can conclude that our 21 samples contain five polymorphs and two mixtures. All this has taken less than 1 min of computer time on a 2.5 GHz PC.

Amorphous samples are an inevitable consequence of high throughput experiments, and need to be handled correctly. To do this we estimate the total background for each pattern and integrate its intensity; at the same time we also calculate the integrated intensity of the non-background signal. If the ratio of the two falls below a pre-set limit (usually 5%) the sample is treated as amorphous. The distance matrix is then

UM00011892
NOVARTIS EXHIBIT 1017
Novartis v. Regents, IPR2023-01346
Page 638 of 4460

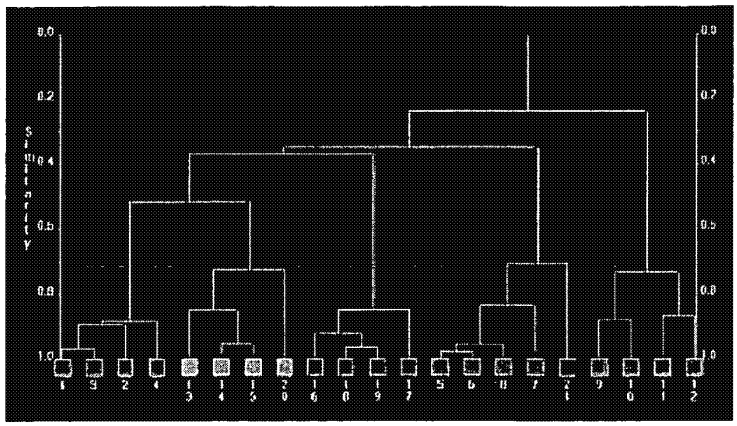


FIGURE 7 A typical dendrogram arising from the cluster analysis of 21 pharmaceutical powder data patterns involving five polymorphs and two mixtures.

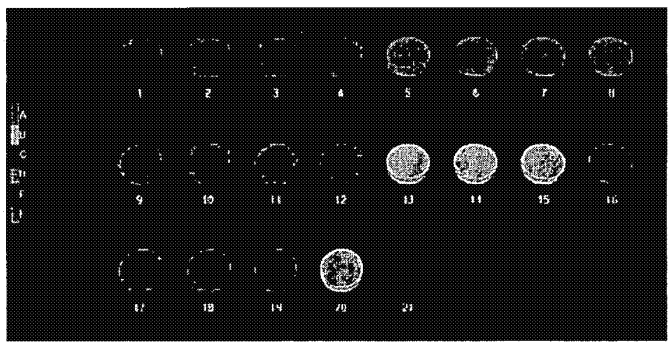


FIGURE 8 Pie chart showing the well contents using colours derived from the dendrogram in Fig. 5.

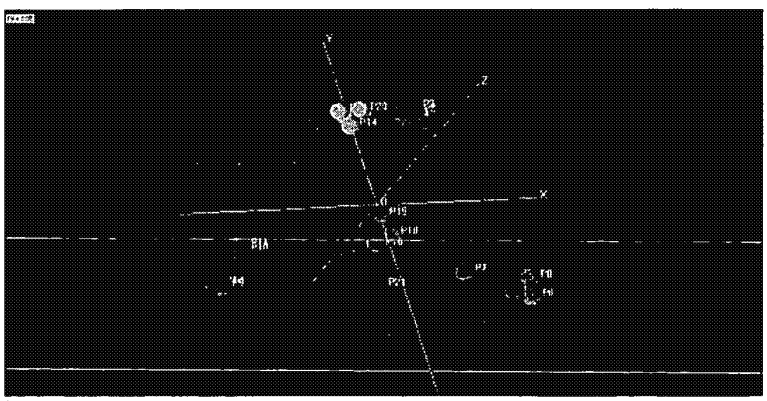


FIGURE 9 A metric multi-dimensional scaling plot of the polymorph data used to generate the dendrogram in Fig. 5. The colours match those of the dendrogram.

UM00011893
NOVARTIS EXHIBIT 1017
Novartis v. Regents, IPR2023-01346
Page 639 of 4460

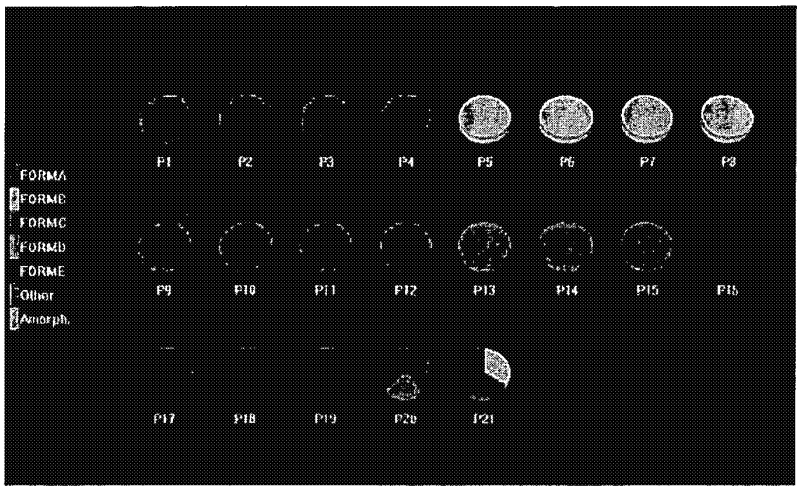


FIGURE 10 The pie chart corresponding to Fig. 3 but using a database of most representative as a reference followed by quantitative phase analysis.

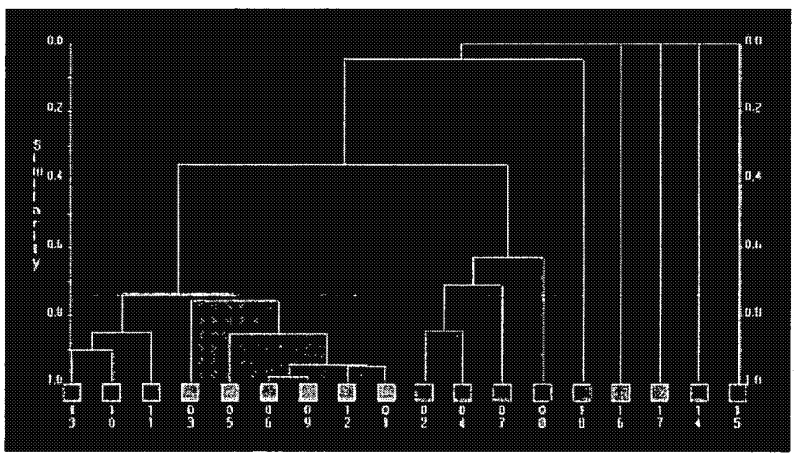


FIGURE 11 A typical dendrogram with amorphous data present. The five amorphous patterns are isolated at the right hand end of the dendrogram and thus clearly identified.

modified so that each amorphous sample is given a distance of 1.0 from every other sample, and a correlation coefficient of zero. This automatically excludes the samples from the clustering until the last amalgamation steps, and also limits their effect on the estimation of the number of clusters. A typical dendrogram with five amorphous samples present is shown in Fig. 11.

This methodology of pattern matching and data visualisation should work with any one-dimensional data set. Techniques which should be amenable to this approach thus include Raman, IR and solid-state NMR spectroscopies. Preliminary tests on Raman data have proved encouraging.

UM00011894
NOVARTIS EXHIBIT 1017
Novartis v. Regents, IPR2023-01346
Page 640 of 4460

As part of the data import process the sample preparation details are also included in the display. This allows rapid access to how particular forms have been manufactured. It also allows the operator to investigate which of the variables investigated in a screen are important in the production of a particular solid form and the edges of failure in a process.

6. CONCLUSIONS

High throughput systems provide a significant increase in the number of experiments performed on a given system, and are becoming a central feature of drug research especially in areas concerned with crystallinity and polymorphs. Properly designed robotic systems coupled with suitable powder X-ray and Raman facilities maximise the amount of data produced with the amount of bulk available. In addition, a correctly implemented automated sample preparation and analysis procedure ensures no sample backlog, and the automatic transfer of sample information maintains sample integrity. The design of high throughput systems must ensure minimal user input in an attempt to avoid bottlenecks, and the automation of best practices using current theory and state of the art technology is essential. There is still a role for manual experimentation – high throughput is not a substitute for thinking!

An essential component of the process outlined here is a suitable software that can provide sound statistical techniques for interpreting the large amounts of data produced. These are not infallible, and visualisation techniques can assist in identifying problem areas that need further investigation. The goal here is, for example, to take 1000 or more patterns and analyse them such that 95% can be effectively ignored, and the experimenter can then focus on the remaining 5% whose behaviour seems anomalous. There is no doubt that with experience, and the increasing prevalence of robotic systems, the software will become increasingly sophisticated.

The high throughput nature of these systems, linked with the data generated by manual screening, informatics and theoretical considerations, can ultimately be used for the production of an expert system. This will allow subsequent polymorph screening to be guided using previous learning, ensuring extra robustness in the screening procedures and providing increased confidence on scale-up.

Acknowledgements

CJG and GB wish to acknowledge support from Pfizer Pharmaceutical Sciences Global R&D, UK for data, many useful discussions and suggestions, and for pioneering and supporting the software project, and the Ford Motor Company, Detroit for funding earlier work, especially Charlotte Lowe-Ma whose input and support has been invaluable.

References

Almarsson (2003). Orn Application of HT Crystallisation Technology to the Study of Polymorphism of Pharmaceuticals at ACS Prospectives: Polymorphism in Crystals, Fundamentals, Predictions and Industrial Practice, February 23–26.

UM00011895
NOVARTIS EXHIBIT 1017
Novartis v. Regents, IPR2023-01346
Page 641 of 4460

Barr, G., Dong, W. and Gilmore, C.J. (2004). High throughput powder diffraction: II applications of clustering methods and multivariate data analysis. *J. Appl. Crystallogr.*, **37**, in press.
Bernstein, J. (2002). *Polymorphism in Molecular Crystals*. Oxford Science Publications.
Byrn, S.R., Pfeiffer, R. and Stowell, J.G. (1999). *Solid State Chemistry of Drugs*, SSCI Inc.
Byrn, S.R., Pfeiffer, R. and Stowell, J.G. (2002 Fall). *Am. Pharm. Rev.*
Calinski, T. and Harabasz, J. (1974). *Commun. Statistics*, **3**, 1–27.
Chemburker, S.R., Bauer, J., Deming, K., Spiwek, H., Patel, K., Morris, J., Henry, R., Spanton, S., Dziki, W., Porter, W., Quick, J. Bauer, P., Donaubauer, J., Narayananan, B.A., Soldani, M., Riley, D. and McFarland, K. (2000). *Organic Process Res. Dev.*, **4**, 413–417.
Davey, R.J., Blagden, N., Potts, G.D. and Docherty, R. (1997). *J. Am. Chem. Soc.*, **119**, 1767–1772.
DeCamp, W.H. (2001). *Am. Pharm. Rev.*
Desiraju, G.R. (1991). *Chem. Commun.*, 426.
Gavezzotti, A. (1997). *Theoretical Aspects and Computer Modelling of the Molecular Solid State*. New York: John Wiley and Sons.
Gilmore, C.J., Barr, G. and Paisley, J. (2004). High throughput powder diffraction: I full-profile qualitative and quantitative powder diffraction pattern analysis. *J. Appl. Crystallogr.*, **37**, in press.
Glaxo Inc. and Glaxo Group Limited versus Novopharm Limited No 5:94-CV-527-BO(1) 931 F. Supp 1280 and 96-1466 DCT 94-CV-527.
Goodman, L.A. and Kruskal, W.H. (1954). *J. Am. Stats. Assoc.*, **49**, 732–764.
Gordon, A.D. (1999). *Classification*, 2nd Edn. Boca Raton, FL: Chapman and Hall/CRC.
Jobson (1992). *Applied Multivariate Data Analysis Volume II: Categorical and Multivariate Methods*. New York: Springer.
McCrone, W. (1965). *Polymorphism, Physics and Chemistry of the Organic Solid State*, Vol. 2, pp. 725–767. New York: Wiley Interscience.
Milligan, G.W. and Cooper, M.C. (1985). *Psychometrika*, **50**, 159–179.
Morissette, S.L., Soukasene, S., Levinson, D., Cima, M.J. and Almarsson, O. (2003). *Proc. Natl. Acad. Sci. USA*, **100**, 2180–2184.
Peterson, M.L., Morissette, S.L., McNulty, C., Goldsweig, A., Shaw, P., LeQuesne, M., Monagle, J., Encina, N., Marchionna, J., Johnson, A., Gonzalez-Zugasti, J., Lemmo, A.V., Ellis, S.J., Cima, M.J. and Almarsson, O. (2002). *J. Am. Chem. Soc.*, **124**, 10958–10959.
Stahly G.P (2003). SSCI Inc. 'Rational Exploration Of Solid Space' at ACS Prospectives: Polymorphism in Crystals, Fundamentals, Predictions and Industrial Practice Feb 23–26.
Wu, E. and Desrosiers, P. (2002 June 9–14). '*High Throughput Screening in Pre-formulation Polymorph and Salt Selection Studies*', IWPCPS-3. Oxford, UK.
Wu, E. and Desrosiers, P. (2003). 'High Throughput Screening in Pre-formulation Polymorph and Salt Selection Studies' at ACS Prospectives: Polymorphism in Crystals, Fundamentals, Predictions and Industrial Practice, February 23–26.

UM00011896
NOVARTIS EXHIBIT 1017
Novartis v. Regents, IPR2023-01346
Page 642 of 4460

This Page is Inserted by IFW Indexing and Scanning Operations and is not part of the Official Record

BEST AVAILABLE IMAGES

Defective images within this document are accurate representations of the original documents submitted by the applicant.

Defects in the images include but are not limited to the items checked:

- ☐ BLACK BORDERS
- ☐ IMAGE CUT OFF AT TOP, BOTTOM OR SIDES
- ☐ FADED TEXT OR DRAWING
- ☐ BLURRED OR ILLEGIBLE TEXT OR DRAWING
- ☐ SKEWED/SLANTED IMAGES
- ☐ COLOR OR BLACK AND WHITE PHOTOGRAPHS
- ☐ GRAY SCALE DOCUMENTS
- ☐ LINES OR MARKS ON ORIGINAL DOCUMENT
- ☐ REFERENCE(S) OR EXHIBIT(S) SUBMITTED ARE POOR QUALITY
- ☐ OTHER: _____

IMAGES ARE BEST AVAILABLE COPY.
As rescanning these documents will not correct the image problems checked, please do not report these problems to the IFW Image Problem Mailbox.

ELSEVIER

Journal of Molecular Structure 416 (1997) 145–160

Journal of
MOLECULAR
STRUCTURE

Molecular structures and hydrogen bonding in the 1 : 1 and 1 : 2 complexes of pyridine betaine with 2,6-dichloro-4-nitrophenol; an example of strongly coupled hydrogen bonds, O–H···O=C–O–H···O⁻

Mirosław Szafran[a,*], Zofia Dega-Szafran[a], Grzegorz Buczak[a], Andrzej Katrusiak[a,b], Marek J. Potrzebowski[c], Anna Komasa[a]

[a]*Faculty of Chemistry, A. Mickiewicz University, ul Grunwaldzka 6, 60780 Poznań, Poland*
[b]*Instrumental Laboratory, A. Mickiewicz University, 60780 Poznań, Poland*
[c]*Centre of Molecular and Macromolecular Studies, Polish Academy of Sciences, 90363 Łódź, Poland*

Received 24 October 1996; accepted 22 November 1996

Abstract

Crystalline complexes of pyridine betaine (PBET) with one and two molecules of 2,6-dichloro-4-nitrophenol (DCNP) were prepared and characterized by single-crystal X-ray analysis and Fourier transform IR (FTIR), Raman, ^{13}C CP/MAS NMR and UV spectroscopies. Both complexes are monoclinic, space group $P2_1/c$, with $Z = 4$. In PBET·DCNP, the proton from DCNP is transferred to PBET and both residues are linked by an O–H···O⁻ hydrogen bond of length 2.419(3) Å and angle 165(4)°. In PBET·$(DCNP)_2$, the COOH group is engaged in two hydrogen bonds, resulting in a short O–H···O⁻ bond of length 2.452(4) Å and angle 178(4)° and a long C=O···H–O bond of length 2.623(4) Å and angle 160(6)°. The ^{13}C NMR spectra in the solid state show signals at 167.7 and 170.2 ppm due to the carboxyl group in PBET·DCNP and PBET·$(DCNP)_2$ respectively. The powdered FTIR spectrum of PBET·DCNP shows a broad absorption with a maximum at 806 cm^{-1} tentatively assigned to ν_{OH}. Although in PBET·$(DCNP)_2$ the analogous hydrogen bond is longer than in the 1 : 1 complex, the absorption is shifted to lower wavenumbers (773 cm^{-1}). The absorption due to the longer hydrogen bond is at 2832 cm^{-1} and is shifted towards higher wavenumbers relative to the analogous hydrogen bond in the complex of PBET with two molecules of pentachlorophenol (PBET·$(PCP)_2$; O···O = 2.582(6) and 2.611(6) Å; ν_H = 2725 cm^{-1}). The observed absorption shifts suggest that, in PBET·$(DCNP)_2$, the hydrogen bonds perturb each other. Two peaks near 300 and 420 nm in the UV spectra of the title complexes in acetonitrile confirm the presence of phenol and phenolate residues in equilibrium. © 1997 Elsevier Science B.V.

Keywords: 2,6-Dichloro-4-nitrophenol (DCNP); Hydrogen bonding; Molecular structure; PBET–DCNP complexes; Pyridine betaine (PBET)

1. Introduction

Betaines, inner salts and zwitterionic compounds, containing a carboxylate group and a quaternary ammonium group, are important from a biological point of view, since they are widely distributed in

* Corresponding author. Tel.: +48 61 699181; fax: +48 61 658008; e-mail: szafran@chem.amu.edu.pl

Dedicated to Professor G. Zundel on the occasion of his 65th birthday.

0022-2860/97/$17.00 © 1997 Elsevier Science B.V. All rights reserved
PII S0022-2860(97)00041-0

UM00011898
NOVARTIS EXHIBIT 1017
Novartis v. Regents, IPR2023-01346
Page 644 of 4460

plants and animal tissue as products of the methylation of α- or ω-amino acids or pyridine carboxylic acids in the presence of methylating agents such as methionine or S-adenylomethionine [1–3]. Betaines can also be biologically demethylated by transferring their methyl group to L-homocysteine [1].

Due to their basic properties, betaines form complexes (adducts) with various acids and cations, exhibiting phase transitions with ferroelectric, antiferroelectric and ferroelastic behaviour [4,5]. Numerous structural X-ray analyses of betaine compounds of this type, such as $Me_3NCH_2CO_2 \cdot H_2O$ [6], $C_5H_5NCH_2CO_2$ [7], $(Me_3NCH_2CO_2H)Cl$ [8,9], $(C_5H_5NCH_2CO_2H)Cl$ [10], $(Me_3NCH_2CO_2H)Cl \cdot H_2O$ [11], $(Et_3NCH_2CO_2H)Cl \cdot 2H_2O$ [12], $(C_5H_5NCH_2CO_2)_2 \cdot H]Cl \cdot H_2O$ [13], $(Me_3NCH_2CO_2H)Br \cdot H_2O$ [14], $(Me_3NCH_2CO_2)_2 \cdot H_2SO_4$ [15], $(C_5H_5NCH_2CO_2)_2 \cdot H_2SO_4$ [16], $(Me_3NCH_2CO_2)_2 Te(OH)_6$ [17], $(Me_3NCH_2CO_2H)HSeO_4 \cdot H_2O$ [18] and $(Me_3NCH_2CO_2H)(HOOCCH{=}CHCOO)$ [19], have been carried out to explain the interaction of the proton with the carboxylate groups.

Two types of complex are known with betaine–acid stoichiometries of 1 : 1 and 2 : 1. The 2 : 1 complexes form centrosymmetric dimers bonded by short hydrogen bonds, characterized by very broad absorption in the IR spectra [20,21].

In this study, we have prepared a third type of complex of pyridine betaine (PBET) with two molecules of 2,6-dichloro-4-nitrophenol (DCNP) ([PBET·$(DCNP)_2$]), and have performed X-ray crystallographic, Fourier transform IR (FTIR), Raman, ^{13}C CP/MAS and UV studies to determine its structure and hydrogen bonding.

2. Experimental details

Pyridine betaine, 1-(carboxymethyl)pyridinium inner salt (PBET), was prepared by a modified procedure of von Gerichten as described previously [22].

The 1 : 1 complex of PBET with DCNP (PBET·DCNP) was prepared by adding a stoichiometric amount of phenol in acetonitrile solution to a methanol solution of PBET. The resulting yellow precipitate was washed with acetonitrile, recrystallized from a CH_3CN–CH_3OH mixture (1 : 1) and dried over P_2O_5 (m.p., 155–156 °C decomp.). Analysis for $C_{13}H_{10}Cl_2N_2O_5$: calculated: C, 45.24%; H, 2.92%; N, 8.12%; found: C, 45.51%; H, 2.93%; N, 7.88%. The complex of PBET with two molecules of DCNP (PBET·$(DCNP)_2$) was obtained by adding 2 mol of DCNP in acetonitrile solution to 1 mol of PBET in methanol. The resulting orange product was recrystallized from a CH_3CN–CH_3OH mixture (1 : 1) and dried over P_2O_5 (m.p., 160–162 °C decomp.). Analysis for $C_{19}H_{13}Cl_4N_3O_8$: calculated: C, 41.25%; H, 2.37%; N, 7.60%; found: C, 41.24%; H, 2.47%; N, 7.44%.

During recrystallization of PBET·DCNP, some PBET·$(DCNP)_2$ may be formed; however, these complexes are easily distinguished by the colour and shape of their crystal forms.

The solvents CH_2Cl_2 and CH_3CN were purified by standard methods, stored over 4 Å and 3 Å molecular sieves respectively and, finally, were freshly distilled over P_2O_5 before use.

The FTIR spectra were recorded using Bruker IFS 113v and IFS 88 spectrometers with a resolution of 1 cm^{-1}. The FTIR spectra at low temperature (300–14 K) were measured using a closed cycle helium cryostat (Displex Closed Cycle Cryogenic Refrigeration System Model CSW-202 and Lakeshore Model 330-11 Dual Sensor Temperature Controller). Solutions ($c = 2 \times 10^{-3}$ mol dm^{-3}) were measured in a KBr cell (l = 1.0 mm). The solid state spectra were recorded in Nujol and Fluorolube suspensions using KBr plates.

The centre of gravity of the broad absorption was estimated using the following equation: $\nu_H = \int \nu \log(I_0/I)\, d\nu / \int \log(I_0/I)\, d\nu$ (in cm^{-1}), where I_0 is the intensity of radiation incident on the sample at wavenumber ν, I is the transmitted intensity and $d\nu = 0.964$ cm^{-1}.

Raman spectra were recorded on a Bruker IFS66 spectrometer equipped with an FRA 106 Raman module operating at the 1064 nm excitation line of an Nd:YAG laser (power, approximately 150 mW).

UV–visible spectra were determined on a Carl Zeiss Jena Specord M 40 spectrometer.

^1H – – ^{13}C CP/MAS NMR spectra were recorded on a Bruker MSL 300 NMR spectrometer at 75.496 MHz with high-power proton decoupling. Powdered samples of PBET·DCNP and PBET·$(DCNP)_2$ were placed in a cylindrical rotor and spun at 2.0–10.5 kHz. For the ^{13}C experiments,

UM00011899
NOVARTIS EXHIBIT 1017
Novartis v. Regents, IPR2023-01346
Page 645 of 4460

the field strength for ^1H decoupling was 1.05 mT; a contact time of 1 ms, a repetition time of 6 s and a spectral width of 50 kHz were used. 8K data points represented the Free Induction Decay (FID). Spectra were accumulated 1000 times, giving a reasonable signal-to-noise ratio. The ^{13}C chemical shifts were calibrated indirectly using the glycine set at 176.34 ppm. The principal elements of the ^{13}C chemical shift tensor and the shielding parameters for the carbonyl groups were determined employing the WIN-MAS program [23]. The details of the fitting routine have been fully discussed elsewhere [24,25]. The principal components δ_{ii} were used to calculate the anisotropy ($\Delta\delta$), asymmetry (η), span (Ω) and skew (κ) [26] according to the following: if $|\delta_{11}-\delta_{iso}| > |\delta_{33}-\delta_{iso}|$ and $\delta_{11} > \delta_{22} > \delta_{33}$, then $\Delta\delta = \delta_{11} - (\delta_{22}+\delta_{33})/2$ and $\eta = (\delta_{22}-\delta_{33})/(\delta_{11}-\delta_{iso})$; if $|\delta_{11}-\delta_{iso}| < |\delta_{33}-\delta_{iso}|$ and $\delta_{11} > \delta_{22} > \delta_{33}$, then $\Delta\delta = \delta_{33} - (\delta_{11}+\delta_{22})/2$ and $\eta = (\delta_{22}-\delta_{11})/(\delta_{33}-\delta_{iso})$.

Single crystals of PBET·DCNP and PBET·$(DCNP)_2$ were grown by slow evaporation of an acetonitrile–methanol (1 : 1) solution. X-Ray measurements were carried out at room temperature on a KUMA diffractometer with a graphite monochromator, and the ω–2Θ scan mode was applied. The structure was solved by direct methods [27] and refined by full-matrix least squares using the SHELXL 93 program [28]. Anisotropic thermal factors were refined for all non-hydrogen atoms. The hydrogen atoms were located from a difference Fourier map and their positions and isotropic thermal parameters were refined. The crystal data and details concerning the data collections and structural refinement are given in Table 1.

Table 1
Crystal data and details of X-ray diffraction measurements and structural refinements for PBET·DCNP (1 : 1) and PBET·$(DCNP)_2$ (1 : 2)

	PBET·DCNP	PBET·$(DCNP)_2$
Molecular formula	$C_{13}H_{10}Cl_2N_2O_5$	$C_{19}H_{13}Cl_4N_3O_8$
Molecular weight	345.13	553.12
Crystal system	Monoclinic	Monoclinic
Space group	$P2_1/c$	$P2_1/c$
Unit cell dimensions		
a (Å)	12.676(3)	9.272(7)
b (Å)	14.260(3)	10.452(7)
c (Å)	8.343(2)	22.978(9)
β (°)	105.30(3)	93.39(6)
V (Å^3)	1454.6(6)	2223(2)
Z	4	4
Density (calculated) (g cm^{-3})	1.576	1.653
Absorption coefficient (mm^{-1})	0.471	0.586
Temperature (K)	293(2)	293(2)
Wavelength (Å)	0.71073	0.71073
F(000)	704	1120
θ_{max} (°)	25.07	22.04
Index ranges	$-14 \le h \le 15$	$-9 \le h \le 9$
	$0 \le k \le 16$	$0 \le k \le 13$
	$-9 \le l \le 0$	$-24 \le l \le 22$
Reflections collected	2769	2945
Independent reflections	2577 (R_{int} = 0.0205)	2740 (R_{int} = 0.0190)
Observed reflections	2576	2740
Refinement method	Full-matrix least squares on F^2	Full-matrix least squares on F^2
	$w = \sigma_1^{-2}$	$w = \sigma_1^{-2}$
Data parameters	2576/240	2740/360
Goodness-of-fit on F^2	1.085	1.029
Final R indices ($I > 2\sigma(I)$)	R_1 = 0.0379, wR_2 = 0.0896	R_1 = 0.0335, wR_2 = 0.0863
Extinction coefficient	0.037(2)	0.0046(5)
Largest ΔF peak and hole (e Å^{-3})	0.384 and –0.330	0.169 and –0.175

UM00011900
NOVARTIS EXHIBIT 1017
Novartis v. Regents, IPR2023-01346
Page 646 of 4460

Table 2
Atomic coordinates ($\times 10^4$ and, for H atoms, $\times 10^3$) and equivalent isotropic displacement parameters ($Å^2 \times 10^3$) for PBET·DCNP and PBET·$(DCNP)_2$. U(eq) is defined as one-third of the trace of the orthogonalized U_{ij} tensor. The dimensions of the unit cells are listed in Table 1

	x	y	z	U(eq)
PBET·DCNP				
C(1)	6552(2)	6101(2)	4538(3)	36(1)
O(1)	7456(1)	5687(1)	4545(2)	47(1)
C(2)	6468(2)	6924(2)	5426(3)	40(1)
Cl(1)	7658(1)	7419(1)	6659(1)	57(1)
C(3)	5492(2)	7358(2)	5361(4)	46(1)
C(4)	4545(2)	6947(2)	4420(3)	45(1)
N(2)	3507(2)	7390(2)	4358(3)	58(1)
O(4)	2667(2)	6972(2)	3693(3)	79(1)
O(5)	3514(2)	8174(2)	4958(4)	93(1)
C(5)	4559(2)	6135(2)	3536(3)	42(1)
C(6)	5544(2)	5736(2)	3578(3)	39(1)
Cl(2)	5586(1)	4737(1)	2419(1)	60(1)
C(7)	10076(2)	6214(2)	5317(3)	35(1)
O(2)	9907(2)	6534(2)	3924(2)	59(1)
O(3)	9365(1)	5886(2)	5992(2)	52(1)
C(8)	11236(2)	6200(2)	6420(3)	39(1)
N(1)	11320(2)	5864(1)	8121(2)	35(1)
C(9)	10880(2)	6393(2)	9120(3)	45(1)
C(10)	10935(3)	6097(3)	10695(4)	61(1)
C(11)	11454(3)	5279(3)	11254(4)	70(1)
C(12)	11898(3)	4754(3)	10224(4)	66(1)
C(13)	11812(2)	5053(2)	8645(4)	48(1)
H(1)	845(4)	590(3)	528(5)	120(15)
H(3)	545(3)	800(3)	589(4)	70(10)
H(5)	392(3)	585(2)	287(4)	64(9)
H(81)	1153(2)	683(2)	646(4)	55(8)
H(82)	1171(2)	579(2)	599(3)	47(8)
H(9)	1058(2)	694(2)	869(4)	48(8)
H(10)	1062(3)	649(2)	1137(4)	71(10)
H(11)	1151(3)	508(3)	1239(6)	107(14)
H(12)	1231(3)	422(3)	1061(5)	83(12)
H(13)	1207(3)	477(2)	791(4)	58(9)
PBET·$(DCNP)_2$				
C(1)	1745(4)	−1186(3)	1053(1)	41(1)
O(1)	1959(3)	−1140(2)	1619(1)	51(1)
C(2)	2739(4)	−608(3)	690(2)	41(1)
Cl(1)	4226(1)	147(1)	1020(1)	61(1)
C(3)	2587(4)	−643(3)	95(2)	45(1)
C(4)	1399(4)	−1237(3)	−165(1)	41(1)
N(2)	1243(4)	−1286(3)	−796(1)	57(1)
O(4)	2203(4)	−851(3)	−1079(1)	83(1)
O(5)	169(4)	−1789(3)	−1023(1)	83(1)
C(5)	365(4)	−1784(4)	160(2)	47(1)
C(6)	542(4)	−1752(3)	760(1)	43(1)
Cl(2)	−763(1)	−2433(1)	1168(1)	70(1)
C(7)	1814(4)	−3943(4)	2203(2)	49(1)
O(2)	2787(3)	−4211(3)	1886(1)	70(1)
O(3)	1251(3)	−2857(3)	2271(1)	62(1)
C(8)	1164(4)	−4977(4)	2565(2)	49(1)
N(1)	2011(3)	−6161(3)	2553(1)	42(1)
C(9)	1593(5)	−7104(4)	2202(2)	59(1)

UM00011901
NOVARTIS EXHIBIT 1017
Novartis v. Regents, IPR2023-01346
Page 647 of 4460

Table 2 Continued

	x	y	z	U(eq)
C(10)	2403(6)	−8197(5)	2184(3)	79(1)
C(11)	3639(7)	−8278(5)	2523(3)	87(2)
C(12)	4077(6)	−7282(6)	2880(2)	80(1)
C(13)	3239(5)	−6235(5)	2887(2)	60(1)
C(1′)	3821(3)	−3791(3)	388(1)	40(1)
O(1′)	4166(3)	−3659(3)	953(1)	54(1)
C(2′)	4728(4)	−3222(3)	−7(2)	42(1)
Cl(1′)	6206(1)	−2396(1)	278(1)	60(1)
C(3′)	4473(4)	−3312(4)	−596(2)	48(1)
C(4′)	3279(4)	−3972(4)	−808(2)	47(1)
N(2′)	2988(5)	−4074(4)	−1444(2)	68(1)
O(4′)	3877(4)	−3665(4)	−1756(1)	104(1)
O(5′)	1858(4)	−4582(4)	−1617(1)	95(1)
C(5′)	2370(4)	−4567(4)	−444(2)	51(1)
C(6′)	2662(4)	−4488(3)	146(2)	44(1)
Cl(2′)	1573(1)	−5283(1)	617(1)	70(1)
H(1)	156(5)	−205(4)	196(2)	85(13)
H(3)	323(4)	−32(3)	−11(1)	34(9)
H(5)	−47(4)	−218(3)	−2(1)	47(10)
H(81)	17(5)	−516(4)	240(2)	70(12)
H(82)	116(4)	−470(4)	295(2)	60(12)
H(9)	67(5)	−693(4)	194(2)	73(12)
H(10)	200(5)	−874(5)	184(2)	110(18)
H(11)	410(5)	−897(5)	52(2)	77(15)
H(12)	505(6)	−735(5)	311(2)	122(19)
H(13)	350(5)	−551(5)	315(2)	91(15)
H(1′)	362(6)	−394(6)	119(2)	123(23)
H(3′)	510(4)	−286(4)	−84(2)	61(11)
H(5′)	156(4)	−494(3)	−61(2)	48(10)

3. Results and discussion

3.1. X-Ray structural analyses

The fractional atomic coordinates and equivalent isotropic thermal parameters for the crystal structures of PBET·DCNP and PBET·$(DCNP)_2$ are presented in Table 2. The bond lengths and bond angles are listed in Table 3.

As illustrated in Fig. 1(a), in the crystalline state, the proton is transferred from DCNP to PBET. The observed hydrogen bond (O···O = 2.419(3) Å) is "very strong" [29]. The O···O distance is compatible with that found in analogous hydrogen-bonded complexes of betaine with DCNP [30]. The C(1)–O(1) bond length and C(2)–C(1)–C(6) bond angle (Table 3) are very close to those in phenolate residues [31], in agreement with proton transfer from DCNP to PBET. In the 1 : 2 complex, both oxygen atoms of PBET are linked to DCNP by two different hydrogen bonds: O(1)···O(3) of 2.452(4) Å and O(1′)···O(2) of 2.623(4) Å (Fig. 1(b), Table 4). The shorter hydrogen bond is that in which the proton is transferred from DCNP to PBET. It is notable that the interaction of two molecules of DCNP with one PBET molecule leads to a lengthening of the shorter hydrogen bond by approximately 0.03 Å. In PBET·$(DCNP)_2$, the C(1)–O bonds and C(2)–C(1)–C(6) angles in the A and B moieties (Table 3) are different, but very close to those in phenolate and phenol respectively [31].

The conformations of the investigated complexes can be described by five planes, A–E, fitted to the pyridine ring of PBET, carboxyl group of PBET, two phenyl rings of DCNP and to the O(2), O(3), C(7), C(8), N(1) and C(11) atoms of PBET respectively (see Fig. 1). The mean deviation of the atoms from coplanarity and the dihedral angles between the planes are listed in Table 5. In PBET·DCNP,

UM00011902
NOVARTIS EXHIBIT 1017
Novartis v. Regents, IPR2023-01346
Page 648 of 4460

Table 3
Bond lengths (Å) and valence angles (°) for PBET·DCNP and PBET·$(DCNP)_2$

	PBET·DCNP	PBET·$(DCNP)_2$		PBET·DCNP	PBET·$(DCNP)_2$
Bond lengths			Bond angles		
C(1)–O(1)	1.288(3)	1.305(4)	O(1)–C(1)–C(6)	120.2(2)	124.3(3)
C(1)–C(6)	1.415(3)	1.399(5)	O(1)–C(1)–C(2)	124.8(2)	120.4(3)
C(1)–C(2)	1.407(4)	1.414(5)	C(6)–C(1)–C(2)	115.0(2)	115.2(3)
C(2)–C(3)	1.371(4)	1.367(5)	C(3)–C(2)–C(1)	123.3(2)	123.1(3)
C(2)–Cl(1)	1.737(2)	1.725(4)	C(3)–C(2)–Cl(1)	118.3(2)	119.0(3)
C(3)–C(4)	1.380(4)	1.370(5)	C(1)–C(2)–Cl(1)	118.4(2)	117.9(3)
C(4)–C(5)	1.374(4)	1.375(5)	C(2)–C(3)–C(4)	118.1(3)	118.8(4)
C(4)–N(2)	1.448(3)	1.449(4)	C(3)–C(4)–C(5)	122.0(2)	121.3(3)
N(2)–O(5)	1.224(4)	1.216(4)	C(3)–C(4)–N(2)	118.7(3)	118.9(3)
N(2)–O(4)	1.219(3)	1.221(4)	C(5)–C(4)–N(2)	119.3(2)	119.8(3)
C(5)–C(6)	1.365(4)	1.379(5)	O(5)–N(2)–O(4)	123.0(3)	122.5(3)
C(6)–Cl(2)	1.730(3)	1.726(4)	O(5)–N(2)–C(4)	118.4(3)	118.4(4)
C(7)–O(2)	1.213(3)	1.225(4)	O(4)–N(2)–C(4)	118.6(3)	119.1(3)
C(7)–O(3)	1.271(3)	1.263(5)	C(4)–C(5)–C(6)	118.6(2)	119.2(3)
C(7)–C(8)	1.516(4)	1.511(5)	C(5)–C(6)–C(1)	123.0(2)	122.3(3)
C(8)–N(1)	1.475(3)	1.467(5)	C(5)–C(6)–Cl(2)	119.5(2)	119.1(3)
N(1)–C(9)	1.348(4)	1.318(5)	C(1)–C(6)–Cl(2)	117.6(2)	118.6(3)
N(1)–C(13)	1.333(4)	1.336(5)	O(2)–C(7)–O(3)	126.6(2)	127.1(4)
C(9)–C(10)	1.364(4)	1.370(7)	O(2)–C(7)–C(8)	119.0(2)	119.7(4)
C(10)–C(11)	1.359(5)	1.349(8)	O(3)–C(7)–C(8)	114.4(2)	113.1(3)
C(11)–C(12)	1.367(5)	1.373(8)	N(1)–C(8)–C(7)	113.6(2)	111.2(3)
C(12)–C(13)	1.361(4)	1.343(6)	C(9)–N(1)–C(13)	121.1(2)	121.2(4)
C(1′)–O(1′)		1.327(4)	C(9)–N(1)–C(8)	118.5(2)	120.2(3)
C(1′)–C(6′)		1.387(5)	C(13)–N(1)–C(8)	120.4(2)	118.5(3)
C(1′)–C(2′)		1.405(5)	N(1)–C(9)–C(10)	119.9(3)	120.0(4)
C(2′)–C(3′)		1.365(5)	C(11)–C(10)–C(9)	119.5(3)	118.9(5)
C(2′)–Cl(1′)		1.716(4)	C(10)–C(11)–C(12)	119.8(3)	120.6(5)
C(3′)–C(4′)		1.368(5)	C(13)–C(12)–C(11)	119.7(3)	118.3(5)
C(4′)–C(5′)		1.371(5)	N(1)–C(13)–C(12)	120.0(3)	121.0(5)
C(4)–N(2′)		1.475(5)	O(1′)–C(1′)–C(6′)		125.6(3)
N(2′)–O(4′)		1.203(5)	O(1′)–C(1′)–C(2′)		118.0(3)
N(2′)–O(5′)		1.220(5)	C(6′)–C(1′)–C(2′)		116.3(3)
C(5′)–C(6′)		1.370(5)	C(3′)–C(2′)–C(1′)		122.4(3)
C(6′)–Cl(2′)		1.733(4)	C(3′)–C(2′)–Cl(1′)		120.1(3)
			C(1′)–C(2′)–Cl(1′)		117.5(3)
			C(2′)–C(3′)–C(4′)		118.4(4)
			C(3′)–C(4′)–C(5′)		121.8(3)
			C(3′)–C(4′)–N(2′)		119.0(4)
			C(5′)–C(4′)–N(2′)		119.2(4)
			O(4′)–N(2′)–O(5′)		124.5(4)
			O(4′)–N(2′)–C(4′)		118.3(4)
			O(5′)–N(2′)–C(4′)		117.3(4)
			C(6′)–C(5′)–C(4′)		118.9(4)
			C(5′)–C(6′)–C(1′)		122.1(3)
			C(5′)–C(6′)–Cl(2′)		120.0(3)
			C(1′)–C(6′)–Cl(2′)		117.9(3)

UM00011903
NOVARTIS EXHIBIT 1017
Novartis v. Regents, IPR2023-01346
Page 649 of 4460

Table 4
Geometry of hydrogen bonds between PBET and DCNP in the title compounds

	PBET·DCNP	PBET·$(DCNP)_2$
O(1)···O(3) (Å)	2.419(3)	2.452(4)
O(1')···O(2) (Å)		2.623(4)
O(1)···H (Å)	1.28(5)	1.30(5)
O(1')–H (Å)		0.83(6)
O(3)–H (Å)	1.16(5)	1.16(5)
O(2)···H (Å)		1.83(5)
O(1)–H–O(3) (°)	165(4)	178(4)
O(1')–H–O(2) (°)		160(6)

PBET·$(DCNP)_2$, PBET·H_2O and PBET·HCl, the betaine residues form quasi-planar molecules comprising all non-hydrogen atoms except the α,α' and β,β' carbon atoms of the pyridine ring. The latter are arranged symmetrically with respect to plane E (Table 5). The dihedral angle between the carboxymethyl groups and the pyridine ring varies with the complexes: PBET·DCNP, 68.3°; PBET·$(DCNP)_2$, 82.7°; PBET·H_2O, 84.5°; PBET·HCl, 84.6°. Planes A and C form dihedral angles of 75.9° in PBET·DCNP and 86.5° in PBET·$(DCNP)_2$. In PBET·$(DCNP)_2$, the two DCNP residues are nearly parallel; the dihedral angle is 3.80°.

3.2. FTIR and Raman spectra

The FTIR powder spectra of PBET-DCNP and PBET·$(DCNP)_2$ at two different temperatures show a broad absorption which extends from 1600 cm^{-1} down to 400 cm^{-1} (Fig. 2); however, in the Raman spectra (Fig. 3) this feature is absent. Broad absorption is typical of compounds with strong hydrogen bonds and arises from the stretching (strong absorption) and bending (much weaker absorption) vibrations of the O–H group involved in the short OH···O hydrogen bonds. A similar broad absorption has been observed in the spectra of pyridine *N*-oxide hemi-perchlorate, bis(pyridine betaine) hydrochloride hydrate and several acid salts of carboxylic acids

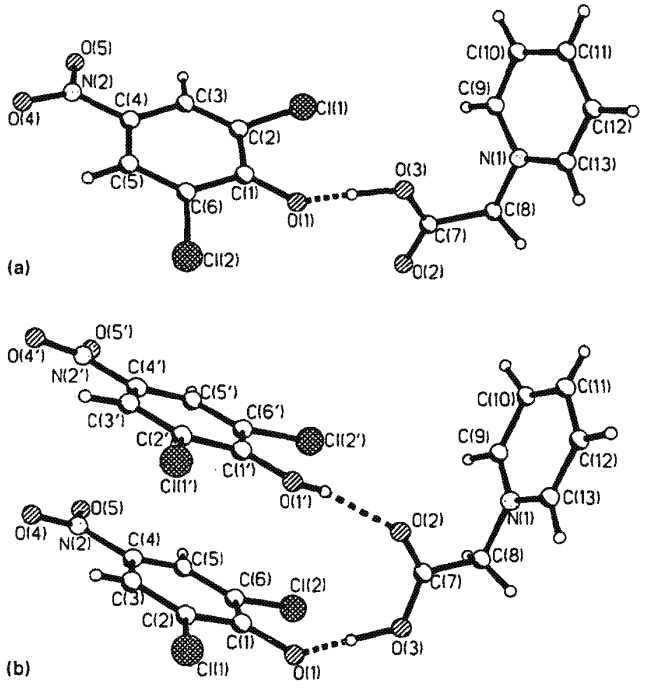


Fig. 1. Perspective view of the arrangement of the complexes of PBET with DCNP with the atomic numbering scheme: (a) 1 : 1 complex; (b) 1 : 2 complex.

UM00011904
NOVARTIS EXHIBIT 1017
Novartis v. Regents, IPR2023-01346
Page 650 of 4460

Table 5
Mean deviation from the least-squares planes and dihedral angles between the planes[a]

	PBET·DCNP	PBET·$(DCNP)_2$	PBET·H_2O	PBET·HCl
Mean deviation from coplanarity (Å)[a]				
A	0.007	0.005	0.004	0.004
B	0.002	0.0	0.006	0.001
C	0.009	0.010	–	
D	–	0.011	–	
E	0.045	0.094	0.005	0.008
Dihedral angles between planes (°)				
AB	68.3	82.7	84.5	84.6
AC	75.9	86.5		
AD	–	89.2		
BC	81.0	81.7		
BD	–	79.5		
CD	–	3.8		

[a]Atoms used for the planes: A: N(1), C(9)–C(13); B: O(2), O(3), C(7), C(8); C: C(1)–C(6); D: C(1')–C(6'); E: O(2), O(3), C(7), C(8), N(1), C(11).

[32,33]. An additional less intense broad absorption in the 3300–2100 cm^{-1} region, due to the ν_{OH} vibration of the long hydrogen bond, is present in the PBET·$(DCNP)_2$ spectrum (Fig. 5).

According to the reasonably good correlation between the ν_{OH} frequencies and $R(O\cdots O)$ distances [33], the frequency shifts to lower wavenumbers with shortening of the hydrogen bond. In the investigated

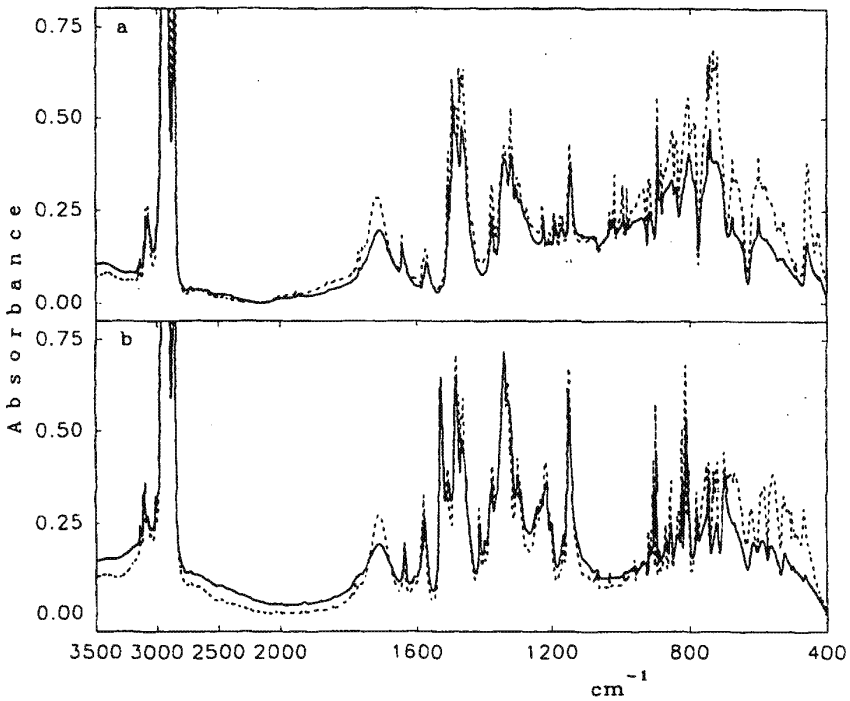


Fig. 2. Nujol FTIR spectra of PBET·DCNP (a) and PBET·$(DCNP)_2$ (b): full line, 299 K; dotted line, 14 K.

UM00011905
NOVARTIS EXHIBIT 1017
Novartis v. Regents, IPR2023-01346
Page 651 of 4460

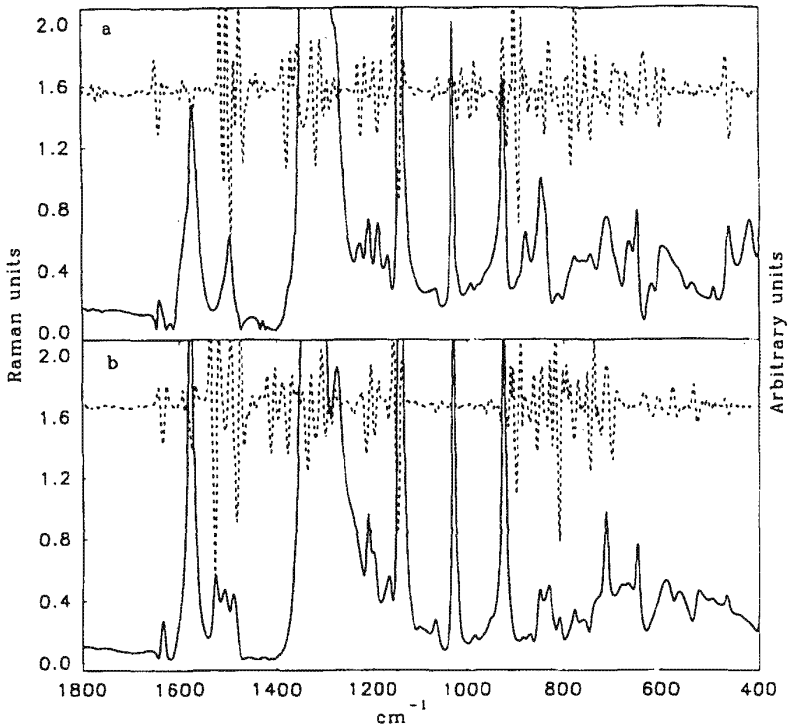


Fig. 3. Powdered FT-Raman (full lines) and second-derivative FTIR (dotted lines) spectra of PBET·DCNP (a) and PBET·$(DCNP)_2$ (b).

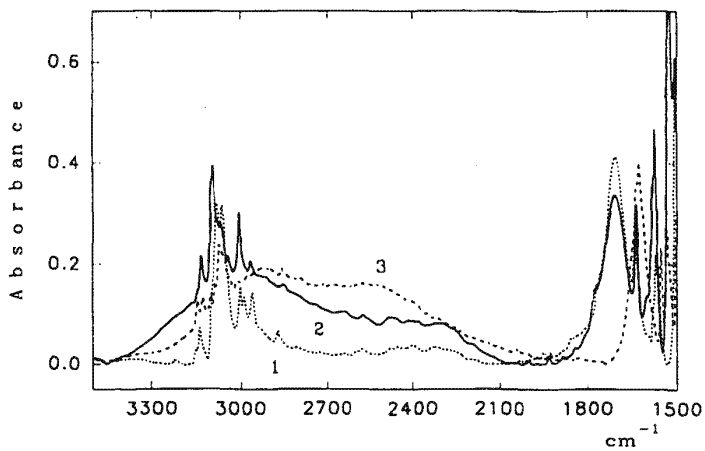


Fig. 4. FTIR spectra in Fluorolube of PBET·DCNP (1), PBET·$(DCNP)_2$ (2) and PBET·$(PCP)_2$ (3).

UM00011906
NOVARTIS EXHIBIT 1017
Novartis v. Regents, IPR2023-01346
Page 652 of 4460

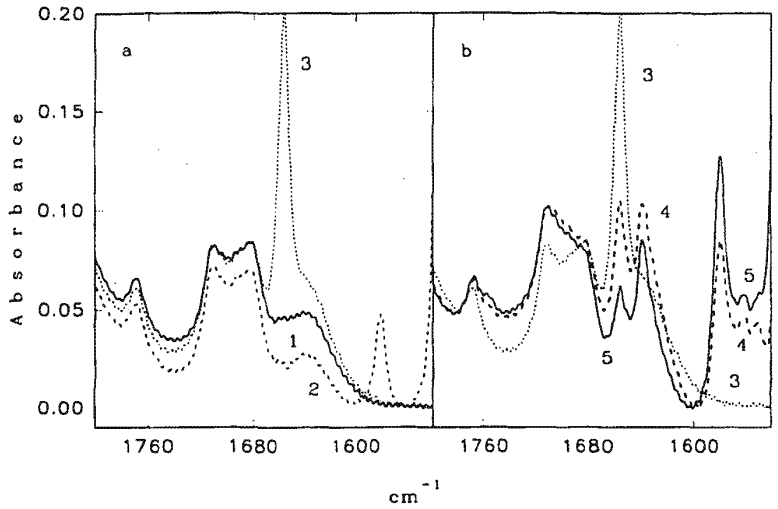


Fig. 5. FTIR spectra of: (1) CD_3CN; (2) DCNP + CD_3CN; (3) PBET + CD_3CN; (4) PBET·DCNP + CD_3CN; (5) PBET·$(DCNP)_2$ + CD_3CN. c~0.004 mol dm^{-3}; l = 1.04 mm.

complexes, this general rule is broken. The short hydrogen bond in PBET·$(DCNP)_2$ is longer than that in PBET·DCNP, but the broad absorption is at lower wavenumbers (Fig. 2, Table 6). On the other hand, the longer hydrogen bond can be compared with the hydrogen bonds in PBET·$(PCP)_2$ (PCP, pentachlorophenol) [34], but as shown in Fig. 4 and Table 6, this band in PBET·$(DCNP)_2$ is shifted to higher frequency. The observed shifts in absorption suggest that, in PBET·$(DCNP)_2$, the hydrogen bonds perturb each other.

The $\nu_{C=O}$ stretching mode in carboxylic acids and their acid salts appears as a very strong band around 1740 cm^{-1} in the IR spectra. As shown in Fig. 2, in the investigated complexes, the $\nu_{C=O}$ bands are weak: PBET·DCNP (at 14 K): 1712 cm^{-1}, $\Delta\nu_{1/2}$ = 69 cm^{-1}; PBET·$(DCNP)_2$ (at 14 K): 1710 cm^{-1}, $\Delta\nu_{1/2}$ = 64 cm^{-1}. In the Raman spectra, these bands are very weak and difficult to localize [16]. The low intensity and relatively large half-width of the $\nu_{C=O}$ bands suggest that the proton dynamics in the investigated complexes are slower than those in acid salts and 2 : 1 complexes of PBET with mineral acids.

In complexes with short hydrogen bonds, the broad absorption overlaps the skeletal vibrations. In order to visualize the narrow bands due to the skeletal vibrations, the second-derivative spectra were calculated (Fig. 3). In the second-derivative spectra, the minima have the same wavenumbers as the maxima in the absorption spectra [35–37]. The relative amplitudes

Table 6
Centre of gravity (ν_H) of selected absorption (due to the hydrogen bond and skeletal vibrations) for PBET·DCNP, PBET·$(DCNP)_2$ and PBET·$(PCP)_2$

Compound	O···O distance (Å)	Region of integration (cm^{-1})	Temperature(K)	ν_H (cm^{-1})
PBET·DCNP	2.419(3)	1130–400	299	806
		1130–400	14	772
PBET·$(DCNP)_2$	2.452(4)	1130–400	299	773
		1130–400	14	723
	2.623(4)	3400–2000	299	2832
PBET·$(PCP)_2$	2.582(6)	3400–2000	299	2725
	2.611(6)	3400–2000	299	2725

UM00011907
NOVARTIS EXHIBIT 1017
Novartis v. Regents, IPR2023-01346
Page 653 of 4460

of the bands in the second-derivative spectra vary inversely with the square of the half-width of the absorption bands.

The origin of the ν_{OH} bandwidth and its frequency in hydrogen-bonded systems is a long-standing problem. It is probable that this unusual spectroscopic feature originates from the strong anharmonic coupling between the high-frequency (ν_{AH}) and low-frequency ($\nu_{A-H\cdots B}$) vibrational modes or between ν_{AH} and the low-frequency lattice phonon [38]. The present results show an additional coupling between two different hydrogen bonds.

Although in the carbonyl region acetonitrile-d_3 has four weak overtones (approximately 1766, 1710, 1680 and 1640 cm^{-1}), they cause some difficulties in the subtraction of absorption due to the investigated complexes. Hence Fig. 5 shows the absorption spectra of the samples (almost saturated solutions) and solvent. The band at 1657 cm^{-1} in the spectra is attributed to the ν_{asCOO} vibration. Its intensity decreases in the order PBET > PBET·DCNP > PBET·$(DCNP)_2$. The additional absorption at approximately 1710 cm^{-1} must be due to the $\nu_{C=O}$ vibration of the complexes. The band at 1639 cm^{-1} is due to the pyridine ring vibration. Although the diluted solution spectra are only qualitative, the presence of the ν_{asCOO} band at 1657 cm^{-1} indicates that, in solution, PBET is only partly protonated, and hence the investigated complexes can be described by a prototropic equilibrium, $A-H\cdots B \rightleftarrows A^{-}\cdots H-B^{+}$. It seems that the 1 : 2 complex in solution exists as an equilibrium of the 1 : 1 complex and "free" DCNP.

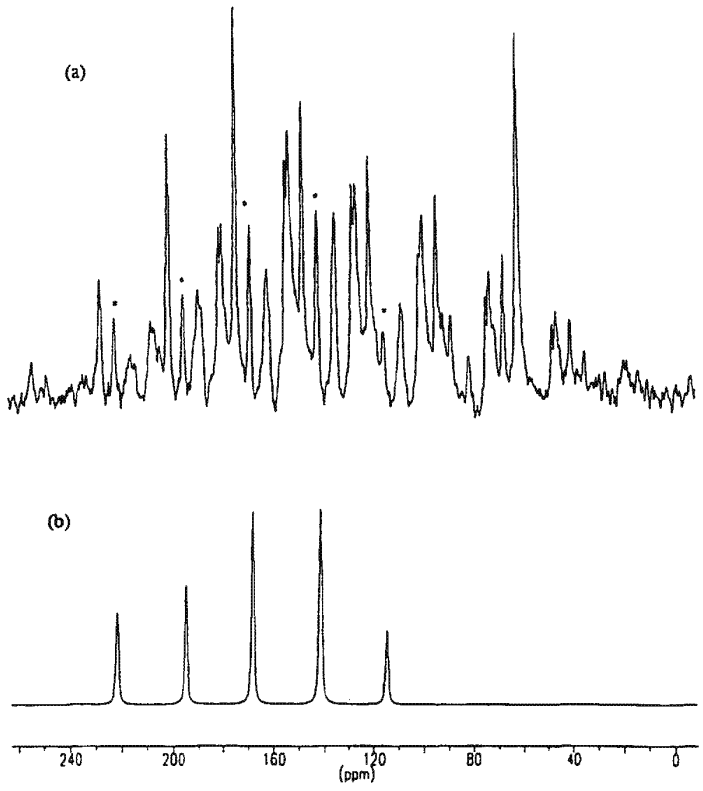


Fig. 6. (a) $^{1}H-\,-^{13}C$ CP/MAS (75.468 MHz) experimental spectrum of PBET·DCNP. The spectrum has 8K data points with 20 Hz line broadening, a contact time of 1 ms, 1000 scans and ν_{rot} = 2 kHz. The spinning sidebands of the carboxyl group are labelled with asterisks. (b) Theoretical spectrum of carboxyl group calculated employing the WIN-MAS program [23]; δ_{11} = 246 ppm; δ_{22} = 153 ppm; δ_{33} = 104 ppm.

UM00011908
NOVARTIS EXHIBIT 1017
Novartis v. Regents, IPR2023-01346
Page 654 of 4460

3.3. ^{13}C CP/MAS NMR spectra

Fig. 6(a) and Fig. 7(a) display the ^{13}C CP/MAS spectra of PBET·DCNP and PBET·$(DCNP)_2$ recorded at room temperature with rotation speeds of 2 kHz and 2.5 kHz respectively. The assignment of the ^{13}C resonances to the carbon atoms of PBET·DCNP and/or PBET·$(DCNP)_2$ from such spectra is ambiguous. Both spectra show a large number of partially overlapped spinning sidebands due to the large chemical shift anisotropy (CSA) of the phenyl rings and carbonyl groups. Furthermore, the presence of the quadrupolar nuclei ^{14}N ($I = 1$), ^{35}Cl ($I = 3/2$) and ^{37}Cl ($I = 3/2$) directly bonded to the carbon atoms causes significant line broadening of the signals.

In order to avoid the problem related to CSA, further results were obtained from spectra monitored with fast sample spinning ($\nu_{rot} = 10$ kHz). The differences between the spectra shown in Fig. 6(a), Fig. 7(a) and Fig. 8 are apparent. Fig. 8 presents only isotropic ^{13}C resonances with a clearly resolved aliphatic region as well as aromatic and carbonyl signals. The CH_2 signals for PBET·DCNP and PBET·$(DCNP)_2$ are found at $\delta = 61.3$ ppm and $\delta = 61.9$ ppm respectively. The resonances are broadened due to the $^{13}C--^{14}N$ quadrupolar effect. Significant differences between the spectra of PBET·DCNP and PBET·$(DCNP)_2$ are observed in the aromatic region covering the chemical shift range from 130 to 148 ppm. The larger number of signals in this region for the complex PBET·$(DCNP)_2$ is related to the presence of two molecules of DCNP in the asymmetric part of the

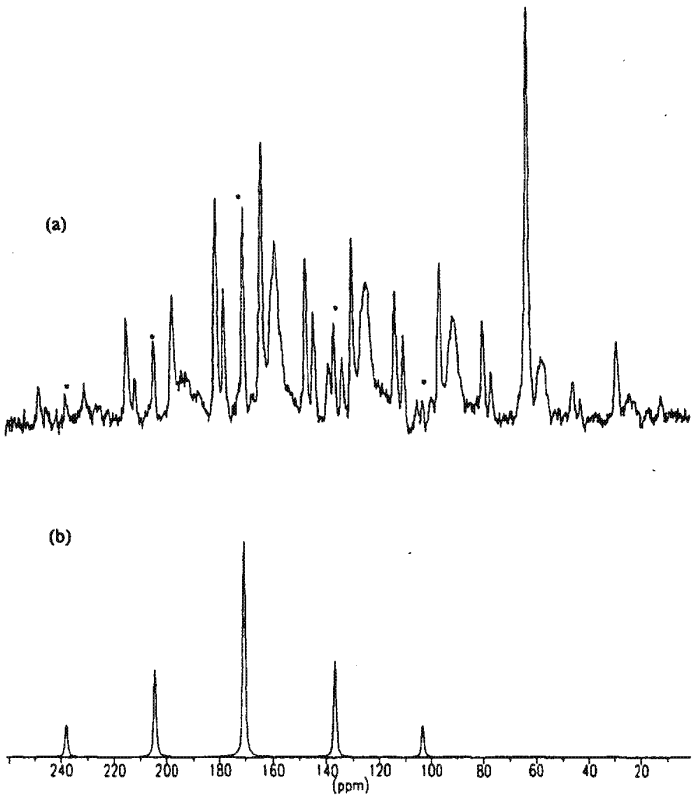


Fig. 7. (a) $^{1}H--^{13}C$ CP/MAS (75.468 MHz) experimental spectrum of PBET·$(DCNP)_2$. The spectrum has 8K data points with 20 Hz line broadening, a contact time of 1 ms, 1000 scans and $\nu_{rot} = 2.5$ kHz. The spinning sidebands of the carboxyl group are labelled with asterisks. (b) Theoretical spectrum of the carboxyl group calculated employing the WIN-MAS program [23]: $\delta_{11} = 237$ ppm; $\delta_{22} = 168$ ppm; $\delta_{33} = 105$ ppm.

UM00011909
NOVARTIS EXHIBIT 1017
Novartis v. Regents, IPR2023-01346
Page 655 of 4460

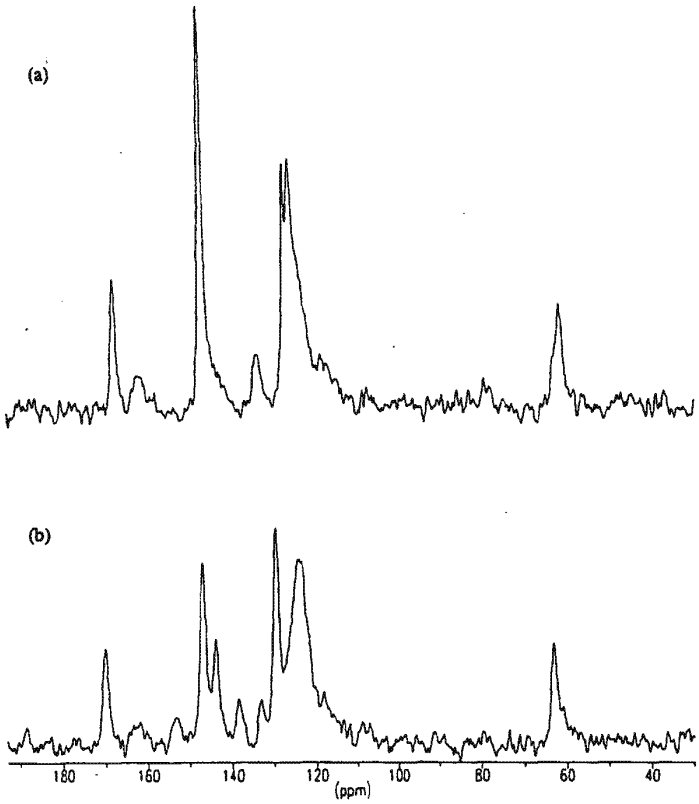


Fig. 8. $^{1}H--^{13}C$ CP/MAS (75.468 MHz) experimental spectra of PBET·DCNP (a) and PBET·$(DCNP)_2$ (b). The spectra have 8K data points with 20 Hz line broadening, a contact time of 1 ms, 1000 scans and ν_{rot} = 10 kHz.

unit cell. These results clearly show how sensitive solid state NMR is to molecular packing. Unfortunately, because of the $^{13}C--^{35}Cl(^{37}Cl)$ and $^{13}C--^{14}N$ line broadening effect, the aromatic resonances cannot be assigned unambiguously.

Interesting information was obtained from a comparison of the ^{13}C chemical shifts of the carboxyl groups. For PBET·DCNP, δ = 167.7 ppm, whereas for PBET·$(DCNP)_2$, the signal is downfield by 2.6 ppm. It is well known that the ^{13}C NMR chemical shift of carboxyl carbon is sensitive to the spatial arrangement of the nuclei comprising the hydrogen bond, since the electronic structure of the carboxyl group is greatly affected by hydrogen bonding. The origin of this effect is related to the decrease in electronic shielding of the carbon as the carboxyl group becomes more polarized during bond formation. It seems that the hydrogen bonding effect is responsible for the small difference observed in the ^{13}C chemical shifts of PBET·DCNP and PBET·$(DCNP)_2$. As shown by the X-ray data, the carboxyl group of PBET·$(DCNP)_2$ is bonded to two molecules of DCNP via hydrogen bonds (2.452 and 2.623 Å). However, in PBET·DCNP, only one shorter hydrogen bond is present (2.419 Å).

Detailed information about the nature of the hydrogen bond can be obtained from an analysis of the principal elements of the chemical shift tensors, δ_{ii}. The graphical method based on the Herzfeld and Berger [25] algorithm was used to establish the δ_{ii} parameters for PBET·DCNP and PBET·$(DCNP)_2$. The intensities of the spinning sidebands corresponding to the carboxyl groups were assigned from the slow spinning spectra (Fig. 6(a) and Fig. 7(a))

UM00011910
NOVARTIS EXHIBIT 1017
Novartis v. Regents, IPR2023-01346
Page 656 of 4460

Table 7
^{13}C chemical shift parameters for PBET·DCNP and PBET·$(DCNP)_2$

Compound	δ_{iso} (ppm)	δ_{11} (ppm)	δ_{22} (ppm)	δ_{33} (ppm)	$\lvert\Delta\delta\rvert$(ppm)	Ω (ppm)	η	κ
PBET·DCNP	167.7	246	153	104	117	142	0.63	−0.31
PBET·$(DCNP)_2$	170.3	237	168	105	102	132	0.94	−0.05

Estimated error in δ_{11}, δ_{22}, δ_{33} and $\Delta\delta$ is ±2.5 ppm; error in δ_{iso} is ±0.2 ppm. The principal components of the chemical shift tensor are defined as follows: $\delta_{11} > \delta_{22} > \delta_{33}$. The isotropic chemical shift is given by $\delta_{iso} = (\delta_{11} + \delta_{22} + \delta_{33})/3$.

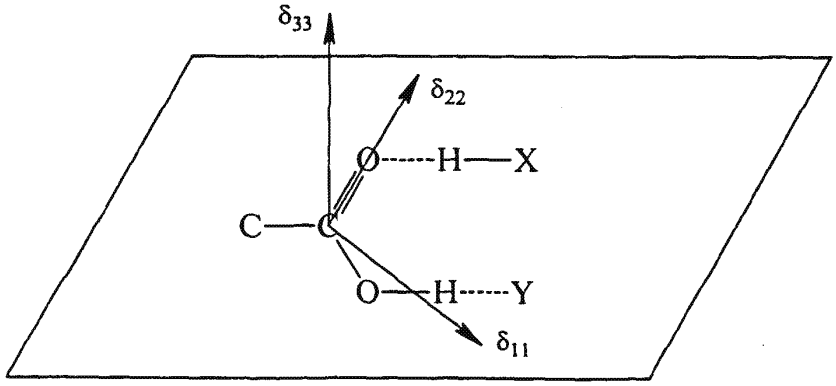
employing a deconvolution procedure. The theoretical spectra of the carboxyl groups for PBET-DCNP and PBET·$(DCNP)_2$ are displayed in Fig. 6(b) and Fig. 7(b). The calculated values of the principal elements δ_{ii}, anisotropy $\Delta\delta$, asymmetry η, span Ω and skew κ are given in Table 7.

From an analysis of the ^{13}C chemical shift parameters, it is apparent that the shielding of the carboxyl groups for the two complexes is different. Moreover, significant differences are observed for the δ_{22} parameters. The orientation of δ_{ii} with respect to the molecular frame of the carboxyl group is shown in Scheme 1. As δ_{22} is oriented along the C=O bond, it can be concluded that the observed downfield shift of approximately 15 ppm in PBET·$(DCNP)_2$ relative to PBET·DCNP is caused by the engagement of the C=O group in the hydrogen bond. The difference in the δ_{11} parameter (9 ppm), which is aligned along the C–O bond, is related to the different strength of C–O–H···O bonding [39]; however, the opposite trend (downfield shift for PBET·DCNP with a stronger hydrogen bond) should be emphasized. The changes in δ_{22} and δ_{11} for PBET·DCNP and PBET·$(DCNP)_2$ correspond very well to small differences in C=O (1.213(3), 1.225(4) Å) and C–O (1.271(3), 1.263(5) Å) bond lengths (see Table 3). The most shielded element δ_{33}, which is orthogonal to the plane containing the C(O)OH group, is very similar for both complexes.

3.4. UV spectra

In the case of nitrophenols, molecular complexes (A–H···B) and hydrogen-bonded ion pairs (A^-···H–B^+) are relatively easily distinguished in the UV spectra, because the ^1L_b transition of nitrophenols is close to 300 nm, whereas that of nitrophenolate ions is close to 400 nm (see, for example, Ref. [40]).

Fig. 9 shows the UV absorption spectra of DCNP, its tetra-(*n*-butyl) ammonium salt and the 1 : 1 and 1 : 2 complexes with PBET. In all the spectra, two bands near 300 and 420 nm are present (Table 8). The band near 420 nm in the DCNP spectrum is very weak and reflects the dissociation in acetonitrile; in less basic and polar solvents, e.g. CH_2Cl_2, this absorption disappears. Another interesting feature is the fine



Scheme 1.

UM00011911
NOVARTIS EXHIBIT 1017
Novartis v. Regents, IPR2023-01346
Page 657 of 4460

Table 8
UV absorption data for DCNP and its complexes in acetonitrile

Compound	λ (nm)	A (cl)
DCNP	233[a]	8990
	302	8520
	421	280
PBET·DCNP	260[b]	7370
	(268)	(6660)
	297	6290
	307	6340
	(320)	(5410)
	423	10240
PBET·$(DCNP)_2$	261[b]	9540
	268	9730
	(297)	(13530)
	306	13820
	421	11300
Bu_4N·DCNP	295[c]	3910
	308	4110
	321	4340
	426	2840

[a] $c = 2 \times 10^{-3}$ M, $l = 0.0525$ cm. [b] $c = 1.25 \times 10^{-3}$ M, $l = 0.0525$ cm. [c] $c = 2 \times 10^{-3}$ M, $l = 0.0151$ cm. Shoulders are given in parentheses.

structure of absorption at 300 nm in the UV spectra of the complexes. The band near 420 nm confirms the presence of the phenolate moiety in solutions of PBET·DCNP and PBET·$(DCNP)_2$. However, the absorption intensity at 420 nm in PBET·DCNP and PBET·$(DCNP)_2$ is much weaker than that in

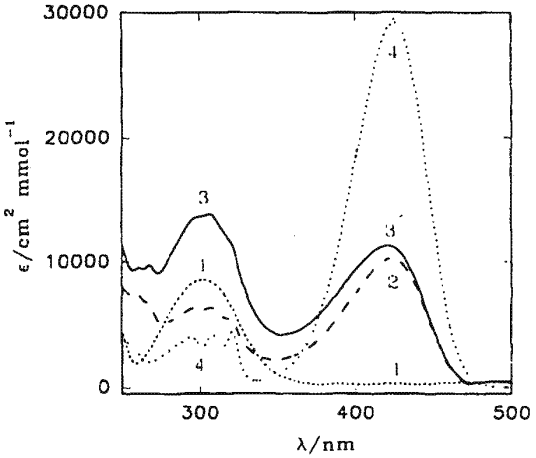


Fig. 9. UV spectra of DCNP and its complexes in acetonitrile: (1) DCNP; (2) PBET·DCNP; (3) PBET·$(DCNP)_2$; (4) Bu_4N^+·$(DCNP)^-$; $c = 2 \times 10^{-3}$ mol dm^{-3}; $l = 0.0525$ cm.

Bu_4N^+·$(DCNP)^-$, whereas the reverse is true for the absorption at 300 nm. This result shows that, in acetonitrile, both phenolate and phenol residues are present and that the acid–base interactions in solution are different from those in the crystal. The comparable absorption intensity at 420 nm in the spectra of PBET·DCNP and PBET·$(DCNP)_2$ suggests a similar degree of proton transfer in these complexes. As shown in Fig. 9, PBET·DCNP in acetonitrile exists in equilibrium: $[O\underline{\cdot\cdot}C\underline{\cdot\cdot}O\cdots H\text{–}O]^- \rightleftarrows O{=}C\text{–}O\text{–}H\cdots O^-$. Both forms can interact with a second molecule of DCNP; however, the interaction of the former species ($[O\underline{\cdot\cdot}C\underline{\cdot\cdot}O\cdots H\text{–}O]^-$) is preferred and lowers the degree of proton transfer. The similar intensity of absorption at 420 nm of the two complexes suggests that PBET·$(DCNP)_2$ is not stable in solution and the equilibrium is shifted towards PBET·DCNP and "free" DCNP.

4. Conclusions

X-Ray studies of the title compounds show that the betaine molecule is protonated and forms very short hydrogen bonds with phenolate anion (PBET·DCNP, O···O = 2.419(3) Å; PBET·$(DCNP)_2$, O···O = 2.452(4) Å). In the 1 : 2 complex, the second molecule of DCNP interacts with the second oxygen atom of betaine with an O···O distance equal to 2.623(4) Å. In the investigated complexes of PBET, a quasi-planar residue is formed comprising all non-hydrogen atoms, except the carbon atoms at the α,α' and β,β' positions of the pyridine ring. The latter are arranged symmetrically with respect to this plane. The dihedral angle between the pyridine and phenol rings varies from 75.9° to 89.2°. In PBET·$(DCNP)_2$, the two phenol rings are nearly coplanar (dihedral angle, 3.8°).

The ^{13}C CP/MAS NMR spectra show signals at 167.7 and 170.3 ppm due to the carboxylate group in PBET·DCNP and PBET·$(DCNP)_2$ respectively, confirming the structures. The most valuable information is obtained from an analysis of the principal elements of the ^{13}C chemical shift tensors; the anisotropic δ_{ii} elements can distinguish even subtle structural differences between the two complexes. The δ_{22} parameter is sensitive to the character of interaction between the C=O group and DCNP, whereas the δ_{11} parameter corresponds to the strength of the

UM00011912
NOVARTIS EXHIBIT 1017
Novartis v. Regents, IPR2023-01346
Page 658 of 4460

C–O–H···O hydrogen bond. The isotropic chemical shift $\delta_{iso}=(\delta_{11}+\delta_{22}+\delta_{33})/3$ "masks" the specific interactions.

The FTIR spectra of the investigated complexes show a broad absorption at approximately 800 cm^{-1} due to the ν_{OH} vibration of the short hydrogen bonds. The long hydrogen bond in PBET·$(DCNP)_2$ absorbs at about 2800 cm^{-1}. In PBET·$(DCNP)_2$, the absorption of the short hydrogen bond is shifted to lower frequencies, whereas that of the longer hydrogen bond is shifted towards higher frequencies when compared with similar hydrogen bonds in PBET·DCNP and PBET·$(PCP)_2$ respectively. These shifts suggest that, in PBET·$(DCNP)_2$, the hydrogen bonds perturb each other.

The two peaks near 300 and 420 nm in the UV spectra of PBET·DCNP and PBET·$(DCNP)_2$, of very different intensity from those of Bu_4N^+·$(DCNP)^-$, demonstrate the prototropic equilibrium of PBET complexes in acetonitrile. The similar absorption intensity at 420 nm in the investigated complexes suggests a similar degree of protonation. PBET·$(DCNP)_2$ in solution can be described as an equilibrium between PBET·DCNP and "free" DCNP. The IR spectra in CD_3CN confirm this conclusion.

Acknowledgements

We thank the State Committee of Scientific Research (Grant KBN/2P303 06907) for financial support, Dr J. Baran for the measurement of the IR spectra at low temperature and Dr M. Połomska for the measurement of the Raman spectra.

References

[1] N. van Thoai, in: M. Florkin, E.H. Stotz (Eds.), Comprehensive Biochemistry, vol. 6, Elsevier, Amsterdam, 1965, p. 224.
[2] H.A. Sober (Ed.), Handbook of Biochemistry. Selected Data for Molecular Biology, 2nd ed., Chemical Rubber Co., Cleveland, OH, 1970, Section B.
[3] G. Blunden, S.M. Gordon, Prog. Phycol. Res. 4 (1986) 39.
[4] S. Haussühl, Z. Kristallogr. 188 (1989) 311.
[5] G. Schaack, Ferroelectrics 104 (1990) 147, and references cited therein.
[6] T.C.W. Mak, J. Mol. Struct. 220 (1990) 13.
[7] M. Szafran, J. Koput, J. Mol. Struct. 381 (1996) 157.
[8] M.S. Fischer, D.H. Templeton, A. Zalkin, Acta Crystallogr., Sect. B 26 (1970) 1392.
[9] W.-H. Yip, R.-J. Wang, T.C.W. Mak, Acta Crystallogr., Sect. C 46 (1990) 717.
[10] M. Szafran, J. Koput, J. Basan, T. Glowiak, J. Mol. Struct. (1997), in press.
[11] X.-M. Chen, T.C.W. Mak, J. Mol. Struct. 240 (1990) 69.
[12] W.-Y. Huang, X.-M. Du, B.-H. Yang, T.C.W. Mak, J. Mol. Struct. 222 (1990) 479.
[13] X.-M. Chen, T.C.W. Mak, J. Mol. Struct. 221 (1990) 265.
[14] X.-M. Chen, T.C.W. Mak, J. Mol. Struct. 245 (1991) 301.
[15] H. Ratajczak, A. Pietraszko, J. Baran, A.J. Barnes, Yu. Tarnavski, J. Mol. Struct. 327 (1994) 297.
[16] J. Baran, Z. Dega-Szafran, M. Jaskólski, M.K. Marchewka, H. Ratajczak, M. Szafran, J. Mol. Struct. in press.
[17] M.M. Ilczyszyn, T. Lis, J. Baran, H. Ratajczak, J. Mol. Struct. 265 (1992) 293.
[18] J. Baran, M. Drozd, T. Lis, M. Śledź, A.J. Barnes, H. Ratajczak, J. Mol. Struct. 372 (1995) 29.
[19] M.M. Ilczyszyn, T. Lis, H. Ratajczak, J. Mol. Struct. 372 (1995) 9.
[20] Z. Dega-Szafran, M. Grundwald-Wyspiańska, M. Szafran, J. Chem. Res. (S) (1993) 316.
[21] Z. Dega-Szafran, M. Gdaniec, M. Grundwald-Wyspiańska, I. Kowalczyk, M. Szafran, J. Mol. Struct. 322 (1994) 297.
[22] Z. Dega-Szafran, I. Kowalczyk, M. Szafran, Bull. Polon. Acad. Sci. Chem. 43 (1995) 303.
[23] WIN-MAS Program, Version 940108, Bruker-Franzen Analytik GmbH, Bremen, 1994.
[24] G. Jeschke, G. Grossman, J. Magn. Res. A 103 (1993) 323.
[25] J. Herzfeld, A.E. Berger, J. Chem. Phys. 73 (1980) 6021.
[26] J. Mason, Solid State Nuclear Magnetic Resonance 2 (1993) 285.
[27] G.M. Sheldrick, Acta Crystallogr., Sect. A 46 (1990) 467.
[28] G.M. Sheldrick, SHELXL 93, Program for the Refinement of Crystal Structures, University of Göttingen, Germany, 1993.
[29] J. Emsley, Chem. Soc. Rev. 9 (1980) 91.
[30] Z. Dega-Szafran, A. Komasa, M. Grundwald-Wyspiańska, M. Szafran, G. Buczak, A. Katrusiak, J. Mol. Struct. 404 (1997) 13.
[31] F.H. Allen, O. Kennard, Cambridge Structural Database, Chemical Design Automation News (1993) 8.1.31–8.1.37.
[32] M. Szafran, Z. Dega-Szafran, J. Mol. Struct. 321 (1994) 57.
[33] A. Novak, Struct. Bonding 18 (1974) 177.
[34] G. Buczak, Z. Dega-Szafran, A. Katrusiak, M. Szafran, J. Mol. Struct. (1997), in press.
[35] W.L. Butler, D.W. Hopkins, Photochem. Photobiol. 12 (1970) 439.
[36] W.F. Maddams, M.J. Southon, Spectrochim. Acta, Part A 38 (1982) 459.
[37] G. Talsky, Derivative Spectroscopy, VGH, Weinheim, 1994.
[38] H. Ratajczak, A.M. Yaremko, Chem. Phys. Lett. 243 (1995) 348.
[39] Z. Gu, R. Zambrano, A. McDermott, J. Am. Chem. Soc. 116 (1994) 6368.
[40] M. Szafran, J. Mol. Struct. 381 (1996) 39.

UM00011913
NOVARTIS EXHIBIT 1017
Novartis v. Regents, IPR2023-01346
Page 659 of 4460

CRYSTAL GROWTH & DESIGN
2003
VOL. 3, NO. 3
369–374

Synchrotron Radiation SAXS/WAXS Study of Polymorph-Dependent Phase Behavior of Binary Mixtures of Saturated Monoacid Triacylglycerols

Morio Takeuchi, Satoru Ueno, and Kiyotaka Sato*

Graduate School of Biosphere Sciences, Hiroshima University, Higashi-Hiroshima, 739-8528, Japan

Received October 3, 2002

ABSTRACT: Polymorphic influences on the phase behavior of three types of binary mixtures of saturated monoacid triacylglycerols (TAGs), trilaurin/trimyristin (LLL/MMM), trilaurin/tripalmitin (LLL/PPP), and trilaurin/tristearin (LLL/SSS), were examined by small- and wide-angle X-ray scattering (SAXS/WAXS) using synchrotron radiation. The carbon numbers (C_n) for the fatty acid chains of the three TAGs are 12 (LLL), 14 (MMM), 16 (PPP), and 18 (SSS). In the LLL/MMM system, miscible phase behavior occurred in metastable α and β' forms, whereas the most stable β form exhibited a eutectic phase. On the other hand, LLL/PPP and LLL/SSS mixtures showed immiscible phases for α, β', and β forms. Therefore, the TAG binary mixtures were miscible in metastable polymorphs of α and β' forms when C_n differed by 2, whereas the immiscible mixtures were constructed in all polymorphic forms when C_n differed by 4 and 6.

Introduction

The phase behavior of triacylglycerol (TAG) mixtures in a crystalline phase is important in foods, pharmaceuticals, and cosmetics[1–3] because the fat structures play dominant roles largely in determining the products' physical properties such as texture, plasticity, and morphology. TAG crystals present in the fat products, such as chocolate, suppository, and lip cream, contain different types of fatty acid.[4,5] Although the physical properties of the fat systems are complex because of polymorphism and mixing behavior of the TAG mixture,[6] these properties are highly crucial in industrial applications of fat blending[7] and solid/liquid separation.[8] Therefore, it is important to precisely analyze the physical and chemical properties of TAGs in multicomponent TAG mixture system.[9,10] For this reason, several groups have studied binary TAG mixtures, but much remains to be done.[11–14]

Organic crystals often have several phases.[15,16] In the case of binary mixtures of TAG molecules, three phase types generally occur: (i) the TAGs with similar chemical structures form a miscible solid-solution phase; (ii) TAGs with different chemical structures form a eutectic phase; and (iii) specific interactions between the TAG molecules result in the formation of a different molecular compound.[12,14,17] In addition, polymorphism of TAG crystals makes the phase behavior more complicated. For example, miscible mixtures are formed between tripalmitin (PPP) and tristearin (SSS) in metastable α and β' polymorphs, whereas the mixtures are eutectic in the most stable β polymorph.[18] Systematic studies using different TAG mixtures have not been done even though this means that the binary TAG mixtures are highly influenced by polymorphism. Synchrotron radiation X-ray diffraction (SR-XRD) is a good tool to monitor polymorphic phase transformations of various TAG mixtures in-situ[13,18–20] and thus was used in the present study.

In the present work, we used an SR X-ray beam to examine the kinetic phase behavior of three binary mixtures of saturated monoacid TAGs, trilaurin/trimyristin (LLL/MMM), trilaurin/tripalmitin (LLL/PPP), and trilaurin/tristearin (LLL/SSS). By controlling the cooling rate of the mixture liquid and by using high-speed monitoring of the SR X-ray beam, we could detect the occurrence of metastable (α and β') and stable (β) polymorphs. Traditional phase behavior studies deal with thermodynamically stable β phase of the mixture in which metastable α and β' forms are not isolated, because of polymorphic transformation to the most stable β form. In contrast, the phase behavior that describes melting temperatures of metastable forms identified during rapid cooling and temperature controlling can be defined as phase behavior kinetically. The carbon number, C_n, of the fatty acid chains of the four TAGs are 12 (LLL), 14 (MMM), 16 (PPP), and 18 (SSS). These TAGs crystallize in three polymorphic forms, α, β', and β, that are characterized by a particular hydrocarbon chain packing and thermal stability.[21–28] α is an unstable form in which the TAG molecules are arranged perpendicular to the lamellar plane and the hydrocarbon chains are packed in a hexagonal subcell. β' form is a metastable form that has an orthorhombic perpendicular subcell and hydrocarbon chains that are inclined with respect to the basal plane by about 108 degrees. β is the most stable form and has a triclinic parallel subcell with the hydrocarbon chains inclined at about 128 degrees. The TAG chains are most densely packed in β, less dense in β', and loosely packed in α. The thermal and structural properties of polymorphic forms of LLL, MMM, PPP, and SSS are listed in Table 1.

Experimental Section

Samples of trilaurin (LLL), trimyristin (MMM), tripalmitin (PPP), and tristearin (SSS) with more than 99% purity were

* Corresponding Author: Kiyotaka Sato, Graduate School of Biosphere Sciences, Hiroshima University, Higashi-Hiroshima, 739-8528, Japan. Phone: +81 824 247935, Fax: +81 824 247910: E-mail: kyosato@hiroshima-u.ac.jp

10.1021/cg025594r CCC: $25.00 © 2003 American Chemical Society
Published on Web 02/20/2003

UM00011914
NOVARTIS EXHIBIT 1017
Novartis v. Regents, IPR2023-01346
Page 660 of 4460

Table 1. Physical Properties of Polymorphic Forms of Each Sample[a]

	LLL			MMM			PPP			SSS		
	α	β′	β	α	β′	β	α	β′	β	α	β′	β
T_m (°C)	15.0	35.0	46.5	33.0	46.5	57.0	44.7	56.6	66.4	54.9	64.0	73.1
LD (nm)	3.5	3.2	3.1	4.1	3.7	3.6	4.6	4.2	4.0	5.1	4.6	4.5
SS (nm)	0.42	0.42	0.46	0.42	0.42	0.46	0.42	0.42	0.46	0.42	0.42	0.46
		0.38	0.39		0.38	0.39		0.38	0.39		0.38	0.39
			0.38			0.38			0.38			0.38

[a] T_m: melting temperature, LD: lamellar distance, SS: short spacing.

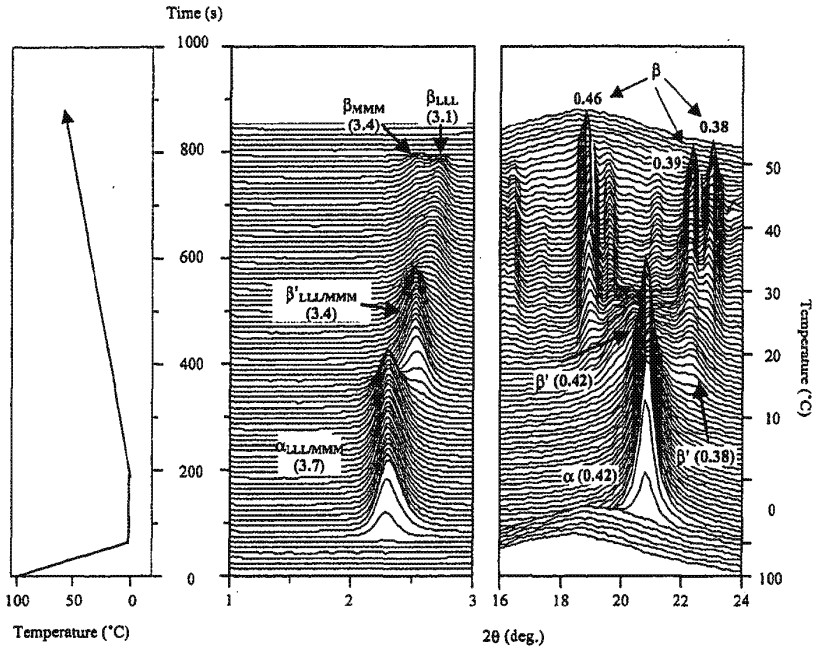


Figure 1. Time-resolved synchrotron radiation X-ray diffraction spectra concentration ratio LLL/MMM = 70/30 (unit; nm). At left, the temperature change with time.

purchased from Sigma Chemical Co. (St. Louis, MO). No further purification was done. The binary mixtures of LLL/MMM, LLL/PPP, and LLL/SSS were prepared by melting the mixtures of weighted samples above 90 °C followed and by rapid cooling to 0 °C. Concentration ratios (molar %) examined for each combination of LLL/MMM, LLL/PPP, and LLL/SSS were 90/10, 80/20, 70/30, 60/40, 50/50, 40/60, 30/70, 20/80, and 10/90.

The SR-XRD measurement was done on beam lines 9C and 15A at the Photon Factory (PF), a synchrotron radiation facility in the National Laboratory for High-Energy Physics (KEK), Tsukuba, Japan. The PF operates at 2.5 GeV and the X-ray wavelength was $\lambda = 0.15$ nm. Both small-angle X-ray scattering (SAXS) and wide-angle X-ray scattering (WAXS) spectra were recorded simultaneously every 10 s with two gas-flown one-dimensional, position-sensitive detectors. The diffraction spectra of SAXS give information about the lamellar distance and those of WAXS give information about subcell packing of the hydrocarbon chains.[27] The temperature of the sample was controlled by LINKAM LK-600PM (Cambridge, UK). The spectra were taken as the sample went through the following temperature program: (i) 100 °C for 5 min, (ii) cooling to 0 °C at a rate of 100 °C/min, (iii) 0 °C for 2 min, (iv) heating to 100 °C at a rate of 5 °C/min.

The phase diagram of TAG mixtures was constructed with the melting and transformation temperatures (T_m and T_t), which were determined when the SAXS (001) reflection spectra appeared and disappeared. The polymorphic structures were determined by the WAXS spectra: in particular, α was identified by a single peak at 0.42 nm, β′ by the closely spaced peaks at 0.42 and 0.38 nm, and β by a strong peak at 0.46 nm and the closely spaced peaks at 0.39 and 0.38 nm.[27,28]

Results and Discussion

(a) LLL/MMM System. Figure 1 shows the SR-XRD spectra of LLL/MMM = 70/30 mixture. After rapid cooling of the sample from 100 to 0 °C, a single peak appeared in SAXS with a lamellar distance of 3.7 nm. In addition to the SAXS peak, a WAXS peak at 0.42 nm appeared. The peak of α in the SAXS spectrum corresponds neither to LLL (α_{LLL}) nor to MMM (α_{MMM}). This indicates that the α form was a miscible solid-solution phase.

An increase of temperature caused a solid-state transformation from α to β′ in the miscible phase at about 15 °C; this was identified by the appearance of a SAXS peak at 3.4 nm and WAXS peaks at 0.42 and 0.38 nm. After further heating of the sample to 35 °C, three WAXS peaks at 0.46, 0.39, and 0.38 nm appeared which identify the β form. In the SAXS region, a single peak of the miscible β′ form (3.4 nm) changed into two peaks at 3.4 and 3.1 nm. The former 3.4-nm peak identifies the β form of MMM (β_{MMM}), and the latter 3.1-nm peak is the β form of LLL (β_{LLL}). This indicates that separa-

UM00011915
NOVARTIS EXHIBIT 1017
Novartis v. Regents, IPR2023-01346
Page 661 of 4460

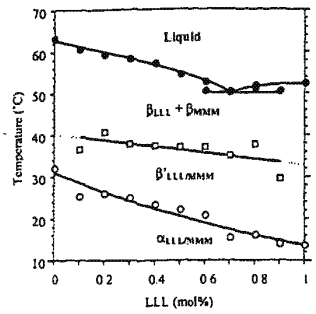


Figure 2. Phase diagram of the LLL/MMM system constructed by using data in Table 2.

tion of β_{LLL} and β_{MMM} occurred after the $\beta'-\beta$ polymorphic transformation. The same results were observed at all of the LLL/MMM mixtures that we examined.

Figure 2 shows the phase diagram obtained from the SR-XRD experiments (Table 2). This phase diagram indicates the following three points: (i) β' was formed in the mixture system, whereas α transformed directly to β in the single component systems of LLL and MMM; (ii) miscible solid-solution phases were formed in the metastable α and β' forms of the mixtures over the entire concentration range; and (iii) a eutectic phase was formed in the most stable β form. These three results are consistent with the results from the PPP/SSS system.[18]

Results of (ii) indicate that the phase behavior of TAG mixtures is remarkably dependent on the methyl end packing of the components. In the LLL/MMM mixture, C_n differs by 2. Hence, irregularity of methyl end packing in the mixture might be so small in α and β' forms, because of their less-dense chain packing, that mixing of LLL and MMM molecules does not cause instability of the methyl end packing. LLL and MMM can, therefore, form a solid-solution phase in the metastable α and β' forms. On the other hand, β has tight hydrocarbon chain packing and the degree of chain inclination with respect to the lamellar plane is high (128 degrees). This might cause instability of the methyl end packing of the mixture systems of LLL and MMM, resulting in the formation of the immiscible β phase.

(b) LLL/PPP System. In this mixture system, the phase behavior is sensitive to the LLL/PPP concentration ratios. The phase diagram is divided into three domains: high LLL concentration domain (LLL > 90%), low LLL concentration domain (LLL < 10%), and intermediate domain (50% ≤ LLL ≤ 90%).

Figure 3 shows the SR-XRD spectra of the LLL/PPP = 90/10 mixture taken during cooling and heating processes. When the mixture liquid was cooled to 0 °C, α_{LLL} with a SAXS peak at 3.5 nm and a WAXS peak at 0.42 nm was crystallized. Soon after the crystallization of α_{LLL}, β'_{LLL} with a SAXS peak at 3.2 nm and two WAXS peaks at 0.42 and 0.38 nm appears. As the temperature increased, α melted at 13.9 °C and β' transformed to β at about 25 °C. The $\beta'-\beta$ transformation was revealed by the conversions of SAXS peak from 3.2 to 3.1 nm and WAXS peak from 0.42 to 0.46, 0.39, and 0.38 nm. Finally, β melted at 51.0 °C. There was no evidence of crystallization of the PPP fraction at any temperature examined, which indicates that the PPP fraction was incorporated into the LLL crystal lattice in this mixture.

Table 2. Transformation and Melting Temperatures (°C) of Binary Mixtures of LLL/MMM, LLL/PPP, and LLL/SSS[a]

(a) LLL/MMM System

LLL (mol %)	T_t (α)	T_t (β')	T_m (β_{LLL})	T_m (β_{MMM})
0.0	32.1			64.7
0.1	25.5	36.7		59.8
0.2	26.2	40.9		59.5
0.3	25.2	38.0		60.3
0.4	23.5	37.5		57.4
0.5	22.3	37.2	54.2	54.7
0.6	21.0	37.2	51.1	52.9
0.7	15.6	35.1	50.3	50.5
0.8	16.4	37.9	51.4	52.0
0.9	14.2	19.7	50.7	
1.0	13.9		52.7	

(b) LLL/PPP System

LLL (mol %)	T_t (α_{LLL})	T_t (β'_{LLL})	T_m (β_{LLL})	T_t (α_{PPP})	T_m (β_{PPP})
0.0				45.2	69.4
0.1				39.9	73.0
0.2				35.4	67.8
0.3				35.4	67.8
0.4				37.7	71.4
0.5		24.9	53.0	35.4	66.7
0.6		25.4	50.8	34.5	63.9
0.7		23.4	48.6	33.7	64.4
0.8		23.6	51.0	32.9	59.5
0.9	13.9	23.7	51.0		
1.0	14.5		52.7		

(c) LLL/SSS System

LLL (mol %)	T_t (α_{LLL})	T_t (β'_{LLL})	T_m (β_{LLL})	T_t (α_{SSS})	T_m (β_{SSS})
0.0				62.3	80.5
0.1				52.5	77.0
0.2				47.5	79.7
0.3				44.9	77.8
0.4				43.7	73.8
0.5		24.7	51.2	43.5	75.0
0.6		23.4	48.1	41.9	70.2
0.7		24.3	49.9	43.3	71.2
0.8		23.1	51.1	42.5	69.8
0.9		21.9	51.1	38.7	64.2
1.0	13.9		52.7		

[a] T_t: transformation temperature; T_m: melting point.

The SR-XRD spectra of the LLL/PPP = 60/40 mixture taken during cooling and heating processes are shown in Figure 4. During cooling, it was clearly shown the β' form of LLL and the α form of PPP were crystallized separately. For LLL fraction, direct crystallization of β'_{LLL} with a SAXS peak at 3.2 nm and two WAXS peaks at 0.42 and 0.38 nm occurred without the crystallization of α_{LLL}. Almost at the same time, α_{PPP} with a SAXS peak at 4.6 nm and a WAXS peak at 0.42 nm appeared at 35.2 °C. Upon heating, β'_{LLL} transformed to β_{LLL} at about 25 °C, as identified by the SAXS peak at 3.1 nm and WAXS peaks at 0.46, 0.39, and 0.38 nm. On the other hand, α_{PPP} transformed to β_{PPP} with a 4.0-nm SAXS peak at 33.7 °C. The intensity of the (001) SAXS peak of β_{PPP} (4.0 nm) started to increase soon after the melting of β_{LLL} at 50.8 °C. This suggests that the presence of β_{LLL} might hinder the transformation from α_{PPP} to β_{PPP}. The same phase behavior as shown in Figure 4 was observed in the concentration ranges for

UM00011916
NOVARTIS EXHIBIT 1017
Novartis v. Regents, IPR2023-01346
Page 662 of 4460

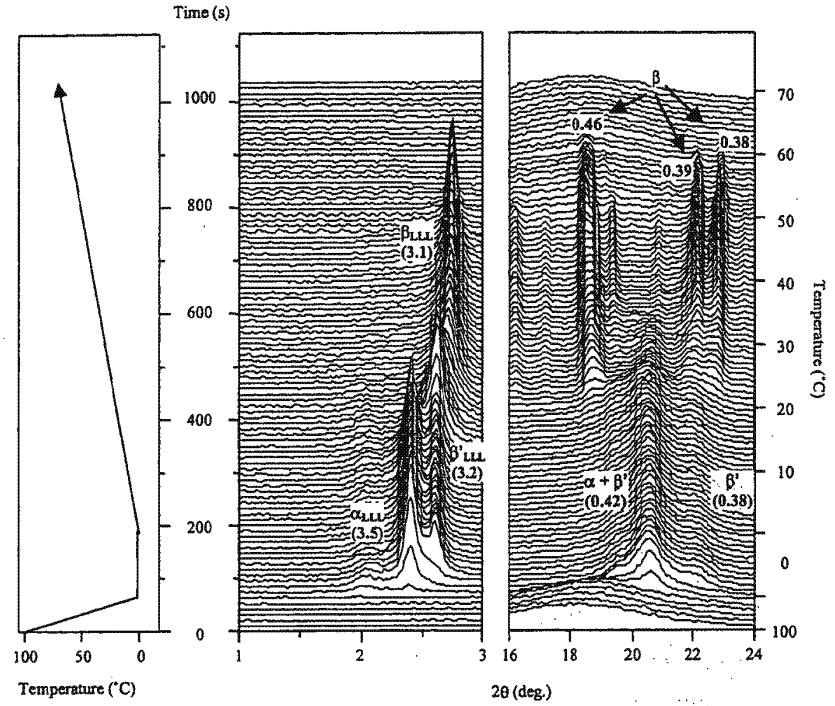


Figure 3. Time-resolved synchrotron radiation X-ray diffraction spectra concentration ratio LLL/PPP = 90/10 (unit; nm). At left, the temperature change with time.

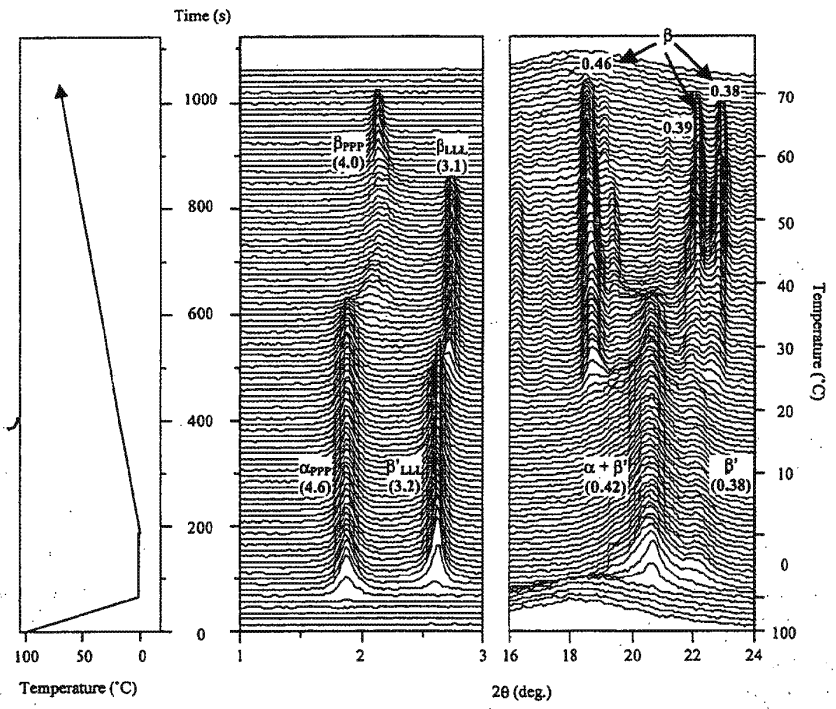


Figure 4. Time-resolved synchrotron radiation X-ray diffraction spectra concentration ratio LLL/PPP = 60/40 (nm). At left, the temperature change with time.

LLL concentrations from 50 to 90%. Hence, the immiscible phases were formed in the LLL/PPP mixture system for the three polymorphic forms. This indicates that the steric hindrance in the mixture is too large to

UM00011917
NOVARTIS EXHIBIT 1017
Novartis v. Regents, IPR2023-01346
Page 663 of 4460

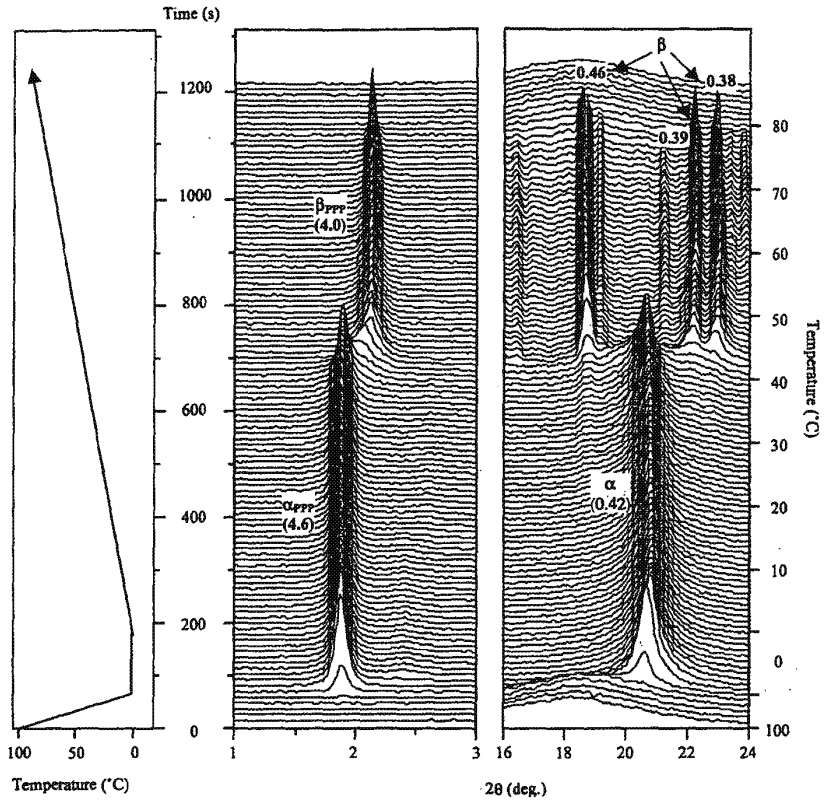


Figure 5. Time-resolved synchrotron radiation X-ray diffraction spectra concentration ratio LLL/PPP = 20/80 (nm). At left, the temperature change with time.

adjust the methyl end packing that might cause the miscible phases, when C_n differs by 4 between the component TAGs.

The SR-XRD spectra of LLL/PPP = 20/80 mixture are shown in Figure 5. No crystallization of the LLL fraction during the cooling and heating processes was observed in this mixture. α_{PPP} with a SAXS peak at 4.6 nm and a WAXS peak at 0.42 nm transformed to β_{PPP} that has a SAXS peak at 4.0 nm and WAXS peaks at 0.46, 0.39, and 0.38 nm. These results show that the LLL fraction is dissolved in the PPP fraction, which revealed the polymorphic crystallization of α and transformation from α to β in the same manner as those of pure PPP. The same behavior occurred for LLL concentrations below 50%.

Figure 6 shows the phase diagram of the LLL/PPP mixture system constructed from the polymorphic transformation and melting temperatures (Table 2). This phase diagram is subdivided into the following three regions: (i) for the LLL concentrations above 90%, the LLL fraction transformed from α to β and no independent PPP crystals were detected; (ii) for LLL concentrations between 50 and 90%, the $\beta'-\beta$ transformation of the LLL fraction and the direct $\alpha-\beta$ transformation of the PPP fraction occurred separately. This indicates that eutectic phases were formed in the three polymorphic forms; (iii) for LLL concentrations below 50%, the LLL fraction was dissolved in the PPP fraction. Hence, the

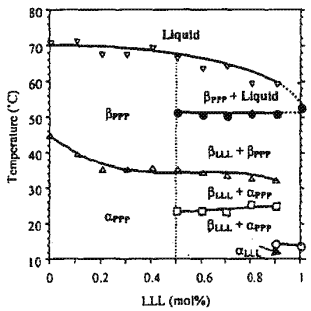


Figure 6. Phase diagram of the LLL/PPP system constructed by using data in Table 2.

phase behavior of the mixture was same as that of pure PPP.

(c) LLL/SSS System. The phase behavior of the LLL/SSS system was similar to that of the LLL/PPP system (the SR-XRD spectra are not shown). Figure 7 is a phase diagram of the LLL/SSS system constructed from the data in Table 2. For LLL concentrations above 50%, α_{SSS} and β'_{LLL} crystallized separately and no crystals of α_{LLL} were observed, when the mixture liquid was cooled to 0 °C. During heating, α_{SSS} transformed to β_{SSS} and β'_{LLL} transformed to β_{LLL}. This shows that LLL and SSS are immiscible in the three polymorphic forms. Below 50% LLL concentration, the SSS fraction involving the LLL

UM00011918
NOVARTIS EXHIBIT 1017
Novartis v. Regents, IPR2023-01346
Page 664 of 4460

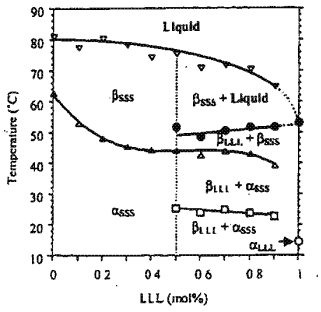


Figure 7. Phase diagram of the LLL/SSS system constructed by using data in Table 2.

fraction transformed from α to β without passing through β'.

In conclusion, it was confirmed that the phase behavior of binary TAG mixtures depended on the difference of C_n. The influences of C_n have been suggested: (i) when C_n differed by 2, the metastable forms had solid-solution phases, but the most stable form had a eutectic phase; (ii) when C_n differed by 4 or 6, both TAGs were not miscible in all polymorphic forms. Unfortunately, due to a lack of relevant thermodynamic data, we can discuss the likely mechanisms for the observed phase transformations. In particular, we need to have more precise knowledge of the conformation of hydrocarbon chains, glycerol backbone structure, methyl end packing, and thermal analyses of the phase transformations.

Acknowledgment. The authors are deeply indebted to Masaharu Nomura, High Energy Accelerator Organization, Hiroshi Takahashi, Gunma University, Shinichi Sakurai, Kyoto Institute of Technology, Shigeru Okamoto, Nagoya Institute of Technology, and Katsuhiro Yamamoto, Nagoya Institute of Technology, for help of synchrotron radiation X-ray diffraction measurements.

References

(1) Padley, F. B. In *Lipid Technology and Applications*; Gunstone, F. D., Padley, F. B., Eds.; Marcel Dekker: New York, 1997; Chapter 15, pp 391–432.
(2) Bunjes, H.; Westesen, K. In *Crystallization Processes in Fats and Lipid Systems*; Garti, N., Sato, K., Eds.; Marcel Dekker: New York, 2001; Chapter 13, pp 457–484.
(3) Matsuda, H.; Yamaguchi, M.; Arima, H. In *Crystallization Processes in Fats and lipid Systems*; Garti, N., Sato, K., Eds.; Marcel Dekker: New York, 2001; Chapter 14, pp 485–504.
(4) Love, J. A. In *Bailey's Industrial Oil & Fat Products*; Hui, Y. H., Eds.; John Wiley & Sons: New York, 1996; Vol. 1, Chapter 1, pp 1–18.
(5) Gunstone, F. D. In *Food Lipids*; Akoh, C. C., Min, D. B., Eds.; Marcel Dekker: New York, 2002; Chapter 24, pp 729–750.
(6) Sato, K. In *Advances in Applied Lipid Research*; Padley, F. B., Eds.; JAI Press: London, 1997; Vol. 2, Chapter 6, pp 213–268.
(7) Timms, R. E. In *Lipid Technologies and Applications*; Gunstone, F. D., Padley, F. B., Eds.; Marcel Dekker: New York, 1997; pp 199–222.
(8) Sato, K. *Chem. Eng. Sci.* **2001**, *56*, 2255–2266.
(9) Rossel, J. B. *Adv. Lipid Res.* **1967**, *5*, 353–408.
(10) Timms, R. E. *Prog. Lipid Res.* **1984**, *23*, 1–38.
(11) Kodali, D. R.; Atkinson, D.; Redgrave, T. G.; Small, D. M. *J. Lipid Res.* **1987**, *28*, 403–413.
(12) Koyano, T.; Hachiya, I.; Sato, K. *J. Phys. Chem.* **1992**, *96*, 10514–10520.
(13) Minato, A.; Ueno, S.; Smith, K.; Amemiya, Y.; Sato, K. *J. Phys. Chem. B* **1997**, *101*, 3498–3505.
(14) Minato, A.; Ueno, S.; Yano, J.; Smith, K.; Seto, E.; Amemiya, Y.; Sato, K. *J. Am. Oil Chem. Soc.* **1997**, *74*, 1213–1220.
(15) Kitaigorodsky, A. I. In *Mixed Crystals*; Cardona, M., Eds.; Springer-Verlag: Berlin, 1984; Chapter 2, pp 17–48.
(16) Mullin, J. W. In *Crystallization*, 4th ed.; Mullin, J. W., Eds.; Butterworth-Heinemann: Oxford, 2001; Chapter 4, pp 135–180.
(17) Engstrom, L. *J. Fat Sci. Technol.* **1992**, *94*, 173–181.
(18) Kellens, M.; Meeussen, W.; Hammersley, A.; Reynears, H. *Chem. Phys. Lipids* **1991**, *58*, 145–158.
(19) Takeuchi, M.; Ueno, S.; Flöter, E.; Sato, K. *J. Am. Oil Chem. Soc.* **2002**, *79*, 627–632.
(20) Takeuchi, M.; Ueno, S.; Sato, K. *Food Res. Int.* **2002**, *35*, 919–926.
(21) Yano, J.; Kaneko, F.; Kobayashi, M.; Kodali, D. R.; Small, D. M.; Sato, K. *J. Phys. Chem. B* **1997**, *101*, 8120–8128.
(22) Hollander, F. F. A.; Boerrigter, S. X. M.; Streek, J. van de; Grimergen, R. F. P.; Meeks, H.; Bennema, P. *J. Phys. Chem. B* **1999**, *103*, 8301–8309.
(23) Streek, J. van de; Verwer, P.; Gelder, R. de.; Hollander, F. F. A. *J. Am. Oil Chem. Soc.* **1999**, *176*, 1333–1342.
(24) Hollander, F. F. A.; Plomp, M.; Streek, J. van de; Enckevort, W. J. P. van. *Surf. Sci.* **2001**, *471*, 101–113.
(25) Evans, J.; Lee, A. Y.; Myerson, A. In *Crystallization and Solidification Properties of Lipids*; Widlak, N., Hartel, R., Narine, S., Eds.; AOCS Press: Champaign. 2001; Chapter 2, pp 17–33.
(26) Bennema, P.; Hollander, F. F. A.; Boerrigter, S. X. M.; Grimbergen, R. F. P.; Streek, J. van de.; Meeks, H. In *Crystallization Processes in Fats and Lipid Systems*; Garti, N., Sato, K., Eds.; Marcel Dekker: New York, 2001; Chapter 3, pp 99–150.
(27) Small, D. M. In *The Physical Chemistry of Lipids*; Small, D. M., Eds.; Plenum Press: New York, 1986; pp 377–382.
(28) Larsson, K. In *Lipids-Molecular Organization, Physical Functions and Technical Applications*; The Oily Press Ltd.: Dundee, 1994; Chapter 2, pp 7–46.

CG025594R

UM00011919
NOVARTIS EXHIBIT 1017
Novartis v. Regents, IPR2023-01346
Page 665 of 4460

O1(G'), 3.8 Å between O1(G) and C1(G'), and 4.6 Å across the gap C4(G')--C4(G). Therefore, the occupancies of G and G' were kept fixed at 0.25, yielding $R = 0.099$, $R_w = 0.097$, and an isotropic U value of 0.077 (3) Å^2 for the guest atoms.

We had assumed for G and G' a cis C_β—C_α—C=O conformation as had been definitely indicated by the difference map in which the oxygen peaks were by far the highest (Figure 14) and by the evidence already provided above in the analysis on DCA–methyl pentyl ketone. Moreover, the acetyl moieties of the ethyl methyl ketone G and G' molecules occupy almost the same locations (relative to steroid host) in the channel as the corresponding $H_3CCOC_2H_4$ moieties of methyl pentyl ketone. Nevertheless, least-squares calculations were carried out to verify the positions of atoms O1 and C1 of ethyl methyl ketone in a procedure akin to that adopted on methyl pentyl ketone. The refinement yielded $R = 0.095$ and $R_w = 0.094$. The refined geometries of the guests, shown in Scheme IX (in angstroms) did not distinguish between the oxygen and methyl groups certainly not in terms of the esd's in the C=O and C—CH_3 bond lengths. Nevertheless, in terms of all the facts presented here, there can be no doubt as to the cis conformation of C_β—C_α—C=O in ethyl methyl ketone.

Structure Determination (at 293 K). The final x, y, and z coordinates of DCA–ethyl methyl ketone at 103 K were used as a starting model for refinement of the room-temperature crystal structure. An R value of 0.097 was obtained. The isotropic thermal parameter of the guest molecules converged to 0.169 (6) Å^2, keeping the occupancies of G and G' each fixed at 0.25.

5.8. DCA–Cyclohexanone (at 293 K). The crystal structure was solved by MULTAN[25] although we had strong reason to believe that the host structure was isomorphous with that of DCA–di-*tert*-butyl diperoxymonocarbonate,[12] as indeed it proved to be. The host structure belongs to the γ motif. The C and O atoms of the guest molecule were unambiguously located, not being subject to disorder by virtue of the 14-Å c axis. The occupancy of the guest molecule was taken to be 0.5, its maximum possible value. Refinement proceeded smoothly to an R value of 0.086; the average U value of the guest C and O atoms was 0.23 Å^2.

5.9. Results of X-ray Crystal Structure Refinements. Details on the final cycle of refinements are given in Table III. The atomic x, y, and z coordinates and U_{eq} of DCA–acetone (at 103 K), APA–acetone, DCA–diethyl ketone, DCA–cyclohexanone, DCA–ethyl methyl ketone (at 103 K), and DCA-methyl pentyl ketone are listed in Tables IV–IX, respectively. Anisotropic temperature factors U_{ij}, bond lengths, and bond angles are listed in supplementary material Tables 4S–9S; the x, y, and z coordinates of DCA–acetone (at 293 K) and DCA–ethyl methyl ketone (at 293 K) are listed in Tables 4S and 8S, respectively.

Acknowledgment. We thank Prof. M. D. Cohen for fruitful discussions. We thank the Israel/U.S. Binational Science Foundation and the Israel Academy of Science and Humanities for financial support.

Registry No. 1, 66014-00-4; **1** (methyl ester), 95484-83-6; **2**, 66014-23-1; **2** (methyl ester), 95484-84-7; **3**, 66971-13-9; **3** (methyl ester), 95615-84-2; **4**, 66014-20-8; **5**, 95484-85-8; **6**, 83035-68-1; **6** (methyl ester), 95484-86-9; **7**, 58678-36-7; **7** (methyl ester), 95484-87-0; **8**, 77522-07-7; **9**, 95484-88-1; **9** (methyl ester), 95484-89-2; **10** (isomer 1), 95586-12-2; **10** (methyl ester) (isomer 1), 95484-90-5; **10** (isomer 2), 95586-13-3; **10** (methyl ester) (isomer 2), 95484-91-6; **11** (isomer 1), 95586-14-4; **11** (isomer 2), 95586-15-5; DCA·$^3/_5$acetone, 83035-57-8; DCA·$^1/_2$(diethyl ketone), 83047-97-6; DCA·$^1/_2$cyclohexanone, 95484-92-7; DCA·$^1/_2$(ethyl methyl ketone), 83035-64-7; DCA·$^1/_3$(methyl pentyl ketone), 95484-93-8; APA·acetone, 66971-12-8.

Supplementary Material Available: Thermal parameters, bond angles, and bond lengths of molecules A and B (26 pages). Ordering information is given on any masthead page.

Reaction Pathways in Crystalline Host–Guest Inclusion Complexes: Rotation by a Net 180° of the Acetyl Group on Photoaddition of Guest–Acetophenone and –*m*-Chloroacetophenone to the Atom C5 of Host Deoxycholic Acid

C. P. Tang,[1a] H. C. Chang,[1a] R. Popovitz-Biro,[1a] F. Frolow,[1a] M. Lahav,*[1a] L. Leiserowitz,*[1a] and R. K. McMullan[1b]

Contribution from the Department of Structural Chemistry, The Weizmann Institute of Science, Rehovot, Israel 76100, and the Department of Chemistry, Brookhaven National Laboratory, Upton, New York 11793. *Received July 11, 1984*

Abstract: The crystalline host–guest channel inclusion complexes 5:2 (DCA) deoxycholic acid–acetophenone ($C_6H_5C'OCH_3$) and 3:1 DCA–*m*-chloroacetophenone ($CLC_6H_4C'OCH_3$) each yield on UV irradiation a photoproduct via addition of guest to the steroid tertiary carbon atom C5 with the formation of a new chiral carbon center C'(OH)(CH_3)(C_6H_5)(DCA) of S configuration. The crystal structures of the two host–guest complexes were determined by low-temperature (103 K) X-ray diffraction; a low-temperature (16 K) neutron study was made on DCA–$C_6H_5COCD_3$. The inclusion compounds DCA–$C_6H_5COCH_3$ and DCA–$CLC_6H_4COCH_3$ each contain two crystallographically independent guest molecules G and G' arranged along the channel axes such that both G and G' should form the same diastereomeric product at C5. A comparison of the stereochemistry of each of the two isolated photoproducts and the host–guest arrangements at the reaction sites in each corresponding complex indicates that photoaddition of the guest molecule to C5 takes place with a net rotation of 180° by the guest acetyl group.

1. Introduction

1.1. Statement of the Problem. In the previous paper in this issue,[2] we described the regiospecific solid-state photoaddition of several guest aliphatic ketones to the host deoxycholic acid (referred to as DCA) in the channels of the bile acids. A comparative analysis of the stereochemistries of the reaction products formed,

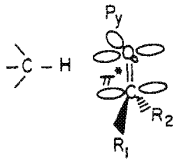
(1) (a) Weizmann Institute of Science. (b) Brookhaven National Laboratory.

(2) Popovitz-Biro, R.; Tang, C. P.; Chang, H. C.; Lahav, M.; Leiserowitz, L. *J. Am. Chem. Soc.*, preceding paper in this issue.

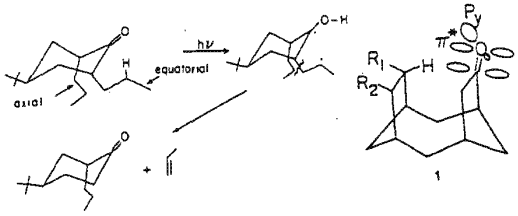
0002-7863/85/1507-4058$01.50/0 © 1985 American Chemical Society

UM00011920
NOVARTIS EXHIBIT 1017
Novartis v. Regents, IPR2023-01346
Page 666 of 4460

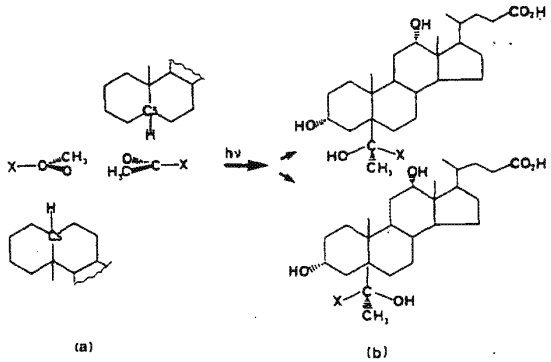
Scheme I



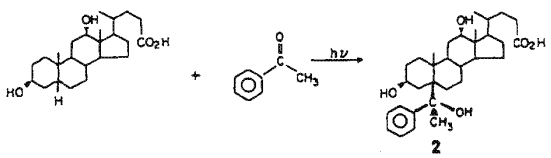
Scheme II



Scheme III



Scheme IV



with the corresponding host–guest arrangements at the sites of reaction prior to photoaddition, demonstrated the topochemical nature of this reaction. In all the complexes where reaction occurred, the plane of the guest carbonyl system >C=O tends to be perpendicular to the C–H bond of the steroid hydrogen to be abstracted. Consequently, in these systems, the P_y orbital of the guest oxygen atom tends to be perpendicular to the C–H bond, and the π^* orbital tends to be parallel to the C–H bond (Scheme I). A number of theoretical and experimental studies have been carried out probing the mechanism of the hydrogen abstraction in terms of the orientation of the to-be-abstracted hydrogen vis-a-vis the carbonyl >C=O system. Zimmerman[3] suggested that the hydrogen abstraction is dominated by the electrophilic attack of the P_y orbital of the $n-\pi^*$ excited carbonyl group. This suggestion was further supported by Salem's symmetry plane assumption,[4] stating that the most favorable orbital interaction is one in which the >C=O and H—X groups are coplanar. On the experimental side, Turro[5] observed that irradiation of 2,6-di-*n*-propylcyclohexanone yields the less stable axial isomer of 2-*n*-propylcyclohexanone, which he rationalized by an in-plane approach of the equatorial C–H bond toward the P_y orbital of the excited carbonyl (Scheme II). From these results, however, the author could not exclude unambiguously the possibility that hydrogen can be abstracted by the π^* orbital as well. In this respect, Sugiyama et al.[6] noticed that in compound **1**, where the π^* orbital is directly aligned toward hydrogen H, the carbonyl oxygen atom does not abstract that atom upon photoirradiation. Scheffer, Trotter, and co-workers,[7] in their studies on the photochemistry of rigid tetrahydro-1,4-naphthoquinones in solution and in the solid state, confirmed that the abstracted hydrogens are almost coplanar with the carbonyl system >C=O, deviating from it by an angle no more than 8°. Recently similar studies were carried out on low-melting α-cyclohexylacetophenones. In these systems, the hydrogen lies outside the mean plane of the carbonyl group. The C–H bond of the to-be-abstracted hydrogen and the carbonyl group tends to be parallel.[8]

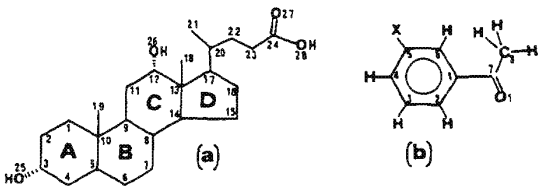


Figure 1. Atom labeling. (a) Deoxycholic acid (DCA). (b) Acetophenone, x = H; *m*-chloroacetophenone x = CL.

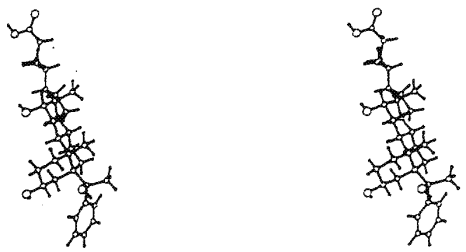


Figure 2. Photoproduct **2** from DCA–acetophenone in its own crystal structure.

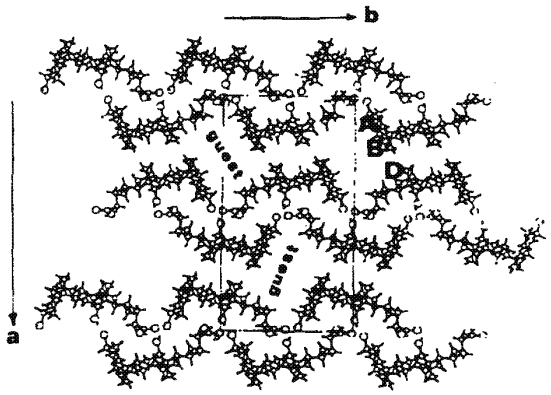


Figure 3. Packing arrangement of DCA molecules in the α motif viewed along the channel *c* axis. The guest molecules are not shown.

(3) Zimmerman, H. E. *Adv. Photochem.* **1963**, *1*, 183 and references cited therein.
(4) Dauben, W. G.; Salem, L.; Turro, J. N. *Acc. Chem. Res.* **1975**, *8*, 41.
(5) Turro, N. J., Weiss; D. W. *J. Am. Chem. Soc.* **1968**, *90*, 2185. Davies, K.; Dalton, J. C.; Turro, N. J. *Mol. Photochem.* **1971**, *3*, 71.
(6) Sugiyama, N.; Nishio, T.; Yamada, K.; Aoyama, H. *Bull. Chem. Soc. Jpn.* **1970**, *43*, 1879.
(7) Scheffer, J. R. *Acc. Chem. Res.* **1980**, *13*, 283. Trotter, J. *Acta Crystallogr, Sect. B* **1983**, *B39*, 373.
(8) Ariel, S.; Ramamurthy, V.; Scheffer, J. R.; Trotter, J. *J. Am. Chem. Soc.* **1983**, *105*, 6959.

UM00011921
NOVARTIS EXHIBIT 1017
Novartis v. Regents, IPR2023-01346
Page 667 of 4460

Table I. ^{13}C NMR Data on Photoaddition Products 2 and 3

	2	3
C1	32.5	32.3
C2	30.9	30.9
C3	69.2	69.3
C4	38.1	38.0
C5	49.3	49.1
C6	29.1	29.7
C7	28.8	28.8
C8	37.5	37.6
C9	36.3	36.4
C10	41.7	41.7
C11	30.8	30.9
C12	75.2	75.2
C13	46.7	46.7
C14	49.2	49.1
C15	24.7	24.7
C16	28.4	28.5
C17	47.9	47.9
C18	13.0	13.0
C19	20.6	20.4
C20	36.4	36.4
C21	17.6	17.6
C22	31.7	31.6
C23	31.7	31.6
$C(OH)CH_3$	85.3	85.1
$C(OH)CH_3$	30.1	30.1
phenyl C's	128.1	127.3
	129.0	128.0
	129.0	128.0
	129.4	128.0
	153.0	154.3

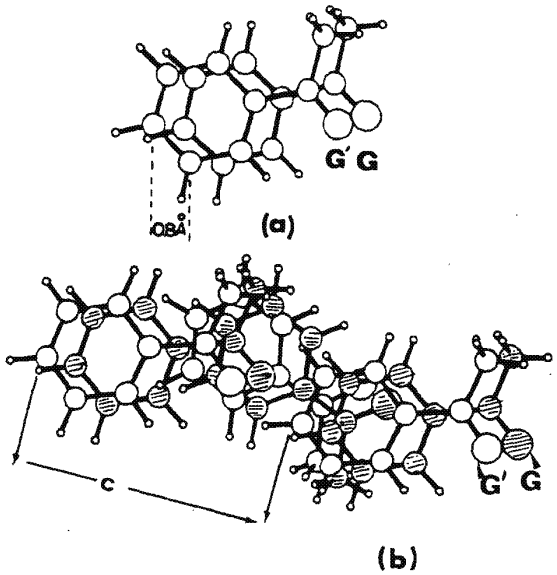


Figure 4. (a) Overlapping pair of guest acetophenone molecules $G(x,y,z)$ and $G'(x,y,z')$ referred to the same molecular site. (b) Molecular overlap of acetophenone guest molecules G (shaded atoms) and G′ (unshaded atoms) in the channel. The arrangement may be derived from the molecular pair in (a) by applying 2_1 symmetry to G and G′ along the channel.

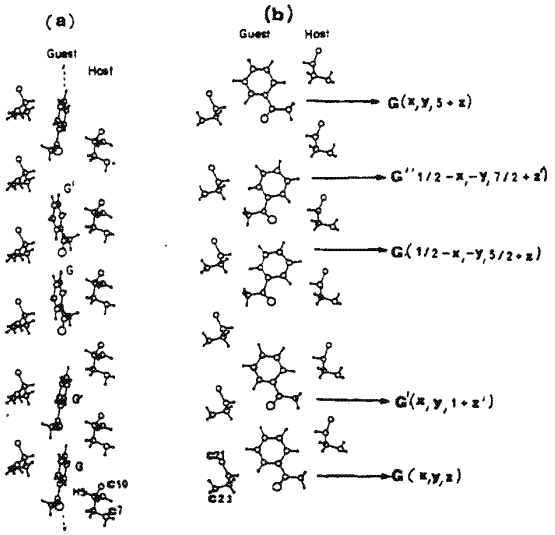


Figure 5. Closest-packed arrangement of acetophenone molecules in a channel derived from the two independent molecules $G(x,y,z)$ and $G'(x,y,z')$ shown in Figure 4. (The coordinates of the channel 2_1 axis are $x = {}^1/_4$, $y = 0$.) (a) View edge-on to plane of guest molecules. The channel walls shown are a part of steroid rings A and B. (b) View perpendicular to plane of guest molecules. The channel walls are a part of the steroid side chain.

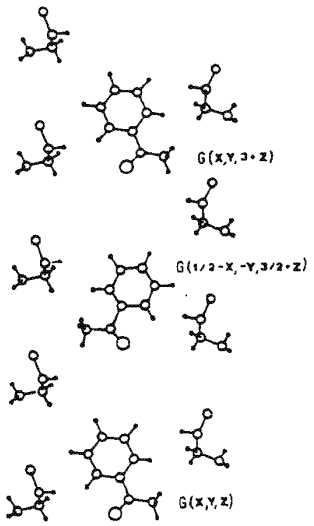


Figure 6. String of nearest neighbor acetophenone G molecules in the channel. The channel 2_1 axis passes through x, $y = {}^1/_4$, 0.

The deoxycholic acid–ketone complexes are ideal for probing the relative roles of the P_y and π^* orbitals in the abstraction process because the carbonyl plane >C=O of the guest–ketone tends to be perpendicular to the steroid C–H bond of the to-be-abstracted H atom. Prochiral ketones are appropriate guests for this purpose because the prochirality allows a correlation to be made between the absolute configuration of the new chiral center of the photoproduct with the relative orientation of the guest >C=O and host H—C groups prior to reaction. Moreover, we have recently observed that the ketone complexes of the bile acids maintain their crystalline integrity on photoreaction. This fact provided a new tool to elucidate the fine details of the molecular pathway of a reaction by allowing one to determine the crystal structure both before and after reaction.

1.2. Selection of the Models. In the previous paper in this issue,[2] it was demonstrated that the prochiral methyl alkyl ketones (H_3C–CO–C_nH_{2n+1}, n = 2–5) are unsatisfactory for the above purpose because these guests from pseudocentrosymmetric pairs (Scheme IIIa) in the channels of DCA arranged in such a way as to yield the two diastereomeric photoproducts (Scheme IIIb). These host–guest arrangements cannot be exploited to elucidate the comparative role of P_y vs. π^* orbitals in the hydrogen ab-

UM00011922
NOVARTIS EXHIBIT 1017
Novartis v. Regents, IPR2023-01346
Page 668 of 4460

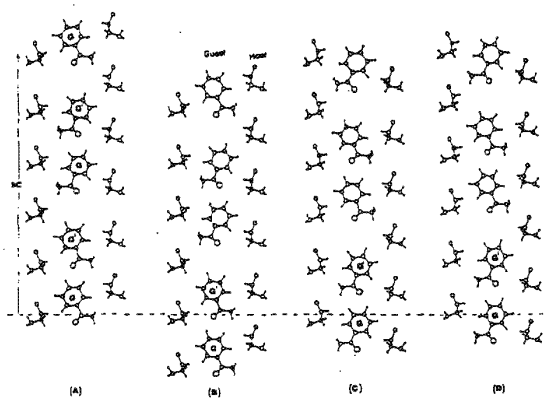


Figure 7. Four disordered guest arrangements in a given channel which differ in their z coordinates. The host–guest contacts are the same for all arrangements.

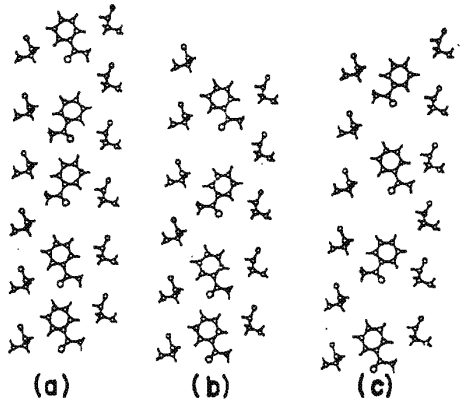


Figure 8. Three guest arrangements for which intermolecular potential energies were calculated: (a) 4:10 guest-host arrangement derived from the X-ray study; (b) 3:8 guest–host arrangement; (c) 1:3 guest–host arrangement.

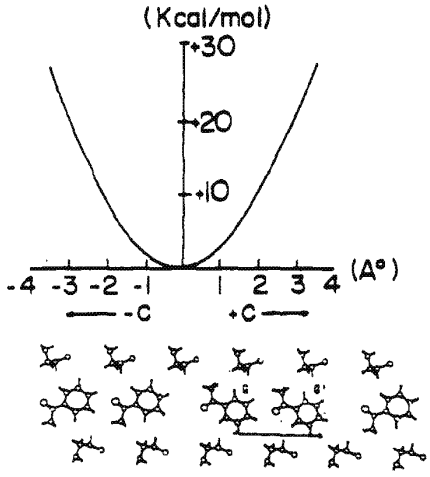


Figure 9. Variation in lattice energy as a result of moving the X-ray-derived chain of acetophenone molecules as a unit along the channel axis.

straction. In an attempt to circumvent such difficulties, we initiated a study with acetophenones as occluded guests, a choice which eventually proved to be auspicious. Here we describe

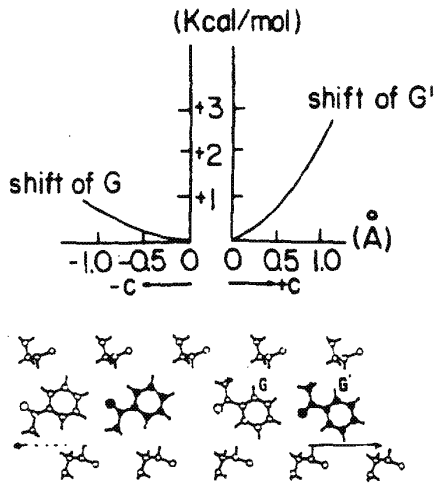


Figure 10. Variation in lattice energy as a result of moving the acetophenone molecules G′ and G separately, along the $+c$ and $-c$ directions respectively.

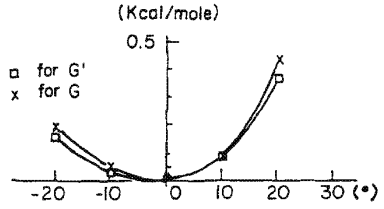


Figure 11. Variation in lattice energy as a result of separately rotating the acetyl groups $COCH_3$ of G and G′.

reactions carried out on complexes of deoxycholic acid (DCA) occluded with acetophenone and with *m*-chloroacetophenone (Figure 1).

2. Crystalline Molecular Complex DCA–Acetophenone

2.1. Solid-State Photochemistry. Crystals of the complex were obtained from a solution of DCA with acetophenone in methanol. Irradiation of these crystals for about 30 days, $\lambda > 300$ nm, yielded a single topochemical addition product **2** with 25% yield, as shown in Scheme IV. The molecular structure of photoproduct **2** (Figure 2) was unambiguously assigned from an X-ray analysis (see section 5.9) and ^{13}C NMR. ^{13}C NMR analysis easily differentiates between the two diastereoisomers, as shown for photoproducts[2] from DCA–ethyl methyl ketone and DCA–methyl propyl ketone. TLC analysis and a ^{13}C NMR analysis of the product (Table I) indicate that only a single diastereoisomer is formed.[9]

2.2. Crystal Structure and the Guest Arrangement in the Channel. The crystal structure of DCA–acetophenone was determined via low-temperature X-ray and neutron diffraction analyses (see sections 5.5 and 5.7). The host DCA molecules are arranged in the α motif[2] (Figure 3), as would be expected for nonbulky guest molecules. Two independent guest molecules, G and G′, were located in the channel. These two molecules nearly coincide in terms of the diffraction analysis; G and G′ differ in position only in the z coordinate along the channel axis by a separation of 0.8 Å as shown in Figure 4. We shall deduce that the guest molecules are arranged along each channel as depicted in Figure 5. They form close-packed pairs GG′ separated by gaps. Within each pair, G and G′ are related along the z direction by

(9) The protons of methyl-19 appear as two singlets due to hindered rotation around the C(5)–$COH(CH_3)(Ph)$ bond. When crystals of the product were dissolved at −60 °C, only one conformation was observed; after heating above 30 °C, the second conformer started to appear.

UM00011923
NOVARTIS EXHIBIT 1017
Novartis v. Regents, IPR2023-01346
Page 669 of 4460

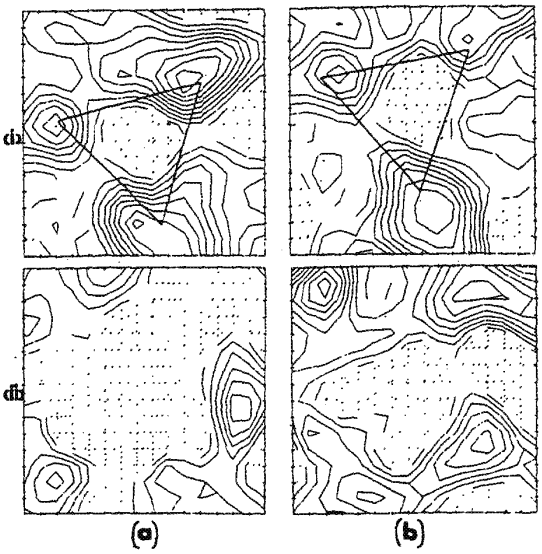


Figure 12. Neutron study of DCA–$C_6H_5COCD_3$. Difference density syntheses using calculated structure factors based on contribution of DCA–C_6H_5COC. The four maps were calculated in planes perpendicular to the C7—C8 (i.e., C—CD_3) and C7—O (i.e., C=O) bonds of guests G and G′. Each plane passes through a point which lies on extension of bond at a distance 1.1 Å sin(110–90)° from atom C8 or O1. (a) Molecule G. (b) Molecule G′. (i) Maps perpendicular to the C7—C8 bond. The three peaks of each map correspond to a symmetric D_3 methyl group as demonstrated by the good fit to the triangles of sides 1.8 Å which is the intramolecular distance between D atoms of a methyl group. (ii) Maps perpendicular to the C7–O1 bond. Neither map shows evidence of a D_3 group.

Table II. Distances *d* (Å) between the Guest C=O Group and the Host DCA

C=O	DCA	*d*, 103 K	*d*, 293 K
	(a) DCA–Acetophenone		
O(G)	H5	3.1	3.1
	$H6_{eq}$	3.2	3.2
	$H6'_{ax}$	3.4	3.2
C(G)	C5	3.8	3.9
	C6	3.8	3.9
O(G′)	H5	2.9	3.0
	H6	3.7	4.0
	H6′	3.9	3.6
C(G′)	C5	3.8	3.9
	C6	4.1	4.0
	(b) DCA–*m*-Cloroacetophenone		
O(G)	H5	2.4	
	H6[a]	3.5	
	H6′[a]	3.3	
C(G)	C5	4.0	
	C6[a]	3.5	
O(G′)	H5	2.4	
	H6	3.8	
	H6′	3.8	
C(G′)	C5	3.6	
	C6	3.9	

[a] Symmetry operation $^1/_2 - x, -y, ^1/_2 + z$ was applied to the guest atom.

a pseudotranslation of $c + 0.8$ Å. The neighboring pairs are related by a $5c/2$ translation plus a rotation about the 2_1 axis which passes along the center of the channel.

Deduction of the Guest Arrangement from the Diffraction Analysis. The occupancies of G and of G′, i.e., the molar ratio of guest to host, were refined by X-ray structure factor least squares to values of 0.202 (6) and 0.215 (8), respectively. These two individual occupancies were kept fixed at 0.2 in the X-ray least-squares refinement. We shall now make use of the principle of closest molecular packing to demonstrate that the maximum total guest occupancy is 0.4, with individual occupancies of G and G′ equal to each other at 0.2. Furthermore, we shall show that the occupancy of 0.4 arises from a unique packing within the channel; any other feasible arrangement would lead to a lower occupancy.

The observed individual occupancies of G and G′ indicate that, on the average, one in every five crystallographic sites of G, and G′, is occupied. First we examine whether the channels are occupied by separate extended strings of G and of G′ molecules, namely GGGGG and G′G′G′G′G′. Let the coordinates of a G molecule be x, y, and z and that of G′ be x, y, and z' where $z' = z + 0.8$ Å/c, G and G′ being referred to the same molecular site as shown in Figure 4a. A generated string of closest-packed

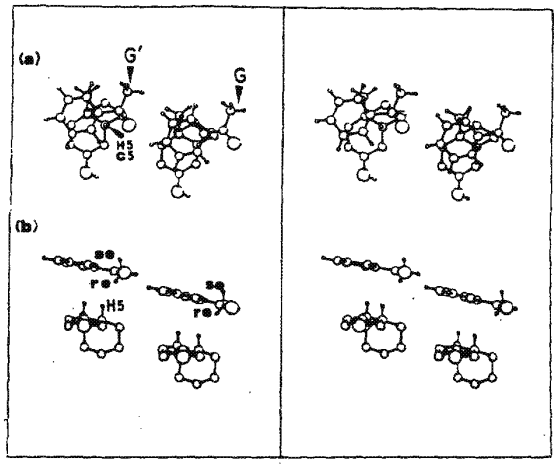


Figure 13. DCA–acetophenone. Host–guest packing at site of reaction. The two guest molecules G and G′ and ring A of the steroid are shown. H atoms omitted on ring A but for H5. (a) View along the steroid H5–C5 bond. (b) View perpendicular to the H5–C5 bond.

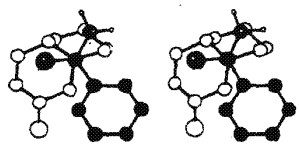
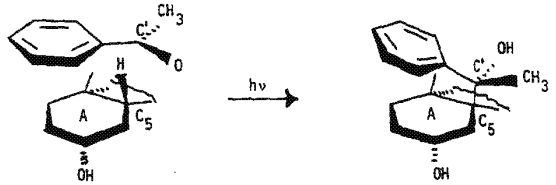
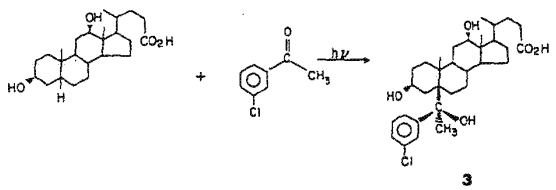


Figure 14. Moiety $C^*OHCH_3C_6H_5$ and rings A and B of photoproduct **2** of DCA–acetophenone in its own crystal structure (see also Figure 2). View along the C^*–C5 bond. C and O of rings A and B in open circles.

Scheme V



Scheme VI



3

UM00011004
NOVARTIS EXHIBIT 1017
Novartis v. Regents, IPR2023-01346
Page 670 of 4460

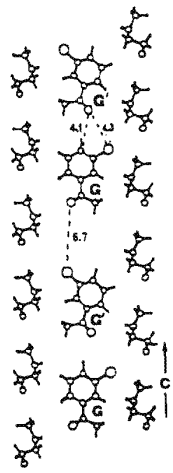


Figure 15. Deduced packing arrangement of chloroacetophenone molecules in the channel viewed perpendicular to the plane of the guest molecule.

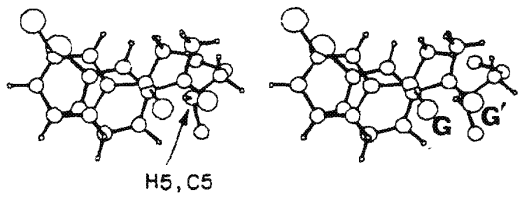


Figure 16. Host–guest packing at site of reaction showing chloroacetophenone molecules G and G′, as referred to the same steroid site, and parts of neighboring rings A and B of steroid. H atoms H5, H6, and H6′ are drawn.

G molecules is shown in Figure 6. The nearest neighbor of $G(x,y,z)$ along the channel would be $G(^1/_2 - x,-y,^3/_2 + z)$ because of the twofold screw symmetry along the channel c axis. In other words, one in three consecutive sites may be occupied in separate strings of G and G′ molecules, resulting in a maximum total occupany of 1:3, which is incompatible with the derived total value of 0.42 (1). Substituting a G′ molecule for G at any molecular site, in the string, i.e., $G'(x,y,z')$ instead of $G(x,y,z)$, would leave the maximum occupancy unchanged at 1:3. It is possible to construct a denser arrangement only if G and G′ form the close-packed pair $G(x,y,z)$ and $G'(x,y,1 + z')$ shown in Figure 5. G and G′, in this pair, are separated by the length of the c axis + 0.8 Å to bring about an acceptable intermolecular H···O contact between C4(G)–H and O(G′) of 3.1 Å. When translation and 2_1 symmetry are applied (the 2_1 axis passes through the channel center at $x = ^1/_4$, $y = 0$), the nearest neighbor that follows $G'(x,y,1 + z')$ in the $+z$ direction is $G(^1/_2 - x,-y,^5/_2 + z)$ followed by $G'(^1/_2 - x,-y,^7/_2 + z')$, the latter two also forming the close-packed GG′ pair. The next nearest molecule, $G(x,y,5 + z)$, is removed by a translation distance of $5c$ from the starting guest $G(x,y,z)$. This guest structure has a total guest occupancy of $2/5 = 0.4$, with values of 0.2 for both G and G′. It is the densest possible arrangement given that the crystal structure contains only the two independent guest molecules $G(x,y,z)$ and $G'(x,y,z')$. This arrangement fits the X-ray structure-factor least-squares results excellently. The guest molecules thus form a one-dimensional superstructure in the channel with a translation repeat of $5c$ = 36 Å. Room-temperature oscillation photographs about the c axis of single crystals of DCA–acetophenone did not appear to reveal any explicit evidence of this superstructure in terms of diffuse reciprocal layers corresponding to the $5c$ repeat distance or, what would appear to be more likely, a $5c/2$ repeat distance which represents the separation along z between the close-packed GG′ pairs in the channel. Nor were we clearly able to discern evidence of this superstructure by low-temperature (103 K) X-ray diffraction measurements. We infer therefore that the diffuse layers were too weak to be observed or that there must be an occasional break of the superstructure pattern along the channel axis. Naturally such faults would reduce the total guest occupancy. In a given channel, there are five different arrangements of the one-dimensional guest superstructure, four of which are shown in Figure 7. Thus, there are 25 different arrangements of the one-dimensional guest superstructure in a disordered unit cell, because there are two symmetry-related channels per unit cell (see Figure 3).

Guest Arrangement by Potential Energy Calculations and Neutron Diffraction. To furnish complementary evidence for the correctness of the guest arrangement derived from the X-ray and neutron diffraction analyses, we examined possible guest arrangement in terms of atom–atom potential energy calculations.[10–13] A similar approach has been recently applied to the inclusion compounds of DCA with phenanthrene and *p*-(dimethylamino)azobenzene to help establish the locations of the guest molecules.[14]

We first consider lattice energies of channel motifs as a function of guest occupancy. The highest possible guest–host molar ratio is 4:9 for an arrangement in which the neighboring guest molecules would be separated along the channel by 8 Å, which is the distance between G and G′ molecules of the close-packed pair (Figure 5) derived from the X-ray diffraction study. The repeat translation distance along the channel would be $9c \simeq 64$ Å $= 8 \times 8$ Å. Such an arrangement may be precluded because it would need to incorporate four independent guest molecules, as against the two (G, G′) derived from the diffraction analysis; moreover, such a motif would incur poor guest–host contacts as shall become evident below. Thus, the motif of the highest guest occupancy examined via lattice energies was that derived from the X-ray study, with an occupancy of 4:10 (Figure 8a). A plausible arrangement with the next most dense packing is found in DCA–*p*-fluoroacetophenone described in the following paper in this series.[15] The motif is shown in Figure 8b, containing a guest occupancy of 3:8 with a G′/G molar ratio of 2:1. We may construct an analogous motif with a G′/G molar ratio of 1:2. A crystal structure containing a random arrangement of these two strings would have a total guest occupancy of 3:8 and a G/G′ molar ratio of 1:1, values close to what was found in the present X-ray study. A third plausible arrangement is the string of G′, or G, molecules (Figure 8c) with a guest occupancy of 1:3. The relative lattice energies of these three crystal structures a, b, and c are 0, +0.4, and +1.1 kcal/mol,[16] respectively. Thus, the most stable structure is the X-ray-derived complex.[17]

Next, the lattice energy was calculated on moving the X-ray derived chain of molecules in the channel in steps of 1 Å. At each

(10) A computer program written by A. T. Hagler and R. Sharon (CMIN2, Department of Chemical Physics, Weizmann Institute, Rehovot, Israel) was used for calculation of lattice energies by atom–atom potentials. Lattice energy minimization was done for several interactions with respect to the nine parameters defining the Cartesian components of the unit cell vectors as well as the six translational and rotational parameters for each, but one, of the molecules in the unit cell. A cutoff distance of 11 Å was used for all minimizations. A 9–6–1 potential was used with energy parameters for the O, C, and H atoms (given in Table 1S, supplementary material) taken primarily from force field studies of amides and carboxylic acids[11] but for the oxygen of the acetyl group and the arom. C–H groups. For the O atom of the acetyl group, we assumed that the net negative charge is 0.38 e instead of 0.46 e found for the corresponding carbonyl O atom. Here we were assisted by quantum chemical calculations on formaldehyde and formic acid.[12] The partial charges of C and H of the phenyl group were taken at −0.08 e and +0.08 e, respectively.[13]

(11) Lifson, S.; Hagler, A. T.; Dauber, P. *J. Am. Chem. Soc.* **1979**, *101*, 5131 and references therein.

(12) Eisenstein, M. Ph.D. Thesis, The Feinberg Graduate School, Weizmann Institute, Rehobot, Israel, 1981.

(13) Williams, D. E. *Acta. Crystallogr., Sect. A* **1974**, *A30*, 71.

(14) De Sanctis, S. C., *Acta Crystallogr., Sect. B* **1983**, *B39*, 366.

(15) Chang, H. C.; Weissenger, Y.; Frolow, F.; Popovitz-Biro, R.; Lahav, M.; Leiserowitz, L., unpublished results.

(16) One mole = one mole of DCA + the molar fraction of guest, which equals 0.4, 0.375, and 0.333 for arrangements a, b, and c, respectively.

UM00011925
NOVARTIS EXHIBIT 1017
Novartis v. Regents, IPR2023-01346
Page 671 of 4460

Table III. Cell Constants and Experimental Data on X-ray and Neutron Intensities of (a),(b) DCA–Acetophenone ($C_6H_5COCD_3$), (c),(d) DCA–Acetophenone ($C_6H_5COCH_3$), (e) DCA–*m*-Chloroacetophenone, (f) 5β-(*S*)(1-Phenylethanol)deoxycholic Acid (Photoproduct 2)

	a	b	c	d	e	f
cryst temp, K	16	83	103	293	103	293
formula[a]	$C_{24}H_{40}O_4$ $^2/_5(C_8H_5D_3O)$	$C_{24}H_{40}O_4$ $^2/_5(C_8H_5D_3O)$	$C_{24}H_{40}O_4$ $^2/_5(C_8H_8O)$	$C_{24}H_{40}O_4$ $^2/_5(C_8H_8O)$	$C_{24}H_{40}O_4$ $^1/_3(C_8H_7OCl)$	$C_{32}H_{48}O_5$
a, $\sigma(a)$, Å[b]	25.199 (6)	25.285 (8)	25.243 (7)	25.589 (6)	25.283 (8)	12.107 (2)
b	13.602 (3)	13.611 (4)	13.606 (2)	13.709 (3)	13.639 (4)	15.115 (5)
c	7.192 (2)	7.192 (3)	7.198 (2)	7.247 (2)	7.198 (4)	7.522 (2)
β, deg						94.08 (3)
Z	4	4	4	4	4	2
V, Å^3	2465	2475	2475	2542	2470	1373
space group	$P2_12_12_1$	$P2_12_12_1$	$P2_12_12_1$	$P2_12_12_1$	$P2_12_12_1$	$P2_1$
D_x, g/cm^3			1.17	1.14	1.17	1.24
mp, °C			177–178	177–178	170–172	216
diffractometer	Brookhaven neutron diffractometer		CAD-4	Siemens	CAD-4	Siemens
crystal size of specimen, (mm × 10^3)	5 × 5 × 22		2 × 3 × 6	2 × 2 × 4	2 × 3 × 5	1 × 1 × 4
radiation[c]	N(=1.1611 Å)		X(Mo Kα)	X(Cu Kα)	X(Mo Kα)	X(Cu Kα)
μ, cm^{-1}	2.95		0.9	6.3	1.0	6.6
θ(maximum)	52		36	70	33	70
ω/θ scan ratio	1/1		3/2	1/1	6/5	1/1
max scan time, s			60	50	80	50
no. of reflects[d]	2564		15196	5425	5930	5415
	1313		6488	2770	5812	2712
R_m[e]	0.033		0.038	0.03	0.025	0.04

[a] The guest–host molar ratios of compounds c and e, equal to 2:5 and 1:3, respectively, were determined by X-ray structure-factor least-squares refinement. [b] λ(Mo Kα$_1$) = 0.70926 Å, λ(Cu Kα$_1$) = 1.54041 Å. [c] N = Neutron radiation; X = X-rays. [d] Two values given for each compound are total and independent number of reflections measured. [e] $R_m = \sum|F^2 - \bar{F}^2|/\sum F^2$ where F is an observed structure factor and $\bar{F}$ the weighted mean of the corresponding symmetry-related set of observed structure factors.

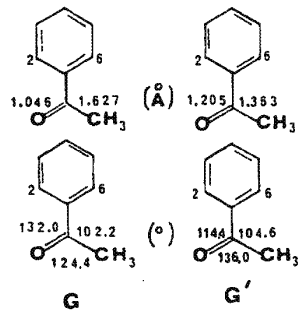


Figure 17. Bond lengths and bond angles of the acetyl groups of acetophenone G and G′ after constrained–restrained refinement.

step, the energy was minimized for two or three cycles. The energy minimum (Figure 9) corresponds to the observed arrangement, and the sharp rise in the curve on both sides of the minimum clearly demonstrates the role played by the host–guest interactions in determining guest packing.[18] The energy was also calculated on a movement of G′ and G separately from their X-ray-derived positions. These energy curves (Figure 10) show not only a rise in energy on guest displacement but that guest G can be more easily displaced along the $-c$ direction than guest G′ can be displaced along the $+c$ direction.

In order to support the results of the X-ray analysis that the acetyl and phenyl moieties of the guest molecules are coplanar, the crystal energy was calculated on rotation of the acetyl groups of G and of G′ separately about the exocyclic C(phenyl)–C(carbonyl) bonds. These calculations (Figure 11) show that planar guest molecules yield the lowest lattice energy.

The oxygen and methyl carbon atoms of G and G′ occupy regions of atomic overlap in the X-ray structure analyses (see

(17) It is relevant that the calculated lattice energy difference between observed and hypothetical crystal structures may be as low as 0.5 kcal/mol. See: Berkovitch-Yellin, Z.; Leiserowitz, L. *J. Am. Chem. Soc.* **1982**, *104*, 4052 and references therein.

(18) One may also infer from this curve that the closest-packed arrangement of guest molecules with a 4:9 guest–host molar ratio would be less stable than the X-ray derived arrangement.

Scheme VII

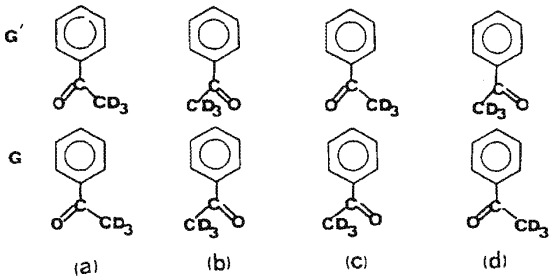


Table IV. X-ray Structure-Factor Refinement of (a) DCA–Acetophenone at 103 K, (b) DCA–Acetophenone at 293 K, (c) DCA–*m*-Chloroacetophenone at 103 K, and (d) Photoproduct 2 at 293 K from DCA–Acetophenone

	a	b	c	d
no. of refined parameters	429	428	407[a]	334
criterion for F_{obsd} exclusion	$F < 3\sigma(F)$	$F < 3\sigma(F)$	$F < 3\sigma(F)$	$F < 2\sigma(F)$
no. of reflect used in refinement	4260	2511	2536	2686
weighing scheme	$1/(\sigma^2(F) + 0.002F^2)$	1	$1/(\sigma^2(F) + 0.002F^2)$	1
R	0.059	0.058	0.075	0.041
R_w	0.051	0.058	0.076	0.041

[a] H atoms belonging to a CH_2 or a CH_3 group of steroid (DCA) constrained for most groups to have same isotropic temperature factor.

Figure 4). Thus, several strategies were adopted by using X-ray structure-factor least squares (see section 5.5) to unambiguously locate these two atoms and to distinguish between them. However, this X-ray study could not definitely establish that there is no minor amount of orientational disorder of the methyl C and O atoms of the guest acetyl group. The neutron study, at a temperature of 16 K on DCA–$C_6H_5COCD_3$ (see section 5.7), confirmed the positions of the oxygen and methyl carbon atoms of

UM00011926
NOVARTIS EXHIBIT 1017
Novartis v. Regents, IPR2023-01346
Page 672 of 4460

Table V. (DCA) Deoxycholic Acid–Acetophenone (at 103 K): (a) x, y, and z Coordinates ($\times 10^4$) and U_{eq}[a] ($\times 10^3$ Å^2) of the C and O Atoms of Deoxycholic Acid (Average $\sigma(U_{eq})$ = 0.001 Å^2), (b) x, y, and z Coordinates ($\times 10^4$) and Isotropic U (Å$^2 \times 10^3$) of H Atoms of Deoxycholic Acid, (c) x, y, and z Coordinates[b] ($\times 10^4$) and U[c] (Isotropic) (Å^2,$\times 10^3$) of the Guest Acetophenone Molecules and G′

(a) x, y, z, and U_{eq} of C and O Atoms of Deoxycholic Acid

atom	x	y	z	U_{eq}	atom	x	y	z	U_{eq}
C(1)	1260 (1)	2124 (2)	3537 (3)	22	C(15)	1616 (1)	5597 (1)	−2477 (3)	21
C(2)	702 (1)	1826 (2)	2977 (3)	22	C(16)	1357 (1)	6620 (2)	−2305 (3)	22
C(3)	725 (1)	1116 (2)	1358 (3)	21	C(17)	1063 (1)	6641 (1)	−407 (3)	17
C(4)	1021 (1)	1561 (2)	−271 (3)	19	C(18)	1864 (1)	6114 (2)	1479 (3)	19
C(5)	1584 (1)	1893 (1)	274 (3)	19	C(19)	2148 (1)	2741 (2)	2702 (4)	26
C(6)	1874 (1)	2337 (2)	−1400 (3)	22	C(20)	1062 (1)	7678 (1)	431 (3)	19
C(7)	1660 (1)	3344 (2)	−1942 (3)	20	C(21)	780 (1)	7742 (2)	2312 (3)	26
C(8)	1646 (1)	4060 (1)	−311 (3)	16	C(22)	836 (1)	8441 (2)	−939 (3)	22
C(9)	1338 (1)	3602 (1)	1333 (3)	16	C(23)	257 (1)	8294 (2)	−1493 (4)	28
C(10)	1580 (1)	2609 (1)	1958 (3)	18	C(24)	83 (1)	9088 (2)	−2807 (3)	23
C(11)	1258 (1)	4348 (1)	2901 (3)	17	O(25)	190 (1)	874 (1)	860 (3)	27
C(12)	999 (1)	5312 (1)	2268 (3)	16	O(26)	469 (1)	5106 (1)	1652 (2)	20
C(13)	1325 (1)	5786 (1)	703 (3)	16	O(27)	91 (1)	9956 (1)	−2444 (3)	39
C(14)	1379 (1)	5019 (1)	−868 (3)	17	O(28)	−84 (1)	8758 (1)	−4420 (2)	24

atom	x	y	z	U	atom	x	y	z	U
	(b) x, y, z, and U of H Atoms of Deoxycholic Acid					(c) x, y, z, and U of Guest Molecules			
H(1)	1246 (9)	2546 (17)	4714 (35)	20 (6)					
H(1′)	1417 (9)	1515 (17)	3925 (33)	18 (6)		Acetophenone Molecule G			
H(2)	483 (10)	2391 (17)	2621 (34)	24 (6)	C(7)	2747	174	−158	33 (1)
H(2′)	501 (10)	1511 (19)	3984 (38)	31 (7)	C(1)	2539	13	1761	33 (1)
H(3)	928 (9)	470 (17)	1710 (34)	21 (6)	C(2)	2074	−522	1976	48 (1)
H(4)	1051 (9)	1066 (17)	−1150 (36)	20 (6)	C(3)	1869	−686	3734	48 (1)
H(4′)	815 (8)	2100 (15)	−783 (29)	4 (5)	C(4)	2125	−321	5285	33 (1)
H(5)	1776 (10)	1280 (20)	691 (40)	36 (7)	C(5)	2588	211	5084	48 (1)
H(6)	1823 (9)	1906 (16)	−2438 (34)	15 (5)	C(6)	2796	379	3321	48 (1)
H(6′)	2267 (11)	2431 (18)	−1088 (36)	30 (7)	H(1)	1896	−777	852	48 (1)
H(7)	1869 (10)	3637 (19)	−2986 (39)	30 (7)	H(2)	1530	−1077	3839	48 (1)
H(7′)	1292 (10)	3309 (17)	−2436 (36)	24 (6)	H(3)	1987	−427	6598	48 (1)
H(8)	2013 (10)	4188 (18)	170 (37)	28 (7)	H(4)	2770	472	6213	48 (1)
H(9)	969 (9)	3456 (16)	800 (32)	15 (5)	H(5)	3136	772	3208	48 (1)
H(11)	1034 (9)	4108 (16)	3816 (34)	15 (5)	C(8)	3269	682	−400	58 (3)
H(11′)	1602 (10)	4506 (16)	3430 (34)	20 (6)	H(6)	3270	1341	148	58 (3)
H(12)	971 (9)	5721 (16)	3272 (33)	16 (6)	H(7)	3354	751	−1743	58 (3)
H(14)	1023 (9)	4879 (15)	−1258 (31)	12 (5)	H(8)	3560	272	203	58 (3)
H(15)	2029 (10)	5635 (18)	−2372 (36)	28 (6)	O(1)	2502	−134	−1491	78 (3)
H(15′)	1537 (9)	5240 (16)	−3655 (34)	16 (5)					
H(16)	1623 (10)	7103 (19)	−2251 (37)	27 (6)		Acetophenone Molecule G′			
H(16′)	1082 (11)	6708 (19)	−3387 (40)	34 (7)	C(7)	2683	10	852	33 (1)
H(17)	687 (8)	6448 (14)	−578 (28)	6 (5)	C(1)	2491	−52	2812	33 (1)
H(18)	2067 (9)	6480 (18)	674 (36)	23 (6)	C(2)	2028	−574	3170	48 (1)
H(18′)	2083 (9)	5543 (17)	1883 (33)	22 (6)	C(3)	1838	−647	4970	48 (1)
H(18″)	1816 (9)	6494 (18)	2567 (37)	25 (6)	C(4)	2106	−204	6421	33 (1)
H(19)	2398 (11)	3074 (19)	1788 (38)	39 (8)	C(5)	2566	315	6077	48 (1)
H(19′)	2307 (10)	2101 (19)	2998 (36)	32 (7)	C(6)	2759	392	4271	48 (1)
H(19″)	2173 (9)	3141 (17)	3891 (37)	25 (6)	H(1)	1842	−885	2116	48 (1)
H(20)	1445 (8)	7830 (15)	577 (30)	12 (5)	H(2)	1501	−1031	5180	48 (1)
H(21)	973 (10)	7455 (18)	3265 (38)	32 (7)	H(3)	1979	−242	7760	48 (1)
H(21′)	428 (11)	7408 (19)	2348 (39)	40 (8)	H(4)	2757	633	7134	48 (1)
H(21″)	715 (10)	8402 (20)	2696 (36)	30 (7)	H(5)	3098	778	4053	48 (1)
H(22)	1046 (10)	8435 (18)	−2044 (39)	31 (7)	C(8)	3203	503	467	58 (3)
H(22′)	892 (9)	9107 (17)	−414 (34)	23 (6)	H(6)	3206	1187	891	58 (3)
H(23)	40 (12)	8357 (21)	−456 (44)	45 (8)	H(7)	3276	504	−890	58 (3)
H(23′)	203 (11)	7675 (21)	−2032 (40)	40 (8)	H(8)	3498	126	1113	58 (3)
H(25)	209 (10)	610 (20)	−192 (42)	36 (7)	O(1)	2427	−365	−393	78 (3)
H(26)	252 (10)	5311 (18)	2416 (38)	26 (7)					
H(28)	−175 (13)	9249 (24)	−5066 (49)	63 (10)					

[a] $U_{eq} = {}^1/_3\sum\sum U_{ij}a_i^*a_j^*a_ia_j$. [b] G and G′ each refined as a rigid body. Thus, all atoms of each molecule have same $\sigma(x)$, $\sigma(y)$, $\sigma(z)$ for G = 3, 6, and 9 ($\times 10^4$), respectively, for G′ = 3, 6, 10 ($\times 10^4$). [c] Atoms within each group [C(7), C(1), C(4)], [C(2)...H(5)], [C(8)...H(8)], and O(1) refined with same U.

G and G′ (see Figure 12) as determined by the X-ray analysis. Moreover, Figure 12 displays no evidence of orientational disorder of the acetyl groups of G and of G′. These results are supported by potential energy calculations. Interchanging oxygen and CH_3 of guest G′ induces relatively unfavorable contacts between the methyl H atoms of G′ and the para H atom of G (see Figure 5); the rise in energy of guest G′ is 1.7 kcal/mol of the guest. Interchanging oxygen and CH_3 of G induces a rise in energy of 1 kcal/mol of the guest. We may conclude that these atom–atom potential energy calculations are completely consistent with the guest structure derived from the X-ray and neutron analyses.

2.3. Structure–Reactivity Relationship in DCA–Acetophenone. The UV irradiation of the crystals was conducted at room temperature, but the crystal structure determined was at 103 K. In order to confirm that the structures at the two temperatures are almost the same, X-ray diffraction data were collected at room temperature, and this structure was refined to an R value of 0.06, (see section 5.6). The guest–host distances at the site of reaction at the two temperatures match to within 0.2 Å (Table IIa) and thus we may safely refer to the low-temperature structure in considering structure–reactivity relationships at room temperature.

The orientation of the G and G′ acetophenone molecules in

UM00011927
NOVARTIS EXHIBIT 1017
Novartis v. Regents, IPR2023-01346
Page 673 of 4460

Table VI. Deoxycholic Acid–*m*-Chloroacetophenone (at 103 K): (a) x, y, and z Coordinates ($\times 10^4$) and U_{eq} (Å^2, $\times 10^3$) the C and O Atoms of Host Deoxycholic Acid (Average $\sigma(U_{eq}) = 0.002$ Å^2), (b) x, y, and z Coordinates ($\times 10^4$) and Isotropic U (Å^2, $\times 10^3$) U (Å^2 $\times 10^3$) of Deoxycholic Acid, (c) x, y, and z Coordinates[a] ($\times 10^4$) of the Guest *m*-Chloroacetophenone Molecules G and G′ (All Atoms Were Refined with an Overall U(Isotropic) = 0.059 (2) Å^2)

(a) x, y, z, and U_{eq} of C and O Atoms of Deoxycholic Acid

atom	x	y	z	U_{eq}	atom	x	y	z	U_{eq}
C(1)	1257 (2)	2095 (4)	3585 (8)	23	C(15)	1621 (2)	5584 (4)	−2402 (8)	24
C(2)	710 (2)	1793 (4)	3014 (8)	24	C(16)	1355 (2)	6596 (4)	−2227 (8)	24
C(3)	742 (2)	1084 (4)	1378 (8)	22	C(17)	1056 (2)	6616 (3)	−339 (7)	16
C(4)	1038 (2)	1537 (3)	−228 (7)	17	C(18)	1853 (2)	6087 (3)	1592 (8)	19
C(5)	1600 (2)	1870 (4)	339 (8)	22	C(19)	2146 (2)	2733 (4)	2802 (9)	27
C(6)	1890 (2)	2329 (4)	−1358 (9)	23	C(20)	1050 (2)	7641 (3)	516 (7)	20
C(7)	1673 (2)	3338 (4)	−1884 (7)	21	C(21)	765 (2)	7702 (4)	2384 (8)	26
C(8)	1655 (2)	4043 (3)	−233 (7)	17	C(22)	830 (2)	8414 (4)	−852 (8)	22
C(9)	1342 (2)	3581 (3)	1393 (7)	15	C(23)	254 (2)	8253 (4)	−1449 (9)	29
C(10)	1582 (2)	2589 (3)	2035 (7)	17	C(24)	86 (2)	9051 (4)	−2797 (8)	26
C(11)	1250 (2)	4314 (3)	2996 (7)	17	O(25)	208 (2)	844 (3)	841 (6)	27
C(12)	990 (2)	5279 (3)	2339 (7)	16	O(26)	461 (1)	5065 (2)	1673 (5)	20
C(13)	1320 (2)	5760 (3)	784 (7)	16	O(27)	108 (2)	9920 (3)	−2466 (7)	45
C(14)	1385 (2)	5002 (3)	−798 (7)	16	O(28)	−100 (1)	8724 (2)	−4383 (5)	25

atom	x	y	z	U	atom	x	y	z	U
	(b) x, y, z, and U of H Atoms of Deoxycholic Acid				(c) x, y, z, and U of the Guest Molecules G and G′				
H(1)	1216 (22)	2619 (43)	4611 (87)	23 (11)					
H(1′)	1373 (23)	1471 (43)	3944 (87)	23 (11)		*m*-Chloroacetophenone Molecule G			
H(2)	504 (20)	2445 (37)	2557 (74)	22 (10)	Cl(1)	2990	656	8033	
H(2′)	530 (21)	1530 (39)	4080 (81)	22 (10)	C(1)	2375	−146	3143	
H(3)	924 (20)	428 (41)	1573 (80)	25	C(2)	1898	−577	3676	
H(4)	1009 (23)	966 (27)	−1053 (61)	30 (10)	C(3)	1761	−623	5560	
H(4′)	811 (21)	2115 (40)	−721 (83)	30 (10)	C(4)	2099	−230	6940	
H(5)	1792 (18)	1267 (22)	655 (78)	30	C(5)	2572	187	6341	
H(6)	1749 (20)	1932 (33)	−2386 (50)	26 (10)	C(6)	2716	244	4485	
H(6′)	2244 (23)	2364 (38)	−1278 (77)	26 (10)	C(7)	2542	−80	1147	
H(7)	1875 (20)	3609 (36)	−2877 (79)	18 (9)	C(8)	3061	394	687	
H(7′)	1322 (22)	3265 (37)	−2423 (77)	18 (9)	O(1)	2265	−403	−95	
H(8)	2039 (19)	4219 (34)	317 (70)	6 (12)	H(1)	1664	−850	2614	
H(9)	980 (20)	3399 (36)	860 (75)	15	H(2)	1407	−940	5973	
H(11)	1563 (11)	4475 (34)	3745 (58)	11 (8)	H(3)	2001	−263	8347	
H(11′)	997 (19)	3966 (33)	3891 (71)	11 (8)	H(4)	3067	558	4075	
H(12)	967 (19)	5701 (28)	3443 (41)	12 (12)	H(5)	3088	1068	1156	
H(14)	1026 (8)	4763 (40)	−1053 (86)	27 (16)	H(6)	3117	426	−694	
H(15)	2015 (22)	5551 (39)	−2099 (80)	24 (10)	H(7)	3363	−11	1235	
H(15′)	1626 (21)	5180 (38)	−3696 (80)	24 (10)					
H(16)	1617 (19)	7046 (35)	−2196 (73)	10 (8)		*m*-Chloroacetophenone Molecule G′			
H(16′)	1089 (19)	6697 (35)	−3140 (75)	10 (8)	Cl(1)	3402	966	9435	
H(17)	667 (21)	6414 (37)	−421 (77)	22	C(1)	2478	−22	5339	
H(18)	2088 (15)	6437 (30)	734 (53)	10 (7)	C(2)	2067	−469	6321	
H(18′)	2082 (18)	5511 (33)	2029 (67)	10 (7)	C(3)	2071	−469	8268	
H(18″)	1763 (18)	6471 (28)	2706 (37)	10 (7)	C(4)	2487	−12	9261	
H(19)	2377 (24)	3150 (44)	2030 (87)	35 (10)	C(5)	2889	419	8220	
H(19′)	2340 (23)	2202 (44)	2612 (86)	35 (10)	C(6)	2893	431	6292	
H(19″)	2140 (23)	3195 (43)	3868 (87)	35 (10)	C(7)	2494	−4	3254	
H(20)	1412 (10)	7727 (47)	981 (92)	44 (19)	C(8)	2949	491	2300	
H(21)	944 (18)	7319 (32)	3354 (50)	22 (8)	O(1)	2145	−382	2333	
H(21′)	409 (21)	7333 (37)	2402 (76)	22 (8)	H(1)	1772	−788	5530	
H(21″)	727 (21)	8323 (41)	2882 (76)	22 (8)	H(2)	1768	−797	9014	
H(22)	1059 (21)	8270 (37)	−1945 (81)	20 (10)	H(3)	2494	−10	10712	
H(22′)	838 (19)	9052 (38)	−345 (75)	20 (10)	H(4)	3194	756	5553	
H(23)	−23 (22)	8244 (38)	−277 (87)	26 (11)	H(5)	2991	1180	2670	
H(23′)	210 (21)	7540 (39)	−1889 (85)	26 (11)	H(6)	2902	485	913	
H(25)	250 (23)	499 (37)	−319 (44)	38 (17)	H(7)	3291	124	2591	
H(26)	192 (14)	5318 (37)	2493 (64)	25					
H(28)	−272 (19)	9254 (25)	−5025 (72)	18 (15)					

[a] *G* and *G*′ each refined as rigid body. Thus, all atoms of each molecule have same $\sigma(x)$, $\sigma(y)$, $\sigma(z) = 5$, 9, and 15 ($\times 10^4$), respectively for G and 4, 8, 16 ($\times 10^4$) for G′.

proximity to the (abstracted) H5 atom of the steroid is shown in Figure 13. The O(G′)···H5 distance is 2.9 Å, less by almost 1 Å than either O(G′)···H6$_{eq}$ or O(G′)···H6$_{ax}$. The carbonyl C7(G′)···C5 and C7(G′)···C6 distances are 3.8 and 4.1 Å, respectively (Table IIa). These distances are completely compatible with the reaction involving addition of G′ to C5 of the steroid. The O(G)···H5 distance of 3.1 Å is 0.1–0.3 Å less than that of O(G)···H6 and O(G)···H6′; the C7(G)···C5 and C7(G)···C6 disstances are equal at 3.8 Å. Thus, purely in terms of distances, one might have expected addition of G to C5 and also to C6. Consequently other factors may play a role, such as differences in ease of abstraction of H5 and H6 and that it appears sterically easier to add a large group at C5 than at C6, C5 being more centrally located on the steroid wall. A comparison of the host–guest arrangement in Figure 13 with the absolute configuration S about the newly generated chiral center C(OHCH$_3$C$_6$H$_5$) of the product, as found in its own crystal structure (Figures 14 and 2), shows that the ketone adds from its Si face, which is the more distant from the steroid in the starting structure, rather than from its Re face. This stereochemical relationship, exemplified in Scheme V, implies the need for unusual motion of the guest acetyl group on reaction. Indeed it indicates that on photoexcitation, the acetyl group of

UM00011928
NOVARTIS EXHIBIT 1017
Novartis v. Regents, IPR2023-01346
Page 674 of 4460

Table VII. Photoproduct 5β-(*S*)(1-Phenylethanol)deoxycholic Acid (2): *x*, *y*, and *z* Coordinates (×10⁴) and U_{eq}/U_{iso} (×10³, Å²) (The Averages $\sigma(x)$, $\sigma(y)$, $\sigma(z)$, and $\sigma(U)$ Values for the H Atoms Are 0.0045, 0.0040, 0.0065, and 0.015 Å², respectively)

	x	*y*	*z*	U_{eq}		*x*	*y*	*z*	U_{iso}
C(1)	4474 (3)	2400 (3)	5079 (6)	39	H(1)	4946	1920	5317	33
C(2)	4904 (3)	2890 (3)	3478 (7)	46	H(1′)	4631	2842	6215	43
C(3)	4204 (4)	3691 (3)	3029 (6)	43	H(2)	4975	2343	1713	57
C(4)	2983 (3)	3418 (3)	2703 (5)	35	H(2′)	5652	2975	3621	50
C(5)	2478 (3)	2944 (2)	4280 (4)	26	H(3)	4231	4094	4274	38
C(6)	1304 (3)	2629 (3)	3595 (6)	38	H(4)	2977	3054	1775	36
C(7)	1269 (3)	1921 (3)	2161 (6)	38	H(4′)	2507	3971	2368	26
C(8)	1923 (3)	1113 (3)	2795 (5)	31	H(6)	858	3198	3098	49
C(9)	3134 (3)	1377 (3)	3337 (5)	31	H(6′)	792	2288	4096	66
C(10)	3245 (3)	2112 (3)	4852 (5)	31	H(7)	1522	2190	942	35
C(11)	3837 (3)	545 (3)	3819 (5)	35	H(7′)	644	1819	2004	37
C(12)	3766 (3)	−187 (3)	2411 (5)	33	H(8)	1437	807	3780	45
C(13)	2546 (3)	−457 (2)	1947 (5)	28	H(9)	3388	1681	2172	32
C(14)	1918 (3)	397 (3)	1359 (5)	31	H(11)	3537	207	4881	29
C(15)	787 (3)	60 (3)	602 (6)	42	H(11′)	4657	666	3974	38
C(16)	1064 (4)	−816 (3)	−315 (8)	46	H(12)	4313	−746	2742	41
C(17)	2290 (3)	−1053 (3)	275 (5)	31	H(14)	2243	631	152	36
C(18)	2073 (3)	−882 (3)	3594 (5)	40	H(15)	432	446	−256	31
C(19)	2972 (4)	1709 (3)	6652 (5)	45	H(15′)	387	−92	1653	34
C(20)	2448 (2)	−2063 (2)	478 (4)	32	H(16)	1020	−828	−1605	45
C(21)	3611 (3)	−2298 (3)	1268 (6)	44	H(16′)	487	−1255	−77	40
C(22)	2177 (3)	−2538 (2)	−1308 (5)	35	H(17)	2849	−914	−608	26
C(23)	1995 (3)	−3540 (3)	−1116 (5)	39	H(18)	1443	−1135	3322	107
C(24)	2994 (3)	−4131 (3)	−891 (5)	38	H(18′)	1979	−507	4649	58
O(25)	4582 (3)	4082 (3)	1456 (6)	65	H(18″)	2550	−1325	3873	59
O(26)	4292 (2)	126 (2)	901 (4)	44	H(19)	2183	1437	6773	67
O(27)	2922 (3)	−4882 (2)	−279 (5)	61	H(19′)	3228	2226	7677	89
O(28)	3904 (2)	−3844 (2)	−1493 (4)	50	H(19″)	3498	1302	6832	67
C(29)	2297 (3)	3662 (2)	5844 (4)	35	H(20)	1824	−2295	1318	35
C(30)	1469 (4)	3390 (3)	7210 (6)	48	H(21)	3689	−2914	1304	59
C(31)	1894 (3)	4571 (3)	5056 (4)	37	H(21′)	3778	−2108	2467	73
C(32)	2638 (4)	5267 (3)	4914 (6)	46	H(21″)	4164	−2045	650	72
C(33)	2277 (5)	6098 (3)	4313 (7)	62	H(22)	2747	−2408	−2109	47
C(34)	1187 (5)	6257 (4)	3875 (7)	64	H(22′)	1438	−2341	−1757	48
C(35)	426 (4)	5570 (4)	3991 (6)	55	H(23)	1646	−3777	−2348	71
C(36)	785 (3)	4737 (3)	4597 (5)	44	H(23′)	1630	−3639	−41	50
O(37)	3345 (3)	3798 (2)	6801 (4)	47	H(25)	4012	4073	766	8
					H(26)	4383	−224	327	44
					H(28)	4405	−4471	−1573	190
					H(30)	657	3288	6667	56
					H(30′)	1495	3848	8100	51
					H(30″)	1895	2837	7683	98
					H(32)	3407	5174	5294	44
					H(33)	2733	6598	4203	112
					H(34)	852	6900	3368	151
					H(35)	−312	5740	3733	63
					H(36)	244	4319	4692	69
					H(37)	3155	3872	7664	197

acetophenone undergoes a net rotation of 180°.

3. Crystalline Molecular Complex of DCA–*m*-Chloroacetophenone

3.1. Choice of Guest. In order to further substantiate the bizarre photochemical result from DCA–acetophenone, we conducted a chemical-crystallographic study on DCA–*m*-chloroacetophenone.

3.2. Solid-State Photochemistry. Crystals of the complex were obtained from a solution of DCA and *m*-chloroacetophenone in methanol. Irradiation of this crystalline material, $\lambda > 300$ nm, for about 30 days led to the formation of one (15%) diastereomeric product 3 of addition to position C5 (Scheme VI). The structure assignment of the product was done by ^{13}C NMR analysis with analogy to product **2** (Table I).

3.3. Guest Packing and Structure Reactivity. The crystal structure of DCA–*m*-chloroacetophenone was determined by low-temperature (103 K) X-ray diffraction (see section 5.8). The host structure is almost identical with that of DCA–acetophenone. Two independent guest molecules G and G′ were located in the channel from the structure-factor least-squares refinement. Their occupancies were refined freely to values of 0.167 (3) and 0.168 (3), respectively, yielding a sum of 0.335 (6). These two occupancies are very close to the value of 1:6. There are only two distinct ways of arranging the guest molecules given their refined positions and occupancies according to which one in six of each of the different G and G′ crystallographic sites is occupied. In the one possible motif, the guest molecules are arranged in separate strings GGGG and G′G′G′G′. In each such string, the nearest-neighbor guest molecules are related by one and a half translations along *c* plus a rotation about the 2_1 axis, as in Figure 6 for acetophenone. In other words, if the coordinates of G be *x*, *y*, and *z*, then its nearest neighbor along the channel will be at $^1/_2 - x, -y, ^3/_2 + z$. Such an arrangement has a maximum total guest occupancy of 1:3, which is completely compatible with the refined individual occupancies. In such an arrangement, the nearest neighbor guest atoms would be separated by approximately 5 Å. In the alternative way of arranging the guest molecules, G(*x*,*y*,*z*) and G′($^1/_2 - x, -y, ^3/_2 + z$′) follow each other alternately, as shown in Figure 15. In this arrangement the maximum total occupancy is 1:3 and the individual occupancies of G and *G′* = 1:6, which is also compatible with experiment. One would tentatively assume that the latter arrangement is the one adopted, otherwise why the necessity for two independent guest molecules G and G′ with equal occupancies and which are arranged to form close-packed pairs. The contact within a closed-packed pair is 4.3 Å between Cl(G) and O(G′). Between pairs there is a gap

UM00011929
NOVARTIS EXHIBIT 1017
Novartis v. Regents, IPR2023-01346
Page 675 of 4460

of 6.7 Å. It is impossible to reduce this large gap to an acceptable value by relating G and G′ by pseudotranslation as in DCA–acetophenone. In such a hypothetical arrangement, G′($^1/_2 - x,-y,^3/_2 + z$) would be followed in the $+c$ direction by G($^1/_2 - x,-y,^5/_2 + z$), instead of by G($x,y,3 + z$); however, the former two molecules would be separated by an prohibitively short Cl(G′)···C(G) contact of 2.3 Å.

According to Figure 16, the C5–H5 bond of the steroid is situated on the Re side of the guest acetyl groups of G and G′, and thus the photochemical addition should follow a similar stereochemical pathway as in DCA–acetophenone. The host–guest distances at the sites of reaction are listed in Table IIb. According to this table and Figure 16, molecule G′ is best positioned to react with atom C5 of the steroid. [O(G′)···H5 2.4 Å, C7(G′)···C5 3.6 Å]. The short O(G)···H5 distance of 2.4 Å as opposed to O(G)···$H6_{eq}$, $H6_{ax}$ distances of 3.3 and 3.5 Å is compatible with the observation that reaction occurs only at C5. However, the relatively long C7(G)···C5 distance of 4.0 Å may preclude photoaddition of G to C5, for we cannot say at this stage whether G reacts as well as G′.

4. Conclusion

This unusual molecular reaction pathway found in DCA–acetophenone and DCA–*m*-chloroacetophenone made it imperative to design a crystalline complex of DCA-substituted acetophenone whose host–guest packing would yield the (missing) diastereomeric photoaddition product, with absolute configuration R at the newly generated chiral carbon. In order to obtain this product, it was necessary to modify the observed guest packing in the channel such that a substituted acetophenone molecule would expose face Si to the steroid C5–H5 bond. This piece of crystal engineering is described in a forthcoming paper.[15]

5. Experimental Section

5.1. General Remarks and Chemical Procedures. Melting points were measured on a Gallenkamp apparatus in capillaries and are uncorrected. ^{1}H NMR spectra were recorded on a Varian A60, HFX-10-Bruker 90-MHZ, and a Bruker WH-270 spectrophotometers by using tetramethylsilane as internal standard. ^{13}C NMR spectra were recorder on a Bruker WH-270 spectrophotometer by using deuterated acetic acid or deuterated methanol as solvents and as an internal lock and tetramethylsilane as internal standard. Mass spectra of the methyl esters of the products were recorded on a Mat 731 high-resolution mass spectrometer. TLC separations were performed on silica gel on aluminum foil, DC-Karten SI (supplied by Riedel de Haen AG, Seelze-Hannover). Column chromatography was performed on Kieselgel 60 (0.063–0.2) supplied by Merck. Irradiation was by Westinghouse sunlamps through Pyrex Petri dishes. Commercial DCA (deoxycholic acid) was purified from fatty acids and cholic acid on a silica gel column eluted by 0.5% acetic acid in ethyl acetate.

All complexes were prepared by cocrystallization of DCA with the guest from methanol by slow evaporation of the solvent. In a typical experiment, 1–2 g of complex was irradiated at room temperature through Pyrex dishes, $\lambda > 300$ nm, for about 30 days. The crystals were generally in the form of powder. Single crystals preserved their integrity during irradiation. The products were separated by chromatography on silica gel 1:100 (eluted with $CH_2Cl_2/CH_3OH/AcOH$ in a ratio of 94.5:5.0:0.5) and by preparative TLC with the same eluent in a ratio of 90.5:9.0:0.5 by using UV detection and phosphomolybdic acid as coloring spray.

5.2. Photoproducts from UV Irradiation of DCA Complexes. Photoproduct 2 from DCA–Acetophenone: TLC $r_f = 0.65$; mp 216–218 °C (methanol/acetic acid); mass spectrum (methyl ester), m/e 404 (M − $C_8H_{10}O$), 273 (M − $C_8H_{10}O$ − H_2O − side chain), 255 (M − C_8H_{10} − $2H_2O$ − side chain), 121 (C_8H_9O); ^{1}H NMR[9] (CD_3OD) δ 0.71 (3 H, s, 18-H), 1.0 (3 H, d, $J = 5$ Hz, 21-H) 1.23 ($^3/_2$ H, s, 19-H), 1.28 ($^3/_2$ H, s, 19-H), 1.73 (3 H, s, $CH_3C(OH)$), 7.18 (5 H, m, $CH_3C(OH)C_6H_5$); UV λ_{max} 258, 290 (ϵ 320, 130); IR 3500, 3440 (OH), 2950 (C—H), 1680 (C=O), 1600 (Ph − H) 770, 720 cm^{-1}. Anal. Calcd for $C_{32}H_{48}O_5$: C, 74.96%, H, 9.44%. Found: C, 74.83%; H, 9.6%.

Photoproduct 3 from DCA–*m*-Chloroacetophenone: TLC $r_f = 0.65$; ^{1}H NMR (CD_3OD) δ 0.72 (3 H, s, 18-H), 0.99 (3 H, d, 21-H), 1.23 ($^3/_2$ H, s, 19-H), 1.28 ($^3/_2$ H, s, 19-H), 1.7 (3 H, s, $CH_3C(OH)C_6H_4Cl$), 7.2 (4 H, m, $CH_3C(OH)C_6H_4Cl$); UV λ_{max} 253 (ϵ 300); IR 3400 (O—H), 2950 (C—H), 1700 (C=O), 1580 (Ph − H) cm^{-1}. Anal. Calcd for $C_{32}H_{47}O_5Cl$: C, 70.24%; H, 8.66%. Found: C, 70.14%; H, 8.61%.

5.3. X-ray Intensity Measurements. DCA Complexes. The X-ray intensities of DCA–acetophenone at room temperature (293 K) were measured on a Siemens three-circle automatic diffractometer. The X-ray data of the DCA–acetophenone and DCA–*m*-chloroacetophenone cooled to ca. 103 K were measured on a CAD-4 diffractometer by using Mo Kα radiation filtered with a graphite monochromator. Cell dimensions (Table III) were determined by least squares using 25 reflections. The X-ray intensities were measured with crystals sufficiently small not to be affected by the inhomogeniety of the X-ray beam due to the graphite monochromator. This was verified by the excellent match between two X-ray data sets on DCA–*p*-fluoroacetophenone described elsewhere;[15] for one of these, the crystal was mounted along its needle direction while for the other the needle was mounted on its side. Details on the X-ray intensity measurements are given in Table III. Absorption corrections were not applied, being negligible.

Photoproduct 2. Needlelike crystals of 5β-(*S*)(1-phenyl-ethanol)-deoxycholic acid (**2**) were obtained by slow evaporation from an ethanol–acetic acid solution. The X-ray diffraction data were measured on a Siemens three-circle diffractometer by using Cu Kα radiation. The cell dimensions (Table III) were determined by least squares from 30 reflections. Absorption corrections[19] were applied to the intensity diffraction data, the crystal exhibited faces {100}, {001}, {101}, and {110} with dimensions given in Table IIIa. The transmission factor applied to the X-ray intensities varied from 1.06 to 1.19.

5.4. General Remarks on X-ray Structure Determination and Refinement. It was obvious from the intensity diffraction data of the two DCA complexes that their host steroid structures are isomorphous, belonging to the known motif.[2] Thus, initial refinement of the host molecule was straightforward. The crystal structure of photoproduct 2 was determined by the use of MULTAN.[20] The least-square refinements were carried out with SHELX.[21] The temperature factors of the C and O atoms of host DCA and of photoproduct 2 were refined anisotropically and their H atoms isotropically. The scattering factors for H, C, and O were taken from ref 22. The function refined was $\sum w(F_o - F_c)^2$ where $w = 1/\sigma^2(F_{obsd})$; $\sigma(F_{obsd})$ was obtained from counting statistics and the match between symmetry-related reflections. Refinement was carried out in two blocks, full matrix not being feasible. The reliability factors given are $R = \sum|F_o - F_c|/\sum F_o$, $R_w = \sum w^{1/2}|F_o - F_c|/\sum w^{1/2}F_o$, $r = \sum w|F_o - F_c|^2/\sum wF_o^2$.

5.5. Refinement of the Low-Temperature (103 K) X-ray Structure of DCA–Acetophenone. The DCA host structure was refined first with isotropic and then anisotropic thermal parameters by using 4260 reflections, for which $F_{obsd} > 3\sigma(F_{obsd})$, yielding $R = 0.13$ (defined above). An electron density diffference map yielded several peaks within the channel, with heights ranging from 1.0 to 1.9 e/Å^3. It was not directly evident from the peak heights and their distribution whether the channel contained more than one guest molecule per asymmetric unit. The peak distribution was coplanar to within 0.2 Å. We proceeded by easily fitting only one guest molecule of acetophenone to the peaks. This molecular model was taken from an accurate low-temperature X-ray diffraction study of crystalline acetophenone.[23] This molecule as guest was refined positionally as a rigid body with a fixed isotropic value of 0.04 Å^2 and an initial occupancy factor of 0.4. The temperature factor of 0.04 Å^2 was assumed reasonable since the average temperature factor of the host atoms was 0.025 Å^2. We had assumed the occupancy of 0.4 for the guest because it was clear at that stage that the molar guest–host ratio could not be higher than 1/2 according to the most hypothetical dense packing of the guest within the channel. On refinement to $R = 0.098$, the occupancy factor of the guest reduced to 0.29, and a difference map yielded seven additional peaks whose heights ranged between 0.8 and 1.1 e/Å^3. These peaks described an acetophenone molecule almost parallel to the original but separated therefrom along the channel axis by approximately 0.8 Å. Therefore, two independent acetophenone molecules, G and G′ as depicted in Figure 4a, were inserted in the channel and refined positionally as rigid bodies.

(19) Coppens, P.; Leiserowitz, L.; Rabinovich, D. *Acta Crystallogr.* **1965**, *18*, 1035.

(20) Main, P.; Hull, S. E.; Lessinger, L.; Germain, G.; Declercq, J.-P.; Woolfson, M. M. "MULTAN 78. A System of Computer Programs for the Automatic Solution of Crystal Structures from X-ray Diffraction Data; University of York, York, England and Louvain, Belgium, 1978.

(21) Sheldrick, G. M. "SHELX: Program for Crystal Structure Determination"; University of Cambridge: England 1976.

(22) Stewart, R. F.; Davidson, E. R.; Simpson, W. T. *J. Chem. Phys.* **1965**, *42*, 3175. Cromer, D. T.; Mann, J. B. *Acta Crystallogr., Sect. A* **1968**, *A24*, 321.

(23) Tanimoto, Y.; Kobayashi, H.; Nagakara, S.; Saito, Y. *Acta Crystallogr., Sect. B* **1973**, *B29*, 1822.

UM00011930
NOVARTIS EXHIBIT 1017
Novartis v. Regents, IPR2023-01346
Page 676 of 4460

Further refinement yielded occupancy factors of 0.215 (8) for G′ and 0.202 (6) for G and a guest thermal parameter of 0.055 Å^2 and an R value of 0.059. Utilizing the result that the crystal structure contains only the two independent guest molecules G and G′, we have demonstrated by packing considerations that the total guest occupancy is maximally 0.4 with individual occupancies of G and G′ maximally 0.2 (see section 2.2). Thus, for further refinement, the occupancies of G and G′ were set equal to 0.2. We replaced the constraint of one isotropic thermal parameter for G and G′ by that in which four different atom groups each had a different isotropic thermal parameter. Refinement yielded the reliability factors $R = 0.059$, $R_w = 0.051$, and $r = 0.0555$. There is pronounced overlap of the G and G′ molecules, due to the small separation of 0.8 Å along the *c* axis, as well as the overlap induced by the twofold screw axis along the channel (Figure 4b). This overlap necessitated a water-tight strategy for unambiguous location of, and differentiation between, atoms oxygen O1 and methyl carbon C8 of each of the guests G and G′. These atoms had been originally located from difference maps by peak heights and peak–peak distances. We adopted the following least-squares procedures to make certain that they are in their deduced sites. Atoms O1 and C8 were removed from both guest molecules G and G′ and the structure was refined with guest tolyl C_7H_5 groups as rigid bodies with their thermal parameters fixed at their original refined values. R was refined to 0.073. A difference map yielded three, rather than four, peaks with heights of 1.37, 1.30, and 1.20 e/Å^3, corresponding to two resolved oxygen peaks and one unresolved carbon peak. We rationalize this result as follows: in the refined crystal structure, the distance between the methyl carbon atoms C8 of molecules G and G′ of 0.65 Å is appreciably shorter than the corresponding distance of 0.82 Å between the oxygen atoms (Figure 4). Insertion of three guest atoms (i.e., two oxygens and one methyl carbon) yielded the remaining methyl C atom by a difference synthesis. However, it was still necessary to prove that we have correctly differentiated between the oxygen and methyl groups. Thus, we refined a structure in which each guest molecule G and G′ had been rotated by 180° about its long molecular axis C7···C1. Namely, we effectively interchanged the oxygen and methyl positions in G and G′. The refinement, which yielded $R = 0.0625$, $R_w = 0.0554$, and $r = 0.0621$ (defined in section 5.4), indicated that *both* acetyl groups should be in their original positions for the following reasons: (a) The temperature factor U of the guest G atoms increased from 0.078 (3) to 0.102 (3) Å^2 and that of the methyl C atoms decreased from 0.058 (3) to 0.047 (3) Å^2. (b) A difference map showed peaks of height 0.6 e/Å^3 near the two oxygen positions of the original unrotated structure. (c) Applying the Hamilton test,[24] the **R** ratio r_2/r_1 (r_1 and r_2 correspond to the original and rotated guest structures, respectively) equals 0.0621/0.0555 = 1.09. We test this **R** ratio of 1.09 against $\mathbf{R}_{16,4260-184,0.005} = 1.004$, where 16 = 2× (six positional + two thermal parameters for each guest molecule), 4260 = the number of reflections used, 184 = the number of parameters refined, 0.005 = the significance level.

We can emphatically reject at a significance level > 99.5% the model structure in which the oxygen and CH_3 groups of *both* independent guest molecules are effectively interchanged.

In the third and most conclusive of the tests based on the X-ray data, the guest molecules were refined with their phenyl rings as rigid bodies and with constraints imposed on their acetyl groups; the bond length of C7–C1 was maintained at 1.49 Å and the 1···3 distance O1···C8 at 2.38 Å. On refinement, $R = 0.0577$ and $R_w = 0.0493$ were obtained. The refined bond lengths and angles of the acetyl groups of G and G′ (Figure 17) demonstrate that the acetyl oxygen and methyl carbon atoms, as inserted in the original rigid body refinement, are in their correct sites. These refinement results could not, however, rule out a minor amount (up to, say, 15%) of conformationally disordered acetyl groups. This ambiguity was removed by a neutron diffraction study described below.

5.6. Refinement of Room-Temperature X-ray Structure of DCA–Acetophenone. The final *x*, *y*, and *z* coordinates of host and guest were used as input for a refinement of the room temperature structure. The R value converged to 0.059. The average temperature factor U for the host C and O atoms is 0.063 Å^2. For the guest atoms, $U = 0.09$ Å^2, which is reasonable considering that at a crystal temperature of 103 K, the average temperature factor of the guest atoms, is also 0.03 Å^2 higher than that of the host atoms.

5.7. Neutron Diffraction Study of DCA–Acetophenone ($C_6H_5COCD_3$). The diffraction data were measured at 16 K with an automated four-circle diffractometer at the Brookhaven High-Flux Beam Reactor. The lattice dimensions were determined at 83 and 16 K (see Table III). The number of reflections that were measurable with significant intensities was severely limited by the size of the crystal (0.56 mm^3), which was less than $^1/_{10}$ of that needed in the present study. A full quadrant of data ($\pm hkl$) was collected in the range $0.023 < \sin\theta/\lambda < 0.40$, giving 1622 observations. An additional 942 ($\pm hkl$) reflections, calculated to be the most intense after preliminary refinement against the low-angle data, were measured in the range $0.40 < \sin\theta/\lambda < 0.68$.

The X-ray-derived crystal structure was refined with individual isotropic temperature factors for all the steroid atoms. The C and O atoms of the guest molecules were refined with the same temperature factor; the H and D atoms of G and G′ were assigned a fixed isotropic U of 0.06 Å^2. The guest acetyl $COCD_3$ was allowed the two possible orientations so that four guest model structures (Scheme VII) were tested.

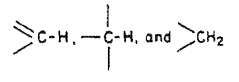
The resulting R and r values for models a–d were (0.1017, 0.1208), (0.1079, 0.1280), (0.1043, 0.1235), and (0.1037, 0.1223), respectively, where a corresponds to the X-ray derived structure. We apply the Hamilton test[24] to compare model a with b, c, and d. r_b/r_a (0.1280/0.1208) = 1.0596, r_c/r_a (0.1235/0.1208) = 1.0224, and r_d/r_a (0.1223/0.1208) = 1.0124. We test these ratios against $R_{13,1317-283,0.005} = 1.015$ and $R_{13,1317-283,0.025} = 1.012$, where 13 = 2x (six positional and one thermal parameter for each guest), 1317 = number of reflections used, 283 = number of refined parameters, and 0.005, 0.025 = confidence levels.

We may reject models b and c at the 99.5% level and model d at approximately the 97.5% level. Thus, the Hamilton test on the four models a–d is consistent with the X-ray results.

Definitive proof of the correctness of model a was provided by Fourier difference maps. All six deuterium atoms were removed from the structure factor calculations of model a, and difference maps were calculated in the four planes perpendicular to the C7–O7 and C7–C8 bonds of G and G′ where the D_3 groups could be expected to be found. The maps (Figure 12a) show peak distributions corresponding to symmetric D_3 groups in the planes perpendicular to the C7–C8 bonds; the maps perpendicular to the C=O bonds (Figure 12b) do not exhibit (symmetric) D_3 methyl groups. Thus, not only do these maps confirm the X-ray-derived guest structure but also that the oxygen and CD_3 groups do not appear to exhibit any conformational disorder.

5.8. Refinement of Low-Temperature (103 K) Structure of DCA–*m*-Chloroacetophenone. The host structure was initially refined with the final coordinates of DCA–acetophenone, yielding an R value of 0.14. A difference map displayed the two strongest peaks of height 2.2 e/Å^3 located within the channel. They were interpreted as two independent Cl atoms each belonging to a guest molecule. These two peaks are far removed from the central axis of the channel and therefore could hardly be interpreted in terms of superposition of the lighter C and O atoms arising from the molecular overlap inherent in these channel structures. When these two Cl positions were utilized as anchor points in the refinement, the orientations of the two guest molecules G and G′ were determined by fitting *m*-chloroacetophenone molecules to the remaining difference map peaks of average height 0.9 e/Å^3. The G and G′ molecules were refined as rigid bodies, where the molecular model of *m*-chloroacetophenone was taken from the crystal structure of bis(*m*-chlorobenzyl)methane.[25] R converged to 0.076 and R_w to 0.078. Refinement of each of the occupancy factors of G and G′ yielded values of 0.167 (3) and 0.168 (3). An analysis of the possible packing arrangements of the guest molecules G and G′ in the channel (see section 3.3) indicates that the maximum guest occupancy is 1:3 which compares excellently with the observed value of 0.167 + 0.168 = 0.335 (4). Thus, we fixed the occupancy factors of the guests G and G′ to 0.16667 each in the final stages of refinement and obtained final values of $R = 0.075$ and $R_w = 0.076$.

5.9. The Crystal Structure of 5β-(*S*)-(1-Phenylethanol)deoxycholic Acid. The C and O atoms of photoproduct **2** were revealed by MULTAN.[20] H atoms belonging to groups



were attached to the C atoms. The subsequent $\Delta\rho(x,y,z)$ maps yielded the positions of all the methyl and hydroxyl H atoms. The R factor converged to 0.04.

6. Results of Refinement

Details on refinement of the crystal structures of deoxycholic acid (DCA) with acetophenone and *m*-chloroacetophenone and of photoproduct 5β-(*S*)-(1-phenylethanol)deoxycholic acid **2** are given in Table IV. The atomic *x*, *y*, and *z* coordinates and

(24) Hamilton, W. C. *Acta Crystallogr.* **1965**, *18*, 502.

(25) Engebreton, G. R.; Rundle, R. E. *J. Am. Chem. Soc.* **1964**, *86*, 574.

UM00011931
NOVARTIS EXHIBIT 1017
Novartis v. Regents, IPR2023-01346
Page 677 of 4460

equivalent thermal parameters of the low-temperature inclusion compounds and of photoproduct **2** are listed in Tables V-VII, respectively. Their bond lengths and angles are listed in supplementary material in Tables 5S, 6S, and 7S, respectively. The x, y, and z coordinates of the room-temperature structure of DCA-acetophenone are listed in Table 5S (d).

Acknowledgment. We thank the Israel/U.S. Binational Science Foundation, Jerusalem, for financial support. Research at Brookhaven National Laboratory was carried out under contract with the U.S. Department of Energy.

Registry No. 2, 95586-16-6; **2** (methyl ester), 95485-48-6; **3**, 95586-17-7; 5DCA·2$C_6H_5COCH_3$, 83035-58-9; 3DCA·m-$C_6H_5COCH_3$, 83047-96-5; 5DCA·2$C_6H_5COCl_3$, 95485-49-7.

Supplementary Material Available: Thermal parameters, bond angles, and bond lengths (13 pages). Ordering of information given on any current masthead page.

Communications to the Editor

Biomimetic Models for Cysteine Proteases. 2. Nucleophilic Thiolate-Containing Zwitterions Produced from Imidazole-Thiol Pairs. A Model for the Acylation Step in Papain-Mediated Hydrolyses

K. I. Skorey and R. S. Brown*

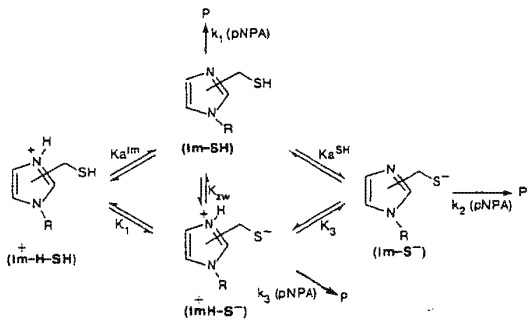
Department of Chemistry, University of Alberta
Edmonton, Alberta, Canada T6G 2G2
Received January 21, 1985

The most widely studied example of the cysteine proteases, papain, cleaves both amide and ester substrates with the formation of the intermediate Cys thiol ester.[1] The pH-rate profile for the hydrolysis of a typical ester substrate (α-*N*-benzoyl-L-arginine ethyl ester) is bell shaped and was interpreted to indicate the involvement of two groups having apparent pK_a's of ~4.3 and 8.2-8.5.[2]

The most recent evidence from spectral and potentiometric titrations and solvent isotope effects[3] indicates that Cys-25 has an unusually low pK_a of 3-4 while that of His 159 is 8.5. These and earlier kinetic studies[4] suggest that Cys-25 and His-159 exist primarily as a zwitterionic imidazolium thiolate ion pair which is catalytically viable at physicological pH.

Although small molecules incorporating both imidazole and thiol units have been studied as nucleophilic catalysts in promoting the hydrolysis of *p*-nitrophenyl acetate (*p*-NPA),[5,6] the kinetic involvement of zwitterions has never been unambiguously demonstrated. Also, there has never been demonstrated a significant cooperative effect in the catalysis of hydrolytic processes by thiol-imidazole intramolecular systems as is thought to occur in the cysteine proteases. Herein we report that **2a** and **3a**[7] (but not

Scheme I



Scheme II

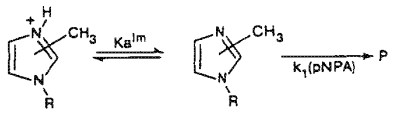


Table I. pK_a Values (Macroscopic and Microscopic) for **1-3**

	macroscopic pK_a[a,b]		microscopic pK_a[c]				
	pK_{a1}	pK_{a2}	pK_1	pK_a^{Im}	pK_3	pK_a^{SH}	K_{Zw}[d]
1a	6.54 (6.68)	9.54 (9.52)	7.72	6.57	8.36	9.51	0.07
2a	6.37 (6.41)	9.26 (9.01)	6.50	6.96	9.13	8.67	2.88
3a	6.31 (6.44)	8.88 (8.83)	6.47	6.83	8.75	8.39	2.29
1b	7.56[e]						
2b	7.94[e]						
3b	7.64[e]						

[a] Values without parentheses are averages of triplicate potentiometric titrations; ±0.05 unit. [b] Bracketed values were obtained as kinetic pK_a values obtained from computer fit to eq 1a.[11] [c] Values as defined in Scheme I and calculated by methods given in ref 12 using titrimetric macroscopic pK_a's and assuming pK_a^{Im} is that of the corresponding *S*-benzyl derivative.[13] [d] K_{Zw} = [Im$^+$H-S$^-$]/[Im-SH] = K_1/K_a^{Im}. [e] Literature values for **1b**, **2b**, and **3b** are 7.51, 8.00, and 7.85, respectively.[14]

(7) Thiols **1a**, **2a**, and **3a** were synthesized from their corresponding alcohols according to the general procedure of Schneider[8] and exhibited spectral and analytical data consistent with their structures (details to be published).

(1) (a) Glazer, A. N.; Smith, E. L. In "The Enzymes"; Boyer, P. D., Ed.; Academic Press: New York, 1971; Vol. 3, pp 502-546. (b) Drenth, J.; Jansonius, J. N.; Koekoek, R.; Wolthers, B. G. *Ibid.* pp 484-499. (c) Liu, T.-Y.; Elliott, S. D. *Ibid.* pp 609-647. (d) Mitchell, W. M.; Harrington, W. F. *Ibid.* pp 699-719. (e) Brocklehurst, K. *Methods Enzymol.* **1982**, *87c*, 427-469. (f) Polgar, L.; Halász, P. *Biochem. J.* **1982**, *207*, 1-10.

(2) (a) Smith, E. L.; Parker, M. J. *J. Biol. Chem.* **1958**, *233*, 1387-1391. (b) Whitaker, J. R.; Bender, M. L. *J. Am. Chem. Soc.* **1965**, *87*, 2728-2737.

(3) (a) Lewis, S. D.; Johnson, F. A.; Shafer, J. A. *Biochemistry* **1976**, *15*, 5009-5017; (b) *Ibid.* **1981**, *20*, 48-51. (c) Johnson, F. A.; Lewis, S. D.; Shafer, J. A. *Ibid.* **1981**, *20*, 52-58. (d) Sluyterman, L. A. AE.; Wijdehes, J. *Eur. J. Biochem.* **1976**, *71*, 383-391. (e) Creighton, D. J.; Schamp, D. J. *FEBS Lett.* **1980**, *110*, 313-318. (f) Creighton, D. J.; Gessourown, M. S.; Heapes, J. M. *Ibid.* **1980**, *110*, 319-322.

(4) (a) Polgar, L. *Eur. J. Biochem.* **1973**, *33*, 104-109; (b) *FEBS Lett.* **1974**, *47*, 15-18. (c) Jolley, C. L.; Yankeelov, J. A., Jr. *Biochemistry* **1972**, *11*, 164-169.

(5) (a) Schneider, F.; Wenck, H. *Z. Physiol. Chem.* **1969**, *350*, 1653-1661, 1521-1530. (b) Schneider, F.; Schaich, E.; Wenck, H. *Ibid.* **1968**, *349*, 1525-1536. (c) Petz, D.; Schneider, F. *Z. Naturforsch., C* **1976**, *31C*, 534-543. (d) Lochon, P.; Schoenleber, J. *Tetrahedron* **1976**, *52*, 3023-3030. (e) Heller, M. J.; Walder, J. A.; Klotz, I. M. *J. Am. Chem. Soc.* **1977**, *99*, 2780-2785.

(6) (a) Schonbaum, G. R.; Bender, M. L. *J. Am. Chem. Soc.* **1960**, *82*, 1900-1904. (b) Lindley, H. *Biochem. J.* **1960**, *74*, 577-584. (c) Whitaker, J. R. *J. Am. Chem. Soc.* **1962**, *84*, 1900-1904. (d) Ogilvie, J. W.; Tildon, J. T.; Strauch, B. S. *Biochemistry* **1964**, *3*, 754-758. (e) Fersht, A. R. *J. Am. Chem. Soc.* **1971**, *93*, 3504-3515 and references therein. (f) Fersht, A. R. "Enzyme Structure and Mechanisms"; Freeman and Co.: San Francisco, 1977; pp 312-315.

0002-7863/85/1507-4070$01.50/0 © 1985 American Chemical Society

UM00011932
NOVARTIS EXHIBIT 1017
Novartis v. Regents, IPR2023-01346
Page 678 of 4460

Acta Crystallographica Section B
Structural Science
ISSN 0108-7681

Rules governing the crystal packing of mono- and dialcohols

Robin Taylor* and Clare F. Macrae

Cambridge Crystallographic Data Centre, 12 Union Road, Cambridge CB2 1EZ, England

Correspondence e-mail: taylor@ccdc.cam.ac.uk

Received 21 May 2001
Accepted 15 August 2001

In memory of Professor Jan Kroon, a pioneer in the exploitation of crystallographic databases.

A new program, *Mercury*, has been used to survey 144 monoalcohol (C_mH_nOH) and 101 dialcohol [$C_mH_n(OH)_2$] crystal structures. Results show that their hydrogen-bonding patterns are strongly correlated with steric effects. Primary monoalcohols have a strong preference to form infinite $\cdots$OH$\cdots$OH$\cdots$ chains. Secondary monoalcohols form chains and rings of hydrogen bonds with about equal facility. Tertiary monoalcohols very often form isolated OH$\cdots$O hydrogen bonds or structures containing no OH$\cdots$O hydrogen bonds at all. In the latter case, however, the structures almost invariably contain CH$\cdots$O and/or OH$\cdots\pi$ interactions. Substitution on the β-carbon(s) of monoalcohols has a profound effect on packing patterns, with increased substitution disfavouring chains and rings. Dialcohols show a much stronger preference for chains of hydrogen bonds, compared with monoalcohols. This is particularly so when at least one of the hydroxyl groups is primary, in which case chains are overwhelmingly preferred. Once again, substitution on the β-C atoms is influential, heavy substitution tending to lead to packing arrangements that involve isolated or intramolecular OH$\cdots$O hydrogen bonds. Dialcohols almost never crystallize without at least some OH$\cdots$O hydrogen-bond formation. In both monoalcohols and dialcohols, chains show a stronger preference to be helical (usually threefold helices) as steric hindrance increases. Hydrogen-bonded rings usually contain four OH$\cdots$O hydrogen bonds. It is possible that empirical observations such as these may aid crystal-structure prediction.

1. Introduction

Crystal structure prediction is a major scientific challenge and of immense potential interest to the materials, pharmaceutical and agrochemical industries. Some years ago, Gavezzotti (1994) wrote a well known paper entitled 'Are crystal structures predictable?' and gave the simple answer 'No'. Since then, great efforts have been made in the area by several groups, many of which participated in a recent competition to assess the state of the art (Lommerse *et al.*, 2000). The outcome was that all four of the test structures were predicted successfully by at least one of the groups. While no group was 100% successful and the test molecules were much smaller and less flexible than *e.g.* typical drug molecules, the study clearly showed that advances have been made. Nevertheless, reliable prediction of the types of structures in which practising chemists are interested is still far away.

A key complication is that crystallization may often be under kinetic control, which means that a successful prediction

© 2001 International Union of Crystallography
Printed in Great Britain – all rights reserved

UM00011933
NOVARTIS EXHIBIT 1017
Novartis v. Regents, IPR2023-01346
Page 679 of 4460

strategy needs to take account of dynamic processes in the liquid as well as the enthalpic stability of putative solid-state packing arrangements. In principle, molecular dynamics simulations offer a way forward (Gavezzotti & Filippini, 1998). The cost of such calculations, however, is prohibitive, certainly for routine prediction with current computers. We therefore need a cheap way of assessing the effects of the kinetics of crystal nucleation. One possibility is to look at the 230 000 crystal-packing arrangements that have been observed experimentally and are stored in the Cambridge Structural Database (CSD; Allen & Kennard, 1993). These do not tell us anything about the kinetics of crystal nucleation *per se*, but they do tell us something about their end results. If particular packing motifs are seen over and over again, they presumably reflect favourable kinetic processes as well as thermodynamically stable arrangements. Equally, there may be thermodynamically stable arrangements that are infrequently seen because they are kinetically disfavoured.

CSD information has already been used to develop pairwise potentials for use in crystal-structure prediction programs (*e.g. FlexCryst*; Hofmann & Lengauer, 1997). Our emphasis here, however, is on the use of the CSD to develop simple heuristics that can help discriminate between likely and unlikely packing arrangements, or can be used to reduce the search space that must be visited by a crystal-structure prediction program. Previous studies in the area, such as the pioneering work of Leiserowitz (1976), were reviewed recently by Brock (1999) and our present work follows on from one of the investigations mentioned in that review. Specifically, Brock & Duncan (1994) (hereinafter 'B&D') showed that monoalcohols (C_mH_nOH) are particularly likely to crystallize in high-symmetry space groups or with $Z' > 1$. Here we extend that work with the objective of elucidating as many useful rules as possible for aiding the prediction of the crystal packing of both monoalcohols and dialcohols [$C_mH_n(OH)_2$]. These systems were chosen because they are relatively simple and B&D have already had some success: if further rules cannot be discerned here, there can be little hope for more complex molecules.

An additional motive for this work was to test a new program for visualizing crystal structures and analysing packing arrangements. The program *Mercury* will soon be distributed as part of the standard CSD release.

2. Experimental

2.1. Database searches

All searches were performed on Version 5.20 of the CSD (October 2000) with the programs *ConQuest*1.1 and *QUEST*. Monoalcohols of the general formula C_mH_nOH were found subject to the following criteria: alkanols only (no phenols); no heavy-atom disorder; no structures flagged in the CSD as containing errors; no other molecules (*e.g.* solvates) in the structure; only one member of each CSD refcode family (chosen arbitrarily, but generally the first alphanumerically); all non-H atom coordinates available. The monoalcohols were divided into three subsets, depending on whether the hydroxyl group was primary, 1°, RCH_2OH, secondary, 2°, R_2CHOH, or tertiary, 3°, R_3COH.

Dialcohols of the general formula $C_mH_n(OH)_2$ were found subject to the same criteria as above plus the additional criteria: R factor < 5%; average e.s.d. for a C—C bond < 0.005 Å; hydroxyl H atom coordinates available. The additional criteria were possible because the CSD contains more dialcohols than monoalcohols, so we could afford to exert tighter control over experimental precision. (Having said that, it is possible that the use of more stringent criteria for the dialcohols has resulted in a bias, *e.g.* against structures with $Z' > 1$, with high molecular weight, or which are well determined except for the positions of disordered hydroxyl hydrogen atoms. We are grateful to a referee and the co-editor for pointing this out.) The dialcohols were divided into six subsets, depending on the nature (primary, secondary or tertiary) of each of the hydroxyl groups (hence primary–primary, 1°–1°; primary–secondary, 1°–2° *etc.*).

An additional search was performed, using the same criteria as in the dialcohol searches, to find primary monoalcohols containing at least one other O atom, *i.e.* molecules of the general formula $C_mH_nO_p$, where $p > 1$ and exactly one alkanol OH is present. A list of the CSD 'refcodes' of these and all other structures used in this study, together with the hydrogen-bond motifs they form, has been deposited as supplementary material.[1]

2.2. Mercury[2]

Analysis of the alcohol packing arrangements was performed with a pre-release version of a new program, *Mercury*, which owes much in its philosophy to an earlier program, *RPLUTO* (Motherwell & Shields, 2000). *Mercury* is an application for visualizing and analysing small-molecule crystal structures. It is intended for release with the CSD system in 2001, at which time it will be supported on Unix and Windows operating systems. The functionality it offers includes the location and display of intermolecular and/or intramolecular hydrogen bonds and other non-bonded contacts, and the ability to build a network of contacts using the methodology of Motherwell & Shields (2000).

2.3. Identification of hydrogen bonds

No fixed distance criteria were used to define hydrogen bonds. Rather, the environment of each hydroxyl group was studied in order to find the closest contacts it formed, relative to the sum of the van der Waals (vdw) radii of the atoms involved (Bondi, 1964). In the case of OH···O hydrogen bonding, the contact distances were, of course, almost invariably shorter than the sum of vdw radii. Our methodology, however, allowed us to find contacts longer than the sum of vdw radii if no shorter ones existed, in accordance with strictures against the use of fixed distance criteria for

[1] Supplementary data for this paper are available from the IUCr electronic archives (Reference: BK0097). Services for accessing these data are described at the back of the journal.
[2] See http://www.ccdc.cam.ac.uk/prods/mercury.

UM00011934
NOVARTIS EXHIBIT 1017
Novartis v. Regents, IPR2023-01346
Page 680 of 4460

hydrogen bonds (Jeffrey & Saenger, 1991). In a very small minority of cases, the presence of a hydrogen bond was inferred from a short O···O distance even though the reported position of the hydroxyl hydrogen was inconsistent with this conclusion. For example, GUHBIU [2-(1-hydroxy-prop-2-yl)-5-methylcyclohexanol; Korner *et al.*, 2000] contains an intermolecular O···O contact of 2.653 Å, which was held as indicative of a hydrogen bond even though the reported H-atom position implies a hydrogen-bond angle (O—H···O) of only 60°. To this extent, our approach for identifying hydrogen bonds might be criticized as judgmental, but the number of controversial cases is so small that the overall conclusions of our study cannot be significantly affected.

3. Results

3.1. Space group and Z' statistics for the CSD

Space group and Z' statistics for the entire CSD are required as a benchmark for interpreting corresponding statistics for the monoalcohol and dialcohol subsets. The 15 most common space groups in the CSD are 1 ($P1$), 2 ($P\bar{1}$), 4 ($P2_1$), 5 ($C2$), 9 (Cc), 11 ($P2_1/m$), 13 ($P2/c$), 14 ($P2_1/c$), 15 ($C2/c$), ($C2/c$), 19 ($P2_12_12_1$), 29 ($Pca2_1$), 33 ($Pna2_1$), 60 ($Pbcn$), 61 ($Pbca$), 62 ($Pnma$); see Cole (2000) and also Mighell *et al.* (1983). 91.0% (200 659) of entries in the CSD belong to one of these space groups. 9.0% (19735) crystallize in other space groups. These percentage figures neglect 4006 CSD entries for which space groups have not been unambiguously assigned.

91.5% (198 894) of CSD entries have Z' values of 1 or less. 8.5% (18 409) have $Z' > 1$. These percentage figures neglect 7097 entries whose Z' values are unknown.

3.2. Basic types of hydrogen-bond aggregates for monoalcohols

In agreement with the findings of B&D, the monoalcohol crystal structures in our study fall into four basic types: those with infinite ···OH···OH··· hydrogen-bonding chains; those containing rings of ···OH···OH··· hydrogen bonds; those containing isolated OH···O hydrogen bonds (called 'dimers' by B&D); and structures in which no OH···O hydrogen bonds are formed at all. Of 144 monoalcohols, all but two fall into one of these categories. The exceptions are WEYSUO [2-(9-fluorenyl)cyclohexanol; Rieger *et al.*, 1994] and NAMLAO (2-buta-1,3-diynyl-2-adamantanol; Keller *et al.*, 1995), both of which form finite hydrogen-bond chains. No monoalcohol structure contains more than one of the basic motifs (*i.e.* structures containing rings *and* chains or rings *and* isolated OH···O hydrogen bonds *etc.* are not found), except that WEYTAV [9-(2-hydroxy-1-phenylethyl)fluorene; Rieger *et al.*, 1994] forms a curious structure containing a ring of four OH···O hydrogen bonds with two additional OH···O hydrogen bonds above and below the plane of the ring at diagonally opposite corners.

In structures containing no OH···O hydrogen bonds, it is almost invariably the case that the hydroxyl hydrogen points towards a neighbouring π system and/or the hydroxyl oxygen accepts one or more CH···O interaction(s) (Desiraju & Steiner, 1999). There are only three reasonably convincing exceptions to this generalization, *viz.* CIPFEM, epi-β-amyrin (Reyes *et al.*, 1983); HOBPET, (1*Z*)-3-phenyl-1-(2′,6′,6′-trimethylcyclohex-1′-enyl)-1-buten-3-ol (Mori *et al.*, 1998); JAGJOQ, 14-taraxen-3α-ol (Chuah *et al.*, 1998). Few of the intermolecular CH···O and OH···π interactions are shorter than the sum of the van der Waals radii of carbon and oxygen, C···O distances typically being in the range 3.3–3.7 Å (intramolecular contacts are often shorter). The fact that these interactions are almost invariably present when OH···O hydrogen bonds are absent nevertheless suggests that, weak though they are, they must play a significant stabilizing role (Braga *et al.*, 1998). A counter-argument is that monoalcohols forming no OH···O hydrogen bonds are often highly sterically crowded, typically with aromatic rings, and the hydroxyl group often has little choice but to form CH···O and OH···π interactions.

Table 1
Frequency of occurrence of four basic packing motifs in 1°, 2° and 3° monoalcohols.

	Chains	Rings	Isolated OH···O	No OH···O	Other
1°	11	2	1	1	0
	73%	*13%*	*7%*	*7%*	*0%*
2°	19	19	5	6	1
	38%	*38%*	*10%*	*12%*	*2%*
3°	12	27	12	27	1
	15%	*34%*	*15%*	*34%*	*1%*
All	42	48	18	34	2
	29%	*33%*	*13%*	*24%*	*1%*

3.3. Steric effects on monoalcohol structures

Full utilization of hydrogen-bond donor and acceptor capacity in monoalcohols requires that the hydroxyl group both donates and accepts, which in turn should lead to a predisposition for chain and/or ring motifs. Furthermore, it has long been known that a hydroxyl oxygen that donates its hydrogen in a hydrogen bond becomes a better hydrogen-bond acceptor. Therefore, hydrogen bonds in a chain or ring are stronger than an isolated hydrogen bond of the same type (the so-called 'cooperative effect'; Del Bene & Pople, 1970; Ceccarelli *et al.*, 1981). This suggests that monoalcohols should preferentially form chains or rings. In fact, this is true only for 1° and 2° monoalcohols. Thus, Table 1 shows that the percentage of structures containing chains decreases dramatically along the series 1° (73%), 2° (38%), 3° (15%). Rings are most common for 2° monoalcohols (1° 13%, 2° 38%, 3° 34%). Structures containing isolated or no OH···O hydrogen bonds are most common for 3° monoalcohols (1° 13%, 2° 22%, 3° 49%). The obvious explanation is that chains form if steric factors allow (Braga *et al.*, 1997); rings are the next most preferred and isolated OH···O hydrogen bonds, or structures with no OH···O hydrogen bonds at all, which only form if steric hindrance prevents the formation of chains or rings.

The significance of steric effects is confirmed by the results in Table 2, which gives the frequency of occurrence of the four

UM00011935
NOVARTIS EXHIBIT 1017
Novartis v. Regents, IPR2023-01346
Page 681 of 4460

Table 2
Occurrence of monoalcohol packing motifs as a function of the sum of substituents on β-carbon(s).

		Sum of substituents on β-carbon(s)									
		0	1	2	3	4	5	6	7	8	Av. (S.E.)
1°	Chains	1	3	7	0						1.6 (0.2)
	Rings	0	0	1	1						2.5 (0.5)
	Isolated OH···O	0	0	0	1						3.0 (–)
	No OH···O	0	0	1	0						2.0 (–)
2°	Chains	0	0	6	6	5	1	1			3.2 (0.3)
	Rings	0	0	2	4	9	2	2			3.9 (0.3)
	Isolated OH···O	0	0	0	1	3	1	0			4.0 (0.3)
	No OH···O	0	0	1	0	5	0	0			3.7 (0.3)
3°	Chains	1	1	1	3	3	2	1	0	0	3.3 (0.5)
	Rings	0	0	3	8	7	5	4	0	0	4.0 (0.2)
	Isolated OH···O	0	0	0	0	1	5	5	1	0	5.5 (0.2)
	No OH···O	0	0	0	1	1	13	8	1	3	5.6 (0.2)
All	Chains	2	4	14	9	8	3	2	0	0	2.8 (0.2)
	Rings	0	0	6	13	16	7	6	0	0	3.9 (0.2)
	Isolated OH···O	0	0	0	2	4	6	5	1	0	4.9 (0.3)
	No OH···O	0	0	2	1	6	13	8	1	3	5.1 (0.2)

Table 3
Space group and Z' statistics for 1°, 2° and 3° monoalcohols.

	Space groups		Molecules per asymmetric unit	
	Top 15	Other	$Z' = 1$	$Z' > 1$
1°	12	3	7	8
	80%	*20%*	*47%*	*53%*
2°	34	16	26	24
	68%	*32%*	*52%*	*48%*
3°	64	15	44	35
	81%	*19%*	*56%*	*44%*
3° alcohols forming chains or rings	27	12	13	26
	69%	*31%*	*33%*	*67%*
3° alcohols forming isolated OH···O	10	2	6	6
	83%	*17%*	*50%*	*50%*
3° alcohols forming no OH···O	26	1	25	2
	96%	*4%*	*93%*	*7%*

basic packing modes as a function of the quantity *SSBC*, the *sum of substituents on β-C atoms*. The *SSBC* value for a given alcohol is calculated by summing the number of non-H atoms (excluding the α-carbon) which are covalently bonded to the β-carbon atom(s) in the molecule. Thus, a β-carbon of the type $-CH_3$ will contribute zero to the *SSBC* value; $-CH_2R$ (*R* not hydrogen) will contribute one, and other types of β-C atoms will contribute as follows: $-CHR_2$ two, $-CR_3$ three, $-C(H)=R$ one, $-C(R)=R$ two, and $-C\equiv R$ one. For example, the molecule $(CH_3CH_2)_2CHOH$ has an *SSBC* count of two, being one for each of the two β-C atoms of the type $-CH_2R$. As another example, $PhCH_2OH$ has *SSBC* = 2, since the only β-carbon is in a phenyl ring and hence of the type $-C(R)=R$.

Table 2 shows that the average *SSBC* value generally increases along the series: chains, rings, isolated OH···O, no OH···O. The only 1° monoalcohols not forming chains have *SSBC* = 2 or 3, *i.e.* the β-carbon is secondary or tertiary [and both of the molecules with secondary β-C atoms have very bulky substituents on this carbon, *viz.* TELZIT: 2-(7,9-diphenylcyclopenta(a)acenaphthadien-6*b*-yl)-2-phenylethanol; Repo *et al.*, 1996; and WEYTAV: 9-(2-hydroxy-1-phenylethyl)fluorene, Rieger *et al.*, 1994]. Amongst 2° monoalcohols, 18 out of 20 structures with *SSBC* < 4 form chains or rings, whereas the four types of packing arrangements are much more evenly split when *SSBC* is four or greater. The outlier 2° monoalcohol forming no OH···O hydrogen bonds but with *SSBC* equal to only two is the extremely hindered CIYSIM (1-hydroxyethylhexahelicene; van Meerssche *et al.*, 1984). For 3° monoalcohols, rings and (to a smaller extent) chains are predominant when *SSBC* < 5 (27 of 30 structures), whereas isolated or no OH···O hydrogen bonds are more common otherwise (36 out of 48 structures).

3.4. Space groups and Z' statistics for monoalcohols

This topic has already been well addressed by B&D and Gavezzotti & Filippini (1994); our work adds a few details. Results are summarized in Tables 3 and 4. As expected from the earlier work, unusual space groups (more specifically, trigonal and tetragonal groups) and Z' values exceeding one are far more common than in the CSD as a whole (see §3.1). This tendency is not shown, however, by 3° monoalcohols forming no OH···O hydrogen bonds, confirming the earlier workers' hypothesis that the unusual symmetries and Z' values are a direct result of the packing requirements for OH···O hydrogen-bond formation. Interestingly, even the formation of isolated OH···O hydrogen bonds in 3° monoalcohols often seems to require $Z' > 1$ (6 of 12 structures). Formation of chains or rings in 3° monoalcohol structures is almost precluded in low-symmetry space groups (orthorhombic or lower) with $Z' = 1$; there are only three such examples in our data set and two of these form ···OH···OH··· chains with very long O···O distances (*viz.* GUBJAO, $P2_12_12_1$, $Z' = 1$, O···O = 3.483 Å, 1-hydroxy-1,2,5,5,8a-pentamethylperhydronaphthalene; Drew *et al.*, 1999; MNPREY, $P2_12_12_1$, $Z' = 1$, O···O = 3.514 Å, 11β-methyl-19-nor-17α-pregn-4-en-20-yn-17β-ol; Rohrer *et al.*, 1976).

Table 4 shows that ring formation is not observed at all in our data set for structures crystallizing with $Z' = 1$ in one of the 15 most common space groups (all of which are triclinic, monoclinic or orthorhombic).

3.5. Geometries of hydrogen-bond aggregates in monoalcohols

The geometries of ···OH···OH··· chains in monoalcohols can be classified into four groups: planar zigzags; threefold helices; fourfold helices; and a broad category which we have

UM00011936
NOVARTIS EXHIBIT 1017
Novartis v. Regents, IPR2023-01346
Page 682 of 4460

Table 4
Monoalcohol space group and Z' frequencies as a function of packing motif.

	Chains		Rings	
	$Z' = 1$	$Z' > 1$	$Z' = 1$	$Z' > 1$
Top 15 space groups	13	15	0	33
Other space groups	10	4	13	2

called 'wave-like' (not being aware of any more widely accepted term). Table 5 shows that helical chains are only common for 2° and 3° monoalcohols – implying that steric factors are relevant – and threefold helices are much more common than fourfold. Exact threefold helices are observed in trigonal space groups, but approximate helices are also seen frequently, formed by translation with $Z' = 3$. Some of the latter examples are sufficiently close to being exact that refinement in a higher symmetry space group might be successful. One of the four observed fourfold helices is exact, along a fourfold screw, while the other three are approximate, being formed by the arrangement of two crystallographically independent molecules along a 2_1 axis. Planar zigzag chains are usually formed by 2_1 axes or by translation with $Z' > 1$ (Fig. 1: VAFMUK, 9-anthrylmethanol; Sweeting & Rheingold, 1988). The geometry we have called 'wave-like', as it refers to monoalcohols, involves two molecules A and B arranged along a glide to give a chain of type $\cdots A\cdots B\cdots A'\cdots B'\cdots$, where A and A' (and B and B') are related to each other by the glide, and A and B are either crystallographically independent or related to each other by some other symmetry operation of the space group. The resulting $\cdots O\cdots O\cdots O\cdots O\cdots$ torsion angles have the sequence of signs + + − − and the motif can be regarded as a zigzag chain with the points of the zigzag pushed alternately in and out of the plane (Fig. 2: ETANOL, ethanol; Jonsson, 1976).

Virtually all $\cdots$OH$\cdots$OH$\cdots$ rings in our sample are 4-rings (*i.e.* involve four OH$\cdots$O hydrogen bonds; 42 4-rings compared with three 3-rings and three 6-rings). The 4-rings are equally divided in geometry between planar and puckered, with the latter becoming more common along the sequence 1°, 2°, 3° (Table 5). All three 6-rings adopt a chair-like geometry. The 4-rings are formed in tetragonal space groups or in space groups of lower symmetry if there are two or four crystallographically independent molecules.

There has been some discussion in the literature regarding the nature of isolated OH$\cdots$O hydrogen bonds in alcohols. B&D said that 'closed dimers' (non-disordered OH$\cdots$HO contacts across a symmetry element) are highly improbable and that 'open dimers' (one dangling H-atom and one free acceptor) are favoured. Glidewell *et al.* (1996), however, concluded that the closed motif 'is actually rather common in α-ferrocenyl alcohols'. A superficial examination of our data set suggests that both open and closed motifs occur (Table 5), but, given the possibilities of disorder and the uncertainty of H-atom positions, we draw no firm conclusion either way.

3.6. Basic types of hydrogen-bond aggregates for dialcohols

The vast majority of dialcohol crystal structures fall into one of three basic types: those with infinite $\cdots$OH$\cdots$OH$\cdots$ chains, those containing rings of $\cdots$OH$\cdots$OH$\cdots$ hydrogen bonds and those containing isolated OH$\cdots$O hydrogen bonds (Table 6). Of 101 dialcohols, only five do not fall into one of these categories. One of the exceptions is the only dialcohol in our study that forms no OH$\cdots$O hydrogen bonds (the highly hindered YIHJOO: $\alpha,\alpha,\alpha',\alpha'$-tetraphenylcyclohexane-1,2-dimethanol; Ito *et al.*, 1994). The other four form structures containing either a mixture of the basic motifs (chains *and* isolated OH$\cdots$O hydrogen bonds, one example), finite hydrogen-bond chains only (one example) or a mixture of finite and infinite hydrogen-bond chains (two examples). The virtual absence of dialcohols forming no OH$\cdots$O hydrogen bonds, even when both hydroxyl groups are tertiary, is in marked contrast to the monoalcohols. It presumably indicates that

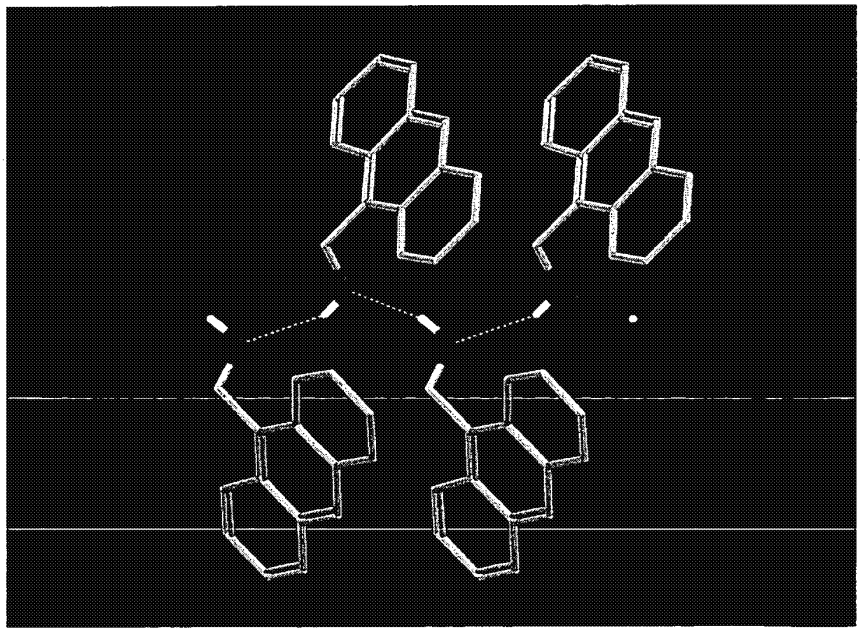


Figure 1
Planar zigzag $\cdots$OH$\cdots$OH$\cdots$ chain in VAFMUK (Sweeting & Rheingold, 1988).

UM00011937
NOVARTIS EXHIBIT 1017
Novartis v. Regents, IPR2023-01346
Page 683 of 4460

Table 5
Geometries of chains, four-membered rings and dimers for 1°, 2° and 3° monoalcohols.

This table excludes five isolated OH···O hydrogen bonds for which no H-atom positions are available.

	Chains				4-Rings		Isolated OH···O	
	Zigzag	Wave	3-helix	4-helix	Planar	Puckered	Open	Closed
1°	4	4	2	1	2	0	0	0
2°	9	2	6	2	10	6	2	2
3°	3	2	6	1	9	15	5	4
All	16	8	14	4	21	21	7	6

dialcohols have more packing possibilities and hence more chance of finding an arrangement that satisfies hydrogen-bonding requirements.

Dialcohols have the possibility of forming intramolecular OH···O hydrogen bonds. This can occur in any of the three basic types of packing, *i.e.* some of the hydrogen bonds in an ···OH···OH··· chain or a hydrogen-bond ring may be intramolecular, or an isolated OH···O hydrogen bond might be intramolecular. All three of these situations occur, although comparatively rarely: 16 of the 60 dialcohol structures containing chains include intramolecular hydrogen bonds; corresponding figures for rings and isolated OH···O hydrogen bonds are two of 21 and three of 15, respectively.

If the two hydroxyl groups (*A*, *B*) of a dialcohol are not chemically equivalent (*i.e.* each is in a different substructural environment), then hydrogen bonds can, in principle, form between a hydroxyl group and its symmetry-generated equivalent (type *A*···*A* and *B*···*B*) or between two non-equivalent hydroxyls (type *A*···*B*). In fact, there is an extremely strong preference for the latter, irrespective of whether the hydrogen bond is isolated, in a ring or in a chain. Thus, in 38 dialcohol structures containing non-equivalent hydroxyl groups, 34 form hydrogen bonds of the type *A*···*B*, and only four form hydrogen bonds of the type *A*···*A* and *B*···*B* (these figures exclude intramolecular hydrogen bonds, which must necessarily be of the type *A*···*B*).

Infinite ···OH···OH··· chains in dialcohols may or may not contain dimers, by which is meant a pair of molecules linked by two hydrogen bonds, *e.g.* compare Fig. 3(*a*) (contains dimers; ZZZKPE01: *trans*-cyclohexane-1,2-diol; Sillanpaa *et al.*, 1984) and Fig. 3(*b*) (does not contain dimers; PUFJIJ: 2,5-hexanediol; Otten *et al.*, 1998). Overall, only a minority of chain structures contain dimers (10 of 60).

3.7. Steric effects on dialcohol structures

Table 6 shows that chains are overwhelmingly favoured for any dialcohol containing at least one primary hydroxyl group (25 chain arrangements in 27 structures). They are also predominant in 2°–2° and 2°–3° dialcohols, although to a smaller extent (27 chains, 10 rings, in a total of 46 structures). Only for 3°–3° dialcohols are structures with isolated OH···O hydrogen bonds as common as chain and ring structures. As with the monoalcohols, the trend is for chains to be formed if steric factors allow, with rings being the next most favoured and isolated OH···O hydrogen bonds only forming when steric hindrance is high. Compared with the monoalcohols, however, the proportion of chains is far higher and only a relatively small minority of structures (< 20%) crystallize without either chains or rings.

The importance of steric factors is confirmed by Table 7, which gives a more detailed breakdown of packing arrangements for the four most common types of dialcohols, *viz.* 1°–1°, 2°–2°, 2°–3°, 3°–3° (all five 1°–2° dialcohols form chains that involve neither dimers nor intramolecular hydrogen bonds; three 1°–3° dialcohols form chains of this type, one forms a chain containing intramolecular hydrogen bonds, the fifth forms

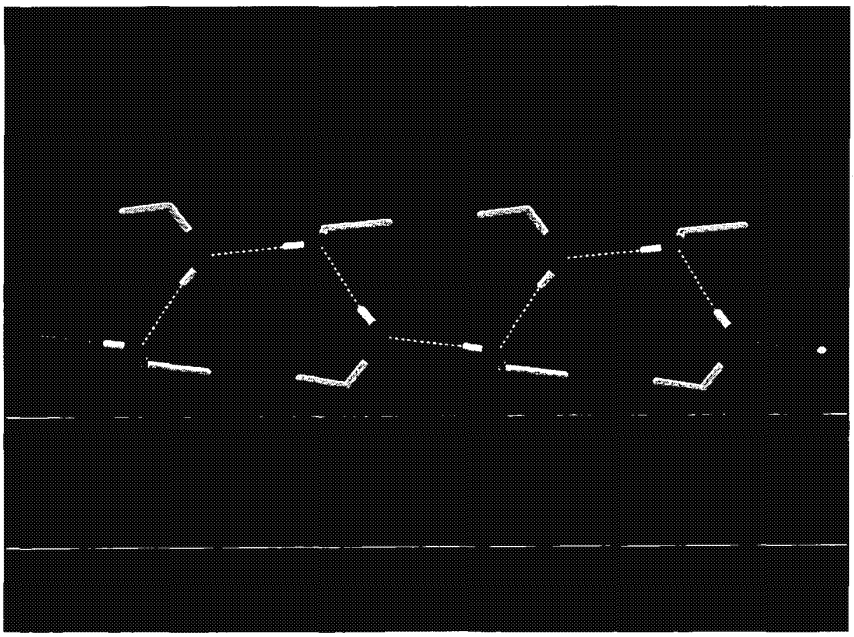


Figure 2
Wave-like ···OH···OH··· chain in ETANOL (Jonsson, 1976).

UM00011938
NOVARTIS EXHIBIT 1017
Novartis v. Regents, IPR2023-01346
Page 684 of 4460

Table 6
Frequency of occurrence of four basic packing motifs in various types of dialcohols.

	Chains	Rings	Isolated OH···O	No OH···O	Other
1°–1°	16	1	0	0	0
	94%	*6%*	*0%*	*0%*	*0%*
1°–2°	5	0	0	0	0
	100%	*0%*	*0%*	*0%*	*0%*
1°–3°	4	1	0	0	0
	80%	*20%*	*0%*	*0%*	*0%*
2°–2°	17	7	1	0	3
	61%	*25%*	*4%*	*0%*	*11%*
2°–3°	10	3	4	0	1
	56%	*17%*	*22%*	*0%*	*6%*
3°–3°	8	9	10	1	0
	29%	*32%*	*36%*	*4%*	*0%*
All	60	21	15	1	4
	59%	*21%*	*15%*	*1%*	*4%*

a ring containing intermolecular hydrogen bonds only). The table also lists the *SSBC* values (*see above*) of all dialcohols in each category. *SSBC* is strongly correlated with packing arrangement. Thus, 40 of the 46 dialcohols in Table 7 with $SSBC < 8$ form intermolecular chains or rings, compared with only 2 of 24 with $SSBC > 8$. Clearly, steric hindrance leads not only to isolated OH···O hydrogen bonds, but also to packing arrangements that include intramolecular hydrogen bonds.

3.8. Space group and Z' statistics for dialcohols

Table 8 summarizes space group and Z' statistics for the dialcohols. The compounds show no abnormal preference for high-symmetry space groups or structures with $Z' > 1$, with the possible exception of 2°–2° and perhaps 3°–3° dialcohols. Of the dialcohols that have $Z' > 1$, three cannot be classified into any of the basic packing categories. Given that there are only four 'unclassified' dialcohols in total (Table 6), this figure is disproportionately high and presumably indicates that these three molecules have difficulty in packing (they are: CIZYOZ, perhydro-1,2-indenediol; Matoba *et al.*, 1984; HINZIN, 9,9-dimethyl-4-phenylbicyclo[4.4.0]decene-5,7-diol; Batey *et al.*, 1999; TETRDO01, *trans*-1,2,3,4-tetrahydro-2,3-naphthalenediol; Lloyd *et al.*, 1998).

3.9. Geometries of hydrogen-bond aggregates in dialcohols

Table 9 summarizes the geometries of intermolecular chains and rings in dialcohol crystal structures. As with monoalcohols, most of the chains can be assigned to one of four categories: planar zigzags, threefold helices, fourfold helices and wave-like chains. Helices are uncommon (six examples in all compared with 11 zigzags and 24 waves). Wave-like chains actually fall into two main groups: the type observed earlier for monoalcohols, generated by glide planes (§3.5); and a geometry generated by a screw axis which can best be described as a zigzag with flattened bottoms. Two slightly different examples are shown in Fig. 4 (FUNCIA, 6-hydroxypropyl-1,7,11,11-tetramethyltricyclo[8.4.0.0^{2,7}]tetradecan-5-ol; Manes *et al.*, 1988; HIYHAY, 1,11-undecanediol; Nakamura *et al.*, 1999).

Table 7
Occurrence of dialcohol packing motifs as a function of sum of substituents on β C atoms.

Table excludes three 2°–2° and one 2°–3° dialcohol structures that cannot be assigned to any of the motifs listed.

	Motif	Total No.	Sum of substituents on β C atoms	Av. (S.E.)
Motifs involving only intermolecular hydrogen bonds				
1°–1°	Chains (no dimers)	10	2, 2, 2, 2, 2, 2, 2, 2, 4, 4	2.4 (0.3)
	Chains (with dimers)	4	2, 4, 4, 6	4.0 (0.8)
	Rings	1	6	6.0 (–)
	Isolated OH···O	0	–	–
	No OH···O	0	–	–
2°–2°	Chains (no dimers)	8	2, 4, 4, 6, 6, 6, 7, 8	5.4 (0.7)
	Chains (with dimers)	5	6, 6, 7, 8, 8	7.0 (0.4)
	Rings	7	4, 6, 6, 8, 8, 8, 9	7.0 (0.7)
	Isolated OH···O	1	9	9.0 (–)
	No OH···O	0	–	–
2°–3°	Chains (no dimers)	5	5, 5, 5, 7, 8	6.0 (0.6)
	Chains (with dimers)	1	8	8.0 (–)
	Rings	3	6,7,8	7.0 (0.6)
	Isolated OH···O	4	5, 9, 11, 11	9.0 (1.4)
	No OH···O	0	–	–
3°–3°	Chains (no dimers)	3	6, 6, 8	6.7 (0.7)
	Chains (with dimers)	0	–	–
	Rings	7	2, 4, 6, 6, 8, 8, 12	6.6 (1.2)
	Isolated OH···O	7	4, 8, 10, 11, 14, 14, 16	11.0 (1.6)
	No OH···O	1	12	12.0 (–)
Motifs involving intramolecular hydrogen bonds				
1°–1°	Chains	2	5, 6	5.5 (0.5)
	Rings	0	–	–
	Isolated OH···O	0	–	–
2°–2°	Chains	4	6, 8, 8, 8	7.5 (0.5)
	Rings	0	–	–
	Isolated OH···O	0	–	–
2°–3°	Chains	4	9, 9, 9, 11	9.5 (0.5)
	Rings	0	–	–
	Isolated OH···O	0	–	–
3°–3°	Chains	5	6, 10, 12, 14, 14	11.2 (1.5)
	Rings	2	12, 12	12.0 (–)
	Isolated OH···O	3	8, 10, 16	11.3 (2.4)

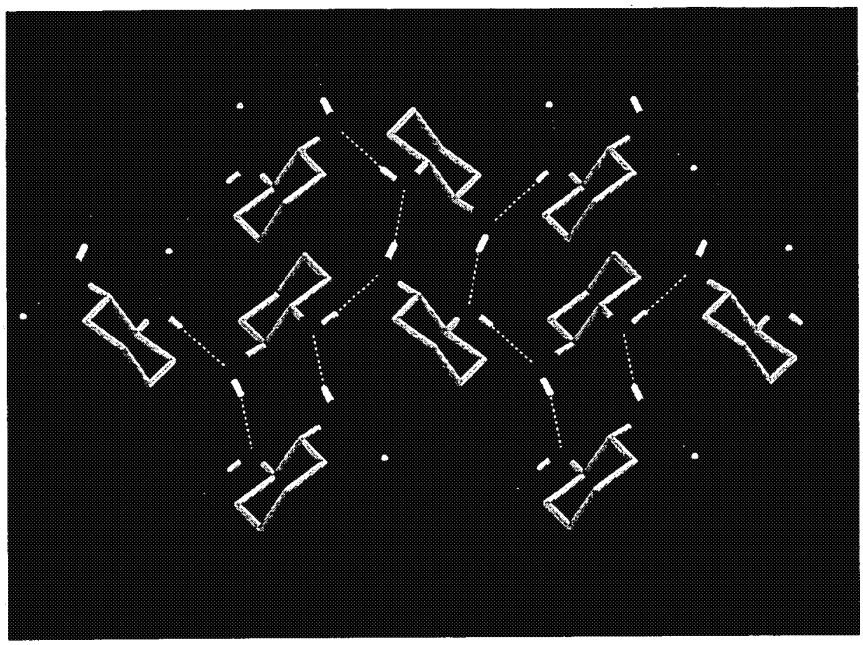
Virtually all the rings in dialcohol structures are 4-rings, *i.e.* contain four OH···O hydrogen bonds (20 of 21, the other is a 6-ring). The majority of these rings are planar, although puckering becomes more likely as steric effects increase.

3.10. Overall topology of hydrogen-bonding networks in dialcohol structures

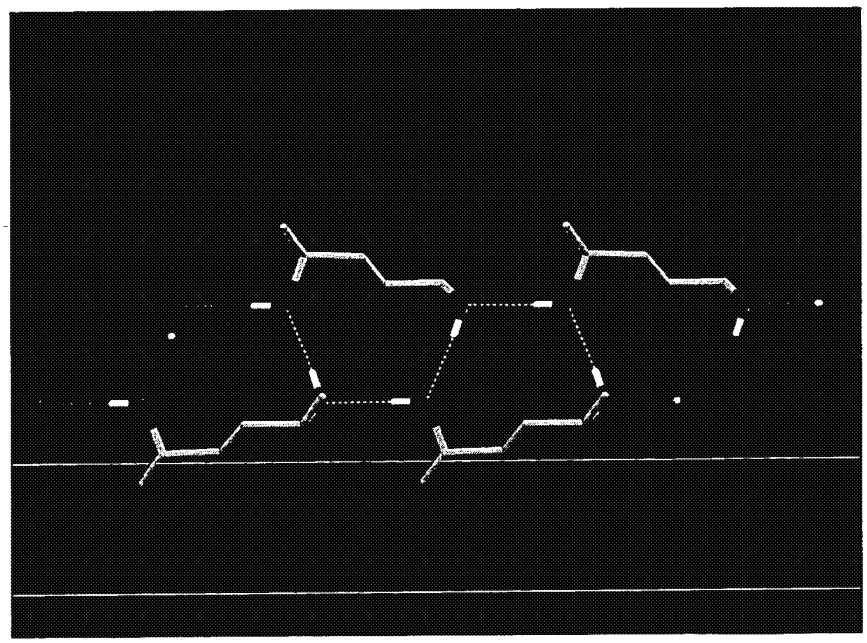
An attempt was made to classify the overall topology of dialcohol networks by removing from the *Mercury* display all atoms other than those on the shortest path between the two hydroxyl groups and expanding the hydrogen-bonded network until an overall pattern emerged (see Batten & Robson, 1998, for a comprehensive review of network topologies). Fig. 5 shows example networks. In the first, the overall topology can be viewed as a network of 6-rings, four sides of each ring being hydrogen bonds, the other two being the covalently linked shortest paths between the hydroxyl groups

UM00011939
NOVARTIS EXHIBIT 1017
Novartis v. Regents, IPR2023-01346
Page 685 of 4460

(CAVDEI, tetradecane-1,14-diol; Nakamura & Sato, 1999). The second is a network of 4- and 8-rings (BCHMOL, 5-*tert*-butylcyclohexane-1,3-dimethanol; van Koningsveld *et al.*, 1981).



(*a*)



(*b*)

Figure 3
Infinite $\cdots$OH$\cdots$OH$\cdots$ chain in dialcohols, (*a*) containing dimers (ZZZKPE01; Sillanpaa *et al.*, 1984) and (*b*) not containing dimers (PUFJIJ; Otten *et al.*, 1998).

One or two of the patterns thus found add insight to dialcohol packing (for example, the arrangement shown in Fig. 4*a* appears to be a common way in which dialcohols form infinite chains). Unfortunately, many overall topologies are impossible to represent in two dimensions and difficult to assimilate even with a three-dimensional graphics terminal. In general, we do not feel confident that they will aid the prediction of dialcohol packing, in contrast to the simpler rules identified in previous sections of this work. This is consistent with the view (Dunitz, 1999) that it is the short-range details that are important ('long-range periodicity is produced by directionally specific short-range interactions, nothing more').

3.11. Packing of primary monoalcohols containing additional oxygen acceptors

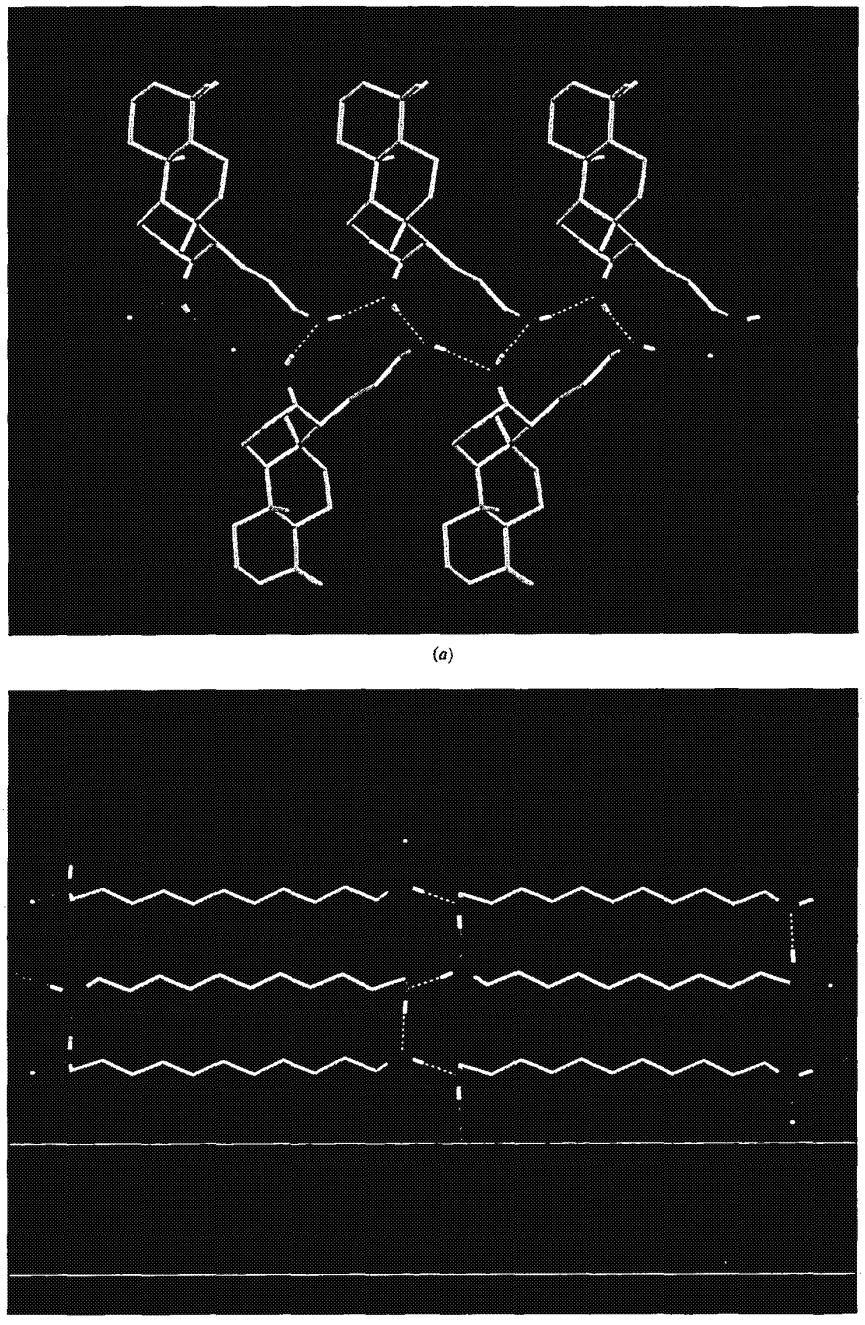
This group of compounds was briefly examined in order to determine the extent to which the packing characteristics of simple monoalcohols, C_mH_nOH, are perturbed when one or more additional (non-hydroxyl) O atoms are present. A count was made of the numbers of different types of O atoms in each molecule, excluding the hydroxyl oxygen. Aromatic and ester (C—O—C) O atoms are also excluded because they are almost incapable of accepting hydrogen bonds (Boehm *et al.*, 1996; Nobeli *et al.*, 1997). The O atom in each structure which acts as the hydrogen-bond acceptor of the hydroxyl hydrogen was then identified. Details of these results have been deposited as supplementary data (see footnote 1).

The analysis shows that hydrogen bonds between hydroxyl groups are rare in these structures, occurring in only four of the 20 examples. When they do occur, they form infinite $\cdots$OH$\cdots$OH$\cdots$ chains in the majority of cases (three

UM00011940
NOVARTIS EXHIBIT 1017
Novartis v. Regents, IPR2023-01346
Page 686 of 4460

out of four), as expected by analogy with the data in Table 1 on 1° monoalcohols. The presence of additional O atoms, however, represents a huge perturbation, since the hydroxyl hydrogen is normally donated to a non-hydroxyl oxygen (usually a carbonyl oxygen if one is present). Lessons learnt from our study of 'pure' monoalcohols, C_mH_nOH, are therefore largely irrelevant for these structures because different types of hydrogen bonds are present.

The space groups and Z' statistics of these compounds are not significantly different from those of the CSD as a whole.



(*a*)

(*b*)

Figure 4
Wave-like ···OH···OH··· chains in (*a*) FUNCIA (Manes *et al.*, 1988) and (*b*) HIYHAY (Nakamura *et al.*, 1999).

4. Conclusions

Rules governing the crystal packing of monoalcohols, C_mH_nOH, are:

(i) Virtually all (142 of 144) monoalcohols form one of four packing motifs, *viz.* infinite ···OH···OH··· chains, ···OH···OH··· rings, isolated OH···O hydrogen bonds or no OH···O hydrogen bonds.

(ii) If a monoalcohol structure contains no OH···O hydrogen bonds, it will almost invariably be stabilized by CH···O and/or OH···π interactions (only three structures found with no OH···O, CH···O or OH···π interactions).

(iii) The occurrence of the basic motifs is strongly correlated with steric effects. Chains form if steric factors permit, rings are next most preferred and sterically hindered monoalcohols form isolated OH···O hydrogen bonds, or no OH···O hydrogen bonds at all. Thus:

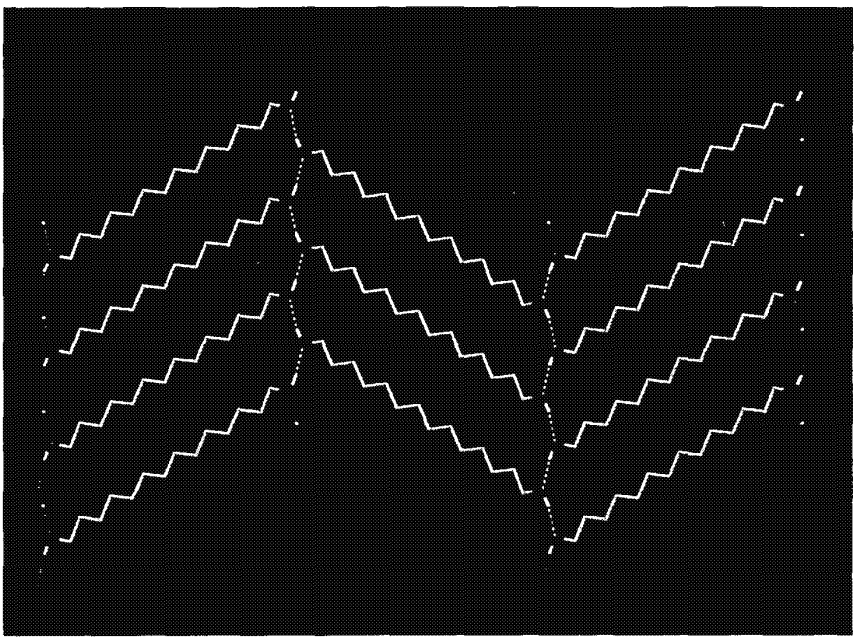
(*a*) 1° monoalcohols always form chains (11 of 15) unless sterically hindered by tertiary substitution on the β carbon, or secondary substitution with very large substituents.

(*b*) 2° monoalcohols form all four of the basic motifs, but are mostly chains (19 of 50) or rings (19 of 50). Chains or rings are highly likely if $SSBC < 4$ (18 of 20).

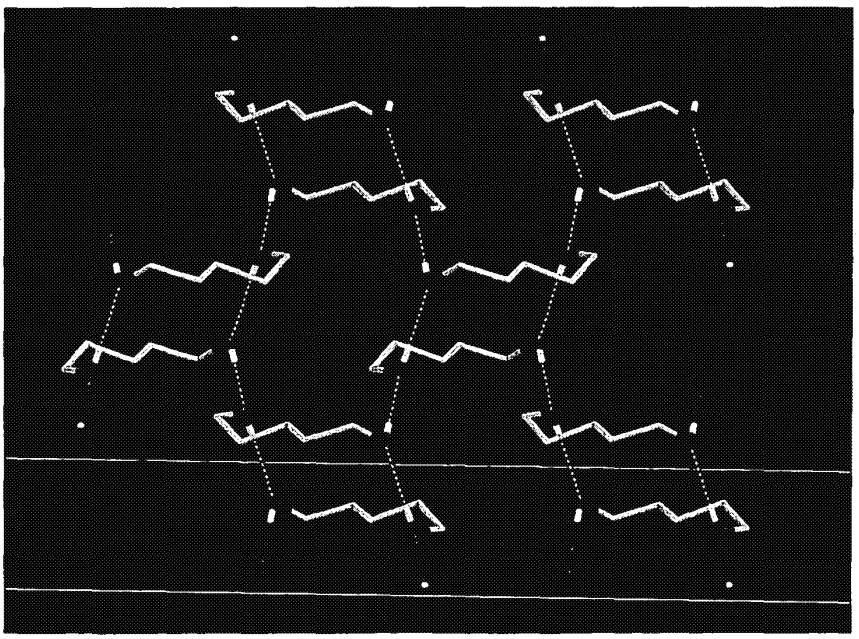
(*c*) 3° monoalcohols usually form rings (27 of 79) or have no OH···O hydrogen bonds at all

UM00011941
NOVARTIS EXHIBIT 1017
Novartis v. Regents, IPR2023-01346
Page 687 of 4460

(27 of 79). Rings or chains are more likely if $SSBC < 5$ (27 of 30), whereas isolated/no OH···O hydrogen bonds are likely otherwise (36 of 48).



(*a*)



(*b*)

Figure 5
Extended hydrogen-bond networks in (*a*) CAVDEI (Nakamura & Sato, 1999) and (*b*) BCHMOL (van Koningsveld *et al.*, 1981).

(iv) Monoalcohols forming chains, rings or isolated OH···O hydrogen bonds have a strongly increased probability (compared with the rest of the CSD) of crystallizing in a high-symmetry (trigonal or tetragonal) space group or with $Z' > 1$. This tendency is not shown by monoalcohols that form no OH···O hydrogen bonds. In particular:

(*a*) It is very unlikely that a ring will occur if $Z' = 1$ and the space group is not high symmetry (no examples in 48 structures forming rings).

(*b*) It is very unlikely that a 3° monoalcohol structure will contain either a chain or a ring if the space group is not high symmetry and $Z' = 1$ (three examples only).

(v) Chains can be zigzag, wave-like or helical, the latter becoming somewhat more predominant as steric hindrance increases. Threefold helices are more common than fourfold (14 *versus* 4).

(vi) A large majority (42 of 48) of ···OH···OH··· rings are 4-rings (*i.e.* contain four OH···O hydrogen bonds). Considering all monoalcohols, such rings are equally likely to be planar or puckered. Puckering becomes more common as steric hindrance increases, *i.e.* for 3° monoalcohols.

Rules governing the crystal packing of dialcohols, $C_mH_n(OH)_2$, are:

(i) A large majority (96 of 101) of dialcohols form one of three packing motifs: infinite ···OH···OH··· chains; ···OH···OH··· rings; isolated OH···O hydrogen bonds. Each of these motifs can involve intramolecular OH···O hydrogen bonds, but in practice this occurs rather infrequently (in 21 of the 101 structures).

(ii) The occurrence of the basic motifs is strongly correlated with steric effects. Intermolecular chains form if steric factors permit, intermolecular rings are next most preferred

UM00011942
NOVARTIS EXHIBIT 1017
Novartis v. Regents, IPR2023-01346
Page 688 of 4460

Table 8
Space group and Z' statistics for different types of dialcohols.

	Space groups		Molecules per au	
	Top 15	Other	$Z' = 1$	$Z' > 1$
1°–1°	16	1	17	0
	94%	*6%*	*100%*	*0%*
1°–2°	5	0	5	0
	100%	*0%*	*100%*	*0%*
1°–3°	4	1	4	1
	80%	*20%*	*80%*	*20%*
2°–2°	26	2	20	8
	93%	*7%*	*71%*	*29%*
2°–3°	15	3	17	1
	83%	*17%*	*94%*	*6%*
3°–3°	25	3	23	5
	89%	*11%*	*82%*	*18%*

Table 9
Geometries of chains and four-membered rings for different types of dialcohols.

	Chains (not involving intramolecular hydrogen bonds)					4-Rings	
	Zigzag	Wave	3-helix	4-helix	Other	Planar	Puckered
1°–1°	6	8	0	0	0	1	0
1°–2°	1	4	0	0	0	0	0
1°–3°	0	1	0	1	1	1	0
2°–2°	3	6	1	2	1	6	1
2°–3°	0	4	0	1	1	2	1
3°–3°	1	1	1	0	0	3	5
All	11	24	2	4	3	13	7

and only sterically hindered dialcohols form crystal structures involving intramolecular hydrogen bonds, isolated OH···O hydrogen bonds, or no OH···O hydrogen bonds at all. Thus:

(*a*) Dialcohols with at least one primary hydroxyl group overwhelmingly favour chains (25 of 27), of which the large majority (22) involve only intermolecular hydrogen bonds.

(*b*) Dialcohols containing at least one secondary hydroxyl group but no primary OH's usually form chains (27 examples out of 46) or rings (10 examples).

(*c*) Chains, rings and isolated OH···O hydrogn bonds are approximately equally likely in dialcohols in which both hydroxyls are tertiary.

(*d*) 2°–2°, 2°–3° and 3°–3° dialcohols with $SSBC < 8$ almost always form intermolecular chains or rings (25 of 29). The same types of dialcohols strongly favour isolated OH···O hydrogen bonds; no OH···O hydrogen bonds or motifs involving intramolecular hydrogen bonds if $SSBC > 8$ (22 of 24).

(iii) Intermolecular hydrogen bonds in the structures of dialcohol molecules containing topologically distinct hydroxyl groups (*A*, *B*) are almost invariably between the non-equivalent groups (*i.e.* *A*···*B* rather than *A*···*A* or *B*···*B*; 34 of 38 structures). This is independent of whether the basic motif is a chain, ring or isolated OH···O hydrogen bond.

(iv) With the possible exception of 2°–2° and 3°–3° dialcohols, the compounds do not show an unusual predilection for crystallizing in high-symmetry space groups or with $Z' > 1$.

(v) Chains are usually zigzag or wave-like. Both threefold and fourfold helices are rare (two and four examples, respectively, in 44 structures forming intermolecular chains).

(vi) Virtually all (20 of 21) ···OH···OH··· rings are 4-rings (*i.e.* contain four OH···O hydrogen bonds). Planar rings are slightly favoured over puckered (13 *versus* 7), but puckering becomes more likely as steric hindrance increases.

Rules governing the crystal packing of primary monoalcohols containing at least one other O atom, $C_mH_n(O)_pCH_2OH$, are:

(i) Hydrogen bonds of the type OH···O=C will usually occur if the molecule contains at least one carbonyl group (seen in 10 of 14 examples).

(ii) Space group and Z' distributions are similar to those seen in the CSD as a whole.

5. Discussion

We have been successful in identifying rules governing the crystal packing of mono- and dialcohols. Moreover, the rules are based on simple quantities that can be rapidly determined from a trivial analysis of molecular connectivity. In this section we now consider whether the rules are of practical value.

In order to be useful, the rules must first add value to what is already achievable in crystal-structure prediction. Common experience suggests that using a state-of-the-art program to predict, say, the structure of a dialcohol will result in a rather large number of possible structures with similar calculated lattice energies. The experimental structure is likely to be amongst them, but cannot be distinguished (Mooij *et al.*, 1999; Lommerse *et al.*, 2000; van Eijck & Kroon, 2000). In this situation, if some of the hypothetical structures fail to match the empirical rules identified in this work, then they can be eliminated with confidence and the rules will have proved useful. Until the experiment is tried, however, we do not know whether this will be the case. If it is not (*i.e.* if all the putative structures obey the rules), then the only way our work can help is by restricting the search space that must be visited by the crystal-structure prediction program. This may allow more time to be spent on higher quality energy calculations which, in turn, may improve predictive ability. Then again, it may not, particularly if kinetic effects are important.

The next issue concerns transferability. Common empirical techniques such as molecular mechanics are successful because they are based on parameters that can be transferred from one situation to another. For example, the same stretching constant can be used for more or less any C—O single bond, irrespective of its molecular environment. In the case under discussion, it is regrettably clear that our rules are far from transferable. Even changing from monoalcohols to dialcohols alters the rules appreciably, and adding an extra type of oxygen acceptor renders them completely inapplicable. Our rules may be fine for the systems from which they

UM00011943
NOVARTIS EXHIBIT 1017
Novartis v. Regents, IPR2023-01346
Page 689 of 4460

were derived, but they are useless for anything else and therefore cannot assist in the solution of problems of real commercial interest.

This does not mean that the CSD itself is of no value in crystal-structure prediction; rather, it means that rules generated from the CSD must be tailored to the problem in hand. At first sight this seems impracticable and, indeed, this would be the case if rules had to be discerned by visual analysis of scores of crystal structures, as we have performed here. Fortunately, the architecture of *Mercury* should make it possible to automate a search for rules: the underlying C++ classes can be put together in a variety of ways to achieve this end. One can imagine the following methodology:

(i) Parse the structure of the molecule of interest to identify the chemical populations to which it belongs (there will normally be more than one – for example, a cyclopentenone with an oxime side chain belongs to the population *of all cyclopentenone derivatives* and the population of *all organic oximes*).

(ii) Find the relevant structures in the CSD and discern packing rules automatically.

(iii) Factor the rules into the crystal-structure prediction process.

The final issue concerns statistical significance and bias. Leusen *et al.* (1999) point out that scoring functions based on the CSD may be incapable of predicting anything novel. While true, this need not greatly concern us. We would be gratified if we could predict the majority of typical structures, never mind the few that are atypical. Bias in the CSD is, however, a problem. For example, the 15 primary monoalcohols used herein do not constitute a very diverse set of molecules. The answer lies in finding a good balance between the relevance of a sample and its size. As we increase the size of a sample by reducing the specificity of the substructure search from which it was generated, the diversity will tend to increase and biases will become less likely. On the other hand, the structures in the sample will, on average, become less similar to the molecule in which we are interested. Finding algorithms for optimizing this balance will be a major challenge in developing an effective methodology for using the CSD in crystal structure prediction.

Mercury was written by one of us (CFM). Significant contributions to the program were also made by Drs Jason Cole, Magnus Kessler and Jonathan Pearson, all present or former members of staff at the Cambridge Crystallographic Data Centre.

References

Allen, F. H. & Kennard, O. (1993). *Chem. Des. Autom. News*, **8**, 31–37.
Batey, R. A., Thadani, A. N. & Lough, A. J. (1999). *J. Am. Chem. Soc.* **121**, 450–451.
Batten, S. R. & Robson, R. (1998). *Angew. Chem. Int. Ed.* **37**, 1460–1494.
Boehm, H.-J., Brode, S., Hesse, U. & Klebe, G. (1996). *Chem. Eur. J.* **2**, 1509–1513.
Bondi, A. (1964). *J. Phys. Chem.* **68**, 441–451.
Braga, D., Grepioni, F. & Desiraju, G. R. (1998). *Chem. Rev.* **98**, 1375–1405.
Braga, D., Grepioni, F., Walther, D., Heubach, K., Schmidt, A., Imhof, W., Goerls, H. & Klettke, T. (1997). *Organometallics*, **16**, 4910–4919.
Brock, C. P. (1999). *Implications of Molecular and Materials Structure for New Technologies*, edited by J. A. K. Howard, F. H. Allen & G. P. Shields, pp. 251–262. Dordrecht, The Netherlands: Kluwer Academic Publishers.
Brock, C. P. & Duncan, L. L. (1994). *Chem. Mater.* **6**, 1307–1312.
Ceccarelli, C., Jeffrey, G. A. & Taylor, R. (1981). *J. Mol. Struct.* **70**, 255–271.
Chuah, C. H., Ng, S. W. & Yap, G. P. A. (1998). *Z. Kristallogr.* **213**, 493–494.
Cole, J. C. (2000). Private communication.
Del Bene, J. & Pople, J. A. (1970). *J. Chem. Phys.* **52**, 4858–4866.
Desiraju, G. R. & Steiner, T. (1999). *The Weak Hydrogen Bond.* Oxford University Press.
Drew, M. G. B., Harwood, L. M., Jahans, A., Robertson, J. & Swallow, S. (1999). *Synlett*, pp. 185–188.
Dunitz, J. D. (1999). *Implications of Molecular and Materials Structure for New Technologies*, edited by J. A. K. Howard, F. H. Allen & G. P. Shields, pp. 175–184. Dordrecht, The Netherlands: Kluwer Academic Publishers.
Eijck, B. P. van & Kroon, J. (2000). *Acta Cryst.* B**56**, 535–542.
Gavezzotti, A. (1994). *Acc. Chem. Res.* **27**, 309–314.
Gavezzotti, A. & Filippini, G. (1994). *J. Phys. Chem.* **98**, 4831–4837.
Gavezzotti, A. & Filippini, G. (1998). *Chem. Commun.* pp. 287–294.
Glidewell, C., Klar, R. B., Lightfoot, P., Zakaria, C. M. & Ferguson, G. (1996). *Acta Cryst.* B**52**, 110–121.
Hofmann, D. W. M. & Lengauer, T. (1997). *Acta Cryst.* A**53**, 225–235.
Ito, Y. N., Ariza, X., Beck, A. K., Bohac, A., Ganter, C., Gawley, R. E., Kuhnle, F. N. M., Tuleja, J., Wang, Y. M. & Seebach, D. (1994). *Helv. Chim. Acta*, **77**, 2071–2110.
Jeffrey, G. A. & Saenger, W. (1991). *Hydrogen Bonding in Biological Structures*, pp. 29–33. Berlin: Springer-Verlag.
Jonsson, P.-G. (1976). *Acta Cryst.* B**32**, 232–235.
Keller, M. B., Rzepa, H. S., White, A. J. P. & Williams, D. J. (1995). *First Electronic Conf. Trends in Org. Chem.*, p. 50, http://www.ch.ic.ac.uk/ectoc.
Koningsveld, H. van, Baas, J. M. A., van de Graaf, B. & Steenks, A. (1981). *Cryst. Struct. Commun.* **10**, 691–697.
Korner, F., Schurmann, M., Preut, H. & Kreiser, W. (2000). *Acta Cryst.* C**56**, 74–75.
Leiserowitz, L. (1976). *Acta Cryst.* B**32**, 775–802.
Leusen, F. J. J., Wilke, S., Verwer, P. & Engel, G. E. (1999). *Implications of Molecular and Materials Structure for New Technologies*, edited by J. A. K. Howard, F. H. Allen & G. P. Shields, pp. 303–314. Dordrecht, The Netherlands: Kluwer Academic Publishers.
Lloyd, M. A., Patterson, G. E. & Brock, C. P. (1998). *Acta Cryst.* C**54**, 1486–1488.
Lommerse, J. P. M., Motherwell, W. D. S., Ammon, H. L., Dunitz, J. D., Gavezzotti, A., Hofmann, D. W. M., Leusen, F. J. J., Mooij, W. T. M., Price, S. L., Schweizer, B., Schmidt, M. U., van Eijck, B. P., Verwer, P. & Williams, D. E. (2000). *Acta Cryst.* B**56**, 697–714.
Manes, L. V., Crews, P., Kernan, M. R., Faulkner, D. J., Fronczek, F. R. & Gandour, R. D. (1988). *J. Org. Chem.* **53**, 570–575.
Matoba, Y., Ishii, Y. & Ogawa, M. (1984). *Acta Cryst.* C**40**, 1735–1736.
Meerssche, M. van, Declercq, J. P., Germain, G., Soubrier-Payen, B., Lindner, H. J. & Kitschke, H. J. (1984). *Bull. Soc. Chim. Belg.* **93**, 445–448.
Mighell, A. D., Himes, V. L. & Rodgers, J. R. (1983). *Acta Cryst.* A**39**, 737–740.
Mooij, W. T. M., van Eijck, B. P. & Kroon, J. (1999). *J. Phys. Chem. A*, **103**, 9883–9890.

UM00011944
NOVARTIS EXHIBIT 1017
Novartis v. Regents, IPR2023-01346
Page 690 of 4460

Mori, H., Ikoma, K., Isoe, S., Kitaura, K. & Katsumura, S. (1998). *J. Org. Chem.* **63**, 8704–8718.
Motherwell, W. D. S. & Shields, G. P. (2000). *RPLUTO*, http://www.ccdc.cam.ac.uk/prods/rpluto.
Nakamura, N. & Sato, T. (1999). *Acta Cryst.* C**55**, 1687–1689.
Nakamura, N., Setodoi, S. & Ikeya, T. (1999). *Acta Cryst.* C**55**, 789–791.
Nobeli, I., Price, S. L., Lommerse, J. P. M. & Taylor, R. (1997). *J. Comput. Chem.* **18**, 2060–2074.
Otten, S., Froehlich, R. & Haufe, G. (1998). *Tetrahedron Asym.* **9**, 189–191.
Repo, T., Klinga, M., Leskele, M., Polamo, M. & Rieger, B. (1996). *Acta Cryst.* C**52**, 2910–2912.
Reyes, J., Hidalgo, C. & Fronczek, F. R. (1983). *Rev. Latinoam. Quim.* **14**, 67–70.
Rieger, B., Jany, G., Steimann, M. & Fawzi, R. (1994). *Z. Naturforsch. Teil B*, **49**, 451–456.
Rohrer, D. C., Hazel, J. P., Duax, W. L. & Zeelen, F. J. (1976). *Cryst. Struct. Commun.* **5**, 543–546.
Sillanpaa, R., Leskele, M. & Hiltunen, L. (1984). *Acta Chem. Scand. Ser. B*, **38**, 249–254.
Sweeting, L. M. & Rheingold, A. L. (1988). *J. Phys. Chem.* **92**, 5648–5655.

UM00011945
NOVARTIS EXHIBIT 1017
Novartis v. Regents, IPR2023-01346
Page 691 of 4460

This Page is Inserted by IFW Indexing and Scanning Operations and is not part of the Official Record

BEST AVAILABLE IMAGES

Defective images within this document are accurate representations of the original documents submitted by the applicant.

Defects in the images include but are not limited to the items checked:

- ☐ BLACK BORDERS
- ☐ IMAGE CUT OFF AT TOP, BOTTOM OR SIDES
- ☐ FADED TEXT OR DRAWING
- ☐ BLURRED OR ILLEGIBLE TEXT OR DRAWING
- ☐ SKEWED/SLANTED IMAGES
- ☐ COLOR OR BLACK AND WHITE PHOTOGRAPHS
- ☐ GRAY SCALE DOCUMENTS
- ☐ LINES OR MARKS ON ORIGINAL DOCUMENT
- ☐ REFERENCE(S) OR EXHIBIT(S) SUBMITTED ARE POOR QUALITY
- ☐ OTHER: _____

IMAGES ARE BEST AVAILABLE COPY.
As rescanning these documents will not correct the image problems checked, please do not report these problems to the IFW Image Problem Mailbox.

Crystal Growth

Polymorphism of 1,3,5-Trinitrobenzene Induced by a Trisindane Additive**

Praveen K. Thallapally, Ram K. R. Jetti, Amy K. Katz, H. L. Carrell, Kuldeep Singh, Kakali Lahiri, Sambasivarao Kotha, Roland Boese, and Gautam R. Desiraju**

Additive-induced polymorphism has always interested the solid-state chemist for fundamental and practical reasons.[1] Polymorphism is, in itself, an enigmatic phenomenon and the reasons for its occurrence are only now beginning to be unraveled.[2] The role of tailor-made additives (auxiliaries) in the control of various aspects of crystallization (nucleation,

[*] Dr. R. K. R. Jetti, Prof. Dr. R. Boese
Institut für Anorganische Chemie
Universität Duisburg-Essen, Standort Essen
Universitätstrasse 5–7, 45177 Essen (Germany)
Fax: (+49) 201-183-2535
E-mail: roland.boese@uni-essen.de

Dr. P. K. Thallapally, Prof. G. R. Desiraju
School of Chemistry
University of Hyderabad
Hyderabad 500 046 (India)
Fax: (+91) 40-2301-0567
E-mail: desiraju@uohyd.ernet.in

A. K. Katz, Dr. H. L. Carrell
The Institute for Cancer Research, Fox Chase Cancer Center, 7701 Burholme Avenue, Philadelphia, PA 19111 (USA)

K. Singh, Dr. K. Lahiri, Prof. S. Kotha
Department of Chemistry, Indian Institute of Technology
Powai, Mumbai, 400 076 (India)

[**] P.K.T thanks the CSIR for a fellowship. G.R.D. is a recipient of the Alexander von Humboldt research award. R.K.R.J. and R.B. are grateful to the DFG for financial assistance. H.L.C. and A.K.K. acknowledge financial support from grant CA-10925 of the NIH. K.S., K.L., and S.R.K. thank RSIC IIT-Mumbai for spectral data.

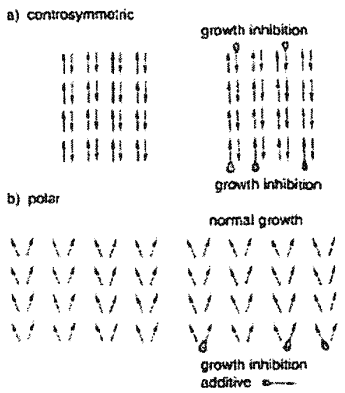
Supporting information for this article (experimental details, spectroscopic data, computational details) is available on the WWW under http://www.angewandte.org or from the author.

 DOI: 10.1002/anie.200352253 © 2004 Wiley-VCH Verlag GmbH & Co. KGaA, Weinheim

UM00011947
NOVARTIS EXHIBIT 1017
Novartis v. Regents, IPR2023-01346
Page 693 of 4460

growth, morphology, dissolution, structure) has been described.[3] Polymorphism is one of the least controllable aspects of crystallization. Therefore it would be extremely useful if there were a reliable and general way of engineering additive-induced polymorphism. These ideas are also relevant in crystal-structure prediction.[4] Three questions are pertinent: 1) Does the presence of an additive change the polymorph that is obtained? 2) If so, can the structure of the polymorph so obtained be correlated with the structure of the additive? 3) What is the mechanism of enhancement/inhibition of a polymorph? Despite the importance of these questions, the number of well-documented examples of additive-induced polymorphism is very limited.

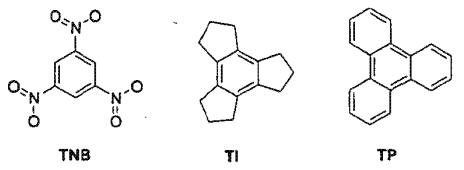
Leiserowitz, Lahav, and co-workers[1f,g] have provided a basic model for additive-induced polymorphism (Scheme 1). The additive is structurally similar to the molecule of interest



Scheme 1. Basic model for additive-induced polymorphism, see text for details.

(host) and it may be selectively adsorbed on its crystal faces. Depending on the degree of similarity between the host and the additive, the latter may selectively inhibit the growth of a few faces of the embryonic crystal of the host. These ideas find a practical application in the preferred crystallization of a noncentrosymmetric polymorph (Scheme 1b, left) at the expense of a centrosymmetric one (Scheme 1a, left). An appropriate tailor-made additive will inhibit growth of the centrosymmetric form at two opposite ends thereby precluding it (Scheme 1a, right), but it will inhibit growth of the polar form at only one end of the crystal (Scheme 1b, right) so that it survives. This concept was demonstrated for *N*-(2-acetamido-4-nitrophenyl)pyrrolidine (PAN) with the 2-nitro and 2-amino derivatives as additives, and for the γ-form of glycine in aqueous solution with racemic hexafluorovaline as an additive.[1f,g] Another clear example is provided by Davey and co-workers[5] who selected trimesic acid and *trans*-glutaconic acid as inhibitors of the stable β-polymorph of L-glutamic acid leading to the metastable α-polymorph. He, Stowell, and co-workers[6] designed isomorphous additives that induced crystallization of a metastable form of 4-methyl-2-nitroacetanilide. The phenomenon has been reviewed.[7,8]

Herein we report on the polymorphism of 1,3,5-trinitrobenzene (TNB) induced by the additive trisindane (TI). TNB has been known for 120 years as an explosive and in the formation of crystalline π–π donor–acceptor complexes.[9] However, and in contrast to the related molecule 2,4,6-trinitrotoluene (TNT),[2a,10] there has been no report of its polymorphism.[11] The only known crystal structure of TNB is that of the centrosymmetric orthorhombic form (space group *Pbca*, $Z' = 2$), which we shall call Form **I**.[12] More recently, TNB has been used as a component of C–H···O hydrogen-bonded molecular complexes for applications in nonlinear optics (NLO). For example, we co-crystallized an equimolar mixture of TNB and triphenylene (TP) to obtain a 1:1



molecular complex, which we studied in detail.[13] Continuing this strategy, we attempted to co-crystallize 1:1 and 2:1 mixtures of TNB and the closely related TI from CCl_4.[14] There was distinct evidence of complex formation in solution in that the solution changed from pale yellow to dark red. However, instead of obtaining the desired 1:1 or 2:1 molecular complexes, we obtained (from a 2:1 experiment in CCl_4) a new polymorph of TNB, henceforth, Form **II**.

Figure 1 shows the crystal structure of the new and unexpected noncentrosymmetric polymorph, in the orthorhombic space group $Pca2_1$, also with $Z' = 2$.[15] Close inspection of this intricate structure shows two patterns generated, respectively, from the two independent molecules in the asymmetric unit. These patterns are shown in green and yellow in Figure 1. The green colored molecules form a V-shaped trough while the yellow colored molecules form a zigzag arrangement. The V-shaped trough and the zigzag chains are linked with weak C–H···O, C–H···N, and $NO_2 \cdots NO_2$ contacts.[16]

We next redetermined the structure of Form **I** because we wished to verify the Lahav–Leiserowitz model for additive induced polymorphism.[15] Figure 2 shows that the *Pbca* structure of Form **I** is closely related to the $Pca2_1$ structure of Form **II**. In both forms, there are V-shaped troughs made up of one of the two symmetry independent molecules in the crystal (green). The major distinction is that the V-shaped troughs point in opposite directions in the centrosymmetric Form **I** crystal and only in one direction in the polar Form **II** crystal. The *Pbca* structure is in effect a doubled version of the $Pca2_1$ structure across an inversion center[18] so that the mechanism in Scheme 1 broadly applies leading to Form **II** crystals. The unit cell parameters (Form **I**, $a = 12.587$, $b = 9.684$, $c = 26.86$; Form **II**, $a = 9.297$, $b = 18.730$, $c = 9.633$) show some relationship in that $b_I \cong c_{II}$ and that $(a_I c_I) \cong 2(a_{II} b_{II})$. While the V-shaped troughs point along [010] and [0−10] in Form **I** they point only along [001] in Form **II**.

 © 2004 Wiley-VCH Verlag GmbH & Co. KGaA, Weinheim

UM00011948
NOVARTIS EXHIBIT 1017
Novartis v. Regents, IPR2023-01346
Page 694 of 4460

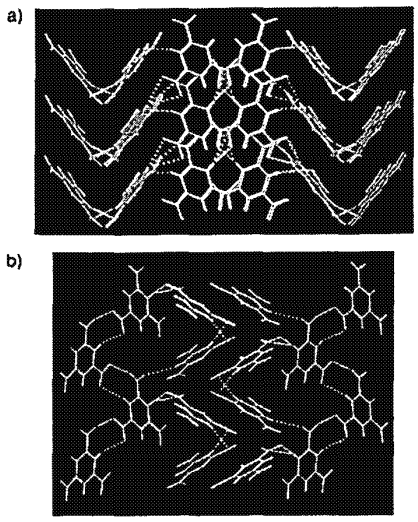


Figure 1. Noncentrosymmetric Form II crystal of TNB. The two symmetry-independent molecules are shown in green and yellow. a) View down the *a* axis showing alternate V-shaped troughs and zigzag chains. b) View down the *c* axis showing TNB tape based on C–H···O and NO_2···NO_2 interactions along the *a* axis (green), and zigzag chains (yellow). For clarity C–H···N and ON–O···NO_2 interactions are removed between the green TNB molecules. Molecular graphics were generated using X-seed and POV-Ray.[17]

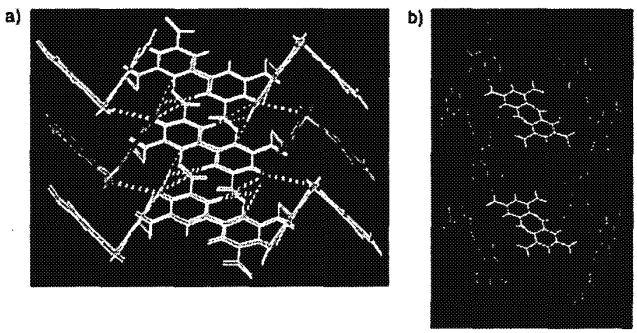


Figure 2. Centrosymmetric Form I crystal structure of TNB (*Pbca*). a) View down the *a* axis. b) View down the *b* axis.

The experimental morphology of the Form **I** crystals was determined. Figure 3 shows the crystal faces in a well-grown specimen. The main faces are (010) and (001) and their centrosymmetrically related equivalents. From the direction of the V-shaped troughs in the two forms, it may be assumed that binding of TI on the (010) faces is likely. If the binding is slightly different on (010) and (0–10) there will be a symmetry reduction from *Pbca* to $Pb2_1a$. A permutation of the *b* and *c* axes ($b_I \cong c_{II}$) leads to space group $Pca2_1$ for Form **II**. According to this model it is not mandatory that $a_I \cong a_{II}$ with $c_I \cong 2\,(b_{II})$. It is sufficient if $(a_I c_I) \cong 2\,(a_{II} b_{II})$ and this condition is achieved by a slight shearing of molecules in the

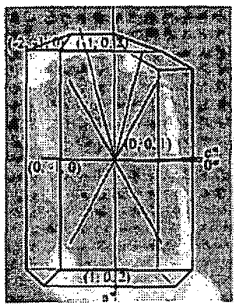


Figure 3. Experimental morphology of Form I crystal of TNB. Note the (010) and (0–10) faces.

(010) planes of the Form **I** crystal. Indeed such shearing is unsurprising. It would have been more exceptional if the preferential growth along +b or –b were accompanied by no change whatsoever in the (010) planes, in effect along the *a* and *c* directions. These results also demonstrate that it is the adsorption of TI additive on (010) and (0–10) that is critical to the formation of the new polymorph because it is the *b* axis of Form **I** that is unchanged in length in going to Form **II** (where it is termed the *c* axis), while the *a* and *c* axes of Form **I** (renamed as the *a* and *b* axes in Form **II**) change in length. The experimental morphology shows that (010) and (001) are major faces, with (001) being more prominent. Yet, only adsorption of TI on (010) is critical to the growth of Form **II** with any possible adsorption on (001) being innocuous.

In considering the growth of Form **II** crystals from a CCl_4 solution of TNB that contains TI additive, an important assumption that is implicit in the Lahav–Leiserowitz model needs to be mentioned,[3a] namely that any solution contains a variety of molecular aggregates, some of which have structures akin to those of the macroscopic crystalline forms. This assumption is a triviality when polymorphs appear concomitantly. However, if say solution *A* normally results in polymorph *A* and one wishes to design an additive that will yield polymorph *B* from this solution, then this assumption must be taken into account. This is pertinent in the present case because both Forms **I** and **II** were obtained from CCl_4 solution. Another consideration that has been utilized in certain layered structures wherein layer stabilities and bulk stabilities are inverted in two polymorphs is to induce nucleation layer by layer so as to obtain the less stable polymorph.[3a] But this is not applicable in the present case because the structures of Forms **I** and **II** are not layered and Form **II** is more stable than Form **I** (see below).

In attempting to reproduce these results we set up a series of crystallization experiments from various solvents (in Essen) with varying mole proportions of TNB and TI.[19] However, we never again were able to obtain the noncentrosymmetric Form **II** (which had appeared originally in Hyderabad), even after nearly 100 crystallization attempts

 © 2004 Wiley-VCH Verlag GmbH & Co. KGaA, Weinheim

UM00011949
NOVARTIS EXHIBIT 1017
Novartis v. Regents, IPR2023-01346
Page 695 of 4460

spread over a six-month period. However, during these experiments, we isolated another polymorph, Form **III**, when TNB (80%) and TI (20%) were taken in EtOAc. This form of TNB crystallizes in the centrosymmetric space group $P2_1/c$ with $Z' = 1$ (Figure 4). Unlike Form **II**, we were

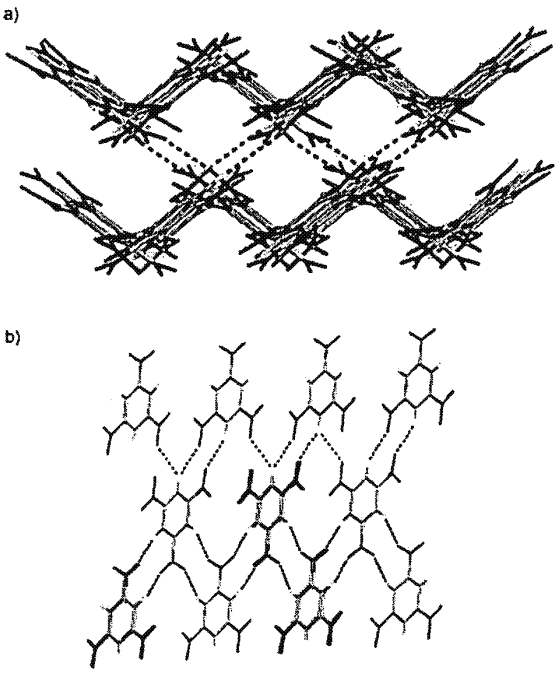


Figure 4. Centrosymmetric Form III crystal of TNB. a) View down the *a* axis. b) View down the *b* axis showing the TNB tape.

able to obtain crystals of Form **III** a second time but only after several attempts. Close inspection of this new(est) structure of TNB shows that it is not obviously related to Form **I** and Form **II**. There are no V-shaped troughs or zigzag chains. The structure is "normal" and emphasizes Kitaigorodskii-type close packing.[20] The TNB tape building block shown in Figure 4b is common in TNB molecular complexes[21] but is not seen in Forms **I** and **II** (see Supporting Information).

These results, unanticipated as they were, open up several lines of discussion. What is the role of TI in inducing the appearance of Form **III** crystals? First, although many crystallization experiments were carried out,[22] Forms **II** and **III** were only obtained when TI was present. An additional indication that TI is indispensable for the production of polymorphic structures is that there is no evidence of any phase transformation of Form **I** crystals, at least as evidenced from differential scanning calorimetry (DSC), thermogravimetric analysis (TGA), and variable-temperature powder diffraction traces. Second, we note that TNB gives stoichiometric molecular complexes with a very large number of planar π donors.[23,24] Thus, TNB readily gives a 1:1 molecular complex with the planar TP. It is possible that the difficulty of formation of a molecular complex between TNB and TI arises from the nonplanarity of the TI molecule. In any event, we observed the formation of small amounts of red microcrystalline material coating the crystals of TNB (shown in a photograph in the Supporting Information) in most of the cocrystallization experiments (regardless of the crystalline form of TNB obtained). We made several attempts to isolate a single crystal from this microcrystalline mass but were unsuccessful. We infer that this material corresponds largely to a TNB–TI molecular complex of unknown structure. Whilst formation of a stoichiometric molecular complex between TNB and TI may be difficult as explained above, there is a close degree of molecular similarity as is revealed in the overlap diagram in Figure 5. This situation leads to the

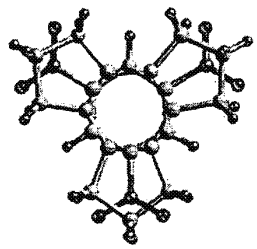


Figure 5. Overlay of TNB and TI molecules.

possibility of nonstoichiometric solid–solution formation at the surface. As very little of this red material was obtained (we estimate less than 5% according to powder X-ray diffractometry) we conclude that the degree of molecular similarity is not high enough.[25,26] In summary, it is this serendipitous duality of events that appears to favor the formation of Form **III**. The nonplanar TI cannot form a stoichiometric molecular complex readily with TNB, for if this were so there would be no other result in the cocrystallization experiments,[9a] and the degree of molecular similarity between TI and TNB is not so high as to lead to the formation of nonstoichiometric solid–solutions. Yet the interaction between TNB and TI is sufficiently good to promote some sort of association. What appears plausible, is an ill-defined outcome with an indiscriminate adsorption of TI molecules over all the faces of the growing TNB crystals.

Such nonselective adsorption of TI on the TNB faces may be rationalized by considerations of molecular and crystal symmetry. It is not straightforward to establish at which faces of the centrosymmetric Form **I** crystal the additive is adsorbed, since TI has molecular threefold symmetry, as does TNB. This issue is resolved for adsorption leading to Form **II**, because it is noncentrosymmetric, but Form **III** is centrosymmetric. How does the additive work in this case? The clue lies in the actual point groups of Forms **I** and **III** which are *2/m 2/m 2/m* and *2/m*, respectively. The idea here is that the higher the crystal point symmetry, the more different orientations in the lattice the constituent molecules may occupy, making the inhibition process less selective, or in other words, more indiscriminate. This principle was enunciated by Weissbuch et al.[3b] but no examples have been found to support this

 © 2004 Wiley-VCH Verlag GmbH & Co. KGaA, Weinheim

UM00011950
NOVARTIS EXHIBIT 1017
Novartis v. Regents, IPR2023-01346
Page 696 of 4460

conjecture until the present case. Here, we may suggest that the threefold symmetric additive molecule may substitute for the threefold symmetric host molecule, of roughly the same size and shape, at several locations because many of the orientations that the host molecule presents in the growing crystal are equivalent.

Finally, let us consider the energetics of the three polymorphs of TNB. To compare the relative stability of the three polymorphs one should consider their lattice energies,[27] melting points, densities, and packing coefficients (see Supporting Information). The crystallographic and physical details are given in Table 1. The data in Table 2 shows that

Table 1: Crystallographic data for the compounds studied

Parameter	I	II	III
crystal system	orthorhombic	orthorhombic	monoclinic
space group	*Pbca*	$Pca2_1$	$P2_1/c$
Z	16	8	4
Z'	2	2	1
ρ_{calcd} [g cm^{-3}]	1.729	1.688	1.717
C_{14}	72.5	71.0	72.5
m.p. [°C]	121.8	119.2	122.7

Table 2: Lattice energy calculations on the polymorphs of TNB

Energy	Form I [Kcal mol^{-1}]	per molecule	Form II [Kcal mol^{-1}]	per molecule	Form III [Kcal mol^{-1}]	per molecule
Van der Waals	−267.830	−16.739	−124.327	−15.541	−65.817	−16.454
electrostatic	−261.686	−16.355	−176.639	−22.079	−82.907	−20.727
hydrogen bond	−43.158	−2.697	−29.152	−3.644	−17.655	−4.414
total energy	−572.67	−35.792	−330.118	−41.265	−166.38	−41.595

Form **III** is the most stable polymorph being more stable than Form **II** by 0.33 kcal mol^{-1} and more stable than Form **I** by as much as 5.80 kcal mol^{-1}.[28] The observed melting points of Forms **I** and **III** support these calculations. Surprisingly, the least stable polymorph (Form **I**) is also the densest. This is not unprecedented but it is uncommon.[29] That a crystal form that is of such high relative energy has been reported after more than a century of experimental work on TNB is noteworthy, and suggests that Form **I** is distinctly favored kinetically.[30] The adsorption of TI on the faces of the kinetic Form **I** crystal leads (in an orderly fashion according to Scheme 1) to Form **II** and the adsorption is selective. If the adsorption is indiscriminate, the growth of all faces of all possible kinetic forms may be affected,[31] and what crystallizes out might be the most stable (thermodynamically favored) Form **III**. The fact that the highest melting Form **III** has a "normal"[20] packing ($P2_1/c$, $Z' = 1$) also corroborates that it is the thermodynamic form, or at any rate close to the thermodynamic form, which may still remain to be isolated. Whether Form **II** is a disappearing form[32] or not is an open question, and we reserve comment at present.[33]

In conclusion, it may be said that the isolation and detection of new polymorphs is still unpredictable. A combination of serendipity and subsequent rigorous observation could well lead to novel and unanticipated polymorphs. For instance, in this work, crystal forms have been found that were hitherto unreported. In general, it would appear that McCrone's dictum[34] is correct but again, perhaps only for some categories of molecules.[35] In the present instance, the fact that molecules of TI can interact with those of TNB, but not too well, seems to be the critical factor that determines the appearance of new polymorphs. But why is so much of additive required? And why is it that while additives change crystal morphology easily,[3] they do not seem to be able to change the polymorph that is obtained so readily? It appears that if the additive completely surrounds the embryonic crystal of the kinetic forms (through an indiscriminate adsorption on all the crystal faces), then only the most stable crystal form is able to survive.[31] Normally, thermodynamic forms are obtained under conditions when nucleation is inhibited (dilute solutions, annealing, supercritical fluids, hydrothermal methods, gel crystallization, high pressure). The present study shows that there may be another way of inhibiting nucleation, namely through the use of additives that bind nonselectively to all crystal faces of all kinetic forms.[36] However, this does not mean that such an additive may be designed, in advance, with our present understanding of the crystallization event although the appearance of Form **II** may be rationalized on the basis of an accepted model. Could one have computed the structure of the stable Form **III**? What would happen if TNB was given as a candidate molecule in a blind test for crystal structure prediction (CSP)?[4] Why is it that the presence of TI in the crystallization vessel does not invariably lead to the formation of Forms **II** or **III**? In other words, why is the formation of these more stable forms much less frequent? We are not particularly disappointed that we obtained Form **II** only once and Form **III** only twice. It is possible that if the crystallization is carried out with TI and also employing some other condition that inhibits nucleation (such as those listed above), the appearance of more stable crystal forms might become much more frequent. We are pursuing these and other related experiments currently. On a more speculative note, is the occurrence of multiple molecules in the crystallographic asymmetric unit for nonpseudosymmetric structures correlated with the appearance of kinetic forms? Perhaps some of the questions posed in this paragraph might appear to be rhetorical, or even fanciful. However, they do show that the phenomenon of polymorphism is one of the most difficult frontiers in the chemistry of the molecular solid state today.

Received: June 27, 2003
Revised: September 22, 2003 [Z52253]

Keywords: additives · crystal growth · inhibition · polymorphism

[1] a) M. Kuhnert-Brandstätter, M. Aepkers, *Mikroskopie* **1961**, *16*, 189–197; b) M. Kuhnert-Brandstätter, M. Aepkers, *Mitt. Mik-*

 © 2004 Wiley-VCH Verlag GmbH & Co. KGaA, Weinheim

UM00011951
NOVARTIS EXHIBIT 1017
Novartis v. Regents, IPR2023-01346
Page 697 of 4460

rochim. Acta **1963**, 360–375; c) A. R. Ebian, M. A. Moustafa, S. A. Khalil, M. M. Motawi, *J. Pharm. Sci.* **1973**, *25*, 13–20; d) A. R. Ebian, M. A Moustafa, S. A. Khalil, M. M. Motawi, *J. Pharm. Sci.* **1975**, *64*, 1481–1484; e) S. N. Black, R. J. Davey, M. Halcrow, *J. Cryst. Growth* **1986**, *79*, 765–774; f) E. Staab, L. Addadi, L. Leiserowitz, M. Lahav, *Adv. Mater.* **1990**, *2*, 40–43; g) I. Weissbuch, L. Leiserowitz, M. Lahav, *Adv. Mater.* **1994**, *6*, 952–956; h) B. D. Chen, J. Garside, R. J. Davey, S. J. Maginn, M. Matsuoka, *J. Phys. Chem.* **1994**, *98*, 3215–3221; i) B. D. Chen, G. D. Potts, R. J. Davey, J. Garside, D. Bergmann, S. Niehoerster, S. Ulrich, *J. Cryst. Growth* **1994**, *144*, 297–303; j) D. Lechuga-ballesteros, N. Rodriguezhornedo, *Int. J. Pharm.* **1995**, *115*, 139–149; k) B. A. Hendriksen, D. J. W. Grant, P. Meenan, D. A. Green, *J. Cryst. Growth* **1998**, *183*, 629–640; l) C.-H. Gu, K. Chatterjee, V. Young, D. J. W. Grant, *J. Cryst. Growth* **2002**, *235*, 471–481.

[2] Selected books and reviews: a) J. Bernstein, *Polymorphism in Molecular Crystals*, *Clarendon*, Oxford, **2002**; b) T. L. Threlfall, *Analyst* **1995**, *120*, 2435–2460; c) "Polymorphism and Pseudo-polymorphism in Organic Crystals: A Cambridge Structural Database Study": by J. A. R. P. Sarma, G. R. Desiraju in *Crystal Engineering* (Eds.: K. R. Seddon, M. Zaworotko), Kluwer, Norwell, MA, **1999**, pp. 325–356; d) G. R. Desiraju, *Science*, **1996**, *278*, 404–405; d) R. J. Davey, *Chem. Commun.* **2003**, 1463–1467; recent papers include: e) R. K. R. Jetti, R. Boese, J. A. R. P. Sarma, L. S. R. Reddy, P. Vishweshwar, G. R. Desiraju, *Angew. Chem.* **2003**, *115*, 2008–2012; *Angew. Chem. Int. Ed.* **2003**, *42*, 1963–1967; f) L. Yu, *J. Am. Chem. Soc.* **2003**, *125*, 6380–6381; g) A. Kálmán, L. Fábián, G. Argay, G. Bernáth, Z. Gyarmati, *J. Am. Chem. Soc.* **2003**, *125*, 34–35.

[3] a) I. Weissbuch, M. Lahav, L. Leiserowitz, *Cryst. Growth Des.* **2003**, *3*, 125–150; b) I, Weissbuch, R. Popovitz-Biro, M. Lahav, L. Leiserowitz, *Acta Crystallogr. Sect. B* **1995**, *51*, 115–148.

[4] a) G. R. Desiraju, *Nat. Mater.* **2002**, *1*, 77–79; b) J. D. Dunitz, *Chem. Commun.* **2003**, 545–548.

[5] R. J. Davey, N. Blagden, G. D. Potts, R. Docherty, *J. Am. Chem. Soc.* **1997**, *119*, 1767–1972.

[6] X. He, J. G. Stowell, K. R. Morris, R. R. Pfeiffer, H. Li, G. P. Stahly, S. R. Byrn, *Cryst. Growth Des.* **2001**, *1*, 305–312.

[7] a) M. R. Caira, *Top. Curr. Chem.* **1998**, *198*, 163–208; b) M. R. Caira, *J. Chem. Crystallogr.* **1994**, *24*, 695–701.

[8] It is possible that additive-induced polymorphism is far more widespread than has been actually documented. In industrial crystallization, it is known, for example, that the crystal form of a substance obtained from the reaction mixture is sometimes different from the forms obtained upon subsequent crystallization of purified material. Considering that the synthetic precursor of a particular molecule of interest is likely to have a related chemical structure, it may well be able to behave as an unintended crystallization auxiliary. For a general reference on industrial crystallization, see *Crystal Growth of Organic Materials* (Eds.: A. S. Myerson, D. A. Green, P. Meenan), ACS Conference Proceedings Series, American Chemical Society, Washington DC, **1996**.

[9] a) R. Foster, *Organic Charge-Transfer Complexes*. Academic, New York, **1969**; b) P. Pfeiffer, *Organische Molekülverbindungen*, 2nd ed., Ferdinand Enke, Stuttgart, **1927**; c) C. Becker, *Ber. Dtsch. Chem. Ges.* **1883**, *16*, 1597.

[10] a) R. M. Vrcelj, H. G. Gallagher, J. N. Sherwood, *J. Am. Chem. Soc.* **2001**, *123*, 2291–2295; b) R. M. Vrcelj, J. N. Sherwood, A. R. Kennedy, H. G. Gallagher, T. Gelbrich, *Cryst. Growth Des.* **2003**, *3*, 1027–1032.

[11] There is solitary report in the patent literature, [G. B. Ravich, O. F. Bogush, *Dokl. Akad. Nauk. SSSR* **1962**, *142*, 831–834] but the forms reported there do not bear a resemblance to the new crystal forms in the present work.

[12] The crystal structure of TNB has been determined by C. S. Choi, J. E. Abel, *Acta Crystallogr. Sect. B* **1972**, *23*, 198–201 using neutron radiation at room temperature. We redetermined the structure using X-ray radiation at 183 K (see ref. [15]), and our analysis is based on this data.

[13] J. Zyss, I, Ledoux, H.-C. Weiss, R. Boese, P. K. Thallapally, V. R. Thalladi, G. R. Desiraju, *Chem. Mater.* **2003**, *15*, 3063–3073.

[14] TI was synthesized by using a literature procedure (S. Kotha, K. Chakraborty, E. Brahmachary, *Synlett* **1999**, 1621–1623). TNB was either synthesized by using a literature procedure (P. Segura, J. F. Bunnett, L. Villanova, *J. Org. Chem.* **1985**, *50*, 1041–1049) or obtained from Dynamit Nobel AG. We attempted to cocrystallize TNB and TI in 1:1 and 2:1 proportions from chloroform, dichloromethane, ethyl acetate, acetonitrile, acetone, dioxane, nitromethane, and from solvent combinations but in none of these cases could we isolate any diffraction-quality crystals of any molecular complexes.

[15] Crystal data for TNB Form **I**: orthorhombic, *Pbca*, $a = 12.587(11)$, $b = 9.684(9)$, $c = 26.86(2)$ Å, $V = 3274(5)$ Å^3, $Z = 16$, $\rho_{calcd} = 1.729$ g cm^{-3}, $T = 183$ K, $\mu = 0.159$ mm^{-1}, $2\theta_{max} = 57.5°$, 36564 measured, 4188 independent, 1396 observed ($I > 2\sigma_I$) reflections, 271 parameters, $R1 = 0.0450$, $wR2 = 0.0985$ (for $I > 2\sigma_I$), residual electron density $+0.188/-0.191$ e Å^{-3} (CCDC-213310); Crystal data for TNB Form **II**: orthorhombic, $Pca2_1$, $a = 9.2970(19)$, $b = 18.730(4)$, $c = 9.6330(19)$ Å, $V = 1677.4(6)$ Å^3, $Z = 8$, $\rho_{calcd} = 1.688$ g cm^{-3}, $T = 120$ K, $\mu = 0.155$ mm^{-1}, $2\theta_{max} = 55.8°$, 2117 measured, 2117 independent, 1924 observed ($I > 2\sigma_I$) reflections, 271 parameters, $R1 = 0.0397$, $wR2 = 0.0985$ (for $I > 2\sigma_I$), residual electron density $+0.240/-0.317$ e Å^{-3} (CCDC-213311); Crystal data for TNB Form **III**: monoclinic, $P2_1/c$, $a = 12.896(5)$, $b = 5.723(2)$, $c = 11.287(5)$ Å, $\beta = 98.190(8)°$, $V = 824.5(6)$ Å^3, $Z = 4$, $\rho_{calcd} = 1.717$ g cm^{-3}, $T = 183$ K, $\mu = 0.158$ mm^{-1}, $2\theta_{max} = 56.60°$, 4936 measured, 2008 independent, 1221 observed ($I > 2\sigma_I$) reflections, 136 parameters, $R1 = 0.0609$, $wR2 = 0.1462$ (for $I > 2\sigma_I$), residual electron density $+0.419/-0.231$ e Å^{-3} (CCDC-213312); Crystal data for TI: monoclinic, $P2_1/c$, $a = 11.920(3)$, $b = 6.0733(13)$, $c = 16.584(4)$ Å, $\beta = 110.670(4)°$, $V = 1123.4(4)$ Å^3, $Z = 4$, $\rho_{calcd} = 1.172$ g cm^{-3}, $T = 203$ K, $\mu = 0.065$ mm^{-1}, $2\theta_{max} = 54°$, 12490 measured, 2443 independent, 1428 observed ($I > 2\sigma_I$) reflections, 136 parameters, $R1 = 0.0559$, $wR2 = 0.1260$ (for $I > 2\sigma_I$), residual electron density $+0.208/-0.139$ e Å^{-3} (CCDC-213313). The data for Form **I**, **III**, and TI were collected on a SMART diffractometer using $Mo_{K\alpha}$ radiation. For Form **II** the instrument used was Nonius FAST area detector. Structure solution by direct methods and refinements on F^2 with SHELXTL (Version 6.10 and 6.12). Non-hydrogen atoms were refined anisotropically and the H atoms of the phenyl groups were generated at idealized geometries and refined isotropically using a riding model. CCDC 213310–213312 contain the supplementary crystallographic data for this paper. These data can be obtained free of charge via www.ccdc.cam.ac.uk/conts/retrieving.html (or from the Cambridge Crystallographic Data Centre, 12 Union Road, Cambridge CB21EZ, UK; fax: (+44) 1223-336-033; or deposit@ccdc.cam.ac.uk).

[16] a) G. R. Desiraju, T. Steiner, *The Weak Hydrogen Bond in Structural Chemistry and Biology*, Oxford University Press, Oxford, **1999**; b) M. Mascal, *Chem. Commun.* **1998**, 303–304; c) K. Wozniak, H. He, J. Klinowski, W. Jones, E. Grech, *J. Phys. Chem.* **1994**, *98*, 13755–13765; d) R. K. R. Jetti, P. K. Thallapally, A. Nangia, C.-K. Lam, T. C. W. Mak, *Chem. Commun.* **2002**, 952–953.

[17] a) L. J. Barbour, *J. Supramol. Chem.* **2001**, *1*, 189–191; b) J. L. Atwood, L. J. Barbour, *Cryst. Growth Des.* **2003**, *3*, 3–8.

[18] See Supporting Information for details of the calculated crystal morphology.

 © 2004 Wiley-VCH Verlag GmbH & Co. KGaA, Weinheim

UM00011952
NOVARTIS EXHIBIT 1017
Novartis v. Regents, IPR2023-01346
Page 698 of 4460

[19] Cocrystallization of TNB with TI in these exhaustive trials was attempted with mole percentages of TI from 10% to 50%. Recrystallization was carried out separately for both TNB and TI and as well as for mixtures from a variety of solvents, such as EtOAc, MeOH, EtOH, CH_2Cl_2, $CHCl_3$, CCl_4, benzene, toluene, *m*-xylene, *p*-xylene, mesitylene, acetone, MeCN, *n*BuOH, *n*PrOH, *i*PrOH, $MeNO_2$, THF, dioxane, Et_2O, DMF, and DMSO. Solvent combinations, such as MeOH–MeCN, benzene–CCl_4, benzene–hexane, EtOAc–hexane, and benzene–MeCN, were also tried. Invariably, we obtained crystals of Form **I** or TI. In all, approximately 100 single crystals from different crystallization experiments were selected for cell measurements. While the crystals very often had different morphologies, all of them turned out to be those of either Form **I** or TI.

[20] A. I. Kitaigorodskii, *Molecular Crystals and Molecules*, Academic Press, New York, **1973**. By "normal" is meant a three-dimensionally close-packed structure without any easily identifiable substructural motifs, such as V-shaped troughs, molecular tapes.

[21] a) P. K. Thallapally, A. K. Katz, H. L. Carrell, G. R. Desiraju, *CrystEngComm* **2003**, *5*, 87–92; b) P. K. Thallapally, K. Chakraborty, H. L. Carrell, S. Kotha, G. R. Desiraju, *Tetrahedron* **2000**, *56*, 6721–6728.

[22] We carried out around 150 crystallization experiments with TNB. In roughly 50 of these trials, we did not use any TI. In these cases, there were two outcomes. For non-aromatic solvents, only Form **I** was obtained. With some aromatic solvents (benzene, toluene, chlorobenzene, *m*-xylene, *p*-xylene, mesitylene) we obtained solvates with a greater or lesser degree of difficulty.[23] With other aromatic solvents (nitrobenzene, bromobenzene, triflurotoluene, pyridine, collidine, picolines), only Form **I** was obtained.

[23] R. K. R. Jetti, P. K. Thallapally, R. Boese, G. R. Desiraju, *Cryst. Growth Des.* **2003**, *3*, 1033–1040.

[24] The current version of the CSD contains 61 (CSD version 5.23, April **2002**) of these molecular complexes; F. H. Allen, O. Kennard, *Chem. Des. Autom. News* **1993**, 8, 1–57.

[25] A. I. Kitaigorodskii, *Mixed Crystals*, Springer, Berlin, **1984** (Springer Series in Solid-State Science 33).

[26] We redetermined the crystal structure of pure TI (the earlier CSD known crystal structure is of limited precision with no hydrogen-atom positions reported; E. R. Boyko, P. O. Vaughan, *Acta Crystallogr.* **1964**, *17*, 152–154; see ref. [15]) but this is quite different from any of the forms of TNB. If the structures were isomorphous, solid-solution formation would be more likely.

[27] The lattice energies were carried out using "Smart Minimizer" option of the Cerius2 package. All molecules in the crystal were treated as rigid entries. Atom–atom potentials were estimated using Dreiding 2.21 force field and atomic charges were estimated using the charge equilibration method. Cerius2, Accelrys, Cambridge (UK). See www.accelrys.com.

[28] These energy values include the small variations in energy owing to the conformational differences between the nitro groups in the three forms.

[29] a) J. M. Robertson, *Proc. R. Soc. London Ser. A* **1936**, *157*, 79–83; b) J. M. Robertson, A. R. Ubbelohde, *Proc. R. Soc. London Ser. A* **1938**, *167*, 122–125.

[30] The relationship between the kinetic accessibility, higher relative energy, and high density of the most common Form **I** and the explosive character of TNB is an aspect that might need to be investigated in the future.

[31] We estimate that at a 20% loading of the additive, the embryonic TNB crystal contains 24580 molecules (crystal radius 107 Å) if the additive coats the crystal at monomolecular thickness, this is reasonable for a crystal in the very early stages of growth. Both TNB and TI are assumed to be spherical and the embryonic crystal is also assumed to be spherical. We thank Mr. T. Omlor for these calculations.

[32] J. D. Dunitz, J. Bernstein, *Acc. Chem. Res.* **1995**, *28*, 193–200.

[33] We do not rule out the possibility that Form **II** may be isolated in another laboratory at a future date, see for example the work on tetraacetyl ribofuransose by P. Bombicz, M. Czugler, R. Tellgren, A. Kálmán, *Angew. Chem.* **2003**, *115*, 2001–2004; *Angew. Chem. Int. Ed.* **2003**, *42*, 1957–1960.

[34] W. C. McCrone, *Polymorphism in Physics and Chemistry of the Organic Solid-State* (Eds.: D. Fox, M. M. Labes, A. Weissberger), Interscience, New York, **1965**.

[35] One of us (GRD) has pointed out on several occasions that despite rigorous experimentation, compounds such as benzoic acid, anthracene, and D-glucose do not yield normal pressure polymorphs.

[36] Leiserowitz et al. made a similar observation with PAN (see refs. [1f, 1g]).

 © 2004 Wiley-VCH Verlag GmbH & Co. KGaA, Weinheim

UM00011953
NOVARTIS EXHIBIT 1017
Novartis v. Regents, IPR2023-01346
Page 699 of 4460

Structure of the caffeine-copper(II) acetate addition compound. Simonov, Yu. A.; Milkova, L. N. USSR. Izvestiya Akademii Nauk Moldavskoi SSR, Seriya Fiziko-Tekhnicheskikh i Matematicheskikh Nauk (1972), (3), 83-4. CODEN: IZFMBL ISSN: 0321-169X. Journal written in Russian. CAN 79:10885 AN 1973:410885 CAPLUS
(Copyright (C) 2006 ACS on SciFinder (R))

Abstract

Caffeine and Cu(OAc)2 reacted in MeOH to give Cu(OAc)2.C8H10O2N4 which was studied by x-ray anal. The crystals are triclinic, space group P1.hivin., with a 7.80, b 9.21, c 10.85 .ANG., α 80°, β 83°, γ 101°, d.(detd.) = 1.68, d. (x-ray) = 1.73, Z = 2.

ANTIMICROBIAL AGENTS AND CHEMOTHERAPY, Aug. 2000, p. 2017–2022 Vol. 44, No. 8
0066-4804/00/$04.00+0
Copyright © 2000, American Society for Microbiology. All Rights Reserved.

In Vitro and In Vivo Activities of SCH 56592 (Posaconazole), a New Triazole Antifungal Agent, against *Aspergillus* and *Candida*

ANTHONY CACCIAPUOTI,* DAVID LOEBENBERG, ERIK CORCORAN,† FRED MENZEL, JR., EUGENE L. MOSS, JR., CHRISTINE NORRIS, MONIKA MICHALSKI, KIMBERLY RAYNOR, JUDITH HALPERN, CARA MENDRICK, BRIAN ARNOLD, BARRY ANTONACCI, RAULO PARMEGIANI, TAISA YAROSH-TOMAINE, GEORGE H. MILLER,† AND ROBERTA S. HARE

Schering-Plough Research Institute, Kenilworth, New Jersey 07033-1300

Received 18 January 2000/Returned for modification 16 February 2000/Accepted 28 April 2000

SCH 56592 (posaconazole), a new triazole antifungal agent, was tested in vitro, and its activity was compared to that of itraconazole against 39 *Aspergillus* strains and to that of fluconazole against 275 *Candida* and 9 *Cryptococcus* strains. The SCH 56592 MICs for *Aspergillus* ranged from ≤0.002 to 0.5 μg/ml, and those of itraconazole ranged from ≤0.008 to 1 μg/ml. The SCH 56592 MICs for *Candida* and *Cryptococcus* strains ranged from ≤0.004 to 16 μg/ml, and those of fluconazole ranged from ≤0.062 to >64 μg/ml. SCH 56592 showed excellent activity against *Aspergillus fumigatus* and *Aspergillus flavus* in a pulmonary mouse infection model. When administered therapeutically, the 50% protective doses (PD_{50}s) of SCH 56592 ranged from 3.6 to 29.9 mg/kg of body weight, while the PD_{50}s of SCH 56592 administered prophylactically ranged from 0.9 to 9.0 mg/kg; itraconazole administered prophylactically was ineffective (PD_{50}s, >75 mg/kg). SCH 56592 was also very efficacious against fluconazole-susceptible, -susceptible dose-dependent, or -resistant *Candida albicans* strains in immunocompetent or immunocompromised mouse models of systemic infection. The PD_{50}s of SCH 56592 administered therapeutically ranged from 0.04 to 15.6 mg/kg, while the PD_{50}s of SCH 56592 administered prophylactically ranged from 1.5 to 19.4 mg/kg. SCH 56592 has excellent potential for therapy against serious *Aspergillus* or *Candida* infections.

Of the estimated 100,000 known species of fungi, only about 180 have been shown to cause disease in humans, and only about 10% of these are encountered in most clinical settings (8). However, fungal infections have substantially increased over the past two decades, and invasive forms are important causes of morbidity and mortality (2, 16). The major increase in fungal infections is related to increased numbers of immunocompromised patients including those with human immunodeficiency virus infection-AIDS or cancer and bone marrow or solid organ transplant recipients, who are at risk of developing invasive fungal infections (5, 7, 12, 16). Disseminated candidiasis, pulmonary aspergillosis, and mycoses caused by emerging opportunistic fungi are the most common of these serious mycoses (7, 16, 38). As a result, there is a developing consensus that prophylactic therapy should be used for these high-risk patients (12). Fluconazole (FLC) is used for prevention of fungal infections in some of these patients, but it is not active against *Aspergillus* or other filamentous fungi. However, there is great concern about the development of resistant *Candida* due to prophylactic use of FLC (4, 10, 15, 18, 23, 35, 37). Clearly, alternative antifungal agents are needed for both therapeutic and prophylactic use. SCH 56592 (SCH; posaconazole) is a new triazole antifungal agent with broad-spectrum activity against fungi including strains of *Aspergillus* and *Candida* resistant to FLC (9, 11, 19, 24, 30, 33). This report describes the in vitro activity of SCH against *Aspergillus* and *Candida* and its efficacy in clinically relevant experimental infection models in mice with both prophylactic and therapeutic dosing regimens.

(Preliminary reports of this research were presented at the 35th Interscience Conference on Antimicrobial Agents and Chemotherapy, San Francisco, Calif., 17 to 20 September 1995 [A. Cacciapuoti, R. Parmegiani, D. Loebenberg, B. Antonacci, E. L. Moss, Jr., F. Menzel, Jr., C. Norris, R. S. Hare, and G. H. Miller, Abstr. 35th Intersci. Conf. Antimicrob. Agents Chemother., abstr. F66, p. 124, 1995], and the 38th Interscience Conference on Antimicrobial Agents and Chemotherapy, San Diego, Calif., 24 to 27 September 1998 [D. Loebenberg, F. Menzel, Jr., E. Corcoran, K. Raynor, J. Halpern, A. F. Cacciapuoti, and R. S. Hare, Abstr. 38th Intersci. Conf. Antimicrob. Agents Chemother., abstr. J-63, p. 469, 1998].)

MATERIALS AND METHODS

Mice. White male CF1 mice from Charles River Laboratories (Wilmington, Mass.) were used in these studies. At the time of infection the mice in the pulmonary infection studies weighed 16 to 18 g and those in the systemic infection studies weighed 18 to 20 g.

Antifungal agents. SCH was prepared at Schering-Plough Research Institute, Kenilworth, N.J., either as a micronized powder or as the clinically formulated suspension. For in vitro susceptibility tests the powder was dissolved in dimethyl sulfoxide, while for in vivo studies it was prepared as a suspension in 0.4% (wt/vol) methylcellulose (MC) containing 0.5% (wt/vol) polysorbate 80 and 0.9% (wt/vol) NaCl. The clinical suspension was diluted as needed in sterile water for injection (sWFI) and used for some in vivo studies. Both forms of SCH were previously tested in our laboratory and were found to have the same in vivo efficacy. FLC powder and Diflucan oral suspension were obtained from Pfizer, Inc., Kent, England. For in vivo use, FLC powder was prepared in MC and Diflucan was diluted as needed in sWFI. Itraconazole (ITC) powder and Sporanox oral solution were obtained from Janssen Pharmaceutica Inc., Beerse, Belgium. For in vivo use only Sporanox was used, and it was diluted as needed in hydroxypropyl-β-cyclodextrin (HPβCD; 40% [wt/vol] in water; Cerestar USA, Inc., Hammond, Ind.).

In vitro antifungal activity. All strains of *Aspergillus*, *Candida*, and *Cryptococcus* were from the Schering-Plough Research Institute fungal culture collection. The MICs for *Candida* and *Cryptococcus* strains were determined by the broth

* Corresponding author. Mailing address: Schering-Plough Research Institute, 2015 Galloping Hill Rd., Kenilworth, NJ 07033-1300. Phone: (908) 740-3139. Fax: (908) 740-3918. E-mail: anthony.cacciapuoti@spcorp.com.

† Present address: Research & Development, Microcide Pharmaceuticals Inc., Mountain View, CA 94043.

UM00011955
NOVARTIS EXHIBIT 1017
Novartis v. Regents, IPR2023-01346
Page 701 of 4460

TABLE 1. In vitro activities of SCH, ITC, and FLC against *Aspergillus*, *Candida*, and *Cryptococcus*

Species	No. of isolates	MIC (μg/ml)								
		SCH			ITC			FLC		
		Range	50%	90%	Range	50%	90%	Range	50%	90%
A. flavus	11	≤0.002–0.125	0.008	0.125	0.008–0.25	0.125	0.25	ND[a]	ND	ND
A. fumigatus	17	≤0.002–0.062	≤0.002	0.031	0.004–0.25	0.125	0.25	ND	ND	ND
Aspergillus species[b]	11	≤0.002–0.5	0.016	0.5	≤0.008–1	0.125	0.5	ND	ND	ND
C. albicans	156	≤0.004–16	≤0.004	0.125	ND	ND	ND	0.062–>64	0.125	16
C. tropicalis	20	≤0.004–8	≤0.016	2	ND	ND	ND	0.125–>64	0.25	>64
C. glabrata	20	≤0.016–2	0.25	1	ND	ND	ND	0.5–>64	4	64
C. krusei	20	0.062–0.5	0.25	0.5	ND	ND	ND	8–64	32	64
Candida species[c]	59	≤0.004–1	≤0.016	0.25	ND	ND	ND	≤0.062–>64	0.25	16
C. neoformans	9	≤0.016–0.5	0.062	ND	ND	ND	ND	≤0.062–16	2	ND

[a] ND, not determined.

[b] Includes the following species and number of strains: *A. niger*, $n = 5$; *A. terreus*, $n = 4$; *A. nidulans*, $n = 1$; species not identified, $n = 1$.

[c] Includes the following species and number of strains: *C. kefyr*, $n = 7$; *C. parapsilosis*, $n = 7$; *C. guilliermondii*, $n = 6$; *C. dubliniensis*, $n = 5$; *C. lusitaniae*, $n = 5$; *C. lambica*, $n = 3$; *C. rugosa*, $n = 3$; *C. famata*, $n = 2$; *C. inconspicua*, $n = 2$; *C. pseudotropicalis*, $n = 1$; *C. stellatoidea*, $n = 1$; species not identified, $n = 17$.

microdilution method according to the procedures of the National Committee for Clinical Laboratory Standards (NCCLS) described in document M27-A, Reference Method for Broth Dilution Susceptibility Testing of Yeasts (26), and those for *Aspergillus* strains were determined by the procedures described in NCCLS document M38-P, Reference Method for Broth Dilution Susceptibility Testing of Conidium-Forming Filamentous Fungi (27).

Therapeutic activity against pulmonary aspergillosis. *Aspergillus fumigatus* strains ND152, ND158, ND159, and ND164 and *Aspergillus flavus* strains ND83, ND134, ND149, and ND168 were grown on malt extract agar for 13 days at 25°C in an inhalation chamber. Mice were compromised with subcutaneous cortisone acetate (100 mg/kg of body weight once daily on the day before infection and the following 2 days) and were exposed to a spore cloud for 0.5 to 1 min in the chamber on the second day of compromise (day 0), as described previously (20). Oral administration of SCH (dose range, 40 to 2.5 mg/kg; 10 mice per dose) began 24 h postinfection, and SCH was given once daily for 4 days. Control mice were administered MC. The 50% protective dose (PD_{50}), defined as the dose which allowed 50% survival, was calculated from the data for the surviving mice on day 7 postinfection by the Hill equation (1).

Prophylactic activity against pulmonary aspergillosis. *A. flavus* ND83 or *A. fumigatus* ND152 or ND158 was grown as described above. Mice were compromised with cortisone acetate and were infected as described above. Cortisone acetate was also administered on days 6 and 12 postinfection to maintain immunosuppression. Oral administration of drugs (25 to 0.025 mg/kg) to groups of eight mice was once (SCH) or three times (ITC) daily beginning at 24 h preinfection (prophylactic) and continuing through day 7 postinfection. Control mice were administered MC or HPβCD. PD_{50}s were determined as described above by use of the data for the surviving mice on day 7 postinfection. Fungal counts in the lungs of mice that survived at the termination of the experiments were determined by spreading aliquots of homogenized suspensions onto Sabouraud dextrose agar (SDA).

Therapeutic activity against systemic candidiasis. *Candida albicans* strains C43, C65, C72, C84, C260, C284, C286, C288, and C342 were grown for 48 h on SDA, and inocula were prepared as described previously (3). Normal mice or immunocompromised mice (which were immunocompromised by exposure to 500 rads 3 days prior to infection in a Shepherd Mark I cesium gamma irradiator) were infected on day 0 by injecting 2.5×10^6 to 1×10^7 CFU as a saline suspension into the tail vein. Groups of 10 mice each were treated with SCH (100 to 0.063 mg/kg) or FLC (200 to 0.63 mg/kg) orally once daily for 4 days beginning at 4 h postinfection. Control mice were administered MC or sWFI. PD_{50}s, calculated as described above, were determined by use of the data for the surviving mice on day 4 postinfection. Survivors were killed 24 h after the last treatment, and the fungal counts in the kidneys were determined as described previously (3).

Prophylactic activity against systemic candidiasis. *C. albicans* strains C43, C284, C288, and C310 were grown as described above. Groups of 10 mice each were immunocompromised, infected (5×10^5 CFU) as described above, and given SCH (50 to 0.025 mg/kg) or FLC (250 to 0.025 mg/kg) orally once daily beginning at 24 h preinfection and continuing through day 7 postinfection. Control mice were administered sWFI. PD_{50}s were calculated by use of the data for the surviving mice on day 7 postinfection as described above.

Statistical analysis. A logistic model was used to determine differences between PD_{50}s by using their 95% confidence bounds. A chi-square test or logistic model was used to determine if the levels of survival among mice in the treatment groups were significantly different from those among mice in the control group. Comparison of survival-versus-time curves in prophylactic activity experiments with mice to determine efficacy differences between drugs at various dose levels was done by log-rank tests. A chi-square test was performed to show significant differences between treatment groups in the clearance of *Aspergillus* from the lungs of the mice.

Statement of animal care and use. These studies were carried out in accordance with the *Guide to the Care and Use of Laboratory Animals* of the National Institutes of Health (28) and the Animal Welfare Act in an Association for Assessment Accreditation of Laboratory Animal Care-accredited program.

RESULTS

In vitro antifungal activity. The in vitro activities of SCH and ITC against 39 strains of *Aspergillus* are shown in Table 1. The MICs of SCH and ITC ranged from ≤0.002 to 0.5 and ≤0.008 to 1 μg/ml, respectively. Against *A. flavus*, *A. fumigatus*, and other *Aspergillus* species, SCH was overall more active (MICs at which 50% of isolates are inhibited [MIC_{50}s], 0.008, ≤0.002, and 0.016 μg/ml, respectively; MIC_{90}s, 0.125, 0.031, and 0.5 μg/ml, respectively) than ITC (MIC_{50}s, 0.125 μg/ml; MIC_{90}s, 0.25, 0.25, and 0.5 μg/ml, respectively).

The in vitro activities of SCH and FLC against 275 strains of *Candida*, including strains which were susceptible (S), susceptible dose-dependent (S-DD), or resistant (R) to FLC on the basis of NCCLS breakpoints (26), are also shown in Table 1. The MICs of SCH and FLC ranged from ≤0.004 to 16 and ≤0.062 to >64 μg/ml, respectively. The potent activity of SCH against FLC-S, FLC-S-DD, and FLC-R strains was reflected in the MIC_{90}s of SCH for *C. albicans*, *C. tropicalis*, *C. glabrata*, *C. krusei*, and other *Candida* species (SCH MIC_{90}s, 0.125, 2, 1, 0.5, and 0.25 μg/ml, respectively compared to those of FLC (16, >64, 64, 64, and 16 μg/ml, respectively). The only resistance to SCH observed was by one strain of *C. albicans*, for which the MIC was 16 μg/ml, and two strains of *C. albicans* and one of *C. tropicalis*, for which the MICs were 8 μg/ml.

SCH was also more active than FLC against nine strains of *Cryptococcus neoformans* (MIC_{50}s, 0.062 and 2 μg/ml, respectively) (Table 1).

Therapeutic activity against pulmonary aspergillosis. The in vivo efficacy of SCH administered therapeutically against pulmonary aspergillosis in immunocompromised mice was examined by using four strains each of *A. fumigatus* and *A. flavus*. The MICs of SCH were ≤0.002 μg/ml for *A. fumigatus* ND158, ND159, and ND164 and *A. flavus* ND134 and ND168, while the SCH MICs were 0.0625, 0.008, and 0.125 μg/ml for *A. fumigatus* ND152 and *A. flavus* ND83 and ND149, respectively. PD_{50}s on the basis of the data for the surviving mice at 7 days postinfection ranged from 3.6 to 29.9 mg/kg against *A. fumiga-*

UM00011956
NOVARTIS EXHIBIT 1017
Novartis v. Regents, IPR2023-01346
Page 702 of 4460

TABLE 2. Efficacy of therapeutic and prophylactic administration of SCH against pulmonary *Aspergillus* infections in immunocompromised mice

Strain	PD_{50} (mg/kg) on day 7		
	Therapeutic administration of SCH[a]	Prophylactic administration of[b]:	
		SCH	ITC
A. fumigatus			
ND152	3.6	2.2, 0.9[c]	>75, >75[c]
ND158	29.9	2.6	>75
ND159	10.9	ND[d]	ND
ND164	22.2	ND	ND
A. flavus			
ND83	5.7	3.9, 9.0[c]	>75, >75[c]
ND134	4.8	ND	ND
ND149	6.5	ND	ND
ND168	5.6	ND	ND

[a] ITC was not tested therapeutically.
[b] The PD_{50} was based on the total daily dose.
[c] Results from experiments 1 and 2.
[d] ND, not done.

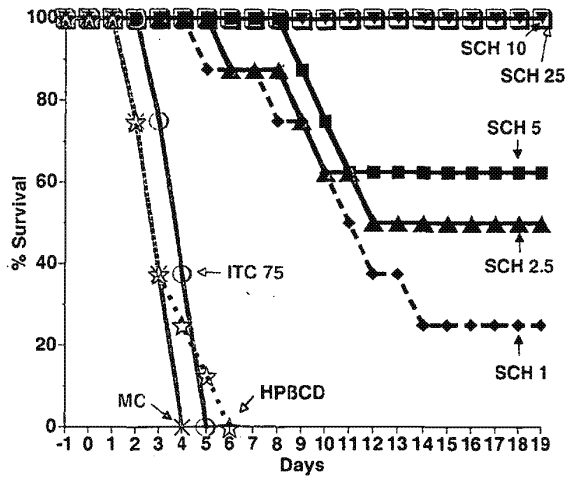


FIG. 1. Effects of SCH (administered orally once daily) and ITC (administered orally three times daily) administered in a prophylactic regimen 1 day preinfection to 7 days postinfection on survival of immunocompromised mice infected (by 1 min of exposure to spores on day 0) with *A. fumigatus* ND152 by the pulmonary route. Total daily doses (in milligrams per kilogram) are indicated. Controls were administered MC or HPβCD.

tus and from 4.8 to 6.5 mg/kg against *A. flavus* (Table 2), and the survival results showed significant differences between treatment groups and controls ($P < 0.05$). The highest PD_{50}s were observed against *A. fumigatus* ND158 (29.9 mg/kg) and ND164 (22.2 mg/kg), although these strains were clearly susceptible to SCH in vitro. All control mice died within 3 to 8 days postinfection.

Prophylactic activity against pulmonary aspergillosis. The in vivo efficacy of SCH against *Aspergillus* in mice was further investigated with a clinically relevant infection model characterized by prophylactic administration preinfection, followed by continued treatment postinfection. SCH administered once daily was compared to ITC administered three times daily, and the results are shown in Table 2. SCH (PD_{50} range, 0.9 to 9.0 mg/kg) was efficacious against strains of *A. fumigatus* and *A. flavus*, while ITC failed to protect the mice (PD_{50}s, >75 mg/kg). The survival-versus-time graph for *A. fumigatus* ND152 is shown in Fig. 1. Against this strain. SCH at 25 and 10 mg/kg protected 100% of mice for 19 days, while control mice and those administered ITC (total daily dose, 75 mg/kg) were all dead by days 4 to 6. SCH at 25, 10, 5, 2.5, and 1 mg/kg was significantly more effective than ITC at 75 mg/kg ($P < 0.01$). The survival-versus-time graphs for the other *Aspergillus* strains tested (data not shown) showed that SCH had significant efficacy compared to that of ITC at 75 mg/kg ($P < 0.01$).

SCH also appeared to be more effective in clearing the infection from the lungs of mice infected with *A. fumigatus* than those of mice infected with *A. flavus*. At 25 and 10 mg/kg, the lungs of 65% of mice infected with *A. fumigatus* ND152 or ND158 were sterilized, but the lungs of only 3% (one mouse) of those infected with *A. flavus* ND83 were sterilized ($P < 0.01$) (Table 3). This differential effect against *A. fumigatus* and *A. flavus* was also evident at the lower doses.

Therapeutic activity against systemic candidiasis. The in vivo efficacy of SCH administered therapeutically against systemic candidiasis was examined in immunocompetent and/or immunocompromised mouse models by using nine strains of *C. albicans*. Included were five FLC-S strains (strains C43, C65, C84, C72, and C286, for which FLC MICs were 0.125, 0.25, 0.25, 0.25, and 4 μg/ml, respectively), two FLC-S-DD strains (strains C288 and C342, for which FLC MICs were 32 and 16 μg/ml, respectively), and two FLC-R strains (strains C260 and C284, for which FLC MICs were >64 μg/ml). The SCH MICs for the strains ranged from ≤0.004 to 0.5 μg/ml; however, the SCH MIC for C260 was 16 μg/ml. The results of these in vivo studies are shown in Table 4. SCH was active against all strains tested, but the PD_{50} against C260 (15.6 mg/kg) was higher than those against the other eight strains (PD_{50} range, 0.04 to 7.1 mg/kg). FLC was active against the FLC-S strains (PD_{50} range, 0.9 to 6.1 mg/kg), less active against the FLC-S-DD strains (PD_{50}s, 25 and 30.5 mg/kg, respectively), and inactive against the FLC-R strains (PD_{50}s, 342 and 417 mg/kg, respectively). In these studies, 80 to 100% of control mice were dead by 4 days postinfection. Statistical analysis of the PD_{50}s of SCH and FLC

TABLE 3. Proportion of mice infected with *Aspergillus* with negative lung cultures following prophylactic treatment with SCH 56592

SCH dose (mg/kg)	Strain	Total no. of mice[a]	% (no.) of mice with negative lung cultures[b]
25	*A. fumigatus* ND152	16	75 (12)
	A. fumigatus ND158	8	62 (5)
	A. flavus ND83	16	6 (1)
10	*A. fumigatus* ND152	16	63 (10)
	A. fumigatus ND158	8	50 (4)
	A. flavus ND83	16	0
5	*A. fumigatus* ND152	16	31 (5)
	A. fumigatus ND158	8	50 (4)
	A. flavus ND83	16	6 (1)
2.5	*A. fumigatus* ND152	16	6 (1)
	A. fumigatus ND158	8	0
	A. flavus ND83	16	0

[a] The surviving mice were killed, and lung homogenates were diluted and spread onto SDA plates. The totals include the mice from two experiments with strains ND152 and ND83 and one experiment with strain ND158.
[b] No growth was detected on SDA plates with a 10^1 dilution.

UM00011957
NOVARTIS EXHIBIT 1017
Novartis v. Regents, IPR2023-01346
Page 703 of 4460

TABLE 4. Efficacies of therapeutic and prophylactic administration of SCH and FLC (both once daily) against systemic *C. albicans* infections in mice

C. albicans susceptibility and strain	Mice	PD_{50} (mg/kg)			
		Therapeutic administration (day 4)[a]		Prophylactic administration (day 7)[b]	
		SCH	FLC	SCH	FLC
FLC S					
C43	Normal	0.3	1.2	ND[c]	ND
C43	Irradiated	1.7	6.1	1.5	5.3
C84	Normal	0.6	4.3	ND	ND
C286	Normal	0.1	0.9	ND	ND
C65	Irradiated	0.04	2.6	ND	ND
C72	Irradiated	0.6	2.4	ND	ND
FLC S-DD					
C288	Normal	0.6	25	ND	ND
C288	Irradiated	ND	ND	7.8	>25
C342	Normal	7.1	30.5	ND	ND
FLC R					
C284	Normal	4.1	342	ND	ND
C284	Irradiated	ND	ND	7.0	431
C260	Normal	15.6	417	ND	ND
C310	Irradiated	ND	ND	19.4	204

[a] PD_{50} determined on day 4 postinfection.
[b] PD_{50} determined on day 7 postinfection.
[c] ND, not done.

on the basis of their 95% confidence bounds indicated that SCH was significantly more active than FLC against FLZ-S-DD strain C288 and the FLC-R strains ($P < 0.05$). The in vivo efficacy of SCH was further reflected in the reduced fungal burdens in the kidneys of the surviving mice (data not shown).

Prophylactic activity against systemic candidiasis. A systemic infection model with immunocompromised mice was used to evaluate the prophylactic efficacy of SCH against *C. albicans*. In these experiments, SCH was compared to FLC (Diflucan) administered once daily beginning at 24 h preinfection and continuing to day 7 postinfection against *C. albicans* C43 (FLC-S), C288 (FLC-S-DD), C284 (FLC-R), and C310 (FLC-R; FLC MIC, >64 μg/ml). The results in Table 4 show that SCH was efficacious against all strains (PD_{50} range, 1.5 to 19.4 mg/kg), while FLC was active against C43 (PD_{50}, 5.3 mg/kg) but not against the less susceptible and resistant strains (PD_{50}s, >25, 431, and 204 mg/kg against strains C288, C284, and C310, respectively). The survival-versus-time graph for FLC-R strain C284 shows that SCH at 50 and 25 mg/kg protected 100% of mice for 12 days postinfection, while FLC at 250 mg/kg was ineffective ($P < 0.01$) (Fig. 2). Other survival-versus-time graphs (data not shown) indicated that SCH at 10 and 25 mg/kg was more efficacious than FLZ at 25 mg/kg against strain C288 and FLZ at 100 mg/kg against strain C310, respectively ($P < 0.01$ for each comparison).

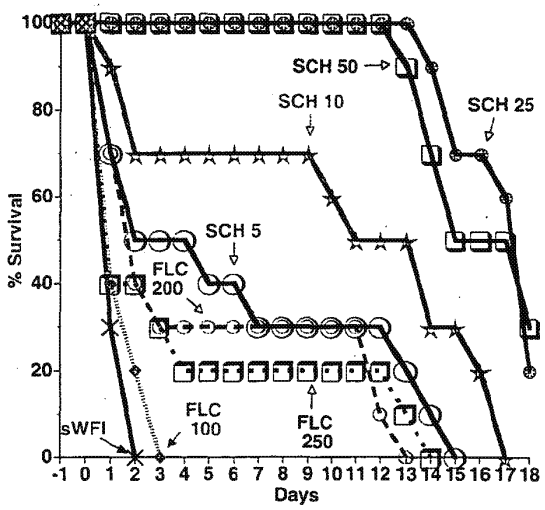


FIG. 2. Effect of SCH and FLC (administered oral once daily) administered in a prophylactic regimen 1 day preinfection to 7 days postinfection on survival of immunocompromised mice systemically infected (with 5×10^6 CFU/mouse on day 0) with *C. albicans* C284 (FLC R). Dose levels (in milligrams per kilogram) are indicated. Controls were administered sWFI.

DISCUSSION

The potent in vitro activity of SCH against *Aspergillus*, *Candida*, and *Cryptococcus* was shown in the study described in this report. Other investigators have found SCH to have broad-spectrum in vitro activity not only against these fungi but also against *Blastomyces dermatitidis*, *Histoplasma capsulatum*, and other filamentous and dimorphic fungi (6, 9, 11, 19, 22, 24, 30, 32, 33, 34, 36).

This report also highlights the in vivo efficacy of SCH against pulmonary *A. fumigatus* and *A. flavus* strains and systemic *C. albicans* strains (including strains with reduced susceptibility or resistance to FLC) in normal or immunocompromised mouse models of infection. In these studies, SCH was effective whether it was initially administered therapeutically after infection or prophylactically before infection. SCH was also reported by Graybill et al. (13) to be more effective than amphotericin B against invasive pulmonary aspergillosis in mice. In addition, Oakley et al. (31) found SCH to be more effective than ITC against disseminated aspergillosis in mice, while Kirkpatrick et al. (17) reported that SCH is more effective than ITC and is as effective as amphotericin B for the clearance of *Aspergillus* from tissues in a rabbit model of invasive aspergillosis.

In experimental infection models SCH was active not only against the more common opportunistic pathogens like *Aspergillus* and *Candida* but also against the less common fungi. Perfect et al. (32) reported that the activity of SCH was comparable to that of FLC against *C. neoformans* in a rabbit model of cryptococcal meningitis. Sugar and Liu (36) found that SCH was more effective than ITC and that the activity of SCH was similar to that of amphotericin B in prolonging survival and sterilizing the lungs of mice infected with *B. dermatitidis*. Lutz et al. (22) showed that SCH, but not FLC or ITC, cured survivors in a mouse model of systemic coccidioidomycosis. Connolly et al. (6) demonstrated in a pulmonary model of histoplasmosis in mice that SCH was more active than ITC and that the activity of SCH was similar to that of amphotericin B for sterilization of the lungs and spleens. SCH was also shown to increase the rate of survival and reduce the organ burdens in mice infected with *Fusarium solani* (21).

Pulmonary aspergillosis and disseminated candidiasis are recognized as serious complications and the leading causes of death among immunosuppressed patients, especially those with AIDS and those who have received bone marrow or liver transplants, for which only inadequate treatment or prophylaxis is available (2, 5, 7, 12, 16). Although prophylaxis with

UM00011958
NOVARTIS EXHIBIT 1017
Novartis v. Regents, IPR2023-01346
Page 704 of 4460

FLC is used to prevent fungal infections in certain patient populations, there are major concerns about the development of resistance (4, 12, 15, 18, 23, 35, 37). ITC was recently evaluated for its prophylactic activity in a clinical trial and was found to reduce the incidence of systemic *Candida* infections and related deaths in neutropenic patients; however, it had no apparent efficacy in the prevention of *Aspergillus* infections (25). The need for more potent, broader-spectrum, longer-acting antifungal agents which are not associated with the emergence of resistance clearly exists. The broad-spectrum activity and experimental efficacy of SCH suggest that it could be effective for the treatment and prevention of severe fungal infections, such as aspergillosis and azole-refractory candidiasis, in high-risk individuals. In addition, the development of resistance to SCH may be a less likely event than with the development of resistance to other azole antifungal agents. Although SCH, like other azoles, blocks fungal sterol biosynthesis by inhibiting C-14 demethylation of lanosterol (H. Munayyer, K. J. Shaw, R. S. Hare, B. Salisbury, L. Heimark, B. Pramanik, and J. R. Greene, Abstr. 36th Intersci. Conf. Antimicrob. Agents Chemother., abstr. F92, p. 115, 1996), Sanglard et al. (D. Sanglard, F. Ischer, and J. Bille, Abstr. 37th Intersci. Conf. Antimicrob. Agents Chemother., abstr. C-11, p. 48, 1997) found that SCH was insensitive to mutations in cytochromes known to hinder the binding of other azole drugs. However, the *C. albicans* ABC transporters Cdr1 and Cdr2 but not the major facilitators Ben and Flu1 were able to use SCH as a substrate when they were expressed in *Saccharomyces cerevisiae* (Sanglard et al., 37th ICAAC).

Preliminary pharmacodynamic analyses suggested that the area under the concentration-time curve is the most important factor in determining the efficacy of SCH in experimental infection models (G. H. Miller, D. Loebenberg, B. Antonacci, A. Cacciapuoti, E. L. Moss, Jr., F. Menzel, Jr., M. Michalski, C. Norris, R. Parmegiani, T. Yarosh-Tomaine, B. Yaremko, and R. S. Hare, Abstr. 36th Intersci. Conf. Antimicrob. Agents Chemother., abstr. F94, p. 116, 1996). Nomeir et al. (29) reported that the concentrations of SCH in serum remained above the MIC for most filamentous fungi and yeasts 24 h following the administration of a single oral dose to various animal species, suggesting that once-daily administration of the compound should be a therapeutically effective dosage regimen. In mice, the mean concentrations of SCH in serum were >2 μg/ml for at least 12 h after oral administration of 20 mg/kg. In addition, SCH achieved a maximum concentration in serum of 6.3 μg/ml at 1 h after dosing, with an area under the concentration-time curve of 63.7 μg · h/ml and bioavailability of 47%. Dose-related increases in both the area under the concentration-time curve and the maximum concentration in serum were also observed in mice over a dose range of 20 to 160 mg/kg. SCH is being evaluated in Phase II and III clinical trials. Preliminary results from a phase II clinical trial indicated that SCH is an effective and well-tolerated alternative treatment for oropharyngeal and esophageal candidiasis in human immunodeficiency virus-infected patients unresponsive to FLC or ITC (D. Skiest, D. Ward, A. Northland, J. Reynes, and W. Greaves, Abstr. 39th Intersci. Conf. Antimicrob. Agents Chemother., abstr. 1162, p. 491, 1999).

ACKNOWLEDGMENT

We thank Ferdous Gheyas for statistical analysis.

REFERENCES

1. **Andes, D., and M. van Ogtrop.** 1999. Characterization and quantitation of the pharmacodynamics of fluconazole in a neutropenic murine disseminated candidiasis infection model. Antimicrob. Agents Chemother. **43**:2116–2120.
2. **Armstrong, D.** 1989. Problems in management of opportunistic fungal diseases. Rev. Infect. Dis. **11**:S1591–S1599.
3. **Cacciapuoti, A., D. Loebenberg, R. Parmegiani, B. Antonacci, C. Norris, E. L. Moss, Jr., F. Menzel, Jr., T. Yarosh-Tomaine, R. S. Hare, and G. H. Miller.** 1992. Comparison of SCH 39304, fluconazole, and ketoconazole for treatment of systemic infections in mice. Antimicrob. Agents Chemother. **36**:64–67.
4. **Cameron, M. L., W. A. Schell, S. Bruch, J. A. Bartlett, H. A. Waskin, and J. R. Perfect.** 1993. Correlation of in vitro fluconazole resistance of *Candida* isolates in relation to therapy and symptoms of individuals seropositive for human immunodeficiency virus type 1. Antimicrob. Agents Chemother. **37**: 2449–2453.
5. **Castaldo, P., R. J. Stratta, R. P. Wood, R. S. Markin, K. D. Patil, M. S. Shaefer, A. L. Langnas, E. C. Reed, S. Li, T. J. Pillen, and B. W. Shaw, Jr.** 1991. Clinical spectrum of fungal infections after orthotopic liver transplantation. Arch. Surg. **126**:149–156.
6. **Connolly, P., J. Wheat, C. Schnizlein-Bick, M. Durkin, S. Kohler, M. Smedema, J. Goldberg, E. Brizendine, and D. Loebenberg.** 1999. Comparison of a new triazole antifungal agent, Schering 56592, with itraconazole and amphotericin B for treatment of histoplasmosis in immunocompetent mice. Antimicrob. Agents Chemother. **43**:322–328.
7. **Denning, D.** 1998. Invasive aspergillosis. Clin. Infect. Dis. **26**:781–805.
8. **Emmons, C. W.** 1977. Medical mycology, 3rd ed. Lea and Febiger, Philadelphia, Pa.
9. **Espinel-Ingroff, A.** 1997. Comparison of in vitro activities of the new triazole SCH 56592 and the echinocandins MK-0991 (L-743,872) and LY303366 against opportunistic filamentous and dimorphic fungi and yeasts. J. Clin. Microbiol. **36**:2950–2956.
10. **Fan-Havard, P., D. Capano, S. M. Smith, A. Mangia, and R. H. K. Eng.** 1991. Development of resistance in *Candida* isolates from patients receiving prolonged antifungal therapy. Antimicrob. Agents Chemother. **35**:2302–2305.
11. **Galgiani, J. N., and M. L. Lewis.** 1997. In vitro studies of activities of the antifungal triazoles SCH 56592 and itraconazole against *Candida albicans*, *Cryptococcus neoformans*, and other pathogenic yeasts. Antimicrob. Agents Chemother. **41**:180–183.
12. **Goodman, J. L., D. J. Winston, R. A. Greenfield, P. H. Chandrasekar, B. Fox, H. Kaizer, R. K. Shadduck, T. C. Shea, P. Stiff, D. J. Friedman, W. G. Powderly, J. L. Silber, H. Horowitz, A. Lichtin, S. N. Wolff, K. F. Mangan, S. M. Silver, D. Weisdorf, W. G. Ho, G. Gilbert, and D. Buell.** 1992. A controlled trial of fluconazole to prevent fungal infections in patients undergoing bone marrow transplantation. N. Eng. J. Med. **326**:845–851.
13. **Graybill, J. R., R. Bocanegra, L. K. Najvar, M. F. Luther, and D. Loebenberg.** 1998. SCH 56592 treatment of murine invasive aspergillosis. J. Antimicrob. Chemother. **42**:539–542.
14. **Gupta, A. K., D. N. Sauder, and N. H. Shear.** 1994. Antifungal agents: an overview. Part II. J. Am. Acad. Dermatol. **30**:911–933.
15. **Havlir, D. V., M. P. Dube, J. A. McCutchan, D. N. Forthal, C. A. Kemper, M. W. Dunne, D. M. Parenti, P. N. Kumar, A. C. White, Jr., M. D. Witt, S. D. Nightingale, K. A. Sepkowitz, R. R. MacGregor, S. H. Cheeseman, F. J. Torriani, M. T. Zelasky, F. R. Sattler, and S. A. Bozzette.** 1998. Prophylaxis with weekly versus daily fluconazole for fungal infections in patients with AIDS. Clin. Infect. Dis. **27**:1369–1375.
16. **Khoo, S. H., and D. W. Denning.** 1994. Invasive aspergillosis in patients with AIDS. Clin. Infect. Dis. **19**:S41–S48.
17. **Kirkpatrick, W. R., R. K. McAtee, A. W. Fothergill, D. Loebenberg, M. G. Rinaldi, and T. F. Patterson.** 2000. Efficacy of SCH 56592 in a rabbit model of invasive aspergillosis. Antimicrob. Agents Chemother. **44**:780–782.
18. **Law, D., C. B. Moore, H. M. Wardle, L. A. Ganguli, M. G. L. Keaney, and D. W. Denning.** 1994. High prevalence of antifungal resistance in *Candida* spp. from patients with AIDS. J. Antimicrob. Chemother. **34**:659–668.
19. **Law, D., C. B. Moore, and D. W. Denning.** 1997. Activity of SCH 56592 compared with those of fluconazole and itraconazole against *Candida* spp. Antimicrob. Agents Chemother. **41**:2310–2311.
20. **Loebenberg, D., A. Cacciapuoti, R. Parmegiani, E. L. Moss, Jr., F. Menzel, Jr., B. Antonacci, C. Norris, T. Yarosh-Tomaine, R. S. Hare, and G. H. Miller.** 1992. In vitro and in vivo activities of SCH 42427, the active enantiomer of the antifungal agent SCH 39304. Antimicrob. Agents Chemother. **36**:498–501.
21. **Lozano-Chiu, M., S. Arikan, V. L. Paetznick, E. J. Anaissie, D. Loebenberg, and J. H. Rex.** 1999. Treatment of murine fusariosis with SCH 56592. Antimicrob. Agents Chemother. **43**:589–591.
22. **Lutz, J. E., K. V. Clemons, B. H. Aristizabal, and D. A. Stevens.** 1997. Activity of the triazole SCH 56592 against disseminated murine coccidioidomycosis. Antimicrob. Agents Chemother. **41**:1558–1561.
23. **Maenza, J. R., W. G. Merz, M. J. Romagnoli, J. C. Keruly, R. D. Moore, and J. E. Gallant.** 1997. Infection due to fluconazole-resistant *Candida* in patients with AIDS: prevalence and microbiology. Clin. Infect. Dis. **24**:28–34.
24. **Marco, F., M. A. Pfaller, S. A. Messer, and R. N. Jones.** 1998. In vitro activity of a new triazole antifungal agent, SCH 56592, against clinical isolates of filamentous fungi. Mycopathologia **141**:73–77.
25. **Menichetti, F., A. Del Favero, P. Martino, G. Bucaneve, A. Micozzi, C. Girmenia, G. Barbabietola, L. Pagano, P. Leoni, G. Specchia, A. Caiozzo, R. Raimondi, and F. Mandelli.** 1999. Itraconazole oral solution as prophylaxis

UM00011959
NOVARTIS EXHIBIT 1017
Novartis v. Regents, IPR2023-01346
Page 705 of 4460

for fungal infections in neutropenic patients with hematologic malignancies: a randomized, placebo-controlled, double-blind, multicenter trial. Clin. Infect. Dis. **28**:250–255.

26. **National Committee for Clinical Laboratory Standards.** 1997. Reference method for broth dilution antifungal susceptibility testing of yeasts. Approved standard. Document M27-A. National Committee for Clinical Laboratory Standards, Wayne, Pa.
27. **National Committee for Clinical Laboratory Standards.** 1998. Reference method for broth dilution antifungal susceptibility testing of conidium-forming filamentous fungi. Proposed standard. Document M38-P. National Committee for Clinical Laboratory Standards, Wayne, Pa.
28. **National Research Council.** 1996. NIH guide to the care and use of laboratory animals. National Academy Press, Washington, D.C.
29. **Nomeir, A. A., P. Kumari, M. J. Hilbert, S. Gupta, D. Loebenberg, A. Cacciapuoti, R. Hare, G. H. Miller, C.-C. Lin, and M. N. Cayen.** 2000. Pharmacokinetics of SCH 56592, a new azole broad-spectrum antifungal agent in mice, rats, rabbits, dogs, and cynomolgus monkeys. Antimicrob. Agents Chemother. **44**:727–731.
30. **Oakley, K. L., C. B. Moore, and D. W. Denning.** 1997. In vitro activity of SCH 56592 and comparison with activities of amphotericin B and itraconazole against *Aspergillus* spp. Antimicrob. Agents Chemother. **41**:1124–1126.
31. **Oakley, K. L., G. Morrissey, and D. W. Denning.** 1997. Efficacy of SCH 56592 in a temporarily neutropenic murine model of invasive aspergillosis with an itraconazole-susceptible and an itraconazole-resistant isolate of *Aspergillus fumigatus*. Antimicrob. Agents Chemother. **41**:1504–1507.
32. **Perfect, J. R., G. M. Cox, R. K. Dodge, and W. A. Schell.** 1996. In vitro and in vivo efficacies of the azole SCH56592 against *Cryptococcus neoformans*. Antimicrob. Agents Chemother. **40**:1910–1913.
33. **Pfaller, M. A., S. Messer, and R. N. Jones.** 1997. Activity of a new triazole, SCH 56592, compared with those of four other antifungal agents tested against clinical isolates of *Candida* spp. and *Saccharomyces cerevisiae*. Antimicrob. Agents Chemother. **41**:233–235.
34. **Pfaller, M. A., S. A. Messer, R. J. Hollis, R. N. Jones, G. V. Doern, M. E. Brandt, and R. A. Hajjeh.** 1998. In vitro susceptibilities of *Candida* bloodstream isolates to the new triazole antifungal agents BMS-207147, SCH 56592, and voriconazole. Antimicrob. Agents Chemother. **42**:3242–3244.
35. **Sangeorzan, J. A., S. F. Bradley, H. Xiaogang, L. T. Zarins, G. L. Ridenour, R. N. Tiballi, and C. A. Kauffman.** 1994. Epidemiology of oral candidiasis in HIV-infected patients: colonization, infection, treatment, and emergence of fluconazole resistance. Am. J. Med. **97**:339–346.
36. **Sugar, A. M., and X.-P. Liu.** 1996. In vitro and in vivo activities of SCH 56592 against *Blastomyces dermatitidis*. Antimicrob. Agents Chemother. **40**:1314–1316.
37. **Troillet, N., C. Durussel, J. Bille, M. P. Glauser, and J. P. Chave.** 1993. Correlation between in vitro susceptibility of Candida albicans and fluconazole-resistant oropharyngeal candidiasis in HIV-infected patients. Eur. J. Clin. Microbiol. Infect. Dis. **12**:911–915.
38. **Walsh, T. J., and P. A. Pizzo.** 1988. Nosocomial fungal infections: a classification for hospital-acquired infections and mycoses arising from endogenous flora and reactivation. Annu. Rev. Microbiol. **42**:517–545.

UM00011960
NOVARTIS EXHIBIT 1017
Novartis v. Regents, IPR2023-01346
Page 706 of 4460

KM

KILDSIG

ci.,

9 (1938).

).

DRUG DEVELOPMENT AND INDUSTRIAL PHARMACY, 8(3), 355-369 (1982)

EQUILIBRIUM MOISTURE CONTENT OF PHARMACEUTICAL EXCIPIENTS

J. C. Callahan, Lederle Laboratories, Inc., Pearl River, NY 10965
G. W. Cleary, Ph.D., Key Pharmaceuticals, Inc., Miami, FL 33169
M. Elefant, Warner Lambert Co., Morris Plains, NJ 07950
G. Kaplan, Ph.D., Johnson & Johnson Products, Inc., New Brunswick, NJ 08903
T. Kensler, Ph.D., Mead Johnson Pharmaceutical Div., Evansville, IN 47721
R. A. Nash, Ph.D., Purdue Frederick Co., Yonkers, NY 10701

ABSTRACT

The equilibrium moisture content (EMC) was determined for thirty pharmaceutical excipients. These data are to be included in the forthcoming publication of the Handbook of Pharmaceutical Excipients. This work was undertaken as a collaborative effort under the sponsorship of the Academy of Pharmaceutical Sciences. The results of this study are being reported herein prior to publication of the Handbook.*

The experimental procedure for determining equilibrium moisture content is included along with a method for classifying the hygroscopic property of solids.

---

* A brief description of the method used in the determination of Equilibrium Moisture Content of pharmaceutical excipients as well as all experimental data will appear in expanded form in the forthcoming "Handbook of Pharmaceutical Excipients" to be published by the APhA Academy of Pharmaceutical Sciences with full copyright protection.

Copyright © 1982 by Marcel Dekker, Inc.

UM00011961
NOVARTIS EXHIBIT 1017
Novartis v. Regents, IPR2023-01346
Page 707 of 4460

Introduction

The sorption of moisture by pharmaceutical solids has been examined by many workers and methods for determining equilibrium moisture content (EMC) have been reported in the literature (1-8). The present method developed by J. Callahan (12) represents a modification of one first described by Scott et al. (5)

EXPERIMENTAL

Materials

Nine plastic desiccators, Nalge/Sybron Corporation, approximately 9 inches in diameter, were obtained from a local laboratory supply house. Glass desiccators of equivalent size may be substituted for the plastic containers.

A supply of glass analytical weighing bottles with standard taper covers (25 mm. O.D. x 40 mm. ht. with 12 ml. capacity were used to contain samples for testing. Samples were weighed on an analytical balance to the nearest 0.1 mg. A series of saturated salt solutions were prepared as described in Table 1.

Procedure

EMC determinations were made by placing accurately weighed samples of each material (100-200 mg) in 2 or 3 open, tared, and numbered weighing bottles and then into a labeled desiccator containing one of the saturated salt solutions described in Table 1. A liberal amount of the saturated salt solution (with excess crystals) was placed in the well of the desiccator.

Samples were stored in each of the nine securely closed individual desiccators, each containing a different moisture atmosphere. At equilibrium (7 days storage at controlled room temperature 25°C ± 2°C) the samples were removed from the desiccators and the moisture increase

UM00011962
NOVARTIS EXHIBIT 1017
Novartis v. Regents, IPR2023-01346
Page 708 of 4460

or decrease determined for each sample by obtaining the final equilibrium weight with the aid of an analytical balance. These data were recorded on moisture analysis data sheets, a sample of which is provided in Table 2.

EMC values were calculated from P (% moisture dry basis) with the aid of the equations given in Table 2. Initial moisture content (A) of each excipient was accurately determined by a suitable method, such as loss on drying to constant weight (see Table 3) and used to caclulate P. EMC values, at each relative humidity tested, were tabulated and presented in Table 2 and plotted, using coordinate graph paper, to obtain EMC vs. relative humidity curves (Figure 2).

TABLE 1

Saturated Salt Solutions for Maintaining Constant Relative Humidity Conditions in Desiccators

Saturated Salt Solution*	Percent Relative Humidity at Temperatures (9-11) 20°C	25°C	30°C	37°C
Lithium Chloride	12	11	11	11
Potassium Acetate	24	23	23	23
Magnesium Chloride	33	33	32	31
Potassium Carbonate	44	43	42	41
Magnesium Nitrate	53	52	52	51
Sodium Nitrite	66	64	63	62
Sodium Chloride	76	75	75	75
Potassium Bromide	84	83	82	81
Potassium Nitrate	94	93	92	91

* Prepared from reagent grade salts dissolved in purified water.

UM00011963
NOVARTIS EXHIBIT 1017
Novartis v. Regents, IPR2023-01346
Page 709 of 4460

Calculation*

$$P = \frac{\left[W \times \frac{A}{100}\right] \pm B \times 100}{W - \left[W \times \frac{A}{100}\right]}$$

Where P = % moisture dry basis

W = initial sample weight in grams

A = % moisture at start

B = weight change at equilibrium in grams

$$EMC = \frac{P}{P + 100} \times 100$$

$$EMC = \frac{24.2\%}{24.2\% + 100} \times 100 = 19.5\%$$

Hygroscopicity Classification

When evaluating the hygroscopic properties of solids, unprotected material is exposed for one week to varying relative humidities from 11 to 93 or 100%. The change in moisture content of the powder depends upon the initial moisture content and the relative humidity of the environmental chamber. Objectionable changes in the physical appearance of the material can occur independent of the moisture increase. For example, physical changes may appear in some materials with little increase in moisture content, whereas no physical change may occur in another product with a large increase in moisture content. These additional physical

* Derivation of the equations used for calculating EMC were provided by Drs. Kaplan and Kensler.

UM00011964
NOVARTIS EXHIBIT 1017
Novartis v. Regents, IPR2023-01346
Page 710 of 4460

TABLE 2

Typical Moisture Analysis Data Sheet

Pharmaceutical Excipient:	Bentonite N.F.
Lot No.:	NG 3977
Source (Manufacturer):	Whittaker, Clark and Daniels, Inc.
Temperature:	
Initial Date:	1.22.80 , 20 °C
Final Date:	1.29.80 , 20 °C
Desiccator No.:	Nine
Salt Solution Used:	Potassium Nitrate
Relative Humidity:	94 Percent
Percent Moisture at Start:	5.74 N.F. XV, page 1210 (2 hrs. at 105°C)

	Replicate No.1	Replicate No.2	Replicate No.3
Bottle No.	17	18	
Wt. Empty Bottle (with cover)	19.6335 g	18.8080 g	
Wt. of Bottle and Sample Before Test (with cover)	19.7386 g	18.9111 g	
Wt. of Bottle and Sample After Test (with cover)	19.7562 g	18.9290 g	
Wt. of Moisture Increase or Decrease	0.0176 g	0.0179 g	
Moisture Content, Dry Basis	23.81%	24.49%	
Average Value		24.2%	

factors are also important in evaluating the hygroscopic nature of a pharmaceutical excipient.

In the case of non-hygroscopic materials, the moisture change at relative humidities below 75% may be negligible, but the increase at high relative humidities may be very large. Though these

UM00011965
NOVARTIS EXHIBIT 1017
Novartis v. Regents, IPR2023-01346
Page 711 of 4460

TABLE 3

Hygroscopicity Classification (See Figure 1)

Class I - Non-Hygroscopic:

Essentially no moisture increases occur at relative humidities below 90%. Furthermore, the increase in moisture content after storage for one week above 90% R.H. is less than 20%.

Class II - Slightly Hygroscopic:

Essentially no moisture increases occur at relative humidities below 80%. The increase in moisture content after storage for one week above 80% R.H. is less than 40%.

Class III - Moderately Hygroscopic:

Moisture content does not increase above 5% after storage at relative humidities below 60%. The increase in moisture content after storage for one week above 80% R.H. is less than 50%.

Class IV - Very Hygroscopic:

Moisture increase may occur at relative humidities as low as 40 to 50%. The increase in moisture content after storage for one week above 90% R.H. may exceed 30%.

---

powders can be adequately protected by suitable packaging, they could change physical form rapidly during actual use under unfavorable high humidity storage conditions. With some very hygroscopic materials the moisture content may increase at relative humidity as low as 40 to 50%. Such powders would require special low humidity areas for processing, in addition to special packaging and storage instructions.

UM00011966
NOVARTIS EXHIBIT 1017
Novartis v. Regents, IPR2023-01346
Page 712 of 4460

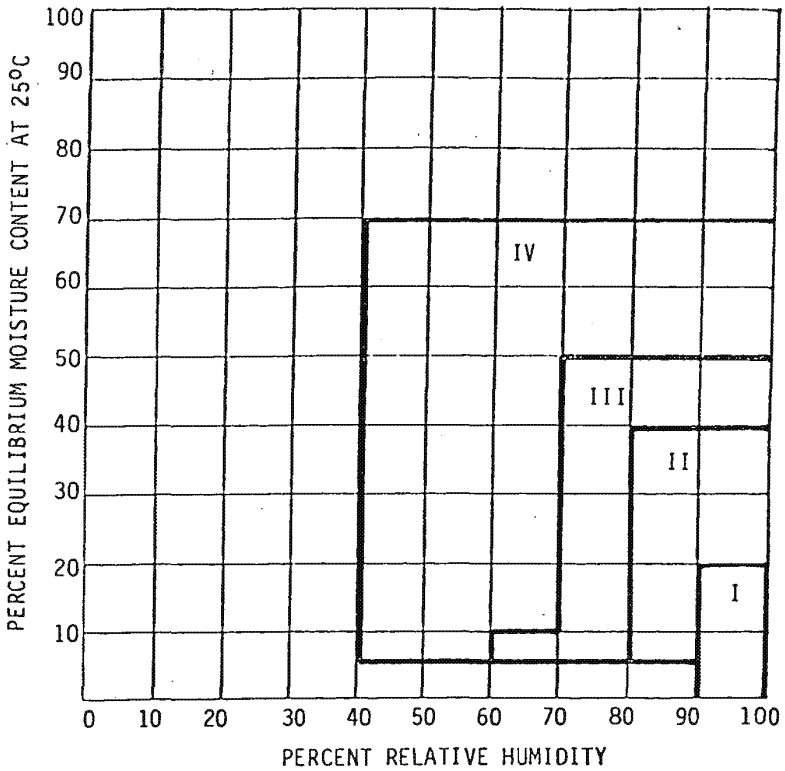


Fig. 1. - Hygroscopicity Classification

Key: Class I - Non-Hygroscopic
Class II - Slightly Hygroscopic
Class III - Moderately Hygroscopic
Class IV - Very Hygroscopic

With these factors in mind, the following classification of hygroscopic materials has been devised (12).

In general most powders are either Class I or Class II excipients. Usually these materials will require only standard packaging and will present no physical stability problems in the field.

Class III materials may or may not require special packaging depending upon the effect of moisture on the physical stability and appearance of the material. Class IV materials, with a few

UM00011967
NOVARTIS EXHIBIT 1017
Novartis v. Regents, IPR2023-01346
Page 713 of 4460

exceptions, should be modified chemically to render them less hygroscopic.

This classification is not applicable if objectionable changes in the physical appearance occur at certain relative humidities. A Class II material would change to a Class III material if an objectionable physical change occurred at relative humidities below 90%. Furthermore, a Class III material would become Class IV if objectionable changes occurred at relative humidities below 75%.

In addition, observations and physical descriptions of materials afer exposure to RH experiments would be useful additional information in such studies.

RESULTS AND DISCUSSION

Powdered excipients and solids may hold water either by physical means (adsorption, absorption, or occlusion, so-called "free water") or by chemical means (water of hydration, or "bound water"). As far as EMC is concerned, sorption or desorption of moisture of water vapor from the surrounding atmosphere is primarily a physical process.

The initial moisture content of the thirty pharmaceutical excipients studied are presented in Table 4. The excipients range in moisture content from less than 0.1 percent for sucrose and anhydrous dicalcium phosphate to more than 10 percent for gelatin and polyplasdone XL. Most of these values were determined by loss on drying in a vacuum oven at 60°C.

The percent EMC at 25°C and different relative humidities for twenty-six excipients together with their hygroscopicity classification

UM00011968
NOVARTIS EXHIBIT 1017
Novartis v. Regents, IPR2023-01346
Page 714 of 4460

are summarized in Table 5. Studies were conducted at 20°C for four other materials: i.e., powdered cellulose, bentonite, gelatin, and polyplasdone XL. The corresponding relative humidities at 20°C are approximately one or two percent higher than the values reported at 25°C. However, the difference in RH values is not considered significant with respect to the EMC values reported.

Almost two-thirds of the excipients tested are either Class I or II materials. These excipients are primarily tablet and capsule fillers, and conditioning agents. The rest, which are more hygroscopic, are primarily tablet binders and tablet disintegrants.

Five cellulosic film formers were also studied. They range from less hygroscopic, ethyl cellulose (I) and cellulose acetate phthalate (II) to more hygroscopic, hydroxypropyl cellulose (III), hydroxypropyl methylcellulose (III), and sodium carboxymethyl cellulose (IV).

Interestingly enough, anhydrous materials, such as dicalcium phosphate and lactose, which were presumed to hydrate rapidly in the presence of high humidity atmospheres, were found to be moisture stable, non-hygroscopic (Class I) diluents.

EMC curves for four representative excipients (anhydrous lactose, cellulose acetate phthalate, magnesium aluminum silicate and povidone) are presented in Figure 2.

CONCLUSIONS

Equilibrium moisture content (EMC) was determined for thirty common pharmaceutical excipients. A method for classifying the hygroscopic properties of powdered materials and solids was presented. Such data and the method described for determining EMC should find application in preformulation work.

UM00011969
NOVARTIS EXHIBIT 1017
Novartis v. Regents, IPR2023-01346
Page 715 of 4460

TABLE 4

INITIAL MOISTURE CONTENT OF PHARMACEUTICAL

Excipient	Supplier & Lot Number
Sucrose U.S.P.	Amstar Co. (51995)
Dicalcium Phosphate, Anhyd. U.S.P.	Monsanto Co. (RNB4768)
Lactose U.S.P., Anhydrous	Humko Products (8NH22-21)
Lactose U.S.P., Monohydrate	Mallinckrodt Chem. (B1523)
Lactose U.S.P., Spray Dried	Foremost Foods (56165)
Lactose U.S.P., Beadlets	Foremost Foods (RB806)
Polyethylene Glycol 3350 N.F.	McKesson Co. (B192-8209)
Poloxamer 188	BASF Wyandotte (WPEA536B)
Silicon Dioxide, Colloidal N.F.	Cabot Corp. (IL288)
Sorbitol U.S.P.	ICI Americas, Inc. (2404J1)
Ethylcellulose N.F.	Hercules (58587)
Dical. Phosphate Dihydrate U.S.P. milled	Monsanto Co. (05587)
Sodium Starch Glycolate N.F.	Edward Mendell Co. (959)
Hydroxypropyl Methylcellulose U.S.P.	Dow Chemical Co. (QP0502-801-E)
Cellulose Acetate Phthalate N.F.	Eastman Chemical (C-2104)
Magnesium Stearate N.F.	S.B. Penick Co. (338 NBS-003)
Hydroxypropyl Cellulose	Hercules (6387)
Cellulose, Microcrystalline N.F.	FMC Corp. (1929)
Povidone U.S.P.	GAF Corp. (690429B)
Cellulose, Powdered N.F.	Brown Co. (30150)
Bentonite N.F.	Whittaker, Clark & Daniels (NG3977)
Magnesium Aluminum Silicate N.F.	R.T. Vanderbilt Co. (NV1640)
Pregelatinized Starch N.F.	National Starch (HJW103)
Starch U.S.P., Corn	National Starch (421)
Dical Phosphate Dihydrate U.S.P. unmilled	Stauffer Chemical Co. (16)
Dextrates	Edward Mendell Co. (M-10)
Dextrose U.S.P.	CPC International (CP44)
Sodium Carboxymethylcellulose U.S.P.	Hercules (76493)
Gelatin U.S.P.	Kind & Knox Gelatin Co.
Polyplasdone XL	GAF Corp. (457-28)

UM00011970
NOVARTIS EXHIBIT 1017
Novartis v. Regents, IPR2023-01346
Page 716 of 4460

LE 4

EUTICAL

EXCIPIENTS USED IN THE STUDY

Initial Moisture Content	Test Method
<0.1%	USPXX Method III, p.960-16 hrs at 105°C
<0.1%	Vacuum Oven - 16 hrs. at 60°C
0.2%	USPXX Method I, p.988 (K. Fischer)
0.2%	Vacuum Oven - 16 hrs. at 60°C
0.2%	Vacuum Oven - 16 hrs. at 60°C
0.2%	Vacuum Oven - 16 hrs. at 60°C
0.3%	Vacuum Oven - 16 hrs. at 60°C
0.3%	Vacuum Oven - 16 hrs. at 60°C
0.6%	Vacuum Oven - 16 hrs. at 60°C
0.7%	USPXX Method I, p.988 (K. Fischer)
0.7%	Vacuum Oven - 16 hrs. at 60°C
1.1%	Vacuum Oven - 16 hrs. at 60°C
1.2%	Vacuum Oven - 20 hrs. at 60°C
2.1%	Vacuum Oven - 16 hrs. at 60°C
2.2%	N.F. XV, p.1219 - 2 hrs. at 60°C
3.0%	N.F. XV, p.1235 - 3 hrs. at 105°C
3.1%	Vacuum Oven - 16 hrs. at 60°C
3.6%	N.F. XV, p.1218 - 4 hrs. at 105°C
4.5%	Vacuum Oven - 16 hrs. at 60°C
5.7%	NF XV, p.1219 - 2 hrs. at 105°C
5.7%	NF XV, p.1210 - 2 hrs. at 105°C
6.0%	Vacuum Oven - 20 hrs. at 60°C
7.0%	Vacuum Oven - 20 hrs. at 60°C
7.1%	Vacuum Oven - 16 hrs. at 60°C
8.0%	Vacuum Oven - 16 hrs. at 60°C
8.2%	Vacuum Oven - 16 hrs. at 60°C
8.3%	USPXX Method III, p.960 - 16 hrs at 105°C
8.5%	USPXX Method III, p.960 - 16 hrs at 105°C
10.6%	AOAC Method, 12th Ed., p.222
11.5%	USPXX Method I, p.988 (K. Fischer)

TABLE 5

EQUILIBRIUM MOISTURE CONTENT OF

Excipient	Percent EMC at 25°C 11%RH	23%RH	33%RH	43%RH
Dicalcium Phosphate, Anhyd. U.S.P.	<0.1	---	<0.1	<0.1
Lactose U.S.P., Beadlets	0.2	---	0.2	0.2
Lactose U.S.P., Monohydrate	0.2	---	0.2	0.2
Lactose U.S.P., Spray Dried	0.5	---	0.5	1.0
Dical. Phosphate Dihydrate, USP milled	1.1	1.5	1.7	1.8
Lactose U.S.P., Anhydrous	0.2	---	0.2	0.2
Ethylcellulose N.F.	0.3	0.6	0.9	0.9
Magnesium Stearate N.F.	3.1	3.6	3.1	3.1
Dical. Phosphate Dihydrate USP unmilled	8.0	8.1	8.1	8.2
Colloidal Silicon Dioxide N.F.	0.0	---	0.6	0.6
Cellulose Microcrystalline N.F.	0.2	2.4	3.7	4.5
Cellulose Acetate Phthalate N.F.	2.2	3.2	3.7	5.1
Sucrose U.S.P.	0.0	0.2	0.3	0.6
Dextrose U.S.P.	7.7	8.6	8.4	8.6
Poloxamer 188	0.4	0.3	0.8	0.6
Powdered Cellulose N.F.*	7.4	---	9.1	7.0
Dextrates	7.7	8.1	8.6	8.8
Polyethylene Glycol 3350 N.F.	0.3	---	<0.3	0.2
Hydroxypropyl Cellulose	0.9	1.9	3.0	3.8
Hydroxypropyl Methylcellulose U.S.P.	1.9	2.6	3.5	4.3
Bentonite N.F.*	2.1	4.5	5.5	5.6
Pregelatinized Starch N.F.	5.3	---	7.8	8.7
Starch U.S.P., Corn	5.5	---	8.0	10.0
Magnesium Aluminum Silicate N.F.	3.7	---	6.0	7.4
Gelatin U.S.P.*	8.2	9.4	10.0	9.6
Sodium Starch Glycolate N.F.	3.8	---	6.2	7.7
Polyplasdone XL*	7.3	13.0	13.1	16.7
Povidone U.S.P.	5.1	8.2	12.2	14.4
Sorbitol U.S.P.	0.7	0.8	1.4	1.2
Sodium Carboxymethylcellulose U.S.P.	7.4	9.2	15.1	14.5

* EMC values determined at 20°C where relative humidities are approximately one percent greater

UM00011972
NOVARTIS EXHIBIT 1017
Novartis v. Regents, IPR2023-01346
Page 718 of 4460

TABLE 5

CONTENT OF PHARMACEUTICAL EXCIPIENTS

MC at 25°C and Different Relative Humidities

H	43%RH	52%RH	64%RH	75%RH	83%RH	93%RH	100%RH	Hygroscopicity Class
	<0.1	<0.1	<0.1	<0.1	<0.1	0.5	7.0	I
	0.2	0.2	0.2	0.2	0.2	1.0	17.0	I
	0.2	0.2	0.2	0.2	0.2	0.2	17.5	I
	1.0	1.0	1.0	1.0	1.0	1.5	21.5	I
	1.8	1.3	1.4	1.4	1.3	1.5	----	I
	0.2	0.2	0.5	1.0	1.5	3.0	27.	I
	0.9	1.3	2.2	2.7	3.3	5.0	----	I
	3.1	3.2	3.3	3.5	5.0	6.9	----	I
	8.2	8.3	8.4	8.4	8.2	8.2	----	I
	0.6	1.7	2.6	3.4	4.8	13.5	34.9	I
	4.5	5.4	6.6	8.1	9.1	13.2	----	II
	5.1	6.0	7.5	8.7	9.5	11.9	----	II
	0.6	1.6	0.2	0.4	0.2	38.7	----	II
	8.6	9.7	9.2	10.0	9.7	31.2	----	II
	0.6	0.9	0.9	1.4	3.8	44.1	----	II
	7.0	7.9	9.3	11.0	12.4	16.0	----	II
	8.8	9.3	10.2	11.7	13.9	51.1	----	II
	0.2	0.6	1.1	2.0	4.0	48.3	62.2	II
	3.8	5.4	7.3	11.0	12.7	21.3	----	III
	4.3	5.9	7.9	10.5	12.8	25.7	----	III
	5.6	6.7	9.9	12.2	13.7	19.5	----	III
	8.7	10.4	12.1	14.7	16.0	22.7	36.4	III
	10.0	11.6	13.2	14.4	19.1	21.5	16.5	III
	7.4	10.1	13.4	15.1	16.7	22.0	39.4	III
	9.6	12.6	15.4	18.4	20.2	33.1	----	III
	7.7	9.5	12.6	17.3	22.4	41.4	60.5	IV
	16.7	19.0	22.2	27.7	29.6	38.0	----	IV
	14.4	17.6	21.8	27.8	31.9	44.8	----	IV
	1.2	1.8	2.7	28.4	36.0	50.8	----	IV
	14.5	19.5	21.4	25.8	30.8	46.2	----	IV

UM00011973
NOVARTIS EXHIBIT 1017
Novartis v. Regents, IPR2023-01346
Page 719 of 4460

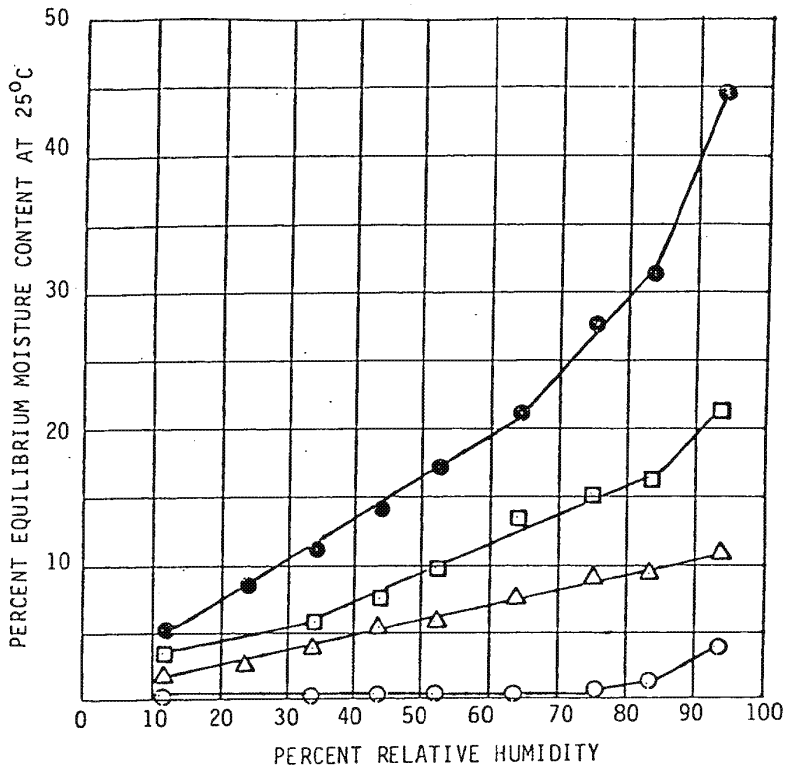


Fig. 2. - EMC Curves for Representative Excipients According to Hygroscopic Classification

Key:
- ○ Class I - Non-Hygroscopic (Anhydrous Lactose USP)
- △ Class II - Slightly Hygroscopic (Cellulose Acetate Phthalate N.F.)
- □ Class III - Moderately Hygroscopic (Magnesium Aluminum Silicate N.F.)
- ● Class IV - Very Hygroscopic (Povidone U.S.P.)

ACKNOWLEDGEMENTS

This work represents a collaborative effort among six scientists in the U.S. pharmaceutical industry. We would like to acknowledge the support and encouragement of Drs. Brooke and Hamlow (Mead Johnson) and Mr. Jack Cooper (Handbook Pharmaceutical Excipients Project Coordinator).

UM00011974
NOVARTIS EXHIBIT 1017
Novartis v. Regents, IPR2023-01346
Page 720 of 4460

REFERENCES

1. G. Edgar and W.O. Swan, J. Am. Chem. Soc., 44, 570 (1922)
2. Browne, J. Ind. Chem. Eng., 14, 712 (1922)
3. Hellman and Melvin, Cereal Chem., 25, 146 (1948)
4. W.A. Strickland Jr., J. Pharm. Sci., 51, 310 (1962)
5. M.W. Scott et al, Ibid., 52, 994 (1963)
6. Czetsch - Linderwold, Amer. Perf. & Cosm., 80, 31 (1965)
7. E. Shotton and N. Harb, J. Pharm. Pharmacol., 17, 504 (1965) and 18, 175 (1966)
8. D. Neville Gore and J. Ashwin, J. Mondial Pharm., 4, 365 (1967)
9. L.B. Rockland, Anal. Chem., 32, 1375 (1960)
10. D.S. Carr and B.L. Harris, Ind. Eng. Chem., 2014 (1949)
11. Technical Bulletin No. 5, Hygrodynamics, Inc., Silver Spring, Maryland 20910
12. J. Callahan and R.A. Nash, Lederle Laboratories, Pearl River, NY 10965, (1968).

.)

.)

in the

support

. Jack

UM00011975
NOVARTIS EXHIBIT 1017
Novartis v. Regents, IPR2023-01346
Page 721 of 4460

This Page is Inserted by IFW Indexing and Scanning Operations and is not part of the Official Record

BEST AVAILABLE IMAGES

Defective images within this document are accurate representations of the original documents submitted by the applicant.

Defects in the images include but are not limited to the items checked:

- ☐ BLACK BORDERS
- ☐ IMAGE CUT OFF AT TOP, BOTTOM OR SIDES
- ☐ FADED TEXT OR DRAWING
- ☐ BLURRED OR ILLEGIBLE TEXT OR DRAWING
- ☐ SKEWED/SLANTED IMAGES
- ☐ COLOR OR BLACK AND WHITE PHOTOGRAPHS
- ☐ GRAY SCALE DOCUMENTS
- ☐ LINES OR MARKS ON ORIGINAL DOCUMENT
- ☐ REFERENCE(S) OR EXHIBIT(S) SUBMITTED ARE POOR QUALITY
- ☐ OTHER: _____

IMAGES ARE BEST AVAILABLE COPY.
As rescanning these documents will not correct the image problems checked, please do not report these problems to the IFW Image Problem Mailbox.

Journal of Antimicrobial Chemotherapy (2001) **47**, 333–340

JAC

Acquired itraconazole resistance in *Aspergillus fumigatus*

Eric Dannaoui*, Elisabeth Borel, Marie-France Monier, Marie-Antoinette Piens, Stéphane Picot and Florence Persat

Laboratoire de Parasitologie, Mycologie Médicale et Pathologie Exotique, Université Claude Bernard Lyon I, 8 avenue Rockefeller, 69373 Lyon Cedex, France

The antifungal susceptibility profiles of four *Aspergillus fumigatus* isolates, recovered at different times from a patient treated with itraconazole for a pulmonary *Aspergillus* infection, were evaluated. Itraconazole MICs against two pre-treatment isolates were 0.5 mg/L, whilst two later isolates, recovered after at least 4 months of itraconazole therapy, had itraconazole MICs of >16 mg/L. *In vivo* susceptibilities to itraconazole and amphotericin B were tested in a murine model of disseminated aspergillosis. Treatment efficacy was evaluated by examining mortality rates and qualitative cultures of brain and kidneys. Itraconazole therapy significantly prolonged survival of mice infected with the initial isolates as compared with untreated controls. The third isolate was only partially susceptible to itraconazole *in vivo*, and the fourth isolate was highly resistant. The four isolates were typed by random amplified polymorphic DNA (RAPD) with four different primers. RAPD patterns obtained with each of them were identical, suggesting that the same strain was recovered over time and had acquired resistance to itraconazole.

Introduction

Aspergillus infections are an important cause of morbidity and mortality, particularly in immunosuppressed patients.[1] For invasive *Aspergillus* infections, amphotericin B remains the drug of choice but the overall success rate is low[2] and amphotericin B therapy may be complicated by nephrotoxicity.[3]

Itraconazole is a triazole antifungal drug with good *in vitro* activity against *Aspergillus* spp.[4] and has been successfully used to treat patients with invasive aspergillosis.[1] Moreover, itraconazole has been used as a long-term therapy for chronic necrotizing aspergillosis and aspergilloma.[5]

The extensive use of azole compounds such as fluconazole has been associated with an increasing number of reports of resistance to this antifungal agent among *Candida* species.[6] Recently, *Aspergillus fumigatus* isolates demonstrating *in vitro* resistance to itraconazole have been described.[4,7,8] For some of these strains, the resistance detected *in vitro* has been confirmed *in vivo* in animal models,[8,9] suggesting that this resistance may have clinical significance.

In this study, we report the acquisition of resistance to itraconazole of *A. fumigatus* isolates in a patient following prolonged itraconazole therapy. The susceptibilities of these isolates to itraconazole were evaluated *in vitro*, and *in vivo* in a murine model of disseminated aspergillosis.

Case report

A 66-year-old man, with a long history of bronchiectasis accompanied by infection and productive cough, presented in mid-May 1997 for dyspnoea and weight loss. *A. fumigatus* (AF 1112) was isolated from a sputum sample. By the end of May the patient was hospitalized. A CT scan of the chest showed multiple cavities in the left lung, the largest being diagnosed as an aspergilloma, with fibrosis and bronchiectasis in the right lung. Surgical resection was not possible due to the poor respiratory function of the patient. A second *A. fumigatus* isolate (AF 1119) was recovered from a sputum specimen taken at this time. Treatment with itraconazole 400 mg daily was started in early June and continued for 5 months. In late September, the patient was hospitalized again and a culture of a bronchoalveolar lavage

*Corresponding author. Tel: +33-4-78-77-72-18; Fax: +33-4-78-75-17-72; E-mail: edanna@rockefeller.univ-lyon1.fr

© 2001 The British Society for Antimicrobial Chemotherapy

UM00011977
NOVARTIS EXHIBIT 1017
Novartis v. Regents, IPR2023-01346
Page 723 of 4460

(BAL) fluid yielded *A. fumigatus* (AF 1237). A chest CT scan revealed that the pulmonary lesions were progressive. In this context, the diagnosis of chronic invasive pulmonary aspergillosis was made and the patient was treated with amphotericin B at 1 mg/kg/day for 2 weeks and then at 1.5 mg/kg/day for 1 week. A BAL fluid taken in mid-October yielded a fourth isolate of *A. fumigatus* (AF 1290) and a bronchial biopsy revealed a glandular carcinoma. Serum itraconazole concentrations determined at various intervals from June to October remained >1 mg/L. All medication was stopped by the end of October, and the patient died a few days later. An autopsy was not performed.

Materials and methods

Organisms

The four isolates of *A. fumigatus* (AF 1112, AF 1119, AF 1237 and AF 1290) isolated in our laboratory were atypical isolates, which sporulated poorly. These strains have been deposited with the IHEM culture collection (Scientific Institute of Public Health, Brussels, Belgium) as IHEM 17905, 17906, 17907 and 17908, respectively. All four isolates sporulated equally poorly and there was no correlation between the degree of itraconazole resistance and the degree of sporulation. Moreover, the four isolates had the same growth rate. Identification was confirmed by E. Guého from the Pasteur Institute, Paris. Isolates were stored as conidial suspensions at –80°C in 10% glycerol until use.

In vitro susceptibility testing

Susceptibility testing was performed by means of a National Committee for Clinical Laboratory Standards (NCCLS)-based broth microdilution technique.[10,11] RPMI 1640 (Gibco-BRL, Uxbridge, UK) with L-glutamine and without sodium bicarbonate, buffered at pH 7.0 with 0.165 M morpholinepropanesulphonic acid (MOPS), was used as the test medium. Amphotericin B (Sigma, St Louis, MO, USA) and itraconazole (Janssen Pharmaceutica, Beerse, Belgium) were provided by the manufacturers as powders. Both drugs were dissolved in dimethylsulphoxide (DMSO; Sigma) to a concentration of 1600 mg/L and stock solutions were stored frozen in aliquots at –80°C. The drug dilutions were prepared by following the standard additive two-fold drug dilution scheme described in the NCCLS reference method for yeasts[12] with the medium as diluent. The final drug concentrations were 0.03–16 mg/L for amphotericin B and itraconazole. The isolates were grown on malt extract agar slants (Sanofi Diagnostics Pasteur, Marnes La Coquette, France) at 35°C for 5 days. The inoculum was prepared by washing the surface of the agar slants with 1 mL of sterile 0.9% saline containing 0.05% Tween 80. The resulting conidial suspensions were counted with a haemocytometer. Sterile microtitre plates with 96 U-shaped wells were used. The conidia were diluted in RPMI and each well of rows 2–12 was inoculated. The final inoculum concentration was 1×10^4 conidia per mL. Row 1 was used as a sterility control and row 12 as a growth control. The determination of MICs for all isolates was performed in duplicate. Microplates were incubated at 35°C for 48 h and after this time the growth in each well was compared with that of the growth control with the aid of a microtitre reading mirror. Each well was given a numerical score:[10] 4, no reduction in growth; 3, growth reduction of 25%; 2, growth reduction of 50%; 1, growth reduction of ≥75%; and 0, absence of growth (optically clear). MIC endpoints were defined as the lowest concentration that had a score of 0 (MIC-0) for amphotericin B. For itraconazole, both MIC-0 and the lowest drug concentration that had a score of 1 (MIC-1) were determined.

In vivo experiments

Mice. Female OF-1 outbred mice (IFFA CREDO, l'Arbresle, France), 5–7 weeks old and weighing 20–22 g, were used throughout the experiments. Mice were housed in groups of 10 and were given food and water *ad libitum*. Animal studies were conducted in accordance with recommendations of the European Community (Directive no. 86/609/EEC, 24 November 1986).

Infection. The inoculum was prepared by culturing the strains on potato carrot agar in cell culture flasks for 10 days at 35°C. Spores were harvested by washing the agar surface with sterile saline containing 0.05% Tween 80, and the resulting spore suspension was counted in a haemocytometer and stored at 4°C until infection. Viability was determined by plating serial 10-fold dilutions prepared in saline with 0.05% Tween 80. Plates were incubated at 35°C and cfu counted at 24 h. The spore suspension was adjusted to the required concentration in saline before administration. Preliminary studies were performed to determine the LD_{90} (90% lethal dose) for each isolate by testing three to four inoculum concentrations. The LD_{90} results were between 5×10^5 and 8×10^5 cfu/mouse for the four isolates. Mice were infected by injection of 0.1 mL of the conidial suspension into a lateral tail vein. After infection, mice were randomized into the different treatment groups.

Drugs and therapy. Amphotericin B desoxycholate (Fungizone, Bristol-Myers Squibb, Paris, France) was given intraperitoneally in 5% glucose and itraconazole (Sporanox oral solution, Janssen Pharmaceutica) was diluted in sterile water and given by gavage. Treatment with both drugs was commenced 2 h after infection and was continued for 10 days. For each isolate, four groups of 10 mice were used. One group was treated with 4.5 mg/kg/day od of amphotericin B by intraperitoneal injection, and one group was treated with 100 mg/kg/day of itraconazole administered bd by gavage. Control mice were infected but received only 5% glucose, one group by intraperitoneal injection and one group by gavage. Animals were checked twice daily for mortality. The mice were observed for a further 12 days after the end of treatment.

UM00011978
NOVARTIS EXHIBIT 1017
Novartis v. Regents, IPR2023-01346
Page 724 of 4460

Organ cultures. Qualitative organ cultures were performed on mice that died before the end of the experiment and on all mice on day 22 post-infection. Surviving mice were killed by cervical dislocation. Brain and kidneys were removed and homogenized with 3 mL of saline in a tissue grinder. A 0.1 mL aliquot of the suspension was plated on to Sabouraud's agar and plates were incubated at 35°C for 3 days for control groups and 5 days for treated groups.

Itraconazole assay. Twelve uninfected mice were given itraconazole by gavage at 100 mg/kg/day. Six mice were killed after 4 days of treatment and six after 6 days of treatment, 6 h after the last dose. Blood was obtained by cardiac puncture and itraconazole serum concentrations were determined by high performance liquid chromatography (HPLC).[13,14]

Data analysis. In each experiment, data for the two control groups were pooled for the analysis. Mortality data were compared by the Kruskal–Wallis test. Qualitative organ cultures were compared by Fisher's exact test.

Molecular typing

Conidia were inoculated into 30 mL of liquid Sabouraud's medium and cultured for 24 h at 35°C. After this time the mycelium was harvested and washed twice with sterile saline. It was then transferred to a 50 mL polypropylene tube containing six glass beads (4 mm diameter). The tube was immersed in liquid nitrogen for 10 s and vortexed vigorously for 1 min. Thereafter, DNA extraction was performed using a QIAmp Tissue Kit (Qiagen, Los Angeles, CA, USA) according to the manufacturer's manual.

Random amplified polymorphic DNA (RAPD)-PCR was performed with primers 2 and 5 (5'-GCTGGTGG and GCGCACGG, respectively)[15] and primers R108 and R151 (5'-GTATTGCCCT and GCTGTAGTGT, respectively).[16] Amplification reactions were performed in 50 μL volumes containing 50 mM KCl, 10 mM Tris–HCl (pH 8.0), 1.5 mM $MgCl_2$, 100 μM (each) dNTPs, 0.2 μM primer, 50 ng of genomic DNA and 2.5 U of *Taq* DNA polymerase (Perkin Elmer, NJ, USA). Amplifications were carried out in a Minicycler (MJ Research, MA, USA) for 1 cycle of 5 min at 94°C, followed by 45 cycles of 1 min at 94°C, 2 min at 35°C and 2 min at 72°C. A final extension was performed at 72°C for 10 min. A blank control tube containing all reagents except the template DNA was also processed. Amplification products were separated by electrophoresis through 1.8% agarose gels containing ethidium bromide. RAPD profiles were compared visually. Both faint and intense bands were included in the interpretation.

Results

In vitro susceptibility testing

The results of susceptibility testing for the four *A. fumigatus* isolates used in the study are shown in Table I. Susceptibility tests were performed at least three times for each strain and MICs were reproducible on re-testing. For isolates AF 1112 and AF 1119, itraconazole was active with an MIC-1 of 0.5 mg/L. Isolates AF 1237 and AF 1290 exhibited high itraconazole MICs of >16 mg/L. For the four isolates, itraconazole MIC-0 and MIC-1 were similar. All four isolates were susceptible *in vitro* to amphotericin B with MICs ≤ 1 mg/L.

In vivo experiments

Survival. Survival curves (Figure 1) demonstrate that each of the four isolates caused an acute and lethal infection in control mice. Median survival time of mice infected with each of the four isolates is shown in Table II.

With strains AF 1112 (Figure 1a) and AF 1119 (Figure 1b) all control mice died within 10 days. Treatment with amphotericin B or itraconazole resulted in 100 and 90% survival, respectively. This was significantly higher than for mice receiving no treatment ($P < 0.001$). Figure 1c shows the survival of mice infected with strain AF 1237. There was 100% mortality in untreated control mice. No mice treated with amphotericin B died, which was significantly

Table I. *In vitro* susceptibility to amphotericin B and itraconazole of four *A. fumigatus* isolates used for *in vivo* studies

Isolate	Amphotericin B MIC-0 (mg/L)	Itraconazole MIC-1 (mg/L)	Itraconazole MIC-0 (mg/L)
AF 1112	0.5	0.5	0.5
AF 1119	1	0.5	1
AF 1237[a]	1	>16	>16
AF 1290[a]	0.5	>16	>16

MICs were determined after 48 h incubation. For itraconazole, MIC-1 (75% inhibition) and MIC-0 (100% inhibition) were determined.
[a]Isolates cultured after at least 4 months of itraconazole therapy.

UM00011979
NOVARTIS EXHIBIT 1017
Novartis v. Regents, IPR2023-01346
Page 725 of 4460

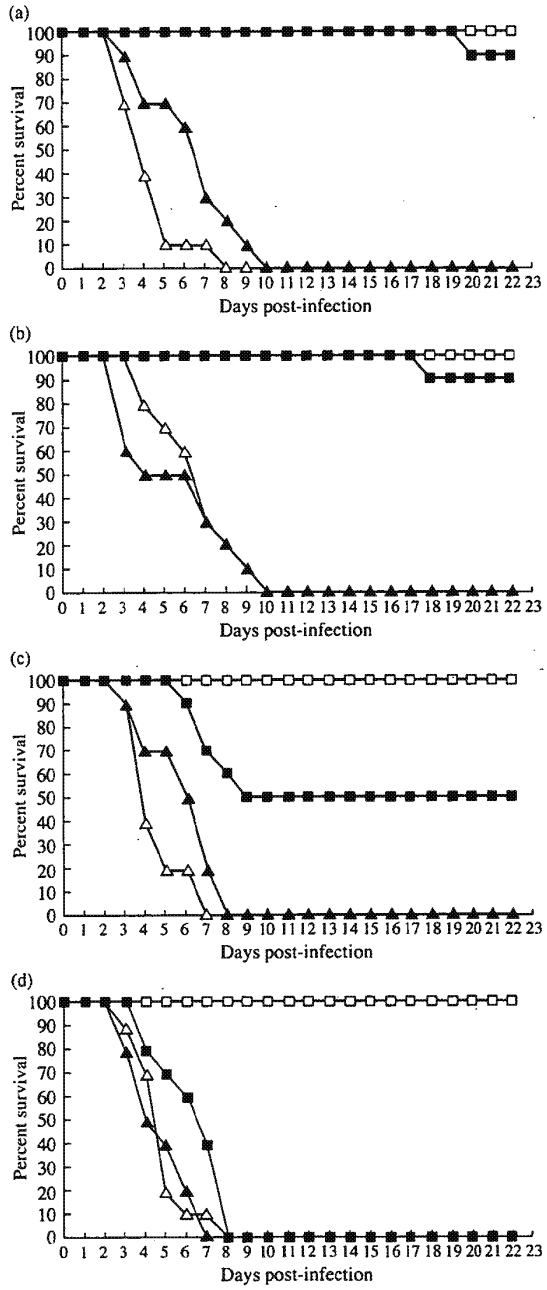


Figure 1. Cumulative mortality for mice infected with strain AF 1112 (a), AF 1119 (b), AF 1237 (c) and AF 1290 (d) in treated and control groups. ■, itraconazole at 100 mg/kg/day; □, amphotericin B at 4.5 mg/kg/day; ▲, 5% glucose control (by gavage); △, 5% glucose control (intraperitoneally).

better than no therapy ($P < 0.001$). In contrast, 50% of mice treated with itraconazole died, which was still better than no therapy ($P < 0.01$).

The survival curves for mice infected with strain AF 1290 are shown in Figure 1 (d). All mice given glucose either by gavage or intraperitoneally died. No mice treated with amphotericin B died, which was significantly better than no therapy ($P < 0.001$). All mice treated with itraconazole died by day 8, which was not significantly different from control mice.

Comparison of the four experiments showed that for groups treated with itraconazole, there was a significant difference in median survival ($P < 0.05$) between mice infected with AF 1290 and those infected with AF 1112 or AF 1119 (Table II).

Culture results. Results of qualitative organ cultures are shown in Table III. For all strains, infection occurred in the kidney tissues of 100% of untreated controls and in the brain of 75–90% of controls. Amphotericin B treatment eradicated or prevented *A. fumigatus* infection in both kidney and brain tissues, whatever the strain tested. For strains AF 1112 and AF 1119, itraconazole significantly reduced kidney and brain infections as compared with controls ($P < 0.0001$ to $P < 0.0005$). In contrast, itraconazole did not significantly reduce the number of infected kidneys in mice infected with strain AF 1237 or AF 1290.

Itraconazole assay. Serum itraconazole concentrations were assessed to ensure adequate absorption of the antifungal agent. Mean itraconazole levels in serum as detected by HPLC are shown in Table IV. The concentration of itraconazole and the active metabolite, hydroxy-itraconazole, in serum was >8 mg/L after 4 days of treatment and only a slight increase was observed after 6 days of treatment.

Molecular typing

The four isolates were typed by means of each of the four primers (primer 2, primer 5, R108 and R151) used separately. The RAPD patterns obtained are shown in Figure 2. Identical patterns were obtained for the four strains, while five unrelated strains, tested in the same conditions, exhibited different RAPD patterns (data not shown). Molecular typing was performed at least twice, with reproducible results.

Discussion

In this study, we tested the antifungal susceptibilities of four isolates of *A. fumigatus* recovered from a patient, both *in vitro* and in an animal model. Two isolates were obtained before treatment with itraconazole and two were post-treatment isolates. The results suggested that the strain acquired resistance to itraconazole during treatment with this antifungal agent.

UM00011980
NOVARTIS EXHIBIT 1017
Novartis v. Regents, IPR2023-01346
Page 726 of 4460

Table II. Survival times for mice infected with four different *A. fumigatus* isolates and treated with amphotericin B 4.5 mg/kg/day or itraconazole 100 mg/kg/day

	Median survival time in days (range)			
Group	AF 1112	AF 1119	AF 1237	AF 1290
Controls	5 (3–10)	7 (3–10)	5 (3–8)	5 (3–8)
Amphotericin B	23 (23)[a]	23 (23)[a]	23 (23)[a]	23 (23)[a]
Itraconazole	23 (20–23)[a]	23 (18–23)[a]	16 (6–23)[b]	7 (4–8)[c]

[a] $P < 0.001$ compared with controls.
[b] $P < 0.01$ compared with controls.
[c] $P < 0.05$ compared with itraconazole treatment of AF1112 or AF1119.

Table III. Qualitative culture results for kidney and brain for all mice

Strain and group (no. of mice in group)	No. of survivors	No. of kidney positive	No. of brain positive
AF 1112			
controls ($n = 20$)	0	20	15
amphotericin B ($n = 10$)	10	0[a]	0[b]
itraconazole ($n = 10$)	9	1[a]	1[c]
AF 1119			
controls ($n = 20$)	0	20	17
amphotericin B ($n = 10$)	10	0[a]	0[a]
itraconazole ($n = 10$)	9	2[a]	0[a]
AF 1237			
controls ($n = 20$)	0	20	15
amphotericin B ($n = 10$)	10	0[a]	0[b]
itraconazole ($n = 10$)	5	8	5
AF 1290			
controls ($n = 20$)	0	20	18
amphotericin B ($n = 10$)	10	0[a]	0[a]
itraconazole ($n = 10$)	0	10	3[c]

[a] $P < 0.0001$ compared with controls.
[b] $P < 0.0005$ compared with controls.
[c] $P < 0.005$ compared with controls.

Table IV. Itraconazole concentration in serum, as measured by HPLC, in non-infected mice after 4 and 6 days of treatment at 100 mg/kg/day

	Itraconazole concentration ± S.D. (mg/L)		
Time (no. of mice)	native	hydroxylated metabolite	native + metabolite
Day 4 (6)	3.13 ± 0.76	5.05 ± 1.51	8.18 ± 2.24
Day 6 (6)	3.37 ± 0.60	6.19 ± 1.30	9.55 ± 1.82

UM00011981
NOVARTIS EXHIBIT 1017
Novartis v. Regents, IPR2023-01346
Page 727 of 4460

BEST AVAILABLE COP

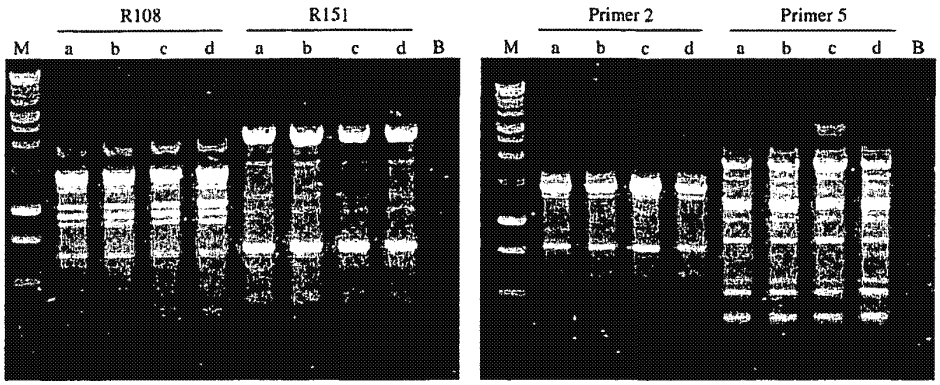


Figure 2. RAPD profiles obtained with four different primers R108, R151, primer 2 and primer 5 for the four strains studied *in vitro* and *in vivo*. M, size marker; a, AF 1112; b, AF 1119; c, AF 1237; d, AF 1290; B, blank.

Although a broth microdilution adaptation of the NCCLS reference method for yeasts has shown good intra- and inter-laboratory reproducibility,[10,11] there is no standardized method for susceptibility testing of filamentous fungi. For this reason we used an animal model of disseminated aspergillosis in immunocompetent mice to confirm the resistance detected *in vitro*. The results of susceptibility testing *in vitro* showed a clear increase in MIC from 0.5 mg/L for isolates recovered before itraconazole therapy, to >16 mg/L for isolates cultured after 4–5 months of therapy. *In vitro* data were confirmed for each of the four isolates in an animal model of disseminated aspergillosis. This model has been used previously to confirm *de novo* resistance of *A. fumigatus* to itraconazole.[9] Although there was good correlation between *in vitro* results and the animal model data, evaluation of the therapeutic efficacy of itraconazole in the patient reported here is difficult. Absence of clinical improvement during itraconazole therapy could be attributed to the resistance of the fungus; however, it could also have been due to the severe underlying respiratory disease.

Previous studies have demonstrated itraconazole resistance of *A. fumigatus in vitro*[4,7,8] and the resistance was confirmed for some strains *in vivo* in animal models of aspergillosis.[8,9] In one study, four itraconazole-resistant strains of *A. fumigatus* were isolated from three patients during long-term itraconazole therapy.[7] However, genotypic analysis of the strains was not performed so it was not possible to determine whether the strains acquired resistance or if the patients were subsequently infected by a resistant strain from the environment.[17] Denning *et al.*[8] reported two patients from whom itraconazole-resistant strains were isolated. In one case, a resistant strain was obtained in culture, although the patient had not been treated with itraconazole. In the other case, a strain was isolated during treatment with itraconazole but was genotypically distinct from the initial strain cultured before treatment.

To our knowledge, the present study is the first to document the acquisition of itraconazole resistance in an *A. fumigatus* strain during prolonged therapy with this antifungal agent.

The genetic diversity of *A. fumigatus* is very important[18] and genetic variations of *A. fumigatus* isolates cultured from respiratory specimens in patients with aspergilloma[19,20] or cystic fibrosis have been demonstrated.[21] Nevertheless, in patients with aspergilloma, although several types could be recovered in the same patient, one predominant genotype is usually found.[19] In the case reported here, the diagnosis of chronic invasive pulmonary aspergillosis was possible. In this context, the disease is probably produced by a single strain of *Aspergillus*, rather than there being multiple strains involved.

Microevolutionary changes within an infecting strain over time have been demonstrated in *Candida albicans*.[22] It is possible, due to microevolution, that some substrains in a colonizing population present altered phenotypes, including changes in susceptibility to antifungal drugs. One can suggest, in a patient with chronic aspergillosis and/or aspergilloma, that the high population density of *A. fumigatus* is a critical factor for strain microevolution or clonal selection of resistant substrains under the drug selection pressure. The situation is probably different in immunosuppressed patients with invasive aspergillosis who have a shorter course and less exposure to the antifungal drug.

Several molecular mechanisms of azole resistance in *Candida* spp. have been reported,[23] but very little is known about the mechanisms of resistance in *Aspergillus* spp. A reduced intracellular accumulation of itraconazole was observed in some strains, possibly due to an efflux pump[8,24] or to a reduced penetration of the drug.[25] In two other strains, the mechanism of itraconazole resistance has been related to a possible modification of the target enzyme 14-α-demethylase.[8]

In the present study we used RAPD to type the isolates.

UM00011982
NOVARTIS EXHIBIT 1017
Novartis v. Regents, IPR2023-01346
Page 728 of 4460

The primers used (2, 5, R108 and R151) have been shown to provide a high level of discrimination between strains of *A. fumigatus*.[15,16,26] The results of RAPD analysis associated with the clinical context strongly suggest the common identity of the four isolates studied.

Further studies have to be done to confirm that *A. fumigatus* could acquire resistance to itraconazole as a result of treatment with this antifungal. Susceptibility studies of *A. fumigatus* strains repeatedly isolated from colonized patients under long-term therapy with itraconazole are needed to evaluate the frequency of this phenomenon.

Acknowledgements

We are indebted to Aline Farille and Lucette Villard for their invaluable help. We thank Eveline Guého from the Pasteur Institute, Paris, for confirmation of the identification of the strains. We also thank Karine Kaiser and Meja Rabodonirina for their advice on molecular typing experiments. This study was supported by a grant from Hospices Civils de Lyon, France.

References

1. Denning, D. W. (1998). Invasive aspergillosis. *Clinical Infectious Diseases* **26**, 781–803.

2. Denning, D. W., Marinus, A., Cohen, J., Spence, D., Herbrecht, R., Pagano, L. *et al.* (1998). An EORTC multicentre prospective survey of invasive aspergillosis in haematological patients: diagnosis and therapeutic outcome. EORTC Invasive Fungal Infections Cooperative Group. *Journal of Infection* **37**, 173–80.

3. Georgopapadakou, N. H. & Walsh, T. J. (1994). Human mycoses: drugs and targets for emerging pathogens. *Science* **264**, 371–3.

4. Dannaoui, E., Persat, F., Monier, M. F., Borel, E., Piens, M. A. & Picot, S. (1999). In-vitro susceptibility of *Aspergillus* spp. isolates to amphotericin B and itraconazole. *Journal of Antimicrobial Chemotherapy* **44**, 553–5.

5. Terrell, C. L. (1999). Antifungal agents. Part II. The azoles. *Mayo Clinic Proceedings* **74**, 78–100.

6. Johnson, E. M. & Warnock, D. W. (1995). Azole drug resistance in yeasts. *Journal of Antimicrobial Chemotherapy* **36**, 751–5.

7. Chryssanthou, E. (1997). In vitro susceptibility of respiratory isolates of *Aspergillus* species to itraconazole and amphotericin B. Acquired resistance to itraconazole. *Scandinavian Journal of Infectious Diseases* **29**, 509–12.

8. Denning, D. W., Venkateswarlu, K., Oakley, K. L., Anderson, M. J., Manning, N. J., Stevens, D. A. *et al.* (1997). Itraconazole resistance in *Aspergillus fumigatus*. *Antimicrobial Agents and Chemotherapy* **41**, 1364–8.

9. Dannaoui, E., Borel, E., Persat, F., Monier, M. F. & Piens, M. A. (1999). In-vivo itraconazole resistance of *Aspergillus fumigatus* in systemic murine aspergillosis. EBGA Network. European research group on Biotypes and Genotypes of *Aspergillus fumigatus*. *Journal of Medical Microbiology* **48**, 1087–93.

10. Espinel-Ingroff, A., Dawson, K., Pfaller, M., Anaissie, E., Breslin, B., Dixon, D. *et al.* (1995). Comparative and collaborative evaluation of standardization of antifungal susceptibility testing for filamentous fungi. *Antimicrobial Agents and Chemotherapy* **39**, 314–9.

11. Espinel-Ingroff, A., Bartlett, M., Bowden, R., Chin, N. X., Cooper, C., Fothergill, A. *et al.* (1997). Multicenter evaluation of proposed standardized procedure for antifungal susceptibility testing of filamentous fungi. *Journal of Clinical Microbiology* **35**, 139–43.

12. National Committee for Clinical Laboratory Standards. (1995). *Reference Method for Broth Dilution Antifungal Susceptibility Testing of Yeasts. Approved Standard M-27A*. NCCLS, Villanova, PA.

13. Michallet, M., Persat, F., Kranzhofer, N., Levron, J. C., Prat, C., Belhabri, A. *et al.* (1998). Pharmacokinetics of itraconazole oral solution in allogeneic bone marrow transplant patients receiving total body irradiation. *Bone Marrow Transplantation* **21**, 1239–43.

14. Warnock, D. W., Turner, A. & Burke, J. (1988). Comparison of high performance liquid chromatographic and microbiological methods for determination of itraconazole. *Journal of Antimicrobial Chemotherapy* **21**, 93–100.

15. Loudon, K. W., Burnie, J. P., Coke, A. P. & Matthews, R. C. (1993). Application of polymerase chain reaction to fingerprinting *Aspergillus fumigatus* by random amplification of polymorphic DNA. *Journal of Clinical Microbiology* **31**, 1117–21.

16. Aufauvre-Brown, A., Cohen, J. & Holden, D. W. (1992). Use of randomly amplified polymorphic DNA markers to distinguish isolates of *Aspergillus fumigatus*. *Journal of Clinical Microbiology* **30**, 2991–3.

17. Verweij, P. E., Voss, A. & Meis, J. F. (1998). Resistance of *Aspergillus fumigatus* to itraconazole. *Scandinavian Journal of Infectious Diseases* **30**, 642–3.

18. Chazalet, V., Debeaupuis, J. P., Sarfati, J., Lortholary, J., Ribaud, P., Shah, P. *et al.* (1998). Molecular typing of environmental and patient isolates of *Aspergillus fumigatus* from various hospital settings. *Journal of Clinical Microbiology* **36**, 1494–500.

19. Girardin, H., Sarfati, J., Kobayashi, H., Bouchara, J. P. & Latge, J. P. (1994). Use of DNA moderately repetitive sequence to type *Aspergillus fumigatus* isolates from aspergilloma patients. *Journal of Infectious Diseases* **169**, 683–5.

20. Denning, D. W., Shankland, G. S. & Stevens, D. A. (1991). DNA fingerprinting of *Aspergillus fumigatus* isolates from patients with aspergilloma. *Journal of Medical and Veterinary Mycology* **29**, 339–42.

21. Verweij, P. E., Meis, J. F., Sarfati, J., Hoogkamp-Korstanje, J. A., Latge, J. P. & Melchers, W. J. (1996). Genotypic characterization of sequential *Aspergillus fumigatus* isolates from patients with cystic fibrosis. *Journal of Clinical Microbiology* **34**, 2595–7.

22. Soll, D. R. (2000). The ins and outs of DNA fingerprinting the infectious fungi. *Clinical Microbiology Reviews* **13**, 332–70.

23. White, T. C., Marr, K. A. & Bowden, R. A. (1998). Clinical, cellular, and molecular factors that contribute to antifungal drug resistance. *Clinical Microbiology Reviews* **11**, 382–402.

24. Slaven, J. W., Anderson, M. J., Sanglard, D., Dixon, G. K., Bille, J., Roberts, I. S. *et al.* (1999). Induced expression of a novel ABC transporter gene *adr1* from *Aspergillus fumigatus* in response to itraconazole. In *Program and Abstracts of the Thirty-Ninth Interscience Conference on Antimicrobial Agents and Chemotherapy, San Francisco, CA, 1999.* Abstract 447. American Society for Microbiology, Washington, DC.

UM00011983
NOVARTIS EXHIBIT 1017
Novartis v. Regents, IPR2023-01346
Page 729 of 4460

25. Manavathu, E. K., Vazquez, J. A. & Chandrasekar, P. H. (1999). Reduced susceptibility in laboratory-selected mutants of *Aspergillus fumigatus* to itraconazole due to decreased intracellular accumulation of the antifungal agent. *International Journal of Antimicrobial Agents* **12**, 213–9.

26. Anderson, M. J., Gull, K. & Denning, D. W. (1996). Molecular typing by random amplification of polymorphic DNA and M13 southern hybridization of related paired isolates of *Aspergillus fumigatus*. *Journal of Clinical Microbiology* **34**, 87–93.

Received 15 May 2000; returned 31 July 2000; revised 6 November 2000; accepted 5 December 2000

UM00011984
NOVARTIS EXHIBIT 1017
Novartis v. Regents, IPR2023-01346
Page 730 of 4460

9. **Garcia-Rodriguez JA, Sanchez JEG, Garcia MIG, Sanchez EG, Bellido JLM:** In vitro activities of new oral β-lactams and macrolides against *Campylobacter pylori*. Antimicrobial Agents and Chemotherapy 1989, 33: 1650–1651.
10. **Barry AL, Jones RN:** Cefixime: spectrum of antibacterial activity against 16016 clinical isolates. Pediatric Infectious Disease Journal 1987, 6: 954–957.
11. **Smith SM, Eng RHK:** Activity of cefixime (FK 027) for gram-negative bacilli. Chemotherapy 1988, 34: 455–461.
12. **Westblom TU, Duriex DE, Madan E, Belshe RB:** Guinea pig model for antibiotic transport across gastric mucosa: inhibitory tissue concentrations of clindamycin against *Helicobacter pylori* (*Campylobacter pylori*) following two separate dose regimens. Antimicrobial Agents and Chemotherapy 1990, 34: 25–28.

In Vitro Activity of Saperconazole (R66 905) Compared with Amphotericin B and Itraconazole against *Aspergillus* Species

D. W. Denning[1,2,3*], L. H. Hanson[1,2], D. A. Stevens[1,2,3]

Twenty isolates of aspergillus were tested against saperconazole and 16 of these against itraconazole and amphotericin B using a macrodilution broth method. For 18 (90 %) of 20 isolates tested against saperconazole, MICs were ≤ 3.1 mg/l and for 15 (75 %) of 20 isolates MFCs were ≤ 3.1 mg/l. For 9 (56 %) of 16 isolates tested against itraconazole, MICs were ≤ 3.1 mg/l, and for 4 (33 %) of 12 isolates MFCs were ≤ 3.1 mg/l. For all 16 isolates tested against amphotericin B MICs and MFCs were ≤ 4.0 mg/l; for 11 of 16 isolates MICs were ≤ 2.0 mg/l. Saperconazole appears to be highly active against *Aspergillus* spp. in vitro, with a bimodal distribution of MICs and MFCs.

[1]Division of Infectious Diseases, Department of Medicine, Santa Clara Valley Medical Center, 751 South Bascom Ave., San Jose, California 95128, USA.
[2]California Institute for Medical Research, San Jose, California 95128, USA.
[3]Division of Infectious Diseases, Department of Medicine, Stanford University School of Medicine, Stanford, California 94305, USA.

Aspergillus infections are an increasing problem as the number of immunocompromised patients continue to grow. Treatment is at present far from satisfactory in many settings in that failure is frequent, relapse occurs and the toxicity of amphotericin B is considerable. New agents with good activity against aspergilli have been developed, the most promising to date being itraconazole (1, 2) and saperconazole (R66 905) (3). Saperconazole [(*cis*)-4-[4-[4-[4-[[2-(2,4-difluorophenyl)-2-(1*H*-1,2,4-triazol-1-ylmethyl)-1,3-dioxolan-4-yl]methoxyl]phenyl]-1-piperazinyl]phenyl]-2,4-dihydro-2-(1-methylpropyl)-3*H*-1,2,4-triazol-3-one] is a new lipophilic fluorinated bis-triazole which is closely related in molecular structure to itraconazole, differing in the substitution of two chlorine atoms by two fluorine atoms on the phenyl ring. The formula of saperconazole is $C_{35}N_{38}F_2N_8O_4$ and its molecular weight is 673. We have undertaken a comparison of its inhibitory and fungicidal activity against aspergilli with that of amphotericin B and itraconazole.

Materials and Methods. All isolates tested were from clinical specimens sent to us for susceptibility testing. All originated in the USA. Isolates were identified by conventional macroscopic and microscopic criteria (4). Isolates (16 each) were tested against amphotericin B and itraconazole directly from media on which they were transported (usually Sabouraud's or Potato Dextrose agar (PDA)); testing against saperconazole (20 isolates) was always done after growth on PDA for four or five days. Selection of isolates was random, i.e. prior or concurrent susceptibility test data was not used in the selection process.

Amphotericin B with 0.41 % deoxycholate was dissolved in sterile water at a concentration of 1.6 mg/ml in glass vials and stored in the dark at – 20 °C. Itraconazole and saperconazole were provided by the manufacturer (Janssen Pharmaceutica, Belgium) as pure powder. Stock solutions were prepared in concentrations of 10 mg/ml in 50 % acetone–50 % 0.2N HCl in a glass tube. To maximize solubility of itraconazole at this concentration, the drug preparation was suspended over hot water (64 °C) for several hours and vortex mixed repeatedly. This was not necessary for saperconazole as it dissolved with vortex mixing alone. Itraconazole and saperconazole stock solutions were stored at room temperature protected from the light.

All drugs were diluted with unbuffered Yeast Nitrogen Base broth containing 0.5 % glucose (YNB). Dilutions for amphotericin B were two-fold from 8 to 0.25 mg/l. For itraconazole and saperconazole dilutions were two-fold from 50 to 0.39 mg/l. Dilutions containing concentrations of saperconazole and itraconazole above

UM00011985
NOVARTIS EXHIBIT 1017
Novartis v. Regents, IPR2023-01346
Page 731 of 4460

12.5 mg/l showed increasing insolubility of the drug. Using 5 ml plastic tubes for susceptibility testing, 1 ml of each drug dilution was pipetted into a series of tubes for each isolate. Control tubes contained YNB without drug.

The inoculum was prepared using YNB to suspend conidia from each test isolate at a concentration of 2000/ml using a hemacytometer. One ml of inoculum was delivered carefully with the tip of the pipette to just below the meniscus to each tube of the drug dilution series and each control tube. A 1:10 dilution was prepared and 0.5 ml plated on a sheep blood agar plate (BAP) to confirm the inoculum size. This plate was incubated at 35 °C for 36 h and a colony count was then done.

The control and drug dilution tubes were incubated on a rotary shaker which held the tubes at an angle of approximately 30° from horizontal with loose caps in ambient air. When growth was evident in the control tube, the MIC was read (40–48 h). The tubes were carefully inspected and the lowest concentration of drug that inhibited growth below the visual threshold was defined as the MIC. A known susceptible organism (for itraconazole and amphotericin B) was assayed periodically during this series of experiments to confirm drug potency and assay reproducibility.

For itraconazole and amphotericin B, from each tube showing no growth or trace growth and the control tube, a 40 µl sample was taken after vigorous mixing and plated on a quadrant of a BAP. For saperconazole, a 40 µl sample from all tubes was taken, vortex mixed and plated on a BAP. Plates were incubated at 35 °C for 48 h. By a criterion used previously in killing studies with clinically useful azoles (5), the lowest drug concentration that produced no growth or one colony on the plate was designated the minimum fungicidal concentration (MFC) and represents ≥ 97.5 % killing. If the MIC was higher than the MFC for an isolate, the MIC value was reduced to equal that of the MFC. To further quantitate killing by saperconazole, from the MIC tubes of four isolates, larger volume samples were plated after vortex mixing; 40, 50, 100, 200 and 1000 µl were plated on BAP. The same criterion (5) was applied to derive the MFC endpoint. "Skip tubes" (tubes which exceeded this endpoint, with higher drug concentrations than others which met the criterion) were occasionally encountered. In such instances, the first tube with a drug concentration higher than the "skip tube" whose plating results met the criterion of less than or equal to one colony was designated the MFC.

Results and Discussion. Fourteen of the isolates were *Aspergillus fumigatus*, three each were *Aspergillus flavus* and *Aspergillus terreus*. The MIC and MFC results are displayed in Table 1. The median (MIC50) and geometric mean MIC

Table 1: MIC and MFC (≥ 97.5 % fungicidal activity) of saperconazole, itraconazole and amphotericin B for 20 isolates of *Aspergillus* spp. Results are in mg/l.

Isolate no.	Saperconazole MIC	Saperconazole MFC	Itraconazole MIC	Itraconazole MFC	Amphotericin MIC	Amphotericin MFC
Aspergillus fumigatus						
5AF	1.6	1.6	3.1	ND	2.0	ND
12AF	1.6	1.6	6.3	ND	4.0	ND
15AF	> 12.5	> 12.5	6.3	6.3	2.0	2.0
19AF	3.1	3.1	6.3	6.3	2.0	2.0
7AF	1.6	1.6	ND	ND	2.0	2.0
88–101	1.6	1.6	3.1	6.3	ND	ND
88–103	0.78	1.6	6.3	> 12.5	ND	ND
88–204	0.78	0.78	1.6	> 12.5	1.0	1.0
88–182	3.1	3.1	1.6	3.1	2.0	ND
87–33	0.78	0.78	12.5	ND	2.0	ND
89–25	1.6	1.6	3.1	3.1	1.0	1.0
44Af	0.78	0.78	ND	ND	ND	ND
89–46	0.78	0.78	6.3	6.3	1.0	1.0
87–51	> 12.5	> 12.5	6.3	ND	4.0	ND
Aspergillus flavus						
5AFL	0.78	> 12.5	1.6	6.3	4.0	ND
89–37	0.78	0.78	3.1	3.1	4.0	4.0
88–110	0.78	0.78	3.1	3.1	ND	ND
Aspergillus terreus						
87–81	1.6	> 12.5	ND	ND	1.0	ND
1AT	1.6	> 12.5	ND	ND	1.0	ND
2AT	0.78	1.6	3.1	> 12.5	2.0	ND

ND = not done.

UM00011986
NOVARTIS EXHIBIT 1017
Novartis v. Regents, IPR2023-01346
Page 732 of 4460

of saperconazole, itraconazole and amphotericin B were 1.5 and 1.7, 3.1 and 3.8, and 2.0 and 2.1 mg/l respectively. The median (MFC50) and geometric mean MFC of saperconazole, itraconazole and amphotericin B were 1.5 and 3.0, 6.3 and 6.6, and 2.0 and 1.6 mg/l respectively. The MIC90 and MFC90 of saperconazole, itraconazole and amphotericin B were 3.1 and > 12.5, 6.3 and > 12.5, and 4.0 and 4.0 mg/l respectively. There were no clear interspecies differences except that for two *Aspergillus fumigatus* isolates the MICs and MFCs of saperconazole were high and the two *Aspergillus flavus* isolates tested showed intermediate susceptibility (MIC 4.0 mg/l) to amphotericin B. With larger numbers of aspergillus isolates, not also tested against saperconazole but tested in our laboratory using the same methods, we have found the itraconazole and amphotericin B results reported here to be representative. For example, we previously reported (1) that in 26 (93 %) of 28 isolates tested against itraconazole the MIC was ≤ 6.3 mg/l (i.e. concentrations below mean steady state serum itraconazole concentrations usually achievable with currently studied doses), compared with 15 (94 %) of 16 isolates reported here. Similarly, in our own unpublished studies of 82 clinical *Aspergillus* spp. isolates tested against amphotericin B, in 53 (65 %) MICs were ≤ 2 mg/l, compared with 12 (75 %) of 16 reported here.

Reproducibility of the assay for saperconazole was assessed by testing one isolate (number 88-204) on four occasions and two isolates (number 87-81 and 5AFL) twice. In all cases the results of the repeat assays were identical or differed by one dilution from the original assay. This observation was valid for both the MICs and MFCs. In addition, interobserver variability was assessed by two observers reading the MICs for six isolates independently. Reading of results for four isolates were identical. In two isolates, differences arose over whether or not a trace or a clump of growth was present in a particular tube – all growth categorized as 1+ was read identically. For these two isolates (number 204-88 and 89-25) the MFCs were 0.78 and 1.6 respectively, suggesting that the very small amount of growth that only one observer classified as present would not alter the final result if an MFC determination was performed.

In most tubes with concentrations above 0.39 mg/l in which growth occurred, growth was evident as a very small clump, or multiple small clumps, tightly adherent to the tube, mostly along one side; little growth occurred at the meniscus.

Quantitative fungicidal activity was further assessed in one experiment with four isolates. Results are displayed in Table 2. For reasons that are not clear, control colony counts for one isolate (number 19AF) were low despite an inoculum that gave a colony count of 1180/2 ml. Some fungicidal activity occurred against all isolates, except isolate 19AF, at 0.39 mg/l. At 0.78 mg/l and higher concentrations, there was apparently almost complete fungicidal activity, and MFCs could be determined in most instances even with a ≥ 99.5 % criterion for killing. However, in no isolate was ≥ 99.9 % killing achieved with ≤12.5 mg/l saperconazole.

The data presented here indicate that saperconazole is highly active against *Aspergillus* spp. in vitro. Our data is bimodal in distribution as for 2 of 20 isolates MICs and MFCs were > 12.5 mg/l and for 18 of 20 MICs were ≤ 3.1 mg/l. It is not clear what serum or tissue levels can be achieved with this agent in humans and therefore no cut-off value for resistance can yet be determined. The median and geometric means of the MICs are approximately half those of itraconazole and lower than those of amphotericin B, indicating saperconazole has greater activity on a weight-for-weight and molar basis than itraconazole and activity approximately equal to that of amphotericin B on a molar basis. Two other reports on the activity of saperconazole have appeared (3, 6). In one, only eight aspergillus isolates were examined by agar dilution and MICs for all isolates were < 0.1 mg/l using two different media (6). In the other study (3), 279 isolates of various *Aspergillus* spp. were tested using tenfold dilutions of saperconazole. In addition to the imprecision of tenfold dilutions, the methodology was at variance with that of most other investigators; brain heart infusion broth was inoculated with an agar block containing hyphae and spores and incubated for two weeks at 25 °C. In 85 % of isolates the MICs were < 0.1 mg/l; only one isolate was not inhibited by 1 mg/l. Neither study examined fungicidal activity in vitro.

Saperconazole also appears to be fungicidal for most isolates of aspergillus. Even in some tubes in which minimal growth was evident, there was no growth on subculture. Using more stringent criteria for activity (≤ 99.0 % and ≤ 99.5 %) a high degree of activity was still observed. The small number of colonies consistently growing in all drug dilutions when half the test sample was plated (1 ml) may or may not indicate a lack of complete killing. It is possible that a few conidia adhering to the tube at the meniscus were inaccessible to saperconazole, and vigorous vortexing prior to plating the MFC allowed them to be plated. Although careful introduction of inocula was used, as in macrodilution broth tests of bactericidal

UM00011987
NOVARTIS EXHIBIT 1017
Novartis v. Regents, IPR2023-01346
Page 733 of 4460

Table 2: Fungicidal activity of saperconazole.

Volume subcultured (ml)	Killing[a] (%)	Control	Colonies in portion removed at given saperconazole concentration (mg/l)[a]					
			0.39	0.78	1.6	3.1	6.3	12.5
Isolate 88–204								
0.04	≥97.5	>200	44	***0***	0	0	0	0
0.05	≥98.0	>200	61	***0***	0	0	0	0
0.10	≥99.0	>400	124	1	1	2	***0***	0
0.20	≥99.5	>500	399	3	***0***	1	1	1
1.00	≥99.9	>1000	>500	8	5	5	2	4
Isolate 19AF								
0.04	≥97.5	6	7	***1***	0	0	1	0
0.05	≥98.0	7	7	6	0	1	1	2
0.10	≥99.0	20	10	***0***	0	1	0	1
0.20	≥99.5	20	36	4	2	8	2	2
1.00	≥99.9	>77	72	11	13	22	6	29
Isolate 89–46								
0.04	≥97.5	90	5	***0***	0	0	0	0
0.05	≥98.0	73	14	***0***	1	0	0	1
0.10	≥99.0	>300	24	***0***	1	0	1	1
0.20	≥99.5	>300	64	1	1	0	4	***1***
1.00	≥99.9	>1500	260	2	3	3	3	8
Isolate 7AF								
0.04	≥97.5	160	16	5	***0***	0	1	1
0.05	≥98.0	73	17	***0***	1	0	1	0
0.10	≥99.0	>400	58	***0***	1	0	0	0
0.20	≥99.5	>400	167	3	4	0	1	2
1.00	≥99.9	>1500	>500	9	5	7	9	4

[a]Criteria used to determine endpoint given in text. Value underlined indicates the lowest concentration meeting these criteria (MFC).

activity, all tubes in this experiment were constantly shaken during incubation, unlike in most bactericidal tests, possibly allowing some conidia to adhere above or at the meniscus.

Our knowledge of the stimuli required for germination of conidia in *Aspergillus* spp. is limited. Although the vast majority of conidia germinate when in contact with a nutrient broth in a warm environment, a small subpopulation may not, but may germinate on solid medium. This could account for the apparent lack of killing, due to germination after plating on blood agar. This would be of little consequence to human infection, particularly since the observation that growth appeared in some tubes but on subculture killing may exceed 99 % suggests that saperconazole may be fungicidal after fungal germination.

Drug carryover from the tubes is almost certainly not pertinent to our data as even the largest plate inoculum (1 ml) and the highest concentration of saperconazole (12.5 mg/l) would give a final saperconazole concentration of 0.4 mg/l on a 30 ml agar plate. Considerably less inhibition and fungicidal activity was evident at this concentration.

Despite the lack of standardization of in vitro susceptibility testing of antifungal agents, the impressive activity of saperconazole observed in vitro was borne out in a serious of studies in aspergillus models in guinea pigs and pigeons (3). Doses of 10 mg/kg orally, or 5 mg/kg intraperitoneally and intravenously sterilized organs in over 93 % of animals and significantly improved survival. The MIC of saperconazole for the organism, *Aspergillus fumigatus*, used for these studies was 1 mg/l in brain heart infusion broth. Further study on the in vivo activity of saperconazole against *Aspergillus* spp. using strains with low and high MICs is required to establish whether the difference in MICs and MFCs we have observed correlates with in vivo outcome.

References

1. **Denning DW, Tucker RM, Hanson LH, Stevens DA:** Treatment of invasive aspergillosis with itraconazole. American Journal of Medicine 1989, 86: 791–800.

UM00011988
NOVARTIS EXHIBIT 1017
Novartis v. Regents, IPR2023-01346
Page 734 of 4460

2. **Van Cutsem J, Van Gerven F, Van De Ven M, Borgers M, Janssen PAJ:** Itraconazole, a new triazole that is orally active in aspergillosis. Antimicrobial Agents and Chemotherapy 1984, 26: 527–534.
3. **Van Cutsem J, Van Gerven F, Janssen PAJ:** Oral and parenteral therapy with saperconazole (R66905) of invasive aspergillosis in normal and immunocompromised animals. Antimicrobial Agents and Chemotherapy 1989, 33: 2063–2068.
4. **Swatek F, Halde C, Rinaldi MJ, Shadomy HJ:** *Aspergillus* species and other opportunistic saprophytic hyaline hyphomycetes. In: Lennette EK, Balows A, Hausler WJ, Shadomy HJ (ed): Manual of clinical microbiology. American Society for Microbiology, Washington, DC, 1985, p. 584–594.
5. **Lefler E, Stevens DA:** Inhibition and killing of *Candida albicans* in vitro by five imidazoles in clinical use. Antimicrobial Agents and Chemotherapy 1984, 25: 450–454.
6. **Odds FC:** Antifungal activity of saperconazole (R66905) in vitro. Journal of Antimicrobial Chemotherapy 1989, 24: 533–537.

In Vitro Activity of the New Semi-Synthetic Polypeptide Cilofungin (LY121019) against *Aspergillus* and *Candida* Species

A. Huang[1], F. Edwards[1], E. M. Bernard[1], D. Armstrong[1], H. J. Schmitt[1, 2, *]

The in vitro activity of cilofungin (LY121019), a new semi-synthetic antifungal agent was evaluated. Potent activity was seen against *Candida albicans* and *Candida tropicalis*, with almost identical MIC and MFC results, whereas no activity was seen against any isolates of *Candida parapsilosis* or three *Aspergillus* spp. However, MICs were dependent on medium and test conditions chosen. It is concluded that cilofungin has good activity against some medically important yeasts in vitro, and that its in vitro activity depends on the method used.

Systemic infections due to *Candida* or *Aspergillus* species are often life-threatening in cancer and transplant patients (1, 2). Unfortunately, the agents available at present for treatment of these infections are toxic and only moderately effective, so that better agents are needed (3). Cilofungin [LY121019; N-*p*-(octyloxybenzoyl)-echinocandin B] is a new semi-synthetic cyclic lipopeptide, an analog of echinocandin B, which inhibits glucan synthesis (4, 5). The aim of this study was to define the range of in vitro antifungal activity of cilofungin against clinically important fungi, to compare several test methods, and to determine the effects of inoculum size and media composition on MICs.

Materials and Methods. Cilofungin (Lilly Research Laboratories, Indianapolis, IN, USA) was prepared as a 1 mg/ml solution in 50 % ethanol and sonicated for 15 min. Microtiter trays were prepared by a standard method (6). Serial two-fold dilutions were made in culture media. The concentrations of cilofungin in the wells were in the range 0.078–40 µg/ml for yeasts and from 0.0125–12.8 µg/ml for aspergilli. A total of 97 yeast strains, predominantly isolated from blood cultures, were tested. A total of 30 *Aspergillus* spp. strains from different clinical sources were tested, including *Aspergillus fumigatus* (n = 16), *Aspergillus flavus* (n = 7) and *Aspergillus niger* (n=7). For testing yeasts different methods were used. Organisms from 24-h slant cultures on Sabouraud (SAB) agar (BBL Microbiology Systems, USA) were suspended in sterile saline, adjusted to 0.55 OD at 660 nm and diluted 1:2000 in SAB broth. Results were read both visually and with an automated photometric plate reader (Titertek Multiskan Type 310C, Flow Laboratories, USA) at 48 h. For strains of *Candida albicans* and *Candida tropicalis*, fungicidal activity of cilofungin was determined by subculturing 10 µl from wells that showed no visible growth on SAB agar plates. Minimal fungicidal concentrations (MFCs) were determined by taking the concentrations in wells showing a 99.9 % reduction in growth compared to the control wells (6). In addition, 20 strains each of *Candida albicans* and *Candida tropicalis* were tested against cilofungin as described above using a high (1×10^5) or a low (2×10^3) inoculum size produced by using a hemacytometer. Either Sabouraud or Yeast-Nitrogen-Glucose (YNG) broth (Difco, USA) were used as medium and results were read at 48 h. *Aspergillus* spp. spores from 4-day-old cultures on SAB agar were harvested using a 0.02 % Tween solution, centrifuged, resuspended in sterile saline and counted in a hemacytometer, and the inoculum was adjusted to 2×10^3 and 1×10^5 spores/ml in YNG broth. Inoculated broth was added in 100 µl portions to the wells of the microtiter trays.

Results and Discussion. Cilofungin exhibited high activity against *Candida albicans* and

[1] Infectious Disease Service, Department of Medicine, Memorial Sloan-Kettering Cancer Center, 1275 York Avenue, New York, New York, USA.
[2] Children's Hospital, Johannes Gutenberg University, Langenbeckstraße 1, 6500 Mainz, FRG.

UM00011989
NOVARTIS EXHIBIT 1017
Novartis v. Regents, IPR2023-01346
Page 735 of 4460

This Page is Inserted by IFW Indexing and Scanning Operations and is not part of the Official Record

BEST AVAILABLE IMAGES

Defective images within this document are accurate representations of the original documents submitted by the applicant.

Defects in the images include but are not limited to the items checked:

- ☐ BLACK BORDERS
- ☐ IMAGE CUT OFF AT TOP, BOTTOM OR SIDES
- ☐ FADED TEXT OR DRAWING
- ☐ BLURRED OR ILLEGIBLE TEXT OR DRAWING
- ☐ SKEWED/SLANTED IMAGES
- ☐ COLOR OR BLACK AND WHITE PHOTOGRAPHS
- ☐ GRAY SCALE DOCUMENTS
- ☐ LINES OR MARKS ON ORIGINAL DOCUMENT
- ☐ REFERENCE(S) OR EXHIBIT(S) SUBMITTED ARE POOR QUALITY
- ☐ OTHER: _____

IMAGES ARE BEST AVAILABLE COPY.

As rescanning these documents will not correct the image problems checked, please do not report these problems to the IFW Image Problem Mailbox.

Pharmaceutical Research, Vol. 15, No. 1, 1998

Review

Dissolution Testing as a Prognostic Tool for Oral Drug Absorption: Immediate Release Dosage Forms

Jennifer B. Dressman,[1,6] Gordon L. Amidon,[2] Christos Reppas,[3] and Vinod P. Shah[4,5]

Received August 20, 1997; accepted September 27, 1997

Dissolution tests are used for many purposes in the pharmaceutical industry: in the development of new products, for quality control and, to assist with the determination of bioequivalence. Recent regulatory developments such as the Biopharmaceutics Classification Scheme have highlighted the importance of dissolution in the regulation of post-approval changes and introduced the possibility of substituting dissolution tests for clinical studies in some cases. Therefore, there is a need to develop dissolution tests that better predict the *in vivo* performance of drug products. This could be achieved if the conditions in the gastrointestinal tract were successfully reconstructed *in vitro*. The aims of this article are, first, to clarify under which circumstances dissolution testing can be prognostic for *in vivo* performance, and second, to present physiological data relevant to the design of dissolution tests, particularly with respect to the composition, volume, flow rates and mixing patterns of the fluids in the gastrointestinal tract. Finally, brief comments are made in regard to the composition of *in vitro* dissolution media as well as the hydrodynamics and duration of the test.

KEY WORDS: dissolution tests; prediction of *in vivo* performance; dissolution test conditions; composition of dissolution media.

INTRODUCTION

An important aspect of the development of a pharmaceutical product is to find an *in vitro* characteristic of potential formulations that reflects their *in vivo* performance. Although immediate release solid dosage forms are routinely subjected to tests such as content uniformity, weight, hardness, friability and disintegration, the test that is most often associated with the assessment of *in vivo* performance is the dissolution test. Currently there are about 500 tablet and capsule monographs in the USP which have dissolution requirements (1), and dissolution testing is an integral component of new drug applications to regulatory bodies worldwide.

In vitro dissolution testing provides useful information at several stages of the drug development process. Formulation scientists use dissolution to assess the dissolution properties of the drug itself and thereby select appropriate excipients for the formulation. Dissolution testing is also employed to assist in choosing among candidate formulations, with the aim of selecting the dosage form with the most suitable and reproducible release profile. However, if these tests are not performed under appropriate conditions, the prediction of which drugs and which dosage forms will exhibit the desired release profiles *in vivo* may be completely erroneous.

Clinical scientists rely on dissolution tests to establish *in vitro/in vivo* correlations between release of drug from the dosage form and drug absorption. When *in vitro* results fail to adequately predict the *in vivo* performance of a drug product, more and larger clinical studies are needed to assess product bioavailability, thus adding substantially to the cost of product development. For drugs and formulations that have release rate limited absorption, it is also of particular interest to know whether the drug will be better absorbed when the product is given with food. Current pharmacopeial tests do not address this need.

From the regulatory scientist's point of view, the evaluation of preclinical and clinical data would be greatly facilitated by the availability of validated, prognostic dissolution methodology for the product. In certain cases, it may be appropriate to use dissolution test results to evaluate the biopharmaceutical implications of a product change, rather than to automatically require a bioequivalence study (2).

Important aspects of the quality assurance of a drug product include the ability to confirm that the correct manufacturing procedures have been followed for a given batch, that batch-to-batch reproducibility of the product meets regulatory requirements, and that the product performs adequately throughout its

[1] Johann Wolfgang Goethe-Universität, Institut für Pharmazeutische Technologie, Marie-Curie-Str. 9, 60439 Frankfurt am Main, Germany.
[2] College of Pharmacy, The University of Michigan, Ann Arbor, Michigan 48109-1065.
[3] Department of Pharmacy, University of Athens, Panepistimiopolis, 157 71 Zografou, Greece.
[4] Office of Pharmaceutical Science, Center for Drug Evaluation and Research, Food and Drug Administration, 5600 Fishers Lane, HFD-350, Rockville, Maryland 20857.
[5] The views and suggestions presented in this article are those of the authors and not of the FDA.
[6] To whom correspondence should be addressed.

0724-8741/98/0100-0011$15.00/0 © 1998 Plenum Publishing Corporation

UM00011991
NOVARTIS EXHIBIT 1017
Novartis v. Regents, IPR2023-01346
Page 737 of 4460

shelf life. Insofar as possible, the *in vitro* test conditions should bear a meaningful relationship to the conditions in the gastrointestinal tract (3). In the case of very poorly soluble drugs, however, the ability to test whether the product is able to release all of the active drug within the desired time-frame under physiologically relevant test conditions may be difficult to achieve with current apparatus.

In summary, there is a real need to develop dissolution tests that better predict *in vivo* performance of drug products. This could be achieved if the conditions in the gastrointestinal tract were successfully reconstructed in *in vitro* test systems. The development of prognostic *in vitro* tests should lead not only to a reduction in the work needed for formulation development, but also in the number and size of clinical studies required, and to more meaningful quality assurance tests.

In this article, we seek first to clarify under which circumstances dissolution testing can be prognostic for *in vivo* performance, then to present physiological data relevant to the design of dissolution tests, particularly with respect to the composition of the medium, the hydrodynamics employed and the duration of the test. In a companion article, examples of drugs for which dissolution is highly dependent on test conditions will be used to illustrate the importance of selecting physiologically relevant test conditions for *in vitro* performance tests.

RATE LIMITING FACTORS TO DRUG ABSORPTION

Essentially, there are four possible sources of incomplete drug absorption following the oral administration of a solid dosage form (4):

1) The drug is not delivered from its formulation over an appropriate time frame in solution form to those sites in the GI tract where it is well absorbed,

2) The drug is decomposed in the gastrointestinal tract or forms a nonabsorbable complex,

3) The drug is not transported efficiently across the gut wall in the apical to basal direction, and/or

4) The drug is metabolized and/or eliminated *en route* to the systemic circulation. These possibilities are illustrated in Figure 1.

Since the gastrointestinal tract is not a static system, the rate at which release, decomposition, complexation and gut wall transport occur must additionally be weighed against the transit rate of the dosage form/drug through the gastrointestinal tract. In order for a drug to be well absorbed, release and uptake must be completed within the time taken for the dosage form/drug to traverse that part of the gastrointestinal tract up to and including the sites at which the drug is absorbed, whereas decomposition and complexation must occur more slowly than either release/uptake or transit.

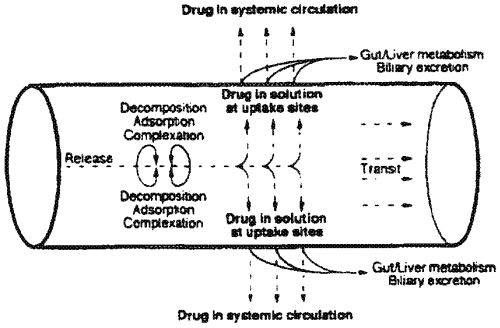


Fig. 1. Steps in drug absorption and sources of incomplete bioavailability following oral administration of a solid dosage form.

THE BIOPHARMACEUTICS CLASSIFICATION SCHEME

Recently, a Biopharmaceutics Classification Scheme (BCS) has been proposed (5). Under this scheme (Table 1), drugs can be categorized into four basic groups according to their solubility properties and their ability to penetrate the gastrointestinal mucosa.

Thus, the BCS addresses two of the potential four limitations to oral drug bioavailability. Of these two, drug solubility recognizes the physicochemical limitations of the drug as a potential source of incomplete release from the dosage form. It is important to understand that the classification is based on the solubility properties of the drug substance throughout the upper GI tract. In the Commentary Section, appropriate media for such studies are suggested. The results of dissolution studies with the drug in the same media can be subsequently used in the development process to assess the influence of formulation on the release rate. Permeability studies are needed to locate the main sites of drug absorption in the gastrointestinal tract, as well as assessing the efficiency of drug transport across the gut wall. A variety of cell culture, tissue and animal models are available for assessing permeability; currently there are also several groups studying permeability of drugs *directly in* humans (6,7). In principle, studies addressing drug stability problems in the lumen of the gastrointestinal tract should be run in media that reproduce the conditions to which the drug is likely to be subjected. In this respect, considerations for design of stability test media parallel those applicable to release and dissolution studies. In the case of drugs that undergo metabolism in the gut wall and/or liver, the rate and extent of the effect must be assessed using tissue preparations or from pharmacokinetic analysis.

Although the BCS is limited to two of the four important factors, it nonetheless provides a useful starting point for recognizing when and how dissolution tests can aid in the design and evaluation of oral dosage forms. Compounds belonging to Class I, i.e. compounds with high solubility and permeability, should go into solution quickly when they are housed in immediate release dosage forms, and also be rapidly transported across

Table 1. The Biopharmaceutics Classification Scheme

Class I: HIGH SOLUBILITY, HIGH PERMEABILITY	**Class II:** LOW SOLUBILITY, HIGH PERMEABILITY
Class III: HIGH SOLUBILITY, LOW PERMEABILITY	**Class IV:** LOW SOLUBILITY, LOW PERMEABILITY

Note: From Ref. 5.

UM00011992
NOVARTIS EXHIBIT 1017
Novartis v. Regents, IPR2023-01346
Page 738 of 4460

the gut wall. Therefore, it is expected that they will be well absorbed unless they are unstable, form insoluble complexes, are secreted directly from the gut wall, or undergo first pass metabolism. Dissolution tests for immediate release formulations of Class I drugs, therefore, need only to verify that the drug is indeed rapidly released from the dosage form under mild aqueous conditions.

For Class II drugs, by contrast, the rate of dissolution of the drug is almost certain to be the principal limitation to its oral absorption. The limitation can be equilibrium or kinetic in nature. In the case of an 'equilibrium' problem there is not enough fluid available in the gastrointestinal tract to dissolve the dose. This can be checked by calculating the dose:solubility ratio (8). For example, at a dose of 500 mg and an aqueous solubility of 15 μg/ml at 37° C, 33 liters of fluid are required to dissolve one dose of griseofulvin. Since the total volume of fluid entering the gastrointestinal tract in a twenty-four hour period is only about five to ten liters (9), there is clearly insufficient volume present at any given time for the entire dose of griseofulvin to be dissolved. In the case of a 'kinetic' problem, the drug dissolves too slowly for the entire dose to become dissolved before the drug has passed by its sites of uptake. Digoxin, for example, with a dose of 0.25 mg and a solubility of 20 μg/ml, has a dose:solubility ratio of just 12.5 ml. Despite the small volume of fluids required to dissolve the drug, digoxin exhibits dissolution rate limited absorption at particle sizes of greater than 10μ in diameter (8) because the poor driving force for dissolution supplied by the solubility, combined with the low surface area of drug at larger particle sizes, is insufficient to ensure timely dissolution. For Class II drugs, it should therefore be possible to establish a strong correlation between the results of dissolution tests and the *in vivo* absorption rate. Establishment of an *in vitro*/*in vivo* correlation and the resultant ability to discriminate between formulations with different bioavailabilities will be dependent on how well the *in vitro* tests are designed. In order to be successful, it is necessary to reproduce the conditions extant in the gastrointestinal tract following administration of the dosage form as closely as possible. Adequate comparison of formulations for Class II drugs requires dissolution tests with multiple sampling times in order to characterize the release profile (2), and in some cases the use of more than one dissolution medium may also be worth considering.

Like compounds belonging to Class I, Class III drugs are rapidly dissolving and the test criterion should be that the formulation can release the drug under mild aqueous conditions within a predetermined time. Rapid dissolution is particularly desirable for Class III drugs, in order to maximize the contact time between the dissolved drug and the absorbing mucosa, and consequently the bioavailability of the compound. Therefore, the duration of the dissolution test should be at least as stringent for Class III drugs as for Class I drugs. Class IV drugs are expected to have poor absorption in general, but it is anticipated that, as in the case of Class II drugs, poor formulation could have an additional, negative influence on both the rate and extent of drug absorption. Thus, for all four categories, it is anticipated that well-designed dissolution tests can be a key prognostic tool in the assessment of both the drug's potential for oral absorption and of the bioequivalence of its formulations.

IMPORTANT CONSIDERATIONS IN DISSOLUTION AND THEIR CORRESPONDING PHYSIOLOGICAL PARAMETERS

From the following equation, based on the Nernst-Brunner and Levich modifications of the Noyes-Whitney model (10–12), the factors important to the kinetics of drug dissolution can be identified:

$$\frac{dX_d}{dt} = \frac{A * D}{\delta} * (C_s - X_d/V)$$

where A is the effective surface area of the solid drug, D is the diffusion coefficient of the drug, δ is the effective diffusion boundary layer thickness adjacent to the dissolving surface, C_s is the saturation solubility of the drug under lumenal conditions, X_d is the amount of drug already in solution and V is the volume of the dissolution medium. Some of these factors are primarily influenced by physicochemical properties of the drugs, but most are also influenced by the conditions in the gastrointestinal tract. A summary of the relevant physicochemical and physiological parameters is given in Table 2.

The key factors in the dissolution of drugs in the gastrointestinal tract are thus the composition, volume and hydrodynamics of the contents in the lumen following administration of the dosage form. Only when these factors are adequately reproduced *in vitro* can we expect to accurately predict dissolution limitations to absorption.

In addition to these factors, the permeability of the gut wall to the compound plays a role in the maintenance of sink (less than 20% of saturation concentration) conditions for dissolution, which are required for the fastest possible dissolution rate. For highly permeable drugs sink conditions are likely to be maintained, in which case the dissolution rate per unit surface area will be constant and close to the initial dissolution rate. For less permeable drugs, the dissolution rate per unit surface area will decrease with time, due to the gradual buildup of drug in solution in the lumen.

The lumenal conditions in the gastrointestinal tract vary widely both within and between subjects. Intersubject variabil-

Table 2. Physicochemical and Physiological Parameters Important to Drug Dissolution in the Gastrointestinal Tract

Factor	Physicochemical parameter	Physiological parameter
Surface area of drug	particle size, wettability	surfactants in gastric juice and bile
Diffusivity of drug	molecular size	viscosity of lumenal contents
boundary layer thickness		motility patterns & flow rate
Solubility	hydrophilicity, crystal structure, solubilization	pH, buffer capacity, bile, food components
Amount of drug already dissolved		permeability
Volume of solvent available		secretions, coadministered fluids

UM00011993
NOVARTIS EXHIBIT 1017
Novartis v. Regents, IPR2023-01346
Page 739 of 4460

ity arises from normal genetic variation in the population (as in the case of heart rate, liver function and other physiological parameters) as well as from disease states implicating the gastrointestinal tract. Intrasubject variability may occur as the result of circadian rhythm, food ingestion, physical activity level and stress level, among others. This variability notwithstanding, the remainder of this Section is devoted to a summary of representative values for key parameters in the fed and fasted states in different segments of the gastrointestinal tract.

Lumenal composition in the GI tract

In addition to food and beverages ingested with the dosage form, various fluids are secreted by the gastrointestinal tract, including hydrochloric acid, bicarbonate, enzymes, surfactants, electrolytes, mucus and, of course, water. Thus, parameters that can profoundly influence the solubility and dissolution rate of a drug, e.g. pH, buffer capacity, presence of surfactant concentration and volume of lumenal contents, may vary widely with position in the gastrointestinal tract and with timing of administration of the drug in relation to meal intake.

pH

Values of gastric pH in the fasted state can fluctuate on a minute-to-minute basis over the range pH 1 to pH 7, but in healthy, young Caucasians gastric pH lies below pH 3 during 90% of the fasted state (13), with an interquartile range of pH 1.4 to pH 2.1. Suitable dissolution media for simulating the fasted state gastric conditions will therefore have pH values between pH 1.5 and pH 2. Fasted state gastric pH values of pH 6 and higher are found in two significant subpopulations: those receiving gastric acid blocker therapy and those over the age of 65 years (about 10–20 % of North Americans (14) and Europeans (15) acquire hypo/achlorhydria; the incidence appears to be much higher in Japan (16)). With ingestion of a meal, the gastric juice is initially buffered to a less acidic pH, which is dependent on the meal composition. Typical gastric pH values immediately following meal ingestion are in the range pH 3 to pH 7. Depending on meal size, the gastric pH returns to fasted state values within two to three hours. Thus, only dosage forms ingested with or soon after meal intake will encounter elevated gastric pH under normal physiological circumstances.

Intestinal pH values (Table 3) are considerably higher than gastric pH values due to the neutralization of incoming acid with bicarbonate ion secreted by the pancreas. Furthermore, there is a pH gradient in the small intestine, with values gradually rising between the duodenum and ileum. pH values in the colon are heavily influenced by products of bacterial exoenzyme reactions. Undigested carbohydrate that is passed into the colon is converted into short chain fatty acids (C_2–C_4) that lower the local pH value to around pH 5 (18). Thus, when suitable carbohydrate substrates are present, the pH in the proximal colon may be 2–3 pH units lower than in the terminal ileum.

Table 3. pH in the Small Intestine in Healthy Humans in the Fasted and Fed States[a]

Location	fasted state pH	fed state pH
mid-distal duodenum	4.9	5.2
	6.1	5.4
	6.3	5.1
	6.4	
jejunum	4.4–6.5	5.2–6.0
	6.6	6.2
ileum	6.5	6.8–7.8
	6.8–8.0 (range)	6.8–8.0
	7.4	7.5

[a] Reproduced from Ref. 17, which summarized results from several studies in the literature.

Table 4. Comparison of Average pH and Buffer Capacity of Chyme Recovered at Midgut From Fistulated Dogs, After Administration of Nonnutrient and Nutrient 'Meals', with Those of Simulated Intestinal Fluid USP, Without Pancreatin

Sample	pH	Buffer capacity (mEq/L/pH unit)
Nonnutrient 'meal' (water)	6.0[a]	0.16 ± 0.16[b]
Nutrient meal (cheeseburger, fries, water)	5.2[a]	76 ± 25[b]
SIFsp (USP)*	7.5	25.8 ± 0.8

Note: Excerpted from Ref. 20.
Shared letters indicate significant differences, [a]$p < 0.05$, [b]$p < 0.005$.
* SIFsp was prepared according to the USP, but without pancreatin. At the time the studies were initiated, the official pH of the medium was 7.5.

Buffer Capacity

The microclimate pH in the diffusion boundary layer adjacent to the dissolving surface is an important determinant to the dissolution of ionizable drugs. In addition to the intrinsic solubility and ionization constant of the drug and the pH of the medium, the buffer capacity of the medium plays an important role in determining the microclimate pH (19). Data obtained in a fistulated dog model (20) suggest that the buffer capacity at midgut is far greater after a cheeseburger/fries/water meal than following administration of water (Table 4).

Surfactants

The surface tension of gastric fluid is considerably lower than that of water, suggesting the presence of surfactants in this region. Usual values in the fasted state lie between 35 and 45 $mN.m^{-1}$ (21). In the small intestine, secretion of bile results in substantial concentrations of bile salts and lecithin, which form mixed micelles even at fasted state concentrations.

Fasting bile salt concentrations of about 3–5 mM have been reported for the proximal small intestine (Table 5). Although

Table 5. Fasting Bile Salt Concentrations in the Human Small Intestine[a]

statistic	duodenum	upper jejunum	lower jejunum
mean ± s.d. (mM)	6.4 ± 1.3	5	6
	4.3 ± 1.2		
median		3	5
range		0–14	0–17

[a] Data from Refs. 22–25.

UM00011994
NOVARTIS EXHIBIT 1017
Novartis v. Regents, IPR2023-01346
Page 740 of 4460

Table 6. Postprandial Bile Salt Concentrations in the Human Small Intestine

Time	Location	Statistic	Reference Number
0–30 min	duodenum	mean 14.5 ± 9.4	29
		range 5.8–39.6	
	upper jejunum	mean 16.2 ± 1.5	30
		mean 15	23
		range 4–34	
30–60 min	duodenum	mean 5.2 ± 2.3	29
	upper jejunum	mean 9.7 ± 1	30
		mean 8	23
		range 3–17	
120–150 min	upper jejunum	mean 6.5 ± 0.9	30

concentrations vary widely between individuals, average values are similar in the duodenum and jejunum. Levels fall rapidly in the ileum where bile salts are absorbed by an active transport mechanism, and are insignificant in the colon in healthy individuals.

After eating, the bile output and lumenal concentration of bile components (Table 6) peak within thirty minutes (26). Thereafter levels gradually decline, mostly because of dilution with chyme. The peak level averages about 15 mM in the proximal small intestine. Since the gallbladder empties into the upper small intestine, duodenal levels tend to fluctuate more with meal ingestion than levels in the distal small intestine (27,28).

Enzymes

The primary enzyme found in gastric juice is pepsin, an exopeptidase. Lipases, amylases and proteases (Table 7) are secreted from the pancreas (31) into the small intestine in response to meal ingestion: these enzymes are responsible for the bulk of nutrient digestion. Pepsin and the pancreatic proteases pose a particular threat to stability of proteins and peptides in the lumen, while lipases may affect release of drugs from fat/oil containing dosage forms.

Bacteria, which mainly populate the distal ileum and the colon, also secrete diverse enzymes. Table 8 (32) illustrates some of the enzymes available, classified according to the reactions that they catalyze. The ability of bacterial exoenzymes to split certain chemical bonds has been used to design dosage forms intended for colonic delivery, such as azo polymers and some hydrogels (33–35).

Volume

The volume of fluids available in the gastrointestinal tract for drug dissolution is dependent upon the volume of coadministered fluids, secretions and water flux across the gut wall. About 2 liters per day are ingested orally, though this varies considerably with climate, body weight, activity and personal habit (9). The volume of the stomach in the fasted state may be as little as 20–30 mL, mostly present as wet mucus rather than as a fluid pool. At the other extreme, gastric pressure starts to rise when a volume of about 1.5 liters is exceeded (36).

The secretions of the para-gastrointestinal organs (salivary glands, liver, pancreas) as well as the secretion of the stomach, are received by the first portion of the duodenum. These endogenous secretions, totalling about 6 liters per day, are essential for the normal lumenal digestion of foodstuffs. Approximately 1–2 L of pancreatic juice are secreted into the duodenum over a 24 hour period (37) while bile output in a 24 hour period totals about 600 mL. Most of the pancreatic and biliary output is secreted postprandially. In addition, the intestine secretes about 1 liter of water per day, mostly as a component of mucus.

According to the perfusion studies of Dillard et al. (38), the volume of fluid in the jejunum and ileum varies from 120–350 mL, depending on the perfusion rate. In a landmark study by Fordtran and Locklear (39) (Figure 2), electrolyte and volume measurements were compared at different sites within the small intestine after ingestion of hypertonic (milk/doughnuts) and hypotonic (steak and water) meals. Volumes were considerably higher following administration of a hypertonic meal than after administration of a hypotonic meal. In the case of a hypertonic meal, net water efflux across the mucosa into the lumen occurs due to the osmotic pressure difference, while in the case of a hypotonic meal, there is net water absorption from the meal.

Table 7. Characteristics of Some Exocrine Pancreatic Enzymes

(pro)enzyme	% output	substrates	products
trypsin(ogen)	33	proteins/polypep	peptides, amino acids
chymotrypsin(ogen)	16	proteins/polypep	peptides, aminoacids
(pro)carboxypeptidase A	12	proteins/polypep	amino acids
(pro)carboxypeptidase B	9	proteins/polypep	amino acids
(pro)elastase	8	proteins/polypep	amino acids
ribonucleases	1	nucleic acids	mono-nucleotides
lipase 1	8.5	triglycerides	fatty acids monoglycerides
lipase 2	3.4	triglycerides	monoglycerides
amylase	3.6	polysaccharides	disaccharides trisaccharides limit dextrins

Note: Excerpted from Ref. 31.

UM00011995
NOVARTIS EXHIBIT 1017
Novartis v. Regents, IPR2023-01346
Page 741 of 4460

Table 8. Bacterial Flora in the Colon and Their Exoenzymes

Bacteria	Reductive Reactions	Hydrolytic Reactions
Bacteroides	nitroreductase	
Clostridia	azoreductase	glucosidase
	hydrogenase	sulfatase
Enterobacteria	nitroreductase	esterase, amidase
	N-oxide-reductase	glucuronidase
	sulfoxide-reductase	sulfatase
Lactobacilli	azoreductase	
	hydrogenase	

Note: Reproduced with permission from Ref. 32.

Fluid levels tend to be lower at more distal locations. Only about 1.5 liters are presented to the colon daily, of which about 1.3 liters are absorbed, with the rest forming a component of the stool (40).

Hydrodynamics in the GI Tract

Mixing Patterns in the Gut

The hydrodynamics in the gastrointestinal tract, that is, how well the lumenal contents are mixed, play an important role in dissolution through their influence on the effective boundary layer thickness, δ. In the upper GI tract, there are basically four motility patterns: no activity (quiescence), segmental movements, propagative movements (short or long range) and tonic contractions (41).

In the fasting stomach, long periods of little or no motor activity occur. About once every two hours, contractions start to occur which gradually become more frequent and more forceful, until they culminate in a burst of activity that clears the contents of the stomach into the intestine (so-called Phase III activity). The quiescent phase can, of course, be modelled by a stagnant system. To date, however, no useful quantitative model of the hydrodynamics of the stomach in the more active phases of the fasted state or in the fed state pattern has been developed.

As far as the small intestine is concerned, some data is available regarding the ratio of segmental to propagative motility as a function of the fed and fasted states. Segmentation is

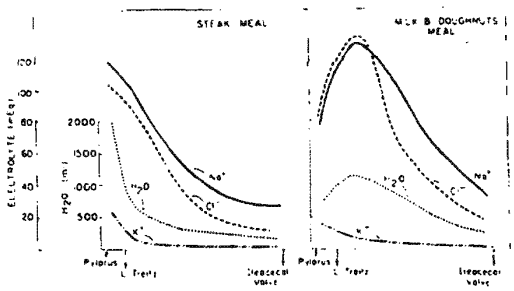


Fig. 2. Water volumes and electrolyte concentrations in the small intestine following ingestion of a hypotonic steak/water meal (Panel A), and a hypertonic milk/doughnuts meal (Panel B). (Reproduced with permission from Ref. 39).

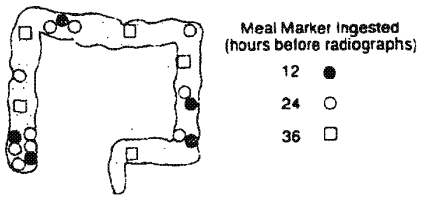


Fig. 3. Distribution of markers in the colon after administration at 12 hour intervals. (Reproduced with permission from Ref. 43).

the predominant mixing pattern in the small intestine, and is characteristic of the fed state. Segmental contractions tend to occur over very short distances, typically less than 2 cm, and serve to mix the lumenal contents thoroughly. Short propulsive movements, on the other hand, provide the main mechanism by which the lumenal contents are moved down the intestine. These usually result in movement of the chyme over distances of 15 cm or less (41).

With the change in the ratio of segmenting to propulsive activity as a function of the phase of the motor pattern and upon meal ingestion, the efficiency of absorption also changes. Absorption is least efficient during Phase III (fasted state long range contractions), is intermediate during Phase I and Phase II and is greatest during the fed state motor pattern (42). Similarly, it is expected that because of better mixing, dissolution will also be most efficient in the fed state.

In the stomach and small intestine, movement of lumenal contents is virtually always in the distal direction. In the proximal colon, however, mixing can occur longitudinally as well as laterally, because some contractions drive the contents in the proximal rather than the distal direction. Figure 3 shows representative results from a study in which subjects ingested radio opaque markers with meals 36, 24, and 12 hours prior to radiography. Some of the markers taken 36 hours earlier are still in the ascending colon while some of the markers taken only 12 hours before are already at the end of the transverse colon (43). Based on these data, one may assume that some degree of mixing of fluids with solids occurs in the colon, although this has not been quantitatively defined.

Flow Rates in the GI Tract

Flow rates out of the stomach and at various locations in the small intestine have been measured in both the fasted and fed states. Emptying rates can be as high as 40 mL/minute immediately after ingestion of a 400 mL volume of normal saline (44). On the other hand, when small volumes are ingested in the quiescent phase of gastric motor activity the emptying rate may be virtually negligible (Table 9) (45). Nutrient fluids empty from the stomach according to zero order kinetics, with emptying dependent on caloric concentration. At a calorie density of 1 kcal/ml, about 2–2.5 mL/minute are emptied, whereas at 0.2 kcal/ml, about 10 mL/min are emptied (44).

Kerlin et al. (46) studied flow rates at various locations in the small intestine. They found that the flow of intestinal content is largely intermittent during fasting, with peaks of flow associated with passage of an activity front through the segment. Values stayed largely between 0 and 2 mL/min, with an average of 0.73 mL/min in the jejunum and 0.43 mL/min in the ileum.

UM00011996
NOVARTIS EXHIBIT 1017
Novartis v. Regents, IPR2023-01346
Page 742 of 4460

Table 9. Lag Times and Time for Half of the Fluid to Empty, for 50 mL and 200 mL Saline Solutions Administered to Healthy Human Subjects

Volume administered	Phase I	Phase II	late Phase II/Phase III
50 mL			
lag time (min)	19	8	4
$t_{0.5}$ (min)	61	17	9
200 mL			
lag time (min)	16	5	2
$t_{0.5}$ (min)	23	12	5

Note: Excerpted from Ref. 45.

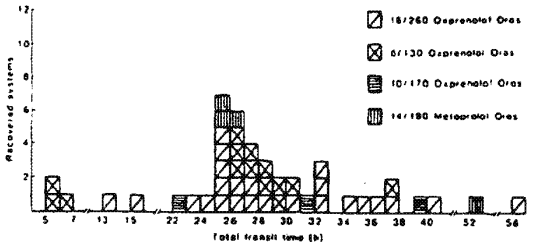


Fig. 4. Total transit time of osmotic pump dosage forms in healthy volunteers. (Reproduced with permission from Ref. 48).

After eating, flow rates increased to average of about 3 mL/min and 2 mL/min respectively, with values ranging from 0–7 mL/min.

Transit Data

Depending on where the drug is absorbed and how long it takes the dosage form to deliver the drug to these sites, the transit time used to calculate the appropriate duration of the dissolution test will differ.

Most drugs are not well absorbed from the stomach, which serves primarily a reservoir function. Because of its anatomical location and permeable mucosa, the small intestine is usually the main site of absorption within the GI tract. Owing to site specificity of transporters and exporters, as well as a tapering off in the unit surface area with distance down the small intestine, many substances are not equally permeable at all sites within the small intestine.

The proximal portion of the large intestine is, like the small intestine, derived embryonically from the midgut (41) and can thus serve as an absorbing organ for drugs. As of this writing, it appears that active transport mechanisms in this section of the gastrointestinal tract are limited primarily to electrolytes. Moreover, the tight junctions are considerably tighter than in the small intestine, restricting the passage of molecules via the paracellular route. Thus, the spectrum of drugs that can be efficiently transported is probably more restricted in the colon than in the small intestine. The distal part of the colon serves as a site for stool formation and storage, and for water conservation and is not generally regarded as being a viable site for drug absorption after oral administration.

Total Residence Time in the Gastrointestinal Tract

The total transit time imposes an overall limit on the duration of the release profile of the dosage form. Total transit time measurements were first reported by Hoelzel (47). He studied the passage of many types of materials, ranging in composition from gases to ball bearings. Total transit times ranged from two to six hours for gases up to 80 hours for high density objects. Materials with densities comparable to pharmaceutical products had transit time on the order of 1–3 days, consistent with the findings of a more recent study (48) (Figure 4) of the total transit times of osmotic pump dosage forms.

The total transit time is comprised of the residence times in the esophagus, stomach, small and large intestines, and rectum. In the absence of pathological conditions, esophageal residence time for most dosage forms is usually on the order of seconds to minutes (49), and thus plays a minor role in the overall transit profile. Gastric residence time is highly variable depending on motility patterns and food intake, whereas the small intestine residence time is relatively constant. In the large intestine, only the proximal residence time is likely to be relevant to drug delivery, since drug release and absorption from the transverse and distal segments is hindered by the paucity of available fluids, and by stool formation and storage.

Residence Times in the Stomach

Gastric residence time can be as short as a few minutes, or as long as half a day, depending on the fed/fasted status of the individual and the conformation of the dosage form. Fastest emptying of fluids occurs when they are taken without food, and in sufficient volumes. Emptying profiles of nonnutrient fluids administered at various phases of the fasted state motility cycle are presented in Table 9 (45).

In the *fasted state*, emptying of solids depends mostly on the phase of the motility cycle operative at the time of administration, and partly on the volume of fluid that is ingested along with the solid. If a small volume of water is ingested with the solid in Phase I (the quiescent phase of motility), first order emptying may not be induced, and consequently there may be a long lag time before either the water or the solid is emptied. For disintegrating solids, the ability of the particles to become suspended in the emptying fluid, along with the emptying pattern of the fluid, will be important to its emptying rate. For nondisintegrating solids greater than about 1 mm in diameter, emptying occurs mostly in late Phase II or Phase III (period of greatest activity) of the motility cycle. Since the average duration of the cycle is about 2 hours, average emptying time will be on the order of one hour, with a range of values between immediate emptying and a delay of two hours. The lack of size dependency in the emptying behavior for particles >1 mm is reflected by the gastric emptying times shown in Table 10 (50,51).

In the fed state, the motility cycle is replaced by a more regular contraction pattern in terms of both frequency and amplitude. Emptying of nutrient fluids is zero-order and calorie dependent, with about 2 kcal/minute emptied (44). Twelve ounces of soda pop contains about 140 kcal, so a ballpark estimate of emptying time in this case would be about 70 minutes. A specialized pattern of antral and pyloric contractions

UM00011997
NOVARTIS EXHIBIT 1017
Novartis v. Regents, IPR2023-01346
Page 743 of 4460

Table 10. Emptying Times of Various Sized Dosage Forms in the Fasted State in Humans

Dosage form	Method	GRT[a]	Reference Number
25u microspheres	γ-scintigraphy	32–87 min	50
1 mm pellets	γ-scintigraphy	60–150 min	51
3 mm pellets	γ-scintigraphy	15–420 min	51
14 mm pellets	γ-scintigraphy	15–210 min	51

[a] GRT = Gastric residence time.

limits the size of the particles which are passed into the duodenum in the postprandial period to those smaller than about 1–2 mm in diameter (52). Ninety % of meal solids are emptied as particles less than 0.25 mm in diameter and almost none are greater than 2 mm. The distal stomach reduces the particle size of ingested solids to a fluid-like consistency. Undigested particles too big to stay suspended in this chyme are retained in the stomach until the reappearance of the fasted motor pattern (53).

Emptying times for nondigestible solids from the stomach in the fed state can vary widely because emptying depends on both the size of the solid particles and the meal that is coadministered. Representative results are shown in Table 11. Meyer et al. (52) calculated that the cutoff diameter for emptying in concert with the solid fraction of the meal is about 1.4 mm.

A second very important factor is the size of the meal. This is because meal emptying depends on the calorie content. Moore et al. (56) showed that the half-emptying times for meals containing 196 (fat: carbo:protein 18:15:67), 621 (6:14:80) and 1920 ± 206 (45:21:34) kcal. had half-emptying times of 77, 145 and 277 minutes respectively. Davis et al. (57) showed that the half-emptying time of 0.7 to 1.2 mm pellets was about twice as long when given with a heavy (900 kcal) as compared to a light (400 kcal) meal.

For a solid that is too large to empty with the meal, a delay of several hours prior to its delivery to the small intestine is likely, since in this case the food has to be cleared from the stomach before the fasted state motility cycle can be reestablished and the dosage form emptied under the auspices of Phase III activity.

Small Intestine Residence Time

In general, there is little difference in the mean transit times through the small intestine for liquids and solids, between

Table 11. Representative Data for Emptying of Nondigestible Solids in the Fed State

Particle size	Method	GRT[a]	Reference Number
0.16-0.4 mm	γ-scintigraphy	34–75 min	54
1 mm	γ-scintigraphy	101 (±53)	52
1.6mm	γ-scintigraphy	152 (±69)	52
2.4mm	γ-scintigraphy	164 (±60)	52
3.2mm	γ-scintigraphy	152 (±40)	52
9 mm	x-ray	105 to >600	55
14 mm	γ-scintigraphy	180 to >780	51

[a] GRT = Gastric residence time.

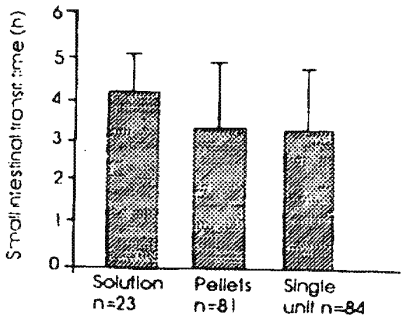


Fig. 5. Transit times of various dosage form types through the small intestine. Data for the fed and fasted state have been pooled. (Reproduced with permission from Ref. 59).

the fed and fasted states, or for different types of dosage forms. Malagelada et al. (58) showed that the intestinal residence profiles for liquid and solids components of a meal are not significantly different, and that the transit time is on the order of one to three hours. Figure 5 summarizes the Nottingham data bank (59,60) for small intestinal residence times of various dosage forms in the fed and fasted states. As with the case of digestible materials, it seems that the small intestine has little capacity to differentiate between dosage forms with different sizes and densities, in sharp contrast to their residence behavior in the stomach.

Residence Times in the Colon

Whereas the transit through the stomach and small intestine are on the order of minutes to hours, and each meal proceeds through without mixing with previous or subsequent meals, transit through the colon can be on the order of hours to days and there is extensive mixing of the contents (see Figure 3). Most of the mixing occurs in the proximal colon. Unlike the remainder of the GI tract, where the electrical waves that underlie the contraction patterns move almost exclusively in the *aborad* direction, in the proximal colon the direction is reversed, promoting delay of transit and facilitating the mixing required for the efficient absorption of water and electrolytes (41).

In the distal half of the colon, the final stages of fluid absorption occur, leading to the formation of feces for defecation. Therefore, the transit time of interest for calculating drug availability for absorption in the colon is the transit time across the proximal and transverse colon. In general, it seems that the size of the dosage form has little effect on the transit time, which is in any case quite variable. Values have been variously reported as 7 to 20 hours (60). Part of the variability appears to be attributable to the time of dosing, i.e. whether the dosage form is ingested in the morning or in the evening. Wilson et al. (61) have recently shown that there is little movement of single unit dosage forms in the colon during sleep.

COMMENTARY

Media Composition

Based on the physiological parameters presented in the previous Section, the following media can be suggested to

UM00011998
NOVARTIS EXHIBIT 1017
Novartis v. Regents, IPR2023-01346
Page 744 of 4460

simulate gastric and small intestinal conditions in the fed and fasted state.

Gastric Media

Table 12 shows the composition of a test medium simulating gastric conditions in the fasted state. Gastric juice already in the stomach and secreted in response to fluid intake will result in an acid pH value in most volunteers. The sodium lauryl sulphate is present to reduce the surface tension to the reported values, since the components that lower the surface tension *in vivo* have not been unequivocally identified (62). Assuming that the coadministered fluid is water, the osmolality and buffer capacity of the medium will be low. Since secretions are at baseline values in the fasted state, the primary determinant of the volume will be the quantity of fluid that is ingested with the dosage form. In most bioavailability studies, 200–300 mL of water is given with the dose.

In the fed state, the lumenal composition in the stomach will be highly dependent on the composition of the meal ingested. A suitable starting point for design of a dissolution medium would be to homogenize the meal to be used in the clinical studies with the coadministered volume of water, and measure the pH, buffer capacity and osmolarity. A volume of oil reflecting the fat content of the meal can be added to an aqueous buffer simulating the afore-mentioned parameters, to produce an appropriate test medium. The use of long-life milk (63) and Ensure® (64) have been variously suggested as media suitable for simulating fed state in the stomach, in that they contain appropriate ratios of fat:protein:carbohydrate.

Intestinal Media

Key differences between gastric and intestinal conditions are the presence of bile and the higher pH value. Bile salts and lecithin facilitate the wetting of solids and the solubilization of lipophilic drugs (65) into mixed micelles. Thus, the dissolution of drugs may be enhanced considerably over the rate observed in plain aqueous solution. Sodium taurocholate was chosen as a representative bile salt because cholic acid is one of the most prevalent bile salts in human bile. Further, since the taurine conjugate has a very low pKa, there is little likelihood of precipitation or a change in the micellar size with minor variations in pH value. A suitable concentration of bile salt for simulating fasted state conditions would be between 3 and 5 mM (Table 13). Lecithin is present in an approximately 1:3 ratio with the bile salt, representative of the *in vivo* ratio which usually lies between 1:2 and 1:5.

Phosphate buffer is used as a substitute for the physiological buffer, bicarbonate, to avoid instability in the pH value due to reaction with oxygen. The pH value chosen is pH 6.8, which is generally representative of values measured from the mid-duodenum to the ileum (Table 3). Buffer capacity data (20) indicate that the buffer capacity in the fasted state is much lower than in the fed state or in the official dissolution medium, so the medium given in Table 13 is only lightly buffered. A volume of 500 mL would be consistent with the values reported in the literature for the volume in the fasted state.

Table 12. Dissolution Medium to Simulate Gastric Conditions in the Fasted State

HCl		0.01–0.05 N
Sodium Lauryl Sulfate		2.5 G
Sodium Chloride		2 G
Distilled Water	qs	1000 mL

Table 13. Medium Simulating Fasted State Conditions in the Small Intestine

KH_2PO4		0.029 M
NaOH	qs	pH 6.8
NaTaurocholate		5 mM
Lecithin		1.5 mM
KCl		0.22 M
distilled water	qs	1 L

pH = 6.8.
osmolarity 280–310 mOsm.
buffer capacity 10 ± 2 mEq/L/pH.

Many drugs that are very lipophilic (e.g. danazol, griseofulvin, BCS Class 2) are better absorbed when given with a meal than in the fasted state. Although changes in transit rate and increased volume in the fed state as well as specific food interactions may contribute to this increase, the increase in bile output could also be a key factor. The dissolution medium presented in Table 14 would be suitable for evaluating this effect. The medium contains acetate buffer instead of phosphate buffer, in order to achieve the higher buffer capacity and osmolarity while maintaining the lower pH value representative of fed state duodenal conditions. The taurocholate and lecithin are present in considerably higher concentrations than for the fasted state medium, and because of meal-induced secretions, a volume of up to 1 L would be reasonable.

After meal ingestion, fats and oils and their digestion products are also present, which may further modify the ability of some drugs to interact with the micelles (66). If the dosage form contains fatty excipients (e.g. some soft gelatin capsule formulations) and/or the drug is very lipophilic, it may therefore be worth considering the addition of mono- and diglycerides and lipase to the medium to simulate oily phase partitioning and digestion.

Duration of Dissolution Tests

The duration of the dissolution test must be tailored to not only the sites of absorption for the drug but also the timing of

Table 14. Medium Simulating Fed State Conditions in the Duodenum

Acetic acid		0.144 M
NaOH	qs	pH 5
NaTaurocholate		15 mM
Lecithin		4 mM
KCl		0.19 M
distilled water	qs	1L

pH = 5.
osmolarity 485–535 mOsm.
buffer capacity 76 ± 2 mEq/L/pH.

UM00011999
NOVARTIS EXHIBIT 1017
Novartis v. Regents, IPR2023-01346
Page 745 of 4460

administration. If a drug is best absorbed from the upper small intestine and is to be administered in the fasted state, dissolution tests in a medium simulating fasted gastric conditions with a duration of 15 to 30 minutes are appropriate. On the other hand, if a drug is administered with food, and well absorbed throughout the small intestine and proximal large intestine, a duration of as long as 10 hours (with appropriate changes to the composition of the medium) could be envisaged.

Perhaps the most common case, though, is that of a drug that is reasonably well absorbed in the small intestine but less well absorbed in the colon, and which is given under fasted state conditions. In order to allow 1–2 hours for absorption in the small intestine, dissolution of such a compound would need to be completed under gastric conditions in 15 to 30 minutes and/or under proximal small intestinal conditions in one hour. In these circumstances, criteria of 85% dissolved after fifteen minutes in a gastric medium; after a combination of fifteen minutes in a gastric medium and fifteen minutes in a medium representative of conditions in the proximal small intestine; or after thirty minutes in a medium representative of conditions in the proximal small intestine would all be reasonable.

Hydrodynamic Model

Overall, most of the data available regarding hydrodynamics in the GI tract are qualitative in nature and not conducive to interpretation in terms of being able to select a representative flow pattern for dissolution test apparatus. The ability of the conventional dissolution testers to simulate hydrodynamics and flow patterns in the GI tract is open to question, since the studies that have been used to compare the testers with the *in vivo* conditions have consisted mainly of empirical *in vivolin vitro* correlations. The recent work of Katori et al. (67), for example, indicated that for controlled release acetaminophen preparations, low agitation conditions correlated best with *in vivo* results. A lot more research in this area is sorely needed to establish suitable testing conditions for both immediate and controlled release products. In addition, the wide variety of mixing patterns found in the GI tract indicate that it is unlikely that a single setting (e.g. of flow rate or rotation speed) or apparatus can be used to simulate all motility conditions in the GI tract.

The flow-through tester is designed to simulate the flow patterns in the GI tract. Flow rates tend to be highest shortly after ingestion of a large volume of fluid into the stomach, and lowest during Phase I of motor activity in the stomach, and in the ileum. The flow rates suggested for application in the USP flow-through tester (1) are rather high (8 or 16 mL/min) compared to the physiological values, and unidirectional flow pattern is probably unrepresentative of the segmental mixing patterns in the small intestine and proximal colon. In the case of paddle and basket apparatus, the relationship between the hydrodynamics in the apparatus and those in the GI tract is even less clear. All-in-all, the simulation of the hydrodynamics in the GI tract is the remaining unknown in our quest to establish dissolution tests that are representative of the physiological conditions.

Summary

The parameters important to design of dissolution tests prognostic for *in vivo* dissolution behavior are the composition, volume and hydrodynamics of the dissolution medium and the duration of the test. Choice of dissolution test conditions should be based on where the drug is best absorbed in the gastrointestinal tract, and on whether it is to be dosed in the fed or fasted state. Although with our current knowledge of the physiology representative media can be selected to simulate gastric and intestinal conditions, and appropriate test durations can be chosen based on a knowledge of the drug's permeability profile in the gastrointestinal tract, the simulation of the in vivo hydrodynamics remains problematic and further research is needed in this area. Because of this deficiency, the dissolution test selected for a given product should be validated in terms of its ability to discriminate adequately between dosage forms that are not bioequivalent, as well as to exhibit similar release profiles for products that are bioequivalent.

ACKNOWLEDGMENTS

Support of this project by the FDA is gratefully acknowledged.

REFERENCES

1. The United States Pharmacopeia (USP 23). United States Pharmacopeial Convention, Inc., Rockville, MD (1995).
2. Guidance for Industry, *Immediate Release Solid Oral Dosage Forms, Scale-Up and Post-Approval Changes: Chemistry, Manufacturing and Controls, In Vitro Dissolution Testing, and In Vivo Bioequivalence Documentation*, CDER, Food and Drug Administration, USA, 1995.
3. *Dissolution Testing of Solid Oral Products:* Joint Report of the Section for Official Laboratories and Medicines Control Services and the Section of Industrial Pharmacists of the FIP, *Dissolution Tech.* 4:5–14 (1997).
4. P. Macheras, C. Reppas, and J. B. Dressman. *Biopharmaceutics of Orally Administered Dosage Forms*. Ellis Horwood Ltd., Series in Pharmaceutical Technology, Chichester, ISBN 0-13-108093-8, UK, 1995.
5. G. L. Amidon, H. Lennernäs, V. P. Shah, and J. R. A. Crison. Theoretical Basis for a Biopharmaceutic Drug Classification: The Correlation of *In Vitro* Drug Product Dissolution and *In Vivo* Bioavailability, *Pharm. Res.* 12:413–420 (1995).
6. H. Lennernäs, Ö. Ahrenstedt, R. Hällgren, L. Knutson, M. Ryde, and L. K. Paalzow. Regional Jejunal Perfusion, a New *In Vivo* Approach to Study Oral Drug Absorption in Man. *Pharm. Res.* 9:1243–51 (1992).
7. T. Gramatte. Die Lokalisationsabhängigkeit der Arzneistoffresorption im Dünndarm des Menschen. Shaker Verlag, Aachen, ISBN 3-8265-1435-1, Germany, 1996.
8. J. B. Dressman and D. Fleisher. Mixing-tank Model for Predicting Dissolution Rate Control of Oral Absorption. *J. Pharm. Sci.* 75:109–116 (1986).
9. H. W. Davenport. Intestinal Absorption of Water and Electrolytes, in: *Physiology of the Gastrointestinal Tract*. 5th. Edition, Chapter 13, Year Book Medical Publishers, Chicago ISBN 0-8151-2330-2, USA, 1982.
10. W. Nernst and E. Brunner. Theorie der Reaktionsgeschwindigkeit in Heterogenen Systemen. Z. Physik. Chem. 47:52–110 (1904).
11. V. G. Levich. *Physicochemical Hydrodynamics*, Englewood Cliffs, Prentice Hall, New Jersey, 1962.
12. A. S. Noyes and W. R. Whitney. The Rate of Solution of Solid Substances in Their Own Solutions. *J. Am. Chem. Soc.* 19:930–934 (1897).
13. J. B. Dressman, R. R. Berardi, L. C. Dermentzoglou, T. L. Russell, S. P. Schmaltz, J. L. Barnett, and K. Jarvenpaa. Upper Gastrointestinal pH in Young, Healthy Men and Women. *Pharm. Res.* 7:756–761 (1990).
14. T. L. Russell, R.R. Berardi, J. L. Barnett, L. C. Dermentzoglou, K. M. Jarvenpaa, S. P. Schmaltz, and J. B. Dressman. Upper Gastrointestinal pH in Seventy-nine Healthy, Elderly North American Men and Women. *Pharm. Res.* 10:187–196 (1993).

15. P. Christiansen. The Incidence of Achlorhydria in Healthy Subjects and Patients with Gastrointestinal Diseases. *Scand. J. Gastroenterology* 3:497–508 (1968).
16. H. Ogata, N. Aoyagi, A. Kaniwa, A. Ejima, K. Suzuki, T. Ishioka, M. Morishita, K. Ohta, Y. Takagishi, Y. Doi, and T. Ogura. Development and Evaluation of a New Peroral Test Agent GA-Test for Assessment of Gastric Acidity. *J. Pharmacobio-Dyn.* 7:656–664 (1984).
17. V. Gray and J. B. Dressman. Simulated Intestinal Fluid, TS-Change to pH 6.8. *Pharmacopeial Forum* 22: 1943–1945 (1996).
18. J. H. Cummings, E. W. Pomare, W. J. Branch, C. P. E. Naylor, and G. T. MacFarlane. Short Chain Fatty Acids in Human Large Intestine, Portal, Hepatic and Venous Blood. *Gut* 28: 1221–1227 (1987).
19. S. S. Ozturk, B. O. Palsson, and J. B. Dressman. Dissolution of Ionizable Drugs in Buffered and Unbuffered Solutions. *Pharm. Res.* 5:550–565 (1988).
20. D. G. Greenwood. *Small Intestinal pH and Buffer Capacity: Implications for Dissolution of Ionizable Compounds*, Doctoral Thesis, University of Michigan, Ann Arbor, Michigan, USA, 1994.
21. P. Finholt and S. Solvang. Dissolution Kinetics of Drugs in Human Gastric Juice: The Role of Surface Tension. *J. Pharm. Sci.* 57:1322–1326 (1968).
22. G. P. van Berge Henegouwen and A. F. Hofmann. Nocturnal Gallbladder Storage and Emptying in Gallstone Patients and Healthy Subjects. *Gastroenterology*, 75: 879–885 (1978).
23. A. Tangerman, A. van Schaik, and E. W. van der Hoek. Analysis of Conjugated and Unconjugated Bile Acids in Serum and Jejunal Fluid of Normal Subjects. *Clin. Chim. Acta* 159:123–132 (1986).
24. T. L. Peeters, G. Vantrappen, and J. Janssens. Bile Acid Output and the Interdigestive Micgrating Motor Complex in Normals and in Cholecystectomy patients. *Gastroenterology* 79:678–681 (1980).
25. L. Marzio, M. Neri, F. Capone, F. Di Felice, C. De Angelis, A. Mezzeti, and F. Cuccurullo. Gallbladder Contraction and Its Relationship to Interdigestive Duodenal Motor Activity in Normal Human Subjects. *Dig. Dis. Sci.* 33:540–544 (1988).
26. H. W. Davenport. Secretion of the Bile, in: *Physiology of the Gastrointestinal Tract*, 5th. Edition, Chapter 11, Year Book Medical Publishers, Chicago, ISBN 0-8151-2330-2, USA, 1982.
27. B. Borgstrom, A. Dahlqvist, G. Lundh, and J. Sjovall. Studies of Intestinal Digestion and Absorption in the Human, *J. Clin. Invest.* 36:1521–1536 (1957).
28. J. Sjovall. On the Concentrations of Bile Acids in the Human Intestine During Absorption. *Acta Physiol. Scand.* 46:339–345 (1959).
29. O. Fausa. Duodenal Bile Acids After a Test Meal. *Scand. J. Gastroenterol.* 9:567–570 (1974).
30. M. Rautureau, A. Bissali, and J.-C. Rambaud. Bile Salts and Lipids in Aqueous Intraluminal Phase During the Digestion of a Standard Meal in a Normal Man. *Gastroenterol. Clin. Biol.* 5:417–425 (1981).
31. T. E. Solomon. Exocrine Pancreas: Pancreatitis, Unit 16 in: *Undergraduate Teaching Series (American Gastroenterological Association)*, Milner-Fenwick Inc., Maryland, 1984, USA.
32. A. S. Uch and J. B. Dressman. Improving Bioavailability by Colonic Administration, in: *Formulation of Poorly-Available Drugs for Oral Administration (Minutes of the European Symposium)*, Editions de Sante, Paris, ISBN 2-86411-096-2, 1996.
33. H. Bronsted and J. Kopecek. Hydrogels for site-specific drug delivery to the colon: *in vitro* and *in vivo* degradation. *Pharm. Res.* 9:1540–1545 (1992).
34. J. Kopecek, P. Kopeckova, H. Bronsted, R. Rathi, B. Rihova, P.-Y. Yeh, and K. Ikesue. Polymers for colon-specific drug delivery. *J. Controlled Release* 19:121–130 (1992).
35. G. Van de Mooter, C. Samyn, and R. Kinget. Azo Polymers for colon-specific drug delivery. *Int. J. Pharm.* 87:37–46 (1992).
36. H. W. Davenport. Gastric Motility and Emptying, in: *Physiology of the Gastrointestinal Tract*, 5th. Edition, Chapter 4, Year Book Medical Publishers, Chicago, ISBN 0-8151-2330-2, USA, 1982.
37. K. Diem and C. Lentner. Documentia Geigy: Scientific Tables, Geigy Pharmaceuticals, Seventh Edition p. 651, Ardsley, New York, 1970.
38. R. L. Dillard, H. Eastman, and J. S. Fordtran. Volume-Flow Relationship During the Transport of Fluid Through the Human Small Intestine. *Gastroenterology* 49:58–66 (1965).
39. J. S. Fordtran and T. Locklear. Ionic Constituents and Osmolarity of Gastric and Small Intestinal Fluids After Eating. *Am. J. Dig. Dis.* 11:503–521 (1966).
40. D. W. Powell. Intestinal Water and Electrolyte Transport, in: *Physiology of the Gastrointestinal Tract*, 2nd. Edition, Chapter 46, Ed. LR Johnson, Raven Press, New York, 0-88167-282-3, USA, 1987.
41. T. R. Hendrix, D. O. Castell, and J. D. Wood. Alimentary Tract Motility; Stomach, Small Intestine, Colon and Biliary Tract, Unit 10B in: *Undergraduate Teaching Series (American Gastroenterological Association)*, Milner-Fenwick Inc., Maryland, 1987, USA.
42. M. G. Sarr, K. A. Kelly, and S. F. Phillips. Canine Jejunal Absorption and Transit During Interdigestive and Digestive Motor States. *Am. J. Physiol.* 239:G167–G172 (1980).
43. H. S. Wiggins and J. H. Cummings. Evidence for the Mixing of Residue in the Human Gut. *Gut* 17:1007–1011 (1976).
44. W. Brener, T. R. Hendrix, and P. R. McHugh. Regulation of the Gastric Emptying of Glucose. *Gastroenterology* 85:76–82 (1983).
45. R. L. Oberle, T.-S. Chen, C. Lloyd, J. L. Barnett, C. Owyang, J. Meyer, and G. L. Amidon. The Influence of the Interdigestive Migrating Myoelectric Complex on the Gastric Emptying of Liquids. *Gastroenterology* 99:1275–1282 (1990).
46. P. Kerlin, A. Zinsmeister, and S. Phillips. Relationship of Motility to Flow of Contents in the Human Small Intestine. *Gastroenterology* 83:701–706 (1982).
47. F. Hoelzel. The Rate of Passage of Inert Materials Through the Gastrointestinal Tract. *Am. J. Physiol.* 92:466–497 (1930).
48. V. A. John, P. A. Shotton, J. Moppert, and W. Theobold. Gastrointestinal Transit of Oros® Drug Delivery Systems in Healthy Volunteers: A Short Report. Br. J. Clin. Pharmacol. 19:203S–206S (1985).
49. P. J. Howard and R. C. Heading. The Role of Oesophageal Transit in Relation to Drug Delivery, in: *Drug Delivery to the Gastrointestinal Tract*, Hardy JG, Davis SS, Wilson CG (Editors), Chapter 2, Ellis Horwood, Chichester, ISBN 0-7458-0656-2, UK, 1989.
50. E. Hunter, J. T. Fell, and H. Sharma. The Gastric Emptying of Pellets Contained in Hard Gelatin Capsules. *Drug Dev. Ind. Pharm.* 8:751–757 (1982).
51. U. E. Jonsson, M. Alpsten, C. Bogentoft, R. Eriksson, and J. Sjögren. Gastric Emptying of Pellets and Tablets in Healthy Subjects Under Fasting and Nonfasting Conditions. 10th International Symposium on the Controlled Release of Bioactive Materials (CRS), p. 241 (1983).
52. J. H. Meyer, J. Elashoff, V. Porter-Fink, J. Dressman, and G. L. Amidon. Human Postprandial Gastric Emptying of 1–3 Millimeter Spheres. *Gastroenterology* 94:1315–1325 (1988).
53. R. A. Hinder and K. A. Kelly. Canine Gastric Emptying of Solids and Liquids. *Am. J. Physiol.* 233:E335–E340 (1977).
54. M. C. Theodorakis, G. A. Digenis, R. M. Beihn, M. B. Shambhu, and F. H. DeLand. Rate and Pattern of Gastric Emptying in Humans Using ^{99m}Tc-Labeled Triethylenetetraamine-Polystyrene Resin. *J. Pharm. Sci.* 69:568–571 (1980).
55. R. K. Blythe, G. M. Grass, and D. R. MacDonnell. The Formulation and Evaluation of Enteric Coated Aspirin Tablets. *Am. J. Pharm.* pp. 206–216 (1959).
56. J. G. Moore, P. E. Christian, and R. E. Coleman. Gastric Emptying of Varying Meal Weight and Composition in Man. Evaluation by Dual Liquid- and Solid-Phase Isotopic Method. *Dig. Dis. Sci.* 26:16–22 (1981).
57. S. S. Davis, J. G. Hardy, M. J. Taylor, D. R. Whalley, and C. G. Wilson. A Comparative Study of the Gastrointestinal Transit of a Pellet and Tablet Formulation. *Int. J. Pharm.* 21:167–177 (1984).
58. J.-R. Malagelada, J. S. Robertson, M. L. Brown, M. Remington, J. A. Duenes, G. M. Thomforde, and P. W. Carryer. Intestinal Transit of Solid and Liquid Components of a Meal in Health. *Gastroenterology* 87:1255–1263 (1984).
59. S. S. Davis, J. G. Hardy, and J. W. Fara. Transit of Pharmaceutical Dosage Forms Through the Small Intestine. *Gut* 27:886–892 (1986).
60. C. G. Wilson and N. Washington. *Physiological Pharmaceutics-BiologicalBbarriers to Drug Absorption*, Chapter 6, Ellis Hor-

UM00012001
NOVARTIS EXHIBIT 1017
Novartis v. Regents, IPR2023-01346
Page 747 of 4460

wood Series in Pharmaceutical Technology, Chichester, ISBN 0-7458-0543-4, UK, 1989.
61. C. G. Wilson. Physiology of the GI Tract-Issues for the Absorption of Poorly-Soluble Drugs, in: *Formulation of Poorly-Available Drugs for Oral Administration (Minutes of the European Symposium)*, Editions de Sante, Paris, ISBN 2-866411-096-2, France, 1996.
62. M. Efentakis and J. B. Dressman. Gastric Juice as a Dissolution Medium: Surface Tension and pH. *Eur. J. Drug Metab. Pharmacokin.* (in press).
63. P. Macheras, M. Koupparis, and E. Apostelelli. Dissolution of Four Controlled-Release Theophylline Formulations in Milk. *Int. J. Pharm.* **36**:73–79 (in press).
64. L. J. Ashby, A. E. Beezer, and G. Buckton. *In Vitro* Dissolution Testing of Oral Controlled Release Preparations in the Presence of Artificial Foodstuffs. I. Exploration of Alternative Methodology: Microcalorimetry. *Int. J. Pharm.* **51**:245–251 (1989).
65. S. D. Mithani, V. Bakatselou, C. N. TenHoor, and J. B. Dressman. Estimation of the Increase in Solubility of Drugs as a Function of Bile Salt Concentration. *Pharm. Res.* **13**:163–167 (1996).
66. C. M. O'Driscoll. Micellar Solubilization (Self-emulsifying Systems for Improved Absorption of Drugs), in: *Formulation of Poorly-Available Drugs for Oral Administration (Minutes of the European Symposium)*, Editions de Sante, Paris, ISBN 2-866411-096-2, France, 1996.
67. N. Katori, N. Aoyagi, and T. Terao. Estimation of Agitation Intensity in the Gi Tract in Humans and Dogs Based on *In Vitro-In Vivo* Correlation. *Pharm. Res.* **12**:237–243 (1995).

Soft elastic gelatin capsules: a unique dosage form

WILLIAM R. EBERT

THE TECHNOLOGY for manufacturing soft elastic gelatin (SEG) capsules has come a long way since the middle of the 19th century, when this dosage form was produced in leather molds. In fact, the rotary die method, introduced in 1933 as an alternative to the plate process, was the first continuous method of encapsulation to be implemented by the industry. (Refinements of this system have since made the process completely automatic.)

The original rotary die machine is now housed in the Smithsonian Institute in Washington, D.C. (Figure 1). Various aspects of the modern version are shown in Figures 2, 3, and 4. As is illustrated in Figure 2, two tanks are hung over the encapsulation machine, one containing the mass of molten gelatin, the other containing liquid fill material. The molten gelatin flows simultaneously through two spreader boxes and over two cool casting drums, where gelatin ribbons are formed and fed to the die rolls. Accurately metered volumes of liquid fill material are injected between the gelatin ribbons through the wedge seen in Figure 3. The injection of the liquid forces the gelatin ribbon to expand into the die pockets that determine the capsule shape. The capsule, heat sealed and automatically cut out between the two dies, is transported through a naphtha wash cycle and thence through infrared drying baskets. Final drying is accomplished by spreading the capsules in trays and drying them at a relative humidity of approximately 20%. When sufficiently dry, they are inspected for possible "leakers" (Figure 5), graded according to size specifications (Figure 6), and packaged for distribution in bulk shippers.

Prior to the invention of the rotary die process, the SEG capsule was held to be of no particular value as a dosage form. For one thing, it could not be filled with accuracy beyond ±20%. Furthermore, poor yields rendered this process uncommercial. Today, the rotary die process achieves a fill accuracy of ±1-3%. Yields are in the range of 98%-99% of theory. Hence, the SEG capsule competes costwise with both sugarcoated tablets and two-piece hard-shell capsules.

The Capsule Fill

The Scherer process described herein is designed to fill liquids only. These may be suspensions of the drug or other solid material in vehicles such as vegetable or mineral oils, triglycerides, glycols such as polyethylene glycols and pro-

UM00012003
NOVARTIS EXHIBIT 1017
Novartis v. Regents, IPR2023-01346
Page 749 of 4460

pylene glycol, surfactants such as polysorbates, or combinations of these. Solutions of the solid in oils, glycols, triglycerides, surfactants, and combinations of these are also widely employed. Drugs, vitamins, and other materials that naturally occur as liquids are ideally suited for SEG encapsulation; two or more miscible liquids may also be encapsulated. There are, of course, limitations to the use of certain vehicles. Some of these are indicated in Table I. Other limitations to be observed include the following:

pH. Liquid pH should not be below 2.5 or above 7.5. Acids hydrolyze gelatin and will cause leaking, while alkalis cause gelatin to tan, which decreases the solubility of the shell.

Emulsions. All emulsions, whether oil/water or water/oil, will eventually "break," thereby releasing water, which will dissolve the gelatin shell.

Aldehydes. These compounds will tan gelatin, affecting its solubility.

Salts of strong acids and bases. This category includes sodium, potassium ammonium, choline chlorides, etc. – all destructive to the gelatin shell.

Miscellaneous. Compounds that readily hydrolyze – aspirin, for example – are not stable.

Solids dispersed in a liquid must have a particle size that does not exceed 80 mesh, for the encapsulation equipment will not function properly with coarser matter. This particle size will generally produce a relatively stable suspension – a requisite in achieving good content uniformity throughout the batch. Of course, in order to obtain optimal content uniformity of a drug, the best possible liquid form is a true solution. This form cannot always be achieved, however, since it is often not possible to dissolve the drug in a volume of solvent small enough to produce a capsule that is appropriate from the standpoints of economics and patient acceptance.

Vehicle	Limitations
1. Water-immiscible, volatile, and nonvolatile liquids:	None
Vegetable oils	
Aromatic oils	
Aromatic and aliphatic hydrocarbons	
Chlorinated hydrocarbons	
Ethers	
Esters	
Alcohols	
Organic acids	
2. Water-miscible, nonvolatile liquids:	None
Polyethylene glycols	
Nonionic surfactants	
3. Miscellaneous:	
Glycerin	Not more than about 5–10%
Propylene glycol	Not more than about 5–10%
Water	Not more than about 5%
Low-molecular-weight alcohols, ketones, acids, amines, esters	Not more than about 5%

Table I: SEG-capsule vehicles.

The rotary die process depends upon gravity fill at a temperature of 35°C or less. This parameter is quite important, as the sealing temperature on the wedge is between 37° and 40°C. Though liquids with a wide range of viscosity – 0.222–3000 cp at 25°C – may be satisfactorily encapsulated, there are materials whose viscosity is within the appropriate range but which cannot be encapsulated because their tackiness will cause binding in the pumps and valves. Some solids in suspension will also cause problems in the filling operation. When this occurs, the problem can generally be overcome through proper formulation.

Calculation of fill volumes begins with determining the specific gravity of the liquid to be encapsulated. This in turn determines the capsule size for a preselected shape. Each capsule size and shape has a known fill-volume range, enabling the formulator to select the size most suitable for his formulation. For obvious reasons of economy, the object is to use the smallest capsule size possible.

While the capsules are drying, water from the gelatin shell will migrate into the fill material and then return to the shell; in this process, a certain amount of water will be retained by the fill material. The extent of this water retention depends upon the nature of the fill material. For example, a water-miscible fill can retain up to 5% of its weight – a fact that should be considered when the fill volume of formulations containing a water-miscible vehicle is being calculated. Hydrophilic solids will also retain water – as much as 3% of the weight of the solid(s). It is therefore obvious that readily hydrolyzed materials (aspirin, for example) are not good candidates for SEG encapsulation.

In the formulation of suspension-type fill materials, base absorption of the solid is the first property that must be determined. *Base absorption* is defined as the number of grams of liquid base required to produce a capsulatable mixture when mixed with one gram of solid(s). Base absorption is affected by various parameters – physical state, particle size and shape, moisture content, hydrophilic or lipophilic nature, etc. Therefore, the physical parameters must be clearly defined once the base absorption for the solid(s) has been determined. Otherwise, the flow characteristics of the formulation could vary from lot to lot, presenting difficulties in the encapsulation process.

As is the case with all suspensions, SEG-capsule suspension fills require a suspending agent (1) to ensure homogeneity of the capsule contents throughout the batch (content uniformity), and (2) to ensure good flow characteristics of the liquid during encapsulation. Waxes such as beeswax, paraffin wax, stearates, and cellulose derivatives are employed as suspending agents in oil suspensions. In nonoil suspensions, polyethylene glycols, poloxamers, glycol esters, and acetylated monoglycerides of various molecular weights are generally used.

The Gelatin Shell

Gelatin shell formulations should be chosen in accordance with the product's application. Many are available. Alterations of the formula result in varying degrees of

UM00012004
NOVARTIS EXHIBIT 1017
Novartis v. Regents, IPR2023-01346
Page 750 of 4460

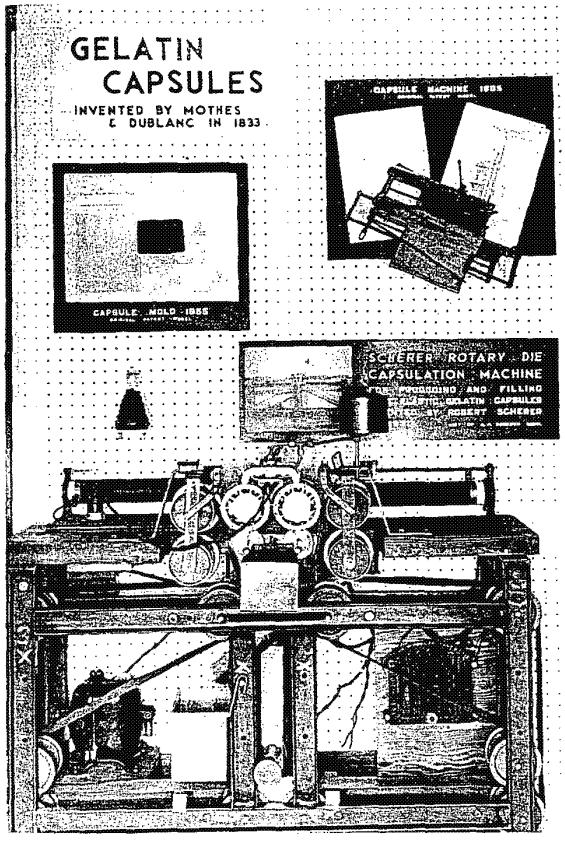


Figure 1: Original rotary die encapsulation machine, on display at the Smithsonian Institute, Washington, D.C.

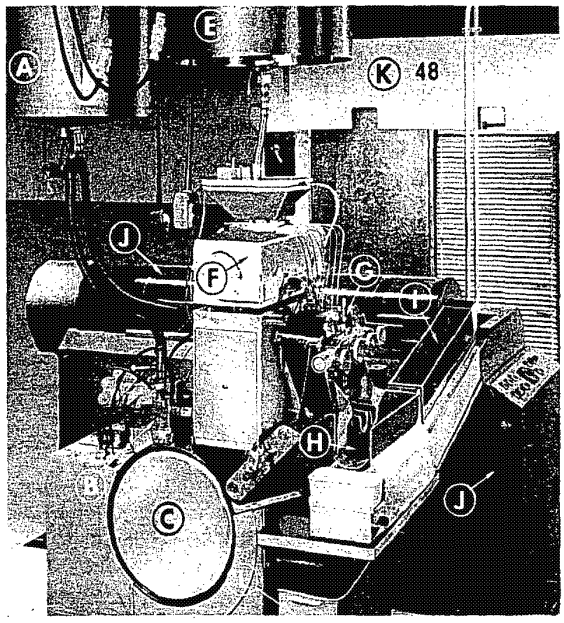


Figure 2: Molten gel mass in tank (A) flows through tubes to spreader box (B) onto gelatin-ribbon casting drums (C). There gelatin is cooled and formed into ribbons that pass through mineral-oil lubricant bath (D) to the encapsulation mechanism (G). Liquid fill material in other tank (E) flows through tube to filling pump (F) and thence to the encapsulation mechanism (G). Filled capsules drop onto capsule conveyor (H) and are carried to capsule washer (I), then to infrared dryer (J), and finally to capsule-drying tunnel (K). Gelatin net falls in gelatin-net receiver (L).

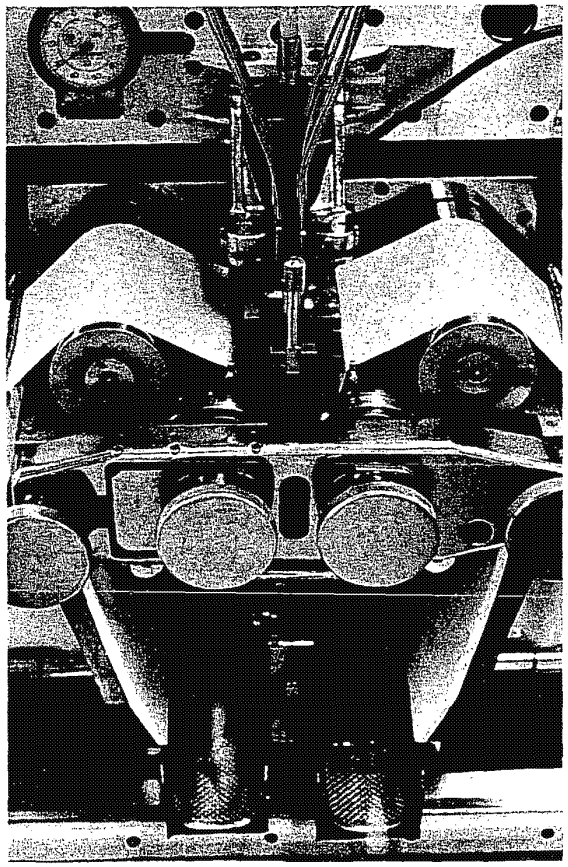


Figure 3: R.P. Scherer rotary die encapsulation machine showing gelatin ribbons, die rolls, and the wedge through which the liquid fill material is injected into the die pockets.

UM00012005
NOVARTIS EXHIBIT 1017
Novartis v. Regents, IPR2023-01346
Page 751 of 4460

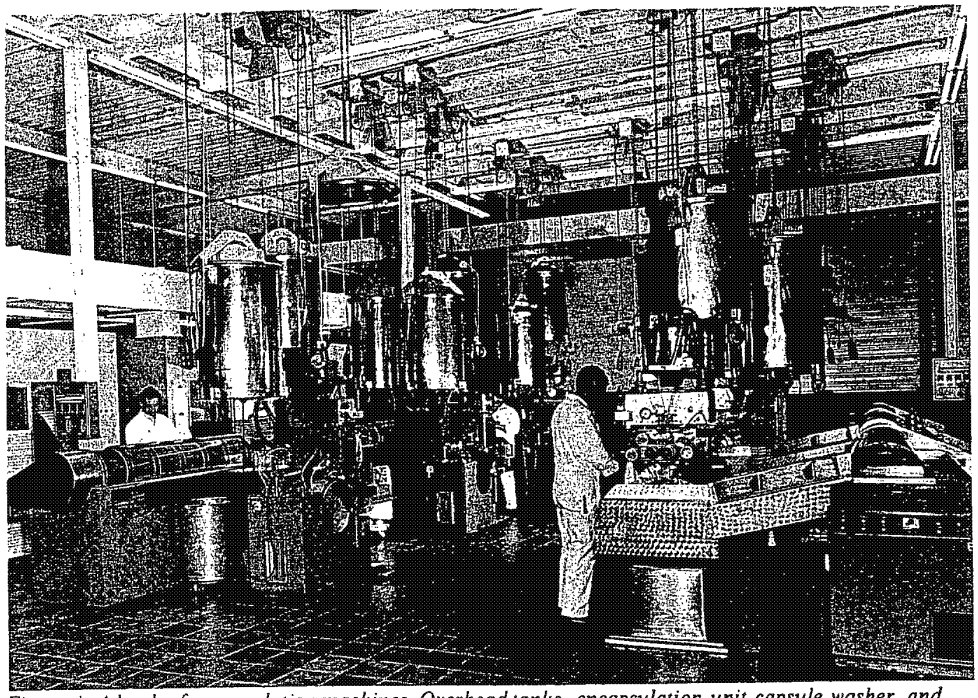


Figure 4: A bank of encapsulation machines. Overhead tanks, encapsulation-unit capsule washer, and infrared drying baskets are seen.

Figure 5: Inspection of finished capsules under a black-light unit.



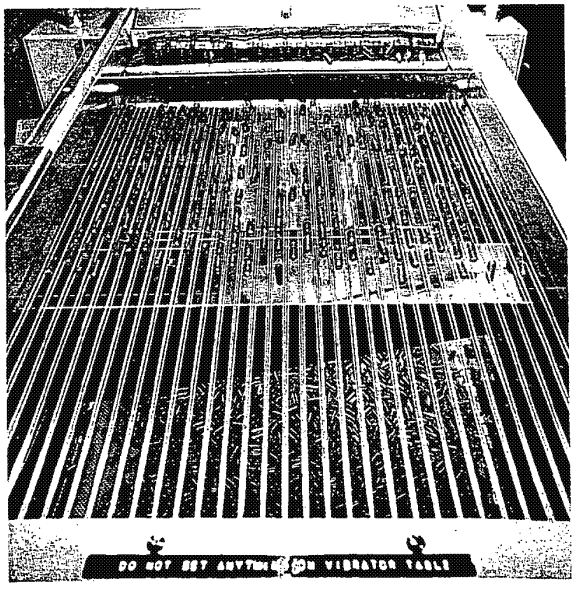


Figure 6: SEG capsules being graded to specifications prior to packaging.

UM00012006
NOVARTIS EXHIBIT 1017
Novartis v. Regents, IPR2023-01346
Page 752 of 4460

plasticity, hard, medium, and soft. The basic ingredients are gelatin, a plasticizer, and water. To obtain the desired properties, the gelatin type and the amounts of plasticizer and water are varied. By gelatin type, we mean the Bloom or gel strength, a measure of the strength – proportional to the molecular weight of the gelatin – of the cross-linking between gelatin molecules. Without a plasticizer, the gelatin shell would be too brittle; therefore, various amounts of plasticizer are added to obtain the degree of plasticity desired. The plasticizers employed are glycerin, sorbitol, and propylene glycol.

Since gelatin can serve as a nutrient medium for microorganisms, a preservative system must be employed. Commonly used preservatives are methyl- and propylparabens and sorbic acid.

FD&C-certified dyes are used when color is desired. If a capsule is to be opaque, titanium dioxide is the opacifier of choice.

It is of course possible to include drugs in the makeup of the shell itself, as well as such flavoring agents as vanillin and volatile oils (menthol, peppermint oil, anethole, etc.).

The Products

The rotary die process allows for a wide choice of size and shape: round, oval, oblong, tube, and suppository. Other shapes can be produced for special applications.

Oral dosage forms are generally formulated so that the heat-seal seam of the gelatin shell opens to release its liquid medication into the stomach less than 5 min after ingestion. However, it is possible to render the gelatin shell enteric so that the capsule will resist gastric juices and pass intact from the stomach to the intestines, where it will release its contents for intestinal absorption. It is also possible to formulate the gelatin shell and its contents so as to produce a palatable chewable product such as a cough capsule, an antacid capsule, an anti-motion-sickness capsule, etc.

Suppositories, both rectal and vaginal, are often produced in the SEG-capsule form. They offer many advantages over conventional molded suppositories designed to melt slowly in body cavities. Molded suppository capsules have bases of polyethylene glycols or of fats and waxes. Since these suppositories melt at body temperature, they must also be protected from melting during storage. In fact, refrigeration is recommended, and costly packaging is generally employed to ensure a reasonable shelf life. An SEG-capsule suppository, on the other hand, does not depend upon heat in order to release its medication. It is the moisture in the body cavity that causes the suppository to come apart at its heat-sealed seam and release its liquid medication. Since this form does not melt at body temperature, it need not be refrigerated during storage; consequently, less costly packaging is required.

A number of veterinary SEG-capsule products are produced – notably, products containing anthelmintics such as dichlorophene, toluene, and butyl chloride. Since these are all organic liquids, they cannot be tableted; nor can they be encapsulated in two-piece hard-shell capsules. These and many other materials that present the same limitations are ideally suited to the SEG capsule. Examples would be alpha-tocopheryl acetate (a vitamin E supplement), which is a liquid; chloral hydrate (a sedative-hypnotic), which is hygroscopic; clofibrate (an anticholesteremic), which is a liquid; and guaifenesin (an expectorant), whose melting point is too low for tableting.

The tube-shaped SEG capsule is used for such special applications as ophthalmic and otic ointments, topical and rectal ointments, veterinary mastitis ointments, etc.

Other special applications include encapsulation of cosmetics such as bath oils, shampoos, and suntan oils. Use in industrial products – paint capsules, ether capsules, room-deodorant capsules, toilet-sanitizing capsules, etc. – is also widespread.

Stability

Oxidation. Since air is excluded during the processing of SEG capsules, and since the gelatin shell offers an excellent barrier to oxygen,[1] oxidation of the fill material is negligible. Hence, vitamins – many of which are susceptible to loss in potency due to oxidation – are generally produced in SEG-capsule form. Vitamins, multivitamins, and multivitamins with minerals can be produced with shelf lives exceeding those attainable for tablets. Any material whose potency would be adversely affected by oxidation is an excellent candidate for SEG encapsulation.

Photosensitivity. As mentioned earlier, the gelatin shell can be rendered opaque by means of the opacifier titanium dioxide. In this manner, photosensitive drugs or other materials may be protected from light.

Bioavailability and Content Uniformity

The pharmaceutical literature of the past decade has shown notable preoccupation with the subject of bioavailability of oral dosage forms. Probably no other area has been more comprehensively studied than this; and rightly so, since it deals with the most important parameters of a dosage form – i.e., the rate and extent of drug absorption after administration. Many factors influence these parameters, including drug-particle size, drug form, and dosage-form adjuvants (binders, lubricants, disintegrants, suspending agents, etc.). Drugs that are poorly soluble in water are often beset by bioavailability problems. This likelihood is increased if the drug's median effective dose and median lethal dose are not far apart (i.e., if the drug has a low therapeutic index) and if the median effective dose is low. This problem is compounded by the fact that it is technically difficult to distribute a very small amount of a drug uniformly throughout a batch of tablets and therefore to obtain an acceptable level of content uniformity from tablet to tablet. A good example of a relatively water-insoluble drug whose dose is very small and whose therapeutic index is low is the cardiac glycoside digoxin. This drug is commercially available in tablets of 0.0625, 0.125, and 0.25 mg. A pediatric liquid is also available, but it is the tablet that causes concern. Studies over the past several years have shown that many brands on the market had bioavailability and/or content-uniformity problems which have since been resolved through the efforts of the Food and Drug Administration and the United States Pharmacopeia. Nevertheless, these products at best exhibit an absorption of only about

UM00012007
NOVARTIS EXHIBIT 1017
Novartis v. Regents, IPR2023-01346
Page 753 of 4460

75%–80% of the drug administered. We at Scherer theorized that if we could formulate digoxin in a solution that would not dissolve the gelatin shell, we might obtain a product whose digoxin was absorbed 100% and whose content uniformity was superior to that achievable by tableting technology. It seemed that both of these objectives could be attained if the digoxin were in a true solution rather than in a heterogeneous tablet-powder mixture. We found that we could dissolve digoxin in a solution containing polyethylene glycol 400, USP (89.4% w/w); alcohol, USP (6.5% w/w); propylene glycol, USP (3.4% w/w); and purified water, USP (0.6% w/w).

Capsules containing 0.05 mg, 0.10 mg, and 0.20 mg of digoxin were submitted to various investigators to be tested for bioavailability. Interesting and unexpected results were obtained. Binnion et al. compared the blood levels obtained in human volunteers when administered the SEG capsules to blood levels obtained after administration of brand-name tablets or of a nonencapsulated solution of digoxin.[2] These investigators found that the SEG-capsule product was better absorbed than either the tablets or the solution, and concluded that the SEG digoxin capsule was the most effective preparation of digoxin available for oral ingestion.

Mallis et al. carried out both single- and multiple-dose crossover studies in human volunteers.[3] Their test preparations were (1) digoxin SEG capsules, (2) digoxin tablets with a 78% dissolution rate, (3) digoxin tablets with a 97% dissolution rate, (4) digoxin solution, and (5) digoxin elixir. No difference in bioavailability was found between the two tablet products; the solution and the elixir were found to be superior to the tablets; and the SEG capsules proved to be even superior to the elixir and the solution. These authors suggested that the SEG digoxin capsule preparation deserved to be considered as a replacement for the tablets currently being marketed.

Marcus et al. also conducted a comparative bioavailability study of digoxin preparations, using (1) digoxin SEG capsules, (2) digoxin tablets, (3) digoxin solution, and (4) digoxin intravenous preparation.[4] Again it was found that bioavailability of the SEG-capsule product was superior to both tablets and solution. Binnion,[5] Johnson et al.,[6] Ghirardi et al.,[7] Lindenbaum,[8] and Johnson et al.[9] all confirmed the superiority of the digoxin SEG-capsule dosage form over commercially available tablets.

The most surprising finding in all of these studies was that the SEG digoxin capsules exhibited a more rapid and complete absorption than did the same solution not encapsulated. This phenomenon has yet to be explained. We can, however, theorize that due to the rapid rupture of the SEG capsule in the stomach, the entire digoxin dosage is instantaneously presented to the absorption site, creating a high concentration gradient which drives the digoxin quickly and completely through the stomach mucosal cells for transport to the blood. Ingestion in SEG-capsule form may also prevent degradation of digoxin in the stomach prior to absorption, while oral administration of the solution might cause the digoxin to be dispersed throughout the esophagus and stomach. This theory has yet to be proved, however.

In any event, the studies with digoxin demonstrate that it is possible to improve the bioavailability of a drug – and therefore to reduce the usual dosage – through SEG encapsulation. In the case of digoxin, a dose reduction of 20% can be achieved without altering the therapeutic effect. This is of significant importance, especially when the drug is relatively toxic, as is digoxin. Surely, current investigations into the nature of this dosage form will uncover other similar situations.

As has already been mentioned, the SEG-capsule dosage form is ideally suited to encapsulation of materials that are impossible or difficult to produce in tablet or two-piece hard-shell gelatin capsules. This category includes those materials whose natural form is a liquid, those that will readily pick up water during processing (hygroscopic materials), and those whose melting points are too low to allow for the heat generated by compression into tablets. Further advantages should also be mentioned:

1. Since the fill material is protected by the gelatin shell, bad-tasting substances are rendered completely palatable.
2. For the same reason that objectionable taste is masked by the gelatin shell, so are objectionable odors.
3. When moistened by saliva, an SEG capsule is easier to swallow than a compressed tablet of the same size. In fact, it is less difficult to swallow a rather large SEG capsule than a smaller tablet. This makes things considerably less complicated for the formulator who is dealing with a drug whose dose is large (e.g., 250 mg or more).
4. There can be little argument about the brilliance and elegance of an SEG capsule.

Considering the virtues of this dosage form, it is hardly surprising that each year more and more SEG-capsule preparations appear among the products of the food, drug, cosmetic, and other industries.

References

1. Hom, F.S., Veresh, S.A., and Ebert, W.R., "Soft Gelatin Capsules II: Oxygen-Permeability Study of Capsule Shells," *J. Pharm. Sci.*, Vol. 64, No. 5, 1975, pp. 851–857.
2. Binnion, P.F., and Klopp, R.W., "Improving the Bioavailability of Digoxin," *Lancet*, Vol. 1, 1975, pp. 1422–1423.
3. Mallis, G.I., Schmidt, D.H., and Lindenbaum, J., "Superior Bioavailability of Digoxin Solution in Capsules," *Clin. Pharmacol. Ther.*, Vol. 18, No. 6, 1975, pp. 761–768.
4. Marcus, F.I., Dickerson, J., Pippin, S., Stafford, M., and Bressler, R., "Digoxin Bioavailability: Formulations and Rates of Infusion," *Clin. Pharmacol. Ther.*, Vol. 20, No. 3, 1976, pp. 253–259.
5. Binnion, P.F., "A Comparison of the Bioavailability of Digoxin in Capsule, Tablet, and Solution Taken Orally with Intravenous Digoxin," *J. Clin. Pharmacol.*, Vol. 16, No. 10, 1976, pp. 461–467.
6. Johnson, B.F., Bye, C., Jones, G., and Sabey, G.A., "A Completely Absorbed Oral Preparation of Digoxin," *Clin. Pharmacol. Ther.*, Vol. 19, 1976, pp. 746–751.
7. Ghirardi, P., Catenazzo, G., Mantero, O., Merotti, G.C., and Marzo, A., "Bioavailability of Digoxin in a New Soluble Pharmaceutical Formulation in Capsules," *J. Pharm. Sci.*, Vol. 66, No. 2, 1977, pp. 267–269.
8. Lindenbaum, J., "Greater Bioavailability of Digoxin Solution in Capsules: Studies in the Postprandial State," *Clin. Pharmacol. Ther.*, Vol. 21, No. 3, 1977, pp. 278–282.
9. Johnson, B.F., Smith, G., and French, J., "The Comparability of Dosage Regimens of Lanoxin Tablets and Lanoxicaps," *Br. J. Clin. Pharmac.*, Vol. 4, 1977, pp. 209–211.

UM00012008
NOVARTIS EXHIBIT 1017
Novartis v. Regents, IPR2023-01346
Page 754 of 4460

This Page is Inserted by IFW Indexing and Scanning Operations and is not part of the Official Record

BEST AVAILABLE IMAGES

Defective images within this document are accurate representations of the original documents submitted by the applicant.

Defects in the images include but are not limited to the items checked:

- ☐ BLACK BORDERS
- ☐ IMAGE CUT OFF AT TOP, BOTTOM OR SIDES
- ☐ FADED TEXT OR DRAWING
- ☐ BLURRED OR ILLEGIBLE TEXT OR DRAWING
- ☐ SKEWED/SLANTED IMAGES
- ☐ COLOR OR BLACK AND WHITE PHOTOGRAPHS
- ☐ GRAY SCALE DOCUMENTS
- ☐ LINES OR MARKS ON ORIGINAL DOCUMENT
- ☐ REFERENCE(S) OR EXHIBIT(S) SUBMITTED ARE POOR QUALITY
- ☐ OTHER: _____

IMAGES ARE BEST AVAILABLE COPY.
As rescanning these documents will not correct the image problems checked, please do not report these problems to the IFW Image Problem Mailbox.

Eur J Clin Pharmacol (1991) 41: 573–578

European Journal of Clinical Pharmacology
© Springer-Verlag 1991

In vitro forecasting of drugs which may interfere with the biotransformation of midazolam*

M.-P. Gascon and P. Dayer

Division of Clinical Pharmacology, University Hospital, Geneva, Switzerland

Received: February 14, 1990/Accepted in revised form: November 22, 1990

Summary. The biotransformation of midazolam is mediated by a cytochrome P-450 isozyme (P-450 IIIA) whose activity is highly variable. The kinetics of the 1′- and 4-hydroxylation of midazolam, the major routes of midazolam oxidation, by human liver microsomes have been examined to characterize further the cytochrome isozyme(s) catalysing these reactions, and to screen for drugs that might interfere with them.

In hepatic microsomal preparation from two kidney donors (extensive and poor metabolisers of debrisoquine) K_M values for 1′-hydroxylation were 4.2 and 6.1 μM (extensive and poor metabolisers, respectively), and for the 4-hydroxylation they were 14.7 and 18.1 μM, respectively. The corresponding V_{max} values were 25.8 and 29.8 and 17.0 and 18.1 nmol · mg $P^{-1} \cdot h^{-1}$. Both reactions appeared to be catalysed by the same or by coregulated isozymes.

Midazolam hydroxylations in vitro are inhibited by many drugs, including nifedipine and other dihydropyridine-type calcium channel blockers, ergot alkaloids, cyclosporine, erythromycin and phenothiazine-type neuroleptics.

A clinical case report illustrates the consequence of such a drug-drug interference with hepatic biotransformation; midazolam-induced sleep in a patient lasted for 6 days ($t_{1/2}$ = 25 h).

Key words: Midazolam; drug metabolism, cytochrome P-450, P-450 IIIA, drug interaction, adverse effect

Midazolam is a short acting, water soluble benzodiazepine with growing popularity as a hypnotic, a surgical premedication, and an anaesthetic induction agent. Its reported brief duration of action in healthy volunteers is due to intense biotransformation via hepatic microsomal oxidation, which results in an elimination half-life of 1.5 to 2.5 h [1–3]. The two major oxidative metabolites are 1′-, and 4-hydroxymidazolam. Under normal conditions they do not contribute to the pharmacological effect, since they are rapidly conjugated before being excreted through the kidney. Some authors have reported a longer half-life of midazolam [4–8]. Dundee et al. [7], for instance, mentioned a markedly prolonged elimination half-life of midazolam, ranging from 8 to 22 h in 6% of surgical patients, and Maitre et al. [8] found an average terminal half-life of 10.6 h in 12 patients recovering from cardiac surgery. Although true genetic polymorphism of midazolam oxidation was not identified, the available data showed a broad unimodal distribution of the kinetic parameters [9].

Evidence that the cytochrome P-450 system catalyses the metabolism of midazolam was recently provided by Kronbach et al. [10]. Through the use of in vitro inhibition studies, it was shown that formation of both midazolam metabolites was more than 90% inhibited by a polyclonal antibody raised against rat P-450 PCN1 (corresponding to the human isozyme P-450 NF or P-450 IIIA; [10]), suggesting that a single P-450 isozyme is involved in the formation of these two metabolites. This isozyme, which is closely related or identical to nifedipine oxidase (P-450 NF), was further identified by cDNA expression as a member of the cytochrome P-450 IIIA subfamily [11]. The same selective antibody was also able to inhibit microsomal biotransformation of nifedipine [12], cyclosporine [13], quinidine [14], and lidocaine [15], which strongly suggests that these reactions are mediated by a unique monooxygenase.

As the marked interindividual variation in the response to this widely used benzodiazepine seems due to variation in hepatic metabolism, the kinetics of midazolam hydroxylation in vitro by human liver microsomes have been investigated in order i) to define the function of the cytochrome P-450 isozyme catalysing the reactions, and ii) to screen drugs for their propensity to interfere with the reaction. The clinical relevance of interference with this hepatic biotransformation is illustrated by a clinical case report.

* Presented in part at the Fifty-seventh Annual Meeting of the Swiss Society for Internal Medicine, Interlaken, May 1989, and at the Fourth World Conference on Clinical Pharmacology and Therapeutics, Mannheim, July 1989.

UM00012010
NOVARTIS EXHIBIT 1017
Novartis v. Regents, IPR2023-01346
Page 756 of 4460

Table 1. Some inhibitors of midazolam 1'-hydroxylase

Inhibitors	IC_{50} (μM) (* K_i)	Inhibitors	IC_{50} (μM) (* K_i)
Amiodarone	15	Levomepromazine	10
Azithromycine	170	Mefloquine	250
Bromocryptine	40	Methylergometrine	5
Caffeine	480*	Nicardipine	8
Chloroquine	150	Nifedipine	5*
Cyclosporine	2*	Primaquine	160
Cimetidine	550	Quinine	250
Clarithromycine	330	Quinidine	120
Clotrimazole	<1	Ranitidine	>1000
Dihydroergotamine	7	SKF 525A	110
Ergotamine	0.5*	Theophylline	>1000
Erythromycin	148*	Verapamil	100
Itraconazole	1	Troleandomycin	180
Ketoconazole	0.1*		

Material and methods

Preparation of microsomes

Liver samples from human organ transplant donors were obtained according to a protocol approved by the institutional Ethics Committee (Department of Medicine, University of Geneva). Preparation and storage was as described [16]. For microsome preparation [17], small samples (50–150 mg wet weight) were homogenised in 0.25 mol·l^{-1} phosphate buffer 5 vol. with a Polytron homogenizer (Kinematica, Kriens, Switzerland), 3 times for 30 s, at 17,000 rpm, with 1 min cooling intervals in between. The homogenate was centrifuged for 5 min in an Eppendorf 5414 centrifuge at 10,000 × g. The pellet was resuspended in the same buffer and again centrifuged. Both supernatants were pooled and fractionated in 180 μl aliquots before being centrifuged for 12 min at 148,000 g (Airfuge, Beckman, Palo Alto, CA). The pellets were resuspended in 0.1 mol·l^{-1} Na pyrophosphate pH 7.4 and were centrifuged for 12 min at 148,000 × g. This washing step was repeated and the final pellet was resuspended in 0.1 M sodium phosphate buffer pH 7.4 and stored at −80°C. The entire procedure was carried out in a cold room to prevent tissue degradation. The protein content of the microsomal fractions, estimated by the Lowry method, ranged from 4 to 7 mg·ml^{-1}, depending on the preparation [18].

Incubation conditions

The kinetic experiments were performed with microsomes prepared from liver from an extensive (KDGE-02) and a poor (KDGE-03) metaboliser of the debrisoquine type polymorphism [19].

Microsomal protein 100 mg was incubated in a final volume of 200 μl sodium phosphate buffer 0.1 mol·l^{-1} containing a NADPH regenerating system (1 mmol·l^{-1} NADP, 5 mmol·l^{-1} isocitrate, 5 mmol·l^{-1} $MgCl_2$, 1U isocitrate dehydrogenase, Type IV; Sigma Chemical Co., St. Louis, MO). The system was preincubated at 37°C for 5 min before the addition of midazolam in final concentrations ranging from 0.5 to 60 μmol·l^{-1}.

Under those conditions the rates of formation of 1'- and 4-hydroxymidazolam were linear for up to 15 min. The reaction was terminated after 10 min by cooling on ice and the addition of 200 μl methanol. Denatured protein was removed by centrifugation at 10,000 × g for 1 min and the supernatant was stored at −80° until analysed.

For competition experiments, inhibitors (see Table 1 and the figures) were dissolved in 0.1 mol·l^{-1} sodium phosphate buffer pH 7.4. Various concentrations of inhibitors were added at the same time as the substrate. For screening experiments, the range of concentrations of the inhibitors used for the calculation of IC_{50} values varied according to the drug being used (0.1–1000 μmol·l^{-1}) against a 20 μmol·l^{-1} concentration of substrate. All inhibition studies were performed with microsomes prepared from the same liver (extensive metaboliser).

Assay of 1'- and 4-hydroxymidazolam

The production of 1'- and 4-hydroxymidazolam was determined by reverse-phase HPLC. The system consisted of a pump (Spectroflow 400; Kratos, Ramsey, NJ, USA), a 100 μl^{-1} injection loop (Rheodyne, Supelco, Bellefonte, PA, USA) and a variable wavelength UV detector operated at 254 nm (HP 1050; Hewlett Packard, Palo Alto, CA, USA). Aliquots of supernatants (50 to 100 μl) were injected directly on to a Spherisorb 3 μm Octodesil column (4.6 × 75 mm; Supelco). The mobile phase was 10 mmol·l^{-1} potassium phosphate buffer pH 7.4, methanol and acetonitrile (38/40/22, vol/vol/vol) and was delivered at 0.7 ml·min^{-1}. Chromatograms were analyzed by an SP 4290 integrator (Spectra-Physics Inc., Mountain View, CA, USA). The limit of detection of midazolam metabolites was 3 ng per injection.

The same analytical method was employed to measure the plasma concentrations of midazolam and its metabolites after extraction with ether/dichloromethane (7/3, vol/vol).

Analysis of kinetic data and statistics

Untransformed kinetic data were analysed by a nonlinear extended least squares curve fitting program with observer-independent weighting of the data [20], assuming Michaelis-Menten kinetics over the substrate range studied. The non-parametric Spearman rank test was applied to correlations in the fixed substrate concentration inhibition studies.

Results

Kinetics of midazolam hydroxylations

The kinetics of formation of 1'- and 4-hydroxymidazolam by microsomes from an extensive metaboliser (KDGE-02) and a poor (KDGE-03) metaboliser of debrisoquine

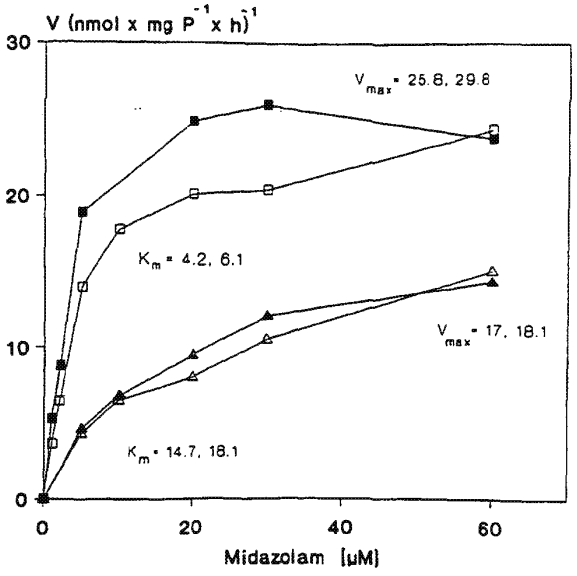
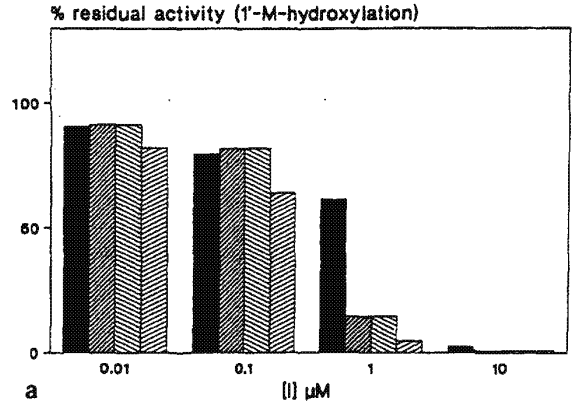


Fig. 1. Kinetics of midazolam 1'- and 4-hydroxylation by microsomes from the liver of an extensive (debrisoquine phenotype) (EM) and a poor (PM) metaboliser.
▲ 4-OH-M EM (db1) △ 4-OH-M PM (db1)
■ 1'-OH-M EM □ 1'-OH-M PM

UM00012011
NOVARTIS EXHIBIT 1017
Novartis v. Regents, IPR2023-01346
Page 757 of 4460



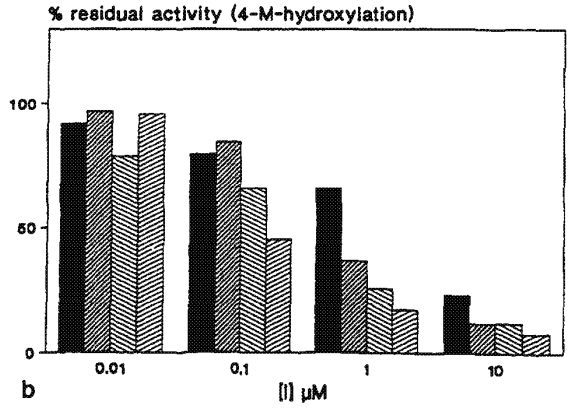


Fig. 2 a, b. Inhibition of midazolam 1'-(**a**) and 4-hydroxylation (**b**) by four azole antifungal agents. From left to right: itraconazole ($P < 0.01$), econazole ($P < 0.001$), ketoconazole ($P < 0.01$), and clotrimazole ($P < 0.001$). Results are expressed as percentage of control activity (in the absence of inhibitor). Each point is the mean of four determinations

are shown in Fig. 1. The pattern of metabolite formation was in accordance with Michaelis-Menten type kinetics. Midazolam was preferentially metabolised its 1'-hydroxy-derivative. Despite slightly different K_M values (4.2 and 6.1 μM in extensive and poor metabolisers, respectively, versus 14.7 and 18.1 μM for the 4-hydroxylation), the calculated V_{max} for both pathways had the same order of magnitude ($V_{max} = 25.8$ and 29.8 nmol · mg $P^{-1} \cdot h^{-1}$ and 17.0 and 18.1 nmol · mg $P^{-1} \cdot h^{-1}$ respectively).

Inhibition of midazolam 1'- and 4-hydroxylations in vitro

Inhibition of midazolam biotransformation by various compounds is presented in Fig. 2 to 4. The effect of four azole antifungal agents is shown in Fig. 2, and that of five compounds structurally related to quinidine in Fig. 3. The pattern of 1'- and 4-hydroxylations inhibition was similar in all experiments (Fig. 2).

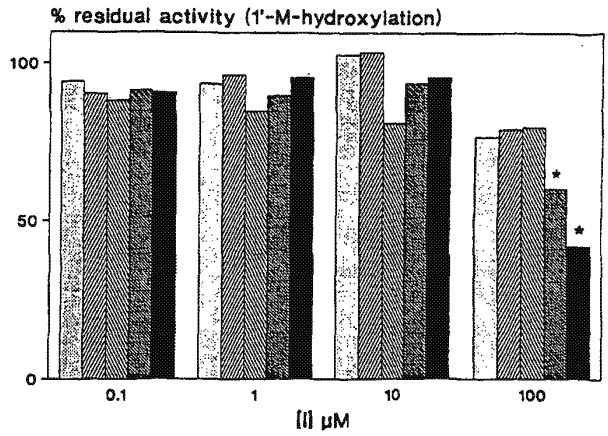


Fig. 3. Inhibition of midazolam 1'-hydroxylation by five compounds, structurally related to quinidine. From left to right: cinchonine, cinchonidine, quinine, hydroquinidine, and quinidine. Results are expressed as percentage of control activity (in the absence of inhibitor). Each point is the mean of four determinations. Hydroquinidine * ($P < 0.05$) and quinidine * ($P < 0.05$) only inhibited the reaction at these concentrations

In inhibition studies at various substrate concentrations, nifedipine and cyclosporine displayed a competitive inhibition-type of kinetics for midazolam 1'-hydroxylation, both K_i being calculated at 2 μM (Fig. 4). The extent of inhibition (IC_{50} or K_i) by the screened drugs is shown in Table 1.

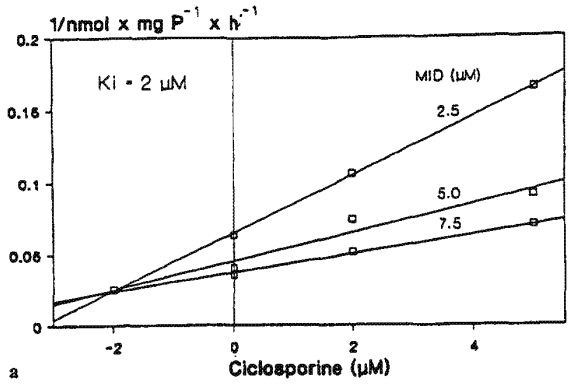
Clinical case report

A 61 year old man was admitted to the coronary care unit of the hospital for acute chest disease associated with intermittent atrial fibrillation. He received erythromycin 4 g · d^{-1} for suspected legionnaire's disease and amiodarone 1.7 g over 3 days for the control of his arrhythmia. Other drugs intermitently administered in the course of therapy were furosemide, digoxin, ranitidine, nitroglycerine and amoxycillin. During electrical cardioversions, sedation was achieved with intravenous midazolam (total dosage 300 mg iv over 14 h). Despite an expected elimination half-life of 1.5 to 2.5 h [21], midazolam-induced sleep lasted for about 6 days. On two occasions, the administration of flumazenil (1 mg) produced a brief awakening. The measured terminal half-life in the patient was (all data set) 24.8 h. His plasma concentrations are shown in Fig. 5.

Discussion

The in vitro biotransformation of midazolam observed here is consistent with known in vivo data: the amount of 1'-hydroxymidazolam excreted as a conjugate in the urine of healthy volunteers reached 75% of the administered dose versus 3% of the 4-hydroxy metabolite [22]. 1'-4-dihydroxymidazolam, another minor metabolite in vivo, was not detected in vitro. This is not surprising, as the 1'-4-

UM00012012
NOVARTIS EXHIBIT 1017
Novartis v. Regents, IPR2023-01346
Page 758 of 4460



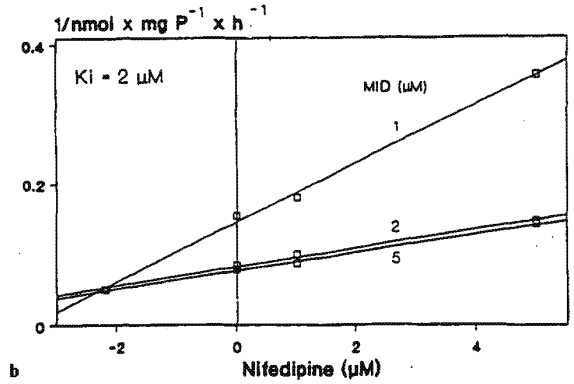


Fig. 4a, b. Competitive inhibition of midazolam 1′-hydroxylation (Dixon plot) by cyclosporin (**a**) and nifedipine (**b**). Each point is the mean of two determinations. MID, midazolam concentration

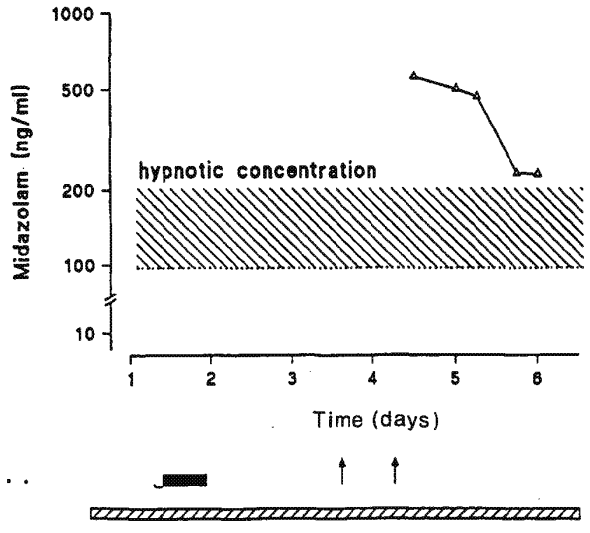


Fig. 5. Time course of a plasma midazolam concentrations in a patient with extremely low biotransformation (calculated half-life 24.8 h). The *black rectangle* shows midazolam infusion (300 mg over 14 h), the hatched rectangle shows erythromycin administration (4 g/day), and the *arrows* show flumazenil administration (1 mg i.v. on each occasion)

derivative results from further oxidation of the first step metabolites, which would not reach a sufficient concentration in vitro to be oxidized in a detectable amount.

In microsomes from KDGE-02 (extensive metaboliser of debrisoquine), the observation of distinct apparent affinity constants for the formation of 1′- and 4-hydroxymidazolam may indicate either that two cytochrome P-450 isozymes are involved in these reactions, or that there is more than one way of binding to a single isozyme, thus leading to the formation of two distinct metabolites. V_{max} values of the same order of magnitude for both the 1′- and 4-hydroxylations, as well as parallel variation in midazolam 1′- and 4-hydroxylation in all drug inhibition experiments, suggest that only one cytochrome P-450 isozyme is involved in the formation of both metabolites. The similar inhibition of both reactions by the same specific rabbit antiserum directed against rat P-450 PCN1 (P-450 IIIA) in the Kronbach study supports this hypothesis [10].

It has been suggested that genetic polymorphism of the debrisoquine-type could have a major impact on the variability of midazolam biotransformation [7]. However, a study in two groups of phenotyped volunteers did not show any influence of the debrisoquine/sparteine phenotype on midazolam kinetics [23]. The lack of influence of the poor metaboliser phenotype on microsomal midazolam metabolism observed here also argues against this hypothesis.

In inhibition experiments, numerous compounds appeared to inhibit midazolam hydroxylase. Immunoinhibition studies have shown that nifedipine [12], cyclosporin [13], and lidocaine [15] are oxidized by an identical or closely related isozyme of the cytochrome P-450 IIIA subfamily. The competitive inhibition by nifedipine and cyclosporin in the present study (Fig. 4) also provide indirect evidence that the same P-450 isozyme is involved in the biotransformation of these three drugs. However, direct extrapolation from in vitro inhibition studies to the clinical situation is not warranted. Indeed, the importance of in vivo interactions is the result not only of affinities (relative K_i and K_M) as relative concentrations at the enzyme site must also be considered.

Both erythromycin and quinidine, a very selective and powerful inhibitor of cytochrome P-450 DB1 [17, 24–25], also act as competitive inhibitors of midazolam 1′-hydroxylation (Table 1). These findings are in agreement with published data showing that the in vitro metabolism of quinidine and erythromycin are catalysed by an isozyme of the P-450 NF family [14, 26].

The inhibitory effect of quinine, a diastereoisomer of quinidine, was less marked (Fig. 3), and another isomer, cinchonine, did not inhibit the reaction, suggesting that the methoxy side chain on the quinoline ring is required to block the hydroxylation of midazolam.

Drugs such as phenothiazine-type neuroleptics (e.g. levomepromazine), H_2-antihistaminics (e.g. cimetidine), amiodarone, verapamil and other nonspecific monooxygenase blockers (e.g. SKF 525-A) are also able to inhibit this reaction (Table 1). These P-450 blockers include the potent "azole" antifungal agents (e.g. ketoconazole and itraconazole). They also inhibit a wide variety of liver monooxygenases, thanks to their ability to

UM00012013
NOVARTIS EXHIBIT 1017
Novartis v. Regents, IPR2023-01346
Page 759 of 4460

bind directly and with very high affinity, to the cytochrome P-450 component of the monooxygenase system [27–29].

The 4-quinolone antibiotics may interfere with the in vivo cytochrome P-450 mediated biotransformation of caffeine and theophylline [30, 31]. Under the present experimental conditions, the lack of an in vitro effect of these drugs on midazolam oxidation provides additional indirect evidence that the hydroxylation of midazolam is mediated by a distinct isozyme.

Potential clinical consequences

A competitive inhibitor may either interact with other drugs that are metabolised by the isoenzyme, or itself be liable to biotransformation by the isozyme. All the drugs mentioned in Table 1 might interfere with midazolam biotransformation in vivo, depending on their respective affinities for the enzyme and the dose administered. In the case of the patient cited, the increase in midazolam concentration was due both to amiodarone, a known inhibitor of the metabolism of phenytoin, quinidine, flecainide and theophylline [32], and to competitive inhibition between midazolam and erythromycin, whose biotransformation seems to be mediated by the same cytochrome P-450 IIIA isozyme [26]. Significant prolongation of the very short half-life of midazolam will not usually have major consequences. However, in certain extreme conditions, the interactions may have a dramatic result, as illustrated by the present clinical report. Due to the very large doses of midazolam administered to the patient, the potential contribution of non-linear kinetics cannot be excluded.

In conclusion, the present data indicate that the major biotransformation route of midazolam is mediated by a monooxygenase which is independent of the polymorphic cytochrome P-450 DB1 isozyme. In vitro inhibition experiments indicate that the disposition of other widely used drugs is also controlled by this distinct metabolic pathway, and that many compounds are capable of interfering with it. This may lead to drug-drug interactions involving either the response to midazolam or to the interacting compound.

Acknowledgements. We are grateful to Professor F. Waldvogel, Geneva University Hospital, for referring the patient described in the clinical case report.

References

1. Smith MT, Eadie MJ, O'Rourke T (1981) The pharmacokinetics of midazolam in man. Eur J Clin Pharmacol 19: 271–278
2. Dundee JW, Halliday NJ, Fee JPH (1984) Midazolam in intensive care. Br Med J 289: 1540
3. Heizmann P, Eckert M, Ziegler WH (1983) Pharmakokinetics and bioavailability of midazolam in man. Br J Clin Pharmacol 16: 43S–49S
4. Byatt CM, Lewis LD, Dawling S, Cochrane GM (1984) Accumulation of midazolam after repeated dosage in patients receiving mechanical ventilation in intensive car unit. Br Med J 289: 799–800
5. Byrne AJ, Yeoman PM, Mace P (1984) Accumulation of midazolam in patients receiving mechanical ventilation (letter). Br Med J 289: 1309
6. Greenblatt DJ, Abernethy DR, Locniskar A, Harmatz JS, Limjuco RA, Shader RI (1984) Effect of age, gender, and obesity on midazolam kinetics. Anesthesiology 61: 27–37
7. Dundee JW, Collier PS, Carlisle RJT, Harper KW (1986) Prolonged midazolam elimination half-life. Br J Clin Pharmacol 21: 425–429
8. Maitre PO, Funk B, Crevoisier C, Ha HR (1989) Pharmacokinetics of midazolam in patients recovering from cardiac surgery. Eur J Clin Pharmacol 37: 161–166
9. Kassai A, Toth G, Eichelbaum M, Klotz U (1988) No evidence of a genetic polymorphism in the oxidative metabolism of midazolam. Clin Pharmacokinet 15: 319–325
10. Kronbach T, Mathys D, Umeno M, Gonzalez FJ, Meyer UA (1989) Oxidation of midazolam and triazolam by human liver cytochrome P450IIIA4. Molec Pharmacol 36: 89–96
11. Nebert DW, Nelson DR, Adesnik M, Coon MJ, Estabrook RW, Gonzalez FJ, Guengerich FP, Gunsalus IC, Johnson EF, Kemper B, Levin W, Phillips IR, Sato R, Waterman MR (1989) The P450 superfamily: Updated listing of all genes and recommended nomenclature for the chromosomal loci. DNA 8: 1–13
12. Beaune PH, Umbenhauer DR, Bork RW, Lloyd RS, Guengerich FP (1986) Isolation and sequence determination of a cDNA clone related to cytochrome P-450 nifedipine oxidase. Proc Natl Acad Sci USA 83: 8064–8068
13. Kronbach T, Fischer V, Meyer UA (1988) Cyclosporine metabolism in human liver: identification of a cytochrome P450 of the human P450III gene family as the major cyclosporine metabolizing enzyme explains enteractions of cyclosporine with other drugs. Clin Pharmacol Ther 43: 630–635
14. Guengerich FP, Müller-Enoch D, Blair IA (1986) Oxidation of quinidine by human liver cytrochrome P-450. Molec Pharmacol 30: 287–295
15. Bargetzi MJ, Aoyama T, Gonzalez FJ, Meyer UA (1989) Lidocaine metabolism in human liver microsomes by cytochrome P450IIIA4. Clin Pharmacol Ther 46: 521–527
16. Von Bahr C, Groth CG, Jansson H, Lundgren G, Lind M, Glaumann H (1980) Drug metabolism in human livers in vitro: Establishment of a human liver bank. Clin Pharmacol Ther 27: 711–725
17. Dayer P, Kronbach T, Eichelbaum M, Meyer UA (1987) Enzymatic basis of the debrisoquine/sparteine-type genetic polymorphism of drug oxidation- characterization of bufuralol 1′-hydroxylation in liver microsomes of in vivo phenotyped carriers of the genetic deficiency. Biochem Pharmacol 36: 4145–4152
18. Lowry OH, Rosebrough NJ, Farr AL, Randall RJ (1951) Protein measurement with the Folin-phenol reagent. J Biol Chem 193: 265–275
19. Dayer P, Leemann T, Striberni R (1989) Dextromethorphan O-demethylation in liver microsomes as a prototype reaction to monitor P-450DB1 activity. Clin Pharmacol Ther 45: 34–40
20. Sheiner LB (1983) ELSFIT (version 3.0) A program for extended least squares fit, UCSF, San Francisco, CA, USA
21. Pentikäinen PJ, Välisalmi L, Himberg JJ, Crevoisier C (1989) Pharmacokinetics of midazolam following intravenous and oral administration in patients with chronic liver disease and in healthy subjects. J Clin Pharmacol 29: 272–277
22. Heizmann P, Ziegler WH (1981) Excretion and metabolism of ^{14}C-midazolam in human following oral dosing. Arzneim Forsch (Drug Res) 31: 2220–2223
23. Klotz U, Mikus G, Zekorn C, Eichelbaum M (1986) Pharmacokinetics of midazolam in relation to polymorphic sparteine oxidation. Br J Clin Pharmacol 22: 618–620
24. Otton SV, Inaba T, Kalow W (1984) Competitive inhibition of sparteine oxidation in human liver by β-adrenoceptor antagonists and other cardiovascular drugs. Life Sci 34: 73–80
25. Leemann T, Dayer P, Meyer UA (1986) Single-dose quinidine treatment inhibits metoprolol oxidation in extensive metabolizers. Eur J Clin Pharmacol 29: 739–741

UM00012014
NOVARTIS EXHIBIT 1017
Novartis v. Regents, IPR2023-01346
Page 760 of 4460

26. Fabre G, Crevat-Pisano P, Dragna S, Covo J, Barra Y, Cano JP (1988) Involvement of the macrolide antibiotic inducible cytochrome P-450 LM_{3c} in the metabolism of midazolam by microsomal fractions prepared from rabbit liver. Biochem Pharmacol 37: 1947–1953
27. Rodrigues AD, Gibson GG, Ioannides C, Parke DV (1987) Interactions of imidazole antifungal agents with purified cytochrome P-450 proteins. Biochem Pharmacol 36: 4277–4281
28. Pasanen M, Taskinen T, Iscan M, Sotaniemi EA, Kairaluoma M, Pelkonen O (1988) Inhibition of human hepatic and placental xenobiotic monooxygenase by imidazole antimycotics. Biochem Pharmacol 37: 3861–3866
29. Back DJ, Stevenson P, Tjia JF (1989) Comparative effects of two antimycotic agents, ketoconazole and terfenadine on the metabolism of tolbutamide, ethinyloestradiol, cyclosporin and ethoxycoumarin by human liver microsomes in vitro. Br J Clin Pharmacol 28: 166–170
30. Thomson AH, Thomson GD, Hepburn M, Whiting B (1987) A clinically significant interaction between ciprofloxacin and theophylline. Eur J Clin Pharmacol 33: 435–436
31. Harder S, Staib AH, Beer C, Papenburg A, Stille W, Shah PM (1988) 4-Quinolones inhibit biotransformation of caffeine. Eur J Clin Pharmacol 35: 651–656
32. Nolan PE, Marcus FI, Hoyer GL, Bliss M, Gear K (1989) Pharmacokinetic interaction between intravenous phenytoin and amiodarone in healthy volunteers. Clin Pharmacol Ther 46: 43–50

Prof. P. Dayer
Division of Clinical Pharmacology
University Hospital
CH-1211 Geneva 4
Switzerland

UM00012015
NOVARTIS EXHIBIT 1017
Novartis v. Regents, IPR2023-01346
Page 761 of 4460

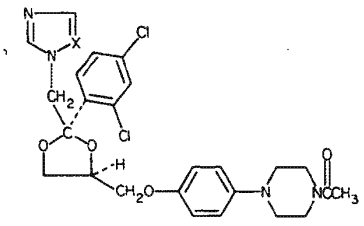
Antimycotic Azoles. 7. Synthesis and Antifungal Properties of a Series of Novel Triazol-3-ones

J. Heeres,* L. J. J. Backx, and J. Van Cutsem

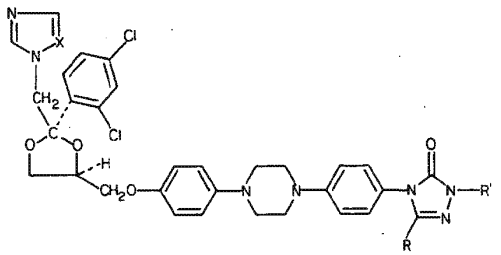
Research Laboratories, Janssen Pharmaceutica N. V., B-2340, Beerse, Belgium. *Received July 5, 1983*

A series of novel triazol-3-ones have been synthesized, and their in vitro and in vivo antifungal properties are reported. Compound **68** (itraconazole), which displays a pronounced oral activity against vaginal candidosis in rats and against microsporosis in guinea pigs, has been selected for clinical evaluation.

With the advent of ketoconazole (Ia), which was dis-



Ia, X = CH (ketoconazole)
b, X = N



IIa, X = CH
b, X = N

covered approximately 30 years after the development of the first orally active broad-spectrum antibiotics, the first oral broad-spectrum antimycotic became available for medical practice. This introduction may be considered a milestone in the treatment of fungal diseases with azoles. The in vitro spectrum of ketoconazole covers a wide variety of yeasts, dermatophytes, and other fungi.[1,2] Its potential in the therapy of dermatomycoses, candidosis of the mouth and the vagina, systemic candidosis, chronic mucocutaneous candidosis and candiduria, as well as of deep and subcutaneous mycoses by dimorphic and other fungi has extensively been reviewed.[1-6]

Notwithstanding the promising results obtained in the oral treatment of mycoses with ketoconazole and the convenience for the patient, there still is a need for more potent and better antimycotic drugs. The present paper deals with the synthesis and antifungal properties of the title compounds IIa,b, and some of them fulfill these criteria in animal models.

Chemistry. The synthesis, starting from *cis*-[2-(2,4-dichlorophenyl)-2-(1*H*-imidazol-1-ylmethyl)-1,3-dioxolan-4-yl]methyl methanesulfonate (**1a**)[6] and *cis*-[2-(2,4-dichlorophenyl)-2-(1*H*-1,2,4-triazol-1-ylmethyl)-1,3-dioxolan-4-yl]methyl methanesulfonate (**1b**),[7] is outlined in Scheme I.

Ketoconazole (**3a**) and the corresponding triazole analogue **3b** were prepared from **1a,b** and **2** according to the method described in a previous paper.[6] These compounds were deacylated at reflux temperature with NaOH in *n*-BuOH to the piperazines **4a** and **4b**, respectively. Both compounds, as well as 1-(4-methoxyphenyl)piperazine (**5**) were arylated with 1-chloro-4-nitrobenzene to the corresponding nitroaryl compounds **6a–c**. Catalytic reduction with 5% Pt/C afforded the anilino derivatives **7a–c**, which were acylated with phenyl chloroformate to the phenyl carbamates **8a–c**. Conversion of these carbamates with hydrazine hydrate at reflux temperature yielded the semicarbazides **9a–c**, which were cyclized to the triazol-3-ones IIIa–c. Alkylation of these triazol-3-ones with alkyl bromides or with dimethyl sulfate gave the target compounds IIa,b (method A) and IIc, respectively. Phenols IId were prepared by demethylation with a 48% HBr solution of compounds IIc. Methanesulfonates **1a,b** in a suspension of NaH (50% dispersion in mineral oil) were coupled either with the sodium salt of phenols IId, generated in situ from IId, to give IIa,b (method B) or with compound **2** to give **3a,b**.

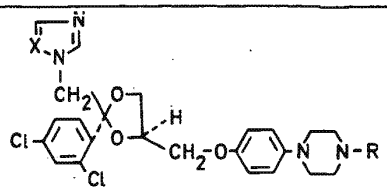
Biological Methods. The title compounds were tested against a large number of microorganisms. Preliminary in vitro experiments were conducted according to the method described by Godefroi[8] with the fungi *Microsporum canis* (*M.c.*), *Trichophyton mentagrophytes* (*T.m.*), *Trichophyton rubrum* (*T.r.*), *Phialophora verrucosa* (*Ph.v.*), *Cryptococcus neoformans* (*Cr.n.*), *Candida tropicalis* (*C.tr.*), *Candida albicans* (*C.a.*), *Mucor* sp. (*Muc.*), *Aspergillus fumigatus* (*A.f.*), *Sporothrix schenckii* (*Sp.s*), and *Saprolegnia* sp. (*Sapr.*). In vivo, the compounds were tested in experimental vaginal candidosis in rats[6] and in experimental microsporosis.[9] For oral treatment, the compounds were formulated in polyethylene glycol (PEG) 200. In vaginal candidosis, the animals were treated therapeutically (treatment starting 3 days after infection) o.d. for 3 consecutive days with doses ranging from 0.63 to 10 mg/kg. Vaginal candidosis in ovarectomized and hysterectomized Wistar rats, kept in pseudopregnancy by weekly injections of 0.1 mg of oestradiol undecylate, was induced by infection with 8×10^5 cells of *C. albicans* (strain B 2630) Experimental microsporosis was treated prophylactically (treatment starting the day of infection

(1) Levine, H. B. "Ketoconazole in the Management of Fungal Disease"; ADIS Press: Australia, 1982.
(2) Van Cutsem, J. *Am. J. Med.* **1983**, *74*(1B), 9.
(3) Restrepo, A.; Stevens, D. A.; Utz, J. P. *Rev. Inf. Dis.* **1980**, *2*, 519.
(4) Graybill, J. R., *Am. J. Med.* **1983**, *74*(1B).
(5) Symoens, J.; Cauwenberg, G., to be published in *Prog. Drug. Res.*
(6) Heeres, J.; Backx, L. J. J.; Mostmans, J. H.; Van Cutsem, J. *J. Med. Chem.* **1979**, *22*, 1003.
(7) Heeres, J.; Hendrickx, R.; Van Cutsem, J. *J. Med. Chem.* **1983**, *26*, 611.
(8) Godefroi, E. F.; Van Cutsem, J.; Van der Eycken, C. H. M.; Janssen, P. A. J. *J. Med. Chem.* **1967**, *10*, 1160.
(9) Van Cutsem, J.; Thienpont, D. *Chemotherapy* **1972**, *17*, 392.

0022-2623/84/1827-0894$01.50/0 © 1984 American Chemical Society

UM00012016
NOVARTIS EXHIBIT 1017
Novartis v. Regents, IPR2023-01346
Page 762 of 4460

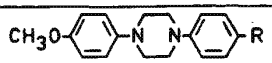
Table I



Compd.	X	R	M.p. °C	Formula	Cryst. solv.	Mr	Yield	Anal.[a]
3a[c]	CH	$-C(=O)CH_3$	146	$C_{26}H_{28}Cl_2N_4O_4$	MIK		59	
3b	N	$-C(=O)CH_3$	176.4	$C_{25}H_{27}Cl_2N_5O_4$	MIK/*i*-Pr_2O	532.42	58	C, H, N
4a	CH	-H	171.7	$C_{24}H_{26}Cl_2N_4O_3$	MIK	489.39	71	C, H, N
4b	N	-H	130.6	$C_{23}H_{25}Cl_2N_5O_3$	*i*-Pr_2O	490.38	79	C, H, N
6a	CH	$-C_6H_4-NO_2$	181	$C_{30}H_{29}Cl_2N_5O_5$	*n*-BuOH	610.48	54	C, H, N
6b	N	$-C_6H_4-NO_2$	167.8	$C_{29}H_{28}Cl_2N_6O_5$	*n*-BuOH	611.47	50	Cl, N
7a	CH	$-C_6H_4-NH_2$	174.4	$C_{30}H_{31}Cl_2N_5O_3$	*i*-PrOH	580.50	97	Cl, N
7b	N	$-C_6H_4-NH_2$	186.8	$C_{29}H_{30}Cl_2N_6O_3$	*n*-BuOH	581.49	80	Cl, N
8a	CH	$-C_6H_4-NHC(=O)O\phi$	198.8	$C_{37}H_{35}Cl_2N_5O_5$	dioxane	700.60	82	C, H, N
8b	N	$-C_6H_4-NHC(=O)O\phi$	203.1	$C_{36}H_{34}Cl_2N_6O_5$		701.61	86	C, H, N
9a	CH	$-C_6H_4-NHC(=O)NHNH_2$	225.9	$C_{31}H_{33}Cl_2N_7O_4$		638.53	98	C, H, N
9b	N	$-C_6H_4-NHC(=O)NHNH_2$	199.7	$C_{30}H_{32}Cl_2N_8O_4$		639.54	99	N

[a] Unless otherwise stated, the analyses are within ±0.4% of the theoretical values. [b] MIK = $CH_3C(=O)CH_2CH(CH_3)_2$. [c] Reference 5.

Table II

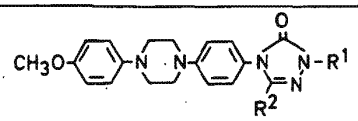


Compd.	R	M.p. °C	Formula	Cryst. solv.	Mr	Yield	Anal.[a]
6c	$-NO_2$	195.1	$C_{17}H_{19}N_3O_3$	dioxane	313.35	67	N
7c	$-NH_2$	191.8	$C_{17}H_{21}N_3O$	*n*-BuOH	283.36	74	C, H, N
8c	$-NHC(=O)O\phi$	204.5	$C_{24}H_{25}N_3O_3$	*n*-BuOH	403.46	61	N
9c	$-NHC(=O)NHNH_2$	>300	$C_{18}H_{23}N_5O_2$	DMF	341.40	63	N

[a] Unless otherwise stated, the analyses are within ±0.4% of the theoretical values.

UM00012017
NOVARTIS EXHIBIT 1017
Novartis v. Regents, IPR2023-01346
Page 763 of 4460

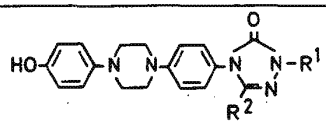
Table III



Compd.	R^1	R^2	m.p.	Formula	Crystn. solv.	Mr.	Yield	Anal.[a]
10	H	H	>300	$C_{19}H_{21}N_5O_2$	DMF	351.40	28	C,H,N
11	CH_3	H	245.2	$C_{20}H_{23}N_5O_2$	dioxane	365.42	35	N
12	C_2H_5	H	210.2	$C_{21}H_{25}N_5O_2$	*n*-BuOH	379.45	44	C,H,N
13	*n*-C_3H_7	H		$C_{22}H_{27}N_5O_2$	*n*-BuOH	393.48	65	—[b]
14	*i*-C_3H_7	H	209.5	$C_{22}H_{27}N_5O_2$	*n*-BuOH	393.48	47	C,H,N
15	*n*-C_4H_9	H	171.6	$C_{23}H_{29}N_5O_2$	*n*-BuOH	407.51	61	C,H,N
16	*i*-C_4H_9	H	203.0	$C_{23}H_{29}N_5O_2$	*n*-BuOH	407.51	57	N
17	H	CH_3	298.4	$C_{20}H_{23}N_5O_2$	dioxane	365.42	34	C,H
18	CH_3	CH_3	196.7	$C_{21}H_{25}N_5O_2$	*n*-BuOH	379.45	31	C,H,N
19	C_2H_5	CH_3	179.8	$C_{22}H_{27}N_5O_2$	*i*-PrOH	393.48	80	C,H,N
20	*n*-C_3H_7	CH_3	144.5	$C_{23}H_{29}N_5O_2$	*i*-PrOH	407.50	83	C,H,N
21	*i*-C_3H_7	CH_3	192.7	$C_{23}H_{29}N_5O_2$	*i*-PrOH	407.50	51	C,H,N
22	*n*-C_4H_9	CH_3	150.1	$C_{24}H_{31}N_5O_2$	*i*-PrOH	421.54	59	N
23	*i*-C_4H_9	CH_3	139.0	$C_{24}H_{31}N_5O_2$	*i*-PrOH	421.54	53	C,H,N

[a] Unless otherwise stated, the analyses are within ±0.4% of the theoretical values. [b] Product was used without further purification.

Table IV

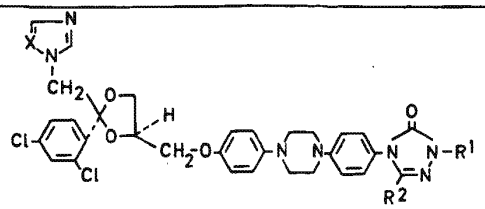


Compd.	R^1	R^2	m.p. °C	Formula	Crystn. solv.	Mr.	Yield	Anal.[a]
24	CH_3	H	>260	$C_{19}H_{21}N_5O_2$	DMF	351.40	96	—[b]
25	C_2H_5	H	217	$C_{20}H_{23}N_5O_2$	DMF	365.42	95	C,H,N
26	*n*-C_3H_7	H		$C_{21}H_{25}N_5O_2$	DMF	379.45	83	—[b]
27	*i*-C_3H_7	H	208.4	$C_{21}H_{25}N_5O_2$	DMF	379.45	86	C,H,N
28	*n*-C_4H_9	H	221.6	$C_{22}H_{27}N_5O_2$	*i*-PrOH	393.49	69	N
29	*i*-C_4H_9	H	211.4	$C_{22}H_{27}N_5O_2$	*i*-PrOH	393.49	38	C,H,N
30	CH_3	CH_3	>260	$C_{20}H_{23}N_5O_2$	DMF	365.42	96	C,H,N
31	C_2H_5	CH_3	287.8	$C_{21}H_{25}N_5O_2$	DMF	379.45	92	C,H,N
32	*n*-C_3H_7	CH_3	258.2	$C_{22}H_{27}N_5O_2$	*i*-PrOH	393.49	88	C,H,N
33	*i*-C_3H_7	CH_3	251.3	$C_{22}H_{27}N_5O_2$	*n*-BuOH	393.49	100	C,H,N
34	*n*-C_4H_9	CH_3	262.0	$C_{23}H_{29}N_5O_2$	*n*-BuOH	407.51	84	C,H,N
35	*i*-C_4H_9	CH_3	268.7	$C_{23}H_{29}N_5O_2$	*i*-PrOH	407.51	89	C,H,N

[a] Unless otherwise stated, the analyses are within ±0.4% of the theoretical values. [b] Products were used without further purification.

UM00012018
NOVARTIS EXHIBIT 1017
Novartis v. Regents, IPR2023-01346
Page 764 of 4460

Table V

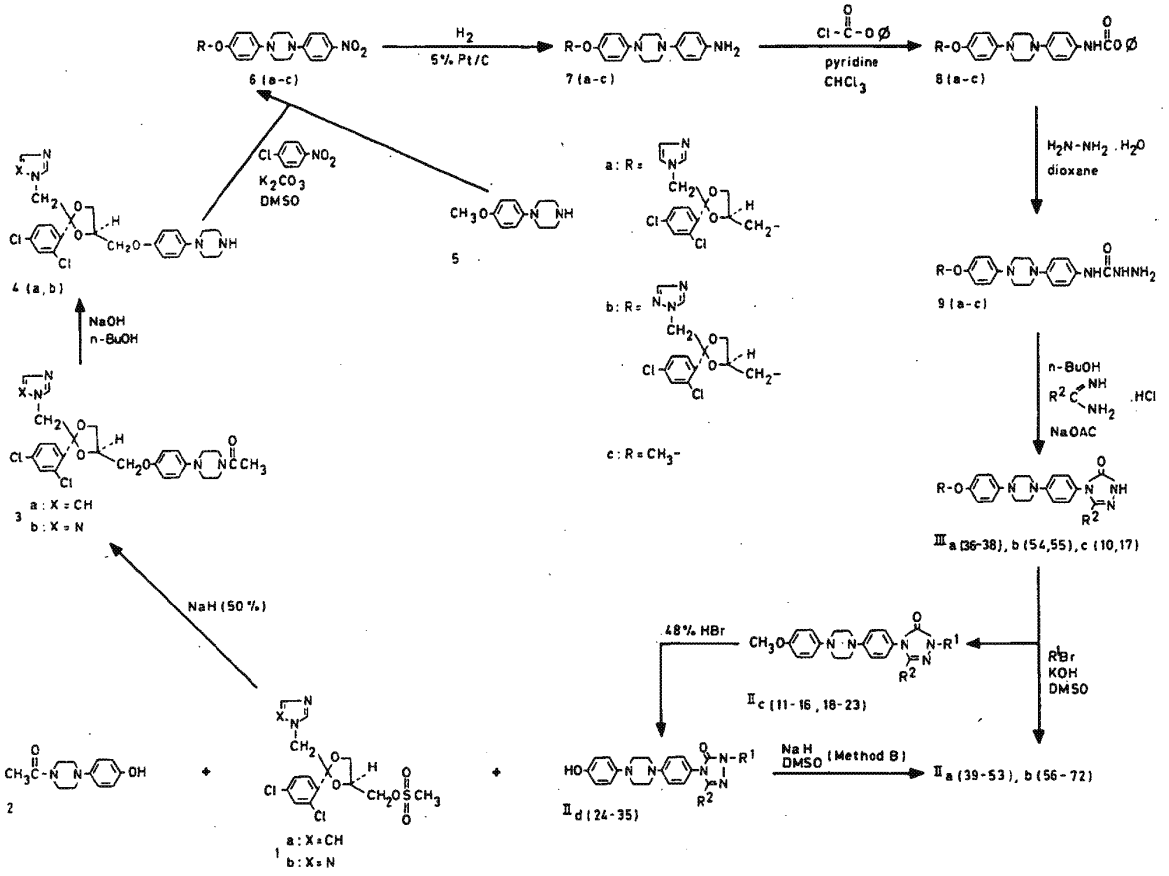


Compd	Stereochem.	X	R^1	R^2	m.p.°C	Formula	Crystn. solv.	Mr.	Yield	Method	Anal.[a]
36	cis	CH	H	H	255.0	$C_{32}H_{31}Cl_2N_7O_4$	*n*-BuOH	648.53	30	-	N
37	cis	CH	H	CH_3	295.7	$C_{33}H_{33}Cl_2N_7O_4 \cdot 1/2\,C_3H_8O$	*i*-PrOH	692.62	44	-	C[c],H,N[c],Cl
38	cis	CH	H	C_2H_5	275.6	$C_{34}H_{35}Cl_2N_7O_4$	*n*-BuOH	676.58	26	-	N
39	cis	CH	CH_3	H	212.8	$C_{33}H_{33}Cl_2N_7O_4$	*n*-BuOH	662.55	44	B	C,H,N
40	cis	CH	CH_3	CH_3	147.3	$C_{34}H_{35}Cl_2N_7O_4$	MIK	676.58	74	B	Cl,N
41	cis	CH	C_2H_5	H	204.7	$C_{34}H_{35}Cl_2N_7O_4$	*n*-BuOH	676.58	53	B	C,H,N
42	cis	CH	C_2H_5	CH_3	135.5	$C_{35}H_{37}Cl_2N_7O_4 \cdot H_2O$ [d]	*i*-PrOH	708.63	51	B	C,H,N
43	cis	CH	*n*-C_3H_7	H	185.7	$C_{35}H_{37}Cl_2N_7O_4$	MIK	690.61	51	B	C,H,N
44	cis	CH	*n*-C_3H_7	CH_3	153.9	$C_{36}H_{39}Cl_2N_7O_4 \cdot H_2O$ [e]	*n*-BuOH	722.67	61	B	N,C[e],H
45	cis	CH	*n*-C_3H_7	C_2H_5	170.4	$C_{37}H_{41}Cl_2N_7O_4$	MIK / *i*-Pr_2O	718.68	70	B	C,H,N
46	cis	CH	*i*-C_3H_7	H	222.1	$C_{35}H_{37}Cl_2N_7O_4$	MIK	690.61	37	A	C,H,N
47	cis	CH	*i*-C_3H_7	CH_3	146.1	$C_{36}H_{39}Cl_2N_7O_4 \cdot H_2O$ [f]	MIK / *i*-Pr_2O	722.67	71	A	C,H,N
48	cis	CH	*n*-C_4H_9	H	199.2	$C_{36}H_{39}Cl_2N_7O_4$	MIK	704.65	45	A	C,H,N
49	cis	CH	*n*-C_4H_9	CH_3	172.6	$C_{37}H_{41}Cl_2N_7O_4$	$PhCH_3$ / *i*-Pr_2O	718.68	70	A	Cl,N
50	cis	CH	*i*-C_4H_9	H	195.0	$C_{36}H_{39}Cl_2N_7O_4$	MIK	704.65	35	B	C,H,N
51	cis	CH	*i*-C_4H_9	CH_3	150.3	$C_{37}H_{41}Cl_2N_7O_4$	MIK	718.68	23	A	N
52	cis	CH	$CH_2CH{=}CH_2$	H	181.3	$C_{35}H_{35}Cl_2N_7O_4$	MIK	688.61	49	A	C,H,N
53	cis	CH	*s*-C_4H_9	H	170.7	$C_{36}H_{39}Cl_2N_7O_4$	MIK	704.65	74	-	C,H,N
54	cis	N	H	H	254.4	$C_{31}H_{30}Cl_2N_8O_4$	DMF / *i*-Pr_2O	652.31	62	-	C,H,N
55	cis	N	H	CH_3	212.4	$C_{32}H_{32}Cl_2N_8O_4 \cdot 1/2\,C_2H_6O$ [g]	EtOH	686.59	38	-	Cl,C[g],H,N
56	cis	N	CH_3	H	212.8	$C_{32}H_{32}Cl_2N_8O_4$	*n*-BuOH	663.55	42	B	C,H,N
57	cis	N	CH_3	CH_3	161.9	$C_{33}H_{34}Cl_2N_8O_4 \cdot H_2O$ [h]	MIK	695.60	71	B	Cl
58	cis	N	C_2H_5	H	184.4	$C_{33}H_{34}Cl_2N_8O_4$	*n*-BuOH	677.57	74	B	C,H,N
59	cis	N	C_2H_5	CH_3	178.3	$C_{34}H_{36}Cl_2N_8O_4$	*n*-BuOH	691.60	71	B	N,Cl
60	cis	N	*n*-C_3H_7	H	176.3	$C_{34}H_{36}Cl_2N_8O_4$	MIK	691.60	53	B	N,Cl
61	cis	N	*n*-C_3H_7	CH_3	165.5	$C_{35}H_{38}Cl_2N_8O_4 \cdot H_2O$ [i]	*n*-BuOH	723.64	52	B	C,H,N
62	cis	N	*i*-C_3H_7	H	200.4	$C_{34}H_{36}Cl_2N_8O_4$	MIK	691.62	64	B	Cl,N
63	cis	N	*i*-C_3H_7	CH_3	158.6	$C_{35}H_{38}Cl_2N_8O_4 \cdot H_2O$ [j]	MIK	723.66	68	B	Cl,N,C[i],H
64	cis	N	*n*-C_4H_9	H	180.5	$C_{35}H_{38}Cl_2N_8O_4$	*n*-BuOH	705.62	70	B	C,H,N
65	cis	N	$(CH_3)_2CHCH_2$-	CH_3	140.0	$C_{36}H_{40}Cl_2N_8O_4$	MIK	719.67	50	B	C,H,N
66	cis	N	$(CH_3)_2CHCH_2$-	H	155.8	$C_{35}H_{38}Cl_2N_8O_4$	MIK	705.62	54	B	C,H,N
67	cis	N	$-CH_2CH{=}CH_2$	H	159.2	$C_{34}H_{34}Cl_2N_8O_4$	$PhCH_3$	689.60	54	A	Cl
68	cis	N	*s*-C_4H_9	H	166.2	$C_{35}H_{38}Cl_2N_8O_4$	$PhCH_3$	705.64	46	A	C,H,N
69	cis	N	$(CH_3)_2CHCH_2CH_2$-	H	183.4	$C_{36}H_{40}Cl_2N_8O_4$	$PhCH_3$	719.67	68	A	C,H,N
70	cis	N		H	197.3	$C_{36}H_{38}Cl_2N_8O_4$	$PhCH_3$	717.66	43	A	C,H,N
71	cis	N	$-CH_2$- 	H	174.5	$C_{35}H_{36}Cl_2N_8O_4$	MIK	703.63	40	A	N,Cl
72	cis	N	*s*-C_4H_9	CH_3	146.1	$C_{36}H_{40}Cl_2N_8O_4$	MIK / *i*-Pr_2O	719.67	68	A	C,H,Cl

[a] Unless otherwise stated, the analyses are within ±0.4% of the theoretical values. [b] MIK = $CH_3C(=O)CH_2CH(CH_3)_2$. [c] C = calcd, 59.82; found, 58.80. N: calcd, 14.80; found, 14.16. [d] NMR for H_2O δ 1.86. [e] C: calcd, 59.84; found, 59.16; NMR for H_2O δ 1.86. [f] NMR for H_2O δ 1.82. [g] C: calcd, 57.73; found, 56.81; NMR for C_2H_5OH δ 1.20 (CH_3), 3.71 (CH_2). [h] NMR for H_2O δ 1.84. [i] NMR for H_2O δ 1.75. [j] C: calcd, 58.09; found, 58.64. NMR for H_2O δ 1.75.

UM00012019
NOVARTIS EXHIBIT 1017
Novartis v. Regents, IPR2023-01346
Page 765 of 4460

Scheme I



or the day before) o.d. for 14 consecutive days with doses ranging from 1.25 to 20 mg/kg. Experimental microsporosis was induced in guinea pigs by artificial infection on the back with *M. canis*. Substances showing more than a 50% cure rate were tested at lower doses.

Results and Discussion

The test results are summarized in Table VI. The in vitro results represent the lowest dose levels for total inhibition of growth. Compared with the title compounds, ketoconazole demonstrates the highest in vitro activity and is also clearly more active than its triazole analogue. The low in vitro activity of the triazol-3-ones may be associated with their low solubility in the test medium. Compound **68**, when tested in Me_2SO solution in Sabouraud broth at pH 7.4, was active against dermatophytes at concentrations ranging from 0.1 to 1 μg/mL and against *Candida* spp., *Cr. neoformans*, *A. fumigatus*, *S. schenckii*, and *Ph. verrucosa* at 0.1 μg/mL.[10] Some compounds (**39**, **53**, **58**, and **67**) appear to be active at rather low concentrations (1–10 μg/mL) against dermatophytes, such as *T. rubrum*, *T. mentagrophytes*, and yeasts, such as *Cr. neoformans* and *C. tropicalis*. It is striking that even at 100 μg/mL none of the tested compounds showed significant activity against *Mucor* sp., and only one compound (**40**) showed significant activity against *M. canis*. Three compounds (**39**, **40**, and **53**) inhibit the growth of *A. fumigatus* at 100 μg/mL.

Compound **67** was active against *T. mentagrophytes*, *T. rubrum*, *Cr. neoformans*, and *C. tropicalis* and was the only compound that had an inhibitory effect on the growth of *S. schenckii* at 100 μg/mL. By comparison, it can be concluded that in vitro and in vivo activity are very poorly correlated. Although none of the triazol-3-ones displays any in vitro activity against *M. canis* at 100 μg/mL, when tested under the conditions described, several compounds (**39**, **47**, **62** and **66–68**) demonstrated significant oral activity against experimental microsporosis, even at low doses (2.5 mg/kg). None of the nonalkylated triazol-3-ones was found to be active in established vaginal candidosis and microsporosis at the indicated doses. N-Alkylation has a pronounced enhancing effect on in vivo activity. In the prophylactic experiments against vaginal candidosis as well as against microsporosis, it was seen that nonalkylated triazol-3-ones were less potent than the alkylated analogues.[11] Moreover, the in vivo results prove that it is favorable to substitute a triazole ring for the imidazole moiety (**46** < **62** and **53** < **68**). Introduction of a methyl group in the 5-position of the triazol-3-one ring (R^2) tends to decrease the oral activity, in particular in microsporosis (**66** > **65** and **62** > **63**, and **68** > **72**). No definite conclusions can be drawn concerning the influence of alkyl chain variation (R^1) on biological activity in the imidazole derivatives, since the gained in vivo results are too heterogeneous. Only minor effects on activity in vaginal candidosis have been observed after elongation of the alkyl chain (R^1) from methyl to *n*-propyl (**56**, **58**, and **60**) in the

(10) Van Cutsem, J.; Van Gerven, F.; Zaman, R.; Heeres, J; Janssen, P. A. J. 13th International Congress of Chemotherapy, Vienna, Aug 28–Sept 2, 1983.

(11) Van Cutsem J., unpublished results.

UM00012020
NOVARTIS EXHIBIT 1017
Novartis v. Regents, IPR2023-01346
Page 766 of 4460

Table VI. In Vitro and in Vivo Antifungal Activity

Compd.	IN VITRO [a]											IN VIVO [b]							
	M. c.	T.m.	T.r.	Ph.v.	Cr.n.	C.tr.	C.a.	Muc.	A.f.	Sp.s.	Sapr.	VAGINAL CANDIDOSIS IN RATS				MICROSPOROSIS GUINEA PIGS			
												DOSE (mg/kg)				DOSE (mg/kg)			
												10	2.5	1.25	0.63	20	10	2.5	1.25
36	>100	100	>100	>100	>100	100	>100	>100	>100	>100	>100		0/2						
37	>100	10	10	>100	100	10	100	>100	>100	>100	>100						0/2		
38	>100	>100	>100	>100	>100	100	100	>100	>100	>100	>100							0/2	
39	>100	1	1	>100	1	1	>100	>100	100	>100	100	5/6	4/11	3/12	0/4		4/4	2/6	0/6
40	100	10	100	>100	>100	>100	100	>100	100	>100	>100	3/4	0/2			2/2	0/2		
41	>100	100	10	>100	>100	100	100	>100	>100	>100	>100		0/2						
42	>100	100	>100	>100	>100	100	>100	>100	>100	>100	>100		0/2					0/2	
43	>100	100	100	>100	>100	>100	>100	>100	>100	>100	>100	4/4	0/2						
44	>100	>100	>100	>100	>100	100	100	>100	>100	>100	>100		0/2						
45	>100	10	100	>100	>100	10	100	>100	>100	>100	>100		1/2				1/4		
46	>100	100	100	>100	>100	100	100	>100	>100	>100	>100		0/2				2/4	0/2	
47	>100	100	>100	>100	>100	1	100	>100	>100	>100	>100		1/6				5/6	1/6	0/6
48	>100	100	10	>100	>100	100	100	>100	>100	>100	>100		4/6	0/2					
49	>100	10	10	>100	100	1	100	>100	>100	>100	>100		4/8	1/6	0/4		4/6	0/6	0/2
50	>100	100	>100	>100	>100	>100	100	>100	>100	>100	>100		1/2				0/2		
51	>100	100	100	>100	100	100	>100	>100	>100	>100	>100		2/4				2/2	0/2	
52	>100	10	1	>100	>100	10	100	>100	>100	>100	>100		0/2				1/2	0/2	
53	>100	1	1	100	10	1	>100	>100	100	>100	>100		1/2				1/2	2/4	
54	>100	>100	>100	>100	>100	>100	>100	>100	>100	>100	>100						0/2		
55	>100	10	100	100	100	1	>100	>100	>100	>100	>100						0/2		
56	>100	1	10	100	100	10	100	>100	>100	>100	>100	2/2	4/6	5/6	4/8		1/8	0/2	0/2
57	>100	>100	>100	>100	>100	>100	>100	>100	>100	>100	>100	1/2	1/2			0/2			
58	>100	1	1	>100	10	1	100	>100	>100	>100	>100	10/12	13/15	16/18	4/12		4/8	3/10	0/8
59	>100	>100	>100	>100	>100	>100	>100	>100	>100	>100	>100		9/10	1/4	1/6		0/4		
60	>100	100	1	>100	100	100	>100	>100	>100	>100	>100	6/6	9/10	9/10	3/10		1/8	0/5	0/6
61	>100	1	>100	>100	100	100	100	>100	>100	>100	>100		1/4		0/2				
62	>100	100	>100	>100	>100	>100	>100	>100	>100	>100	>100	5/6	20/24	12/22	2/12		6/6	7/12	2/6
63	>100	100	>100	>100	>100	10	>100	>100	>100	>100	>100		1/2				0/2		
64	>100	100	>100	>100	>100	>100	>100	>100	>100	>100	>100		0/2				1/6		
65	>100	10	>100	>100	100	1	100	>100	>100	>100	>100		6/6	6/6	4/11		2/6	0/8	0/8
66	>100	10	10	>100	100	10	100	>100	>100	>100	>100		7/10	7/10	4/10		2/2	5/8	3/6
67	>100	1	10	>100	10	1	>100	>100	>100	100	>100		3/6	1/2	1/6		2/2	4/6	0/4
68	>100	10	10	>100	100	100	>100	>100	>100	>100	>100	12/12	29/34	13/33	7/40		6/6	11/12	12/15
69	>100	100	>100	>100	>100	>100	100	>100	>100	>100	>100		0/2				1/2		
70	>100	100	>100	>100	>100	>100	>100	>100	>100	>100	>100		1/2				2/2	0/2	
71	>100	10	10	100	>100	>100	100	>100	>100	>100	>100		1/2				2/2	0/2	
72	>100	100	>100	>100	>100	>100	10	>100	>100	>100	>100		2/2		0/2		2/2	0/2	
3b	100	1	10	100	10	>100	>100	>100	>100	100	10	1/2	0/2			0/2			
3a	100	1	1	10	10	10	100	>100	100	10	10	173/181	2/8	0/12		30/30	4/34	0/14	

[a] Lowest level of total inhibition (micrograms per milliliter). [b] Ratio of animals cured/animals infected.

triazoles, whereas the *n*-butyl derivative (**64**) is devoid of activity.

Replacement of the *n*-propyl (**60**) by an allyl chain (**67**) tends to decrease the activity against vaginal candidosis, but, on the other hand, an important increase in activity against microsporosis is noticed. Branching of the alkyl chain gives rise to a dramatic increase of activity against vaginal candidosis, as well as against microsporosis (**62**, **66**, and **68**). Introduction of a cyclopropylmethyl group (**71**) for isobutyl (**66**) leads to a decreased activity in both in-

UM00012021
NOVARTIS EXHIBIT 1017
Novartis v. Regents, IPR2023-01346
Page 767 of 4460

fection models. Based on the results,[10] also gained from other animal models, one compound [**68**, (itraconazole, proposed international nonproprietary name)] has been selected for clinical studies.

Experimental Section

Melting points are measured with a Mettler FP_1 melting point apparatus and are uncorrected. New compounds were routinely checked for their structure by UV and/or IR and NMR spectrometry (UV, Hewlett-Packard HP-8450; IR, Perkin-Elmer 580B; NMR, Brucker WP 200).

***cis*-1-Acetyl-4-[4-[[2-(2,4-dichlorophenyl)-2-(1*H*-1,2,4-triazol-1-ylmethyl)-1,3-dioxolan-4-yl]methoxy]phenyl]piperazine (3b).** To a suspension of NaH (50% dispersion) (37.0 g, 0.772 mol) in Me_2SO (1500 mL) was added compound **2** (168.0 g, 0.772 mol). After the solution was stirred for 1 h, **1b** (286.0 g, 0.7 mol) was added, and stirring was continued for 5 h at 80 °C. The reaction mixture was cooled, and water was added. After extraction with CH_2Cl_2, the organic layer was dried ($MgSO_4$) and evaporated to afford an oily residue, which was crystallized from 4-methyl-2-pentanone to give **3b** (240.0 g, 64%), mp 176.4 °C. Anal. ($C_{22}H_{27}Cl_2N_5O_4$) C, H, N.

***cis*-1-[4-[[2-(2,4-Dichlorophenyl)-2-(1*H*-1,2,4-triazol-1-ylmethyl)-1,3-dioxolan-4-yl]methoxy]phenyl]piperazine (4b).** A solution of **3b** (240.0 g, 0.450 mol) and NaOH pellets (22.0 g, 0.54 mol) in *n*-BuOH (1000 mL) was refluxed with stirring overnight. The reaction mixture was cooled, whereupon water was added. The mixture was subsequently extracted with $CHCl_3$; the organic layer was dried ($MgSO_4$) and evaporated in vacuo. The solid residue was crystallized from 4-methyl-2-pentanone/isopropyl ether to give **4b** (156.0 g, 70%), mp 130.6 °C. Anal. ($C_{23}H_{25}Cl_2N_5O_3$) C, H, N.

***cis*-1-[4-[[2-(2,4-Dichlorophenyl)-2-(1*H*-1,2,4-triazol-1-ylmethyl)-1,3-dioxolan-4-yl]methoxy]phenyl]-4-(4-nitrophenyl)piperazine (6b).** A solution of **4b** (150.0 g, 0.306 mol) and 1-chloro-4-nitrobenzene (56.0 g, 0.356 mol) in Me_2SO (400 mL) was stirred overnight at 120 °C in the presence of K_2CO_3 (22.4 g, 0.160 mol). The reaction mixture was cooled and diluted with water. The crystallized product was filtered and taken up in $CHCl_3$. The solution was dried ($MgSO_4$) and evaporated in vacuo, yielding **6b** (180.0 g, 96%), mp 165.0 °C. Recrystallization from *n*-BuOH afforded an analytical sample, mp 167.8 °C. Anal. ($C_{29}H_{28}Cl_2N_6O_5$) C, H, N.

***cis*-4-[4-[4-[[2-(2,4-Dichlorophenyl)-2-(1*H*-1,2,4-triazol-1-ylmethyl)-1,3-dioxolan-4-yl]methoxy]phenyl]-1-piperazinyl]benzenamine (7b).** A solution of **6b** (175.0 g, 0.286 mol) in $MeOCH_2CH_2OH$ (1000 mL) was hydrogenated at 50 °C in the presence of a solution of thiophene (4%) in MeOH (1 mL) with 5% Pt/C (2.0 g) as the catalyst. When hydrogen uptake was complete, the mixture was heated to reflux, and, subsequently, the catalyst was filtered off. While the mixture was cooling, the product crystallized and then filtered off to give **7b** (134.4 g, 81%), mp 180.0 °C. Recrystallization from *n*-BuOH afforded an analytical sample, mp 186.8 °C. Anal. ($C_{29}H_{30}Cl_2N_6O_3$) C, H, N.

***cis*-Phenyl [4-[4-[4-[[2-(2,4-Dichlorophenyl)-2-(1*H*-1,2,4-triazol-1-ylmethyl)-1,3-dioxolan-4-yl]methoxy]phenyl]-1-piperazinyl]phenyl]carbamate (8b).** To a solution of **7b** (129.0 g, 0.222 mol) in $CHCl_3$ (1000 mL) and pyridine (300 mL) was added dropwise over a period of 15 min phenyl chloroformate (36.3 g, 0.232 mol). The reaction mixture was stirred for 3 h, and subsequently, H_2O and petroleum ether were added. The product crystallized and was filtered off. The crystals were subsequently washed with H_2O, *i*-PrOH, and finally with isopropyl ether to give, after drying, **8b** (133.0 g, 86%), mp 203.0 °C. Anal. ($C_{36}H_{34}Cl_2N_6O_5$) C, H. N.

***cis*-*N*-[4-[4-[4-[[2-(2,4-Dichlorophenyl)-2-(1*H*-1,2,4-triazol-1-ylmethyl)-1,3-dioxolan-4-yl]methoxy]phenyl]-1-piperazinyl]phenyl]hydrazinecarboxamide (9b).** Hydrazine hydrate (50.0 g, 1.0 mol) and **8b** (130.0 g, 0.185 mol) in 500 mL of dioxane were stirred and refluxed for 3 h. Subsequently, the reaction mixture was poured into H_2O, whereupon the product crystallized. The crystalline solid was filtered, washed with H_2O and *i*-PrOH, and dried to give **9b** (170.0 g, 99%), mp 199.7 °C. Anal. ($C_{30}H_{32}Cl_2N_8O_4$) C, H, N.

***cis*-4-[4-[4-[4-[[2-(2,4-Dichlorophenyl)-2-(1*H*-1,2,4-triazol-1-ylmethyl)-1,3-dioxolan-4-yl]methoxy]phenyl]-1-piperazinyl]phenyl]-2,4-dihydro-3*H*-1,2,4-triazol-3-one (10b).** Formamidine acetate (83.2 g, 0.800 mol) and **9b** (115.0 g, 0.179 mol) in DMF (300 mL) were stirred at 130 °C for 3 h. The product crystallized on dilution with water. The solid was filtered off and recrystallized from DMF/*i*-Pr_2O, yielding **10b** (72.0 g, 62%), mp 254.4 °C. Anal. ($C_{31}H_{30}Cl_2N_8O_4$) C, H, N.

***cis*-4-[4-[4-[4-[[2-(2,4-Dichlorophenyl)-2-(1*H*-1,2,4-triazol-1-ylmethyl)-1,3-dioxolan-4-yl]methoxy]phenyl]-1-piperizinyl]phenyl]-2,4-dihydro-2-(1-methylpropyl)-3*H*-1,2,4-triazol-3-one (68).** To a suspension of KOH powder (0.7 g, 0.01 mol) and **10b** (5.0 g, 0.0077 mol) in Me_2SO (100 mL) was added 2-bromobutane (1.23 g, 0.009 mol). Stirring was continued for 14 h, whereupon the reaction mixture was diluted with water. Extracting with $CHCl_3$, drying ($MgSO_4$), and evaporating in vacuo afforded a solid,which was chromatographed on silica with $CHCl_3/CH_3OH$ (98:2) as the eluent. The pure compound was recrystallized from toluene to give **68** (2.5 g, 46%), mp 166.2 °C. Anal. ($C_{36}H_{38}Cl_2N_8O_4$) C, H, N.

2,4-Dihydro-4-[4-[4-(4-hydroxyphenyl)-1-piperazinyl]phenyl]-2-(1-methylethyl)-3*H*-1,2,4-triazol-3-one (27). A mixture of **14** (4.7 g, 0.012 mol) and 48% HBr solution (50 mL) was refluxed overnight. The reaction mixture was cooled, whereupon a product crystallized. The solid was filtered off and dissolved in a water/MeOH mixture (50:50). After neutralization of the solution with $NaHCO_3$, the product was extracted with $CHCl_3$ (500 mL). The organic layer was dried ($MgSO_4$) and evaporated to afford a residue, which was crystallized from DMF to give **27** (3.9 g, 86%), mp 208.4 °C. Anal. ($C_{21}H_{25}N_5O_2$) C, H, N.

***cis*-4-[4-[4-[4-[[2-(2,4-Dichlorophenyl)-2-(1*H*-1,2,4-triazol-1-ylmethyl)-1,3-dioxolan-4-yl]methoxy]phenyl]-1-piperazinyl]phenyl]-2,4-dihydro-2-(1-methylethyl)-3*H*-1,2,4-triazol-3-one (62).** To a suspension of NaH (50% dispersion in mineral oil) (0.4 g, 0.0083 mol) in dry Me_2SO (100 mL) was added **27** (3.0 g, 0.0079 mol). after the solution was stirred at 50 °C for 1 h, **1b** (3.2 g, 0.0079 mol) was added, and stirring at 100 °C was continued for 3 h. After dilution with water, the mixture was extracted with CH_2Cl_2; the organic layer was washed with water, dried ($MgSO_4$), and evaporated in vacuo to leave a solid residue. Purification on silica with $CHCl_3/CH_3OH$ (98:2) as the eluent, followed by recrystallization from 4-methyl-2-pentanone, gave **62** (3.5 g, 64%), mp 200.4 °C. Anal. ($C_{34}H_{36}Cl_2N_8O_4$) Cl, N.

Acknowledgment. The authors thank the "Instituut tot Aanmoediging van het Wetenschappelijk Onderzoek in Nijverheid en Landbouw" for financial support. Dr. M. Janssen and H. Vanhove are thanked for helpful suggestions in the preparation of this manuscript.

Registry No. **1a**, 61397-61-3; **1b**, 67914-86-7; **2**, 67914-60-7; **3a**, 65277-42-1; **3b**, 67915-35-9; **4a**, 67914-61-8; **4b**, 67915-50-8; **6a**, 89848-07-7; **6b**, 89872-79-7; **6c**, 74852-61-2; **7a**, 89848-08-8; **7b**, 89848-09-9; **7c**, 74852-62-3; **8a**, 89848-10-2; **8b**, 89848-11-3; **8c**, 74853-06-8; **9a**, 89848-12-4; **9b**, 89848-13-5; **9c**, 74852-89-4; **10**, 74853-07-9; **11**, 74852-91-8; **12**, 74852-95-2; **13**, 74852-92-9; **14**, 89848-14-6; **15**, 89848-15-7; **16**, 89848-16-8; **17**, 74852-90-7; **18**, 74853-02-4; **19**, 74852-93-0; **20**, 74852-94-1; **21**, 89848-17-9; **22**, 89848-58-8; **23**, 89848-18-0; **24**, 79538-92-4; **25**, 74853-20-6; **26**, 79538-91-3; **27**, 89848-19-1; **28**, 89848-20-4; **29**, 89848-21-5; **30**, 74853-17-1; **31**, 74853-18-2; **32**, 74853-19-3; **33**, 89848-22-6; **34**, 89848-23-7; **35**, 89848-24-8; **36**, 89848-25-9; **37**, 89848-26-0; **38**, 89848-27-1; **39**, 89872-80-0; **40**, 89848-28-2; **41**, 89848-29-3; **42**, 89872-81-1; **43**, 89848-30-6; **44**, 89848-31-7; **45**, 89848-32-8; **46**, 89848-33-9; **47**, 89848-34-0; **48**, 89848-35-1; **49**, 89848-36-2; **50**, 89848-37-3; **51**, 89848-38-4; **52**, 89848-39-5; **53**, 89848-40-8; **54**, 89848-41-9; **55**, 89848-42-0; **56**, 89848-43-1; **57**, 89848-44-2; **58**, 89848-45-3; **59**, 89848-46-4; **60**, 89848-47-5; **61**, 89848-48-6; **62**, 89848-49-7; **63**, 89848-50-0; **64**, 89848-51-1; **65**, 89848-52-2; **66**, 89848-53-3; **67**, 89848-54-4; **68**, 84625-61-6; **69**, 89848-55-5; **70**, 89848-56-6; **71**, 89848-57-7; **72**, 89848-59-9; $NH{=}CHNH_2$, 463-52-5; $NH{=}C(CH_3)NH_2$, 143-37-3; *p*-$NO_2C_6H_4Cl$, 100-00-5; 1-(4-methoxyphenyl)piperazine, 38212-30-5.

UM00012022
NOVARTIS EXHIBIT 1017
Novartis v. Regents, IPR2023-01346
Page 768 of 4460

This Page is Inserted by IFW Indexing and Scanning Operations and is not part of the Official Record

BEST AVAILABLE IMAGES

Defective images within this document are accurate representations of the original documents submitted by the applicant.

Defects in the images include but are not limited to the items checked:

- ❑ BLACK BORDERS
- ❑ IMAGE CUT OFF AT TOP, BOTTOM OR SIDES
- ❑ FADED TEXT OR DRAWING
- ❑ BLURRED OR ILLEGIBLE TEXT OR DRAWING
- ❑ SKEWED/SLANTED IMAGES
- ❑ COLOR OR BLACK AND WHITE PHOTOGRAPHS
- ❑ GRAY SCALE DOCUMENTS
- ❑ LINES OR MARKS ON ORIGINAL DOCUMENT
- ❑ REFERENCE(S) OR EXHIBIT(S) SUBMITTED ARE POOR QUALITY
- ❑ OTHER: _____

IMAGES ARE BEST AVAILABLE COPY.
As rescanning these documents will not correct the image problems checked, please do not report these problems to the IFW Image Problem Mailbox.

Itraconazole Affects Single-Dose Terfenadine Pharmacokinetics and Cardiac Repolarization Pharmacodynamics

Peter K. Honig, MD, MPH, Dale C. Wortham, MD, Robert Hull, MD, Kaveh Zamani, PhD, Julie E. Smith, BSN, and Louis R. Cantilena, MD, PhD

The object of this study was to examine prospectively the effects of itraconazole on the pharmacokinetics and electrocardiographic repolarization pharmacodynamics (QTc intervals) of single-dose terfenadine in six healthy volunteers. It was designed as a prospective cohort study with each subject serving as his own control, set in an outpatient cardiology clinic. The participants were six healthy volunteers (two men, four women; ages 24–35) not taking any prescription or over-the-counter medications. Single-dose terfenadine administration (120 mg) was accompanied by pharmacokinetic profiles and serial determination of the QTc interval for 12 hours. The subjects then began daily oral itraconazole (200 mg each morning) for 7 days. Repeat pharmacokinetic and pharmacodynamic determinations were made after administration of a second dose (120 mg) of terfenadine while receiving itraconazole. The main outcome measures were terfenadine and acid metabolite serum concentrations; corrected QT intervals as determined by 12-lead electrocardiogram (ECG); and presence or absence of late potentials as determined by signal-averaged ECGs over 150 cardiac cycles. There were significant changes in the pharmacokinetic parameters of acid metabolite after treatment with itraconazole. All subjects had detectable levels of unmetabolized terfenadine after addition of itraconazole, which was associated with QT prolongation. There was no evidence of late depolarization as manifested by an increase in QRS duration found using signal-averaged electrocardiography. Itraconazole influences the metabolism of terfenadine in normal volunteers and results in the accumulation of unmetabolized parent drug associated with altered cardiac repolarization. This drug combination should be avoided.

The metabolism of terfenadine is significantly influenced by concomitant administration of ketoconazole and some of the macrolide antibiotics.[1–3] The inhibition of the biotransformation of terfenadine allowing the accumulation of unmetabolized terfenadine is accompanied by altered cardiac repolarization. In vitro, parent terfenadine is a potent inhibitor of the delayed rectifier potassium current (I_k) in isolated cardiac myocytes.[4] This is a feature shared by other drugs, such as quinidine, that prolong the QT interval.[5] The potential seriousness of such drug interactions involving terfenadine is well illustrated by a case in which a young woman taking terfenadine and ketoconazole concomitantly had repeated symptomatic episodes of the serious ventricular arrhythmia, torsades de pointes.[6] The spontaneous reporting of other similar serious events to the Food & Drug Administration (FDA) and the results of prospective, controlled pharmacokinetic-pharmacodynamic studies resulted in a labeling change that contraindicated the concomitant use of terfenadine with either ketoconazole or erythromycin.[1,2,7]

Itraconazole is a recently approved oral systemic antifungal agent with an enhanced spectrum of activ-

From the Division of Clinical Pharmacology (Drs. Honig, Zamani, Cantilena, and Ms. Smith), the Uniformed Services University of the Health Sciences, Bethesda, Maryland; and Division of Cardiology (Drs. Wortham and Hull), Walter Reed Army Medical Center, Washington, D.C. The views expressed in this article are those of the authors and do not reflect the official policy of the Uniformed Services University, Walter Reed Army Medical Center, Department of Defense or the Food and Drug Administration. Supported by FDA interagency agreement: FDA 224-88-3006, the Departments of Cardiology and Clinical Investigation of the Walter Reed Army Medical Center. Dr. Honig is a FDA/USUHS Fellow in Clinical Pharmacology. Address for reprints: Louis R. Cantilena, MD, PhD; Division of Clinical Pharmacology, Departments of Pharmacology and Medicine, Uniformed Services University of the Health Sciences, Bethesda, MD 20814-4799.

UM00012024
NOVARTIS EXHIBIT 1017
Novartis v. Regents, IPR2023-01346
Page 770 of 4460

ity over ketoconazole in the treatment of aspergillosis, sporotrichosis, and other mycotic infections.[8] In vitro experiments demonstrate itraconazole to be a weaker, noncompetitive inhibitor of hepatic microsomal oxidation than ketoconazole[9]; however, several reports describe a significant interaction between itraconazole and cyclosporine.[10,11] Because cyclosporin and terfenadine may share metabolic pathways (Personal communication, FP Guengerich, March 1992), a terfenadine interaction with itraconazole seemed plausible. The purpose of this study was to examine prospectively the magnitude of the effects of oral itraconazole on the pharmacokinetics and electrocardiographic pharmacodynamics of single-dose terfenadine in humans and to determine if there exists significant inter-individual variability for this drug–drug interaction.

METHODS

Study Site

This study was conducted at the Division of Cardiology at Walter Reed Army Medical Center, Washington, DC. Determination of plasma terfenadine and metabolite concentrations were performed at the Division of Clinical Pharmacology, Uniformed Services University of the Health Sciences, Bethesda, Maryland. Approval to conduct the study was obtained from the Human Use Committee of the Department of Clinical Investigation of the Walter Reed Army Medical Center.

SUBJECTS

Healthy adult male and female volunteers between the ages of 18 and 65 were eligible. Exclusion criteria were the use of prescription or over-the-counter medications or the presence of cardiac, hepatic, renal, or other systemic illnesses. A negative serum human chorionic gonadotropin (β-HCG) was required for exclusion of pregnancy for all female subjects.

Enrollment Protocol

Six volunteers were enrolled. No volunteering subjects were excluded. After informed consent was obtained, a complete screening history and physical examination were performed. Laboratory studies included a complete blood count, serum electrolytes, and chemistry panel including serum calcium and magnesium, urinalysis, and baseline resting 12-lead ECG at 25 mm/second and 50 mm/second paper speed.

Study Protocol

Patients reported to the study area after an overnight fast and had sterile catheters placed in a forearm vein, kept patent with heparin, to facilitate repeated blood sampling. Blood was collected with ethylenediaminetetra-acetic acid (EDTA) as an anticoagulant after a waste sample was drawn to minimize any potential effects of the heparin on the sample. Plasma was separated and frozen for later analysis. A predose (trough) blood sample was obtained, and a 12-lead ECG was performed. A single dose (120 mg) of terfenadine was administered, and blood samples were drawn at 0.5, 1, 2, 4, 6, 8 and 12 hours afterwards. All medications were administered with 4 to 6 ounces of water and no food was allowed for 1 hour after dosing. Twelve-lead ECGs were performed at 1, 2, 4, 6, 8, and 12 hours after dosing. Signal-averaged ECGs of 150 cardiac cycles were obtained before dosing and at 2, 6, and 12 hours after terfenadine administration. Itraconazole (200 mg by mouth every morning) was administered beginning at 8:00 AM the next day (Day 9). After having taken itraconazole for 6 days, the subjects reported for the second pharmacokinetic profile and electrocardiographic evaluation after receiving the second dose of terfenadine and final dose of itraconazole.

Terfenadine and Acid Metabolite Assays

Plasma was separated from blood cells by centrifugation at 1000g within 30 minutes of phlebotomy and stored frozen at −70°C. Concentrations of terfenadine and acid metabolite were determined within 30 days of collection. A solid-phase extraction was used to prepare the samples for quantification by automated high-performance liquid chromatography with fluorescence detection.[12] The lower limit of quantification in plasma for both parent terfenadine and its acid metabolite was 5 ng/mL. The coefficients of variation for this assay were 6% for terfenadine and 12% for acid metabolite at the lowest control point.

Analysis of Electrocardiograms

All 12-lead ECG tracings were performed using a Marquette MAC 15 Series (Milwaukee, WI) machine by the same individual during the study to maintain uniformity of technique. All identifying information was removed from the tracings, which were then coded, randomized, and blinded for ECG interval determination by another investigator. The rate-corrected QT interval (QTc) was determined using the formula of Bazett[13] after cycle lengths (R-R inter-

UM00012025
NOVARTIS EXHIBIT 1017
Novartis v. Regents, IPR2023-01346
Page 771 of 4460

val) and QT intervals were ascertained from the average measurements of three distinct leads (II, aVF, V2) over a minimum of three cycles. For the analysis of T-U complex morphology, the ECG tracings were grouped by subject, blinded, and serially compared.

Signal-averaged ECGs were obtained over 150 cardiac cycles using an ART (Arrhythmia Research Technologies; Austin, TX) recorder. Data were digitally stored before quantitative analysis of total QRS duration and for evidence of late potentials.

Statistical Analysis

Wilcoxon signed-rank tests were used to compare the maximum concentration (Cmax), time to maximum concentration (tmax), half-life ($t_{1/2}$), and areas under the concentration–time curve ($AUC_{0-\infty}$) of acid metabolite before and after the addition of itraconazole.[14] The elimination rate constant (k) was calculated for acid metabolite as the slope of a log-linear regression of the terminal elimination phase. The acid metabolite half-life in each subject was calculated by the formula: $t_{1/2} = .693/k$. Area under the curve was calculated by the trapezoidal rule for the measured concentrations during the dosing interval plus the last time point/k[15]. Electrocardiographic data (ECG_{max}) of the two treatment periods and baseline were compared using the Scheffe-F test for repeated measures.[14] Area under the curve of the QTc over the 12-hour terfenadine dosing interval before and after the addition of itraconazole were compared using the Wilcoxon signed-rank test. A value of $P < .05$ was required to reject the null hypothesis for all statistical comparisons.

RESULTS

Subject Demographics and Laboratory Results

No subjects were excluded during the screening and enrollment process. Laboratory values for potassium, magnesium, and calcium were within the normal range for all subjects. Table I shows the demographic characteristics of the six subjects.

TABLE I

Subject Demographics

Subject Number	Age (Years)	Gender (M/F)	Height (inches)	Weight (kg)
1	24	F	67	52
2	35	M	65	68
3	33	F	67	61
4	29	F	66	75
5	31	M	72	79
6	31	F	65	73

Pharmacokinetics

After the first dose of terfenadine, the mean Cmax ± standard error of the mean of the acid metabolite was 469 ng/mL ± 136 (range, 243–1136 ng/mL), which is in accordance with published values for single 120-mg dosing (Figure 1).7 The tmax of acid metabolite was 2.3 ± .3 hours (range, 2–4 hours). After 1 week of itraconazole, the pharmacokinetic parameters (Cmax, tmax, and AUC_t) for the acid metabolite were significantly changed. Maximum peak plasma concentration of the acid metabolite ranged from 126 to 380 ng/mL (mean = 272 ± 37 ng/mL), and time to maximum concentration increased to 5.7 ± 0.6 hours (range, 4–8 hours). The mean acid metabolite $AUC_{0-\infty}$ increased 30% (2732 ng·hr/mL to 3549 ng·hr/mL, Figure 1 and Table II); however, this change was not statistically significant.

Three (Subjects 1, 3, and 6) of the six volunteers had quantifiable maximum concentrations of unmetabolized terfenadine (Cmax = 8.0, 8.0, and 6.9 ng/mL, respectively) during the first pharmacokinetic profile. In contrast, at the time of the second pharmacokinetic profile, all six subjects demonstrated easily quantifiable concentrations of unmetabolized terfenadine. Subjects 1, 3, and 6 had higher concentrations of unmetabolized terfenadine (Cmax = 17.2, 10.0, and 17.7 ng/mL, respectively) after the addition of itraconazole. Figure 2 shows the individual concentration–time curves for unmetabolized terfenadine administered after 1 week of itraconazole, demonstrating marked intersubject variability in AUC and Cmax.

Pharmacodynamics

Symptoms. None of the six subjects displayed any unusual reactions or offered any subjective complaints during administration of terfenadine and itraconazole individually or in combination. Subjects were specifically questioned for any dizziness, palpitations, chest discomfort, shortness of breath, headaches, drowsiness, sleep disturbances, or gastrointestinal distress, and all denied such problems.

Electrocardiographic Findings

There was no significant change in the corrected mean QT interval or AUC of the corrected QT intervals after terfenadine alone. For the group, the mean

UM00012026
NOVARTIS EXHIBIT 1017
Novartis v. Regents, IPR2023-01346
Page 772 of 4460

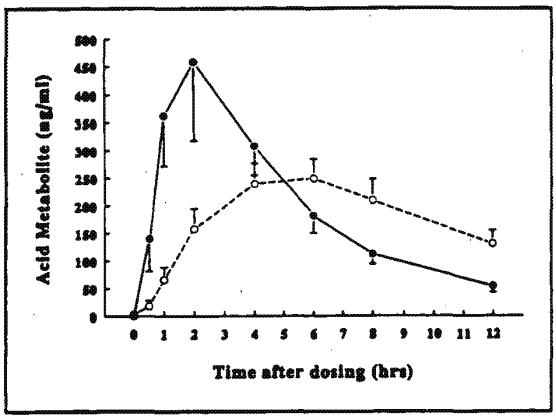


Figure 1. Mean acid metabolite concentration–time graph of six subjects receiving single-dose terfenadine along (solid line and markers) and with concomitant itraconazole (broken line and open markers). Error bars represent standard error of the mean.

maximum baseline QTc was 410 ± 9.1 msec (Mean ± SEM), which increased to 425 ± 9.0 msec after the single dose of terfenadine. The addition of itraconazole to terfenadine resulted in a significant increase from baseline to 432 ± 11.5 msec, which was associated with detectable levels of unmetabolized terfenadine in the blood (Table III). Figure 3 shows the mean QTc intervals during the dosing interval after a single dosing of terfenadine before and after 1 week of itraconazole. The difference in areas under each curve (AUC) was also statistically significant (Table III).

Qualitative morphologic analysis of the 12-lead ECGs did not demonstrate significant changes. The signal-averaged electrocardiograms failed to show increases in QRS duration or evidence of late potentials.

DISCUSSION

Itraconazole was approved by the FDA in 1992 for the treatment of severe systemic mycotic infections.[16] Based on its chemical and structural similarity to ketoconazole, labeling included a contraindication for concomitant use of terfenadine. This decision did not reflect the results of prospective clinical studies investigating this drug combination in a controlled fashion; however, the FDA has four well-documented reports of severe cardiac complications resulting from this interaction (Personal Communication: M. Sevka, FDA). One case involved a 28-year-old woman who had prolonged QT intervals and torsades de pointes accompanied by measurable concentrations (28 ng/mL) of unmetabolized terfenadine. This patient was rechallenged with a single 120-mg dose of terfenadine without itraconazole and had no quantifiable concentrations of unmetabolized terfenadine. Another report involved the death of a 21-year-old woman receiving both terfenadine and itraconazole who had quantifiable (10.8 ng/mL) antemortem blood concentrations.

This study demonstrates the pharmacokinetic interaction as shown by the accumulation of the unmetabolized parent drug and, more importantly, shows the consequences of this accumulation, which are changes in electrocardiographic repolarization. The effect may have been more profound if dosing to steady-state had been performed, as in the design of a terfenadine–ketoconazole interaction study in which comparable concentrations of unmetabolized terfenadine were accompanied by profound alterations in cardiac repolarization.[1]

TABLE II

Acid Metabolite Pharmacokinetic Parameters

Subject Number	C_{max} (ng/mL) T alone	C_{max} (ng/mL) T + Itraconazole	AUC (ng*hr/mL) T Alone	AUC (ng*hr/mL) T + Itraconazole	t 1/2 (hr) T Alone	t 1/2 (hr) T + Itraconazole
1	1136	319	5666	3441	3.7	6.1
2	294	126	1853	1602	3.1	6.1
3	337	273	2213	2809	3.1	4.7
4	421	380	2143	4058	3.3	4.4
5	243	219	1792	3215	3.7	6.4
6	388	317	2724	6171	3.6	10.3
Mean ± SEM	470 ± 136	272 ± 37*	2732 ± 603	3549 ± 622	3.4 ± .12	6.3 ± .86*

** Indicates significant difference ($P < .05$)*

UM00012027
NOVARTIS EXHIBIT 1017
Novartis v. Regents, IPR2023-01346
Page 773 of 4460

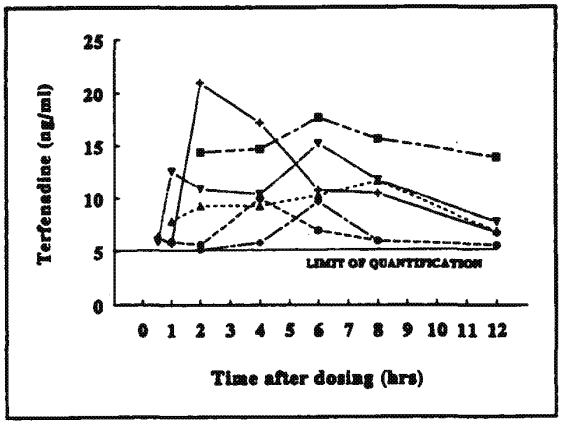


Figure 2. Individual single-dose terfenadine concentration–time profiles of the six subjects after receiving itraconazole for 1 week.

Marked intersubject variability in the magnitude of itraconazole-induced changes in terfenadine pharmacokinetics was found. This may be due to several factors, including intersubject variability of the bioavailability of itraconazole or terfenadine. Alternatively, the cytochrome responsible for the oxidative metabolism of terfenadine may be variably expressed in the human population. Nifedipine has a large intersubject pharmacokinetic variability and is thought to share metabolic pathways with terfenadine.[17] It is certainly plausible that the wide population variability in the metabolic capability of this cytochrome may explain the detection of small quantities of unmetabolized parent compound while on terfenadine alone and the wide variability in the magnitude of inhibition by itraconazole across this relatively small group.

The design of this single-dose interaction study produced a different pattern in the before/after concentrations of acid metabolite than seen in previous steady-state terfenadine interaction studies.[1–3] An explanation is offered by the fact that the acid metabolite is further oxidatively metabolized to an inactive second metabolite.[18] A steady-state interaction study may allow for inhibition of this second process and accumulation of the acid metabolite. This hypothesis is substantiated by analysis of the extrapolated single-dose AUC data that shows an increase after the addition of itraconazole (Table II).

This study shows that itraconazole alters the metabolism of terfenadine, leading to the accumulation of the cardiotoxic unmetabolized parent compound and alteration of cardiac repolarization in all subjects studied. Prolongation of the QT interval suggests an increased risk for torsades de pointes.[19] Signal-averaged electrocardiography was performed in an attempt to detect any effect on conduction as determined by total QRS duration and late potentials that may be a marker for individual susceptibility to reentrant ventricular tachycardia. No evidence of late potentials was found in this study; however, most of the literature demonstrating the predictive utility of this technique involves studies with post-myocardial infarction patients and may not apply to this drug-induced condition.[20]

An itraconazole-only arm to control for the effects of this antifungal agent on the electrocardiogram was not performed throughout the entire dosing interval because itraconazole is not known to have clinically significant effects on cardiac repolarization. Because the predose electrocardiograms and signal-averaged studies after 1 week of itraconazole were unchanged from baseline, we believe that the likelihood of itraconazole confounding the electrocardiographic findings is small.

TABLE III

Electrocardiographic Outcome Parameters

Subject Number	Baseline QTc (msec)	QTc MAX (msec) T Alone	QTc MAX (msec) T + Itraconazole	AUC of ECG T Alone	AUC of ECG T + Itraconazole
1	355	377	416	4887	5003
2	372	371	385	4670	4660
3	398	416	441	5296	5612
4	378	410	418	5009	5067
5	388	382	409	4867	4928
6	366	388	431	4968	5046
Mean ± SEM	376 ± 6.3	390 ± 7.5	417 ± 7.9*	4950 ± 84	5053 ± 127†

* *Indicates significant difference from baseline and terfenadine alone periods.* † *Indicates significant difference from AUC during terfenadine alone period.*

UM00012028
NOVARTIS EXHIBIT 1017
Novartis v. Regents, IPR2023-01346
Page 774 of 4460

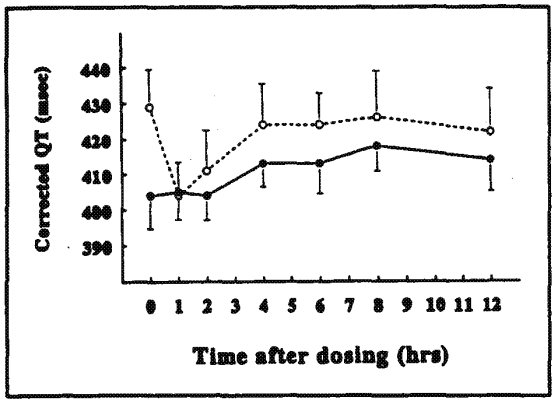


Figure 3. Mean QTc measurements of the six subjects during the dosing interval (12 hours) for single-dose terfenadine alone (solid line, solid markers) and after 1 week of itraconazole (broken line, open markers). Error bars represent standard error of the mean.

It is still unknown what factors are responsible for the individual susceptibility to cardiac arrhythmia in patients concomitantly receiving itraconazole and terfenadine. Terfenadine is known to have other metabolites that also may contribute to the electrocardiographic effects we have described.[18]

Furthermore, as demonstrated in this study, there exists large interindividual pharmacodynamic variability in QT response as well as the wide variability in the pharmacokinetic effect of itraconazole on terfenadine. It is imperative that awareness of this potentially fatal drug–drug interaction in the prescribing community be achieved. It is important to disseminate the knowledge of this drug–drug interaction to health care practitioners through continuing education and appropriate product labeling.[16,21]

The authors thank Drs. Gregory Burke and Michael Sevka of the FDA for their cooperation in this study. They thank Ms. Kristine Hoffman for her excellent technical assistance. They are grateful to Al Szkutnik and the Pharmacy staff, WRAMC.

REFERENCES

1. Honig PK, Wortham DC, Zamani K, Conner DP, Mullin JC, Cantilena LR: Terfenadine-ketoconazole interaction: pharmacokinetic and electrocardiographic consequences. *JAMA* 1993;269: 1513–1518.

2. Honig PK, Woosley RL, Zamani K, Conner DP, Cantilena LR: Changes in the pharmacokinetics and electrocardiographic pharmacodynamics of terfenadine with concomitant administration of erythromycin. *Clin Pharmacol Ther* 1992;52:231–238.

3. Honig PK, Wortham DC, Zamani K, Conner DP, Cantilena LR: Effect of the erythromycin, clarithromycin and azithromycin on the pharmacokinetics of terfenadine. *Clin Pharmacol Ther* 1993;53:161.

4. Woosley RL, Chen Y, Freiman JP, Gillis RA: Mechanism of the cardiotoxic actions of terfenadine. *JAMA* 1993;269:1532–1536.

5. Schwartz PJ, Locati E, Priori SG, Zaza A: The long QT syndrome, in Zipes DP, Jaliffe J (eds.): Cardiac electrophysiology; From cell to bedside. Philadelphia: Saunders, 1990.

6. Monahan BP, Ferguson CL, Killeavy ES, Lloyd BK, Troy J, Cantilena LR: Torsades de pointes occurring in association with terfenadine use. *JAMA* 1990;264:2788–2790.

7. Matthews DR, McNutt B, Okerholm R, Flicker M, McBride G: Torsades de pointes occurring in association with terfenadine use (letter). *JAMA* 1991;266:2375–2376.

8. Cleary JD, Taylor JW, Chapman SW: Itraconazole in antifungal therapy. *Ann Pharmacother* 1992;26:502–508.

9. Back DJ, Tjia JF: Comparative effects of the antimycotic drugs ketoconazole, fluconazole, itraconazole and terbinafine on the metabolism of cyclosporin by human liver microsomes. *Br J Clin Pharmac* 1991;32:624–6.

10. Kwan JTC, Foxall PJD, Davidson DGC, Bending MR, Eisinger AJ: Interaction of cyclosporin and itraconazole (letter). *Lancet* 1989;2:282.

11. Trenk D, Brett W, Jahnchen E, Birnbaum D: Time course of cyclosporin/itraconazole interaction. *Lancet* 1987;2:1335–1336.

12. Coutant JE, Westmark PA, Nardella PA, Walter SM, Okerholm RA: Determination of terfenadine and terfenadine acid metabolite in plasma using solid-phase extraction and high-performance liquid chromatography with fluorescence detection. *J Chromatogr* 1991;570:139–148.

13. Bazett HC. An analysis of the times relations of electrocardiograms. Heart 1920;7:353–370.

14. Bethea RM, Duran BS, Boullion TL: Statistical methods for engineers and scientists. 2nd ed. New York: Marcel Dekker, 1985.

15. Gibaldi M: Biopharmaceutics and clinical pharmacokinetics. Philadelphia: Lea and Febiger, 1984.

16. Sporonox® Product Labelling. Piscataway, NJ: Janssen Research Foundation. 1992.

17. Breimer DD, Schellens JHM, Soons PA: Nifedipine: Variability in its kinetics and metabolism in man. *Pharmacol Ther* 1989;44:445–454.

18. Garteiz DA, Hook RA, Walker BJ, Okerholm RA: Pharmacokinetics and biotransformation studies of terfenadine in man. *Arzneimittelforshung* 1982;32:1185–1190.

19. Algra A, Tijssen JGP, Roelandt JRTC, Pool J, Lubsen J: QTc prolongation measured by standard 12-lead electrocardiography is an independent risk factor for sudden death due to cardiac arrest. *Circulation* 1991;83:1888–1894.

20. Kelen G: Ambulatory electrocardiography signal averaging: Practicalities, clinical value, and potential applications. *Cardiol Clin* 1992;10:539–549.

21. Seldane® Product Labelling. Marion Merrell Dow, Inc. Kansas City, MO. 1993.

UM00012029
NOVARTIS EXHIBIT 1017
Novartis v. Regents, IPR2023-01346
Page 775 of 4460

□ CASE REPORT □

Successful Treatment of Cerebral Aspergillosis with a High Oral Dose of Itraconazole after Excisional Surgery

Tomihiro IMAI, Toshiyuki YAMAMOTO, Shingo TANAKA, Motoi KASHIWAGI, Susumu CHIBA, Hiroyuki MATSUMOTO and Teiji UEDE*

We report a case of cerebral aspergillosis which originated from the sphenoid sinus, and involved a progressive decrease of visual acuity. The neurological signs indicated a cavernous sinus invasion. After extensive intracranial surgery we treated the residual aspergillosis with a high oral dose of itraconazole (800 mg/d for 4 months, followed by 400 mg/d for 5 months). The neurological impairments of the patient gradually subsided with the resolution of the fungal lesion shown on MRI. The successful therapy indicated that itraconazole has a significant role in the treatment of advanced cerebral aspergillosis if it is used in high doses (16 mg/kg/d for adults). (Internal Medicine 38: 829–832, 1999)

Key words: fungus infection, sphenoid sinus, brain abscess, MRI

Introduction

Cerebral aspergillosis due to a primary infection of the nasal sinuses is common in hot and dry areas such as the Sudan, but it is rare in Japan (1, 2). This form of cerebral aspergillus infection has a very poor prognosis in spite of intracranial surgery and conventional antifungal therapy. Recent reviews suggest that high-dose itraconazole (ITZ) is a suitable treatment for cerebral aspergillosis (3). We report a case of a skull base aspergillus infection which originated from the sphenoid sinus. It was successfully treated with high-dose ITZ.

Case Reports

In September 1996 a 47-year-old man with a history of poorly controlled diabetes mellitus was admitted to the Department of Ophthalmology in our hospital. He presented with a loss of left visual acuity which had developed in 1 month. Following a tentative diagnosis of optic neuritis, he received high doses of intravenous corticosteroids as a treatment. However subsequent cranial computed tomography (CT) showed an enhanced lesion in the left sphenoid sinus and also the left optic canal. An external sphenoidectomy was performed and a thick pasty material was aspirated. When the aspirated material was examined microscopically numerous aspergilli were evident. The treatment was then changed to intravenous fluconazole (FLCZ) at 200 mg/d (equivalent to 2 mg/kg of body weight) for 1 week, and then increased to 600 mg/d (equivalent to 12 mg/kg of body weight) for the next 2 weeks, but no clinical improvement was observed. Cranial magnetic resonance imaging (MRI; GE Signa 1.5 tesla system) of the patient revealed a direct extension of the lesion from the left sphenoid sinus to the left frontal lobe (Fig. 1 and 2A). The patient was transferred to the Department of Neurology in October 1996. On admission he complained of a dull pain in the left frontal area which subsided after nonsteroidal anti-inflammatory drug administration. The patient was afebrile, completely conscious and well-orientated, but blind in the left eye with a Marcus-Gunn pupil. Neither extraocular muscle weakness nor ptosis were observed. The other cranial nerves and the cerebellum were intact and abnormalities in the trunk and limbs were not detected. The results of routine hematological and biochemical investigations were within normal limits. The erythrocyte sedimentation rate was normal, and the result of a test for C-reactive protein was negative. The total protein and cell count in the CSF were 65 mg/dl, and 1 lymphocyte and 2 neutrocytes per mm^3, respectively. The patient's diabetes mellitus was controlled by insulin therapy and repeat electroencephalograms indicated the absence of any abnormality. After admission he developed ptosis and weak extraocular muscles due to a left oculomotor palsy, but he did not complain of double vision (due to left blindness).

Treatment with ITZ was started initially at 200 mg/d, po, together with FLCZ (600 mg/d, iv). An incomplete recovery of the left extraocular muscles was obtained by this regimen within 2 weeks. Subsequently the FLCZ was reduced and he

From the Departments of Neurology and *Neurosurgery, School of Medicine, Sapporo Medical University, Sapporo
Received for publication October 30, 1998; Accepted for publication May 17, 1999
Reprint requests should be addressed to Dr. Tomihiro Imai, the Department of Neurology, School of Medicine, Sapporo Medical University, South 1 West 16 Chuo-ku, Sapporo 060-8543

UM00012030
NOVARTIS EXHIBIT 1017
Novartis v. Regents, IPR2023-01346
Page 776 of 4460

was kept on ITZ at 200 mg/d for 2 months. Proliferation in the dura adjacent to the left ethmoid and sphenoid sinuses and an intensity-enhanced cyst at the frontal lobe base (Fig. 2A and B) were consistently shown in serial cranial MRIs. Due to a sudden increase in headaches in the left forehead and decreased visual acuity of the right eye, he returned to our department in February 1997. Cranial CT scans revealed a new fungal lesion which had expanded beyond the midline to the right optic canal and involved the right optic nerve. The CT scans did not reveal a granulomatous lesion or fluid retention within the right sphenoid and ethmoid sinuses. On the basis of these findings, we concluded that the sudden loss of right visual acuity was probably caused by constriction of the optic nerve by the granulomatous aspergillus lesion within the right optic canal.



Figure 1. Axial postcontrast T1-weighted image by Gd-DTPA show an invasive aspergillosis from the left sphenoid sinus to the skull base involving the orbital apex.

A right frontotemporal craniotomy was immediately performed to decompress the right optic nerve. It was observed that the dura over the medial part of the right pterion, tuberculum sella and planum sphenoidale was covered with a thick, soft and grayish-granulomatous tissue. The lesion around the right optic nerve was removed meticulously and the roof of the right optic canal was also removed so that the optic nerve was sufficiently decompressed. Although cranial MRIs demonstrated an aspergillus brain abscess in the deep medial frontal

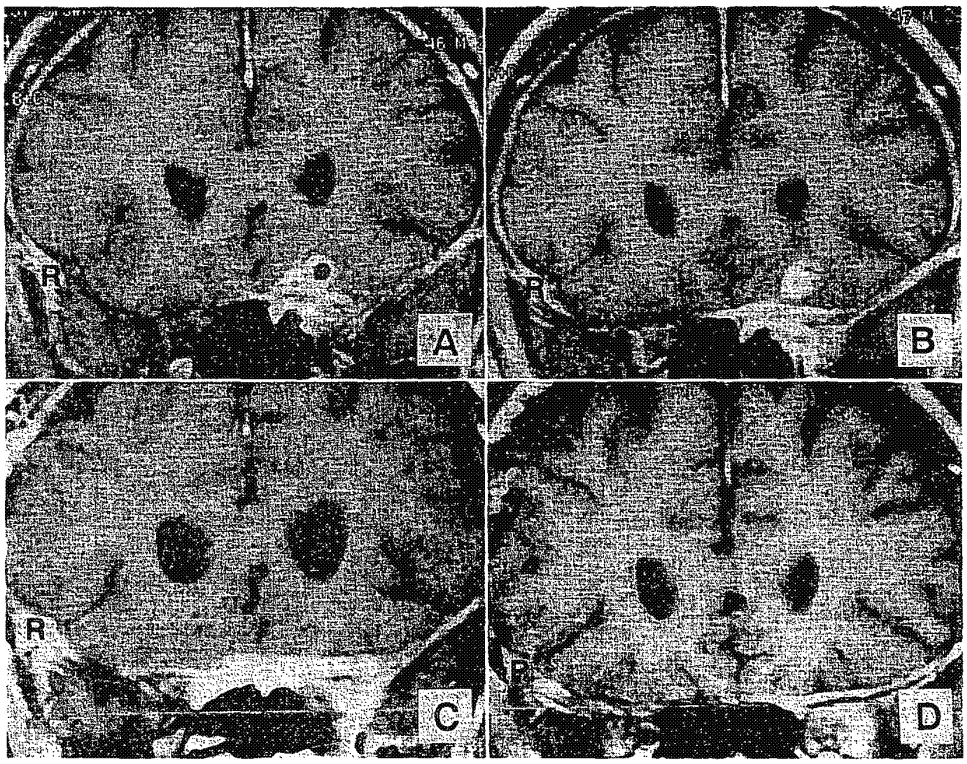


Figure 2. Coronal postcontrast T1-weighted images by Gd-DTPA displayed a cyst and an intensity-enhanced dura at the left frontal lobe base during ITZ therapy of 200 mg/d (A. October 8, 1996; B. November 1, 1996). Repeated MRIs failed to show the enhanced cyst (C. March 3, 1997) and the thickness of the dura (D. July 7, 1997) while the therapy was 400 mg/d of ITZ.

UM00012031
NOVARTIS EXHIBIT 1017
Novartis v. Regents, IPR2023-01346
Page 777 of 4460

lobe (Fig. 2A and B), excisional surgery did not approach the abscess so that the dura remained intact. A histopathological examination of the resected tissue showed the presence of aspergillus hyphae with reactive inflammatory cells. Mucormycosis, which is more common in poorly controlled diabetes mellitus (4), was not present in the tissue.

His visual acuity and right eye movements recovered immediately after the excisional surgery. The dose of ITZ was increased to 600 mg/d (equivalent to 12 mg/kg of body weight) for the next 4 weeks, and then to 800 mg/d (equivalent to 16 mg/kg of body weight). The serum concentration of the antifungal drugs, measured by high power liquid chromatography (5), ranged from 213–866 ng/ml for ITZ and 714–2,355 ng/ml for hydroxyitraconazole (hydroxy-ITZ) at a dose of 200–600 mg/d ITZ (equivalent to 4–12 mg/kg of body weight). After the dose of ITZ was increased to 800 mg/d, the concentrations rose dramatically to 2,561 ng/ml (ITZ) and 4,962 ng/ml (hydroxy-ITZ). Mainly because of their lipophilic characteristics, neither ITZ nor hydroxy-ITZ was detectable in the CSF until the oral ITZ dose reached 800 mg/d. When the patient received 800 mg/d of ITZ for 4 weeks, the CSF concentrations of ITZ and hydroxy-ITZ were 16 and 83 ng/ml, respectively. The left extraocular muscle movements gradually improved with high therapuetic doses of ITZ (800 mg/d) but the left eye remained blind. The patient received 800 mg/d of ITZ for 4 months, followed by 400 mg/d for 5 months. Complete recovery of bilateral extraocular muscle movements was achieved within 3 months after the surgery. Cranial MRIs showed neither a fungal abscess in the frontal lobe (Fig. 2C) nor thickening of the adjacent dura (Fig. 2D) and the cavernous sinus was not enhanced. The patient developed facial pigmentation, eruption of the skin on the upper limbs and trunk, and postural hand tremor during high therapeutic doses of ITZ. Laboratory findings revealed a moderate serum ACTH elevation at 800 mg/d ITZ. All these changes were side effects due to the high dose of ITZ. The skin changes and postural hand tremor eventually disappeared, and the serum ACTH level returned to normal when the dose was reduced.

Discussion

Invasive aspergillosis is usually either a serious complication of immunosuppressive treatment or diseases which profoundly impair normal immunity. Aspergillus infection has been noted in almost every organ and system of the human body (6). Involvement of the lung, sinus, bone and brain was relatively common in the review of 2,121 published cases with invasive aspergillosis (6). Histologically, 20 of 32 necropsies of invasive aspergillosis showed a wide range beyond the lungs, with the brain being the most common site (7).

Invasive aspergillosis from the sinuses into the skull base often affects the orbits, the cavernous sinuses, and involves the cranial nerves. In an advanced stage it causes carotid arteritis, carotid occlusion, meningitis and brain abscesses. The mortality rate is very high in the advanced condition (2). At present, there is no completely effective treatment for aspergillus brain abscesses. Aspergillus abscesses with capsules are often surgically drained or removed, depending on the size and location of a lesion, yet this is rarely curative. Any successful outcome in the reported cases with cerebral aspergillosis can be attributed to a combination of aggressive surgery supplemented by the use of antifugal drugs, including ITZ (8).

Amphotericin B is the only antifungal agent licensed in the United States of America for the treatment of aspergillosis (9). The side effects of this agent frequently include febrile reactions and nephrotoxicity (10), and its efficacy is said to be suboptimal (9). To attain a significantly higher tissue level with less toxicity than conventional amphotericin B (8), a lipid formulation of amphotericin B has been recommended as the first-line therapy for cerebral aspergillosis. However this drug has not been available in Japan. A significant efficacy of miconazole and FLCZ for human aspergillus infections (6) has not been demonstrated. Indeed in the present case, even at high doses, FLCZ did not prevent progression of the disease.

Itraconazole is a triazole derivative with a broad antifungal spectrum which includes the aspergillus species (11–13); it is been available as an oral preparation. Its distribution in human tissues has been studied after single or repeated oral administrations of 100 mg or 200 mg (14). Although concentrations of ITZ were below 1–2 ng/ml in most body fluids, the tissue concentrations of ITZ were much higher, indicating extensive distribution of the drug to the tissues. In humans neither the brain nor meningeal concentration has been determined, however in dogs, during long-term administration the amount of the drug at either site was slightly more than that in the plasma (14). In general ITZ appears to be tolerated well (15) and most of the reported adverse reactions are transient. Gastrointestinal reactions, mild dyspepsia, heart burn, nausea, vomiting, diarrhea and epigastric pain are not uncommon. Administration of high doses gives rise to an increased incidence of side effects: among those documented are severe hypokalemia, reversible adrenal insufficiency and arrythmias. The latter is connected with an interaction with terfenadine. Skin rashes and pruritus have also been reported as hypersensitivity reactions (15). Consequently it is necessary to watch for possible side effects, and to monitor serum concentrations of ITZ during high dose administration. The bioassay technique employed in the present study measured both ITZ and its major active metabolite, hydroxy-ITZ (16). There are no defined concentrations of ITZ and hydroxy-ITZ that consistently yield a predictable and favorable response against invasive aspergillosis (9). In general, however, higher concentrations appear to be desirable. Recent reports have recommended the use of high dose ITZ for high-risk patients with cerebral aspergillosis for whom conventional therapy has failed (3, 17). On the basis of our experience, we strongly recommend high doses of ITZ combined (if necessary) with radical surgery for the treatment of advanced cerebral aspergillosis.

References

1) Lowe J, Bradley J. Cerebral and orbital aspergillus infection due to inva-

UM00012032
NOVARTIS EXHIBIT 1017
Novartis v. Regents, IPR2023-01346
Page 778 of 4460

sive aspergillosis of ethmoid sinus. J Clin Pathol **39**: 774–778, 1986.
2) Tsuboi K, Higuchi O, Nose T, Maki Y. Intracranial aspergillus granuloma originating in the sphenoidal sinus: case report. Neurol Med Chir (Tokyo) **28**: 1014–1019, 1988
3) Sanchez C, Mauri E, Dalmau D, Quintana S, Aparicio A, Garau J. Treatment of cerebral aspergillosis with itraconazole: do high doses improve the prognosis? Clin Infect Dis **21**: 1485–1487, 1995.
4) deShazo RD, O'Brien M, Chapin K, Soto-Aguilar M, Gardner L, Swain R. A new classification and diagnostic criteria for invasive fungal sinusitis. Arch Otolaryngol Head Neck Surg **123**: 1181–1188, 1997.
5) Heykants J, Van Peer A, Van de Velde V, et al. The clinical pharmacokinetics of itraconazole: an overview. Mycoses **32** (Suppl 1): 67–87, 1989.
6) Denning DW, Stevens DA. Antifugal amd surgical treatment of invasive aspergillosis: review of 2121 published cases. Rev Infect Dis **12**: 1147–1201, 1990.
7) Boon AP, O'Brien D, Adams DH. 10 year review of invasive aspergillosis detected at necropsy. J Clin Pathol **44**: 452–454, 1991.
8) Coleman JM, Hogg GG, Rosenfeld JV, Waters KD. Invasive central nervous system aspergillosis: Cure with liposomal amphotericin B, itraconazole, and radical surgery ? case report and review of the literature. Neurosurgery **36**: 858–863, 1995.
9) Dennings DW, Lee JY, Hostetler JS, et al. NIAID mycoses study group multicenter trial of oral itraconazole therapy for invasive aspergillosis. Am J Med **97**: 135–144, 1994.
10) Bennett JE. Antimicrobial agents. Antifungal agents. in: The Pharmacological Basis of Therapeutics, 8th ed, Gilman AG, Rall TW, Nie AS, Taylor P. Eds. Pergamon Press, New York, 1990: 1165–1181.
11) Schmitt HJ, Edwards F, Andrade J, Niki Y, Armstrong D. Comparison of azoles against aspergilli in vitro and in an experimental model of pulmonary aspergillosis. Chemothcrapy **38**: 118–126, 1992.
12) Bailey EM, Krakovsky DJ, Rybak MJ. The triazole anti-fungal agents: a review of itraconazole and fluconazole. Pharmacotherapy **10**: 146–153, 1990.
13) Grant SM, Clissold SP. Itraconazole: a review of its pharmacodynamic and pharmacokinetic properties, and therapeutic use in superficial and systemic mycoses. Drugs **37**: 310–344, 1989.
14) Heykants J, Michiels M, Meuldermans W, et al. The pharmacokinetics of itraconazole in animals and man: an overview. in: Recent Trends in the Discovery, Development and Evaluation of Antifugal Agents, Fromtling RA, Ed. J.R Prous Science Publishers, Barcelona, 1987: 223–249.
15) Tester-Dalderup CBM. Antifungal drugs. in: Meyler's Side Effects of Drugs, 13th ed, Dukes MNG, Ed. Elsevier, Amsterdam, 1996: 774–798.
16) Hostetler JS, Heykants J, Clemons KV, Woestenborghs R, Hanson LH, Stevens DA. Discrepancies in bioassay and chromatography determinations explained by metabolism of itraconazole to hydroxyitraconazole: studies of interpatient variations in concentrations. Antimicrob Agents Chemother **37**: 2224–2227, 1993.
17) Kloss S, Schuster H, Schroten H, Lamprecht J, Wahn V. Control of proven pulmonary and suspected CNS aspergillus infection with itraconazole in a patient with chronic granulomatous disease. Eur J Pediatr **150**: 483–485, 1991.

UM00012033
NOVARTIS EXHIBIT 1017
Novartis v. Regents, IPR2023-01346
Page 779 of 4460

This Page is Inserted by IFW Indexing and Scanning Operations and is not part of the Official Record

BEST AVAILABLE IMAGES

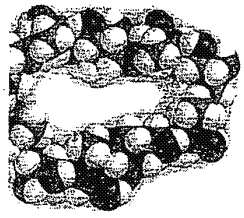
Defective images within this document are accurate representations of the original documents submitted by the applicant.

Defects in the images include but are not limited to the items checked:

- ☐ BLACK BORDERS
- ☐ IMAGE CUT OFF AT TOP, BOTTOM OR SIDES
- ☐ FADED TEXT OR DRAWING
- ☐ BLURRED OR ILLEGIBLE TEXT OR DRAWING
- ☐ SKEWED/SLANTED IMAGES
- ☐ COLOR OR BLACK AND WHITE PHOTOGRAPHS
- ☐ GRAY SCALE DOCUMENTS
- ☐ LINES OR MARKS ON ORIGINAL DOCUMENT
- ☐ REFERENCE(S) OR EXHIBIT(S) SUBMITTED ARE POOR QUALITY
- ☐ OTHER: _____

IMAGES ARE BEST AVAILABLE COPY.
As rescanning these documents will not correct the image problems checked, please do not report these problems to the IFW Image Problem Mailbox.

PU/US04/28156



34

(n = 5).

nbers of sugar units in their
rsors playing the roles of
ses. The success of these
cedure, *ii)* the similarities of
e of the cyclodextrins giving
ar chain prior to cyclisation,
ntersaccharide bonds which
charides are not the same in
redominate very much in the
2 can be explained in terms
-deoxymannose) structures.
es with a diameter of *ca.* 1

lining of the X-ray crystal
elling study, and Mr. P. R.
pported in the UK by the
Research Council, and the

ures and functional units, *Angew.*

dextrins, *Tetrahedron*, 39, 1417-

glycosylation of a (1→4)-linked
d cyclo-*lacto*decaose *Carbohydr.*

ure, *Tetrahedron*, 43, 2389-2436

kov, N. K., Synthesis of 1,2-*O*-
Ser. Khim., 2751-2758 (1978)
hesis of a common antigen of
Res., 193, 75-90 (1989)
ture of uncomplexed hydrated

NEW TYPE OF BRIDGED MONOAMINO-β-CYCLODEXTRINS

J. KOVÁCS[1], Fl. SALLAS[2], I. PINTÉR[1], A. MARSURA[2] and L. JICSINSZKY[3]

[1]*Central Research Institute for Chemistry, H.A.S., H-1525 Budapest, P.O.B. 17, Hungary*

[2]*G.E.V.S.M. EA N° 1123, Université Henri Poincaré, Nancy-1, 5 rue A. Lebrun, B.P. 403, F-54000 Nancy, France*

[3]*Cyclolab, Cyclodextrin Res. and Dev. Laboratory Ltd., H-1525 Budapest, P.O.B. 435, Hungary*

ABSTRACT

The synthesis of new urea-bridged ß-cyclodextrin dimers (CDs) has been successfully achieved by a one-pot transformation of 6-monoazido-6-monodeoxy-ß-CDs (**1** and **2**) *via* the phosphinimines. Pseudo-first-order rate constants for hydrolysis of bis-(*p*-nitrophenyl)-phosphate (BNPP) by metal-complexes of **7** have been measured.

1. INTRODUCTION

Although a large number of synthetic compounds have been designed as biomimetic host molecules [1], only few of them reproduce characteristics of enzymatic action.

In the design of artificial enzymes cyclodextrin hosts are highly available compounds and have interesting properties. Hydrophobic binding of non-polar substrates in water can be achieved with hydrophobic cavities of natural or modified cyclodextrins (CDs). Among numerous published cyclodextrin conjugates [2] cyclodextrin dimers have a special status and notably can bind appropriate substrates very strongly [3].

Another important feature of CD dimers is that the doubly-bound substrate is normally stretched along the linker. In the case of linkers containing a catalytic group, this leads to striking rate acceleration. A representative example was recently reported by Breslow [4]. The dimer including bipyridine moiety is able to coordinate La^{3+} ion and hydrogen peroxide molecule to result in oxidative hydrolysis of phosphate anion or neutral phosphate triester with high rate acceleration.

Considering the increasing interest of this field and the necessity to develop new systems to improve the properties of the previously described enzyme mimics (*e.g.*, selectivity, rate acceleration, chelation) we decided to bring a new contribution with the synthesis of a full family of novel ß-cyclodextrin dimers.

Journal of Inclusion Phenomena and Molecular Recognition in Chemistry **25**: 53–56, 1996.

© 1996 *Kluwer Academic Publishers. Printed in the Netherlands.*

Material may be protected by copyright law (Title 17, U.S. Code)

UM00012035
NOVARTIS EXHIBIT 1017
Novartis v. Regents, IPR2023-01346
Page 781 of 4460

2. MATERIALS AND METHODS

6-Monoazido-6-deoxy-ß-cyclodextrin (**1**) was prepared according to the literature [5, 6] but with only a slight excess of sodium azide (1.2 mol). Acetylation of **1** with pyridine/ acetic anhydride at 80°C afforded the peracetylated **2** as white powder (m.p. 155-157°C) in 91% yield. Phenanthroline-2,9-bis-(2-aminoethyl)-carboxamide (**5**) was obtained as yellow powder from phenantroline-2,9-dicarboxylic acid dimethyl ester with ethylene diamine in 90% yield. Hydrocortison, Ketoconazole and Itraconazole were isolated from commercially available drug formulations by extraction with organic solvents.

Solubility isotherms were measured at 25 ± 1°C, with 48 h equilibration in a Millipore reverse osmotic purified water. Stability constants were determined for 1 : 1 complex composition by linear curve fitting to the solubility isotherms (Table 1). Kinetic measurements were carried out in HEPES buffer (pH 7.06) at room temperature, using dimer **7** (0.2mM), $CuCl_2$, $ZnCl_2$ or $EuCl_3$ (0.2mM), H_2O_2 (48mM) and bis-(*p*-nitrophenyl)-phosphate (BNPP) (0.06mM). Concentration of *p*-nitrophenol, resulted by the hydrolysis, was determined by UV/vis spectrometer at λ_{max} = 400 nm and the rate constants were calculated (Table 2).

3. RESULTS AND DISCUSSION

Hitherto, CD dimers bridged with carbon-sulfur single bonds were obtained by direct condensation of dithiols with 6-monoiodo-6-mono-deoxy-ß-cyclodextrin [7].

We report here the synthesis and characterization of four original symmetrical CD dimers with urea linkage or with a spacer which contains diamino and urea moieties.

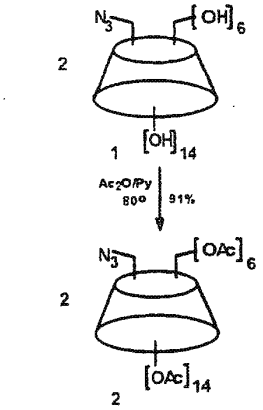
For the synthesis we used the sugar phosphinimine reaction, *i. e.*, conversion of azido sugars with triphenylphosphine and CO_2. From protected azidosugars the reaction leads to the formation of carbodiimides [8] in which two sugar units are linked with carbodiimide bridge. In contrast, from unprotected sugar azides cyclic carbamates [9] were obtained. Both syntheses were carried out either in two steps or under one-pot conditions. Recently, we have found that similar transformation of azidosugars, in the presence of amines, furnishes urea derivatives of the aminosugars corresponding to the starting azides [10].

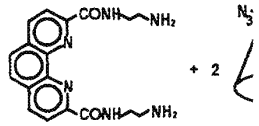
Application of the reaction to 6-monoazido-6-monodeoxy-ß-cyclodextrin (**1**) gave readily the dimer **3** in which the two CD units are bound with urea linkage (Scheme 1). Similarly, the peracetyl compound **2** afforded the acetylated urea-linked dimer (**4**) and not the corresponding carbodiimide. Formation of **4** can be attributed, very probably, to the presence of water molecules complexed by ß-CD. Dimer **4** was also obtained by acetylation of **3** in pyridine/acetic anhydride at 80°C providing evidence for the structure of both molecules (Scheme 1).

Under similar conditions, but in the presence of phenantroline-2,9-bis-(2-aminoethyl)-carboxamide (**5**) **2** gave a new dimer (**6**) in which the two ß-CD units are linked symmetrically to the phenantroline-bis-carboxamide moiety with urea units. Deacetylation of **6** by the Zemplén method gave the hydroxy derivative **7** (Scheme 2).

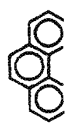
The structures of the new dimers were corroborated by NMR showing the characteristic signals of the CD, phenantrolyl and urea moieties. Data of FABMS analyses matched

also the proposed structure





5



Stability constants of dime
(Table 1).

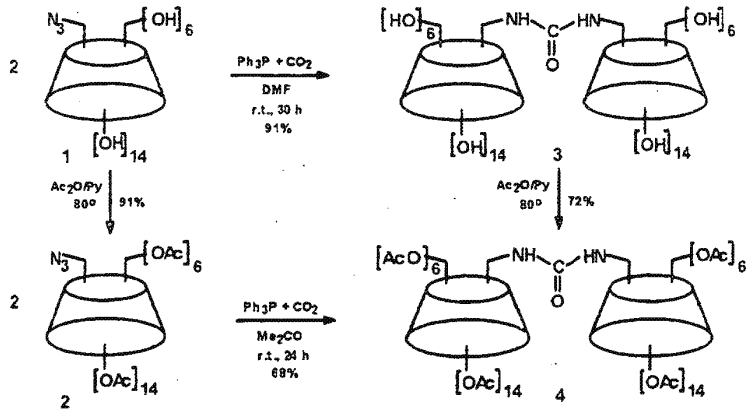
Material may be protected by copyright law (Title 17, U.S. Code)

rding to the literature [5, 6]
tylation of 1 with pyridine/
e powder (m.p. 155-157°C)
amide (5) was obtained as
ethyl ester with ethylene di-
onazole were isolated from
organic solvents.
equilibration in a Millipore
ermined for 1 : 1 complex
s (Table 1). Kinetic measu-
temperature, using dimer 7
nd bis-(*p*-nitrophenyl)-pho-
resulted by the hydrolysis,
nd the rate constants were

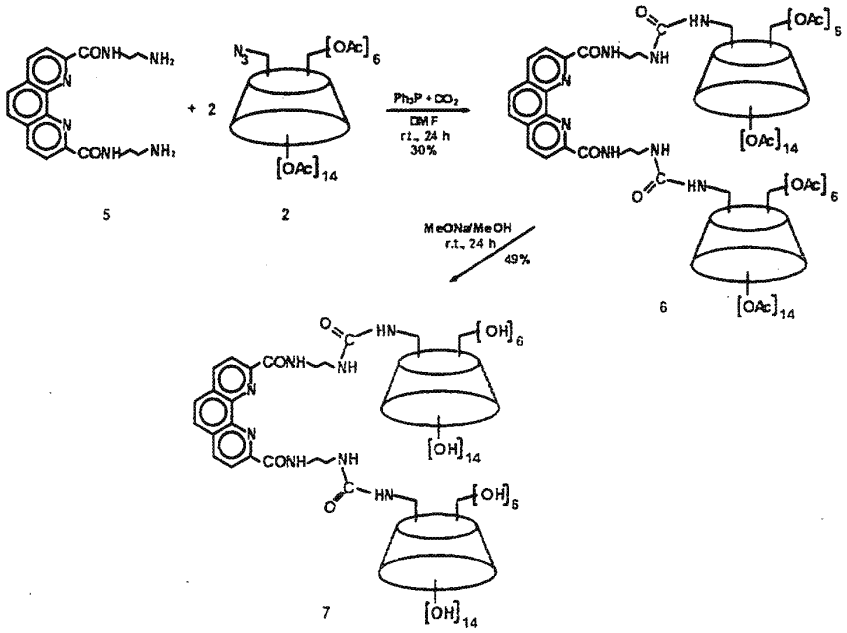
ds were obtained by direct
cyclodextrin [7].
inal symmetrical CD dimers
d urea moieties.
. *e.*, conversion of azido su-
sugars the reaction leads to
re linked with carbodiimide
bamates [9] were obtained.
one-pot conditions. Recent-
, in the presence of amines,
o the starting azides [10].
-cyclodextrin (1) gave rea-
rea linkage (Scheme 1). Si-
ea-linked dimer (4) and not
outed, very probably, to the
as also obtained by acetyla-
nce for the structure of both

line-2,9-bis-(2-aminoethyl)-
ß-CD units are linked sym-
urea units. Deacetylation of
eme 2).
R showing the characteristic
ABMS analyses matched

also the proposed structures.



Scheme 1



Scheme 2

Stability constants of dimers **3** and **7** were determined and compared with those of ß-CD (Table 1).

Material may be protected by copyright law (Title 17, U.S. Code)

UM00012037
NOVARTIS EXHIBIT 1017
Novartis v. Regents, IPR2023-01346
Page 783 of 4460

Table 1. Stability constants of urea-bridged ß-CDs and ß-CD with various drugs

	K [$dm^3.mole^{-1}$]		
CD-compound	Ketoconazole	Itraconazole	Hydrocortisone
3	131	101	2481
7	55	28	
ß-CD	939	250	6111

Complexes of dimer 7 with cations were formed and the rate constants of BNPP hydrolysis were measured under pseudo-first-order conditions (Table 2).

Table 2. Rate constants of BNPP hydrolysis by dimer 7

Compounds	Time(s)	$k_1(s^{-1})$	Time(s)	$k_2(s^{-1})$
7-Cu^{2+}	$0<t<180$	9.55×10^{-4}	$180<t<7.2.10^3$	1.60×10^{-5}
Cu^{2+}	$0<t<10.8\times10^3$	8.62×10^{-6}	$64.8\times10^3<t<97.2\times10^3$	5.69×10^{-8}
7-Eu^{3+}	$0<t<240$	3.10×10^{-4}	$300<t<90\times10^3$	2.10×10^{-6}
Eu^{3+}	$0<t<70.2\times10^3$	6.45×10^{-7}	$75.6\times10^3<t<163.8\times10^3$	2.39×10^{-7}
7-Zn^{2+}	$0<t<7.2\times10^{-3}$	8.03×10^{-6}	$9.0\times10^3<t<14.4\times10^3$	1.80×10^{-7}
Zn^{2+}	no hydrolysis after 72 h			

4. CONCLUSION

Structures of the new CD dimers allow to conclude positively for the scope of this methodology in the synthesis of such derivatives. The calculated complex constants for 1:1 complex compositions are in a similar range to those of ß-CD. Complexation of Hydrocortison by the dimer **7**, however, is more complicated. The low solubility of the complexes are the limits of their application to steroids and conazole-like drugs.

5. ACKNOWLEDGEMENTS

The National Fund for Scientific Research (Hungary, OTKA T014458 and T014939) and the ARC association are acknowledged for financial support and Roquette S.A. (Lestrem France) for providing ß-cyclodextrin.

6. REFERENCES

[1] Bender, M.L., Komiyama, M., in *Cyclodextrin Chemistry*, Springer Verlag, Berlin, 1978; Gutsche, C.D., *Calixarenes*, in *Monographs in Supramolecular Chemistry*, (Ed. Stoddart, J.F.) The Royal Society of Chemistry, Cambridge, 1989; Gokel, G.W., in *Crown Ethers and Cryptands*, The Royal Society of Chemistry, Cambridge, 1991
[2] Breslow, R., *Acc. Chem. Res.*, **28**, 146-153 (1995)
[3] Breslow, R., *Rec. Trav. Chim. Pays-Bas*, **13**, 493-498 (1994)
[4] Breslow, R., Zhang, B., *J. Am. Chem. Soc.*, **116**, 7893-7894 (1994)
[5] Tsujihara, K., Kurita, H., Kawazu, M., *Bull. Chem. Soc. Jpn.*, **50**, 1567-1571 (1977)
[6] Jicsinszky, L., *J. Inclusion Phenom. Mol. Recogn. Chem.*, **18**, 247-254 (1994)
[7] Breslow, R., Halfon, S., Zhang, B., *Tetrahedron*, **51**, 377-388 (1995)
[8] Messmer, A., Pintér, I., Szegő, F., *Angew. Chem.*, **76**, 227-228 (1964); Kovács, J., Pintér, I., Messmer, A., Tóth, G., Duddeck, H., *Carbohydr. Res.*, **166**, 101-111 (1987)
[9] Kovács, J., Pintér, I., Messmer, A., Tóth, G., *Carbohydr. Res.*, **141**, 57-65 (1985)
[10] Pintér, I., Kovács, J., Tóth, G., *Carbohydr. Res.*, **273**, 99-108 (1995)

A NEW SYNTHETIC S

CYCLODEXTRIN-DERI
α (1→4)-LINKED ALT

Y. NOGAMI,[1]
C. SHINOHAR

[1] *Daiichi Colle*
[2] *Faculty of Ph*
Japan

ABSTRACT

An effective synthetic strate
proposed and along this pla
α(1→4)-linked D-altropyra.
yields from the correspondi

1. INTRODUCTION

For the syntheses of the nov
than glucose, there are two t
naturally occurring open cha
oligosaccharides which wer
According to the former stra
intrinsic disadvantages of th
lowers the general applicabi
often lacks control of the re
homologues which are diffi
According to the latter strat
these cases, there are difficu
pure oligomer in each steps
To overcome these difficult
cyclooligosaccharides using
high possibility of the short
easily available in large amo
sized analogues.
Along this project, an appr
altropyranoses, was intende
Scheme 1.

Journal of Inclusion Phenomena an
© 1996 *Kluwer Academic Publisher*

Material may be protected by copyright law (Title 17, U.S. Code)

UM00012038
NOVARTIS EXHIBIT 1017
Novartis v. Regents, IPR2023-01346
Page 784 of 4460

Nor are Hunter and colleagues' PCR data convincing. It would have been surprising not to find trypanosomal DNA in the brain of patients who died only 3–19 days after initiation of therapy, and these workers have no arguments supporting their contention that this implies the presence of live trypanosomes.

It was shown four decades ago that in *T brucei rhodesiense* sleeping sickness, graded dosing of melarsoprol decreases the frequency of PTRE.[5] This has not yet been proved in gambiense trypanosomiasis, and it is still standard practice to initiate treatment with the full dose on the first injection (3·6 mg/kg), to reduce the risk of treatment failures. The minimum effective dose of melarsoprol is not known, and studies with another animal model have suggested that 0·9 to 1·8 mg/kg daily may be sufficient,[6] so that the currently used daily dose may already be overcurative. This finding highlights that what is urgently needed is more aggressive research, with properly designed trials involving large numbers of patients, to answer these very simple questions.

As clinicians who have treated more than 1500 patients with gambiense trypanosomiasis, we are very well aware that melarsoprol treatment is much like playing Russian roulette. We believe that the more aggressive treatment regimens that Hunter et al propose would be equivalent to increasing the number of bullets in the cylinder—perhaps killing the parasites more rapidly but at what cost to the patient?

Université de Montréal,
Montréal, Québec, H1N 1A2 Canada — FRANÇOIS MILORD

Université de Sherbrooke,
Sherbrooke, Québec — JACQUES PEPIN

1. Jennings FW, McNeil PE, Ndung'u JM, Murray M. Trypanosomiasis and encephalitis: possible aetiology and treatment. *Trans R Soc Trop Med Hyg* 1989; 83: 518–19.
2. Pepin J, Milord F. African trypanosomiasis and drug-induced encephalopathy: risk factors and pathogenesis. *Trans R Soc Trop Med Hyg* 1991; 85: 222–24.
3. Clarkson AB, Bienen EJ, Bacchi CJ, et al. New drug combination for experimental late-stage African trypanosomiasis: DL-alpha-difluoromethylornithine (DFMO) with suramin. *Am J Trop Med Hyg* 1984; 33: 1073–77.
4. Hardenberg J, Cawerie N, Tell GP. Eflornithine (Ornidyl) treatment of *Trypanosoma brucei gambiense* sleeping sickness; report of 711 patients treated up to March 1991 (Presented at the 21st meeting of the International Scientific Council for Trypanosomiasis Research and Control, Yamoussoukro, Cote d'Ivoire, October, 1991).
5. Apted FIC. Four years' experience of melarsen oxide/BAL in the treatment of late-stage Rhodesian sleeping sickness. *Trans R Soc Trop Med Hyg* 1957; 51: 75–86.
6. Bouteille B, Darde ML, Pestre-Alexandre M, et al. Traitement de la trypanosomiase expérimentale du mouton à *Trypanosoma brucei brucei*: recherche d'une dose minimale active de melarsoprol. *Bull Soc Pathol Exp Fil* 1988; 81: 548–54.

Eosinophilia, clozapine, and pancreatitis

SIR,—Clozapine has fewer extrapyramidal side-effects than conventional neuroleptics, although it has a particular spectrum of adverse reactions.[1] Acute pancreatitis associated with clozapine has been reported.[2] We report a second case of pancreatitis that also seems to have been caused by clozapine.

A 17-year-old woman who continued to have psychotic symptoms despite treatment with conventional neuroleptic was started on clozapine. After 2 weeks at 100 mg per day, her psychotic symptoms diminished. Other medications were lithium, propranolol, haloperidol, and valproic acid. She had pyrexia, nausea, vomiting, right upper quadrant pain, and tachycardia. Gallbladder studies were normal. Leucocytes ($18·5 \times 10^9$/l), eosinophils (19%), amylase (231 U/ml, normal = 16–108), alkaline phosphatase (147 IU/l, 0–41), and erythrocyte sedimentation rate (60 mm/h) were increased. We presumed clozapine-induced pancreatitis. Because of the association between valproic acid and pancreatitis,[3] valproic acid was stopped with no change in her symptoms. Clozapine was then stopped and her somatic symptoms resolved within a few days. Her psychiatric status deteriorated and 30 days later, clozapine was restarted. Her somatic symptoms recurred within 2 weeks. Leucocyte count rose to $14·8 \times 10^9$/l (no differential was done). Clozapine was stopped and her somatic symptoms resolved. The patient has been off clozapine for the past 2 years with no recurrence of pancreatitis.

There was a temporal relation between the use of clozapine and two episodes of abdominal symptoms with pyrexia and increased leucocyte count, with a clear "on-off-on" pattern. The patient also had an eosinophilia (which has been reported with clozapine)[4,5] at the time of the first episode of pancreatitis, suggesting a possible allergic aetiology.

McLean Hospital,
Belmont,
Massachusetts 02178-9106, USA — FRANCES R. FRANKENBURG
JUDY KANDO

1. Baldessarini RJ, Frankenburg FR. Clozapine: a novel antipsychotic agent. *N Engl J Med* 1991; 324: 746.
2. Martin A. Acute pancreatitis associated with clozapine use. *Am J Psychiatry* 1992; 149: 714.
3. Murphy MJ, Lyon LW, Taylor JW, Mitts G. Valproic acid associated pancreatitis in an adult. *Lancet* 1981; i: 41–42.
4. Stricker BHC, Tielens JAE. Eosinophilia with clozapine. *Lancet* 1991; 338: 1520.
5. Tiihonen J, Paanila J. Eosinophilia associated with clozapine. *Lancet* 1992; 339: 488.

Hepatic injury associated with itraconazole

SIR,—Liver enzyme may be slightly raised during treatment with the antimycotic itraconazole.[1,2] We describe three cases of symptomatic hepatic injury associated with this drug.

Case 1 (62/F, itraconazole 100 mg twice daily for onychomycosis)—5 weeks later she complained of malaise, nausea, pain in right flank, pale stools, and dark urine. Itraconazole was stopped. There was no history of alcohol abuse, operations, or transfusions and she did not use other drugs. Laboratory values are shown in the table. Ultrasonography revealed a mildly enlarged liver. 2 weeks later she had pruritus, weight loss, and jaundice. Total bilirubin and conjugated bilirubin increased to 97 μmol/l and 80 μmol/l, respectively, whereas the other values gradually decreased. 2 months later all laboratory indices were normal.

Case 2 (75/M itraconazole 200 mg twice daily for bronchopulmonary aspergillosis)—In the sixth week of treatment he was jaundiced. There was no history of transfusions or operations and he did not use other drugs. Itraconazole was discontinued. Echography of the liver and biliary tract showed no abnormalities. Serum bilirubin increased to a maximum of 183 μmol/l. 10 weeks later all liver function tests were normal.

Case 3 (57/F itraconazole 100 mg twice daily for chronic mycosis of soles and toe nails)—5 weeks later she had a temperature of 40·2°C, anorexia, headache, and insomnia. She used topical imidazole but no other drugs and there was no history of transfusions or operations. Itraconazole was stopped and the patient received 30 mg prednisone for 5 days, which resulted in disappearance of pyrexia and subjective symptoms. After discontinuation of itraconazole, alkaline phosphatase and γ-GT increased slightly during 10 days to 392 U/l and 275 U/l, respectively. 1 month later, laboratory data were almost normal.

LABORATORY AND SEROLOGICAL INDICES

—	Case 1	Case 2	Case 3	Normal
Alkaline phosphatase (U/l)	593	716	280	40–120
Asparate aminotransferase (U/l)	124	58	182	<25
Alanine aminotransferase (U/l)	227	106	272	<25
γ-GT (u/l)	307	485	227	<35
Total bilirubin (μmol/l)	37	130	–	8–16
Conjugated bilirubin (μmol/l)	27	–	–	<5
Lactate dehydrogenase (U/l)	292	–	409	110–270
Hepatitis A	–	–	–	..
Hepatitis B	–	–	–	..
Toxoplasmosis	IgG + /IgM –	ND	–	..
Epstein-Barr virus	IgG + /IgM –	–	IgG + /IgM –	..
Chlamydia virus	ND	–	ND	..
Cytomegalovirus	–	–	IgG + /IgM –	..
Coxiella burnetii	ND	–	ND	..

γ-GT = gamma-glutamyl transferase. ND = not done. – = negative.

UM00012039
NOVARTIS EXHIBIT 1017
Novartis v. Regents, IPR2023-01346
Page 785 of 4460

07019901

Itraconazole was probably the cause of liver damage in these three patients because other common causes of hepatic injury were excluded and because there was a clear temporal relation between intake and onset of the reaction. Moreover all patients recovered after discontinuation of treatment. Itraconazole is related to miconazole and ketoconazole, for which several cases of symptomatic hepatic injury have been reported.[3] The mild and transient liver enzyme elevations, the paucity of immunoallergic signs, the delayed latent period, and delayed reaction to rechallenge are compatible with metabolic idiosyncrasy to a mildly intrinsic hepatotoxin.

Although the structures of itraconazole and ketoconazole are similar there are pharmacodynamic differences. Whereas ketoconazole influences microsomal cytochrome P-450-dependent monooxygenases,[4] a similar effect has not been demonstrated for itraconazole.[4] But both drugs may increase cyclosporin blood concentrations.[5,6] We conclude that it is highly likely that itraconazole can cause liver injury. It may be advisable to monitor serum liver enzymes in patients who receive (long-term) therapy with itraconazole.

Department of Dermatology, University Hospital, Leiden — A. P. M. LAVRIJSEN

Department of Dermatology, Ziekenhuis Sint Antoniushove, Leidschendam — K. J. BALMUS

Department of Dermatology, Beatrix Ziekenhuis, Gorinchem — W. M. NUGTEREN-HUYING

Department of Medicine, Bronovoziekenhuis, The Hague — A. C. ROLDAAN; J. W. VAN'T WOUT

Netherlands Centre for Monitoring of Adverse Reactions to Drugs, Rijswijk — B. H. CH. STRICKER

1. Restrepo A, Robledo J, Gómez I, Tabares AM, Gutiérrez R. Itraconazole therapy in lymphangitic and cutaneous sporotrichosis. *Arch Dermatol* 1986; 122: 413–17.
2. Legendre R, Esola-Macre J. Itraconazole in the treatment of tinea capitis. *J Am Acad Dermatol* 1990; 23: 559–60.
3. Stricker BHC, Blok APR, Bronkhorst FB, Van Parijs GB, Deamet VJ. Ketoconazole-associated hepatic injury: a clinicopathological study of 55 cases. *J Hepatol* 1986; 3: 399–406.
4. Lavrijsen K, van Houdt J, Thijs D, Meuldermans W, Heykants J. Induction potential of antifungals containing an imidazole of triazole moiety: miconazole and ketoconazole, but not itraconazole are able to induce hepatic drug metabolizing enzymes of male rats at high doses. *Biochem Pharmacol* 1986; 35: 1867–78.
5. Kwan JTC, Foxall PJD, Davidson DGC, Bending MR, Elsinger AJ. Interaction of cyclosporin and itraconazole. *Lancet* 1987; ii: 282.
6. Back DJ, Fjia JF. Comparative effects of the antimycotic drugs ketoconazole, fluconazole, itraconazole and terbinafine on the metabolism of cyclosporin by human liver microsomes. *Br J Clin Pharmacol* 1991; 32: 624–26.

Loss of taste and terbinafine

SIR,—Professor Juhlin (June 13, p 1483) reported loss of taste in a 46-year-old woman receiving treatment with 250 mg terbinafine (Lamisil, Sandoz) for *Trichophyton rubrum* infection of her toenails. Since the only other drug taken by the patient was a combined oral contraceptive (lynestrenol plus ethinyloestradiol) Juhlin considered the possibility of drug interaction, and in so doing misinterpreted a paper from my research group.[1] This paper presented data from an in-vitro study in which two antimycotic drugs, the azole ketoconazole and the allylamine terbinafine, were examined for their effects on the metabolism of several drugs including ethinyloestradiol (EE_2). At 50 µmol/l terbinafine, the enzyme hydroxylating the steroid (EE_2 2-hydroxylase) was inhibited by 30%. We speculated that terbinafine and EE_2 may be substrates for the same cytochrome P-450 isoenzyme but that it is noteworthy that maximum plasma concentrations following 250 mg terbinafine are only 3 µmol/l (ie, 16 times less than concentrations used in vitro). We were therefore looking specifically at the effect of terbinafine on EE_2 metabolism and not vice-versa; we have no evidence that EE_2 is inhibitory towards terbinafine (as stated by Juhlin). We still await definitive identification of the specific isoenzyme(s) responsible for terbinafine metabolism.

Terbinafine has a low potential for interactions with other drugs. The only interactions reported[2] are decreased elimination with cimetidine (400 mg twice daily) and increased elimination with rifampicin (600 mg/day).

Department of Pharmacology and Therapeutics, University of Liverpool, Liverpool L69 3BX, UK — DAVID BACK

1. Back DJ, Tjia JF. Azoles and allylamines: the clinical implications of interaction with cytochrome P-450 enzymes. *J Dermatol Treat* 1990; 1 (suppl 2): 11–13.
2. Jensen JC. Pharmacokinetics of Lamisil in humans. *J Dermatol Treat* 1990; 1 (suppl 2): 15–18.

Immunisation of infants in Iceland against *Haemophilus influenzae* type b

SIR,—In May, 1989, a national vaccination programme against *Haemophilus influenzae* type b (Hib) was started in Iceland with the first conjugate vaccine available, a capsular polysaccharide of Hib linked to diphtheria toxoid (PRP-D, Connaught Laboratories). Children aged 3 months to 3 years were offered this vaccine during the first year (about 17 000 children). PRP-D was given to infants at age 3, 4, 6, and 14 months with triple vaccine. Children who were 4–14 months when the programme started received two or three doses according to age, and those who were 15 months to 3 years were given one dose. The age groups up to and including 2½ years received PRP-D at a regular visit to a health centre, but children over that age had to come in for an extra visit, and not all came. In Reykjavik (about 50% of the population) a few hundreds older than 2½ years did not attend although twice invited by letters to their parents.[1] Infant immunisations in Iceland are free. If an infant does not turn up as scheduled, parents are called and reminded of the visit. Coverage of infant immunisations generally reaches 95–97%. Parents, however, have an option whether to accept immunisation for their children or not. Occasional parents did not want this new vaccine.

During 1974–88 *H influenzae* meningitis was confirmed in 135 children under 5, an incidence of 43 per 100 000. About 70% were under 2, 9% under 6 months, and 7% were 4–9 years. Their median age was 16 months. 1 of these children died and a few were left with sequelae. During this period Hib bacteraemia without meningitis was confirmed in 64 children under 5; many had accompanying focal infections but all survived. Their median age was the same as those with Hib meningitis.[1]

In 1989 Hib meningitis was confirmed in 8 children, all of whom were unvaccinated except 1 baby aged 3 months who had received one dose of vaccine 12 days before the illness. These children all survived, but 1 had total hearing loss. Hib bacteraemia without meningitis was confirmed in 4 children in 1989; all survived. 3 of these children were unvaccinated, but 1 had received one dose at 7 months and developed epiglottitis at 12 months.[1] Since 1989 no case of Hib meningitis has been confirmed in Iceland, but 2 children have had Hib bacteraemia (besides 2 newborn babies). 1 was in January, 1990, at age 4 years (unvaccinated), the other in December, 1991—a 9-month-old child who had received three doses of PRP-D.

During 3 months in 1984 and 1986 and from autumn of 1990 until spring of 1992, *H influenzae* strains isolated from children under 6, swabbed because of respiratory, throat, ear, or conjunctival infections, were typed. The percentage of type b strains diminished during the second and third trimester in 1991. Out of 415 strains

H INFLUENZAE STRAINS ISOLATED FROM SWABS FROM CHILDREN AGED 0–5

—	Total no	No of Hib strains *(%)*
Jan-April, 1984	144	15 *(10)*
Aug-Nov, 1986	117	12 *(10)*
Sept-Dec, 1990	116	18 *(16)*
1991		
Jan-March	89	9 *(10)*
April-June	131	4 *(3)*
July-Sept	89	2 *(2)*
Oct-Dec	172	0
Jan-May, 1992	243	1

UM00012040
NOVARTIS EXHIBIT 1017
Novartis v. Regents, IPR2023-01346
Page 786 of 4460

Itraconazole drastically increases plasma concentrations of lovastatin and lovastatin acid

Background: Lovastatin is a cholesterol-lowering drug that can cause myopathy as a rare side effect. Concomitant use of certain drugs (e.g., cyclosporine) increases the risk of skeletal muscle toxicity. Lovastatin is metabolized by CYP3A4. Because itraconazole is a potent inhibitor of CYP3A4, we wanted to study a possible interaction between these drugs.

Methods: In this double-blind, randomized, two-phase crossover study, 12 healthy volunteers received either 200 mg itraconazole or placebo orally once a day for 4 days. On day 4, each subject ingested a single 40 mg dose of lovastatin. Plasma concentrations of lovastatin, lovastatin acid, itraconazole, hydroxyitraconazole, and creatine kinase were measured up to 24 hours.

Results: On average, itraconazole increased the peak concentration (C_{max}) of lovastatin and the area under the lovastatin concentration–time curve (AUC) more than twentyfold ($p < 0.001$). The mean C_{max} of the active metabolite, lovastatin acid, was increased 13-fold (range, tenfold to 23-fold; $p < 0.001$) and the AUC(0-24) twentyfold ($p < 0.001$). In one subject plasma creatine kinase was increased tenfold within 24 hours of lovastatin administration during the itraconazole phase but not during the placebo phase. No increase in creatine kinase was observed in the other subjects.

Conclusions: Itraconazole greatly increases plasma concentrations of lovastatin and lovastatin acid. Inhibition of CYP3A4-mediated metabolism probably explains the increased toxicity of lovastatin caused not only by itraconazole but also by cyclosporine, erythromycin, and other inhibitors of CYP3A4. Their concomitant use with lovastatin and simvastatin should be avoided, or the dose of 3-hydroxy-3-methylglutaryl coenzyme A reductase inhibitors should be reduced accordingly. (Clin Pharmacol Ther 1996;60:54-61.)

Pertti J. Neuvonen, MD, and Kirsi-Maija Jalava, MD *Helsinki, Finland*

Inhibitors of 3-hydroxy-3-methylglutaryl coenzyme A (HMG-CoA) reductase, widely used to treat hypercholesterolemia, reduce clearly mortality from coronary disease and overall mortality.[1] Lovastatin (mevinolin) is an inactive lactone pro-drug converted in vivo to the corresponding open hydroxy acid, lovastatin acid, which is a competitive inhibitor of HMG-CoA reductase, the rate-limiting step in cholesterol synthesis.

Skeletal muscle toxicity is a rare side effect of HMG-CoA reductase inhibitors: its incidence is 0.1% to 0.2% with lovastatin monotherapy.[2] A considerably increased risk of diffuse myalgia, and even cases of severe rhabdomyolysis, have been reported after the combined use of lovastatin and certain other drugs, for example, cyclosporine and erythromycin.[3-5] According to the product information for lovastatin (Mevacor, Merck & Co., Inc., Whitehouse Station, N.J.), the incidence of myopathy has been as high as 30% within 1 year when patients have used lovastatin together with immunosuppressive therapy, including cyclosporine. The mechanism of these interactions has remained unclear, although higher-than-expected concentrations of HMG-CoA reductase inhibitors have been observed.[6,7]

Lovastatin is metabolized in the liver by CYP3A.[8] Cyclosporine and erythromycin are inhibitors of, for example, CYP3A4.[9] Itraconazole, a widely used antimycotic, is a very potent inhibitor of CYP3A4, and

From the Department of Clinical Pharmacology, University of Helsinki.

Received for publication Dec. 4, 1995; accepted Feb. 19, 1996.

Reprint requests: Pertti J. Neuvonen, MD, Department of Clinical Pharmacology, University of Helsinki, Paasikivenk. 4, FIN-00250 Helsinki, Finland.

Copyright © 1996 by Mosby–Year Book, Inc.

0009-9236/96/$5.00 + 0 13/1/72922

UM00012041
NOVARTIS EXHIBIT 1017
Novartis v. Regents, IPR2023-01346
Page 787 of 4460

Table I. Characteristics of the subjects

Subject No.	*Sex*	*Age (yr)*	*Weight (kg)*	*Other drugs*
1	Male	27	60	No
2	Female	22	53	No
3	Female*	24	53	Levonorgestrel 0.15 mg + ethinylestradiol 30 μg
4	Female	21	53	No
5	Female*	29	65	Gestodene 75 μg + ethinylestradiol 30 μg
6	Male	23	60	No
7	Male	22	65	No
8	Female	20	48	No
9	Female†	22	52	No
10	Female	23	57	No
11	Male	23	62	No
12	Male	23	67	No

* Using contraceptive steroids.
† A tenfold increase in creatine kinase during the itraconazole phase.

it increases the AUC values of certain orally administered substrates of this enzyme (midazolam[10] and triazolam[11]) up to tenfold to a hundredfold, that is, more than erythromycin does in similar experimental conditions.[12] We wanted to study the effect of itraconazole on the pharmacokinetics of lovastatin to find their possible interaction and to clarify the mechanism of myopathies associated with HMG-CoA reductase inhibitors.

METHODS

Study design. Five male and seven female volunteers (age range, 20 to 29 years; weight range, 48 to 67 kg; Table I) participated in the study after each gave written informed consent. The study was approved by the Ethics Committee of the Department of Clinical Pharmacology, University of Helsinki. The subjects were ascertained to be healthy by means of a clinical examination and laboratory tests (e.g., blood count, glucose, serum potassium, creatinine, alanine amino transferase, and creatine kinase). All subjects were nonsmokers, and none of them was receiving continuous medication except for two female subjects who were using contraceptive steroids (Table I).

A randomized, double-blind, crossover study design in two phases was used, at intervals of 4 weeks. The volunteers were given either 200 mg itraconazole (Sporanox, Janssen Pharma, Beerse, Belgium) or placebo orally at 7:30 AM for 4 days. On day 4, each subject ingested a single 40 mg dose of lovastatin (Lovacol, Orion, Espoo, Finland, license of Merck & Co., Inc.) with 150 ml water at 8:30 AM. The subjects fasted for 1 hour before the ingestion of lovastatin and had a standard meal 4 hours afterward.

Blood sampling and determination of drug concentrations. On the day of administration of lovastatin, a forearm vein of each subject was cannulated with a plastic cannula and kept patent with an obturator. Blood was sampled into tubes that contained ethylenediaminetetraacetic acid. Timed blood samples (10 ml) were collected immediately before administration of lovastatin and ½, 1, 2, 3, 4, 6, 8, 12, and 24 hours after administration. Plasma was separated within 30 minutes and stored at −40° C until analyzed.

Plasma concentrations of lovastatin and lovastatin acid were quantified by HPLC.[13] A 10 cm × 4.6 mm internal diameter column packed with 3 μm particle-sized Shandon HyperSil C_{18} BDS (Alltech, Deerfield, Ill.) was used. The detection limit was 5 ng/ml. The coefficient of variation was 5.5% for lovastatin (at 20 ng/ml) and 3.7% for lovastatin acid (at 33 ng/ml). The standard curves were linear between 5 and 2000 ng/ml. Itraconazole or its metabolites in plasma did not interfere with the analytical method.

The concentrations of itraconazole and hydroxyitraconazole were determined by HPLC.[14,15] A 10 cm × 4.6 mm internal diameter column, packed with 3 μm particle-sized Shandon HyperSil C_{18} BDS was used. Ammonium acetate-acetonitrile (35:65) was used as a mobile phase. The detection limit was 5 ng/ml. The coefficient of variation was 1% for itraconazole (at 96 ng/ml) and 7.7% for hydroxyitracon-

UM00012042
NOVARTIS EXHIBIT 1017
Novartis v. Regents, IPR2023-01346
Page 788 of 4460

azole (at 98 ng/ml). Creatine kinase was quantified with use of a routine photometric method in the hospital laboratory.

Pharmacokinetic calculations. The pharmacokinetics were characterized by peak (C_{max}) and minimum (C_{min}; for itraconazole and hydroxyitraconazole) concentrations in plasma, concentration peak times (t_{max}), elimination half-lives ($t_{1/2}$), and areas under the drug plasma concentration–time curves up 24 hours [AUC(0-24)]. The AUC(0-24) values of itraconazole and hydroxyitraconazole refer to the time between 0 and 24 hours after the ingestion of lovastatin, that is, between 1 and 25 hours after the last dose of itraconazole.

Statistical analysis. All data are expressed as mean values ± SEM. Data were analyzed by the Student *t* test for paired values or the Wilcoxon signed-rank test. Differences were regarded statistically significant when p values were <0.05.

RESULTS

Lovastatin and lovastatin acid. Itraconazole greatly increased the plasma concentrations of both lovastatin and lovastatin acid (Fig. 1; Table II). The mean C_{max} of the parent lovastatin was increased more than twentyfold by itraconazole (from less than 5 $ng \cdot ml^{-1}$ during the placebo phase to 128 ± 14 $ng \cdot ml^{-1}$; $p < 0.001$). During the itraconazole phase, the AUC(0-24) of lovastatin was 546 ± 55 $ng \cdot ml^{-1} \cdot hr$ (Table II), and the $t_{1/2}$ was 3.6 ± 1.1 hours. During the placebo phase these variables could not be determined because plasma concentration of lovastatin was higher than the detection limit in only three subjects.

During the itraconazole phase, the plasma concentrations of lovastatin acid in each subject were much higher than those during the placebo phase. On average, the C_{max} was increased 13-fold (range, tenfold to 23-fold; $p < 0.001$) and the AUC(0-24) was increased about twentyfold ($p < 0.001$). The $t_{1/2}$ of lovastatin acid was 6.0 ± 1.1 hours during the itraconazole phase; during the placebo phase it could not be determined.

Itraconazole and hydroxyitraconazole. The mean plasma concentrations of itraconazole and its active metabolite hydroxyitraconazole on the day of lovastatin ingestion are given in Fig. 2. The AUC(0-24) of hydroxyitraconazole was about twofold higher than that of itraconazole. There were fourfold to fivefold interindividual differences in the C_{max}, C_{min}, and AUC(0-24) values of itraconazole and threefold to sixfold differences in the respective values of hydroxyitraconazole (Table III). The lowest C_{max} values of plasma itraconazole and hydroxyitraconazole were associated with the lowest increases in the concentrations of lovastatin and lovastatin acid (subject 12). Subject 9, in whom the creatine kinase level was increased, had the lowest AUC(0-24) values of itraconazole and hydroxyitraconazole.

Creatine kinase. In one subject (subject 9), plasma creatine kinase was increased tenfold within 24 hours of lovastatin administration during the itraconazole phase but not during the placebo phase (Fig. 3). No increase in creatine kinase was observed in the other 11 subjects.

Side effects. No clinical side effects were reported by the subjects after the ingestion of lovastatin during the placebo phase or the itraconazole phase.

DISCUSSION

The results of this study indicate that concomitant ingestion of itraconazole increases greatly the concentrations of the pro-drug lovastatin and its active metabolite lovastatin acid in the systemic blood circulation. The concentrations of lovastatin acid were increased in each subject about tenfold to thirtyfold. The concentrations of lovastatin were increased even more, but the exact figures for the inactive parent drug could not be determined because its concentrations during the placebo phase were often below the detection limit of 5 ng/ml. Lovastatin acid is a competitive inhibitor of HMG-CoA reductase; that is, the activity of this enzyme in plasma and peripheral tissues must have been reduced accordingly, although it was not measured in this study.

The systemic bioavailability of the pharmacologically active lovastatin acid is normally only about 5%. The major part of oral lovastatin is taken up by the liver and metabolized during the first pass.[16] Accordingly, the concentrations of lovastatin acid in peripheral blood and tissues are low and the systemic side effects are rare with lovastatin monotherapy when conventional doses are used.[2] On the other hand, high doses and, in particular, coadministration of cyclosporine, erythromycin, or certain other drugs increase the incidence and severity of skeletal muscle side effects of the HMG-CoA reductase inhibitors.[3-7]

The parent lovastatin is an inactive lactone prodrug, of which a part is hydrolyzed to the active lovastatin acid. This metabolic step is not dependent on cytochrome P450. In contrast to this, the other main routes of the biotransformation of lovastatin, that is, the formation of 6′-β-hydroxylovastatin, 3″-

UM00012043
NOVARTIS EXHIBIT 1017
Novartis v. Regents, IPR2023-01346
Page 789 of 4460

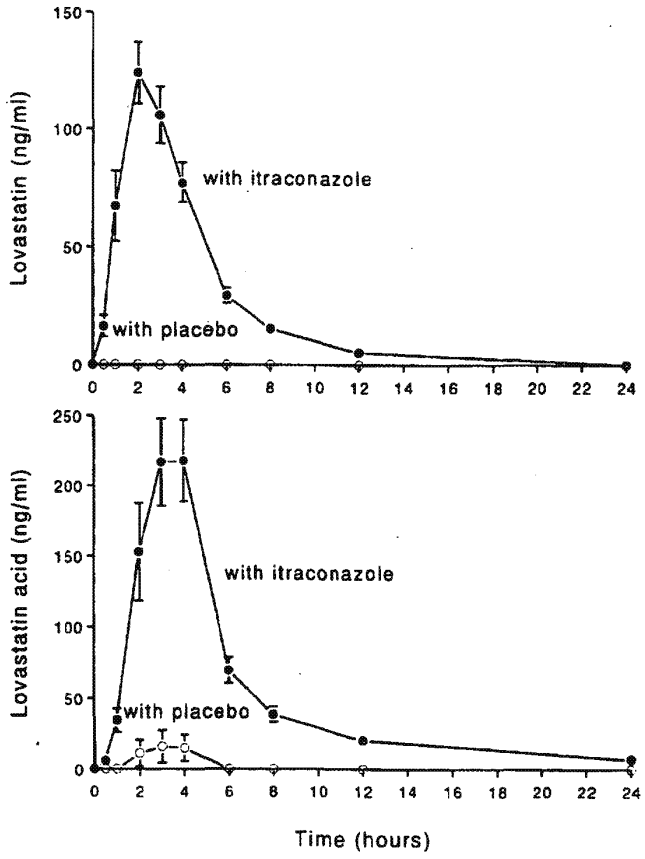


Fig. 1. Mean ± SEM concentrations of lovastatin **(upper panel)** and lovastatin acid **(lower panel)** in the plasma of 12 healthy volunteers after a single oral dose of 40 mg lovastatin following daily use of oral 200 mg itraconazole *(solid circles)* or placebo *(open circles)* for 4 days.

hydroxylovastatin, and 6'-exomethylene-lovastatin, are cytochrome P450 dependent, and CYP3A enzymes are primarily responsible for their formation.[8] In the present study, itraconazole increased the plasma concentrations of the parent lovastatin more than twentyfold, obviously by inhibiting its CYP3A-mediated biotransformation. On the other hand, because the hydrolysis of lovastatin to lovastatin acid is independent of CYP3A, the concentration of lovastatin acid was increased greatly along with the increased level of lovastatin. Furthermore, it can be suggested that metabolism of lovastatin acid to its further metabolites is CYP3A dependent, because the $t_{1/2}$ of lovastatin acid was prolonged during the itraconazole phase (up to a mean of 6 hours).

Many of those drugs reported to have increased the toxicity of lovastatin are inhibitors of CYP enzymes. At least itraconazole, cyclosporine, and erythromycin are all potent inhibitors of CYP3A4,[9] and their concomitant use increases the plasma concentration of several drugs that are substrates of CYP3A4. In particular, drugs that have a low oral bioavailability due to an extensive first-pass metabolism either in the gut wall and or in the liver (e.g., terfenadine,[17,18] triazolam,[11] and midazolam[10]) are liable to interact with the inhibitors of CYP3A4. In this study the increases in the C_{max} and AUC(0-24) of lovastatin and lovastatin acid obviously were caused mainly by inhibition by itraconazole of the first-pass metabolism. The $t_{1/2}$ values of lovastatin

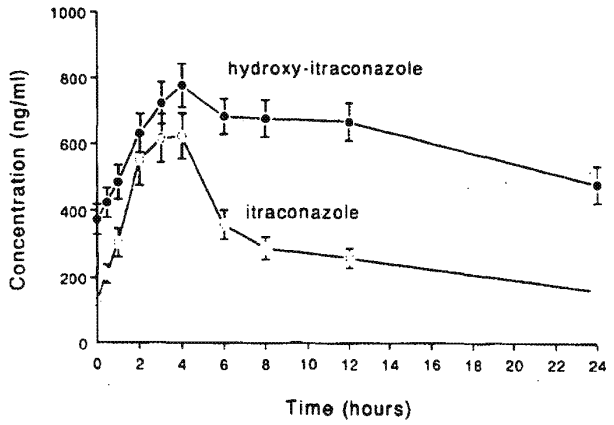


Fig. 2. Mean ± SEM concentrations of itraconazole *(open circles)* and hydroxyitraconazole *(solid circles)* in the plasma of 12 healthy volunteers after daily use of 200 mg oral itraconazole for 4 days.

Table II. C_{max}, t_{max}, and AUC(0-24) of lovastatin and lovastatin acid in plasma during the itraconazole and placebo phases

	Lovastatin			*Lovastatin acid*		
Subject No.	C_{max} *(ng · ml^{-1})*	t_{max} *(hr)*	*AUC(0-24) (ng · ml^{-1} · hr)*	C_{max} *(ng · ml^{-1})*	t_{max} *(hr)*	*AUC(0-24) (ng · ml^{-1} · hr)*
1	168 (<5)	2	811 (*)	135 (8.8)	4 (6)	735 (54)
2	148 (9.6)	2 (1)	565 (*)	99 (7.7)	3 (2)	486 (8)
3	168 (<5)	2	619 (*)	288 (20.7)	3 (4)	1370 (69)
4	176 (<5)	2	813 (*)	391 (33.4)	4 (4)	2086 (118)
5	156 (<5)	2	651 (*)	159 (12.3)	3 (2)	1007 (43)
6	86 (<5)	3	392 (*)	267 (19.1)	4 (4)	1286 (71)
7	171 (<5)	3	691 (*)	284 (17.7)	3 (4)	1351 (50)
8	70 (5.2)	3 (2)	325 (*)	216 (13.1)	4 (4)	1367 (31)
9	116 (<5)	2	430 (*)	192 (8.5)	4 (3)	751 (33)
10	116 (8.7)	2 (1)	574 (*)	473 (43.1)	2 (3)	2439 (126)
11	140 (<5)	2	510 (*)	247 (25.5)	3 (3)	1179 (93)
12	25 (<5)	2	173 (*)	62 (5.1)	4 (3)	488 (5)
Mean	128† (<5)	2.3	546† (*)	234† (17.9)	3.4 (3.5)	1212† (54.8)
SEM	14	0.1	55	34 (3.3)	0.2 (0.3)	171 (11.2)

The data within parentheses refer to the corresponding values during the placebo phase.
C_{max}, Peak plasma concentration; t_{max}, time to reach peak concentration; AUC(0-24), area under the plasma concentration–time curve from 0 to 24 hours.
* Less than 15 but could not be calculated exactly.
† Significantly different from the placebo phase, $p < 0.001$.

and lovastatin acid during the itraconazole phase (3.6 hours and 6.0 hours) are two to three times longer than those described in the literature.[16] Thus, itraconazole also seems to decrease their elimination, although the elimination $t_{1/2}$ values (or clearances) could not be determined during the placebo phase.

In this study healthy volunteers ingested a single therapeutic dose of 40 mg lovastatin during the placebo and itraconazole phases. Even this short exposure to high concentrations of lovastatin and lovastatin acid (and to itraconazole and hydroxyitraconazole) caused a tenfold increase in creatine kinase in one healthy young woman. There was no increase in her creatine kinase level when she ingested the same dose of lovastatin 4 weeks later

UM00012045
NOVARTIS EXHIBIT 1017
Novartis v. Regents, IPR2023-01346
Page 791 of 4460

Table III. Pharmacokinetic parameters of itraconazole and hydroxyitraconazole in plasma on the fourth day on itraconazole, that is, on the day of lovastatin ingestion

	Itraconazole					*Hydroxyitraconazole*				
Subject No.	C_{max} *(ng · ml^{-1})*	t_{max} *(hr)*	C_{min} *(ng · ml^{-1})*	$t_{1/2}$ *(hr)*	*AUC(0-24) (ng · ml^{-1} · hr)*	C_{max} *(ng · ml^{-1})*	t_{max} *(hr)*	C_{min} *(ng · ml^{-1})*	$t_{1/2}$ *(hr)*	*AUC(0-24) (ng · ml^{-1} · hr)*
1	974	2	131	17.1	10,070	832	4	412	35.2	17,990
2	693	4	89	11.4	7,080	823	4	259	14.8	14,170
3	1,041	3	226	17.6	11,680	1,114	4	596	39.0	20,510
4	753	4	133	25.2	8,460	904	4	461	48.8	18,500
5	437	4	87	25.7	4,620	621	4	286	20.8	10,850
6	741	4	193	19.5	8,320	1,059	4	649	41.5	19,160
7	743	3	70	12.9	7,750	866	4	217	21.5	16,820
8	475	4	107	19.0	4,610	655	4	314	21.4	10,990
9	318	3	48	21.5	2,960	419	4	108	17.9	6,730
10	694	2	102	14.0	6,410	755	4	398	28.4	14,460
11	846	4	136	26.7	9,630	957	6	397	36.3	18,980
12	213	6	111	18.7	3,790	448	8	255	18.0	8,760
Mean	661	3.6	119	19.1	7,115	788	4.5	363	28.6	14,826
SEM	73	0.3	50	1.4	782	63	0.4	45	3.2	1,318

C_{min}, Minimum plasma concentration; $t_{1/2}$, elimination half-life.

during the placebo phase. She had a slight allergic rhinitis and atopy in her medical history, but there were no abnormalities in her laboratory parameters when studied 2 weeks before the ingestion of itraconazole and lovastatin. However, her creatine kinase was already slightly elevated (from 143 IU/L to 385 IU/L) after 3 days' use of itraconazole, and it was 3640 IU/L 24 hours after the ingestion lovastatin (and the fourth itraconazole dose). A prolonged concomitant use of lovastatin and itraconazole obviously would have led to a more severe myopathy in this subject. During the itraconazole phase her concentrations of itraconazole, hydroxyitraconazole, lovastatin, and lovastatin acid were on the same level as or even less than those in the other subjects in whom no elevation of creatine kinase was observed. Thus some additional factors, in addition to a tenfold increase in the concentration of HMG-CoA reductase inhibitor, seem to have contributed to the rapid increase in creatine kinase.

Quite recently (i.e., during the final preparation of this article) a case of severe rhabdomyolysis was reported to have occurred in a patient within 2 weeks of the addition of itraconazole to a therapy that contained lovastatin.[19] Furthermore, we are aware of another patient in whom a severe rhabdomyolysis developed while receiving treatment with the combination of itraconazole and lovastatin. Thus the findings of the present study are in a good agreement with these clinical case reports.

In the prolonged concomitant use of itraconazole and lovastatin, the concentrations of HMG-CoA reductase inhibitors in the peripheral blood and tissues would be at least ten to thirty times higher than the concentrations during the lovastatin monotherapy. Because of the dose-dependent nature of lovastatin toxicity, use of lovastatin in conventional doses together with itraconazole or with other potent inhibitors of CYP3A4 carries an obvious risk of a systemic toxicity. Itraconazole is extensively metabolized to pharmacologically active hydroxyitraconazole. The AUC(0-24) values of this metabolite were about two times higher than those of the parent drug. Because hydroxyitraconazole is equally potent or even more potent than itraconazole as an inhibitor of CYP3A4, this metabolite may contribute significantly to the observed itraconazole-lovastatin interaction. Ketoconazole, erythromycin, clarithromycin, verapamil, and diltiazem are among other commonly used drugs that cause a clinically significant inhibition of CYP3A4 in humans and can elevate the plasma concentrations of its substrates.[9-12,17,18,20] Furthermore, in addition to several drugs, even grapefruit juice might increase the plasma levels of lovastatin acid by inhibition of CYP3A4 in humans.[21,22]

Most of the clinically used HMG-CoA reductase inhibitors are extensively metabolized, and the biotransformation of simvastatin closely resembles that of lovastatin.[23] The formation of simvastatin acid is not dependent on cytochrome P450, whereas CYP3A enzymes probably are primarily responsible for other

UM00012046
NOVARTIS EXHIBIT 1017
Novartis v. Regents, IPR2023-01346
Page 792 of 4460

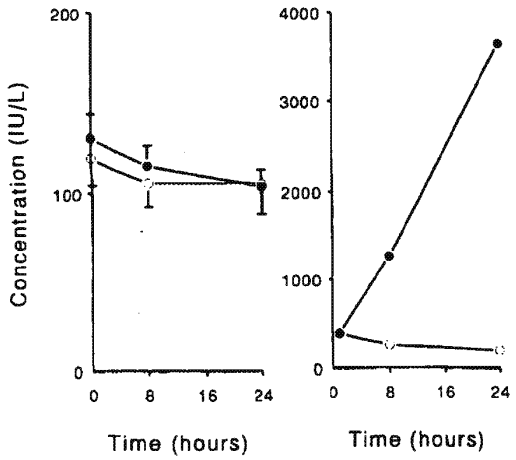


Fig. 3. Mean ± SEM concentrations of creatine kinase **(left panel)** in the plasma of eleven healthy volunteers after a single oral dose of 40 mg lovastatin following daily use of 200 mg oral itraconazole *(solid circles)* or placebo *(open circles)* for 4 days. The **right panel** shows the creatine kinase values for subject 9. Note the different scales on the *y*-axis.

routes of metabolism. Accordingly, the interaction between CYP3A4 inhibitors and lovastatin probably can be extended to simvastatin and, possibly, to some other "statins." Interaction between itraconazole and other potent CYP3A4 inhibitors and HMG-CoA reductase inhibitors is clearly of major clinical significance. Thus, care should be taken when, for example, systemic antimycotics are prescribed to patients taking lovastatin or simvastatin.

We are grateful to Janssen Pharmaceuticals (Beerse, Belgium) for the determination of plasma drug concentrations.

References

1. Scandinavian Simvastatin Survival Study Group. Randomized trial of cholesterol lowering in 4444 patients with coronary heart disease: the Scandinavian Simvastatin Survival Study (4S). Lancet 1994;344:1383-9.
2. Bradford RH, Shear CL, Chremos AN, et al. Expanded Clinical Evaluation of Lovastatin (EXCEL) Study Results. Arch Intern Med 1991;151:43-9.
3. Tobert JA. Efficacy and long-term adverse effect pattern of lovastatin. Am J Cardiol 1988;62:28J-34J.
4. Norman DJ, Illingworth DR, Murson J, Hosenpud J. Myolysis and acute renal failure in a heart-transplant patient receiving lovastatin [letter]. N Engl J Med 1988;318:46-7.
5. Marinella MA. More on lovastatin [letter]. West J Med 1995;162:176-7.
6. Smith PF, Eydelloth RS, Grossman SJ, et al. HMG-CoA reductase inhibitor-induced myopathy in the rat: cyclosporine A interaction and mechanism studies. J Pharmacol Exp Ther 1991;257:1225-35.
7. Arnadottir M, Eriksson LO, Thysell H, Karkas JD. Plasma concentration profiles of simvastatin 3-hydroxy-3-methyl-glutaryl-coenzyme A reductase inhibitory activity in kidney transplant recipients with and without ciclosporin. Nephron 1993;65:410-3.
8. Wang RW, Kari PH, Lu AYH, Thomas PE, Guengerich FP, Vyas KP. Biotransformation of lovastatin; IV: identification of cytochrome P-450 3A proteins as the major enzymes responsible for the oxidative metabolism of lovastatin in rat and human liver microsomes. Arch Biochem Biophys 1991;290:355-61.
9. Gascon MP, Dayer P. In vitro forecasting of drugs which may interfere with the biotransformation of midazolam. Eur J Clin Pharmacol 1991;41:573-8.
10. Olkkola KT, Backman JT, Neuvonen PJ. Midazolam should be avoided in patients receiving systemic antimycotics ketoconazole or itraconazole. Clin Pharmacol Ther 1994;55:481-5.
11. Varhe A, Olkkola KT, Neuvonen PJ. Oral triazolam potentially hazardous to patients receiving systemic antimycotics ketoconazole or itraconazole. Clin Pharmacol Ther 1994;56:601-7.
12. Olkkola KT, Aranko K, Luurila H, et al. A potentially hazardous interaction between erythromycin and midazolam. Clin Pharmacol Ther 1993;53:298-305.
13. Stubbs RJ, Schwartz M, Bayne WF. Determination of mevinolin and mevinolic acid in plasma and bile by reversed-phase high-performance liquid chromatography. J Chromatogr 1986;383:438-43.
14. Woestenborgshs R, Lorreyne W, Heykants J. Determination of itraconazole in plasma and animal tissues by high-performance liquid chromatography. J Chromatogr 1987;413:332-7.
15. Heykants J, Van-Peer A, Van-de-Velde V, et al. The clinical pharmacokinetics of itraconazole: an overview. Mycoses 1989;32(suppl 1):67-87.
16. Dollery C, editor. Therapeutic drugs; vol 2. Edinburgh: Churchill Livingstone, 1991:L66-71.
17. Honig PK, Wortham DC, Zamani K, et al. Terfenadine-ketoconazole interaction: pharmacokinetic and electrocardiographic consequences. JAMA 1993;269:1513-8.
18. Pohjola-Sintonen S, Viitasalo M, Toivonen L, Neuvonen PJ. Itraconazole prevents terfenadine metabolism and increases risk of torsades de pointes ventricular tachycardia. Eur J Clin Pharmacol 1993;45:191-3.
19. Lees RS, Lees AM. Rhabdomyolysis from the coadministration of lovastatin and the antifungal agent itraconazole [letter]. New Engl J Med 1995;333:664-5.
20. Backman JT, Olkkola KT, Aranko K, Himberg JJ, Neuvonen PJ. Dose of midazolam should be reduced

UM00012047
NOVARTIS EXHIBIT 1017
Novartis v. Regents, IPR2023-01346
Page 793 of 4460

during diltiazem and verapamil treatments. Br J Clin Pharmacol 1994;37:221-5.
21. Bailey DG, Arnold MO, Strong A, Munoz C, Spence JD. Effect of grapefruit juice and naringin on nisoldipine pharmacokinetics. Clin Pharmacol Ther 1993; 54:589-94.
22. Hukkinen SK, Varhe A, Olkkola KT, Neuvonen PJ. Plasma concentrations of triazolam are increased by concomitant ingestion of grapefruit juice. Clin Pharmacol Ther 1995;58:127-31.
23. Vickers S, Duncan CA, Vyas KP, et al. In vitro and in vivo biotransformation of simvastatin, an inhibitor of HMG CoA reductase. Drug Metab Dispos 1990;18: 476-83.

ANTIMICROBIAL AGENTS AND CHEMOTHERAPY, Mar. 2000, p. 727–731 Vol. 44, No. 3
0066-4804/00/$04.00+0
Copyright © 2000, American Society for Microbiology. All Rights Reserved.

Pharmacokinetics of SCH 56592, a New Azole Broad-Spectrum Antifungal Agent, in Mice, Rats, Rabbits, Dogs, and Cynomolgus Monkeys

AMIN A. NOMEIR,[1]* PRAMILA KUMARI,[1] MARY JANE HILBERT,[2] SAMIR GUPTA,[1] DAVID LOEBENBERG,[3] ANTHONY CACCIAPUOTI,[3] ROBERTA HARE,[3] GEORGE H. MILLER,[3] CHIN-CHUNG LIN,[1] AND MITCHELL N. CAYEN[1]

Departments of Drug Metabolism and Pharmacokinetics,[1] Biotechnology,[2] and Chemotherapy and Molecular Genetics,[3] Schering-Plough Research Institute, Kenilworth, New Jersey

Received 16 February 1999/Returned for modification 20 September 1999/Accepted 24 November 1999

SCH 56592 is a new broad-spectrum azole antifungal agent that is in phase 3 clinical trials for the treatment of serious systemic fungal infections. The pharmacokinetics of this drug candidate were evaluated following its intravenous (i.v.) or oral (p.o.) administration as a solution in hydroxypropyl-β-cyclodextrin (HPβCD) or oral administration as a suspension in 0.4% methylcellulose (MC) in studies involving mice, rats, rabbits, dogs, and cynomolgus monkeys. SCH 56592 was orally bioavailable in all species. The oral bioavailability was higher with the HPβCD solution (range, 52 to ~100%) than from the MC suspension (range, 14 to 48%) and was higher in mice (~100% [HPβCD] and 47% [MC]), rats (~66% [HPβCD] and 48% [MC]), and dogs (72% [HPβCD] and 37% [MC]) than in monkeys (52% [HPβCD] and 14% [MC]). In rabbits, high concentrations in serum suggested good oral bioavailability with the MC suspension. The i.v. terminal-phase half-lives were 7 h in mice and rats, 15 h in dogs, and 23 h in monkeys. In rabbits, the oral half-life was 9 h. In species given increasing oral doses (mice, rats, and dogs), serum drug concentrations were dose related. Food produced a fourfold increase in serum drug concentrations in dogs. Multiple daily doses of 40 mg of SCH 56592/kg of body weight for eight consecutive days to fed dogs resulted in higher concentrations in serum, indicating accumulation upon multiple dosing, with an accumulation index of approximately 2.6. Concentrations above the MICs and minimum fungicidal concentrations for most organisms were observed at 24 h following a single oral dose in MC suspension in all five species studied (20 mg/kg for mice, rats, and rabbits and 10 mg/kg for dogs and monkeys), suggesting that once-daily administration of SCH 56592 in human subjects would be a therapeutically effective dosage regimen.

The incidence of fungal infections has substantially increased over the past 2 decades, and invasive forms are important causes of morbidity and mortality (1). Of the estimated 100,000 known species of fungi, about 180 have been shown to cause disease in humans, and only about 10% of these are encountered in most clinical settings (2). Disseminated candidiasis, pulmonary aspergillosis, and infections caused by emerging opportunistic fungi are the most common of the serious mycoses (12). Aggressive immunosuppression, myelotoxic therapeutic regimens, AIDS, cancer, and organ transplantation have opened the door for these organisms. Although amphotericin B has been the gold standard in antifungal therapy for half of a century, newer chemical agents, such as azoles, have emerged in recent decades. These entities are generally active by more than one route of administration, have a broader spectrum of activity, and are less toxic than amphotericin B. The ideal antifungal agent would be broad spectrum, fungicidal, active against resistant strains, and active by various routes of administration and would have a good safety profile.

SCH 56592 has been shown to be active against both yeasts and filamentous fungi, including *Aspergillus*, *Candida* (including fluconazole-resistant *Candida krusei*), *Cryptococcus*, *Blastomyces*, *Coccidioides*, and other opportunistic fungi (5, 7–11; V. M. Girijavallabhan, A. K. Saksena, R. G. Lovey, F. Bennett, R. E. Pike, H. Wang, P. Pinto, Y. T. Liu, N. Patel, and A. K. Ganguly, Abstr. 35th Intersci. Conf. Antimicrob. Agents Chemother., abstr. F61, 1995). The MIC at which 90% of the isolates are inhibited and the minimal concentrations at which 90% of the isolates are killed for various strains of *A. flavus*, *A. fumigatus*, *C. albicans*, and *C. tropicalis* were in the ranges of 0.03 to 0.25 and 0.5 to 2.0 μg/ml, respectively. Preliminary studies suggest that SCH 56592 binds to the plasma protein of rats, dogs, and humans. SCH 56592 is expected to be clinically effective in both immunocompetent and immunocompromised patients as prophylactic, therapeutic, and maintenance treatment for fungal infections.

The objectives of the present studies were to characterize the pharmacokinetics of SCH 56592 following intravenous (i.v.) and/or oral (p.o.) administration to mice, rats, rabbits, dogs, and cynomolgus monkeys. In addition, the effect of dose on serum drug concentrations was evaluated in mice, rats, and dogs.

MATERIALS AND METHODS

Animals. Male CF-1 mice (18 to 20 g), male CRL-CD-BR rats (180 to 220 g), and male New Zealand White rabbits (approximately 3 kg) were purchased from Charles River Laboratories (Wilmington, Mass.). Male beagle dogs (7 to 15 kg) and male cynomolgus monkeys (3 to 9 kg) were obtained from the Schering-Plough Research Institute colony. Animals were kept in temperature-, humidity-, and light cycle-controlled rooms. Animals were randomly assigned to each treatment group and were subjected to fasting (water allowed) for 18 h prior to dosing, unless otherwise indicated.

Bioavailability and pharmacokinetics. SCH 56592 was administered i.v. to mice, rats, dogs, and monkeys as a solution in 40% (wt/vol) aqueous hydroxypro-

* Corresponding author. Mailing address: Department of Drug Metabolism and Pharmacokinetics, Schering-Plough Research Institute, Mail Stop 2880, Kenilworth, NJ 07033-1310. Phone: (908) 740-3190. Fax: (908) 740-3966. E-mail: Amin.Nomeir@sprcorp.com.

UM00012049
NOVARTIS EXHIBIT 1017
Novartis v. Regents, IPR2023-01346
Page 795 of 4460

pyl-β-cyclodextrin (HPβCD) and orally as a solution in HPβCD or as a suspension in an aqueous solution containing 0.4% methylcellulose, 0.5% polysorbate 80, and 0.9% NaCl (MC). Rabbits received SCH 56592 only p.o. in the MC suspension. Mice, rats, and rabbits received a single dose of 20 mg/kg of body weight; dogs and cynomolgus monkeys received a single 10-mg/kg dose. Blood was collected at various intervals following dosing, and serum was frozen at −20°C pending analysis.

Effect of oral dose on serum drug concentrations. Mice were given 20-, 40-, 80-, and 160-mg/kg doses at a constant volume of 5 ml/kg of body weight from MC suspension formulations prepared at 4, 8, 16, and 32 mg/ml, respectively. Additional animals received only the vehicle. Three animals were sacrificed at each time point to determine concentrations of SCH 56592 in serum. In a similar experimental design, rats were given 10-, 20-, 40-, 80-, and 120-mg doses of SCH 56592/kg in MC, and 3 animals were sacrificed at each time point.

An initial study was carried out with dogs to evaluate the effect of food on the oral bioavailability of SCH 56592 following a single 10-mg/kg dose. This was a parallel group study design in which 6 dogs were dosed following an 18-h fast and another 6 animals were dosed following feeding. The results showed that food significantly improved the bioavailability of SCH 56592 (see Table 2); therefore, a study was carried out in fed dogs to evaluate the effect of dose on concentrations of SCH 56592 in serum. Six animals were used in a crossover study design with a 2-week washout period. The oral dose formulation was prepared as a suspension in MC at a concentration of 16 mg/ml, and the animals were dosed at 40, 80, and 120 mg/kg.

A third study was performed to investigate the pharmacokinetics of SCH 56592 in fed dogs following multiple dosing. Six animals were dosed with an MC suspension of SCH 56592 (16 mg/ml) at 40 mg/kg once daily for 8 consecutive days. Blood was collected at various time intervals on days 1 and 8, just prior to the administration of SCH 56592 on days 2 to 7, and once daily on days 9 to 13.

Analysis of serum samples. Serum samples were analyzed for SCH 56592 by high-performance liquid chromatography (HPLC). The HPLC system used consisted of a Hitachi model L-620 pump, a Waters model 715 WISP sample processor, and a Waters 484 tunable absorbance detector set at 262 nm. Two sequential 5-μm Beckman octadecyl silane Ultrasphere 4.6-mm by 15-cm columns, preceded by a 5-μm Beckman octadecyl silane Ultrasphere 4.6-mm by 4.5-cm guard column, were used. The mobile phase was a mixture of 500 ml of acetonitrile, 500 ml of 0.1 M ammonium phosphate monobasic, 5 ml of methylene chloride, and 0.5 ml of triethylamine at a flow rate of 1.5 ml/min. The retention times for SCH 56592 and the internal standard (SCH 56894, a diastereomer analogue of SCH 56592) were approximately 10 and 7.5 min, respectively. Serum was prepared for analysis by the addition of 0.04 ml of the internal standard in methanol (10 μg/ml) and 0.56 ml of methanol to 0.2 ml of serum, mixed for about 1 min, and then centrifuged at 3,000 × *g* for 4 min. The supernatant was transferred into polypropylene tubes and was kept in a refrigerator (4°C) overnight. Samples were then recentrifuged as previously described, and 0.2 ml of the supernatant was analyzed by HPLC. The method was cross validated in all species studied prior to sample analysis. The limit of quantitation was 0.05 μg/ml. Intraday precision (coefficient of variation [CV]) and accuracy (bias) were in the ranges of 2 to 4 and 0 to 6%, respectively. The corresponding interday values were 3 to 5 and 0 to 5%, respectively, indicating that the method was satisfactory. With each analytical run, six quality control samples were analyzed, along with two standard curves prepared in serum.

Pharmacokinetic evaluation. Concentrations of SCH 56592 in serum that were equal to and above the limit of quantitation were used for pharmacokinetic analysis by model-independent methods (3). The maximum concentration in serum (C_{max}), time of C_{max} (T_{max}), and final quantifiable sampling time (tf) were the observed values. The terminal-phase rate constant (k) was the slope of the serum concentration-time curve. The half-life ($t_{1/2}$) was estimated as 0.693/k. The area under the serum concentration-time curve from time zero to tf (AUC_{tf}) was calculated by the trapezoidal rule and was extrapolated to infinity as follows: $AUC_{0-\infty} = AUC_{tf} + C_{tf}/k$, where C_{tf} is the estimated concentration at tf.

RESULTS

Mean serum concentration-time profiles of SCH 56592 following i.v. and p.o. administration to mice are shown in Fig. 1, with mean pharmacokinetic parameters presented in Table 1. SCH 56592 was completely bioavailable (100%) from the HPβCD solution; from the MC suspension, its bioavailability was 47%. Following p.o. administration at 20 mg/kg, the C_{max} range was 6.3 to 7.8 μg/ml, which was attained at a T_{max} range of 1 to 2 h after dosing. It is interesting that serum concentrations remained almost unchanged between 1 and 6 h following i.v. or p.o. administration (Fig. 1). Also, following p.o. administration in MC, mean concentrations of SCH 56592 in serum were >2 μg/ml for at least 12 h after dosing. The $t_{1/2}$ following i.v. administration was 7 h. Table 2 shows the mean C_{max}, T_{max}, and $AUC_{0-\infty}$ following p.o. administration in MC at doses of 20, 40, 80, and 160 mg/kg to mice. There was a dose-related increase in both C_{max} and $AUC_{0-\infty}$ within the dose range studied. Also, as the dose increased, T_{max} shifted toward longer times.

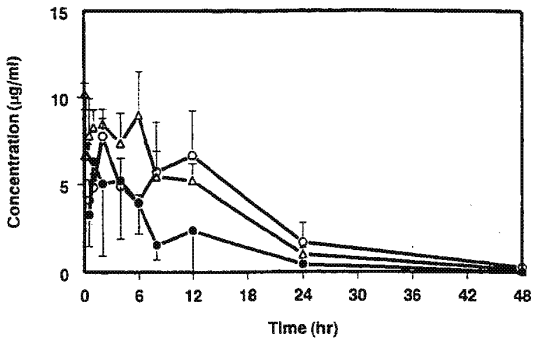


FIG. 1. Serum concentration-time profiles of SCH 56592 in mice following the i.v. or p.o. administration of a 20-mg/kg dose of SCH 56592. △, i.v. as a solution in HPβCD; ○, p.o. as a solution in HPβCD; ●, p.o. as a suspension in MC. Each vertical bar represents 1 standard deviation from the mean.

Mean serum concentration-time profiles of SCH 56592 in rats following i.v. and p.o. administration are shown in Fig. 2, with mean pharmacokinetic parameters shown in Table 1. The oral bioavailability values were approximately 66 and 48% for the HPβCD solution and the MC suspension, respectively. Following p.o. administration, the C_{max} range was 3.0 to 3.5 μg/ml, which was attained at a T_{max} range of 2 to 4 h after dosing. The $t_{1/2}$ following i.v. administration was 7.0 h. The mean C_{max}, T_{max}, and $AUC_{0-\infty}$ of SCH 56592 following p.o. administration at 10, 20, 40, 80, and 120 mg/kg as a suspension

TABLE 1. Mean pharmacokinetic parameters of SCH 56592 in mice, rats, dogs, and cynomolgus monkeys[a]

Species (n)	Parameter	i.v. in HPβCD	p.o. in HPβCD	p.o. in MC
Mouse (3)	C_{max} (μg/ml)		7.8 (13)	6.3 (11)
	T_{max} (h)		2.0	1.0
	$AUC_{0-\infty}$ (μg · h/ml)	137.0	143.0	63.7
	$t_{1/2}$ (h)	7.0		
	Bioavailability (%)		104.0	46.5
Rat (3)	C_{max} (μg/ml)		3.5 (13)	3.0 (20)
	T_{max} (h)		2.0	4.0
	$AUC_{0-\infty}$ (μg · h/ml)	89.4	58.6	43.0
	$t_{1/2}$ (h)	7.0		
	Bioavailability (%)		65.6	48.0
Dog (2)	C_{max} (μg/ml)		3.5	3.0
	T_{max} (h)		2.0	4.0
	$AUC_{0-\infty}$ (μg · h/ml)	89.4	58.6	43.0
	$t_{1/2}$ (h)	7.0		
	Bioavailability (%)		65.6	48.0
Monkey (2)	C_{max} (μg/ml)		1.1	0.4 (18)[b]
	T_{max} (h)		14.0	5.0 (31)
	$AUC_{0-\infty}$ (μg · h/ml)	115.0	59.4	15.9 (20)
	$t_{1/2}$ (h)	22.7		
	Bioavailability (%)		51.7	13.8

[a] Values in parentheses are CVs (in percent).
[b] n = 6.

UM00012050
NOVARTIS EXHIBIT 1017
Novartis v. Regents, IPR2023-01346
Page 796 of 4460

TABLE 2. Mean pharmacokinetic parameters of SCH 56592 following p.o. administration in MC suspensions

Species (n)	Dose (mg/kg)	C_{max} (μg/ml)	T_{max} (h)	$AUC_{0-\infty}$ (μg · h/ml)
Mice (6)	20	4.9 (20)[a]	3.0	82.0
	40	11.5 (45)	7.0	146.0
	80	12.1 (20)	7.0	363.0
	160	17.1 (14)	12.0	508.0
Rats (3)	10	2.7 (51)	4.0	31.4
	20	3.7 (12)	6.0	65.1
	40	6.0 (19)	4.0	119.0
	80	10.2 (26)	6.0	189.9
	120	10.1 (11)	4.0	262.6
Rabbits (6)	20	4.2 (12)	5.1 (21)	77.5 (16)
Dogs (fasting) (5)	10	0.2 (22)	7.6 (121)	7.5 (45)
Dogs (fed) (6)	10	0.7 (28)	8.3 (93)	26.6 (42)
	40	2.1 (31)	9.2 (90)	105.0 (30)
	80	3.1 (20)	9.0 (82)	167.0 (18)
	120	3.3 (27)	15.0 (66)	192.0 (34)

[a] Values in parentheses are CVs (in percent).

in MC are shown in Table 2. There was a dose-related increase in both C_{max} (up to 80 mg/kg) and $AUC_{0-\infty}$ (up to 120 mg/kg), while the T_{max} range was 4 to 6 h.

The mean serum concentration-time profile of SCH 56592 in fed rabbits following p.o. administration of a 20-mg/kg dose in an MC suspension is shown in Fig. 3, with mean pharmacokinetic parameters presented in Table 1. The $t_{1/2}$ was approximately 9 h. The high concentrations of SCH 56592 in serum suggest good oral bioavailability.

Mean serum concentration-time profiles of SCH 56592 following i.v. and p.o. administration to dogs are illustrated in Fig. 4, with mean pharmacokinetic parameters presented in Table 1. The oral bioavailability values were 72 and 37% for the HPβCD solution and the MC suspension, respectively. Following p.o. administration in HPβCD and MC, the C_{max} values were 1.4 and 0.7 μg/ml, and the T_{max} values were 2.5 and 15 h, respectively. The $t_{1/2}$ was 15 h following i.v. administration. Mean pharmacokinetic parameters of SCH 56592 following p.o. administration at 10 mg/kg in fed and fasting dogs are shown in Table 2. Food enhanced the bioavailability of SCH 56592, while the shape of the serum concentration-time profile was not affected by food (data not shown). The data in Table 2 show that both C_{max} and $AUC_{0-\infty}$ were increased approximately fourfold in the fed dogs compared to the fasting dogs. Mean pharmacokinetic parameters of SCH 56592 following p.o. administration of doses of 10, 40, 80, and 120 mg/kg to fed dogs are shown in Table 2. As the dose increased, concentrations of SCH 56592 in serum increased as reflected by dose-related increases in both C_{max} (up to 80 mg/kg) and $AUC_{0-\infty}$ (up to 120 mg/kg).

The mean serum concentration-time profile of SCH 56592 in fed dogs on days 1 to 13 during and after daily p.o. administration at 40 mg/kg for eight consecutive days as a suspension in MC is shown in Fig. 5; mean pharmacokinetic parameters on days 1 and 8 are shown in Table 3. Because of the limited number of blood samples taken after the first dose (day 1), the results of the single dose-exposure study at the 40-mg/kg dose level were included in Table 3 to compare single- and multiple-dose data. Concentrations of SHC 56592 in serum appeared to be at steady state by day 8, since concentrations in serum on days 6, 7, and 9 were similar (Fig. 5). Concentrations in serum

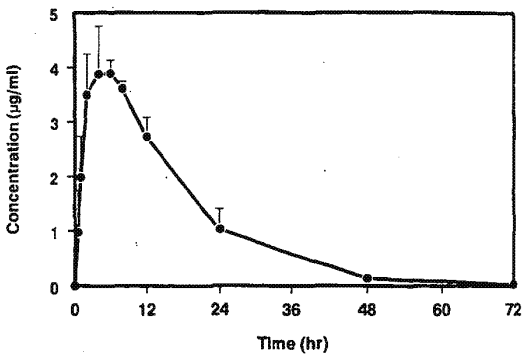


FIG. 3. Serum concentration-time profile of SCH 56592 in rabbits following the p.o. administration of a 20-mg/kg dose of SCH 56592 as a suspension in MC. Each vertical bar represents 1 standard deviation from the mean.

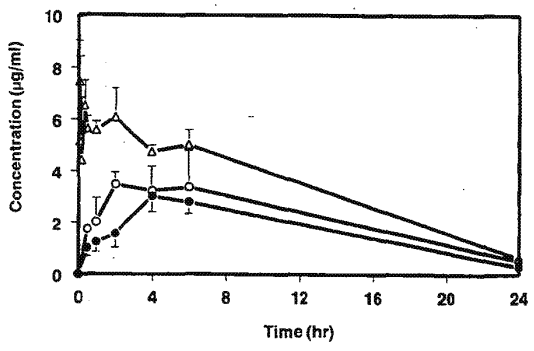


FIG. 2. Serum concentration-time profiles of SCH 56592 in rats following the i.v. or p.o. administration of a 20-mg/kg dose of SCH 56592 △, i.v. as a solution in HPβCD; ○, p.o. as a solution in HPβCD; ●, p.o as a suspension in MC. Each vertical bar represents 1 standard deviation from the mean.

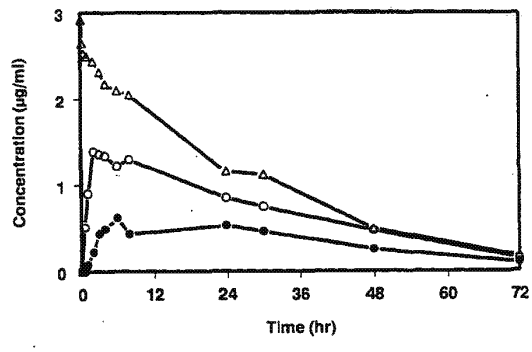


FIG. 4. Serum concentration-time profiles of SCH 56592 in dogs following the i.v. or p.o. administration of a 10-mg/kg dose of SCH 56592 △, i.v. as a solution in HPβCD; ○, p.o. as a solution in HPβCD; ●, p.o as a suspension in MC.

UM00012051
NOVARTIS EXHIBIT 1017
Novartis v. Regents, IPR2023-01346
Page 797 of 4460

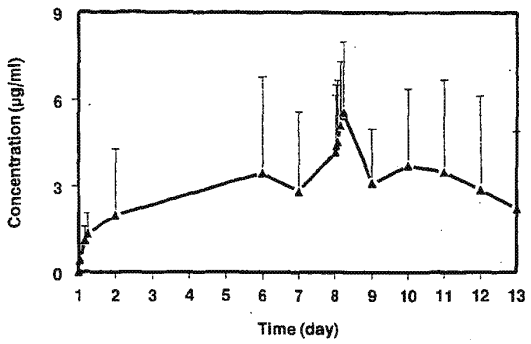


FIG. 5. Serum concentration-time profile of SCH 56592 in dogs during and following daily p.o. administration of 40 mg of SCH 56592 per kg as a suspension in MC for eight consecutive days. Sampling times were at 1, 4, 6, and 8 h on the first day of dosing (day 1), predose on days 2, 6, and 7, and at 0.5, 1, 2, 4, 6, 8, 12, 24, 48, 72, 96, and 120 h after the last dose (administered on day 8). Each vertical bar represents 1 standard deviation from the mean.

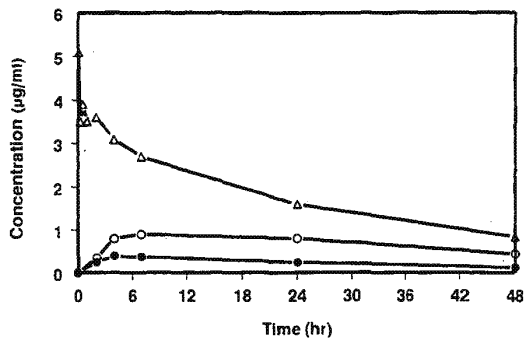


FIG. 6. Serum concentration-time profiles of SCH 56592 in cynomolgus monkeys following the i.v. or p.o. administration of a 10-mg/kg dose of SCH 56592. △, i.v. as a solution in HPβCD; ○, p.o. as a solution in HPβCD; ●, p.o. as a suspension in MC.

were higher upon multiple dosing; the accumulation index was approximately 2.6.

Mean serum concentration-time profiles of SCH 56592 in fasting monkeys following i.v. and p.o. administration at a 10-mg/kg dose level are shown in Fig. 6, with mean pharmacokinetic parameters presented in Table 1. The oral bioavailability values were approximately 52 and 14% from the HPβCD solution and the MC suspension, respectively. Following p.o. administration in HPβCD and MC, the C_{max} values were 1.1 and 0.4 μg/ml, respectively. The $t_{1/2}$ was calculated from the i.v. data to be approximately 23 h.

DISCUSSION

SCH 56592 was bioavailable in all five species studied. The oral bioavailability was higher with the HPβCD solution than with the MC suspension, which was not surprising, since the compound is completely in solution following administration in HPβCD. This also suggests either that SCH 56592 did not precipitate out from the HPβCD solution in the gastrointestinal tract or that it was dissolved quickly in the gastrointestinal tract contents after precipitation. The latter explanation is unlikely because the bioavailability from the MC suspension was always lower than that from HPβCD solution.

Oral bioavailability was higher in mice, rats, and dogs than in monkeys. In rabbits, high concentrations in serum suggested good oral bioavailability from the MC suspension. The $t_{1/2}$ values in mice, rats, and rabbits were 7 to 9 h, while in dogs and monkeys they were 15 and 23 h, respectively. Dose-related increases in serum drug concentrations were observed in mice (dose range, 20 to 160 mg/kg), rats (10 to 120 mg/kg), and fed dogs (10 to 120 mg/kg) following a single p.o. dose in the MC suspension. However, as the dose increased, the increase in the C_{max} was less than that in the AUC, suggesting that absorption is slowed at higher doses. Also, concentrations above the MICs and minimal fungicidal concentrations were observed at 24 h following a single p.o. dose in the MC suspension in all five species studied (data not shown), suggesting that a once-daily administration could be the clinical dose regimen.

Studies in dogs showed that the administration of SCH 56592 as a suspension in MC with food increased both the C_{max} and the $AUC_{0-\infty}$ approximately fourfold. This increase in bioavailability is likely due to a greater dissolution in the presence of food because of increased residence time in the stomach as well as increased gastrointestinal secretions (4, 6, 13, 14). This is supported by the finding that p.o. administration of the same dose of SCH 56592 as a solution in HPβCD with food increased its bioavailability by only 60% compared to administration of the same solution under fasting conditions (data not shown).

Following daily administration of 40 mg/kg for eight consecutive days in an MC suspension to fed dogs, concentrations in serum were higher than those following a single dose, as indicated by an approximately 2.6-fold increase in the C_{max}. However, the $AUC_{0-\infty}$ following a single dose (105 μg · h/ml) was similar to the AUC_{0-24} following multiple doses (107 μg · h/ml) (Table 3), indicating no untoward accumulation upon multiple dosing in the dog.

In conclusion, SCH 56592 was orally bioavailable in mice, rats, rabbits, dogs, and monkeys. Dose-related increases in concentrations of SCH 56592 in serum were observed in mice, rats, and dogs following administration in an MC suspension. Food improved the oral bioavailability in dogs approximately fourfold. SCH 56592 concentrations in serum increased upon multiple dosing with no untoward accumulation.

TABLE 3. Single- versus multiple-dose pharmacokinetics of SCH 56592 in fed dogs following daily administration in an MC suspension of 40 mg/kg for 8 consecutive days

Parameter (unit)	Mean (% CV; $n = 5$)	
	Single dose[a] (day 1)	Multiple dose (day 8)
C_{max} (μg/ml)	2.1 (31)	5.6 (43)
T_{max} (h)	9.2 (90)	5.0 (45)
AUC (μg · h/ml)	105.0 (30)[b]	107.0 (47)[c]

[a] These data are from the dose-response study (Table 2).
[b] $AUC_{0-\infty}$
[c] AUC_{0-24}

REFERENCES

1. **Armstrong, D.** 1989. Problems in management of opportunistic fungal infections. Rev. Infect. Dis. **11**:S1591.
2. **Emmons, C. W.** 1977. Medical mycology, 3rd. ed. Lea and Febiger, Philadelphia, Pa.
3. **Gibaldi, M., and D. Perrier.** 1982. Pharmacokinetics, 2nd ed., p. 409–417. Marcel Dekker, New York, N.Y.
4. **Hebbard, G. S., M. W. Sun, F. Bochner, and M. Horowitz.** 1995. Pharma-

UM00012052
NOVARTIS EXHIBIT 1017
Novartis v. Regents, IPR2023-01346
Page 798 of 4460

cokinetic considerations in gastrointestinal motor disorders. Clin Pharmacokinet. 28:41–66.
5 **Lutz, J. E., K. V. Clemons, B. H. Aristizabal, and D. A. Stevens.** 1997. Activity of the triazole SCH 56592 against disseminated murine coccidioidomycosis. Antimicrob. Agents Chemother. 41:1558–1561.
6 **Nomeir, A. A., P. Mojavarian, T. Kosoglou, M. B. Affrime, J. Nezamis, E. Radwanski, C. C. Lin, and M. N. Cayen.** 1996. Influence of food on the oral bioavailability of loratadine and pseudoephedrine from extended-release tablets in healthy volunteers. J. Clin. Pharm. 36:923–930.
7. **Oakley, K. L., G. Morrissey, and D. W. Denning.** 1997. Efficacy of SCH-56592 in a temporarily neutropenic murine model of invasive aspergillosis with an itraconazole-susceptible and an itraconazole-resistant isolate of *Aspergillus fumigatus*. Antimicrob. Agents Chemother. 41:1504–1507.
8 **Oakley, K. L., C. B. Moore, and D. W. Denning.** 1997. In vitro activity of SCH-56592 and comparison with activities of amphotericin B and itraconazole against *Aspergillus* spp. Antimicrob. Agents Chemother. 41:1124–1126.
9 **Perfect, J. R., G. M. Cox, R. K. Dodge, and W. A. Schell.** 1996. In vitro and in vivo efficacies of the azole SCH56592 against *Cryptococcus neoformans*. Antimicrob. Agents Chemother. 40:1910–1913.
10. **Pfaller, M. A., S. Messer, and R. N. Jones.** 1997. Activity of a new triazole, Sch 56592, compared with those of four other antifungal agents tested against clinical isolates of *Candida* spp. and *Saccharomyces cerevisiae*. Antimicrob. Agents Chemother. 41:233–235.
11. **Sugar, A. M., and X.-P. Liu.** 1996. In vitro and in vivo activities of SCH 56592 against *Blastomyces dermatitidis*. Antimicrob. Agents Chemother. 40:1314–1316.
12. **Walsh, T. J., and P. A. Pizzo.** 1988. Nosocomial fungal infections: a classification for hospital-acquired infections and mycoses arising from endogenous flora and reactivation. Annu. Rev. Microbiol. 42:517.
13. **Welling, P. G.** 1986. Pharmacokinetics: process and mathematics. American Chemical Society, Washington, D.C.
14. **Welling, P. G.** 1977. Influence of food and diet on gastrointestinal drug absorption: a review. J. Pharmacokinet. Biopharm. 5:291–334.

UM00012053
NOVARTIS EXHIBIT 1017
Novartis v. Regents, IPR2023-01346
Page 799 of 4460